

*Perspectives in
Supramolecular
Chemistry*

FOUNDED BY J.-M. LEHN



**Supramolecular Materials
and Technologies**

Edited by

David N. Reinhoudt

Supramolecular Materials and Technologies

Editorial Board

Founding Editor

J.-M. Lehn, Collège de France, Chimie des Interactions Moléculaires, 11 Place Marcelin Berthelot, 75005 Paris, France

Editors

J.-P. Behr, Université Louis Pasteur, Institut le Bel, 4 Rue Blaise Pascal, F-67070, Strasbourg, France

G. R. Desiraju, University of Hyderabad, School of Chemistry, Hyderabad 500134, India

A. D. Hamilton, Yale University, Department of Chemistry, New Haven, CT 06520-8107, USA

T. Kunitake, Kyushu University, Faculty of Engineering, Hakozaki, Fukuoka 812, Japan

D. N. Reinhoudt, University of Twente, Faculty of Chemical Technology, PO Box 217, 7500 AE Enschede, The Netherlands

J.-P. Sauvage, Université Louis Pasteur, Institut le Bel, 4 Rue Blaise Pascal, F-67070 Strasbourg, France

Supramolecular Materials and Technologies

*Perspectives in
Supramolecular Chemistry
Volume 4*

EDITED BY DAVID N. REINHOUDT

University of Twente, Department of Chemistry, Enschede, The Netherlands

JOHN WILEY & SONS

Chichester · New York · Weinheim · Brisbane · Toronto · Singapore

Copyright © 1999 John Wiley & Sons Ltd,
Baffins Lane, Chichester,
West Sussex PO19 1UD, England

National 01243 779777
International (+44) 1243 779777

e-mail (for orders and customer service enquiries): cs-books@wiley.co.uk
Visit our Home Page on <http://www.wiley.co.uk>
or <http://www.wiley.com>

All Rights Reserved. No part of this publication may be reproduced, stored in a retrieval system, or transmitted, in any form or by any means, electronic, mechanical, photocopying, recording, scanning or otherwise, except under the terms of the Copyright, Designs and Patents Act 1988 or under the terms of a licence issued by the Copyright Licensing Agency, 90 Tottenham Court Road, London W1P 9HE, UK, without the permission in writing of the publisher.

Other Wiley Editorial Offices

John Wiley & Sons, Inc., 605 Third Avenue,
New York, NY 10158-0012, USA

WILEY-VCH Verlag GmbH, Pappelallee 3,
D-69469 Weinheim, Germany

Jacaranda Wiley Ltd, 33 Park Road Milton,
Queensland 4064, Australia

John Wiley Sons (Asia) Pte Ltd, Clementi Loop #02-01,
Jim Xing Distripark, Singapore 129809

John Wiley & Sons (Canada) Ltd, 22 Worcester Road,
Rexdale, Ontario M9W 1L1, Canada

Library of Congress Cataloging-in-Publication Data

Supramolecular materials and technologies / edited by David N. Reinhoudt.

p. cm. — (Perspectives in supramolecular chemistry : v. 4)

Includes bibliographical references and indexes.

ISBN 0-471-97367-X (hb : alk. paper)

1. Macromolecules. I. Reinhoudt, D. N. II. Series.

QD381.S87 1999

99-18991

547'.7-dc21

CIP

British Library Cataloguing in Publication Data

A catalogue record for this book is available from the British Library

ISBN 0-471-97367-X

Typeset in 10/12pt Times by Techset Composition Ltd, Salisbury, Wiltshire
Printed and bound in Great Britain by Biddles Ltd, Guildford and King's Lynn
This book is printed on acid-free paper responsibly manufactured from sustainable forestation, for which at least two trees are planted for each one used for paper production.

Contents

Contributors	vii
Preface	ix
1 Self-Assembling Systems on Scales from Nanometers to Millimeters: Design and Discovery Lyle Issacs, Donovan N. Chin, Ned Bowden, Younan Xia and George M. Whitesides	1
2 Dendritic Architectures Marcel H. P. van Genderen and E. W. Meijer	47
3 Supramolecular Structures with Macromolecules Uwe Beginn and Martin Möller	89
4 Chemosensors: Synthetic Receptors in Analytical Sensing Applications Anthony W. Czarnik and Juyoung Yoon	177
5 Selective Ion Recognition with Durable Sensors Ronny J. W. Lugtenberg and David N. Reinhoudt	193
6 Ion Separations in Membrane and Solid Phase Extraction Systems Reed M. Izatt, Jerald S. Bradshaw and Ronald L. Bruening	225
7 Porphyrin- and Expanded Porphyrin-based diagnostic and therapeutic agents Tarak D. Mody and Jonathan L. Sessler	245

Cumulative Author Index	295
Cumulative Title Index	299
Index	301

Contributors

Uwe Beginn, Universität Ulm Abteilung Organische Chemie III/Makromolekulare Chemie, Albert-Einstein-Allee 11, D-89069 Ulm, Germany

Ned Bowden, Department of Chemistry and Chemical Biology, Harvard University, 12 Oxford Street, Cambridge, MA 02138, USA

Jerald S. Bradshaw, Department of Chemistry and Biochemistry, Brigham Young University, Provo, UT 84602, USA

Ronald L. Bruening, IBC Advanced Technologies Inc., American Fork, UT 84003, USA

Donovan N. Chin, Moldyn Inc, 955 Massachusetts Avenue, Cambridge, MA 02139, USA

Anthony W. Czarnik, Illumina, 9390 Towne Centre Drive, STE 200, San Diego, CA 92121-3015, USA

Lyle Issacs, Department of Chemistry and Chemical Biology, Harvard University, 12 Oxford Street, Cambridge, MA 02138, USA

Reed M. Izatt, Department of Chemistry and Biochemistry, Brigham Young University, Provo, UT 84602, USA

Ronny J. W. Lugtenberg, Laboratory of Supramolecular Chemistry and Technology and MESA Research Institute, University of Twente, PO Box 217, 7500 AE Enschede, The Netherlands

E. W. Meijer, Laboratory of Macromolecular and Organic Chemistry, Eindhoven University of Technology, PO Box 513, 5600 MB Eindhoven, The Netherlands

Tarak D. Mody, Pharmacyclics Inc., 995E. Arques Ave. Sunnyvale, CA 94086, USA

Martin Möller, Universität Ulm, Abteilung Organische Chemie III/ Makromolekulare Chemie, Albert-Einstein-Allee 11, D-89069 Ulm, Germany

David N. Reinhoudt, Laboratory of Supramolecular Chemistry and Technology and MESA Research Institute, University of Twente, PO Box 217, 7500 AE Enschede, The Netherlands

Jonathan L. Sessler, The University of Texas at Austin, Department of Chemistry and Biochemistry, Austin, TX 78712, USA

Marcel H. P. Van Genderen, Laboratory of Macromolecular and Organic Chemistry, Eindhoven University of Technology, PO Box 513, 5600 MB Eindhoven, The Netherlands

George M. Whitesides, Department of Chemistry and Chemical Biology, Harvard University, 12 Oxford Street, Cambridge, MA 02138, USA

Younan Xia, Department of Chemistry and Chemical Biology, Harvard University, 12 Oxford Street, Cambridge, MA 02138, USA

Juyoung Yoon, Department of Chemistry, The Scripps Research Institute, La Jolla, CA 92037, USA

Preface

From the early days of supramolecular chemistry the field has been associated with possible applications. This is not surprising as the design of new molecules, and later of assemblies of molecules, is often function driven. Now, after three decades of supramolecular chemistry, it is interesting to reflect on what has really been achieved in terms of applications. This is the field that I have defined as Supramolecular Technology.

In the beginning *molecular recognition was the objective*. From this work on receptors that selectively recognize ionic species, the first applications are now established technologies. They can be found in analytical chemistry, in separation science and in the medical world. Chapters 4 to 7 deal with the various aspects of these technologies.

In more recent years there is a development towards *molecular recognition as a tool*. Based on the increasing understanding of the weak forces between (macro) molecules we now see new concepts of material design. Chapters 1 to 3 cover three aspects of this development: nanostructures that are formed by self-assembly of small molecules (chapter 1), dendritic structures (chapter 2) and polymers (chapter 3). A volume of a series like *Perspectives in Supramolecular Chemistry* can never claim to cover all aspects of a subject. All I can hope is that these chapters are representative of the field of supramolecular technology.

David N. Reinhoudt
Enschede

Chapter 1

Self-assembling Systems on Scales from Nanometers to Millimeters: Design and Discovery

LYLE ISAACS*, DONOVAN N. CHIN†, NED BOWDEN*, YOUNAN XIA*,
AND GEORGE M. WHITESIDES*

* *Harvard University, MA, USA*

† *Moldyn Inc., Cambridge, MA, USA*

1. INTRODUCTION

Self-assembly is the spontaneous organization of molecules or objects into stable aggregates by noncovalent forces [1–5]. Self-assembly is especially evident in biology and much of the early inspiration for studies of self-assembly came from biological aggregates: lipid bilayers, viral capsids, the DNA duplex, and the tertiary and quaternary structure of proteins [6–8]. Chemists have been exploring self-assembly as an alternative to the powerful, but stepwise, methods of synthetic chemistry [2,9–27]. Self-assembly is interesting both for its biological relevance, and because it is a new approach to complex structures having nanometer to millimeter dimensions that are difficult or impossible to prepare by traditional techniques. Figure 1 shows a scale from 1 nm to 10 mm; several examples of natural systems and their corresponding sizes are shown above the scale. Below the scale are pictures of four self-assembling systems that have been investigated in this group, namely hydrogen bonded self-assembled aggregates both in solution and the solid state, patterned self-assembled monolayers (SAMs) of alkanthiolates on gold, and milli-

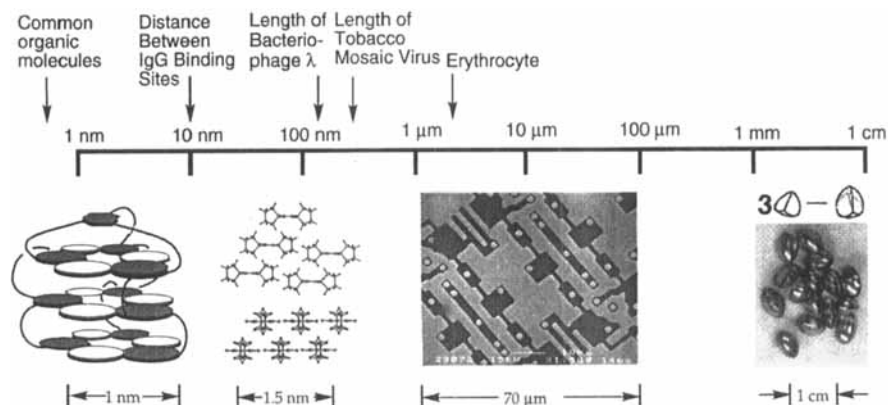


Figure 1 Illustration of the range of sizes of structures that can be formed by self-assembly. The sizes of several natural objects are included above the logarithmic scale for the purpose of comparison

meter-scale two- and three-dimensional self-assembled structures based on capillary forces: these systems form the basis of this review.

Many different types of forces have been explored for their ability to form self-assembled structures including: hydrogen bonds, metal–ligand interactions, hydrophobic interactions, electrostatic forces, and capillary forces. Receptor–ligand interactions and DNA duplex formation have also been used to form self-assembled structures. In this review we describe some of our experiences with self-assembly in four systems: aggregates in solution held together by networks of hydrogen bonds based on the cyanuric acid–melamine lattice [28,29], aggregates held together in the solid state by hydrogen bonds [30], SAMs of alkanethiols on gold [31,32], and mesoscale objects assembled using capillary forces [33–35]. Studies in self-assembly have often proceeded by designing the components, hypothesizing the outcome of the self-assembly process, preparing the components in the laboratory, and observing if a well-ordered assembly results experimentally. If an assembly forms, then it is characterized; if not, the program moves on to the next system. This hit-and-miss approach is inefficient. We have explicitly tried to develop systems that are stable, form reliably, and are amenable to systematic structural variation. The ability to make structural changes, and to observe the process resulting in self-assembly, has begun to allow us to understand the rules of self-assembly governing these systems and to make predictions about related structures.

2. SCOPE AND OBJECTIVES OF THE REVIEW

The scope of this review includes four areas of self-assembly that were investigated in this laboratory; namely self-assembly based on hydrogen bonds in solution, self-

assembly based on hydrogen bonds in organic molecular crystals, self-assembly of monolayers of alkanethiolates on gold, and self-assembly of macroscopic objects using capillary and other forces. The sections on aggregation in solution and the solid state will be limited to those systems where hydrogen bonds are a specific design element, characterization is extensive, and theoretical predictions of stability have been made. Self-assembly in natural systems and self-assembly in solution based on other forces are excluded from the review. The section on self-assembled monolayers will focus on the formation, structure, defects, and applications of SAMs and mixed SAMs of alkanethiols on gold. We do not include SAMs on substrates other than Au(111), or with ligands other than alkanethiols. The section on self-assembly of macroscopic objects will focus on assembly based on lateral capillary forces.

The objectives of this review are: to describe the types of structures that can be formed by self-assembly in these systems, to discuss the current experimental and theoretical issues of self-assembly, to assess the current role of theory in the predicting stability of self-assembled systems, and to highlight important future directions for self-assembled structures.

3. EXPERIMENTAL SYSTEMS

3.1 Soluble Hydrogen-bonded Molecular Aggregates

(a) Introduction

Organic chemistry has traditionally been concerned with the synthesis and characterization of *molecules* held together by *covalent* bonds. The great power and utility of organic synthesis is exemplified by the preparation of complex molecules such as vitamin B₁₂, palytoxin, and brevetoxin [36–39]. In recent years, however, increasing attention has been directed toward larger biomolecules; for example, peptides, proteins, oligosaccharides, RNA, and DNA. Much of the structure and function of these biomolecules is derived from noncovalent forces; namely hydrophobic and electrostatic interactions and hydrogen bonds. Often, these molecules are themselves aggregates of several molecules and are held together exclusively by intermolecular interactions. Based on this impetus, we and others have studied the ability of hydrogen bonds to direct the formation of aggregates [29]. Excellent reviews describing the work of other groups involved in this field are available [2,9,11,15,17,20,23]. The specific goal of this section is to describe the most important current issues in the design, synthesis, and characterization of aggregates based on the network of hydrogen bonds in the cyanuric acid-melamine lattice (CA•M). At the end of this section, the current limitations of and future challenges for self-assembly are discussed.

(b) Design

The focus of our research on hydrogen-bonded aggregates in solution is on one portion of the CA•M lattice, namely the cyclic hexameric “rosette”, which is composed of three molecules of CA and M (Figure 2) [40]. We have concentrated on the hydrogen-bonded CA•M lattice for several reasons: hydrogen bonds are highly directional, the hydrogen-bonds are numerous (18 per rosette) and strong in chloroform solution (1–3 kcal mol⁻¹ per hydrogen bond), and derivatives of CA and M are easily prepared by organic synthesis. The aggregation of several molecules to form a structured aggregate is an entropically disfavored process; the enthalpy of the interaction must overcome losses of translational, rotational, and conformational entropy.

We have used two strategies in the design of stable self-assembled aggregates based on the CA•M lattice; namely, preorganization [40] and peripheral crowding

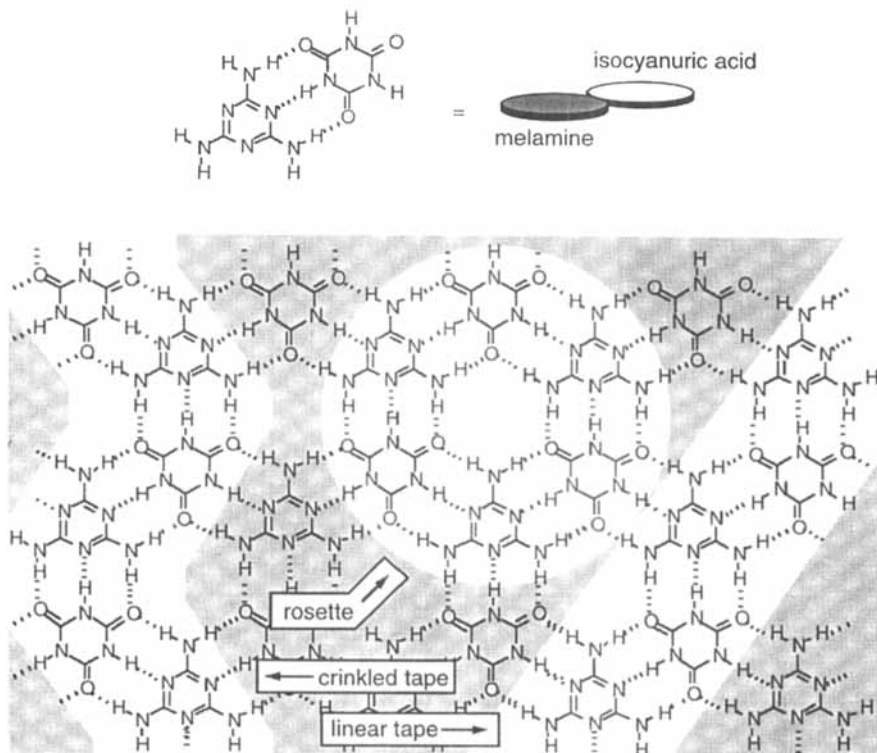


Figure 2 The structure of the hydrogen-bonded CA•M lattice. Three classes of aggregates that we have observed in solution and the solid state are highlighted: the rosette, crinkled tape, and linear tape motifs. The molecular structures of melamine and cyanuric acid and their abbreviated representation as dark and light disks are shown

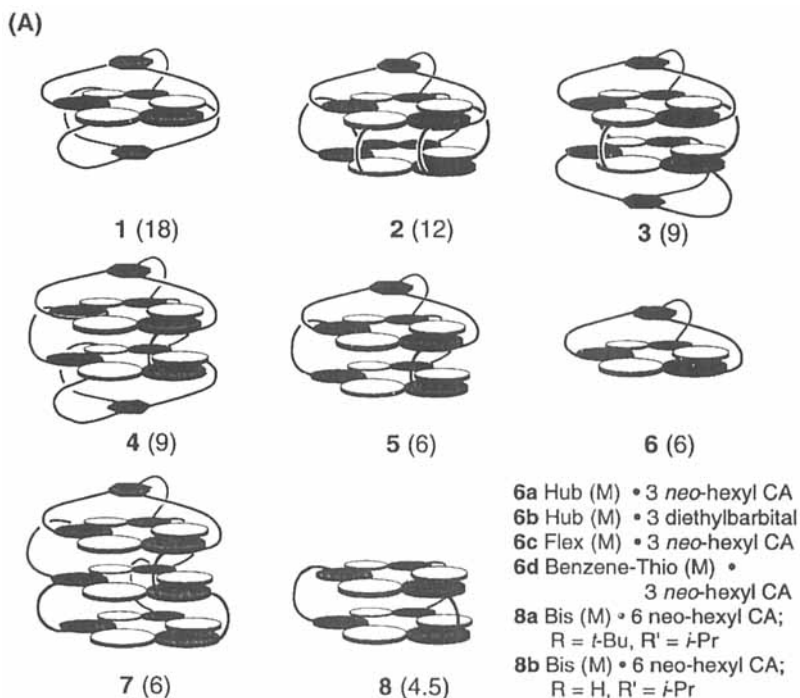


Figure 3 (A) Schematic representations of eight distinct classes of self-assembled structures (1–8). Aggregates 1–8 are arranged in decreasing order of stability; the number in parentheses is the ratio of the number of hydrogen bonds formed (HB) to the number of aggregating molecules minus one ($N - 1$) that we have used as a semiempirical parameter of stability.

[41]. Figure 3A shows eight distinct members (1–8) of this family of aggregates. The molecular structures of the components are shown in Figure 3B [40–48].

Preorganization Preorganization is a qualitative concept introduced by Cram [4] to describe the conformational similarity of a molecule in its uncomplexed relative to its complexed state. We have covalently linked the three melamines of the CA•M rosette by “spokes” to a central benzene-based “hub”; this linkage results in preorganization by reducing unfavorable changes in translational, rotational, and conformational entropy upon formation of the aggregate.

Peripheral crowding Peripheral crowding is a second strategy that produces stable aggregates based on the CA•M lattice [41]. Large substituents on CA and M develop severe steric interactions in certain configurations. These unfavorable steric interactions are less important in the cyclic rosette structure than in the linear or crinkled tape motifs (Figure 4) [41]. These steric interactions can be used to promote the formation of the rosette structure for these aggregates.

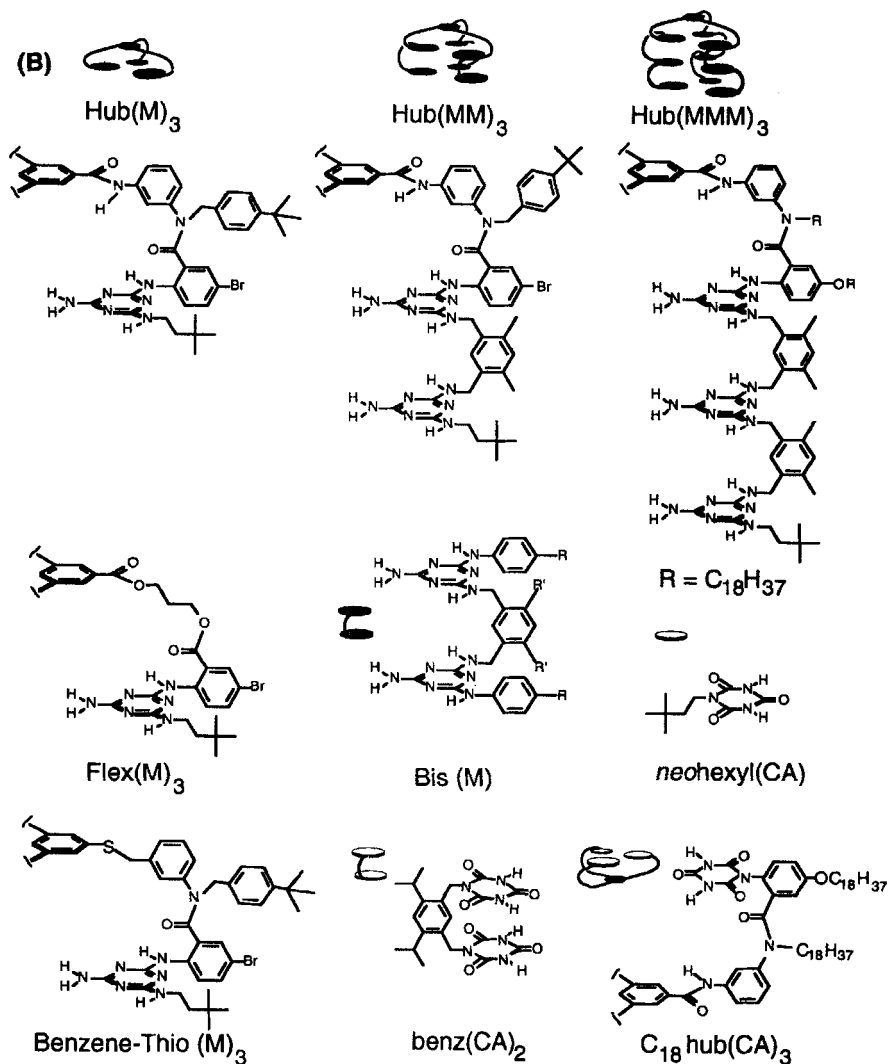


Figure 3 (B) Molecular and schematic representations of the components used in the formation of 1–8

HB/N – 1 The stability of hydrogen-bonded aggregates based on the CA·M lattice is related to the number of hydrogen bonds (*HB*) formed upon aggregation and the total number of aggregating molecules (*N*) [28,49,50]. For the related series of aggregates shown in Figure 2, the quantity *HB/(N – 1)* is very useful predictor of relative stability. This ratio is intuitively reasonable; the enthalpy of aggregation is expected to increase as *HB* increases; the unfavorable losses of translational and

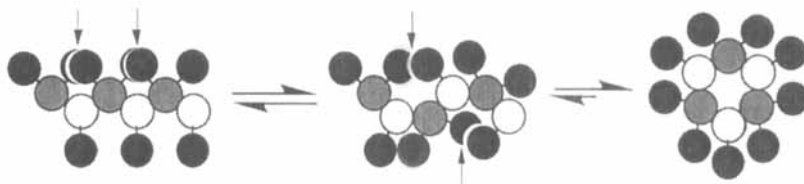


Figure 4 Incorporation of large groups (black disks) on the periphery of CA and M results in steric interaction between these groups in the tape (left) and crinkled tape (center) motifs, the arrows indicate these regions. In the rosette motif (right) these unfavorable steric interactions are minimized

rotational entropy upon aggregation is expected to increase as the number of particles in the assembly increases. In general, our experience suggests that $HB/(N - 1)$ should be equal to or greater than six in order to achieve reasonably stable aggregates in the CA•M series in chloroform solution.

Symmetry In systems based on the CA•M lattice, the three points of connection of the spokes to the edge of the rosette can lead to C_3 or C_1 symmetry. Figure 5A shows a schematic representation of the two enantiomeric forms of C_3 - and C_1 -symmetric (6). It is useful to incorporate one or more potential elements of symmetry in the design of self-assembled aggregates. Products that possess these symmetry elements will show diagnostically simple NMR spectra, whereas structures that do not possess these symmetry elements will show more complex (and more difficult to analyze) spectra. Often, only a single structure for a self-assembled aggregate meets the symmetry considerations imposed by NMR spectral data and in these cases it is possible to use NMR spectroscopy to determine structure with few ambiguities [43,46,51]. Conversely, aggregates which are C_1 symmetric are particularly difficult to characterize; structure determination in these cases would require the powerful NMR techniques used for protein structure determination.

Solubility An important consideration in the design of self-assembled structures is solubility. The cyanuric acid and melamine components are often poorly soluble in chloroform; this insolubility hinders both synthesis and analysis of the self-assembled structure. We have often attached *t*-butyl benzyl, *t*-butyl phenyl, *n*-C₁₈H₃₇, and *neo*-hexyl groups to provide sufficient CHCl₃ solubility.

CPK models CPK models were used to help visualize the geometries of molecules and complexes in the design of aggregates 1–8. These models are useful in identifying aggregates that *cannot* be stable due to impossible geometric constraints. They are *not* useful, in general, in determining the stability of a given aggregate, or even relative stability within a series of aggregates. Since CPK models are not calibrated for the weak intermolecular interactions that are so important in self-

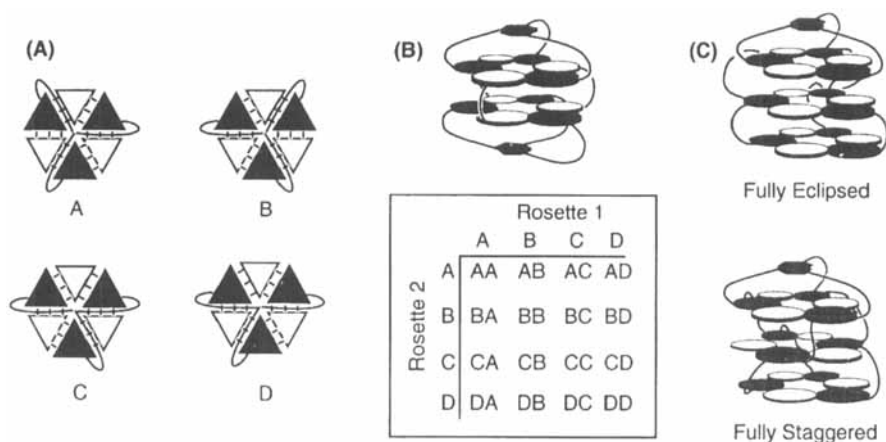


Figure 5 Aggregates 1–8 have the potential to exist as mixtures of isomers. (A) Schematic depiction of the four isomers possible for 6 resulting from different points of attachment of the spokes to the rosette. (B) Aggregate 3, which contains two rosettes, can exist in 16 isomeric forms. This table enumerates the 16 possibilities based on the four isomers for a single rosette shown in (A). (C) Schematic depiction of the fully staggered and fully eclipsed isomers of 7; only these isomers are compatible with the six lines in the imide region of the ^1H NMR spectrum

assembly, one must be cautious not to over-interpret the results inferred from examination of molecular models.

(c) Synthesis

The synthesis of noncovalent hydrogen-bonded aggregates can often be accomplished simply by mixing the components in the correct molar ratio in an appropriate solvent (usually chlorinated hydrocarbons such as chloroform). In some cases, one of the components (usually the cyanuric acids) may be poorly soluble in chloroform; in these cases it may be useful to dissolve the components in a more polar solvent or solvent mixture (e.g. chloroform–methanol), then remove this solvent and redissolve the residue in chloroform. This procedure can overcome kinetic limitations to formation of aggregates associated with solubilities.

(d) Characterization

Synthetic organic chemists have developed a powerful set of tools for the structural elucidation of synthetic or natural products. By applying these techniques it is often possible to provide *definitive proof* for the structure of a covalent molecule. Structural elucidation for aggregates is less direct and we have had to rely on

inference based on data obtained using several characterization methods. The most useful of these methods are nuclear magnetic resonance, gel permeation chromatography, vapor pressure osmometry (VPO), and electrospray mass spectrometry [28,51–53].

Nuclear magnetic resonance Several aspects of the NMR spectra of these hydrogen-bonded aggregates are noteworthy. These features are discussed here for the specific case of **6a** (Hub(M)₃•3 *neo*-hexyl (CA) (Figure 6A) [40].

Peak width The ¹H NMR spectrum of Hub(M)₃ in chloroform is broad and featureless except for solvent and *t*-butyl peaks (Figure 6A). This nondescript spectrum is the result of self-association and restricted rotation around the RNH–triazene bonds.

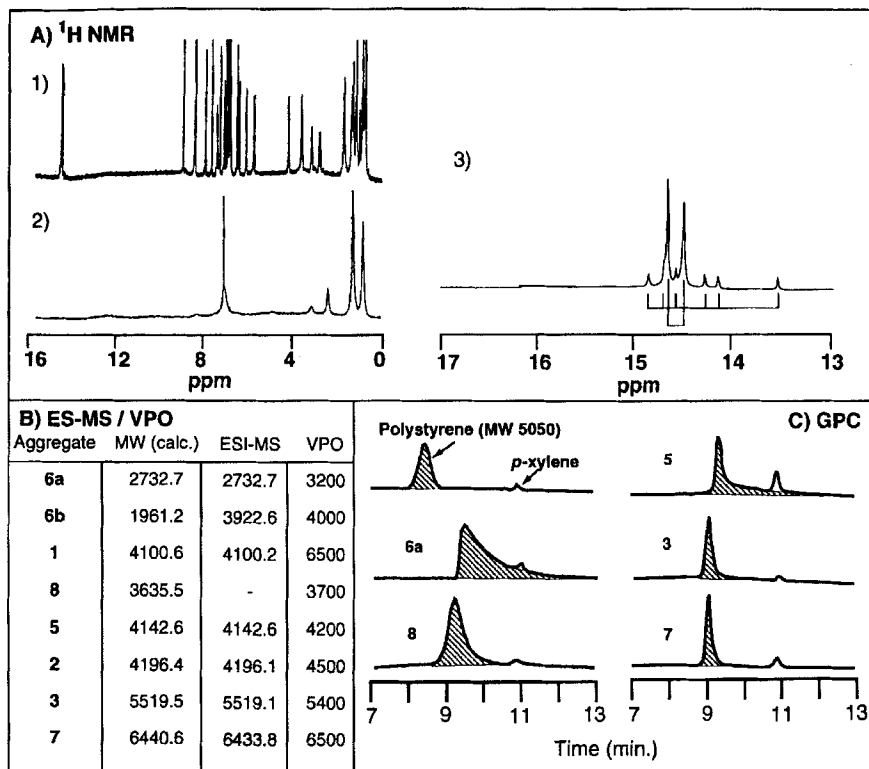


Figure 6 Characterization data for some noncovalent aggregates: (A) ¹H NMR spectra in CDCl₃ for 1) **6a**, 2) Hub(M)₃ and 3) and an expansion of the imide region for **6b**, (B) a table showing the calculated and experimentally determined (ES-MS and VPO) molecular weights for several aggregates; and (C) GPC chromatograms for five aggregates

Stoichiometry by titration The titration of $\text{Hub}(\text{M})_3$ with solid portions of *neo*-hexyl CA can be monitored by ^1H NMR spectroscopy. Upon addition of three equivalents of *neo*-hexyl CA, the broad and featureless spectrum of $\text{Hub}(\text{M})_3$ is transformed into the highly structured spectrum of **6a** (Figure 6A). At intermediate amounts of *neo*-hexyl CA, the spectrum is a combination of **6a** and free $\text{Hub}(\text{M})_3$. Addition of *neo*-hexyl CA beyond three equivalents has no effect on the ^1H NMR spectrum; it is insoluble and visible as a white powder. These experiments are good evidence for the 1 : 3 stoichiometry.

Hydrogen bonded imide protons The hydrogen bonded N-H protons of the isocyanurate resonate in an uncluttered region of the ^1H NMR spectrum (13–16 ppm) [40,51,54]. The location and sharpness of these resonances is consistent with the presence of a highly structured hydrogen-bonded aggregate in solution. The number and intensity of these resonances is diagnostic for the time-averaged symmetry of the aggregate in solution [51]. In particular, only two resonances are observed in this region of the spectrum for **6a**. This observation implies that on the NMR time-scale, this aggregate has C_3 symmetry. The corresponding spectrum for **6b** ($\text{Hub}(\text{M})_3 \cdot 3$ diethylbarbital) shows eight resonances; two of higher intensity and six of lower, but equal intensity (Figure 6A). We rationalize this result by postulating two different aggregates, with C_3 and C_1 symmetries (Figure 5). In principle, these isomers can interconvert by rotation of the melamine about one of the aryl–NH triazine bonds.

^1H NMR: other aspects Two other aspects of the ^1H NMR spectrum of hydrogen bonded aggregates are useful in determining structure. Variable-temperature NMR can reveal dynamic processes that are fast (or slow) on the NMR time scale at room temperature [51]. Nuclear Overhauser effect (nOe) studies can be used to determine relative proximity of the hydrogen bonded protons and the diastereotopic methylene protons [40,43,46]. ^1H NMR competition studies where two different hubs (for example, $\text{Hub}(\text{M})_3$ and $\text{Flex}(\text{M})_3$) compete for only three equivalents of CA allows direct assessment of the relative stability of the competing aggregates [45,55].

Gel permeation chromatography GPC is a size-exclusion technique that provides information on molecular weight and stability of aggregates [41,43,44,46–48]. The pores of the stationary phase (cross-linked styrene/divinylbenzene) readily allow small molecules to enter, whereas larger molecules are excluded from these pores. The direct result is that smaller molecules take longer to pass through the column than larger molecules. Figure 6C shows the GPC traces obtained for **6a**, **8**, **5**, **3**, **7** and polystyrene ($MW = 5050$, polydispersity = 1.05) with added *p*-xylene as standard. The stability of these aggregates is reflected in the extent of their tailing on the column. Stable aggregates (e.g. **3** and **7**) elute from the column as sharp peaks. In contrast, kinetically more labile aggregates (e.g. **6a**, **8**, and **5**) dissociate on the GPC time scale (≈ 8 min) into their components; these components then

separate. These unstable aggregates appear as broadened, tailing peaks by GPC. The order of stability suggested by GPC correlates well with predictions based on the values of $HB/(N - 1)$ and on ^1H NMR competition studies.

Vapor pressure osmometry VPO is a classical colligative property that yields a semiquantitative (number average) estimate of molecular weight in solution. Figure 6B shows the molecular weights determined by VPO for a series of aggregates. In general, the agreement between the calculated and experimentally determined molecular weight is within 20%. In the experiment, the voltage (and hence current) is recorded that is required to maintain a solution at known aggregate concentration at the same temperature as pure solvent while both undergo evaporative cooling. Comparing these voltages to those recorded for a series of standards of known molecular weight (in our case, sucrose octaacetate ($MW = 679$), polystyrene ($MW = 5050$), and perbenzoyl β -cyclodextrin ($MW = 3321$)) gives an estimate of the molecular weight of the unknown.

Electrospray ionization mass spectrometry ES-MS is a powerful tool for the analysis of bimolecular complexes and complexes containing metal cations. The success of these measurements relies on the ability of the complex to be ionized from suitable (usually aqueous) solvent systems. The aggregates described here are unstable in water, so a different ionization system was required. The use of the chloroform-soluble charge carrier tetraphenylphosphonium chloride, in experiments performed by Smith and coworkers, allowed the ionization of **6a** and its detection as $\mathbf{6a}\cdot\text{Cl}^-$ [52,53]. Figure 6B shows the excellent agreement between the calculated and experimental values obtained for several other aggregates. Collision induced dissociation experiments of the m/z selected $\mathbf{6a}\cdot\text{Cl}^-$ complex showed ions corresponding to $\text{Hub}(\text{M})_3\text{Cl}^-$ and $\mathbf{6a}\cdot\text{Cl}^-$; this selectivity supports the suggestion that the self-assembly of **6a** in solution is a cooperative process.

(e) Discussion

Analysis of the spokes Many different mono-rosette aggregates, including (**6a–6d**, **6c**: $\text{Flex}(\text{M})_3\cdot 3$ *neo*-hexyl CA, **6d**: benzene-thio($\text{M})_3\cdot 3$ *neo*-hexyl CA), have been prepared based on the “hub and spoke” architecture. On the basis of the number of hydrogen bonds formed and the number of particles aggregating, one might assume on the basis of the value of $HB/(N - 1)$ that the stability of **6a–6d** would be similar. In fact, the stability of this series of aggregates depends on the nature of the “spokes” [42,49,50,56,57]. Compared to **6a** hubs incorporating thioether linkages (**6d**) or a propane diol linker (**6c**) form less stable aggregates (as determined by ^1H NMR spectroscopy, competition, and GPC studies). These results are readily rationalized; upon formation of the aggregates, larger losses in conformational entropy occur for **6c** and **6d** than for **6a** these losses result in a lower overall free

energy of binding. The entropic cost of freezing a n -fold free rotor in a single conformation can be approximated by Equation 1 [50,57].

$$T\Delta S = -RT \ln n \quad (1)$$

Thus, the rigid amide bonds and benzene rings in HubM₃ are less costly to restrict conformationally than are the three-fold rotors in Flex(M)₃ and benzene-thio(M)₃.

Peripheral crowding and buttressing groups Peripheral crowding refers to the steric interaction between substituents on the periphery of an aggregate; these steric interactions can be used to favor the formation of the rosette over tape and crinkled tape motifs (Figure 4) [41]. For example, aggregate **8a** (Bis(M)•3 *neo*-hexyl CA, R = *t*-Bu, R' = *i*-Pr) is formed and is stable in chloroform solution, while aggregate **8b** (Bis(M)•3 *neo*-hexyl CA, R = H, R' = *i*-Pr), which incorporates the less bulky phenyl group, does not form a well defined aggregate on mixing the components in chloroform. Another important factor governing the stability of **8a** (and also **2–5** and **7**) is the incorporation of the isopropyl (or methyl) groups on the phenylenediamine linker [41]. These isopropyl groups act as buttressing groups and preorganize the melamines (or CA in the case of **2** and **3**) to lie in parallel orientation. When these isopropyl groups are removed (Bis(M)•3 *neo*-hexyl CA, R = *t*-Bu, R' = H) no stable aggregate formed.

Isomers As described above, aggregate **6** can exist in two isomeric forms, namely C₃- and C₁-**6** (Figure 5). An important goal of this research program is the synthesis of large, structurally complex aggregates. Toward this goal, we investigated the design, synthesis, and characterization of aggregates incorporating two or more rosettes stacked in parallel orientation, (**3–5** and **7**) [41–43,46,47]. The potential isomerism in these aggregates is more complex than in aggregates based on a single rosette. For **3**, sixteen isomeric aggregates differing only in the relative orientation of the spokes are possible (Figure 5B). The ¹H NMR spectrum of **3** showed only two resonances in the imide region. Symmetry considerations, therefore, rule out all but three of the possible isomers; namely, the enantiomeric pairs D₃-AA and D₃-BB and the meso compound C_{3h}-AB. It was not possible to distinguish between these possibilities on the basis of NMR spectroscopy, but computational results suggest that C_{3h}-AB is less stable than D₃-AA and D₃-BB due to unfavorable eclipsing interactions between the phenyl groups [54].

The most complicated aggregate that has been prepared to date is **7** [46]. Aggregate **7** consists of a nona-melamine derivative, Hub(MMM)₃, and nine molecules of *neo*-hexyl CA comprising three connected parallel rosettes. Aggregate **7** is held together by 54 hydrogen bonds and has a weight of 6.4 kD – slightly larger than a small protein like insulin. As for **3**, many (16) isomers are possible, but ¹H NMR of the aggregate shows only six resonances in the imide region. These six resonances result from three independent C₃-symmetric rosettes contributing two resonances each. Only the fully eclipsed and fully staggered conformations shown in

Figure 5C are consistent with these symmetry constraints. We have not been able to distinguish between these isomeric forms. These observations serve as a warning: it may be possible to synthesize relatively complex aggregates like 7, but in the absence of symmetry their characterization will remain challenging.

(f) *Attempted synthesis of tetrahedral aggregates*

We have investigated the possibility of forming aggregates in which a CA•M rosette is held on each face of a tetrahedron [55,58]. Such tetrahedral aggregates would be a step toward structurally complex and potentially functional aggregates (the central cavity could, for example, act as a receptor for guest molecules). Figure 7 shows the molecular structure of the two components and a schematic drawing of the proposed tetrahedral aggregate. Each tetrahedron would be composed of ten individual particles; four equivalents of tris-M would be situated at the corners of the tetrahedron, and six equivalents of bis-CA bridge each edge of the tetrahedron. The proposed aggregate would be held together by 72 hydrogen bonds; yielding a value of $HB/(N - 1) = 8$. A homogeneous solution of the components in hot chloroform–methanol could be formed, but upon cooling and concentration only CHCl_3 -insoluble gels were formed. These results were discouraging since we predicted stability for this aggregate *a priori* based on examination of CPK models and $HB/(N - 1)$. We believe that instability in this case is due to two factors: insufficient preorganization, and an unfavorable $\Delta\Delta G$ of solvation; there is a high entropic price to trap solvent molecules inside the tetrahedral cavity.

(g) *Future challenges and unsolved problems*

Despite our success in predicting and understanding the series of aggregates based on connected stacks of CA•M rosettes, we have not yet been able to extend this

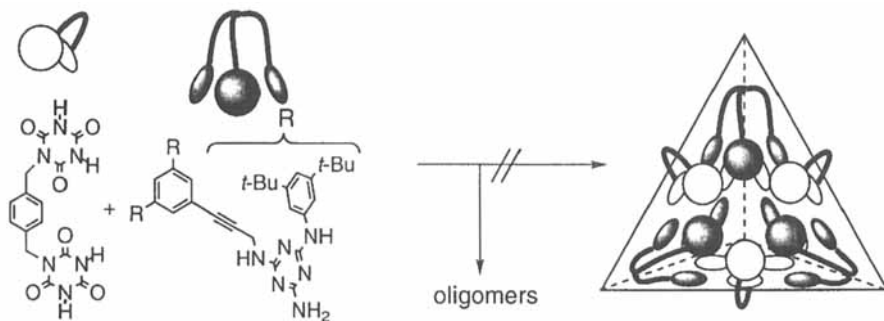


Figure 7 Molecular structures and schematic representations of a bis-CA and a tris-M that do not self-assemble to form the proposed tetrahedral aggregate: oligomers are formed preferentially

platform beyond parallel stacked rosettes [58]. We also have not yet been able to make very large aggregates. Our unsuccessful efforts directed toward the synthesis of tetrahedral aggregates underscore this point; despite our best efforts at design we were unable to synthesize stable aggregates. Clearly, there are terms that contribute to the ΔG of aggregation as well as intra- and intermolecular forces that we do not yet understand well. One particular deficiency is that CPK models are *not* helpful in predicting the stability of structures involving noncovalent forces. Improved methods (computational or otherwise) for the construction, manipulation, and evaluation of potential self-assembled structures as well as improved methods for the characterization of nonsymmetrical aggregates would be useful and important advances.

An important future concern for self-assembly is the construction of aggregates with function. None of the aggregates that we have synthesized to date are functional. Some steps have been taken in this direction by Rebek who has made dimeric aggregates that show molecular recognition properties and by Ghadiri who has made artificial membrane channels [9,12]. Without some demonstrated utility, this type of self-assembly remains an interesting, but academic, exercise in design. An equally important concern for future work in self-assembly is the solvent. Most of the self-assembled hydrogen bonded structures prepared have been designed to assemble in chlorinated hydrocarbons. In contrast, the interesting examples of biological self-assembly take place in water. A clear current limitation of molecular self-assembly is our inability to take advantage of the hydrophobic effect to construct aggregates that are both structured, soluble, and stable in water.

3.2 Molecules on Surfaces: Self-Assembled Monolayers

Self-assembled monolayers (SAMs) are highly ordered molecular assemblies that form spontaneously by chemisorption and self-organization of functionalized long-chain molecules on the surfaces of appropriate substrates [59]. They represent the best developed class of nonbiological systems involving self-assembly. They are robust, relatively stable, and capable of providing the flexibility, both at the individual molecular and materials levels, required to tailor the properties of surfaces [32,60]. Various types of systems of SAMs have been developed (Table 1), and a number of reviews have been devoted to this subject [32,59,61–63]. This section will focus on SAMs of alkanethiolates on thin polycrystalline films of gold since they are the most studied, and certainly the best characterized, system to date [64]. We shall outline the formation, structure, order, and defects of SAMs and their applications in interface engineering and microfabrication.

The process of spontaneous formation of *ordered* structures that occur as reaction, adsorption, and organization of alkanethiols ($X-(CH_2)_n-SH$) on gold is a good example of molecular self-assembly [1,31]. Their construction is driven by the thermodynamically favored segregation of molecules to the phase boundary between *solid gold and solution* (or vapor) of alkanethiols. The chemical bonding between

Table 1 Substrates and ligands that form self-assembled monolayers (SAMs)

Substrate	Ligand or precursor	Binding	Ref.
Au	RSH, ArSH (thiols)	RS–Au	62
Au	RSSR' (disulfides)	RS–Au	87
Au	RSR' (sulfides)	RS–Au	150
Au	RSO ₂ H	RSO ₂ –Au	151
Au	R ₃ P	R ₃ P–Au	152
Ag	RSH, ArSH	RS–Ag	153
Cu	RSH, ArSH	RS–Cu	154
Pd	RSH, ArSH	RS–Pd	155
Pt	RNC	RNC–Pt	156
GaAs	RSH	RS–GaAs	157
InP	RSH	RS–InP	158
SiO ₂ , glass	RSiCl ₃ , RSi(OR') ₃	siloxane	159
Si/Si–H	(RCOO) ₂ (neat)	R–Si	160
Si/Si–H	RCH=CH ₂	RCH ₂ CH ₂ Si	161
Si/Si–Cl	RLi, R–MgX	R–Si	162
metal oxides	RCOOH	RCOO ⁻ ···MO _n	163
metal oxides	RCONHOH	RCONHOH ···MO _n	164
ZrO ₂	RPO ₃ H ₂	RPO ₃ ²⁻ ···Zr(IV)	165
In ₂ O ₃ /SnO ₂ (ITO)	RPO ₃ H ₂	RPO ₃ ²⁻ ···M(n+)	166

sulfur atoms and gold on the surface ($\approx 44 \text{ kcal mol}^{-1}$) drives the assembly; sulfur atoms anchored on the surface bring the alkyl chains of these molecule into close contact, freezing out configurational entropy, and leading the chains to order [62]. The degree of interaction in a SAM increases with the density of molecules on the surface and the length of the alkyl backbones. As a result, only alkanethiolates with $n > 11$ form closely-packed, highly-ordered, and effectively two-dimensional organic quasicrystals on the surfaces of gold [62]. The nomenclature of materials science is not fully in accord with organic chemistry in the use of the term of “self-assembly”: systems in which only chemisorption was involved, and neither monolayers nor ordered structures were formed, have also been called SAMs.

(a) Fundamental studies on SAMs

SAMs of alkanethiolates on gold have been characterized using a wide range of techniques (Table 2). Because optical and diffraction techniques can only reveal the properties of SAMs averaged over probed areas that are typically a few square millimeters in size, scanning probe microscopy (SPM) is increasingly used to study SAMs, and in particular, to characterize their structure and order [62,65]. Application of SPM to SAMs has, however, been more complicated than anticipated. There is still no good model to account for what occurs when a metallic tip approaches a gold surface that has been covered with a 1–2 nm thick layer of insulating SAMs

Table 2 Methods for the characterization of SAMs by alkanethiolates on Au

Property of SAMs	Technique	Refs.
Structure and order	Scanning probe microscopy (STM, AFM, and LFM)	62, 65
	Infrared spectroscopy	61, 167
	Low energy helium diffraction	168
	X-ray diffraction	169
	Transmission electron diffraction	170
	Surface Raman scattering	171
	Sum frequency spectroscopy (SFS)	172, 173
Composition	X-ray photoelectron spectroscopy (XPS)	174
	Temperature programmed desorption (TPD)	175
	Mass spectroscopy (MS)	69, 176
Wettability	Contact angle	177
Thickness	Ellipsometry	178
Coverage and/or degree of perfection	Quartz crystal microbalance (QCM)	71
	Surface acoustic wave device (SAWD)	179
Defects	Electrochemical methods	180, 181
	STM and AFM	62
	Wet etching	78

[62]. Explaining the SPM image requires caution. For example, the hexagonal lattice observed in early scanning tunneling microscopy (STM) studies [66] that used high currents (≈ 1 nA) is now believed to be the image of the sulfur atoms rather than the head groups of a SAM [62]. The structure of the outer surface of a SAM (for example, the superlattice) can only be observed using STM operated at ultralow currents (<10 pA). The contrast in the STM image acquired at a constant current provides a positive record of the topology of the SAM. The SPM technique is now showing a rich variety of surface structures (or phases), and more importantly, it is providing a flood of useful information about the origin and distribution of defects in SAMs [62,65].

Formation of SAMs SAMs of alkanethiolates on gold can be easily prepared by spontaneous adsorption of alkanethiols onto gold, either from solution or vapor phase. Although it is generally accepted that the reaction involved can be expressed as (2),



the mechanistic details of the reaction of alkanethiols with the gold surface are still not completely understood. For example, the fate of the hydrogen atom, and the exact nature of the resulting species on the gold surface is not well-established. A recent X-ray diffraction study suggested that the species on the Au surface is a disulfide (X-R-S-S-R-X) rather than a thiolate (X-R-S⁻), although this suggestion

requires physically unreasonable bond lengths and results from a sample in which the potential radiation damage was high [67]. Recent studies based on mass spectrometry also indicated that SAMs prepared from solutions of alkanethiols in the ambient atmosphere of a laboratory are a mixture of $X-RS^-$, $X-RSO_2^-$, and $X-RSO_3^-$ since air oxidation of alkanethiolate solutions occurs very rapidly [68,69].

The kinetics of the formation of SAMs on gold has been studied using a number of techniques; ellipsometry [70], contact angle [70], quartz crystal microbalance [71,72], and surface acoustic wave [71]. These studies found that the growth rate was proportional to the number of unoccupied sites on gold, and could be described as a first-order Langmuir adsorption process. Most of these techniques were, however, spatially averaging, and thus left questions about the microscopic aspects of self-assembly unanswered. Poirier and Pylant studied the microscopic mechanism for the formation of closely-packed structures of alkanethiolates on the surfaces of gold using ultrahigh vacuum (UHV) STM [73]. They suggested a molecular-scale picture for the self-assembling process in which the alkanethiols form the following phases with increasing coverage: a lattice-gas phase, a low-density solid phase, and a higher density solid phase (Figure 8). This growth model has been observed in several systems, including SAMs of $HSC_6H_{12}COOH$ and $HSC_9H_{18}CH_3$ from the vapor phase, and SAM of $HSC_9H_{18}CH_3$ from the solution; this mechanism appears to be a general one for the self-assembly of alkanethiolates on gold [73].

Structure and order of SAMs It is generally accepted that sulfur atoms form a $\sqrt{3} \times \sqrt{3}$ R 30° overlayer structure on the Au(111) surface [62]. To maximize the van der Waals interactions between adjacent methylene groups (≈ 1.5 kcal mol $^{-1}$ per CH_2) the chains tilt at an angle of $\approx 30^\circ$ from the surface normal [61]. The alkyl chains, however, may have several different conformations, and thus form a “superlattice” at the surface of the monolayer [74,75]. These results indicate that the order in the top part of SAMs is not dictated by the sulfur atoms directly bonded to the gold, but also strongly depends on the intermolecular interaction between the alkyl chains. When alkanethiolates are terminated with head groups other than the methyl group, it becomes even more complicated to predict and determine the structures of the formed SAMs [62]. In fact, it has been shown that the end group (in particular, a bulky end group) may play the most important role in determining the packing and order of a SAM [76].

Defects in SAMs The density of defects in SAMs may ultimately determine the usefulness of the materials in micro- and nanofabrication [77]. Although SAMs are representative self-assembling systems and tend to reject defects, formation of defects in these systems is inevitable because the true thermodynamic equilibrium is never achieved in the preparation of a SAM. A variety of factors have been found to influence the formation and distribution of defects in a SAM, including the molecular structure of the surface, the length of the alkyl chain, and the conditions used to prepare the SAM [78]. A range of techniques have been employed to

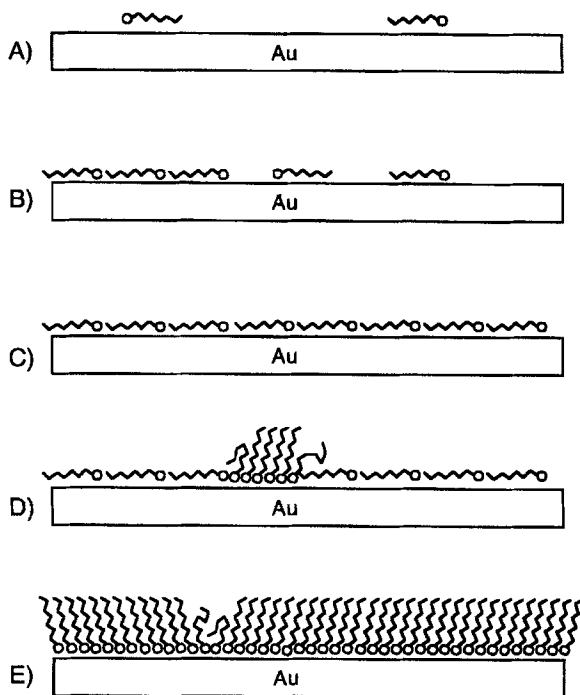


Figure 8 Schematic illustration for the formation of SAMs of alkanethiolates on gold [73]. (A) Alkanethiols adopt the highly mobile lattice-gas phase; (B) above a critical value of coverage, striped-phase islands are formed; (C) surface reaches saturation coverage of striped phase; (D) surface undergoes lateral-pressure-induced solid phase transition: high-density islands nucleate and grow at domain boundaries; (E) high-density islands grow at the expense of the striped phase until the surface reaches saturation

evaluate and characterize the defects in SAMs (Table 2). These techniques are complementary to each other; the electrochemical method only provides a statistical picture of defects over a relatively large area; SPM methods can only collect information over a relatively small area, but can provide useful information about the nature and origin of defects. A combination of these techniques, therefore, seems to be the most appropriate way for the characterization of defects in SAMs.

Figure 9 shows a high resolution STM image of the SAM of dodecanethiolate on the surface of Au(111) [62]. The black lines are now believed to be depressions in the monolayer where neighboring thiols have either tilted over or migrated to cover missing lines of thiols. The inset shows the STM image of a similar sample at a molecular resolution. The gold terrace shown here had five depressions (black “holes”) that are one gold step (≈ 0.24 nm) in depth. These depressions are pits in gold rather than defects in SAMs; they are still covered with an ordered SAM with a lattice characteristic of the packing of molecules in the SAM on the flat surface. The origin of these pits is still under debate; they could originate from a corrosion

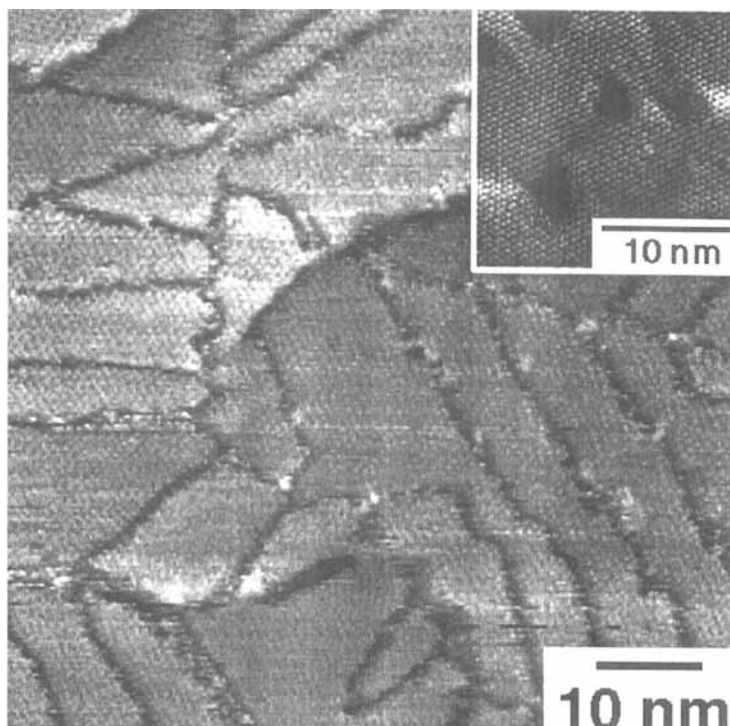


Figure 9 Scanning tunneling microscopy (STM) image of a SAM of dodecanethiolate on Au(111) that shows a gold step, a screw dislocation, and depressed lines in the monolayer due to the accommodation of missing lines of thiols by vicinal molecules. The inset shows five pits in gold that were ≈ 0.24 nm deep and linked by domain boundaries. The monolayer packing corresponds to a phase of the $c(4 \times 2)$ rectangular superlattice. These images were provided by Biebuyck and coworkers [62]

process or from a reconstruction of the gold surface caused by the adsorption of the thiols [79,80].

Current estimates for the number of pinholes in SAMs of hexadecanethiolate on Au range from two to several thousand per square centimeter, with the latter value being more realistic. Thermal annealing induces reorganization of the SAM and the surface, and usually reduces the density of pits in SAMs by migration and coalescence of pits in gold with steps [81]. A recent study using a wet-chemical etchant to amplify the defects in SAMs gave ≈ 90 pits mm^{-2} as a minimum value for the density of defects for a SAM of hexadecanethiolate on 20 nm thick gold [78]. Preparation of truly defect-free SAMs still remains a great challenge in this area.

Mixed SAMs The preparation of SAMs with more than one head groups and/or chain lengths is a prerequisite for many of their uses in the design and synthesis of interfaces with complex properties [32,60,82,83]. With the development of SPM

techniques, more and more information has become available on the structure and order in mixed SAMs [84,85]. In contrast to what is known about mixed Langmuir–Blodgett (LB) films [86], no phase segregation occurs at scales larger than 50 nm for two-component SAMs on gold surface. Asymmetric disulfides (RS–SR') provide a good system for the study of phase segregation in mixed SAMs because the adsorption of disulfide on gold leads to two equal populations of end groups in the formed SAM [84,85,87]. STM images showed that the two components (for example, –CH₃ and –OH) in the SAM are well mixed without disruption of the packing in the monolayer [88].

(b) Applications of SAMs in interface engineering and microfabrication

SAMs of alkanethiolates on gold exhibit many of the features that are most attractive about self-assembling systems: ease of preparation, relatively low density of defects, good stability under ambient laboratory conditions, and amenability to the control over the interfacial (for example, physical, chemical, electrochemical, and biochemical) properties [32,59]. SAMs have been used as active elements to fabricate sensors and biosensors [89,90]; they may also be useful in fabricating capacitors and molecular electronic devices [91]. Equally importantly, SAMs are capable of protecting the underlying surfaces from certain chemical etchants, a characteristic that may have a number of potential technological applications. Early studies showed that SAMs of alkanethiolates on Cu and GaAs can inhibit oxidation by retarding oxygen transport to the surface [92,93]. We, and others, recently demonstrated that SAMs can be directly used as nanometer-thick resists in chemical etching; this capability combined with appropriate printing techniques is the basis for methods of fabricating micro- and nanostructures [77,94,95]. Fabrication procedures involving SAMs are relatively low-cost compared with conventional photolithographic methods.

Patterning SAMs in the plane of the monolayer has been achieved using a wide range of techniques (Table 3). Among these techniques, microcontact printing (μ CP) is the one that seems to offer the most interesting combination of convenience and new capability (Figure 10). Microcontact printing forms patterned SAMs by contact of an elastomeric stamp (usually made from polydimethylsiloxane, PDMS) wetted with (or containing dissolved) alkanethiols, with a gold or silver surface [77]. It provides a superior control over the surface chemistry. Printing has the advantage of simplicity and convenience: multiple copies of the pattern can be easily reproduced using a straightforward procedure. It is an inherent parallel process; areas as large as ≈ 50 cm² can be patterned with submicron features on a single impression [96]. A recent, thoughtful study by Larsen *et al.* showed that μ CP formed SAMs of dodecanethiolate on Au(111) that were indistinguishable from those formed from solutions of dodecanethiol, when the ink concentration was >10 mM and the duration of contact was >0.5 s [74].

Table 3 Methods that have been used for patterning SAMs of thiolates

Technique	SAMs	Resolution ^a	Refs.
Microcontact printing (μ CP)	RSH/Au	≈ 35 nm	97
	RSH/Ag	≈ 100 nm	102
	RSH/Cu	≈ 500 nm	182
Photo-oxidation	RSH/Au	≈ 10 nm	183, 184
Photo-cross-linking	RSH/Au	≈ 10 nm	185, 186
Photoactivation	RSH/Au	≈ 10 nm	187, 188
Electron beam writing	RSH/Au	≈ 75 nm	189
	RSH/GaAs	≈ 25 nm	190
Focused ion beam writing	RSH/Ag	≈ 10 nm	191
Neutral metastable atom writing	RSH/Au	≈ 70 nm	192
SPM lithography	RSH/Au	≈ 10 nm	193
Micromachining	RSH/Au	≈ 100 nm	194
Micropen writing	RSH/Au	≈ 10 nm	195

^a The lateral dimension of the smallest feature that has been generated.

Microcontact printing has been used to form patterned SAMs of alkanethiolates on Au, Ag, Cu and GaAs; and of alkylsiloxanes on Si/SiO₂ and glass [95]. Patterned features as small as ≈ 500 nm in dimensions can be routinely generated using μ CP; smaller features (≈ 35 nm) have also been fabricated with greater difficulty and lower reproducibility [97]. The lower limit for the resolution in this technique, the upper limit of the area that can be patterned on one contact, and the degree to which multiple impressions can be brought into registration, have yet to be established.

The ability to form patterned SAMs allows us to engineer the interfacial properties of a surface with one more degree of freedom, in addition to the flexibility offered by SAMs themselves. It provides immediate opportunities to prepare systems in which structures can be controlled *in* the plane of the interface. SAMs can be used to control the nucleation, adsorption, and wetting of other materials, and thus patterned SAMs can be used as templates to direct and control the assemblies of other materials to form useful structures; they can also be used as patterned resists in directing the dissolution of the substrate to form patterns and structures in the underlying substrates (Au, SiO₂ and Si) [95].

Figure 11A shows an optical micrograph of water drops preferentially condensed on hydrophilic SAMs terminated by carboxylic (COOH) groups; no water condensed on the hydrophobic SAMs terminated by methyl (CH₃) groups [98]. This process shows how the functionality of a SAM influences the condensation of water vapor on a SAM-derivatized surface. It uses self-assembly at two scales: the formation of SAMs at the molecular scale and the directed condensation of water vapor at the macroscopic scale. The organization of liquids into patterned arrays illustrates one of the uses of self-assembly in microfabrication [99].

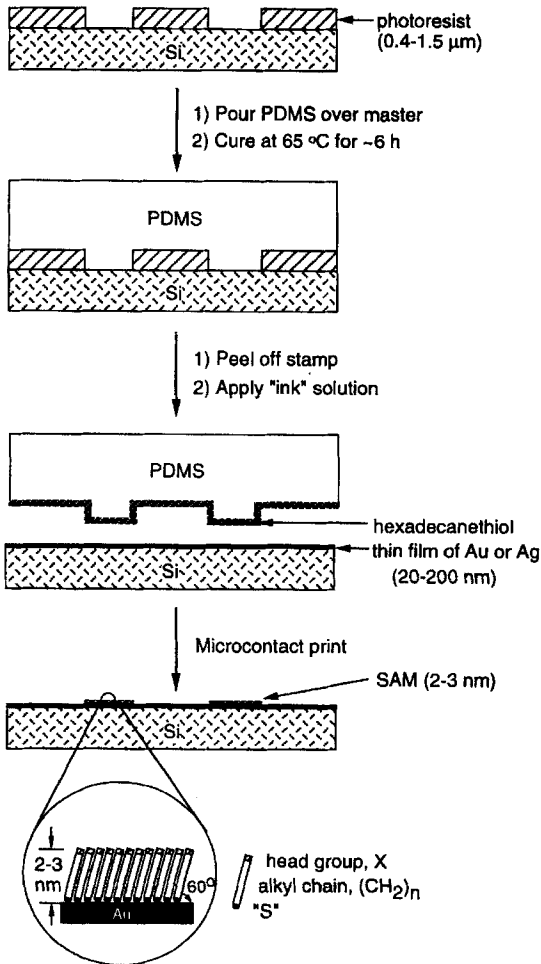


Figure 10 Schematic illustration of the procedure used for microcontact printing of hexadecanethiol on gold

Patterned SAMs can also be used as templates to define and control the adsorption of extracellular matrix proteins, and consequently the attachment of mammalian cells [100,101]. Figure 11B shows an SEM image of cells that have been selectively attached to a surface patterned with SAM. Using a very simple procedure for patterning, it is possible to dictate the shape of a cell that is attached to a surface, and thus partially control cell growth and protein secretion. This technique allows us to examine the influence of cell morphology on cell metabolism, and should be useful for applications in biotechnology that require analysis of individual cells cultured at high density, or for repeated access to cells placed in specified locations.

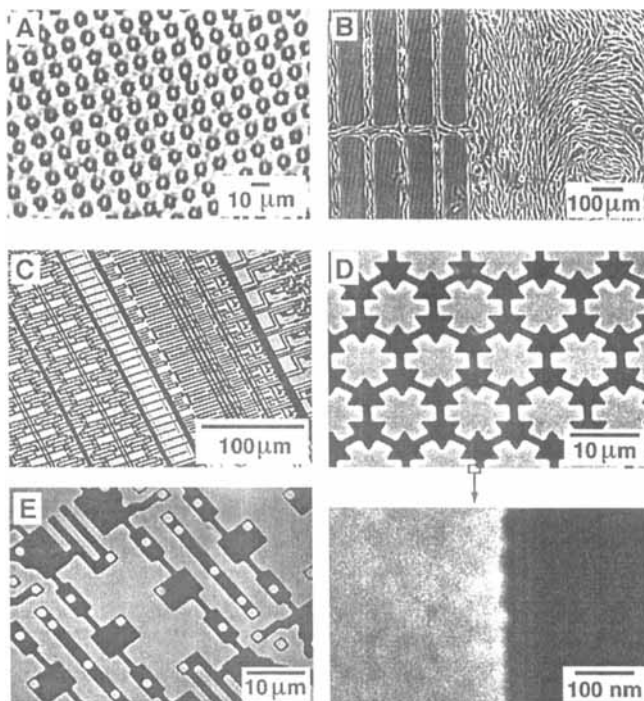


Figure 11 (A) An optical micrograph of water selectively condensed on a SAM-patterned surface of gold [98]; (B) an SEM image of cells selectively attached to a surface using patterned SAMs as templates [100,101]; (C–E) SEM images of test patterns of silver fabricated by μ CP with hexadecanethiol, followed by selective etching in an aqueous ferricyanide solution [102]

Figures 11C–E show SEM images of test patterns of silver that were fabricated using μ CP with hexadecanethiol, followed by selective chemical etching [102]. The SAMs protect the underlying substrates from dissolving by blocking the diffusional access of etchants. The ability to generate arrays of microstructures of coinage metals with controlled shapes and dimensions is directly useful in fabricating sensors and arrays of microelectrodes.

SAMs are prototypical self-assembled systems. They provide a convenient method for forming nanometer-thick “coatings” on solid substrates. Organic synthesis also makes it possible to incorporate different functional groups (with different physical, chemical, electrochemical, and biochemical properties) into and/or at the termini of the alkyl chain. As a result, SAMs themselves are excellent model systems for studies on wetting, adhesion, lubrication, corrosion, nucleation, protein adsorption, and cell attachment [103–105]. The coupling of SAMs with microcontact printing offers a powerful strategy for fabricating small, high-quality

patterns and structures with virtually no specialized equipment. Although the initial pattern is formed in SAMs, subsequent processes such as selective etching and deposition make μ CP a convenient and versatile method for the formation of patterned microstructures of a wide variety of materials. Microfabrication based on μ CP and SAMs offers a higher degree of control over the detailed, molecular-level structure of the interfaces than does photolithography. It can also be readily applied to types of patterning where photolithographic techniques simply fail, for example, patterning nonplanar surfaces [106]. We believe that μ CP will become the major patterning technique in areas where cost or control of surface chemistry is the primary concern. Two issues remain to be solved before μ CP can find applications in microelectronics: systems that form high quality SAMs on semiconductors must be developed; and the formation and distribution of defects in SAMs, especially under the conditions of chemical etching, must be understood.

3.3 Molecular Self-Assembly in the Solid State: Molecular Organic Crystals

The CA·M lattice is a useful starting point for crystal engineering because it predictably forms hydrogen-bonded substructures: tapes or rosettes (Figure 2). The triplet of hydrogen bonds that holds the components together is strong enough to generate these motifs reliably. We were able to rationalize each motif in model systems by identifying the molecular features responsible for promoting each motif. In particular, our clearest success has been in rationalizing general trends in the molecular arrangements *within these motifs* for cocrystals of *para*-substituted diphenylmelamines (**9**) and barbital (**10**) [107]. That is, we were able to control whether the molecules adopted a linear tape, a crinkled tape, or a rosette motif by altering the size of the substituents (Figure 12) [107].

Despite our successes, the potential of CA·M in crystal engineering may be limited. Several features of this system contribute to these limitations. First, growing diffraction-quality crystals in this series remains slow and difficult; in an ideal system, crystallization would be more straightforward. Second, the system does not tolerate polar substituents well. Third, the occurrence of polymorphism decreases the level of control that can be exercised in the system (Figure 13): complexities in packing due to conformational isomerism may be one of the biggest hurdles hindering the rational design of molecular crystals. In principle, each accessible conformation can pack as a separate crystalline phase. While the CA·M system has many attractive characteristics, it is probably too complex to serve as a basis for extensive studies at the current state of development of the field.

We have examined a second system based on 4,5-disubstituted 2-benzimidazolones (cyclic ureas, **11**). Although cyclic ureas were substantially simpler structurally than systems based on CA·M, the tape motif was less robust, and a number of nontape structures formed [108].

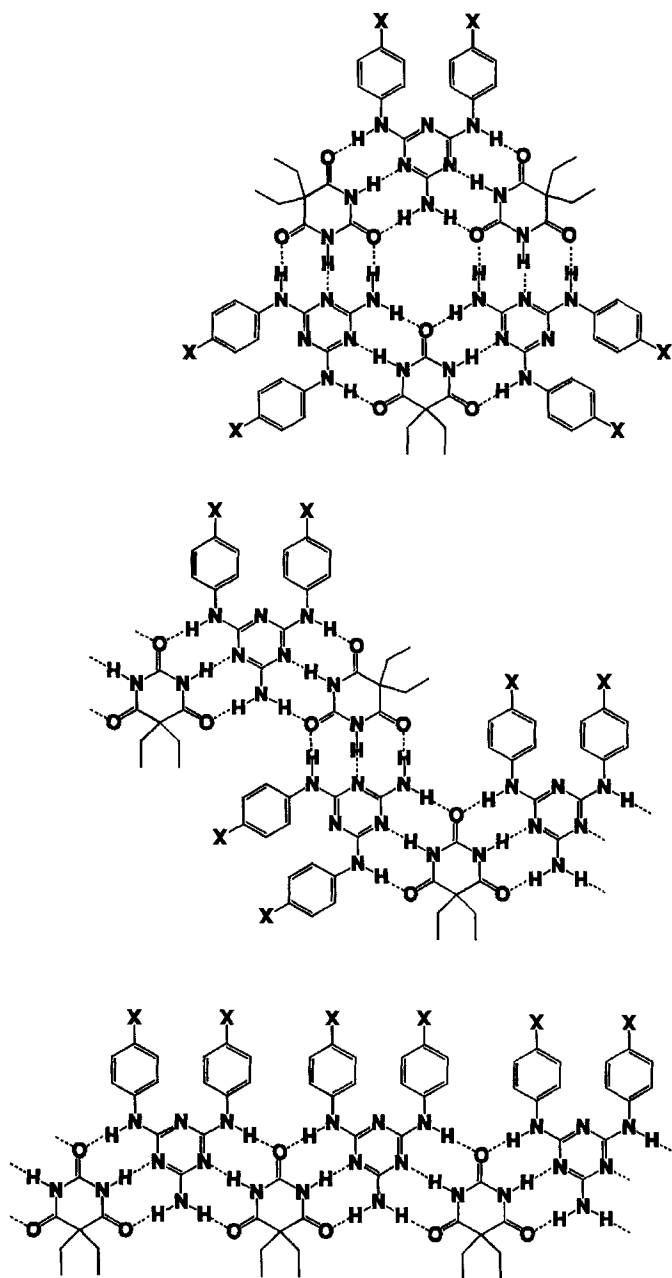


Figure 12 Illustration of three motifs – linear, crinkled, and rosette – that are based on CAM. The size of the para-substituent governs the motif that is formed

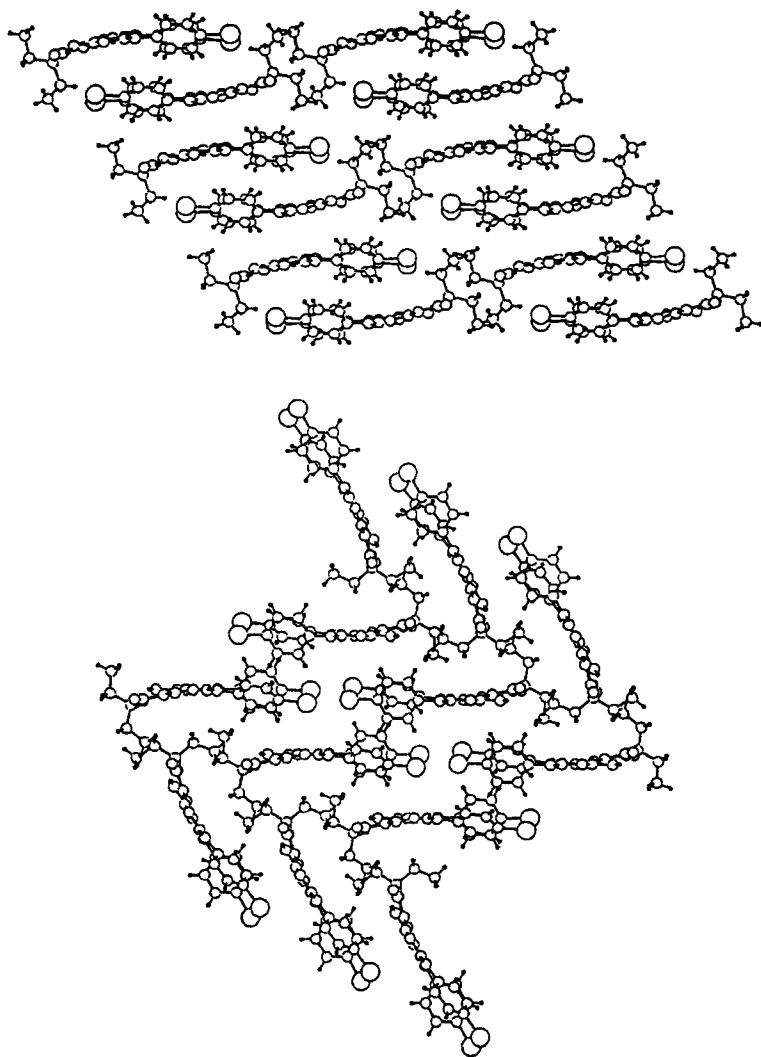


Figure 13 Single crystal X-ray structures of two polymorphic forms of the 1 : 1 cocrystal between diethylbarbital and bis-(*p*-bromophenyl)melamine

Among the classes of molecules able to form hydrogen-bonding-based tapes, the diketopiperazine (DKP) family now appears to be the most attractive [30]. The molecular packing in this system of crystals is less complex than systems based on CA·M or cyclic ureas, because there is only one possible tape. The locations of the 3,6-substituents seems to “protect” the secondary amide groups from interactions

with other amide groups, and thereby constrains the motif to one type of hydrogen-bond network.

More than 40 crystal structures of DKPs (**12**) have already been published [30]. Almost all of these DKPs form linear tapes that pack with their long axis parallel.

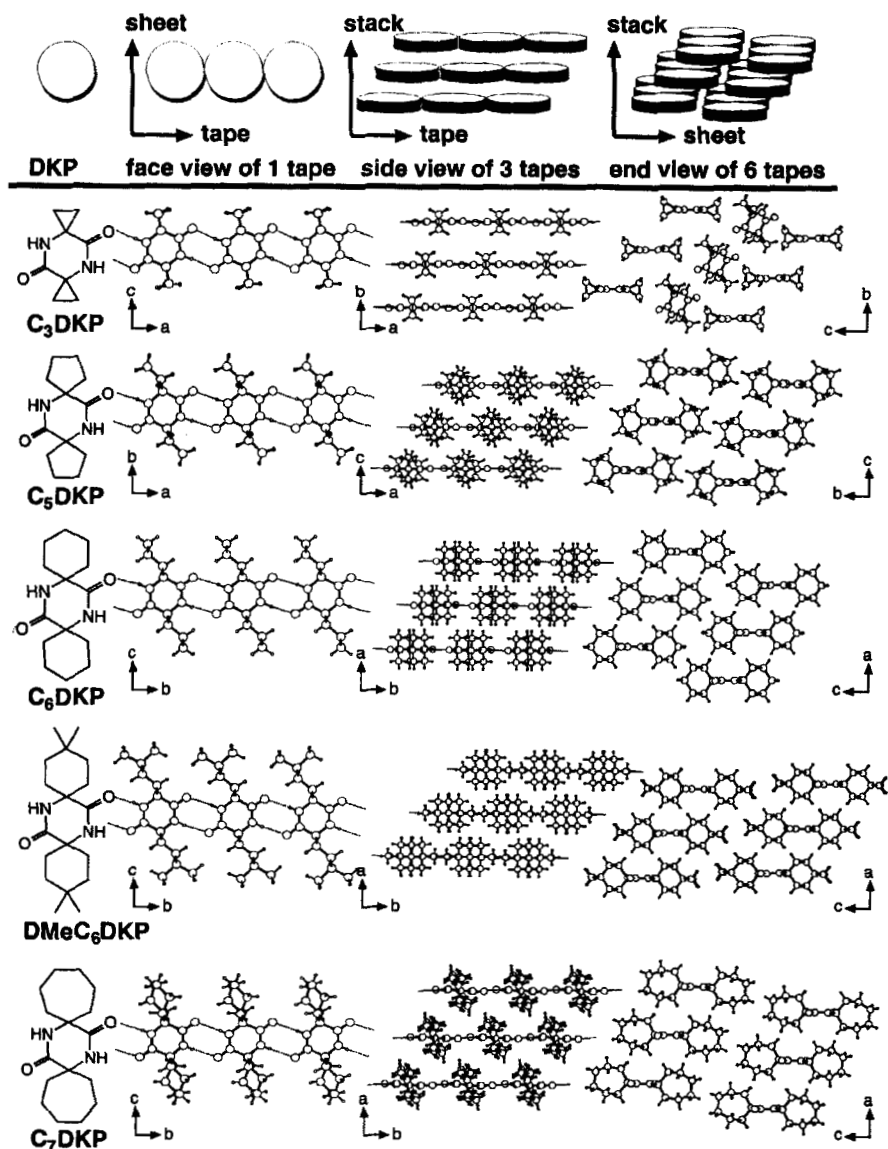


Figure 14 Crystal structures of four different DKP derivatives viewed in three different orientations. All form hydrogen-bonded tapes

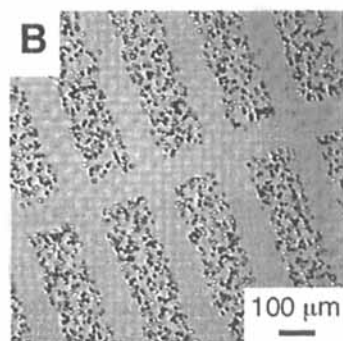
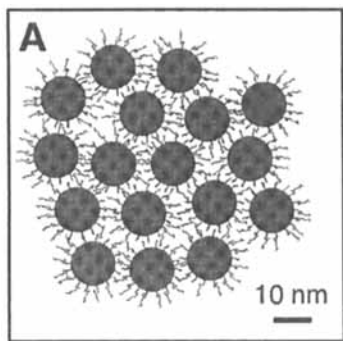
The geometry of the tapes and their packing do not seem to depend strongly on the size, location, and (within some limitations) the type of substituent as is demonstrated in some of the crystals that we have analyzed (Figure 14) [109]. The robustness of the tape motif found in the crystal structures of the DKPs suggests that this system is an excellent platform for studying the packing arrangements of molecules in crystals.

The field of crystal engineering – designing crystals *de novo* based on molecular structures – is still in its prolonged infancy. DKPs do not have the generality to provide the basis for a broad range of different types of crystals, but it provides the most practical system that has been identified to date.

3.4 Mesoscale Self-Assembly

Mesoscopic self-assembly (MESA) is the assembly of *objects* into ordered arrays or units. We define an object as a body whose size is such that its properties can only be considered as those of a material: that is, as collections of many atoms. For example, proteins have a well-defined arrangement of atoms and known molecular weights; we consider them molecules. Colloids, nanotubes, and micron-sized structures fabricated from metals, ceramics, or polymers do not have precisely defined atomic arrangements or molecular weights; we consider them objects. The lower limit on the size of objects considered interesting for use in MESA is set by the upper limit of sizes of molecules that can be made in the laboratory or by nature; the upper limit on the size of the objects for MESA is set by the lower limit of objects that can be better or more easily assembled by the human hand or by machine [1,7]. The size range for the objects varies from several nanometers to centimeters: seven orders of magnitude. Included in this size regime are nanotubes, colloids, cells, transistors, computer chips, bearings, and micromotors, these objects are interesting in fields ranging from biology to microelectronics [110,111].

Mesoscale self-assembly is a new area of research; Figure 15 shows the most notable of these systems [35,112–115]. Gold colloids 13 nm in diameter were assembled into a disordered array based on complementary strands of DNA (Figure 15A) [116]. The colloids were covered in one of two different SAMs terminated in different, noncomplementary DNA sequences. When a soluble linker complementary to both strands was added to an aqueous solution of two colloids the colloids became cross-linked due to DNA duplex formation. The array that formed is not well-characterized but is believed to be densely packed. An example of MESA using micron-scale objects is the electrostatic assembly of gold cylinders onto a gold surface patterned with two different alkanethiols (Figure 15B) [117]. The cylinders are covered with a SAM terminated in $-\text{PO}_3\text{H}_2$. The cylinders selectively assembled onto regions of a patterned gold coated silicon wafer bearing a SAM terminated in $-\text{NMe}_3^+$ groups; the cylinders did not assemble onto regions terminated in $-\text{CO}_2^-$.



↑ $-\text{CO}_2\text{H}$ ↑ $-\text{NMe}_3^+\text{Br}^-$

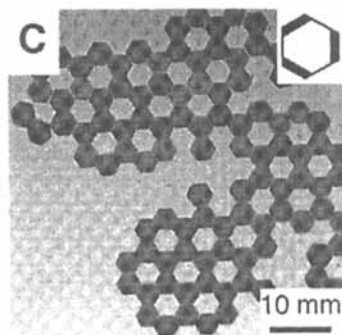


Figure 15 Three examples of mesoscale self-assembly spanning the range from nanometers to millimeters. (A) Gold colloids 13 nm in diameter that are coated with a DNA terminated SAM. The colloids flocculate when a strand of DNA, whose ends are complementary to the DNA on the SAM, is added. (B) Gold cylinders that are 10 μm in diameter, 10 μm high, and are coated with a SAM terminated in PO_3H_2 selectively assemble onto regions on a gold surface where the SAM is terminated in $-\text{NMe}_3^+$ and avoid those regions where the SAM is terminated in $-\text{CO}_2\text{H}$. (C) The hexagons shown assemble due to lateral capillary forces. In the inset the bold sides indicate hydrophobic faces and the thin sides indicate hydrophilic faces. The hexagons are floating at the perfluorodecalin–water interface. The perfluorodecalin wets the hydrophobic faces; when two hydrophobic sides are in close proximity the free energy of the system is lowered and the objects remain in contact

A promising new system for MESA on the millimeter-scale is the assembly of PDMS objects at the water–perfluorodecalin (PFD) interface (Figure 15C) [33]. PDMS objects ($\rho = 1.05 \text{ g cm}^{-3}$) float at the interface between PFD ($\rho = 1.90 \text{ g ml}^{-1}$) and water ($\rho = 1.00 \text{ g ml}^{-1}$); lateral capillary forces between the objects result in self-assembly. By controlling the hydrophobicity of the sides, we can direct the assembly of the objects into different arrays. PFD wets the hydrophobic sides and forms menisci; the menisci are high in energy because they increase the PFD–water surface area [118–120]. The decreased size of the menisci when two hydrophobic sides come into contact lowers the free energy of the system and holds the objects together (Figure 16A). Water wets the hydrophilic sides. The magnitude of this wetting is smaller than when PFD wets hydrophobic faces; thus, two hydrophilic faces are only weakly attractive toward each other (Figure 16B). Hydrophobic and hydrophilic sides exhibit a repulsive interaction due to the increase in perfluorodecalin–water surface area when the two sides come into contact (Figure 16C).

Self-assembly of millimeter-scale objects at the PFD–water interface based on lateral capillary forces is attractive for several reasons. First, the objects are easy to fabricate. Second, even though PDMS is naturally hydrophobic it can be rendered hydrophilic by oxidation in an oxygen plasma [121]. Third, we can control which sides remain hydrophobic by covering them with tape before oxidation; exposed sides become hydrophilic. Fourth, capillary forces are well understood from a theoretical point of view and modeling the assembly process should be possible [119,120]. Fifth, capillary forces are long range and objects are attracted to one another at distances up to several times their heights. Sixth, the assembly is rapid and reversible, a typical assembly is done in less than 30 min. We use this system to illustrate some of the general ideas and issues of MESA in the next section.

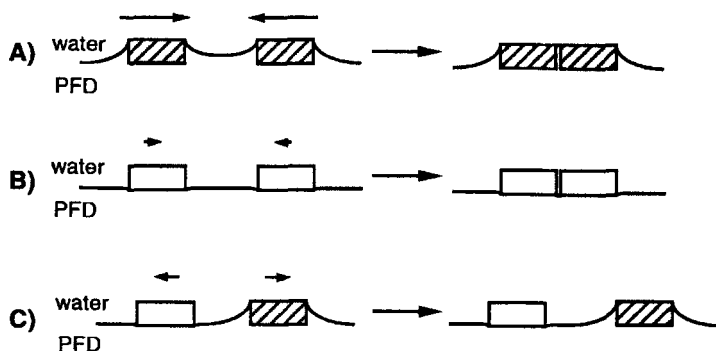


Figure 16 (A) Two hydrophobic objects are strongly attracted to one another due to the large menisci formed when PFD wets the hydrophobic sides of the objects. (B) Two hydrophilic objects are only weakly attracted to one another due to the small menisci formed when water wets the hydrophilic sides of the objects. (C) A hydrophobic object is repelled by a hydrophilic object

The current range of structures that can be made using MESA is limited. From the nanometer to the micron size range it is exceedingly difficult, if not impossible, to design and build complex three-dimensional structures with differentiated recognizing elements. Most of the work in MESA has been limited to making two- and three-dimensional close-packed arrays of colloids [116,122,123]. Several techniques exist on the micron to the millimeter size range that allow fabrication of complex three-dimensional objects, for example: photolithography, soft lithography, and molding. At this point we can assemble a variety of simple arrays, in the future we intend to assemble large, complex arrays.

(a) *Experimental issues*

In the following paragraphs we will discuss some of the important problems and issues that are faced in designing a MESA system. Some of the most important experimental issues include the choice of material, design and fabrication of the objects, forces, and how the objects are assembled.

Choice of material In the case of the two-dimensional array shown in Figure 15C, the material used to make the objects was chosen primarily based on two criteria: first, the objects had to have a density between that of water and perfluorodecalin, and second, the objects had to have sides that could be selectively rendered hydrophobic or hydrophilic. PDMS fulfills these criteria in addition to being easy to fabricate into many shapes. In other systems a consideration of the Young's modulus, durability, electrical conductivity, hardness, and the range of shapes that can be fabricated may be important. The choice of material in the nanometer to micron size range is currently limited by the method of fabrication.

Design and fabrication of the objects The design and fabrication of the individual objects are two important and closely related problems in this area. Useful techniques for fabrication include the combination of photolithography and electro-deposition of metals (this technique was employed to make the objects in Figure 15B), the use of a mold (this technique was employed to make the objects in Figure 15C), soft lithography, synthesis of colloids, and reactive ion etching. Improved techniques will be needed in the future to make complex objects on a nanometer and micron scale.

In order to form complex arrays, the sides of the objects must be differentiated from one another; without this differentiation only close- or loosely-packed arrays can form. For example, in Figure 17A all of the sides of the hexagons are hydrophobic and a close packed array is formed. Figures 17B and 17C show two examples where the sides of the hexagons are differentiated; different open arrays were assembled with these hexagons. Although the formation of close-packed arrays is interesting and can give important information about MESA, the ability to form a

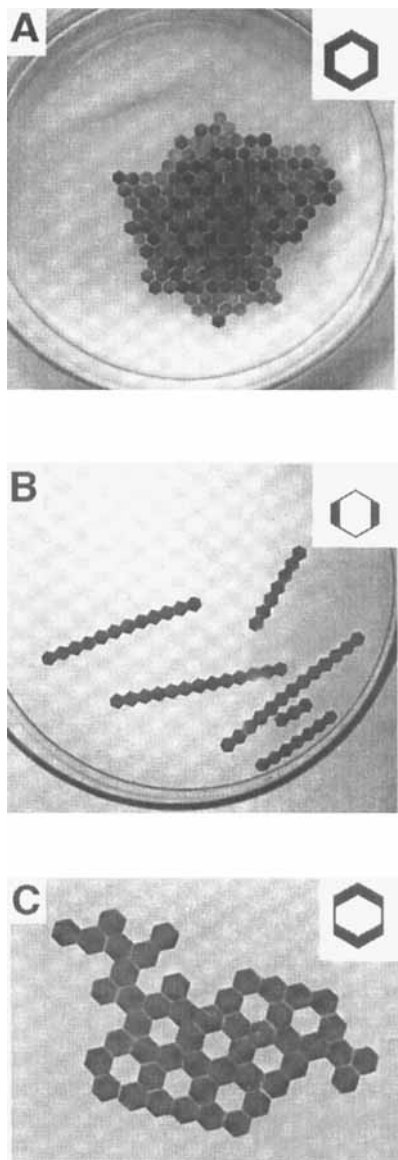


Figure 17 Three examples of two dimensional self-assembly based on one structure, hexagons. In the insets the bold sides indicate hydrophobic faces and the thin sides indicate hydrophilic faces. The hexagons are floating at the perfluorodecalin–water interface. The array shown in (A) results when all the sides are equivalent and hydrophobic; (B) and (C) show two of the arrays possible when the sides are differentiated

variety of arrays by differentiating the sides of the objects will allow us to discern the basic rules of MESA. In our system this problems is solved by physically protecting sides of the hexagons before the oxidation, for smaller systems new techniques may need to be developed.

Forces An important choice in MESA is that of the inter-object forces to be used. The range of forces that can be used has not been established; we surmise that those

Forces Appropriate to use in Mesoscopic Self-Assembly (MESA)

- Capillary
- Surface
- Ferro- and paramagnetic
- Hydrophobic
- Electrostatic
- Van der Waals
- Biospecific
(DNA duplex, protein-ligand)
- Metal-ligand
- Light
- Gravitational
- Shear
- Electrophoretic
- Diaphoretic
- Wave
- Centrifugal

Figure 18 Examples of interactions that may find uses in mesoscale self-assembly. Some interactions can be used to pull objects together that are separated by distances greater than 100 nm, while other forces are strong over short separations (less than 100 nm) but much weaker or nonexistent over longer separations

forces listed in Figure 18 may prove to be useful. The most successful examples that we have achieved are based on lateral capillary forces (Figure 15C). Lateral capillary forces are particularly effective because we can control their strength by altering the height of the object and the hydrophobicity of the sides. Another attractive feature of lateral capillary forces is that they are sufficiently attractive between objects separated by distances equal to several times their heights and are of sufficient magnitude to hold the objects together.

Assembly of objects In the assemblies shown in Figure 15C and Figure 17, the objects were agitated by shaking in a circular motion in the plane of the perfluorodecalin/water interface. The objects at the edge of the dish have more kinetic energy than those in the center of the dish; this distribution in kinetic energy results in a non-Boltzmann distribution of energy. A variety of other methods for supplying energy for the self-assembly process are conceivable, these include: heating, sonication, microwave heating, and vibrational agitation. These methods of supplying energy may result in a non-Boltzmann distribution of energy among the objects, the detailed thermodynamic properties need to be worked out. Two future

critical problems to solve are the duration over which energy is supplied to the system and the development of improved methods for characterization of the final array. Methods for characterizing the arrays include TEM, SEM, diffraction patterns, and optical microscopy. Physical rules describing the association and dissociation processes remain to be established.

3.5 Issues in Theory

(a) *Methods that calculate entropy and enthalpy for molecular systems*

Computations should reliably predict stabilities of complexes in terms of common quantities – enthalpy and entropy – to be broadly useful to physical organic chemists interested in self-assembly. There are extensive reviews on the use of potentials in calculating these quantities [124,125]. Some of the general issues are the following. Enthalpy can be determined accurately from quantum mechanics (QM), but the method is limited to a few atoms: far below the number of interest to the supramolecular chemist. Enthalpy is approximated by empirical potentials (EP). These EP are accurate in some systems where parameterization is of particular high quality, but poor in others, because EP are not easily transferable between systems. EP are currently the only way to study the dynamics of atomistic models of aggregates the size of those discussed in this review. Entropy is determined by evaluating the partition function for vibrational, rotational, and translational degrees of freedom (DOF). Normally, only the vibrational contribution to entropy can be calculated for *atomistic* models of modest flexibility; calculating the contributions to entropy from rotational and translational entropy is prohibitively time consuming. Most popular force fields based on EP are adequate for simple organic compounds; they have been, however, developed primarily for use with biological systems, and may not be appropriate for other problems (for example, crystal engineering) [126].

(b) *Increasing the efficiency of simulations*

The time-dependent mechanism of molecular interactions can be studied, in principle, by solving Newton's equations of motion using a variety of molecular dynamics methods [127]. Simulating the process of aggregation, however, remains an intractable problem for computational supramolecular chemistry. The root of the problem is the relatively short time scale accessible by simulations. Two factors, other than the available computational power, contribute to this limitation: the number of atoms, particularly those systems where solvent is included; the fastest motion in the system (e.g. bond stretches): dynamics algorithms must include the fastest motion in its calculations to be stable energetically. Currently, simulations on the order of nanoseconds are considered cutting edge; this value is far too short to simulate accurately many (and perhaps all) systems of interest.

Some of the new methods that are being developed to reduce the amount of calculations are the following.

- Those that eliminate the high frequency motions by grouping many atoms in a system into rigid or flexible entities, and thereby allow larger time steps (spanning several orders of magnitude) in the simulation [128–130].
- Those that model the effects of solvent without explicitly including each molecule of solvent in the calculations. One such strategy is based on Brownian motion, and has been used to simulate events that happen on the millisecond time scale (but at the expense of much atomistic detail): for example, the diffusion of a ligand into the active site of a protein [131] and the supercoiling of DNA [130]. A second strategy is the handling of the effects of solvent on long range electrostatics interactions by solving the Poisson–Boltzmann equation [132,133].

Many of these methods are being tested on problems in biochemistry (e.g. protein–ligand, and DNA–protein interactions), and their applications to problems in supramolecular chemistry should be straightforward.

(c) Surrogates for ΔG

It is impractical to calculate the complete thermodynamic cycle for the formation of self-assembled molecular systems of the size and complexity of those discussed in this review. Methods that “mutate” the system from one kind to another are not applicable to such large systems [134]. Surrogates for relative stabilities, therefore, must be developed. Two such methods that we have developed are the following.

Deviation from planarity (DP) The values of *DP* measure the extent to which the components of the CA•M motif are out of plane with each other relative to a coplanar geometry that represents a minimum in free energy (Figure 19). The higher the value of *DP*, the more unstable the complex. For aggregates based on CA•M, we have found that *DP* correctly ranks the order of stabilities for a variety of different complexes [55,56], and for conformational isomers of a single aggregate [54]. Values of *DP* are typically calculated from an ensemble of conformations from molecular dynamics simulations. In this way, the effects of enthalpy and *entropy* are implicitly included in the value of *DP*. We have found that *DP* is sensitive to the effects of solvent and conformational flexibility. It remains to be established, however, whether *DP* can be an effective surrogate for ΔG in other systems.

HB/(N – 1) The ratio of the number of hydrogen bonds in the system (*HB*) to the number of particles (*N*), is a convenient and simple first approximation to predicting stability in systems based on CA•M [28,49]. This simple ratio is a coarser metric for ranking stabilities than *DP*, but it does not involve the complexities of setting up an atomistic simulation. The range of systems amenable to *HB/(N – 1)* is, however,

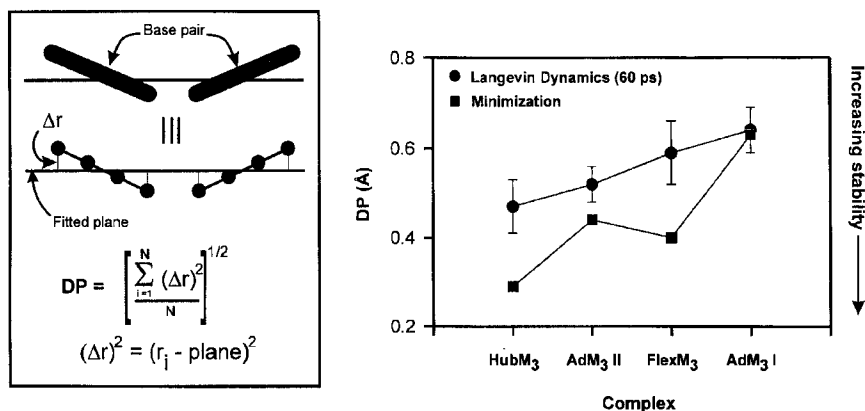


Figure 19 The definition of DP (left) and the results for several complexes based on CA•M (right). Hub(M)₃ and Flex(M)₃ are discussed in the section on soluble aggregates; Ad(M)₃ I and Ad(M)₃ II are similar to Hub(M)₃, the primary difference is that adamantane instead of benzene is the central hub in the tripod [55]. The results from molecular dynamics (circles) and minimization calculations (squares) are shown

limited: that is, for any two different complexes, we assume that $\Delta\Delta H$ is dominated by hydrogen bonds, and the $\Delta\Delta G$ of solvation is close to 0.

(d) Specific computational issues

We have discussed some of the broader issues facing computational supramolecular chemistry, and we will now discuss some of the specific computational issues that we have experienced in the areas explored in this review.

Soluble aggregates New computational tools for assembling supramolecular structures are needed. We have been frustrated by the difficulty of manipulating many molecules in 3D into a plausible aggregate. As we have discussed, CPK models were not useful beyond a basic conceptual stage; new computational tools that easily manipulate many molecules into structures such as the tetrahedral aggregate shown in Figure 7 would be very useful. New and efficient theories for predicting relative stabilities that are generally applicable to systems other than those based on hydrogen bonds, or CA•M, are needed. One question that we have not addressed is the transferability of methods such as DP or $HB/(N - 1)$ to systems other than those for which they were developed.

SAMs Simulations involving SAMs are particularly computationally demanding because the rearrangement of molecules for such close packed systems is slow on the sub-nanosecond time scale [135]. These simulations have been useful to us,

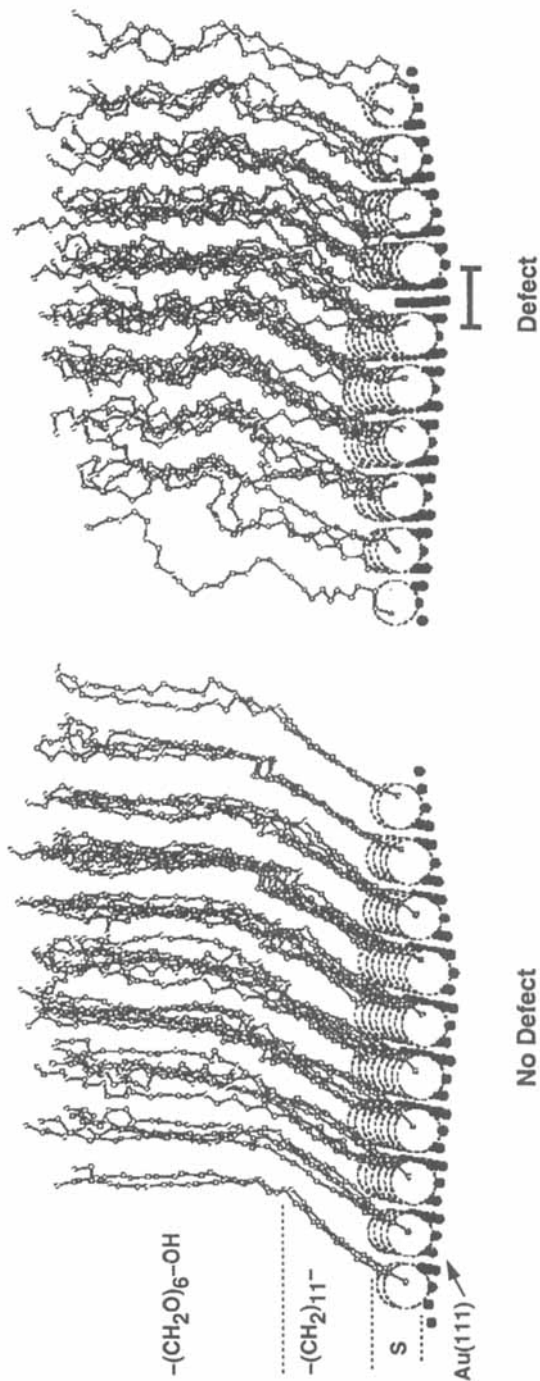


Figure 20 The last frames (representative) of two 600 ps simulations of a self-assembled monolayer (SAM) on Au(111). When a defect was introduced by shifting roughly half of the chains to the next interstitial site on the Au(111) surface (this resulted in the loss of four chains in the system below), the chains reoriented to a helical conformation to fill the voids caused by the defect. A 1.5 nm layer of water was placed on top of the SAM, and the computations were carried out in the presence of 2-D periodic boundaries to mimic an infinite SAM. Only the non-water molecules and atoms of the primary system are shown for clarity

nevertheless, in suggesting new ways of thinking about SAMs (Figure 20) [136]; the large computational efforts involved, however, have limited such simulations from being a routine part of our studies.

Crystal engineering A particularly challenging problem in supramolecular chemistry is predicting the crystalline packing arrangement of a molecule given only the geometrical and chemical information of a single molecule [137–143]. There are two main problems for computations. First, molecules can pack in an astronomical number of different ways, and searching through these arrangements is computationally impossible. Second, many of these crystalline arrangements can be similar in energy – differences on the order of 2 kcal mol^{-1} – and it is unlikely that present-day empirical force fields can accurately separate two polymorphs [140]. One strategy that we have successfully tested and implemented is to reduce the magnitude of the dimensionality problem by constraining the molecules to form hydrogen-bonded tapes. The hydrogen bond is a particularly useful type of constraining force as we and others have reviewed previously [30,144].

We were able to develop some simple rules in predicting the packing of molecules based on CA·M in one dimensional tapes, but not for predicting the three-dimensional packing of these tapes [98,107,145–148]. Conformational polymorphism due to the diphenyl rings, in addition, increased the complexity of the problem in the CAM system. We have found that crystal structures based on diketopiperazines (DKP) are simpler to predict and rationalize than our previous systems, both from observations of existing structures, and from computational methods [30,109].

Predicting the packing of organic crystals is not a completely unachievable goal, however: strategies exist to yield tractable computations by studying systems like DKP that can be predisposed to form tapes. We have used simulated annealing Monte Carlo methods [137] in concert with procedures that restrict the search to those molecular arrangements that have reasonable hydrogen bonds, to predict crystalline structures that compare well with those from experiment (Figure 21) [136].

One area that has not been extensively explored with computations, however, is the nucleation, or kinetics, of crystalline growth. The process of growing crystals is typically the rate limiting step in our studies in crystal engineering.

Mesoscale self-assembly We have not yet modeled MESA by computer, but with the wealth of experimental results we are in a position to develop believable computer simulations calibrated by experiment. The force of attraction between the objects is well understood mathematically in a number of cases [33,120] and in some systems it may be possible to measure these forces experimentally [149]. Some of the problems encountered in modeling molecular systems will also be encountered in modeling MESA. For example, finding global rather than local minima, the availability of computer time limiting how long the assembly can be modeled, and constructing potential functions for interactions that have not been determined

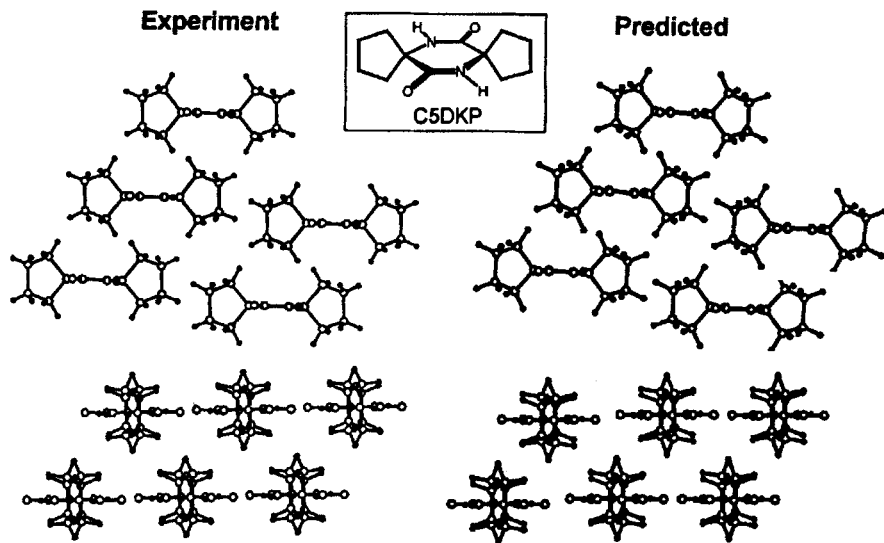


Figure 21 The experimental and predicted crystal structures for C_5DKP

experimentally are all important issues. Computer models already exist, however, that use simple geometric shapes and interactions to build arrays and optimizing these models for MESA may be possible.

The distribution of energy (supplied by shaking, sonication, or heating) in the system and the definition of entropy in MESA may be challenging. The distribution of kinetic energy among the objects will not necessarily follow Boltzmann's distribution and new thermodynamic descriptions will need to be developed. The two-dimensional self-assembly shown in Figure 17 is a good example of a MESA system where the distribution of energy is complex. The objects are agitated in a circular motion and the objects on the outer edge of the array have more kinetic energy than those in the center of the array. Entropy is an important part of all systems, but we have little knowledge of how to model this quantity.

4. SUMMARY AND CONCLUSIONS

We have described our recent work on four different self-assembling systems: self-assembly in solution based on the hydrogen-bonded CA•M rosette, self-assembly in the organic solid state using hydrogen-bonds, self-assembly of monolayers of alkanethiolates on gold, and self-assembly of mesoscale objects floating at the water–PFD interface. We have not yet succeeded in preparing arbitrarily structurally or functionally complex aggregates, although the formation of SAMs on gold shows excellent promise in this regard (mesoscale self-assembly is not yet sufficiently

developed to draw conclusions). Many important problems remain to be addressed in each of these areas. In molecular self-assembly, the lack of convenient computational tools for the construction and evaluation (enthalpic and entropic) of self-assembled structures and the difficulty of preparing self-assembled structures in water using the hydrophobic effect are two important issues to address. For crystal engineering, two of the most important current experimental difficulties are the occurrence of polymorphs and the growth of X-ray quality crystals. Computationally, the most important issue to address is the development of methods that correctly predict crystal structure from molecular structure. For SAMs to find more diverse use in areas like microelectronics, the development of methods for forming them on semiconductors and the control of the number and nature of defects in the SAMs are critical issues. For mesoscale self-assembly, improved methods for the fabrication and selective functionalization of micron sized objects will be of critical importance.

These systems have taught several lessons relevant to future studies in self-assembly. What characteristics should be considered in the design of a self-assembling system? First, the molecules or objects should be designed such that a single motif forms in every case (e.g. CA•M rosette, hydrogen bonded tapes, close packed hexagonal array of alkanethiolates on gold, and mesoscale hydrophobic side-hydrophobic side interactions). Second, the strength of the different interactions used should be of different orders of magnitude. Third, the self-assembled structures should bear several selectively functionalizable sites that do not interfere with the assembly process. Self-assembly based on hydrogen bonds in solution and the solid state meets (partially) the first criteria, but does not meet the second or the third. Specifically, the similar magnitudes of the favorable enthalpies of formation of the hydrogen bonds and the unfavorable conformational, rotational, and translational entropies of aggregation have made it difficult to progress to more complex aggregates. In contrast, SAMs meet all three of these criteria; they form every time, the strong Au-S bond and the weaker interchain packing determine the overall structure whereas the easily synthetically varied headgroup determines the properties of the interface. We believe that mesoscopic self-assembly of PDMS objects at the perfluorodecalin-water interface is another system that meets these three criteria and that this system will become as versatile as SAMs on gold.

5. ACKNOWLEDGMENTS

We are grateful to the NSF (CHE-91-22331), and ONR/DARPA for financial support of the work described in this review. L.I. and N.B. would like to thank, respectively, the NIH and DOD for postdoctoral and doctoral fellowships.

6. REFERENCES

1. G. M. Whitesides, J. P. Mathias and C. T. Seto, *Science*, **254**, 1312 (1991).
2. J.-M. Lehn, *Science*, **260**, 1762 (1993).

3. J.-M. Lehn, *Angew. Chem. Int. Ed. Engl.*, **27**, 89 (1988).
4. D. J. Cram, *Angew. Chem. Int. Ed. Engl.*, **27**, 1009 (1988).
5. C. J. Pederson, *Angew. Chem. Int. Ed. Engl.*, **27**, 1021 (1988).
6. E. L. Shakhnovich, V. Abkevich and O. Ptitsyn, *Nature*, **379**, 96 (1996).
7. A. Klug, *Angew. Chem. Int. Ed. Engl.*, **22**, 565 (1983).
8. D. Voet and J. G. Voet, *Biochemistry*, John Wiley, New York, 1995.
9. M. R. Ghadiri, J. R. Granja, R. A. M. Milligan, D. E. McRee and N. Khazanovich, *Nature*, **366**, 324 (1993).
10. J.-P. Sauvage, *Acc. Chem. Res.*, **23**, 319 (1990).
11. S. C. Zimmerman, F. Zeng, D. E. C. Reichert and S. V. Kolotuchin, *Science*, **271**, 1095 (1996).
12. J. Kang and J. Rebek Jr., *Nature*, **382**, 239 (1996).
13. S. Anderson, H. L. Anderson and J. K. M. Sanders, *Acc. Chem. Res.*, **26**, 469 (1993).
14. R. G. Chapman and J. C. Sherman, *J. Am. Chem. Soc.*, **117**, 9081 (1995).
15. D. Philp and J. F. Stoddart, *Angew. Chem. Int. Ed. Engl.*, **35**, 1154 (1996).
16. T. Beissel, R. E. Powers and K. N. Raymond, *Angew. Chem. Int. Ed. Engl.*, **35**, 1084 (1996).
17. J. Rebek Jr., *Chem. Soc. Rev.*, **96**, 255 (1996).
18. J.-C. Chambron, C. Dietrich-Buchecker and J.-P. Sauvage, in *Comprehensive Supramolecular Chemistry* (Series eds J.-M. Lehn, J. L. Atwood, J. E. D. Davies, D. D. MacNicol and F. Vögtle), Volume 9 (eds J.-P. Sauvage and M. W. Hosseini), Pergamon, New York, 1996, pp. 43–83.
19. P. N. W. Baxter, in *Comprehensive Supramolecular Chemistry* (Series eds J.-M. Lehn, J. L. Atwood, J. E. D. Davies, D. D. MacNicol and F. Vögtle), Volume 9 (eds J.-P. Sauvage and M. W. Hosseini), Pergamon, New York, 1996, pp. 165–211.
20. T. Kunitake, in *Comprehensive Supramolecular Chemistry* (Series eds J.-M. Lehn, J. L. Atwood, J. E. D. Davies, D. D. MacNicol and F. Vögtle), Volume 9 (eds J.-P. Sauvage and M. W. Hosseini), Pergamon, New York, 1996, pp. 351–406.
21. M. Fujita, in *Comprehensive Supramolecular Chemistry* (Series eds J.-M. Lehn, J. L. Atwood, J. E. D. Davies, D. D. MacNicol and F. Vögtle), Volume 9 (eds J.-P. Sauvage and M. W. Hosseini), Pergamon, New York, 1996, pp. 253–282.
22. A. Reichert, H. Ringsdorf, P. Schuhmacher, W. Baumeister and T. Scheybani, in *Comprehensive Supramolecular Chemistry* (Series eds J.-M. Lehn, J. L. Atwood, J. E. D. Davies, D. D. MacNicol and F. Vögtle), Volume 9 (eds J.-P. Sauvage and M. W. Hosseini), Pergamon, New York, 1996, pp. 313–350.
23. D. H. Lee and M. R. Ghadiri, in *Comprehensive Supramolecular Chemistry* (Series eds J.-M. Lehn, J. L. Atwood, J. E. D. Davies, D. D. MacNicol and F. Vögtle), Volume 9 (eds J.-P. Sauvage and M. W. Hosseini), Pergamon, New York, 1996, pp. 451–481.
24. J. R. Fredericks and A. D. Hamilton, in *Comprehensive Supramolecular Chemistry* (Series eds J.-M. Lehn, J. L. Atwood, J. E. D. Davies, D. D. MacNicol and F. Vögtle), Volume 9 (eds J.-P. Sauvage and M. W. Hosseini), Pergamon, New York, 1996, pp. 565–594.
25. X. Wang, M. Simard and J. D. Wuest, *J. Am. Chem. Soc.*, **116**, 12119 (1994).
26. B. Olenyuk, J. A. Whiteford and P. J. Stang, *J. Am. Chem. Soc.*, **118**, 8221 (1996).
27. W. T. S. Huck, F. C. J. M. van Veggel and D. N. Reinhoudt, *Angew. Chem. Int. Ed. Engl.*, **35**, 1213 (1996).
28. E. E. Simanek, M. Mammen, D. M. Gordon, D. N. Chin, J. P. Mathias, C. T. Seto and G. M. Whitesides, *Tetrahedron*, **51**, 607 (1995).
29. G. M. Whitesides, E. E. Simanek, J. P. Mathias, C. T. Seto, D. N. Chin, M. Mammen and D. M. Gordon, *Acc. Chem. Res.*, **28**, 37 (1995).
30. J. C. MacDonald and G. M. Whitesides, *Chem. Rev.*, **94**, 2383 (1994).
31. G. M. Whitesides, *Sci. Am.*, **273**, 146 (1995).

32. G. M. Whitesides and P. E. Laibinis, *Langmuir*, **6**, 87 (1990).
33. N. Bowden, A. T. Terfort, J. Carbeck and G. M. Whitesides, *Science*, **276**, 233 (1997).
34. A. Terfort and G. M. Whitesides, *Adv. Mater.*, **10**, 470 (1998).
35. A. Terfort, N. Bowden and G. M. Whitesides, *Nature*, **386**, 162 (1997).
36. K. C. Nicolaou, F. P. J. T. Rutjes, E. A. Theodorakis, J. Tiebes, M. Sato and E. Untersteller, *J. Am. Chem. Soc.*, **117**, 10252 (1995).
37. Y. Kishi, *Pure Appl. Chem.*, **61**, 313 (1989).
38. A. E. Eschenmoser and C. Wintner, *Science*, **196**, 1410 (1977).
39. R. B. Woodward, *Pure Appl. Chem.*, **33**, 145 (1973).
40. C. T. Seto and G. M. Whitesides, *J. Am. Chem. Soc.*, **112**, 6409 (1990).
41. J. P. Mathias, E. E. Simanek and G. M. Whitesides, *J. Am. Chem. Soc.*, **116**, 4326 (1994).
42. C. T. Seto and G. M. Whitesides, *J. Am. Chem. Soc.*, **113**, 712 (1991).
43. C. T. Seto, J. P. Mathias and G. M. Whitesides, *J. Am. Chem. Soc.*, **115**, 1321 (1993).
44. C. T. Seto and G. M. Whitesides, *J. Am. Chem. Soc.*, **115**, 1330 (1993).
45. C. T. Seto and G. M. Whitesides, *J. Am. Chem. Soc.*, **115**, 905 (1993).
46. J. P. Mathias, E. E. Simanek, C. T. Seto and G. M. Whitesides, *Angew. Chem. Int. Ed. Engl.*, **32**, 1766 (1993).
47. J. P. Mathias, C. T. Seto, E. E. Simanek and G. M. Whitesides, *J. Am. Chem. Soc.*, **116**, 1725 (1994).
48. J. P. Mathias, J. A. Zerkowski, C. T. Seto, E. E. Simanek and G. M. Whitesides, *J. Am. Chem. Soc.*, **116**, 4316 (1994).
49. M. Mammen, E. E. Simanek and G. M. Whitesides, *J. Am. Chem. Soc.*, **118**, 12614 (1996).
50. M. Mammen, E. I. Shakhnovich and G. M. Whitesides, *J. Org. Chem.*, **53**, 3168 (1998).
51. E. E. Simanek, M. I. M. Wazeer, J. P. Mathias and G. M. Whitesides, *J. Org. Chem.*, **59**, 4904 (1994).
52. X. Cheng, Q. Gao, R. D. Smith, E. E. Simanek, M. Mammen and G. M. Whitesides, *Rapid Comm. Mass Spec.*, **9**, 312 (1995).
53. X. Cheng, Q. Gao, R. D. Smith, E. E. Simanek, M. Mammen and G. M. Whitesides, *J. Org. Chem.*, **61**, 2204 (1996).
54. D. N. Chin, E. E. Simanek, X. Li, M. I. M. Wazeer and G. M. Whitesides, *J. Org. Chem.*, **62**, 1891 (1997).
55. D. N. Chin, D. M. Gordon and G. M. Whitesides, *J. Am. Chem. Soc.*, **116**, 12033 (1994).
56. X. Li, D. N. Chin and G. M. Whitesides, *J. Org. Chem.*, **61**, 1779 (1996).
57. M. Mammen, E. I. Shakhnovich and G. M. Whitesides, *J. Org. Chem.*, **63**, 3821 (1998).
58. L. Isaacs and G. M. Whitesides, unpublished results.
59. A. Ulman, *Introduction to Ultra Thin Organic Films: From Langmuir-Blodgett to Self-Assembly*, Academic Press, Boston, 1991.
60. C. D. Bain and G. M. Whitesides, *Angew. Chem. Int. Ed. Engl.*, **28**, 506 (1989).
61. L. H. Dubois and R. G. Nuzzo, *Annu. Rev. Phys. Chem.*, **43**, 437 (1992).
62. E. Delamar, B. Michel, H. A. Biebuyck and C. Gerber, *Adv. Mater.*, **8**, 719 (1996).
63. J. Xu and H.-L. Li, *J. Coll. Interf. Sci.*, **176**, 138 (1995).
64. A. R. Bishop and R. G. Nuzzo, *Curr. Opin. Coll. Interf. Sci.*, **1**, 127 (1996).
65. G. E. Poirier, *Chem. Rev.*, **97**, 1117 (1997).
66. C. A. Widrig, C. A. Alves and M. D. Porter, *J. Am. Chem. Soc.*, **113**, 2805 (1991).
67. P. Fenter, A. Eberhardt and P. Eisenberger, *Science*, **266**, 1216 (1994).
68. Y. Li, J. Huang, R. T. McIver Jr. and J. C. Hemminger, *J. Am. Chem. Soc.*, **114**, 2428 (1992).
69. T. D. McCarley and R. L. McCarley, *Anal. Chem.*, **69**, 130 (1997).
70. C. D. Bain and G. M. Whitesides, *J. Am. Chem. Soc.*, **111**, 7164 (1989).
71. D. A. Buttry and M. D. Ward, *Chem. Rev.*, **92**, 1355 (1992).
72. D. S. Karpovich and G. J. Blanchard, *Langmuir*, **10**, 3315 (1994).
73. G. E. Poirier and E. D. Pylant, *Science*, **272**, 1145 (1996).

74. N. B. Larsen, H. A. Biebuyck, E. Delamarche and B. Michel, *J. Am. Chem. Soc.*, **119**, 3017 (1997).
75. N. Camillone III, C. E. D. Chidsey, P. Eisenberger, P. Fenter, J. Li, K. S. Liang, G.-Y. Liu and G. Scoles, *J. Chem. Phys.*, **99**, 744 (1993).
76. G.-Y. Liu, P. Fenter, C. E. D. Chidsey, D. F. Ogletree, P. Eisenberger and M. Salmeron, *J. Chem. Phys.*, **101**, 4301 (1994).
77. Y. Xia, X.-M. Zhao and G. M. Whitesides, *Microelectron. Eng.*, **32**, 255 (1996).
78. X.-M. Zhao, J. L. Wilbur and G. M. Whitesides, *Langmuir*, **12**, 3257 (1996).
79. C. Schonenberger, J. A. M. Sondag-Huethorst, J. Jorritsma and L. G. J. Fokkink, *Langmuir*, **10**, 611 (1994).
80. C. A. McDermott, M. T. McDermott, J.-B. Green and M. D. Porter, *J. Phys. Chem.*, **99**, 13257 (1995).
81. E. Delamarche, B. Michel, H. Kang and C. Gerber, *Langmuir*, **10**, 4103 (1994).
82. K. L. Prime and G. M. Whitesides, *J. Am. Chem. Soc.*, **115**, 10714 (1993).
83. D. J. Olbris, A. Ulman and Y. Shnidman, *J. Chem. Phys.*, **102**, 6865 (1995).
84. H. Schönherr and H. Ringsdorf, *Langmuir*, **12**, 3891 (1996).
85. T. Ishida, S. Yamamoto, W. Mizutani, M. Motomatsu, H. Tokumoto, H. Hokari, H. Azebara and M. Fujihara, *Langmuir*, **13**, 3261 (1997).
86. R. M. Overney, E. Meyer, J. Frommer, D. Brodbeck, R. Lüthi, H.-J. Güntherodt, L. Howald, M. Fujihara, H. Takano and Y. Gotoh, *Nature*, **359**, 133 (1992).
87. H. A. Biebuyck, C. D. Bain and G. M. Whitesides, *Langmuir*, **10**, 1825 (1994).
88. T. Takami, E. Delamarche, B. Michel, C. Gerber, H. Wolf, and H. Ringsdorf, *Langmuir*, **11**, 3876 (1995).
89. J. J. Hickman, D. Ofer, P. E. Laibinis, G. M. Whitesides and M. S. Wrighton, *Science*, **252**, 688 (1991).
90. S. J. Vigmond, M. Iwakura, F. Mizutani and T. Katsura, *Langmuir*, **10**, 2860 (1994).
91. J. M. Tour, L. Jones II, D. L. Pearson, J. J. S. Lamba, T. P. Burgin, G. M. Whitesides, D. L. Allara, A. N. Parikh and S. V. Atre, *J. Am. Chem. Soc.*, **117**, 9529 (1995).
92. P. E. Laibinis and G. M. Whitesides, *J. Am. Chem. Soc.*, **114**, 9022 (1992).
93. J. F. Dorsten, J. E. Maslar and P. W. Bohn, *Appl. Phys. Lett.*, **66**, 1755 (1995).
94. A. Kumar, H. A. Biebuyck and G. M. Whitesides, *Langmuir*, **10**, 1498 (1994).
95. Y. Xia and G. M. Whitesides, *Angew. Chem. Int. Ed. Engl.*, **37**, 551 (1998).
96. Y. Xia, D. Qin and G. M. Whitesides, *Adv. Mater.*, **8**, 1015 (1996).
97. H. A. Biebuyck, N. B. Larsen, E. Delamarche and B. Michel, *IBM J. Res. Dev.*, **41**, 159 (1997).
98. A. Kumar and G. M. Whitesides, *Science*, **263**, 60 (1994).
99. H. A. Biebuyck and G. M. Whitesides, *Langmuir*, **10**, 2790 (1994).
100. R. Singhvi, A. Kumar, G. P. Lopez, G. N. Stephanopoulos, D. I. C. Wang, G. M. Whitesides and D. E. Ingber, *Science*, **264**, 696 (1994).
101. M. Mrksich, C. S. Chen, Y. Xia, L. E. Dike, D. E. Ingber and G. M. Whitesides, *Proc. Natl. Acad. Sci. USA*, **93**, 10775 (1996).
102. Y. Xia, E. Kim and G. M. Whitesides, *J. Electrochem. Soc.*, **143**, 1070 (1996).
103. A. Ulman, *Mater. Res. Soc. Bull.*, **20**, 46 (1995).
104. M. Mrksich and G. M. Whitesides, *TIBTECH*, **13**, 228 (1995).
105. M. Mrksich and G. M. Whitesides, *Annu. Rev. Biophys. Biomol. Struct.*, **25**, 55 (1996).
106. R. J. Jackman, J. L. Wilbur and G. M. Whitesides, *Science*, **269**, 664 (1995).
107. J. A. Zerkowski, C. T. Seto and G. M. Whitesides, *J. Am. Chem. Soc.*, **114**, 5473 (1992).
108. K. E. Schwiebert, D. N. Chin, J. C. MacDonald and G. M. Whitesides, *J. Am. Chem. Soc.*, **118**, 4018 (1996).
109. S. Palacin, D. N. Chin, E. E. Simanek, J. C. MacDonald, G. M. Whitesides, M. T. McBride and G. T. R. Palmore, *J. Am. Chem. Soc.*, **119**, 11807 (1997).

110. S. Y. Chou, P. R. Krauss and P. Renstron, *J. Appl. Phys. Lett.*, **67**, 3114 (1995).
111. M. C. Wu, L. Y. Lin and S. S. Lee, *SPIE*, **2291**, 40.
112. E. Smela, O. Inganäs and I. Lundström, *Science*, **268**, 1735 (1995).
113. J. H. E. Promislow and A. P. Gast, *Langmuir*, **12**, 4095 (1996).
114. A. W. Simpson and P. H. Hodkinson, *Nature*, **237**, 320 (1972).
115. S. T. Schober, J. Friedrich and A. Altmann, *J. Appl. Phys.*, **71**, 2206 (1992).
116. C. A. Mirkin, R. L. Letsinger, R. C. Mucic and J. J. Storhoff, *Nature*, **382**, 607 (1996).
117. J. Tien, A. Terfort and G. M. Whitesides, *Langmuir*, **13**, 5349 (1997).
118. M. A. Fortes, *Can. J. Chem.*, **60**, 2889 (1982).
119. P. A. Kralchevsky, V. N. Paunov, N. D. Denkov, I. B. Ivanov and K. Nagayama, *J. Coll. Interf. Sci.*, **155**, 420 (1993).
120. P. A. Kralchevsky and K. Nagayama, *Langmuir*, **10**, 23 (1994).
121. D. W. Fakes, M. C. Davies, A. Browns and J. M. Newton, *Surf. Interf. Anal.*, **13**, 233 (1988).
122. M. Yamaki, J. Higo and K. Nagayama, *Langmuir*, **11**, 2975 (1995).
123. N. D. Denkov, O. D. Velev, P. A. Kralchevsky, I. B. Ivanov, H. Yoshimura and K. Nagayama, *Langmuir*, **8**, 3183 (1992).
124. K. B. Lipkowitz and D. B. Boyd, *Rev. Comp. Chem.*, VCH: New York, 1990.
125. K. B. Lipkowitz and D. B. Boyd, *Rev. Comp. Chem.*, VCH: New York, 1991.
126. B. R. Brooks, R. E. Bruccoleri, B. D. Olafson, D. J. States, S. Swaminathan and M. L. Karplus, *J. Comp. Chem.*, **4**, 187 (1983).
127. M. P. Allen and D. J. Tildesley, *Computer Simulations of Liquids*, Clarendon Press, Oxford, 1987.
128. J. D. Turner, P. K. Weiner, H. Chun, V. Lupi, S. Gallion and U. C. Singh, in *Computer Simulation of Biomolecular Systems: Theoretical and Experimental Applications* (eds Gunsteren, W. F., Weiner, P. K. and Wilkinson, A. J.) EXCOM, Leiden, 1993.
129. A. M. Mathiowetz, A. Jain, N. Karasawa and W. A. Goddard, *Proteins*, **20**, 227 (1994).
130. T. Schlick and W. K. Olson, *Science*, **257**, 1110 (1992).
131. S. A. Allison, S. H. Northrup and J. A. McCammon, *Biophys. J.*, **49**, 167 (1986).
132. B. A. Luty, M. E. Davis and J. A. McCammon, *J. Comp. Chem.*, **13**, 768 (1992).
133. A. Nicholls and B. Honig, *J. Comp. Chem.*, **12**, 435 (1991).
134. D. L. Beveridge and F. M. Dicapua, *Annu. Rev. Biophys. Biophys. Chem.*, **18**, 431 (1989).
135. J. I. Siepmann and I. R. McDonald, *Mol. Phys.*, **75**, 255 (1992).
136. D. N. Chin, G. T. R. Palmore and G. M. Whitesides, *J. Am. Chem. Soc.* In press.
137. J. Perlstein, *J. Am. Chem. Soc.*, **114**, 1955 (1992).
138. J. Perlstein, *J. Am. Chem. Soc.*, **116**, 455 (1994).
139. H. R. Karfunkel and R. J. Gdanitz, *J. Comp. Chem.*, **13**, 1171 (1992).
140. A. Gavezzotti, *Acc. Chem. Res.*, **27**, 309 (1994).
141. A. Gavezzotti and G. Filippini, *J. Phys. Chem.*, **98**, 4831 (1994).
142. A. Gavezzotti, *J. Am. Chem. Soc.*, **113**, 4622 (1991).
143. A. Gavezzotti, *J. Phys. Chem.*, **94**, 4319 (1990).
144. M. C. Etter, *J. Phys. Chem.*, **95**, 4601 (1991).
145. J. A. Zerkowski, C. T. Seto, D. A. Wierda and G. M. Whitesides, *J. Am. Chem. Soc.*, **112**, 9025 (1990).
146. J. A. Zerkowski, J. C. MacDonald, C. T. Seto, D. A. Wierda and G. M. Whitesides, *J. Am. Chem. Soc.*, **116**, 2382 (1994).
147. J. A. Zerkowski and G. M. Whitesides, *J. Am. Chem. Soc.*, **116**, 4298 (1994).
148. J. A. Zerkowski, J. P. Mathias and G. M. Whitesides, *J. Am. Chem. Soc.*, **116**, 4305 (1994).
149. C. D. Dushkin, P. A. Kralchevsky, V. N. Paunov, H. Yoshimura and K. Nagayama, *Langmuir*, **12**, 641 (1996).

150. E. B. Throughton, C. D. Bain, G. M. Whitesides, R. G. Nuzzo, D. L. Allara and M. D. Porter, *Langmuir*, **4**, 365 (1988).
151. J. E. Chadwick, D. C. Myles and R. L. Garrell, *J. Am. Chem. Soc.*, **115**, 10364 (1993).
152. K. Uvdal, I. Persson and B. Liedberg, *Langmuir*, **11**, 1252 (1995).
153. P. Fenter, P. Eisenberger, J. Li, N. Camillone III, S. Bernasek, G. Scoles, T. A. Ramnanarayanan and K. S. Liang, *Langmuir*, **7**, 2013 (1991).
154. J. B. Schlenoff, M. Li and H. Ly, *J. Am. Chem. Soc.*, **117**, 12528 (1995).
155. T. R. Lee, P. E. Laibinis, J. P. Folkers and G. M. Whitesides, *Pure Appl. Chem.*, **63**, 821 (1991).
156. J. J. Hickman, P. E. Laibinis, D. I. Auerbach, C. Zou, T. J. Gardner, G. M. Whitesides and M. S. Wrighton, *Langmuir*, **8**, 357 (1992).
157. C. W. Sheen, J.-X. Shi, J. Martensson, A. N. Parikh and D. L. Allara, *J. Am. Chem. Soc.*, **114**, 1514 (1992).
158. Y. Gu, Z. Lin, R. A. Butera, V. S. Smentkowski and D. H. Waldeck, *Langmuir*, **11**, 1849 (1995).
159. M. J. Wirth, R. W. P. Fairbank and H. O. Fatunmbi, *Science*, **275**, 44 (1997).
160. M. R. Linford and C. E. D. Chidsey, *J. Am. Chem. Soc.*, **115**, 12631 (1993).
161. M. R. Linford, P. Fenter, P. M. Eisenberger and C. E. D. Chidsey, *J. Am. Chem. Soc.*, **117**, 3145 (1995).
162. A. Bansal, X. Li, I. Lauermaun, N. S. Lewis, S. I. Yi and W. H. Weinberg, *J. Am. Chem. Soc.*, **118**, 7225 (1996).
163. Y.-T. Tao, M.-T. Lee and S.-C. Chang, *J. Am. Chem. Soc.*, **115**, 9547 (1993).
164. J. P. Folkers, C. B. Gorman, P. E. Laibinis, S. Buchholz, G. M. Whitesides and R. G. Nuzzo, *Langmuir*, **11**, 813 (1995).
165. G. Cao, H.-G. Hong and T. E. Mallouk, *Acc. Chem. Res.*, **25**, 420 (1992).
166. T. J. Gardner, C. D. Frisbie and M. S. Wrighton, *J. Am. Chem. Soc.*, **117**, 6927 (1995).
167. M. R. Anderson, M. N. Evaniak and M. Zhang, *Langmuir*, **12**, 2327 (1996).
168. N. Camillone III, T. Y. B. Leung, P. Schwartz, P. Eisenberger and G. Scoles, *Langmuir*, **12**, 2737 (1996).
169. W. B. Caldwell, D. J. Campbell, K. Chen, B. R. Herr, C. A. Mirkin, A. Malik, M. K. Durbin, P. Dutta and K. G. Huang, *J. Am. Chem. Soc.*, **117**, 6071 (1995).
170. L. Strong and G. M. Whitesides, *Langmuir*, **4**, 546 (1988).
171. M. A. Bryant and J. E. Pemberton, *J. Am. Chem. Soc.*, **113**, 3629 (1991).
172. Q. Du, E. Freysz and Y. R. Shen, *Science*, **264**, 826 (1994).
173. C. D. Bain, *J. Chem. Soc. Faraday Trans.*, **91**, 1281 (1995).
174. J. P. Folkers, P. E. Laibinis and G. M. Whitesides, *Langmuir*, **8**, 1330 (1992).
175. L. H. Dubois, B. R. Zegarski and R. G. Nuzzo, *J. Am. Chem. Soc.*, **112**, 570 (1990).
176. M. J. Tarlov and J. G. Newman, *Langmuir*, **8**, 1298 (1992).
177. C. D. Bain and G. M. Whitesides, *J. Am. Chem. Soc.*, **110**, 3665 (1988).
178. C. D. Bain, E. B. Throughton, Y.-T. Tao, J. Evall, G. M. Whitesides and R. G. Nuzzo, *J. Am. Chem. Soc.*, **111**, 321 (1989).
179. M. D. Ward and D. A. Buttry, *Science*, **249**, 1000 (1990).
180. S. Li and R. M. Crooks, *Langmuir*, **9**, 1951 (1993).
181. A. Badia, R. Back and R. B. Lennox, *Angew. Chem. Int. Ed. Engl.*, **33**, 2332 (1994).
182. Y. Xia, E. Kim, M. Mrksich and G. M. Whitesides, *Chem. Mater.*, **8**, 601 (1996).
183. J. Huang and J. C. Hemminger, *J. Am. Chem. Soc.*, **115**, 3342 (1993).
184. M. J. Tarlov, D. R. F. Burgess Jr. and G. Gillen, *J. Am. Chem. Soc.*, **115**, 5305 (1993).
185. K. C. Chan, T. Kim, J. K. Schoer and R. M. Crooks, *J. Am. Chem. Soc.*, **117**, 5875 (1995).
186. T. Kim, K. C. Chan and R. M. Crooks, *J. Am. Chem. Soc.*, **119**, 189 (1997).
187. E. W. Wollman, C. D. Frisbie and M. S. Wrighton, *Langmuir*, **9**, 1517 (1993).
188. D. J. Pritchard, H. Morgan and J. M. Cooper, *Angew. Chem. Int. Ed. Engl.*, **34**, 91 (1995).

189. J. A. M. Sondag-Huethorst, H. R. J. van Helleputte and L. G. Fokkink, *Appl. Phys. Lett.*, **64**, 285 (1994).
190. M. Lercel, R. C. Tiberio, P. F. Chapman, H. G. Craighead, C. W. Sheen, A. N. Parikh and D. L. Allara, *J. Vac. Sci. Technol. B*, **11**, 2823 (1993).
191. G. Gillen, S. Wight, J. Bennett and M. Tarlov, *J. Appl. Phys. Lett.*, **65**, 534 (1994).
192. K. K. Berggren, A. Bard, J. L. Wilbur, J. D. Gillaspay, A. G. Helg, J. J. McClelland, S. L. Rolston, W. D. Phillips, M. Prentiss and G. M. Whitesides, *Science*, **269**, 1255 (1995).
193. C. B. Ross, L. Sun and R. M. Crooks, *Langmuir*, **9**, 632 (1993).
194. N. L. Abbott, A. Kumar and G. M. Whitesides, *Chem. Mater.*, **6**, 596 (1994).
195. A. Kumar, H. A. Biebuyck, N. L. Abbott and G. M. Whitesides, *J. Am. Chem. Soc.*, **114**, 9188 (1992).

Chapter 2

Dendritic Architectures

MARCEL H.P. VAN GENDEREN AND E.W. MEIJER

Eindhoven University of Technology, The Netherlands

1. INTRODUCTION

For many years organic chemists have been enamoured of the synthesis of aesthetically pleasing molecules, based on their symmetry (e.g. Buckminsterfullerene and tetraethynylmethane) or resemblance to macroscopic structures (e.g. cubane and olympiadane). In the realm of natural shapes, recent years have seen a great interest in tree shapes: whether called dendrimers (Greek *δενδρον*) or arborols (Latin *arbor*), the synthesis of these regularly branched macromolecules has been investigated by various groups. The interest in dendritic macromolecules arises from the unique properties of these highly branched structures, which have a defined number of generations and functional end groups [1–4]. The high degree of control over molecular weight and shape has led to the synthesis of unimolecular micelles [5], spherical and cone-shape mesostructures [6], as well as stratified dendrimers possessing generations of different structure [7]. Diameters of the spherical dendrimers are in the range 3–10 nm, enabling these structures to be building blocks of a new chemistry set [8], and molecular containers in host–guest systems such as the dendritic box (Plate 1) [9].

Routes have been developed for growth-type (divergent) and Lego-type (convergent) syntheses, both with their advantages and disadvantages. Whereas convergent methods (in the organic synthesis tradition) yield well-defined products, they are time-consuming [2,3]. On the other hand, though divergent routes can be more easily scaled up, they accumulate errors due to the exponentially increasing number of reactions at each step [1,3,5]. Nevertheless, the products obtained in the latter way are of extremely low dispersity in terms of polymer chemistry.

Polymer chemists have known branched macromolecules for a long time, of course, and a lot of work has been performed on starbranched polymers [10] and (more recently) on hyperbranched polymers [11]. These latter systems are close cousins of dendrimers: they share the highly branched topology and the multiplicity of end groups. The one defining aspect of dendritic systems is absent, though: the (potential) dense packing of end groups on the curved two-dimensional exterior of the molecule. This is due to the combination of exponential branching and geometrical increase in size. This feature also has consequences for the density of the dendrimer: since the mass doubles every generation while the volume increases cubically, the density goes through a minimum and then increases strongly. This is clearly seen when the intrinsic viscosity (which is calculated as a viscosity divided by mass density) is plotted as a function of generation. Whereas a linear polymer shows the familiar Mark–Houwink–Sakurada rise in viscosity, dendrimers typically display a maximum in the curve [11].

Although there is still a lot of discussion in the literature about the density profile *within* a dendrimer (maximum at the centre of periphery, or in between [12–14]), it seems clear that dendritic systems harbour the potential for encapsulating guest molecules. This feature, combined with the large number of functional groups in close proximity, is where the supramolecular aspects meet the dendrimer world: one can make host–guest complexes with dendrimers, and one can study interactions between functional end groups in dendritic systems. The latter allows for discriminating between *intra*- and *intermolecular* interactions, i.e. between different branches in a molecule and between different dendrimers. It has even been possible to assemble dendrimers spontaneously on the basis of secondary interactions [15–17].

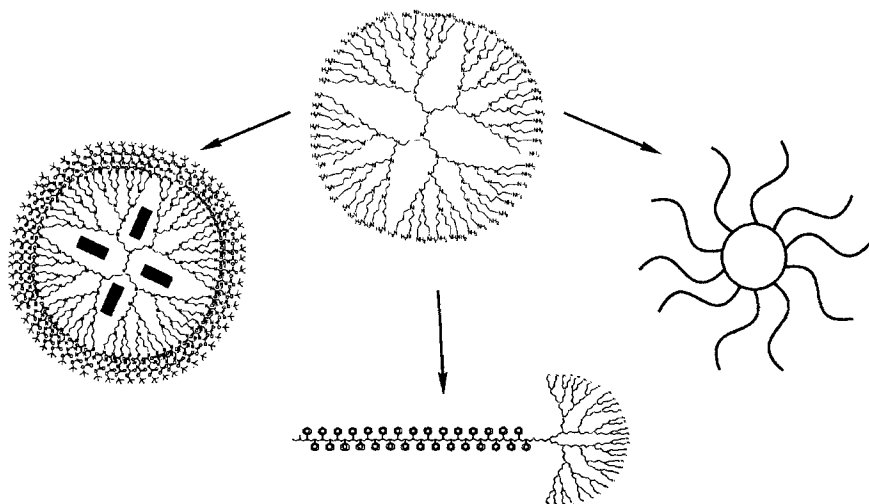


Figure 1 Overview of the three systems that will be treated in this chapter

For supramolecular *technologies*, however, it is necessary to manipulate dendrimers in large quantities. Large-scale syntheses of dendrimers do not abound: only the StarburstTM, poly(aminoamide) dendrimers of Dendritech and the AstramolTM, poly(propylene imine) dendrimers as synthesized by DSM Research (Geleen, The Netherlands) are commercially available.

For a general review on supramolecular chemistry with dendrimers, the reader is referred to an excellent paper of Zimmerman *et al.* [18]. Because of our acquaintance with the poly(propylene imine) dendrimers, we will restrict ourselves in this Chapter to some examples of supramolecular behaviour of these systems as investigated in our laboratory. Three systems will be discussed (Figure 1): the dendritic box, which can encapsulate guest molecules, the polystyrene–poly(propylene imine) block copolymer superamphiphiles, and alkyl-decorated dendrimers, which function as unimolecular micelles, and show surprising aggregation behaviour. However, first the synthesis and properties of the poly(propylene imine) dendrimers will be discussed to demonstrate some typical dendrimer features.

2. POLY(PROPYLENE IMINE) DENDRIMERS

The oligo(propylene imine) cascade structures made by Vögtle *et al.* in 1978 are generally accepted to be the first, low generation dendrimers ever made [19]. Their synthetic approach is based on a repetitive reaction sequence of the double Michael addition of an amine to acrylonitrile, followed by the reduction of the nitriles to primary amines. The yields of both steps are reasonable, but the procedures are tedious and no structures beyond what we now call the second-generation dendrimer were synthesized. Until recently, this elegant reaction sequence was regarded as useless for the synthesis of well-defined high-generation dendrimers, despite the simplicity of the structure as well as the chemistry involved.

Totally independent from each other, two research groups (Wörner/Mülhaupt and de Brabander-van den Berg/Meijer) disclosed their modifications of the original Vögtle approach [20,21]. Major improvements in the synthesis of poly(propylene imine) dendrimers were made by applying knowledge of the highly efficient industrial manufacturing of bulk chemicals for nylons, to wit a Michael addition of acrylonitrile and the heterogeneous hydrogenation of nitriles to primary amines, which resulted in the first synthesis of dendrimers on a large, pilot-plant scale of approximately 10 kg per batch, up to the fifth generation. The availability of large quantities of structurally well-defined poly(propylene imine) dendrimers of all generations up to 64 amine or nitrile end groups, paved the way for exploring the scope and limitations of these globular three-dimensional architectures.

2.1 Large-scale Synthesis

The synthetic scheme for the so-called poly(propylene imine) dendrimers is shown in Figure 2 and consists of a repetition of a double Michael addition of acrylonitrile to primary amines, followed by the heterogeneously catalysed hydrogenation of the nitrile groups [21]. This sequence results in a doubling of the number of end groups in every generation. 1,4-Diaminobutane has been used as the core-molecule in the studies presented in this paragraph, but a variety of molecules with primary or secondary amino groups can be used as the core as well, as will be demonstrated for a polystyrene core. In most cases poly(propylene imine) dendrimers up to the fifth generation are prepared on a routine basis. The following nomenclature for the dendrimers is used: DAB-*dendr*-(NH₂)_n and DAB-*dendr*-(CN)_n for the amine- and nitrile-functionalized dendrimers, respectively. "DAB" stands for the core molecule 1,4-diaminobutane, "*dendr*" refers to the dendritic structure, and (NH₂)_n and (CN)_n represent the type and number of end groups.

All Michael reactions are performed in water at a concentration of up to 50 wt% of amine, to which 2.5–4 moles of acrylonitrile per mole of primary amine are added. In the double cyanoethylation, the first acrylonitrile molecule reacts at room temperature, while the reaction temperature has to be raised to 80°C to accomplish the double Michael adduct. The reaction time required to achieve complete conversion increases with generation from 1 h for DAB-*dendr*-(CN)₄ to 3 h for DAB-*dendr*-(CN)₆₄. After completion of the reaction the excess acrylonitrile is removed by distillation, making use of the water–acrylonitrile azeotrope.

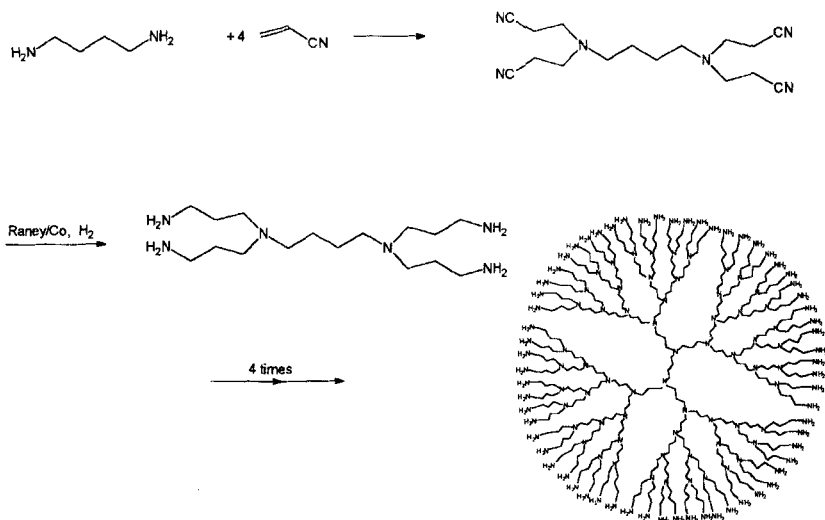


Figure 2 Synthetic scheme for poly(propylene imine) dendrimers using 1,4-diaminobutane as core

The hydrogenations of the cyanoethylated structures with Raney Co as catalyst and applying H₂ pressures of more than 30 bar, were initially performed in water as well. However, the selectivity, the productivity and the yields are all enhanced dramatically by changing the solvent from water to methanol and adding ammonia to the reaction mixture. After reduction, the reaction mixtures are filtered and the primary amine-terminated dendrimers are isolated by evaporating the solvent. The reaction time required for complete hydrogenation increases with generation, but even DAB-*dendr*-(NH₂)₆₄ can be obtained via this procedure within 3 h. The main purpose of adding ammonia in the hydrogenation step is to prevent secondary amine formation, which occurs via the addition of a primary amine to an aldimine, followed by hydrogenation [22]. Secondary amine formation is possible both intra- and intermolecularly, leading to eight-membered rings and dendrimer dimerization, respectively. Detailed analysis showed that there is no evidence of intermolecular reactions. The intramolecular reaction is diminished significantly by adding NH₃. Generally, the formation of eight-membered rings is less than 1% (see later). Another important aspect of the use of ammonia in the dendrimer synthesis is the increase in hydrogenation reaction rate, thereby preventing retro-Michael reaction of the nitrile-terminated dendrimers during the hydrogenation. Retro-Michael reaction results in elimination of acrylonitrile, yielding defect dendrimers missing one or more branches. However, this side reaction also is found to be less than 1% (see later). Furthermore, in the presence of ammonia the amount of catalyst required can be lowered by an order of magnitude, the catalyst needs no pretreatment with sodium hydroxide and the dendrimer concentration can be increased eight times, thus making this procedure very suitable for the large scale synthesis.

2.2 Characterization

Dendrimers are regarded as macromolecules with a structural precision comparable to organic compounds. Accurate analysis and quantitative identification of side products are furthermore required to optimize and adjust the reaction conditions of the synthesis of DAB-*dendr*-(NH₂)_{*n*} and DAB-*dendr*-(CN)_{*n*}. Therefore, it is necessary to characterize the products obtained unambiguously. To achieve the complete molecular characterization of the poly(propylene imine) dendrimers and the possible side-products nuclear magnetic resonance (NMR) and infrared (IR) spectroscopy, high pressure liquid chromatography (HPLC), gel permeation chromatography (GPC) and electrospray mass spectroscopy (MS) are used.

NMR spectroscopy appears to be a very suitable technique for detecting and assigning failures in the outermost layer of the dendrimer structure at each generation. All three nuclei present in the dendrimers have been used in ¹H-, ¹³C- and ¹⁵N-NMR spectroscopy [23–25].

IR spectroscopy is used on a routine basis to follow the hydrogenation of DAB-*dendr*-(CN)_n. It is a useful technique for the detection of functional groups, e.g. nitrile absorptions at 2247 cm⁻¹ or the characteristic double peaks due to NH₂ groups at 3356 and 2280 cm⁻¹. The IR spectra of the various generations with identical end groups are very similar.

Electrospray MS was performed on both series of nitrile- and amine-terminated poly(propylene imine) dendrimers [26]. The actual and reconstructed spectra of DAB-*dendr*-(NH₂)₆₄ are given in Figure 3. The measured spectrum shows a repetition of different clusters of peaks, corresponding to dendrimers with 4–12 charges per dendrimer (m/z with $z = 4-12$), while no counter-ion interactions are observed. Deconvolution yields a spectrum in which the largest peak at $M_r = 7168$ corresponds to the perfect DAB-*dendr*-(NH₂)₆₄ and a series of peaks with lower abundance is found with regular intervals of $\Delta M = 57.1$ (missing propyl amine units) from the perfect dendrimer. Furthermore, the peak at $M_r = 7151$ (missing ammonia via the intramolecular ring closure) is assigned to the dendrimer with 62 primary amine groups and one cyclic secondary amine functionality, while there is also a series of peaks with intervals of 57.1 from $M_r = 7151$. After performing this analysis for all dendrimers within the synthetic scheme, it was possible to simulate the electrospray MS spectra in detail. These simulations show that the dendrimers possess statistical defects in their structures as the result of the many consecutive reactions that are performed to prepare these highly branched structures. The poly(propylene imine) dendrimers with 64 amine end groups, the result of 248 of

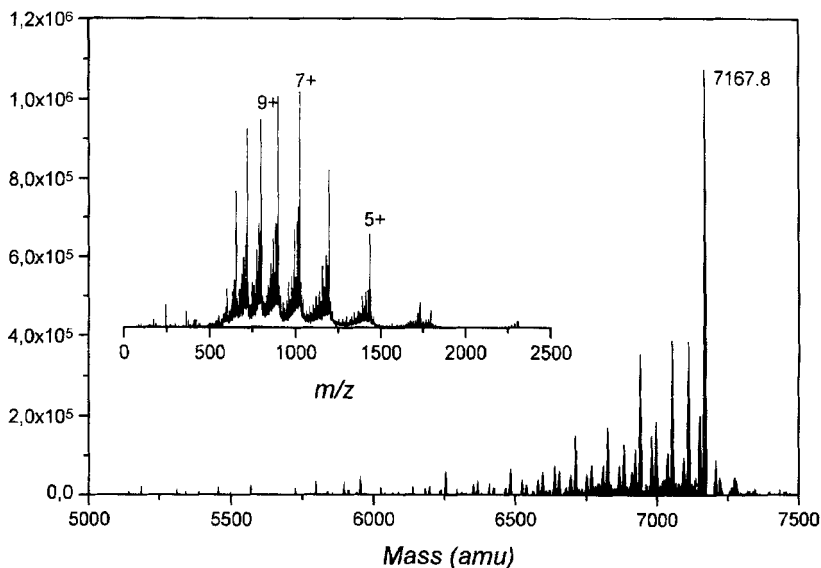


Figure 3 Deconvoluted ES-MS spectrum of DAB-*dendr*-(NH₂)₆₄. Inset: actual data

these reactions, possess a dendritic purity of around 20% and have a polydispersity of around 1.002. These results show that the divergent synthesis, once optimized to the extreme, compares to the best results obtained in the Merrifield synthesis of polypeptides etc., while the polydispersities are unprecedented in polymer synthesis. Throughout this Chapter, we will use the perfect structures in figures, but the recent electrospray MS results show that the logical statistical defects are present, though only in a low concentration.

2.3 Physical Properties

Apart from DAB-*dendr*-(CN)₄, which is a white crystalline solid, all generations are colourless to slightly yellow oils. The amine-terminated dendrimers are transparent, whereas the nitrile-terminated ones are somewhat turbid. The solubility of the dendrimers is determined primarily by the nature of the end group: DAB-*dendr*-(NH₂)_n is soluble in H₂O, methanol and toluene, DAB-*dendr*-(CN)_n in a variety of common organic solvents. The viscosity of the poly(propylene imine) dendrimers is investigated both in THF (intrinsic viscosity, Figure 4) and in the neat form. A maximum in $-\log[\eta]$ is observed in the plot, which is characteristic for dendrimers [11].

Thermal analysis of DAB-*dendr*-(CN)_n and DAB-*dendr*-(NH₂)_n shows a number of interesting aspects. The glass transition temperature (T_g) has been derived from

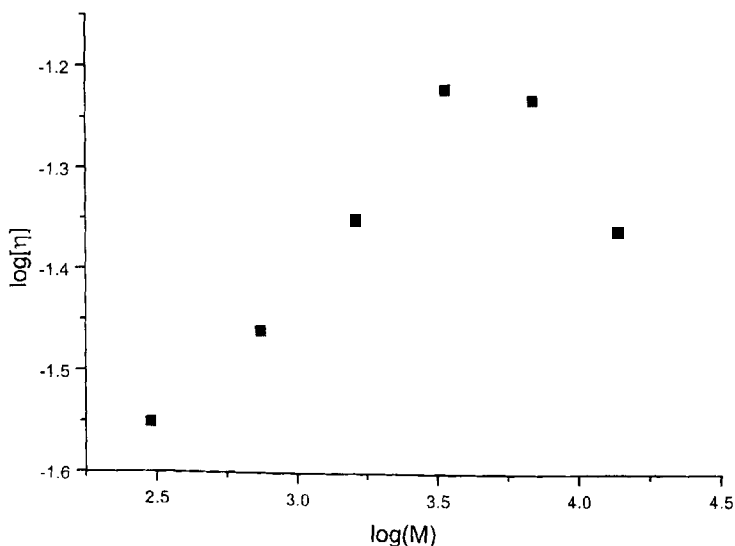


Figure 4 Plot of $[\eta]$ versus logMW of the various nitrile-terminated poly(propylene imine) dendrimers (in THF)

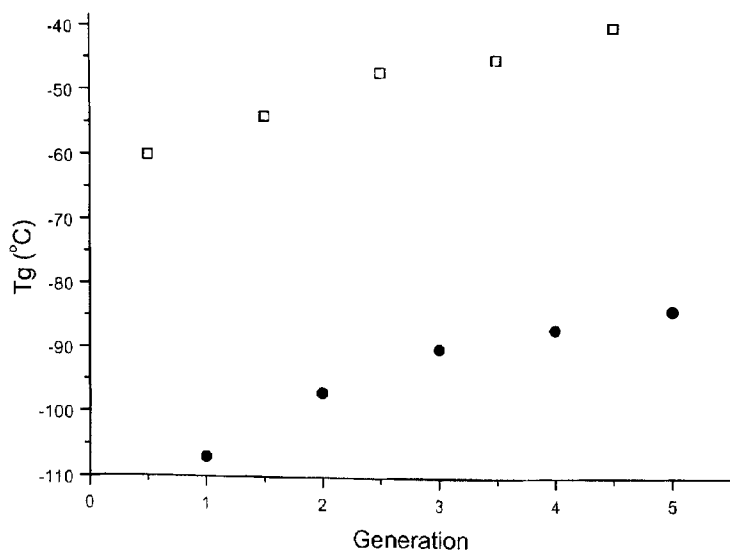


Figure 5 Plot of the glass transition temperatures of the poly(propylene imine) dendrimers with nitrile (□) and amine (●) end groups

differential scanning calorimetry (DSC) and the results are presented in Figure 5. In both series of amine- and nitrile-terminated dendrimers, the T_g -values observed are low and from generation three onwards independent of the generation. In all cases the nitrile-terminated dendrimers show higher T_g -values than the amine-terminated structures, which can be attributed to the dipole–dipole interactions between the nitrile groups. There exists some confusion as to the meaning of a T_g for this kind of molecules. Since in all cases only one T_g is observed, we are tempted to assume that this value is linked to the mobility of segments within a single molecule. In any case, the low T_g -values indicate that the dendrimers possess a large degree of conformational freedom.

The thermal stability, determined by thermogravimetric analysis (TGA), of the amine-terminated dendrimers is unexpectedly high and increases with increasing molecular weight. The TGA_{max} (temperature at which the weight loss is maximal) for *DAB-dendr*-(NH₂)₄, *DAB-dendr*-(NH₂)₈, *DAB-dendr*-(NH₂)₁₆, *DAB-dendr*-(NH₂)₃₂ are 330, 378, 424, and 470°C, respectively (measured at a heating rate of 20°C min⁻¹ under nitrogen). For *DAB-dendr*-(NH₂)₈ less than 1.0% weight loss is observed at 310°C. The nitrile-terminated dendrimers are less stable, but in this case too the stability increases with higher generations. Using TGA–MS a thermally induced retro-Michael reaction could be identified to be the major degradation mechanism for the nitrile-terminated dendrimers.

All dendrimers consist of inner tertiary amines, located at the branching points of the different dendritic layers. The amine-terminated dendrimers furthermore have

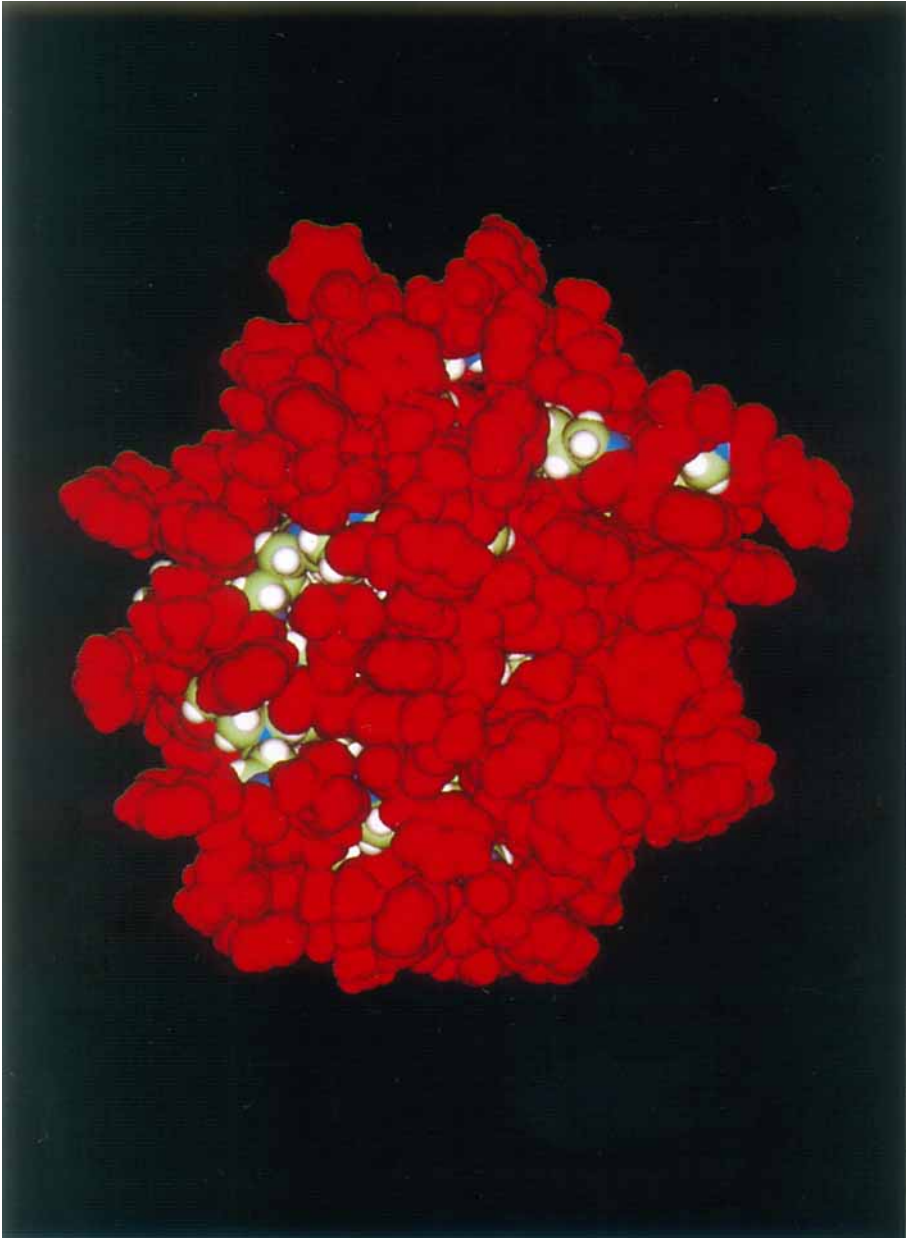


Plate 1. Molecular model of the dendritic box.

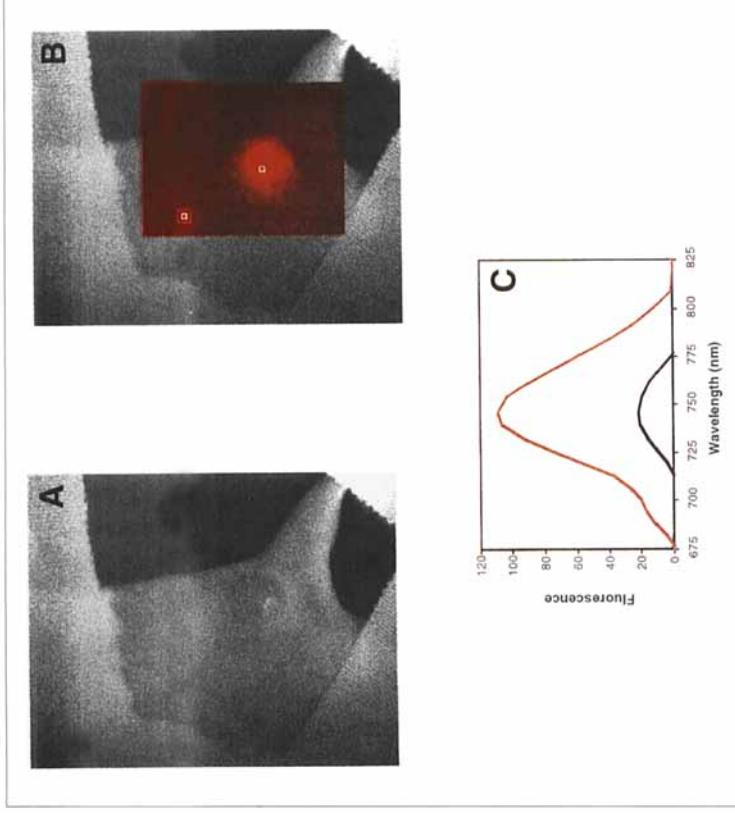


Plate 2. Fluorescence spectral bioimaging of lutetium(III) texaphyrin **PCI-0123** in an EMT6-bearing mouse. The mouse is lying in the prone position; the right flank bearing the subcutaneous EMT6 tumour is exposed. The mouse received a tail vein injection of 10 μ mol **PCI-0123** per kg and then was imaged 4.5 h postinjection. The fluorescence spectral typing measurement (**B**) was overlaid on the pre-imaged black and white photo (**A**). Two pixels denoting the tumour (red) and nontumour (black) regions, as shown by boxes in (**B**), were processed to yield fluorescence emission profiles (**C**).

basic primary amine endgroups. Basicity is therefore one of the most marked properties of the poly(propylene imine) dendrimers, and has been studied via titration experiments and calculations. Titration experiments of the dendrimers have been performed in water using 1 M hydrochloric acid. Only two equivalence points are observed for DAB-*dendr*-(NH₂)₄ in a ratio of 2 : 1. From these titrations, pK_a values of 10.0 (primary amine groups) and 6.7 (tertiary amine groups) have been derived. These results agree with the well-documented solvent dependence of the relative basicity of primary and tertiary amine groups. For DAB-*dendr*-(NH₂)₈ and DAB-*dendr*-(NH₂)₁₆ there is no big difference in the observed pK_a values compared to DAB-*dendr*-(NH₂)₄. Titration experiments in water showed that it is possible to protonate all nitrogen atoms up to DAB-*dendr*-(NH₂)₆₄. Also, ¹⁵N-NMR titrations of the amine-terminated dendrimers in water, in combination with Ising model calculations on the protonation of branched polyamines, show the protonation sequence of the different layers of nitrogens [25]: first the primary amines are protonated, followed by the most central tertiary amines, and finally the other tertiary amines in such a way that Coulombic interactions are minimized.

Titration experiments on the nitrile-terminated dendrimers in water show for DAB-*dendr*-(CN)₄ pK_a values of 3.2 and 4.8. The corresponding calculated pK_a values are 3.1 and 4.1 respectively (using the pKalc program, version 2.0, CompuDrug chemistry). For DAB-*dendr*-(CN)₈ only the two inner nitrogen atoms can be protonated in acetonitrile, due to the low basicity of the four other ones. This is confirmed with calculated pK_a values of the four outer tertiary nitrogen atoms in DAB-*dendr*-(CN)₈, ranging from 2.0 to 3.2. The presence of the electropositive nitrile-functions and the protonated inner tertiary amines can explain this phenomenon.

2.4 Shape of the Poly(propylene imine) Dendrimers

Following the first synthetic attempts toward dendrimers, theoretical investigations [13] predicted molecular dimensions, limits of growth, and intramolecular configurational details of dendrimers, which afterwards were indeed confirmed experimentally, like for instance the maximum of the intrinsic viscosity as a function of the generation number [11,27]. In the same spirit, simulation techniques were employed by Lescanec *et al.* [14]. The internal structure predicted by the simulations differs strongly from the proposed analytical model of de Gennes *et al.* [13]. The Lescanec model predicts a (segment) density maximum near the centre of the dendrimer, whereas de Gennes argues for a density minimum in the centre. Recent results based on Monte Carlo simulations [28], calculations of the intrinsic viscosity [29], as well as ²H and ¹³C NMR studies [30] are in favour of the model of Lescanec *et al.*

Surprisingly, there is still a lack of experimental data on the generation dependence of molecular size to discriminate between the two models. Some experimental studies on various other dendrimers have been reported using, e.g. size exclusion

Table 1 Radii of gyration of DAB-*dendr*-(CN)_n and DAB-*dendr*-(NH₂)_n, as determined from neutron scattering [34]

DAB- <i>dendr</i> -(NH ₂) _n n	Radius (nm)	DAB- <i>dendr</i> -(CN) _n n	Radius (nm)
4	0.44	—	—
8	0.69	8	0.60
16	0.93	16	0.80
32	1.16	32	1.01
64	1.39	64	1.22

chromatography (SEC), viscometry [1,27], small-angle neutron scattering (SANS) [31] and diffusion-ordered spectroscopy [32], but the overall quantity of data is limited. Scherrenberg *et al.* have studied 1% (v/v) solutions of the amine-terminated poly(propylene imine) dendrimers in deuterated water at the SANS facility of the Risø National Laboratory, Roskilde, Denmark [34]. The obtained radii of gyration for the nitrile- as well as for the primary amine-terminated dendrimers are depicted in Table 1. An excellent linear relationship is found between the radius of gyration (R_g) and the generation number. Such a linear relationship has already been predicted by Monte Carlo simulations for other dendrimer systems [28] and these results are therefore additional proof for the Lescanec-model.

Molecular modelling techniques are a powerful tool for obtaining a very detailed insight in the three-dimensional structure of dendrimer molecules at the atomic level. They have been applied to calculate sizes of the poly(propylene imine) dendrimers and radial density profiles in order to estimate the amount of free volume inside the dendrimers, and to make a prediction about the starburst-dense packed generation. The molecular modelling work by Coussens *et al.* [33,34] was focussed on the generations 1–5 of the DAB-*dendr*-(CN)_n and DAB-*dendr*-(NH₂)_n ($n = 4, 8, 16, 32, 64$).

The sizes of the dendrimers have been determined by calculating the molecular volumes, as defined by the Van der Waals radii of the atoms, and by calculating the radii of gyration for several configurations of the dendrimers, as obtained from a molecular dynamics simulation at room temperature. The solvent influence on the calculated radii was estimated by scaling the non-bonded interactions between the atoms. Molecular volumes and average radii for ensembles of 500 conformations of the DAB-*dendr*-(NH₂)_n dendrimers have been collected in Table 2. The calculated radii with all interactions included are somewhat smaller than the radii measured with SANS, whereas the radii obtained with only the Van der Waals repulsions taken into account are somewhat larger. As could be anticipated, the sizes of the dendrimers are of course dependent on the pH of the solution. As both the primary and the tertiary amine groups can be protonated, they start repelling each other when the pH of the solution is decreased.

Table 2 Molecular volumes and radii of gyration of the DAB-*dendr*-(NH₂)_n dendrimers as obtained by molecular modelling in the gas phase [34]

Generation dendrimer	$V^{a,b}$ (nm ³)	$\langle R_g \rangle^a$ (nm)	$\langle R_g \rangle^c$ (nm)
1	1.06	0.49	0.50
2	1.95	0.60	0.76
3	3.65	0.74	1.01
4	9.01	1.00	1.29
5	17.60	1.25	1.59

^a All interactions (Coulombic and Van der Waals) taken into account.

^b The hydrodynamic radius ($= (5/3)^{1/2} R_g$) was used for calculating this volume.

^c Only repulsive Van der Waals interactions taken into account.

2.5 Conclusions

As has been shown, large-scale synthesis of the poly(propylene imine) dendrimers is possible, and leads to well-characterized products. Both the nitrile and amine groups at the periphery of the poly(propylene imine) dendrimers lend themselves for modification via classical organic reactions: nitriles can be converted to carboxylic acids, and amines can be changed to amides, ureas, imines, etc. (Figure 6). Also, other amines can be used as the core molecule.

Physical properties of poly(propylene imine) dendrimers are determined by the nature of the end group and the number of generation. The effect of the end group is clearly noticed from, for example, DSC and TGA measurements, in which the amine-terminated structures show a higher thermal stability and a lower T_g than the nitrile-terminated dendrimers. Naturally, a different pH-dependent behaviour between the two types of dendrimers is observed. Generation-dependence is noticed for the optimum in the plot of intrinsic viscosity vs. molecular weight and is a common feature for dendrimers. The cavities observed with molecular modelling studies are typical for high generation dendrimers. The radius of gyration increases linearly with generation. This is in harmony with the predictions based on Monte Carlo simulations of dendrimers.

3. DENDRITIC BOX

After the initial reports on dendritic molecules [19], proposals have been made for the construction and applications of guest–host systems made out of dendrimers [1,2,35]. The concept of topological trapping by core–shell molecules is based on

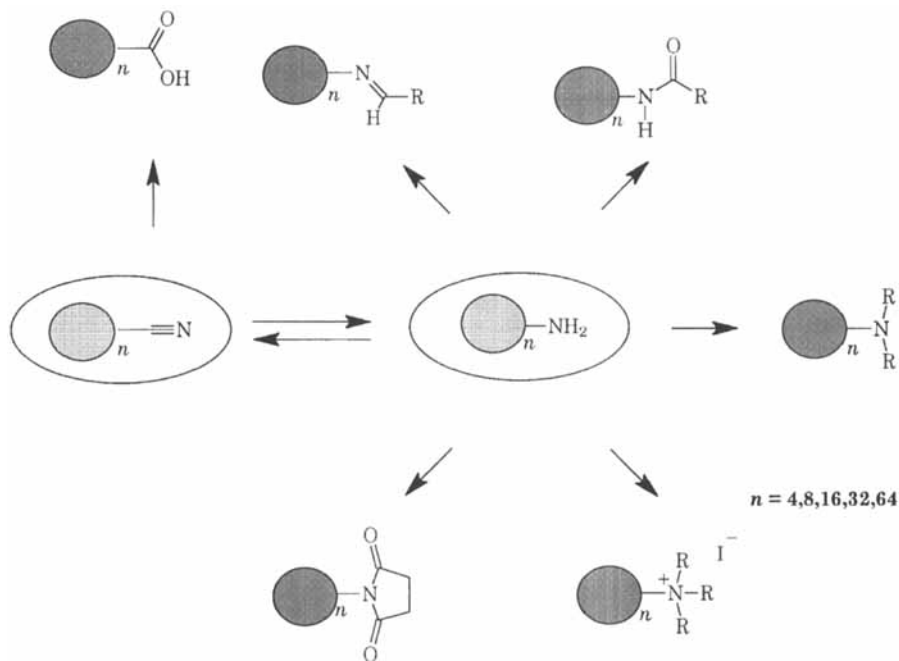


Figure 6 A number of modifications of the poly(propylene imine) dendrimers that have been explored in our laboratory

the fact that, at some stage in the synthesis of dendrimers, the space available for the new generation or end group modification is not sufficient to accommodate all the atoms required for complete conversion (the so-called sterically induced stoichiometry) [1]. We have discussed the synthesis of a dendritic box consisting of a flexible core with a rigid shell [9]. These boxes have internal cavities available in which guest molecules can be physically entrapped due to the rigid shell.

The flexible core of our dendritic box is based on poly(propylene imine) dendrimers which were synthesized as discussed above. For the construction of the rigid shell of the dendritic box a critical end group modification of the cascade polyamine with an appropriate bulky group is performed. For instance, the *N*-hydroxy-succinimide ester of a *tert*-butyloxycarbonyl (*t*-BOC)-protected L-phenylalanine is allowed to react with the fifth generation poly(propylene imine) dendrimer in a CH_2Cl_2 -triethylamine mixture (Figure 7). Extended washing procedures were used to obtain pure dendritic box with a molecular weight of almost 24 kg mol^{-1} [9].

Structure elucidation of the dendritic box was performed with a variety of characterization techniques; IR, ultraviolet (UV), ^1H and ^{13}C NMR spectroscopy data are all in agreement with the structure assigned. However, the resonances in the ^{13}C NMR spectra showed a significant line broadening for the higher generations. Spin-lattice (T_1) and spin-spin (T_2) relaxation measurements were performed and

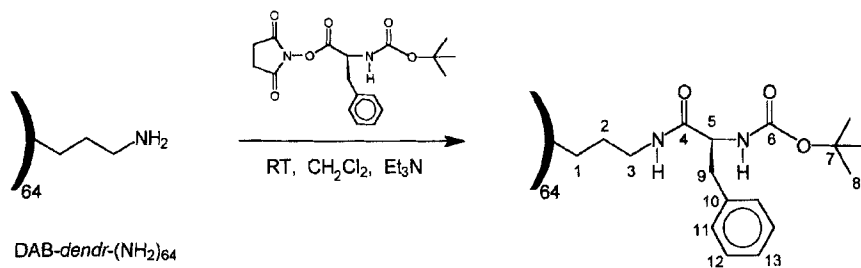


Figure 7 Schematic presentation of the synthesis of the amino acid-terminated poly(propylene imine) dendrimers, including an atomic numbering of the shell of the dendritic box

the results for the shell atoms were compared with the corresponding data of the other lower generations (Figure 8). The observed increase of T_1 relaxation times after the third generation is indicative of a decrease in molecular motion for the higher generations; an almost solid-phase behaviour of the shell in solution is proposed. Further evidence for this close packing of the shell is found from chiroptical studies. Presumably, intramolecular hydrogen bonding between several L-Phe residues in the shell is contributing to this solid-phase character. Unfortunately, MALDI-TOF-MS (matrix-assisted laser desorption time of flight mass spectroscopy) and electrospray mass spectrometry studies have not been successful yet.

Molecular mechanics calculations with the CHARMM program of the DAB-dendr-(NH-*t*-BOC-L-Phe)₆₄ are performed to get insight into the three-dimensional

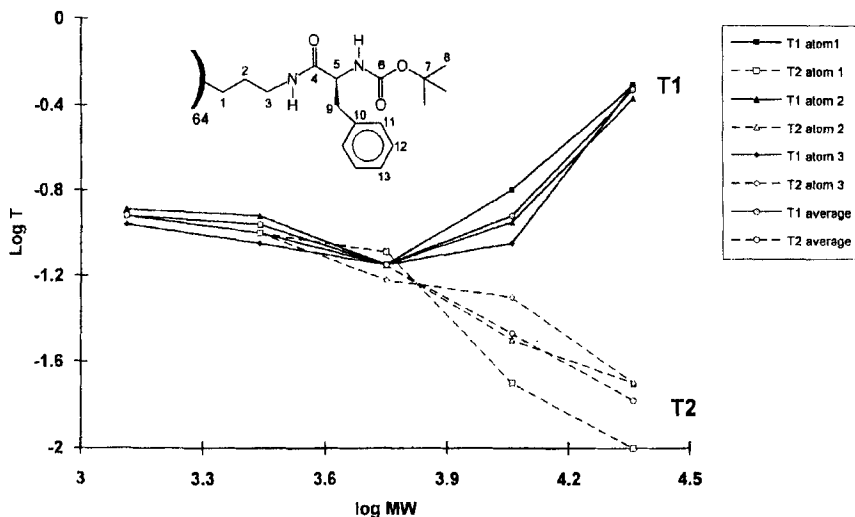


Figure 8 Double logarithmic graph of relaxation data (carbon T_1 and T_2) versus molecular weight (generation) for the carbon atoms 1, 2, and 3 as recorded at 75 MHz in chloroform

structure. A globular architecture is found with an estimated radius of 2.3 ± 0.3 nm (see Plate 1). Dynamic light scattering studies of the dendritic box in solution showed single particle behaviour with a radius of gyration of 1.7 ± 0.4 nm (which resembles a radius of the box of 2.2 nm). Finally, small-angle X-ray scattering (SAXS) measurements gave a radius of gyration of 1.8 nm for the dendritic box.

Single-crystal X-ray studies of a model compound for the dendritic box showed the formation of an intramolecular hydrogen-bonded network within the shell [73]. Hence, in the case of strong secondary interactions between end groups, they are forced to form a shell-like periphery. The increase of intramolecular hydrogen bonds is also observed in IR spectroscopy.

The choice of L-Phe as the amino-acid component of the shell has been made from a study in which we compared a variety of amino acids of different size. By using larger amino acids like L-Trp it is no longer possible to modify all the end groups due to the restricted space available, verifying the sterically induced stoichiometry principle [1,8]. On the other hand, by performing the modification reaction with smaller amino acids, like L-Ala and L-Leu, such a dense packing is not achieved, as concluded from NMR and modelling studies, as well as the encapsulation experiments described in the next paragraph. L-Tyr in the *t*-BOC protected form is comparable with L-Phe as shell component with respect to dense packing, but lacks the good solubility in most organic solvents. Therefore, we selected the DAB-dendr-(NH-*t*-BOC-L-Phe)₆₄ as the dendritic box, being a nanometer-sized host system for a variety of guest molecules [9].

3.1 Encapsulation of Guest Molecules into the Dendritic Box

The experimental and modelling results prompted us to propose that we prepared molecules with a solid shell and a flexible core that will have internal cavities available for guest molecules. As the shell is constructed in the last step, it is possible to perform this coupling reaction in the presence of guest molecules. In fact, we encapsulated molecules with some affinity for tertiary amines within the dendritic box. Excess of guest and/or traces of guests adhering to the surface are removed by extensive washing and/or dialysis. When a dendrimer of lower generation was used, the shell is not dense enough to capture the guests and they were removed by extraction. A large variety of guest molecules have been encapsulated and this opens a plethora of interesting chemical and biochemical applications. We will discuss some of these nanometer-sized guest–host systems here as well as the properties of the guest molecules that are so critically influenced by the dendritic box.

By carrying out the encapsulation reaction in the presence of a varying concentration of 3-carboxy-PROXYL, the number of entrapped radicals could be varied from 0.3 to 6.0 molecules per dendritic box as determined by electron spin resonance (ESR) spectroscopy [36]. The number of 3-carboxy-PROXYL radicals in the dendritic box does not increase above six (Figure 9), clearly demonstrating that

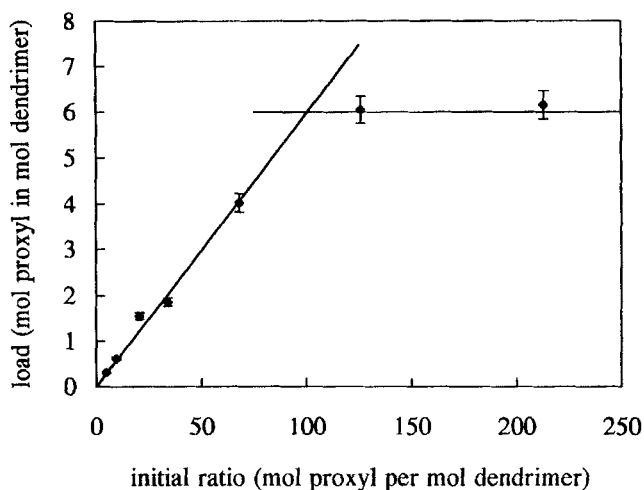


Figure 9 Number of 3-carboxy-PROXYL radicals trapped in the dendritic box, as determined by ESR spectroscopy, versus the molar ratio of radical and dendrimer in the initial solution prior to the encapsulation reaction

the maximum attainable number of radicals is restricted by the shape of the cavities in the box. The ESR spectra of 3-carboxy-PROXYL@DAB-*dendr*-(NH-*t*-BOC-L-Phe)₆₄ dissolved in 2-methyltetrahydrofuran are strongly temperature dependent. At 305 K an essentially isotropic ¹⁴N-coupled ESR spectrum is observed, characteristic for a rapid rotational diffusion of the radical spin probes. Lowering the temperature results in a decreasing intensity of the isotropic spectrum and the appearance of an anisotropic ESR spectrum, consistent with a more restricted motion of the spin probe. In the temperature range 150–250 K, a superposition of the motionally narrowed (isotropic with $A_{\text{iso}}(\text{N}) = 1.40\text{--}1.42$ mT) and the slow-motion (anisotropic with $A_{\text{zz}}(\text{N}) = 3.38$ mT) spectrum is observed. This superposition indicates that the micro-environment of the encapsulated 3-carboxy-PROXYL molecules is not uniform over the interior of the dendritic box. A solid sample of 3-carboxy-PROXYL@DAB-*dendr*-(NH-*t*-BOC-L-Phe)₆₄ with more than 1.6 molecules per box shows at lower temperatures a (partial) ferromagnetic alignment of the radicals. The observation of a $\Delta_{\text{ms}} = 2$ ESR transition exhibiting a partially resolved 1:2:3:2:1 hyperfine coupling pattern due to two ¹⁴N nuclei with $A(\text{pair}) = 1/2A(3\text{-carboxy-PROXYL})$ showed unambiguous spectral evidence of the presence of a triplet-state radical pair (Figure 10). The intensity of the $\Delta_{\text{ms}} = 2$ signal follows the Curie law ($I = C/T$) between 4.2 and 100 K, consistent with a triplet ground state. To the best of our knowledge this is the first observation of an intermolecular ferromagnetic exchange interaction in a non-crystalline guest–host assembly. Since these types of interactions are often observed intramolecularly or in organic crystals, we are prompted to conclude that the dendritic box possesses

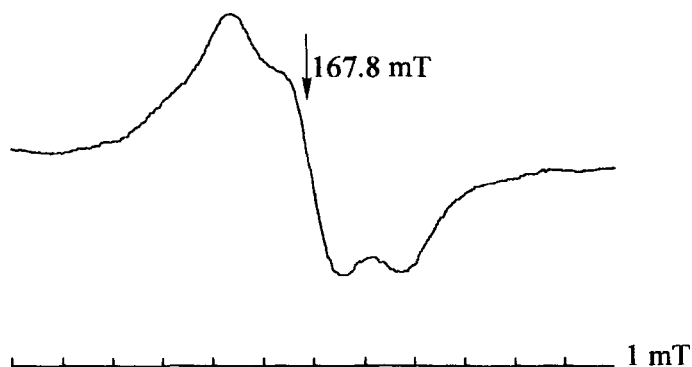


Figure 10 $\Delta_{ms} = 2$ ESR spectrum of a solid sample of 3-carboxy-PROXYL@DAB-dendr-(NH-*t*-BOC-L-Phe)₆₄ at 4.2 K

some peculiar ordering properties apparently dictated by the architecture of the dendritic skeleton.

As another example we have encapsulated a variety of organic dye molecules into the dendritic box [9]. Rose Bengal is encapsulated in a similar fashion as the spin probe described above. The number of Rose Bengal molecules encapsulated could be estimated after prolonged dialysis by comparison of the UV spectra of guests that are inside or outside of the box. The relation between the number of encapsulated molecules of Rose Bengal as a function of the concentration of Rose Bengal used in the shell-forming reaction is depicted in Figure 11. Also in this case the maximum

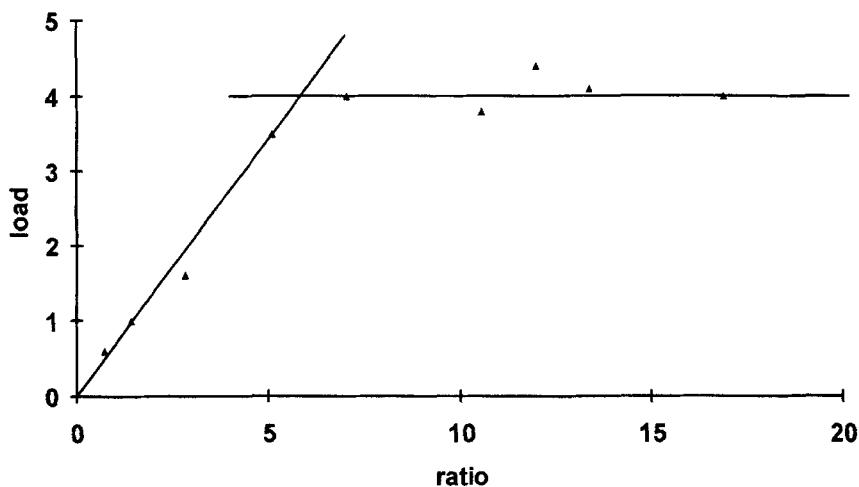


Figure 11 Number of Rose Bengal molecules encapsulated in one dendritic box, as determined by UV-vis spectroscopy, versus the molar ratio of Rose Bengal and dendrimer during the encapsulation reaction

number of guest molecules attainable is limited, in this case to four. It is tempting to propose that each of the four guest molecules is occupying one large cavity present in the dendritic box. Although the absorption spectra of Rose Bengal and Rose Bengal@DAB-*dendr*-(NH-*t*-BOC-L-Phe)₆₄ are identical, there is a large difference in the fluorescence spectra as recorded in CHCl₃. The strong fluorescence at $\lambda_{\text{max}} = 600$ nm for Rose Bengal@DAB-*dendr*-(NH-*t*-BOC-L-Phe)₆₄ is completely absent in the case of the supramolecular isomer of Rose Bengal outside the box. In the latter the fluorescence is quenched effectively. The emission of the guest–host system is relatively insensitive to solvent effects, hence, we believe that we have prepared a fluorescent sphere with an environment-independent emission profile.

Stimulated by the observation of induced chirality of dyes dissolved into chiral bilayers and micelles [37], the circular dichroism (CD) spectra of a variety of dyes encapsulated in the dendritic box have been recorded. Induced circular dichroism spectroscopy is based on the transfer of chirality from the environment to an achiral dye and could therefore be applicable to these boxes. In Figure 12 the results are given for two samples of Rose Bengal@DAB-*dendr*-(NH-*t*-BOC-L-Phe)₆₄ with one and with four molecules of Rose Bengal per dendritic box on the average. Although both samples show identical UV spectra, a dramatic difference is observed in their induced CD spectra. The dendritic box with one molecule of Rose Bengal encapsulated exhibits an induced CD spectrum related to the UV spectrum, in which all bands possess a negative Cotton effect. However, an exciton-coupled spectrum is observed when four molecules of Bengal Rose are encapsulated on average in a single dendritic box. This exciton coupling indicates the close proximity of chromophores with a certain fixed orientation [38]. All explanations for the

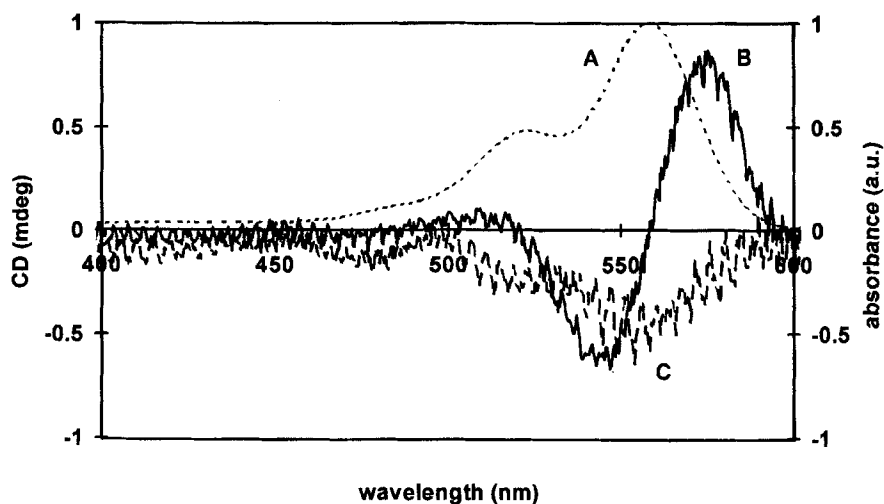


Figure 12 UV (A) and CD spectra of Bengal Rose@DAB-*dendr*-(NH-*t*-BOC-L-Phe)₆₄ containing one (C) and four (B) molecules of Bengal Rose

induced CD observed are speculative, however, it is reasonable to assume that some chirality is present in the cavities of the dendritic box, despite the vanishing optical activity of the shell [39].

Eriochrome Black T is a pH-dependent dye that is very soluble in polar solvents and can be encapsulated in the box. Due to the many (62) tertiary amines present in the interior of the box, Eriochrome Black T shifts its absorption spectrum from $\lambda_{\text{max}} = 280$ nm for free dye in CH_2Cl_2 to $\lambda_{\text{max}} = 360$ and 570 nm for dye in the box and in CH_2Cl_2 . As soon as the absorption spectrum of free dye and encapsulated dye are different it is not possible to accurately determine the number of molecules encapsulated in a simple way. Since Eriochrome Black T is very soluble in water or acetonitrile, while the dye@box is insoluble in these solvents, we used this system to study the diffusion of the dye out of the box. Even after prolonged heating, dialysis or sonification the aqueous phase of the dispersion did not become coloured due to diffusion. Therefore, it was concluded that the diffusion of dye out of the box is unmeasurably slow.

By comparing the encapsulation results of a large variety of dye molecules, it became apparent that many coplanar dye molecules with an ionic group can be encapsulated into the dendritic box. For concentrated solutions of large dyes in the encapsulation reaction the maximum number of dye molecules entrapped is four, which is related to the architecture of the dendritic box. Large three-dimensional dyes or coplanar dyes without ionic or polar groups are hard to encapsulate and only small numbers of the ratio guest per host are observed, typically around 0.1. Smaller polar guests can be encapsulated with maximum numbers beyond four, but in almost all cases an integer number of six or ten is found.

Recent theoretical studies of Goddard *et al.* confirmed the encapsulation of Rose Bengal in the dendritic box [74]. A maximum number of 4–6 molecules could be entrapped and a rationale was given for the encapsulation.

These results suggest that the procedure employed here produces a unimolecular compartmented structure in which guest molecules can be encapsulated and for which the diffusion out of the box is unmeasurably slow.

3.3 Shape-selective Liberation of Encapsulated Guests

So far, the dendritic box has been used to encapsulate guest molecules into the internal cavities present. The rigid, densely packed shell of the DAB-*dendr*-(NH-*t*-BOC-L-Phe)₆₄ limits the diffusion out of the box of almost all guest molecules studied up to now. Obviously, it is difficult to determine the diffusion of solvent molecules accurately, but all experimental data available so far show that small molecules like CH_2Cl_2 can penetrate through the rigid shell. If a dendritic box is made from the *t*-BOC protected glycine amino acid, a semi-permeable box is made. This idea of tuning the density of the shell by decreasing the size of the end groups

has been used to obtain a shape-selective liberation of guests from the dendritic box made from L-Phe [40].

After encapsulation of four molecules of Rose Bengal and 8–10 molecules of para-nitrobenzoic acid together in a dendritic box, hydrolysis of the *t*-BOC groups with formic acid (95% HCOOH, 16 h) was performed. Subsequent dialysis of the reaction mixture (5% water in acetone) yielded a perforated dendritic box in which only the four molecules of Rose Bengal are entrapped, whereas all *p*-nitrobenzoic acid was dissolved in the acetone/water mixture. Rose Bengal cannot be liberated from the perforated box, not even after the addition of 12 N hydrochloric acid. However, hydrolysis of the outer shell using 12 N HCl under reflux for 2 h liberated Rose Bengal after dialysis (100% water) and the starting poly(propylene imine) dendrimer was recovered in 50–70% yield. By applying this two-step hydrolysis procedure to a variety of different mixtures of guest molecules, it was shown that this shape-selective liberation is a general principle [34]. Furthermore, by changing the amino acids in the shell and the protecting group of the amino acid it proved to be possible to fine-tune this pathway of liberation completely.

3.4 Conclusions

We have discussed the synthesis of dendritic boxes possessing a unimolecular compartmented structure in which guest molecules are physically locked. Evidence is presented that the encapsulation is dominated by the architecture of the dendrimer and that some supramolecular ordering is present. Furthermore, a shape-selective liberation of guests can be accomplished by a two-step process.

It is envisaged that the binding between guests and dendritic box can be used as a new tool in modular chemistry. Therefore, we are working on large guest molecules that are partly inside and partly outside the dendritic box. The inside part is functionalized with an anchoring group and a spacer is used to make these large guests compatible with the shell [41]. When the large part that is outside the box becomes functional or possesses functional groups, it should be possible to build larger structures, comparable with the key-and-lock principle, recently published by Newkome *et al.* [42]. It is very appealing to us to exploit the functionality of four as is found for the maximum number of many encapsulated guests. The approach described here based on the dendritic box will lead to modular chemistry at the nanoscopic level by using mechanical bonding between modules.

4. SUPERAMPHIPHILES BASED ON DENDRIMERS

Dendrimers are a type of molecules that can make a positive contribution to a better understanding of the structure–property relation of amphiphiles. These well-defined highly branched macromolecules have gained a growing scientific interest as

building blocks in new molecular architectures [1,2,43]. They have been applied, for example, in unimolecular micelles and structures containing dendrimers and linear macromolecules [5,7,44,45]. Chapman's hydraamphiphiles [46] and the amphiphilic polymers as described by Zhong and Eisenberg [47], which can be regarded as the first approach toward polystyrene–dendrimer structures with variable polar head group size, already show the versatility of the introduction of dendrimers into amphiphilic molecules. Recently, we have reported hybrid polystyrene–dendrimer block copolymers (see Figure 13) that fill the gap between the low molecular weight surfactants and amphiphilic polymers [20,48]. These structures show a generation-dependent aggregation behaviour, which is consistent with Israelachvili's theory of the effect of amphiphile geometry on type of aggregation. The dendritic architectures presented here can be regarded as a new type of amphiphiles in between the traditional organic surfactants and amphiphilic block copolymers. Finally, they are important structures in the emerging field of self-assembled dendrimers [49].

4.1 Synthesis

In order to synthesize poly(propylene imine) dendrimers onto polystyrene via the divergent method, well-defined primary amine functionalized polystyrene had to be prepared as the core molecule. The anionic polymerization technique was chosen for the preparation of polystyrene (PS), because of the possibility of control over molecular weight and end group functionalization. An indirect amination procedure was developed [50]. In this procedure a standard quantitative end-cap reaction with CO_2 is used and a spacer is created between polystyrene and the primary amine function. The obtained polystyrene–COOH (PS–COOH), with M_n around 3 kg mol^{-1} and M_w/M_n values around 1.05, could be quantitatively reduced to the corresponding alcohol (PS–CH₂–OH) with LiAlH_4 . Onto PS–CH₂–OH a cyanoethylation with acrylonitrile was performed, followed by hydrogenation of the nitrile to a primary amine. After optimization of this four-step procedure, an interesting indirect route has been developed toward PS–CH₂–O–CH₂–CH₂–CH₂–NH₂.

To obtain polystyrene–poly(propylene imine) block copolymers, the divergent dendrimer synthesis as described in 2.1 was performed onto the PS–CH₂–O–CH₂–CH₂–CH₂–NH₂ core molecule, with $M_n = 3.2 \text{ kg mol}^{-1}$ (based on GPC of PS–CH₂–OH).

All nitrile and amine products, with the exception of PS–*dendr*–(NH₂)₃₂, could be purified by precipitation techniques. The polarity of the medium that was used for precipitation had to be increased with increasing generation, from MeOH to ammonia, although PS–*dendr*–(NH₂)₃₂ was too polar to be precipitated even in ammonia. Column-chromatographic purification of the nitrile intermediates was possible up to PS–*dendr*–(CN)₁₆. With this technique, side products as for example

poly(acrylonitrile) and acetylated PS-CH₂-O-CH₂-CH₂-CH₂-NH₂ could easily be removed. All of the products were obtained in good yields after work-up.

From the nitrile intermediates, we were able to obtain a series of acid-modified head groups also: by acid hydrolysis the PS-*dendr*-(COOH)_{*n*} (*n* = 2–32) series was synthesized (Figure 14). Due to the amphiphilic character of these structures, the reactions had to be performed in a toluene–concentrated HCl mixture. The amphiphiles were obtained after workup as their HCl-salt [51].

4.2 Amphiphilic Behaviour

The development of amphiphilic and aggregation behaviour as a function of dendrimer generation of PS-*dendr*-(NH₂)_{*n*} and PS-*dendr*-(COOH)_{*n*} was studied with several different techniques: the amphiphilic character at a toluene–water interface was investigated with conductivity measurements, and at a water–air interface with monolayer experiments. Dynamic light scattering (DLS) and transmission electron microscopy (TEM) were used to examine the aggregates formed by the different generations in aqueous solutions, while the critical association concentrations were determined with the pyrene-probe luminescence technique.

With ¹³C NMR spectroscopy, it was also possible to follow the development of the amphiphilic behaviour as a function of the dendrimer generation. In CDCl₃ only the polystyrene part of PS-*dendr*-(COOH)_{*n*} with *n* = 4–16 was discernible, thereby indicating inverted micellar behaviour. The higher generations with *n* = 8–32 could easily be dissolved in D₂O at high pH. In this solvent only the dendrimer block was visible using ¹³C-NMR spectroscopy. The polystyrene block was confined inside the aggregation in this solvent and therefore long relaxation times resulted in broad peaks, which made it impossible to identify this part of the amphiphile.

(a) Conductivity measurements

To a stirred 0.3 mM dispersion of PS-*dendr*-(NH₂)_{*n*} in a 0.01 M KCl solution, a 0.3 mM amphiphile solution in toluene was added dropwise. By measuring the conductivity of the system as a function of the ratio toluene–water, it could be estimated whether toluene or water was the continuous phase. At the point where the conductivity dropped to zero, the phase inversion point was reached and toluene became dispersing phase. The effect of dendrimer generation on the position of this inversion point was investigated with PS-*dendr*-(NH₂)_{*n*} with *n* = 2–16. PS-*dendr*-(NH₂)₃₂ could not be measured in the same manner, because this product proved to be insoluble in toluene. The conductivity measurements show a distinct difference between PS-*dendr*-(NH₂)₁₆ and the lower generations. For PS-*dendr*-(NH₂)_{*n*} with *n* = 2–8 there is a strong tendency to stabilize toluene as a continuous phase. PS-*dendr*-(NH₂)₂ even showed a remarkable phase inversion at 2 vol% of toluene. This can be explained by the fact that polystyrene is the dominant part in the amphiphilic

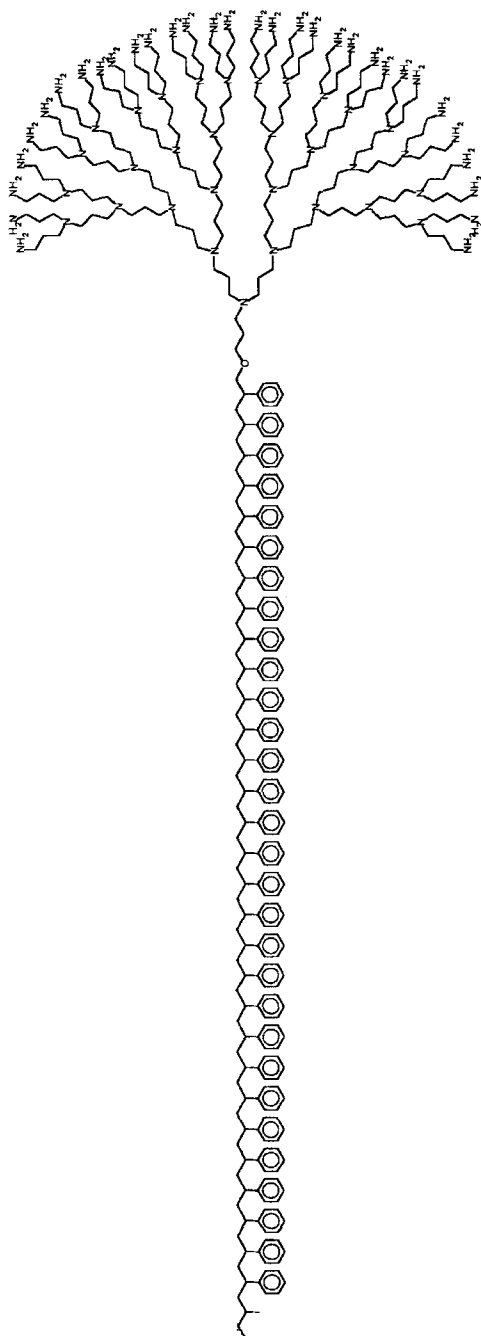


Figure 13 The polystyrene–poly(propylene imine) block copolymer

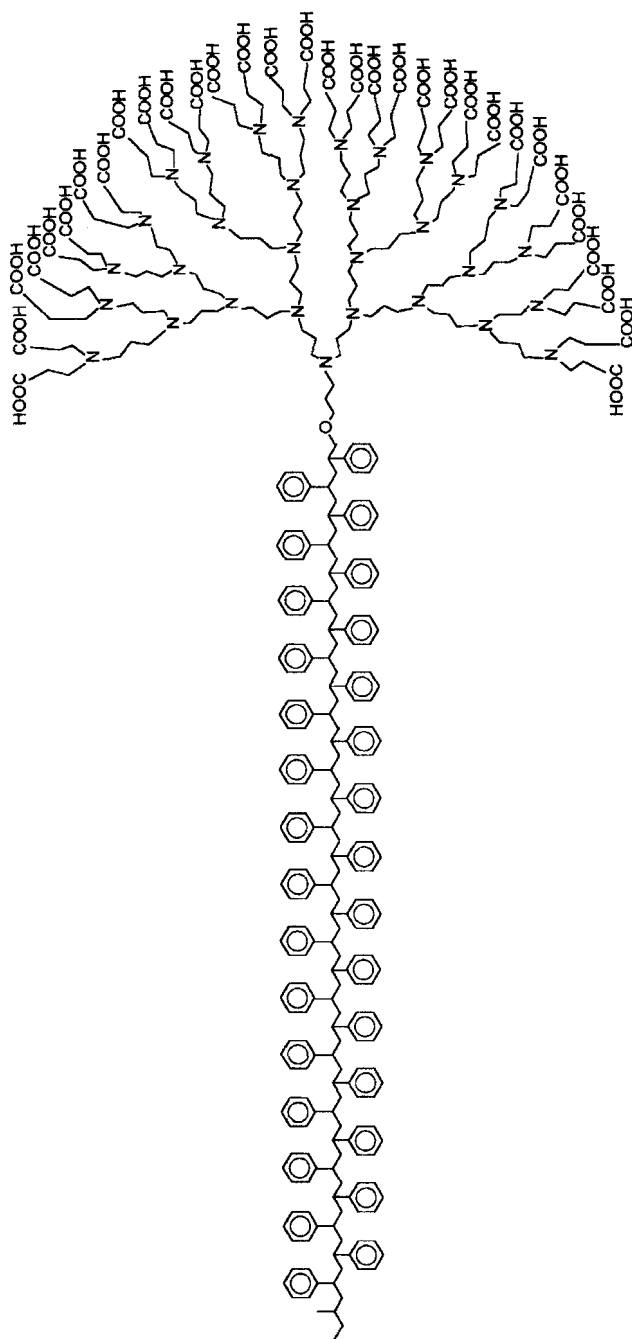


Figure 14 The head group modified superamphiphile with acid end groups

structure and, according to the empirical rules of Bancroft [52] the organic phase as continuous phase is preferred. PS-*dendr*-(NH₂)₁₆ is a much more balanced amphiphile and is therefore equally capable of stabilizing toluene as well as water as dispersing phase.

The behaviour of PS-*dendr*-(COOH)_{*n*} in a 0.01 M KCl solution is comparable to results of the amines above. The apolar PS chain is the dominant block for the low-generations PS-*dendr*-(COOH)_{*n*} (*n* = 2–8). Therefore there is a strong preference for these structures to stabilize toluene as continuous phase. For PS-*dendr*-(COOH)₁₆ a balance is obtained between the apolar and polar parts of the amphiphile, resulting in a strongly increased phase inversion point. This structure is equally capable of stabilizing toluene as water as a dispersing phase. At low and high pH, PS-*dendr*-(COOH)_{*n*} with *n* = 2–8 show, compared to the KCl system, a much better ability to stabilize water as a continuous phase. At low pH the tertiary amines of PS-*dendr*-(COOH)_{*n*} are protonated and a polycationic structure is obtained, while at high pH the tertiary amines and the carboxylic acid end groups are not protonated, resulting in a negative charge on the dendrimer surface. Both processes result in a net charge and therefore follow Newkome's observations for spherical acid-functionalized dendrimers of a sharp increase of dendrimeric diameter due to repulsive interactions [45b]. Therefore, the measured behaviour is in line with the increased polarity of these structures. Because of the already good water-stabilizing properties of PS-*dendr*-(COOH)₁₆, its behaviour is less influenced by a change of pH. The remarkable upswing in conductivity of PS-*dendr*-(COOH)₁₆ in the KCl solution is accompanied by a strong viscosity increase of the system. The conductivity increase can therefore be explained by the formation of a lamellar phase that allows conductivity paths to sustain.

(b) Monolayer experiments

Amphiphilic behaviour at an air–water interface was studied using monolayer experiments. Surface pressure–area isotherms were recorded for PS-*dendr*-(NH₂)_{*n*} with *n* = 1–16. The formed monolayers were also investigated with a Brewster angle microscope (BAM) [53], which made it possible to investigate the type of structures that are formed in the monolayer. The results are shown in Figure 15.

The development of amphiphilic character is also noticed from the monolayer experiments. Only for PS-*dendr*-(NH₂)_{*n*} with *n* = 8 and 16, a normal pressure–area isotherm is obtained, which shows a transition from gaseous through the liquid to the solid-like state. For these two generations an estimation of head group dimensions is possible (PS-*dendr*-(NH₂)₈: head group area = 4.4 nm², head group diameter = 2.37 nm; PS-*dendr*-(NH₂)₁₆: head group area = 5.7 nm², head group diameter = 2.69 nm). The lower generations all show the same type of curves and directly go to solid-state behaviour. In these cases solid polystyrene films are formed, that, at the point of increase or surface pressure, collide and cover the total area

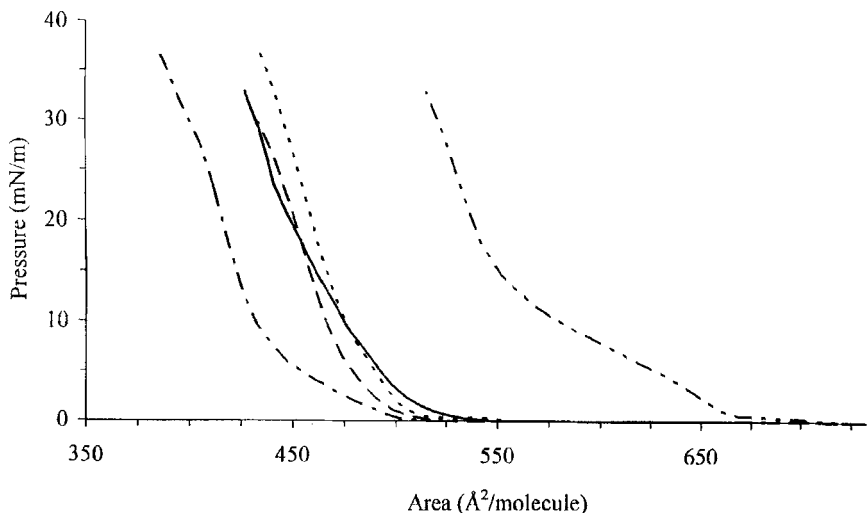


Figure 15 Pressure–area isotherms: — PS-O-CH₂-CH₂-CH₂-NH₂; - - - PS-dendr-(NH₂)₂; - · - PS-dendr-(NH₂)₄; - - - PS-dendr-(NH₂)₈; - - - PS-dendr-(NH₂)₁₆

between the barriers. With BAM these colliding plateaux were also observed. These films are formed because of the dominance of the polystyrene-chain interactions over the dendrimer head group interactions. The areas per molecule that can be estimated are more determined by polystyrene than by the dendrimer head group. This explains that for PS-dendr-(NH₂)₈ a lower value is found for the pressure–area isotherm. This is the first generation for which the influence of the head group on the behaviour at the air–water interface has to be taken into account.

(c) Critical association concentrations

Many techniques can be used for the determination of critical association concentrations (CACs), however, not all of them are sensitive enough to detect the onset of aggregation if this occurs at very low concentrations. Since the CACs of block copolymers are usually much lower than those of low molecular mass surfactants [54], we used pyrene as a fluorescent probe and calculated the effective CACs from the changes in the spectral characteristics of pyrene [55] as a function of surfactant concentration. If we represent the intensity of the emission spectra as a function of the block copolymer concentration, we directly obtain CAC_1 [56]. From the excitation spectra we obtain CAC_2 by representing the ratio I_{340}/I_{335} vs. $\log C$.

The experimental results for PS-dendr-(NH₂)_n with $n = 8$ and 16 obtained from excitation spectra are shown in Figure 16, with CACs of 4 and 5×10^{-7} M, for $n = 8$

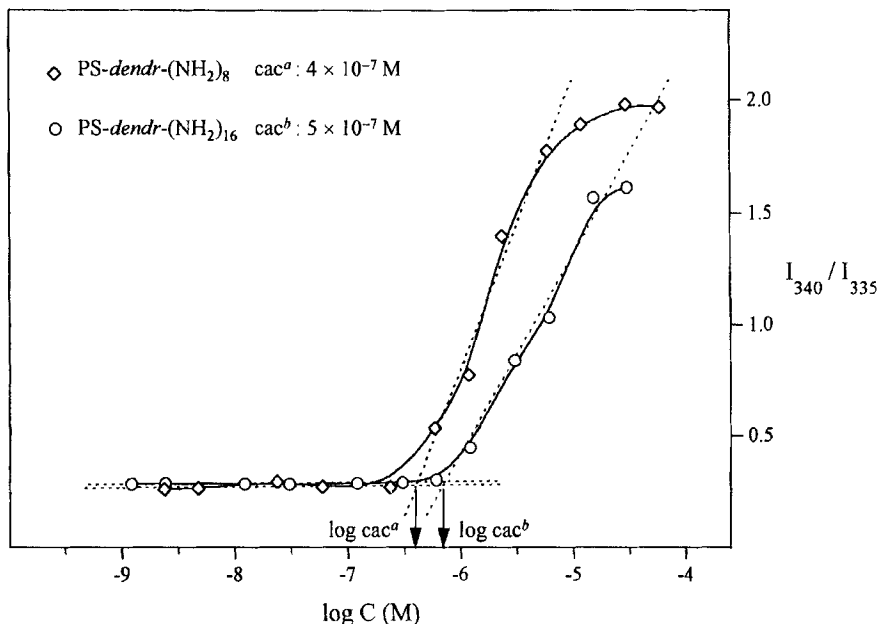


Figure 16 Plots of fluorescence intensity ratio I_{340}/I_{335} from excitation spectra of pyrene in aqueous solutions in presence of —◇— PS-*dendr*-(NH₂)₈ and —○— PS-*dendr*-(NH₂)₁₆

and 16, respectively. The CAC values obtained from excitation data are always lower than those found by emission spectra. No CACs could be measured for the lower generations because these products are insoluble in water. Only the higher generations are soluble in water, while small dendritic head groups are not able to differences were found between the CACs for different generations as the length of the hydrophobic chain remains the same for all the block copolymers. It has been pointed out before [56,57], that the onset of micellation in amphiphilic block copolymers is mainly determined by the nature and the length of the hydrophobic block. Also for most low molecular mass surfactants in aqueous solutions, the free energy of micellation is proportional to the length of the alkyl chain [58–60].

Preliminary measurements have been performed to obtain CACs of PS-*dendr*-(COOH)_{*n*} (*n* = 8, 16, 32). These experiments gave values of 10⁻⁶–10⁻⁷ M.

(d) Dynamic light scattering

Dynamic light scattering (DLS) measurements were performed for PS-*dendr*-(NH₂)₄ in toluene and for PS-*dendr*-(NH₂)_{*n*}, with *n* = 8–32 in water. Concentrations of all of the aggregates were 0.3 mM. For the aqueous aggregates turbid systems were obtained, except for PS-*dendr*-(NH₂)₃₂. PS-*dendr*-(NH₂)₄ showed single particle

behaviour in toluene. A hydrodynamic radius of 3.4 nm could therefore be estimated. The aqueous aggregates were much more difficult to interpret. For PS-*dendr*-(NH₂)₁₆ complicated structures were observed that could be identified as large threadlike structures with a hydrodynamic radius of 120 nm. This type of aggregation remained unchanged even after extreme dilution. The other structures, however, showed so much clustering of the aggregates that no particle dimensions could be estimated. Dilution of the samples did not improve the experiments.

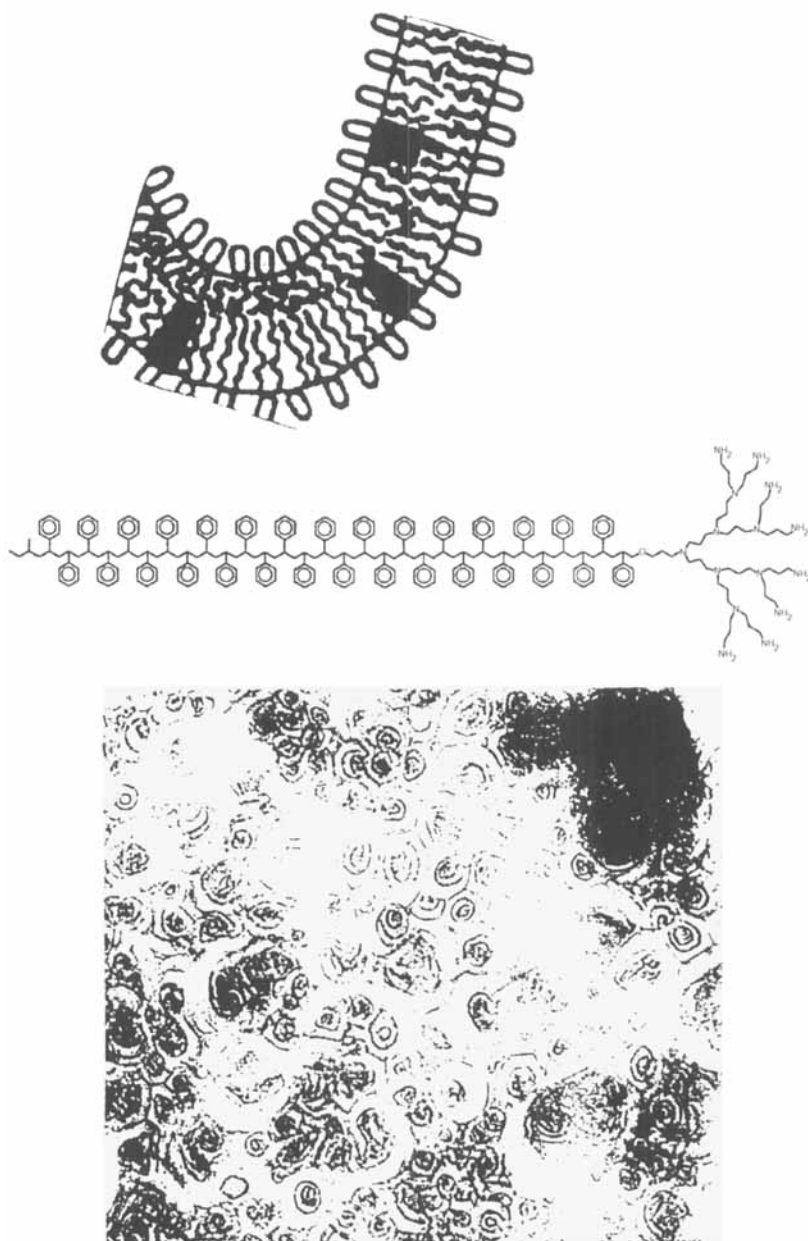
Clustering occurs when the dendritic head groups are directed towards the periphery of the aggregates, where they are able of forming electrostatic interactions. These interactions are also noticed for the normal poly(propylene imine) dendrimers (A. Moussaid, personal communication). The fact that even after extreme dilution the aggregates and clusters remain intact, means that these intermolecular interactions are very strong. They can only be reduced by modification of the dendrimers or by inverted micellar behaviour. This is the case for PS-*dendr*-(NH₂)₄ in toluene. Single particle behaviour points in the direction of inverted micellar structures, in which case the head groups are shielded off from the environment by the polystyrene chains.

(e) Transmission electron microscopy studies

Aqueous aggregates of PS-*dendr*-(NH₂)_{*n*} with *n* = 8, 16 and 32 (0.3 mM) were studied with three different TEM techniques: negative staining with uranyl acetate, Pt-shading and freeze fracture. All three techniques gave consistent results: in the case of PS-*dendr*-(NH₂)₈ flexible bilayers were formed (Figure 17) [61], PS-*dendr*-(NH₂)₁₆ showed rodlike micelles with a diameter of 12 nm (Figure 18), and PS-*dendr*-(NH₂)₃₂ gave spherical micelles with diameters in the range 10–20 nm (Figure 19). For this last sample no freeze fracture results could be obtained. Acidification of PS-*dendr*-(NH₂)₈ from pH = 7 to pH = 1 did not influence the aggregation type. Also after 4 weeks the same aggregates were still observed for PS-*dendr*-(NH₂)₈.

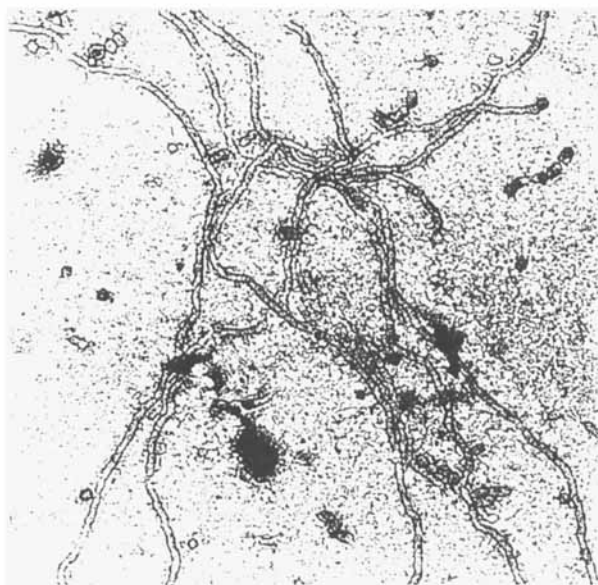
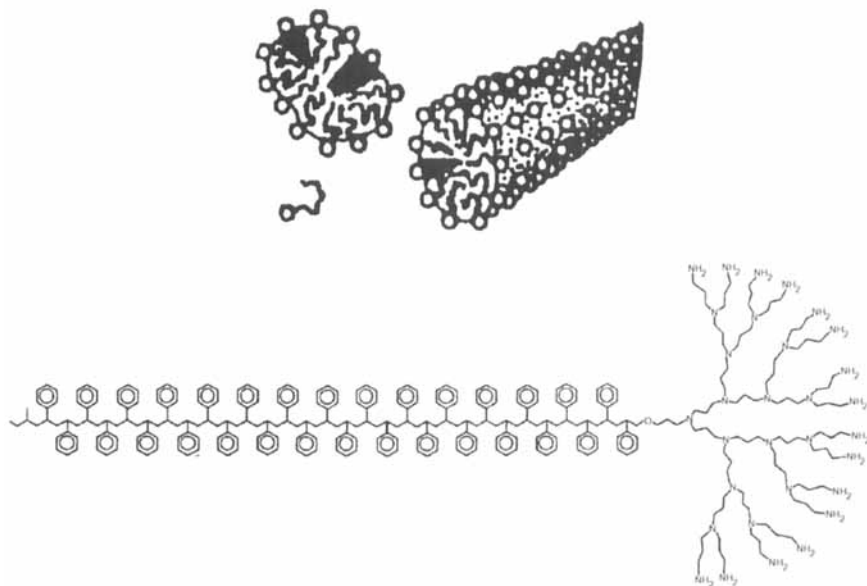
The observed diameters of rodlike and spherical micelles are of the same order of magnitude as can be expected from a bilayer of the diblock copolymers. With respect to clustering and stability of aggregates TEM is consistent with the DLS measurements. The stability of the aggregates formed is remarkable: spherical micelles can be made visible with the TEM techniques used [62]. The well-known transition behaviour for simple amphiphiles [63] from micellar cylinders towards micelles upon dilution is in this case not observed. The aggregates formed of PS-*dendr*-(NH₂)₈ are shown to be stable in time, for at least a month. This structure also shows pH-independent behaviour. This can be explained by the fact that at pH = 7 the primary amines are already partly protonated, so that a change to lower pH does not have a drastic effect on head group charge and size.

TEM was also used to study aggregates of PS-*dendr*-(COOH)_{*n*} with *n* = 8–32, made of samples from aqueous solutions (pH = 14; 0.3 μM). Large network



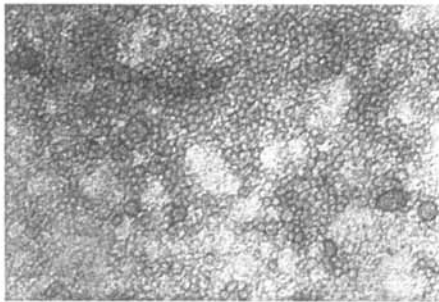
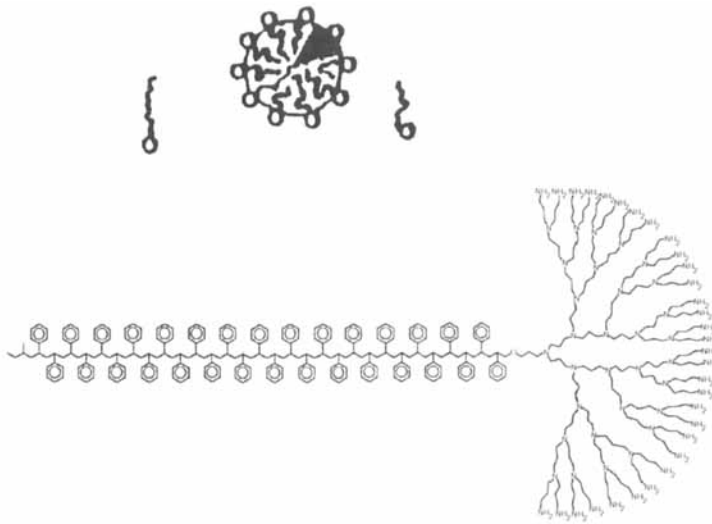
negative staining, 107,500x

Figure 17 TEM photograph of the vesicular structures formed by PS-dendr-(NH₂)₈; negative staining, $\times 107\,500$

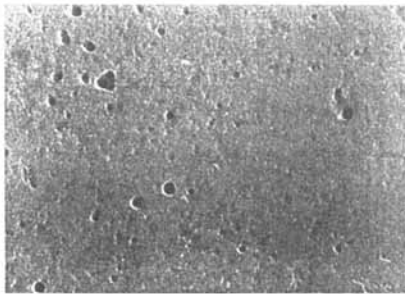


negative staining, 86,000x

Figure 18 TEM photograph of the micellar rods formed by $PS\text{-}dendr\text{-}(NH_2)_{16}$; negative staining, $\times 86\,000$



negative staining, 135,000x



shadowing 24,400x

Figure 19: TEM photographs of the spherical micelles formed by *PS-dendr*-(NH₂)₃₂; Pt-shadowing, ×24 400; negative staining, ×135 000

structures were observed due to clustering of the aggregates. Only in the case of PS-*dendr*-(COOH)₈ could the single aggregation structures be identified as curved, “worm-like” micelles. This aggregation form is thought to be in between the structures observed for PS-*dendr*-(NH₂)₈ and PS-*dendr*-(NH₂)₁₆, which respectively form flexible bilayers and micellar rods.

4.3 Discussion

The results obtained with both TEM and DLS are in perfect qualitative agreement with the theory of Israelachvili [64] about surfactant assembly. He describes how the geometry of the amphiphile determines what kind of aggregates is formed. Starting with a small head group, compared to the chain, inverted micelles are to be expected.

With increasing head group size, aggregates change from planar bilayers, through vesicles, rodlike micelles to spherical micelles. This process is exactly what is observed going from PS-*dendr*-(NH₂)₄ to PS-*dendr*-(NH₂)₃₂. Changing head group size and not the chemical nature of the amphiphilic structures is only possible using dendrimers and results in proof for Israelachvili’s theory of shape-dependent aggregation behaviour. A model for traditional surfactants is now qualitatively applicable for this special kind of amphiphilic block copolymers.

By comparing the polystyrene–poly(propylene imine) dendrimer amphiphiles with low molecular weight surfactants and traditional amphiphilic block copolymers, it becomes clear that our structures combine properties of both. A shared feature with surfactants is the ability of changing the type of aggregation by adjusting amphiphile geometry. For surfactants this is a well-known phenomenon, and forms the basis of Israelachvili’s theory [64]. For amphiphilic block copolymers the possibilities are much more restricted. An advantage that our systems share with block copolymers is the stability of the aggregates formed. This also points in the direction of low critical association concentration (CAC) values. The CAC values found are comparable to those of traditional block copolymer systems. Our systems are therefore very interesting for use as stabilizers for vesicle and emulsion polymerization.

4.4 Conclusions

It is possible to prepare a new series of amphiphilic diblock copolymers by a divergent poly(propylene imine) dendrimer synthesis onto a primary amine functionalized polystyrene core molecule. Every intermediate of this ten-step reaction procedure can be characterized in great detail. Study of the behaviour of these amphiphiles at toluene–water and air–water interfaces clearly demonstrates the development of amphiphilicity with increasing generation. The change of aggregation type from inverted micellar structures for PS-*dendr*-(NH₂)₄, through vesicles, rodlike micelles to spherical micelles for PS-*dendr*-(NH₂)₃₂ is in qualitative agree-

ment with the theory of Israelachvili concerning surfactant assembly. The amphiphiles described in this Chapter are similar in shape but different in size as compared with traditional block copolymers. This new class of amphiphiles shows that dendritic structures can self-assemble to larger constructs, and it is the amphiphilic character that will give numerous possibilities for dendrimers in supramolecular technologies.

5. SELF-ASSEMBLY OF INVERTED UNIMOLECULAR DENDRITIC MICELLES

The construction of molecular architectures having well-defined shapes and dimensions by self-assembly of molecules is a topic of great interest [65,66]. Applications of these supramolecular structures can be foreseen in fields such as information storage, catalysis and sensors. Dendrimers are attractive building blocks to form such molecular materials because they are well-defined, highly-branched macromolecules with unusual behaviour and unique properties [2,9,67]. Dendrimers can be considered as unimolecular micelles with a static structure and all end groups covalently bonded to the central core, and are stable under a variety of experimental conditions [7,44,45b,68]. Recently we successfully prepared a new class of unimolecular structures: inverted unimolecular dendritic micelles (Figure 20) [69]. These fully characterized macromolecules were based on hydrophilic poly(propylene imine) dendrimers (DAB-*dendr*-(NH₂)_n) in which 4–64 primary amines were decorated with hydrophobic chains by reaction with long-chain alkyl acid chlorides (ClCOC_m with C_m = (CH₂)_{m-1}CH₃ with *m* = 5, 9–15) in THF in the presence of Et₃N as an external base. Structural characterization of the dendritic amides DAB-*dendr*-(NHCOC_m)_n with NMR, IR and MALDI-TOF-MS showed that all of the dendrimer end groups were amidated.

5.1 Properties of Unimolecular Dendritic Micelles

Evidence for the development of dendritic character (i.e. higher packing of end groups) by increasing generation from DAB-*dendr*-(NHCOC_m)₄₋₆₄ was obtained by ¹H-NMR spectroscopy. A significant shift for the NHCO proton to lower fields with increasing generation was observed. The low generations, *n* = 4–6 also showed a concentration dependence of the NHCO position, which was absent for the two higher generations, *n* = 32 and 64. The shift of the amide proton is a result of the change from predominantly concentration-dependent, but weak, intermolecular hydrogen bonding to concentration-independent strong intramolecular H-bonding for the higher generations. Dynamic light scattering also confirms the absence of clustering between DAB-*dendr*-(NHCOC₁₅)₆₄ molecules: single particle behaviour was observed with a hydrodynamic diameter of 2–3 nm in dichloromethane.

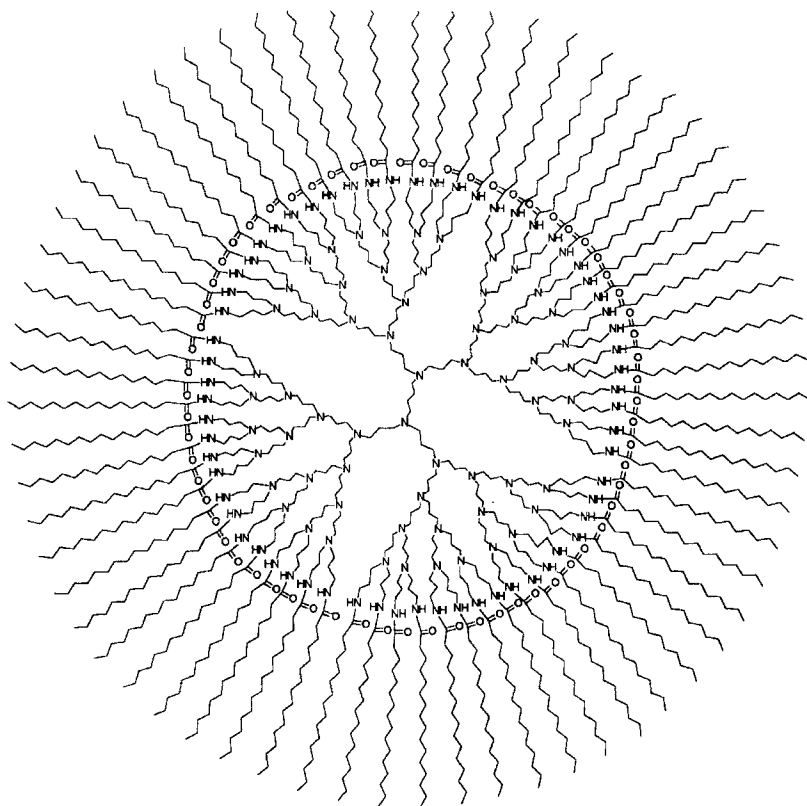


Figure 20 The unimolecular dendritic inverted micelle

We presented evidence that these compounds were able to encapsulate guest molecules [69]. DAB-*dendr*-(NHCOC_{5,9,15})_{8,64} were used as dynamic hosts for guest molecules like Rose Bengal. The hydrophilic dye was trapped into the inverted unimolecular micelles by first dissolving micelle and dye in ethanol, allowing the dye to enter the dendritic core. Precipitation of the complex in acetonitrile, followed by an extensive washing procedure with acetonitrile until no colouration of solvent occurred, resulted in the removal of untrapped and adhered dye. The $n = 64$ compounds were further purified by dialysis with water. The number of dye molecules entrapped (varying from an average of one for $n = 8$ up to seven for $n = 64$) was determined with UV spectroscopy. It was possible to strongly improve the compatibility between Bengal Rose and an apolar solvent such as *n*-hexane by first encapsulating the dye into the inverted micelle. It was impossible to release the dye from the solution by washing with water; however, the addition of toluene to Bengal Rose@DAB-*dendr*-(NHCOC_{*m*})₆₄ in *n*-hexane released the dye from the micelle.

Recently, we are also able to perform liquid–liquid extractions of water-soluble dyes from water to organic solvents like toluene using the unimolecular dendritic micelles as extractants. These guest–host properties of the modified poly(propylene imine) dendrimers make use of the basic nature of the interior of the dendrimer. Therefore, it is possible to transfer dyes like Bengal Rose into toluene. Although simple tri-octylamines are capable of transferring these dyes as well, it is evident from the experiments that unimolecular dendritic inverted micelles are much more selective, probably due to the shielding effect of the apolar shell [70].

5.2 Self-assembly of the Inverted Micelles

It is also of interest to study the self-assembly of these inverted unimolecular dendritic micelles into vesicles in water at $\text{pH} = 1$ and at the air–water interface. In these vesicles, the dendrimers adopt a distorted conformation, far from spherical. These dendritic amphiphiles form a novel class of vesicle-forming surfactants [71] and introduce new perspectives towards a better understanding of the structure–property relation of amphiphiles on the one hand and dendrimers on the other hand.

When the different generations of amphiphilic dendrimers were dispersed in buffered acid water ($\text{pH} = 1$), opalescent solutions were obtained. Dispersions of the first and second generation dendrimer precipitate within one day whereas the higher generation aggregates were stable for several weeks, as was judged by measuring the time dependent change in turbidity at 450 nm. Transmission electron micrographs showed for all generation dendrimers vesicular structures with diameters that varied in the range 20–200 nm (Table 3, Figure 21).

The values obtained by dynamic light scattering (DLS) for the diameter of these vesicles are larger due to aggregation. The critical aggregation concentration (CAC) was determined with pyrene as probe molecule [56] and were for all generations

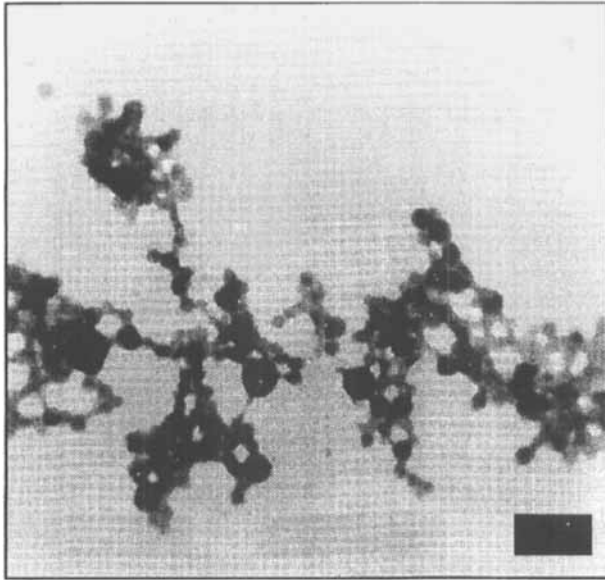
Table 3 Characteristics of the different generations dendrimeric amphiphile

Generation dendrimer	Vesicle diameter (nm) from EM ^a	Vesicle diameter (nm) from DLS ^a	CAC (μM) ^a	Bilayer thickness (nm) ^b	Molecular area (nm^2) ^c
1	—	330	1.0	5.1	1.07
2	—	340	0.62	5.1 (4.1)	2.14
3	35–200	350	0.63	4.8 (4.2)	4.42
4	35–130	330	0.63	5.7 (5.0)	8.14
5	20–140	160	0.22	5.4	16.0

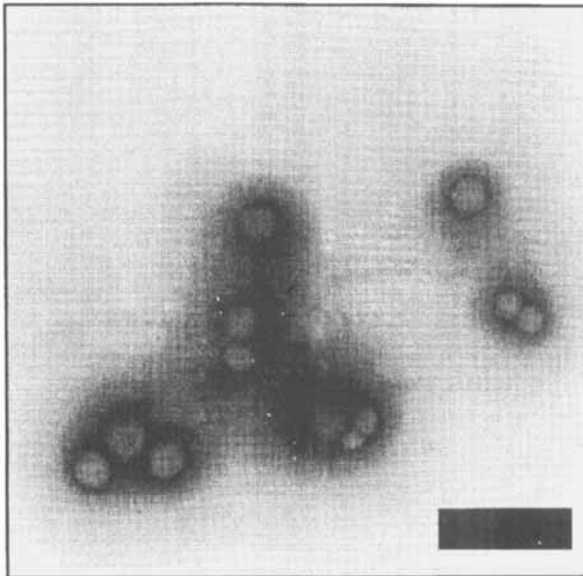
^a Vesicles were prepared by dissolving the dendrimers in 100 μl of methanol/THF (1 : 2, v/v) and injecting this solution into 5 ml of a buffer solution at $\text{pH} = 1$.

^b Determined from X-ray scattering. Secondary reflections are given in brackets.

^c Determined by extrapolating the slopes of the isotherms in the liquid condensed region to zero pressure.



A



B

Figure 21 Transmission electron micrograph of a 10^{-4} M dispersion of fifth generation amphiphilic dendrimer in buffered water (pH = 1). (A) Sample shaded with Pt. (B) Sample stained with uranyl acetate. Bars represents 300 nm

dendrimer low (10^{-6} – 10^{-7} M). X-ray diffraction was carried out on cast films of a vesicle dispersion of the various amphiphiles dried on a silicon plate *in vacuo*. The diffraction patterns displayed for the different generations show a clear periodicity in the range 4.8–5.4 nm, with in some cases additional periodicities (Table 3). Since the extended molecular length of a palmitoyl chain as estimated from space-filling CPK (Corey–Pauling–Koltun) models is 2.2 nm, the observed thickness can correspond to that of a bilayer in which the dendrimers possess an asymmetric conformation. The additional periodicities in the diffraction pattern can be due to domains in which the bilayers are tilted or interdigitated.

Monolayer experiments were performed on the different generations of dendritic amphiphiles to estimate the molecular area. The pressure–area isotherms show a linear increase of the molecular area with the number of alkyl chains attached to the different generations dendrimer (Figure 22, Table 3).

The molecular area per alkyl chain is approximately 0.25 nm^2 which is a value often found in X-ray structures of hydrocarbon chains. These results indicate that the higher generation dendrimer have a more flat conformation because in that case all the attached chains can count for the observed molecular area.

After adjusting at a fixed pressure, no decrease in area per molecule was observed during several hours which indicates that the monolayers of our amphiphilic dendrimers are stable. Decompression isotherms of the monolayers showed irreversibility due to the formation of aggregates on the surface. The progressive increase of the surface pressure is probably due to the formation of films on the water surface that remain in the proximity of the platinum plate when the barrier is moved

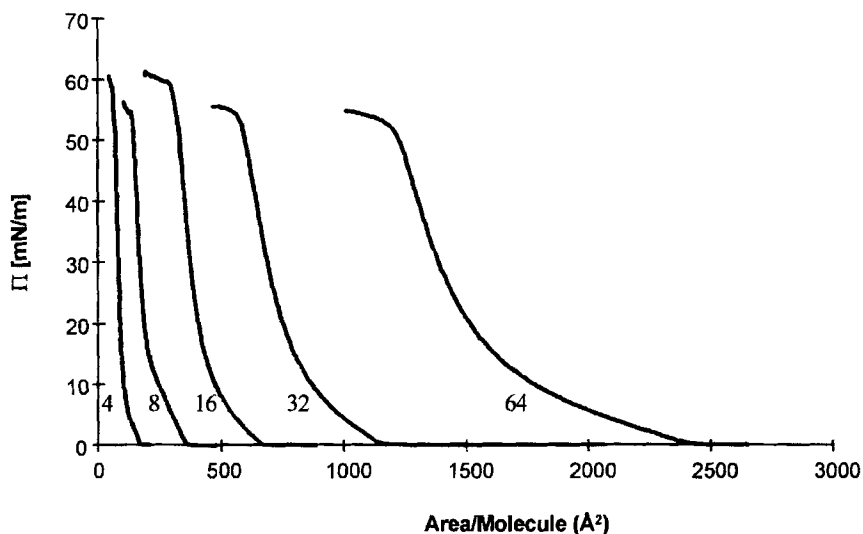


Figure 22 Compression isotherms of different generations of unimolecular inverted micelles in water at 25 °C. The number of alkyl chains is indicated

backwards. When the Pt plate was removed and cleaned and the compression was run again, a curve very similar to the first one was obtained. This could indicate that the increase in the surface pressure was due to the formation of aggregates on the metal surface, but not on the water surface.

Preliminary studies showed that it was possible to transfer monolayers composed of the fifth generation dendrimer to hydrophilic glass substrates. A Z-type deposition (deposition takes place during upstroke dipping) was observed with remarkably high transfer ratios in the range 0.8–1.0 (five layers were deposited).

Based on the data above we propose that the vesicles of the various dendritic molecules have a structure in which the amphiphilic dendrimers are aligned with their hydrophilic, protonated dendritic unit facing the aqueous phase and in which the aliphatic chains are forming a bilayer (Figure 23).

Hence, protonation of the poly(propylene imine)s leads to a more extended conformation of the dendritic core, resulting in a more loosely packed shell. At that moment the dendritic interior moves to the outside, while the hydrophobic chains tumble and form a bilayer. If we assume that this architecture is correct we can calculate the molecular volumes of the amphiphiles by multiplying the length of the amphiphiles by the molecular area (Table 4).

The result matches very well with the theoretical values based on CPK models and molecular simulation of the various dendrimers in the gas phase [33,34,72]. This similarity implicates that the hydrophilic core of the higher generation dendrimers has a more ellipsoidal conformation. The results obtained from the monolayer experiments also indicate that the higher generation dendrimer has a more flat conformation, because in that case all the attached chains can count for the observed molecular area.

The radius of the spherical fifth generation dendrimers is about 1.25 nm [33,34]. If we assume that the molecular area of 16 nm^2 of this macromolecule (Table 3) measured by the monolayer experiments is the area of the head group [73], then a radius of 2.26 nm is calculated. This means an increase of a factor 1.8 compared with the theoretical value. It is generally believed that higher generation dendrimer are spherical. Our results show in acidic water the dendrimers have a more elliptical conformation.

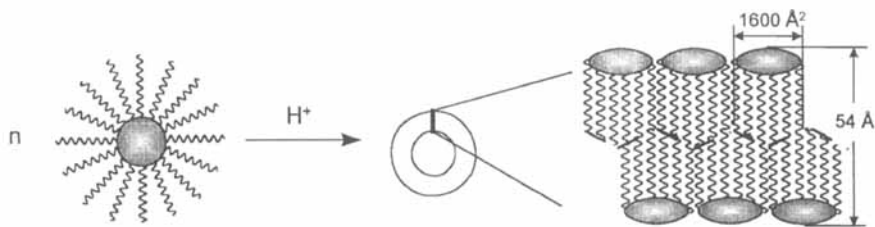


Figure 23 Schematic representation of the vesicle formation of the fifth generation inverted unimolecular dendritic micelles

Table 4 Molecular volumes of the dendrimers and dendrimer amphiphiles

Generation dendrimer	Molecular volume (nm ³) ^a	Molecular volume (nm ³) ^b	Major radius (nm) ^c	Minor radius (nm) ^d	Molecular volume (nm ³) ^e
1	3.00	2.73	0.58	0.23	2.27
2	5.82	5.46	0.83	0.23	4.54
3	11.40	10.60	1.19	0.13	8.53
4	24.50	20.35	1.61	0.20	17.66
5	48.58	43.20	2.26	0.33	38.04

^a Theoretical volume of the amphiphiles calculated as the sum of the alkyl volumes (from CPK models: 1 chain = 0.484 nm³) and the dendrimer volume (see Table 2).

^b Obtained by multiplying half the bilayer thickness with the molecular area (Table 3).

^c Calculated from the molecular area, assuming a circular head group cross-section.

^d Calculated by assuming all alkyl chains to be in an all-trans conformation.

^e Calculated by adding the volume of the dendrimer amphiphile, considered as an oblate spheroid, and the alkyl chain CPK volume.

In summary, we have shown that molecular objects based on a novel class of surfactants, e.g. amphiphilic dendrimers, can be formed in which the hydrophilic dendritic core of the unimolecular micelle acts as head group and the long aliphatic chains as hydrophobic part of the molecule.

6. OUTLOOK

Dendritic architectures have attracted the interest of many scientists recently. The aesthetically pleasing tree-like molecules combine advanced synthesis and unique properties with the prospects of supramolecular technologies. The guest–host properties of these well-defined macromolecules are of great interest, because they resemble the interactions of small molecules with biomacromolecules like proteins, and they are able to close the gap between the “traditional” supramolecular interactions of smaller molecules and the interactions in larger (phase-separated) macromolecular systems. In recent years a large number of interesting results have been reported, in which supramolecular interactions and dendritic architectures are combined.

We have been inspired by the many possibilities of dendritic technologies to investigate the supramolecular interactions of dendritic architectures. In our view, it is of utmost interest to have large quantities of well-defined dendrimers available in order to explore the different possibilities for applications. Although reports on dendritic structures are ubiquitous, data on the commercially available dendrimers are more scarce. Our poly(propylene imine) dendrimers combine high purity with specific properties due to the highly polar structure of a polyimine. Some of the

properties reported are unique for dendritic architectures. Some others, however, are also present in more simple hyperbranched or linear (macro)molecular structures. The current status of research with poly(propylene imine) dendrimers enables us to discriminate between “unique” and “normal” properties or between successful and unsuccessful multiple modifications. In this Chapter, we have discussed a selection of recent results from studies that make use of the cavities present within the dendrimers or that employ the amphiphilic character of the modified dendrimers. In addition to the successful experiments described here, we have encountered during the years also many modifications of the poly(propylene imine) dendrimer end groups that were unsuccessful and a number of applications that can be performed with branched poly(ethylene imine)s as well.

The research of the synthesis, characterization, properties and possible applications of dendrimers shows dendritic growth: each year the number of reports in the literature doubles [76]. Therefore, we suppose that supramolecular technology with dendrimers is only at its beginning. Biocompatibility and biomedical applications, catalysis, specific recognition, phase-transfer properties and amphiphilic character are a few keywords that will appear with increasing frequency within the scientific literature and in patents. With this Chapter we have focussed on our contributions within this field, with special emphasis on guest–host systems and amphiphilic character. Both are thought to be of prime interest for supramolecular technologies with dendritic architectures.

7. ACKNOWLEDGEMENTS

We would like to thank our colleagues for stimulating discussions, experimental assistance and the enthusiasm to enter the field of dendrimers. At the Eindhoven University: Maurice Baars, Tonny Bosman, Danniël van Boxtel, Didier Delnoye, Joost van Dongen, Cristina Elissen-Román, Jan van Hest, Kees Hummelen, Johan Jansen, René Janssen, Rob Peerlings, Sandra Stevelmans, Bas de Waal, Jan-Willem Weener.

At DSM Research: Ellen de Brabander-van den Berg, Betty Coussens, Jacques Joosten, Peer Froehling, Ynez Mengerink, Abdellativ Moussaid, Manon Muré, Jos Put, Rolf Scherrenberg, Sjoerd van der Wal. At the University of Nijmegen: Huub Geurts, Roeland Nolte. At the University of Wageningen: Dominique Hubert, A. Roelofsens, Edwin Currie.

8. REFERENCES AND NOTES

1. D. A. Tomalia, A. M. Naylor and W. A. Goddard III, *Angew. Chem.*, **102**, 119 (1990).
2. J. M. J. Fréchet, *Science*, **263**, 1710 (1994).
3. G. R. Newkome, C. N. Moorefield and F. Vögtle, *Dendritic Molecules—Concepts, Syntheses, Perspectives*, VCH, Weinheim, 1996.

4. B. I. Voit, *Acta Polym.*, **46**, 87 (1995).
5. G. R. Newkome, C. N. Moorefield, G. R. Baker, M. J. Saunders and S. H. Grossman, *Angew. Chem.*, **103**, 1207 (1991).
6. D. A. Tomalia, H. Baker, J. Dewald, M. Hall, G. Kallos, S. Martin, J. Roeck, J. Ryder and P. Smith, *Polym. J.*, **17**, 117 (1985).
7. K. L. Wooley, G. J. Hawker and J. M. J. Fréchet, *J. Am. Chem. Soc.*, **115**, 11496 (1993).
8. D. A. Tomalia and D. Durst, *Topics in Current Chemistry* (eds E. Weber), Springer-Verlag, Berlin, **165**, 93 (1993).
9. J. F. G. A. Jansen, E. M. M. de Brabander-van den Berg and E. W. Meijer, *Science*, **266**, 1226 (1994).
10. J. Roovers, *Trends Polym. Sci.*, **2**, 294 (1994).
11. J. M. J. Fréchet, C. J. Hawker, I. Gitsov and J. W. Leon, *J. Macromol. Sci., Pure Appl. Chem.*, **A33**, 1399 (1996).
12. D. Boris and M. Rubinstein, *Macromolecules*, **29**, 7251 (1996).
13. P. G. De Gennes and H. J. Hervet, *Phys. Lett. (Paris)*, **44**, 351 (1983).
14. R. L. Lescanec and M. Muthukumar, *Macromolecules*, **23**, 2280 (1990).
15. S. C. Zimmerman, F. Zeng, D. E. C. Reichert and S. V. Kolotuchin, *Science*, **271**, 1095 (1996).
16. C. Moucheron and A. Kirsch-De Mesmaeker, *J. Am. Chem. Soc.*, **118**, 12834 (1996).
17. W. T. S. Huck, R. Hulst, P. Timmerman, F. C. J. M. van Veggel and D. N. Reinhoudt, *Angew. Chem. Int. Ed. Engl.*, **36**, 1006 (1997).
18. F. Zeng and S. C. Zimmerman, *Chem. Rev.*, **97**, 1681 (1997).
19. E. Buhleier, W. Wehner and F. Vögtle, *Synthesis*, 155 (1978).
20. E. M. M. De Brabander-van den Berg and E. W. Meijer, *Angew. Chem.*, **105**, 1370 (1993).
21. C. Wörner and R. Mülhaupt, *Angew. Chem.*, **105**, 1367 (1993).
22. (a) M. Freifelder, *Catalytic Hydrogenation in Organic Synthesis, Procedures and Commentary*, Wiley, New York, 1978, p. 43. (b) P. N. Rylander, *Best Synthetic Methods, Hydrogenation Methods*, Academic Press, London, 1985, p. 94.
23. M. H. P. Van Genderen, M. W. P. L. Baars, J. C. M. van Hest, E. M. M. de Brabander-van den Berg and E. W. Meijer, *Recl. Trav. Chim. Pays-Bas*, **113**, 573 (1994).
24. M. H. P. Van Genderen, M. W. P. L. Baars, C. Elissen-Román, E. M. M. de Brabander-van den Berg and E. W. Meijer, *Polym. Mater. Sci. Eng.*, **73**, 336 (1995); *Abstract Paper Am. Chem. Soc.*, **20**, 179 (1995).
25. G. J. M. Koper, M. H. P. van Genderen, C. Elissen-Román, M. W. P. L. Baars, E. W. Meijer and M. Borkovec, *J. Am. Chem. Soc.*, **119**, 6512 (1997).
26. J. C. Hummelen, J. L. J. van Dongen and E. W. Meijer, *Chem. Eur. J.*, **3**, 1489 (1997).
27. T. H. Mourey, S. R. Turner, M. Rubinstein, J. M. J. Fréchet, C. J. Hawker and K. L. Wooley, *Macromolecules*, **25**, 2401 (1992).
28. M. L. Mansfield and L. I. Klushin, *Macromolecules*, **26**, 4262 (1993).
29. M. L. Mansfield and L. I. Klushin, *J. Phys. Chem.*, **96**, 3994 (1992).
30. (a) A. D. Meltzer, D. A. Tirrell, A. A. Jones, P. T. Inglefield, D. M. Hedstrand and D. A. Tomalia, *Macromolecules*, **25**, 4541 (1992). (b) A. D. Meltzer, D. A. Tirrell, A. A. Jones and P. T. Inglefield, *Macromolecules*, **25**, 4549 (1992).
31. (a) B. J. Bauer, R. M. Briber, B. Hammouda and D. A. Tomalia, *Polym. Mater. Sci. Eng.*, **67**, 428 (1992). (b) R. M. Briber, B. J. Bauer, B. Hammouda and D. A. Tomalia, *Polym. Mater. Sci. Eng.*, **67**, 430 (1992).
32. J. K. Young, G. R. Baker, G. R. Newkome, K. F. Morris and C. S. Johnson Jr., *Macromolecules*, **27**, 3464 (1994).
33. E. M. M. De Brabander, J. Brackman, M. Muré-Mak, H. de Man, M. Hogeweg, J. Keulen, R. Scherrenberg, B. Coussens, Y. Mengerink and S. van der Wal, *Macromol. Symp.*, **102**, 9 (1996).

34. R. Scherrenberg, B. Coussens, P. van Vliet, G. Edouard, J. Brackman, E. de Brabander and K. Mortensen, *Macromolecules*, **31**, 456 (1998).
35. M. Maciejewski, *J. Macromol. Sci. Chem.*, **A17**, 689 (1982).
36. J. F. G. A. Jansen, R. A. J. Janssen, E. M. M. de Brabander-van den Berg and E. W. Meijer, *Adv. Mater.*, **7**, 561 (1995).
37. T. Kunitake, N. Nakashima and K. Moritsu, *Chem. Lett.*, 1347 (1980).
38. J. F. G. A. Jansen, E. M. M. de Brabander-van den Berg and E. W. Meijer, *Recl. Trav. Chim. Pays-Bas*, **114**, 225 (1995).
39. J. F. G. A. Jansen, H. W. I. Peerlings, E. M. M. de Brabander-van den Berg and E. W. Meijer, *Angew. Chem. Int. Ed. Engl.*, **34**, 1206 (1995).
40. J. F. G. A. Jansen, E. M. M. de Brabander-van den Berg and E. W. Meijer, *J. Am. Chem. Soc.*, **117**, 4417 (1995).
41. J. C. M. Van Hest, PhD Thesis, Eindhoven University of Technology, 1996.
42. G. R. Newkome, R. Güther, C. N. Moorefield, F. Cardullo, L. Echegoyen, E. Pérez-Cordero and H. Luftmann, *Angew. Chem. Int. Ed. Engl.*, **34**, 2023 (1995).
43. (a) D. A. Tomalia, *Adv. Mater.*, **6**, 529 (1994). (b) G. R. Newkome, A. Nayak, R. K. Behera, C. N. Moorefield and G. R. Baker, *J. Org. Chem.*, **57**, 358 (1992). (c) C. J. Hawker, K. L. Wooley and J. M. J. Fréchet, *J. Chem. Soc., Perkin Trans I*, 1287 (1993). (d) V. Percec, P. Chu and M. Kawasumi, *Macromolecules*, **27**, 4441 (1994). (e) S. Watanabe and S. L. Regen, *J. Am. Chem. Soc.*, **116**, 8855 (1994). (f) S. C. Zimmerman, F. Zeng, D. E. C. Reichert and S. V. Kolotuchin, *Science*, **271**, 1095 (1996).
44. (a) G. R. Newkome, Z.-Q. Yao, G. R. Baker and V. K. Gupta, *J. Org. Chem.*, **50**, 2003 (1985). (b) D. A. Tomalia, V. Berry, M. Hall and D. Hedstrand, *Macromolecules*, **20**, 1164 (1987). (c) G. R. Newkome, C. N. Moorefield, G. R. Baker, A. L. Johnson and R. K. Behera, *Angew. Chem.*, **103**, 1205 (1991).
45. (a) N. Tanaka, T. Tanigawa, K. Hosoya, K. Kimata, T. Araki and S. Teraba, *Chem. Lett.*, 959 (1992). (b) G. R. Newkome, J. K. Young, G. R. Baker, R. L. Potter, L. Audoly, D. Cooper and C. D. Weiss, *Macromolecules*, **26**, 2394 (1993). (c) G. R. Newkome, C. N. Moorefield, J. Keith, G. R. Baker and G. Escamillo, *Angew. Chem.*, **106**, 701 (1994). (d) S. A. Kuzdzal, C. A. Monning, G. R. Newkome and C. N. Moorefield, *J. Chem. Soc., Chem. Commun.*, 2139 (1994). (e) P. G. H. M. Muijselaar, H. A. Claessens, C. A. Cramers, J. F. G. A. Jansen, E. W. Meijer, E. M. M. de Brabander-van den Berg and S. van der Wal, *J. High Resol. Chrom.*, **18**, 121 (1995). (f) I. Gitsov, K. L. Wooley and J. M. J. Fréchet, *Angew. Chem.*, **104**, 1282 (1992). (g) I. Gitsov, K. L. Wooley, C. J. Hawker, P. Ivanova and J. M. J. Fréchet, *Macromolecules*, **26**, 5621 (1993). (h) I. Gitsov and J. M. J. Fréchet, *Macromolecules*, **26**, 6536 (1993). (i) I. Gitsov and J. M. J. Fréchet, *Macromolecules*, **27**, 7309 (1994).
46. T. M. Chapman, G. L. Hillyer, E. J. Mahan and K. A. Shaffer, *J. Am. Chem. Soc.*, **116**, 11195 (1994).
47. (a) X. F. Zhong and A. Eisenberg, *Macromolecules*, **27**, 1751 (1994). (b) X. F. Zhong and A. Eisenberg, *Macromolecules*, **27**, 4914 (1994).
48. J. C. M. Van Hest, D. A. P. Delnoye, M. W. P. L. Baars, M. H. P. van Genderen and E. W. Meijer, *Science*, **268**, 1592 (1995).
49. (a) S. C. Zimmerman, F. Zeng, D. E. C. Reichert and S. V. Kolotuchin, *Science*, **271**, 1095 (1996). (b) W. T. S. Huck, F. C. J. M. van Veggel and D. N. Reinhoudt, *Angew. Chem. Int. Ed. Engl.*, **35**, 1213 (1996).
50. J. C. M. Van Hest, D. A. P. Delnoye, M. W. P. L. Baars, C. Elissen-Román, M. H. P. van Genderen and E. W. Meijer, *Chem. Eur. J.*, **2**, 161 (1996).
51. J. C. M. Van Hest, M. W. P. L. Baars, C. Elissen-Román, M. H. P. van Genderen and E. W. Meijer, *Macromolecules*, **28**, 6689 (1995).
52. W. D. Bancroft, *J. Phys. Chem.*, **17**, 501 (1913).

53. N. A. J. Sommerdijk, M. C. Feiters, R. J. M. Nolte and B. Zwanenburg, *Recl. Trav. Chim. Pays-Bas*, **113**, 194 (1994).
54. M. Wilhelm, C. L. Zhao, Y. Wang, R. Xu, M. A. Winnik, J. L. Mura, G. Riess and M. D. Croucher, *Macromolecules*, **24**, 1033 (1991).
55. K. Kalyanasundaram and J. K. Thomas, *J. Am. Chem. Soc.*, **99**, 2039 (1977).
56. I. Astafieva, X. F. Zhong and A. Eisenberg, *Macromolecules*, **26**, 7339 (1993).
57. J. F. Marko and Y. Rabin, *Macromolecules*, **25**, 1503 (1992).
58. M. J. Rosen, *Surfactants and Interfacial Phenomena*, 2nd edn, Wiley, New York, 1989.
59. D. Mayers, *Surfactant Science and Technology*, VCH, New York, 1988.
60. B. Lindman and H. Wennerstrom, *Top. Curr. Chem.*, **87**, 1 (1980).
61. The observed vesicular structures show a resemblance with the work of Kunitake *et al.* (a) T. Kunitake, N. Kimizuka, N. Higashi and N. Nakashima, *J. Am. Chem. Soc.*, **106**, 1978 (1984). (b) T. Kunitake, M. Nagai, H. Yanagi, K. Takarabe and N. Nakashima, *J. Macromol. Sci. Chem.*, **A21**, 1237 (1984).
62. For the situation on observing spherical micelles with TEM, see: O. Regev, C. Kang and A. Khan, *J. Phys. Chem.*, **98**, 6619 (1994).
63. E. H. Lucassen-Reijnders, *Anionic Surfactants, Physical Chemistry of Surfactant Action*, Surfactant Series, Vol. 11, Marcel Dekker, New York, 1981.
64. (a) J. N. Israelachvili, D. Mitchell and B. Ninham, *Biochim. Biophys. Acta*, **470**, 185 (1977). (b) J. N. Israelachvili, S. Marcelja and R. Horn, *Rev. Biophys.*, **13**, 121 (1980). (c) J. N. Israelachvili, D. J. Mitchell and B. W. Ninham, *J. Chem. Soc., Faraday Trans II*, **72**, 1525 (1976).
65. (a) G. M. Whitesides, J. P. Mathias and C. T. Seto, *Science*, **254**, 1312 (1991). (b) G. M. Whitesides, E. E. Simanek, J. P. Mathias, C. T. Seto, D. N. Chin, M. Mammen and D. M. Gordon, *Acc. Chem. Res.*, **28**, 37 (1995). (c) S. I. Stupp, V. LeBonheur, K. Walker, L. S. Li, K. E. Huggins, M. Keser and A. Amstutz, *Science*, **276**, 384 (1997).
66. J.-M. Lehn, *Angew. Chem. Int. Ed. Engl.*, **29**, 1304 (1990).
67. (a) J. F. G. A. Jansen and E. W. Meijer, *J. Am. Chem. Soc.*, **117**, 4417 (1995). (b) J. W. J. Knapen, A. W. van der Made, J. C. de Wilde, P. van Leeuwen, P. Wijkens, D. M. Groves and G. van Koten, *Nature*, **372**, 659 (1994).
68. G. R. Newkome, C. N. Moorefield, G. R. Baker, A. L. Johnson and R. K. Behera, *Angew. Chem. Int. Ed. Engl.*, **30**, 1176 (1991).
69. S. Stevelmans, J. C. M. van Hest, J. F. G. A. Jansen, D. A. F. J. Bostel, E. M. M. de Brabander-van den Berg and E. W. Meijer, *J. Am. Chem. Soc.*, **118**, 7398 (1996).
70. M. W. P. L. Baars, P. E. Froehling and E. W. Meijer, *Chem. Commun.*, 1959 (1997).
71. A. P. H. J. Schenning, C. Elissen-Román, J.-W. Weener, M. W. P. L. Baars, S. J. van der Gaast and E. W. Meijer, *J. Am. Chem. Soc.*, **120**, 8199 (1998)
72. It should be mentioned, however, that the radius of the dendrimers in the gas phase will be different from that in solution. Also, protonation will change the radius of the dendrimers. Molecular modelling shows a radius of 2.1 nm for the protonated fifth generation dendrimer, while for the unprotonated form 1.6 nm was calculated.
73. For vesicle-forming surfactants it is believed that the molecular area of the head group is roughly the same as that of the hydrophobic part of the amphiphile: see Ref. 64a.
74. A. W. Bosman, M. J. Bruining, H. Kooymans, A. L. Spek, R. A. J. Janssen and E. W. Meijer, *J. Am. Chem. Soc.*, **120**, 8547 (1998).
75. R. Miklis, T. Çagin and W. A. Goddard III, *J. Am. Chem. Soc.*, **119**, 7458 (1997).
76. (a) O. A. Mathews, A. N. Shipway and J. F. Stoddart, *Prog. Polym. Sci.*, **23**, 1 (1998). (b) H.-F. Chow, T. K.-K. Mong, M. F. Nongrum and C.-W. Wan, *Tetrahedron*, **54**, 8543 (1998). (c) H. M. Janssen and E. W. Meijer, *Synthesis of Polymers* (ed. A.-D. Schüter), Vol. 20 in *Materials Science and Technology* (eds. R. W. Chan, P. Haasen, E. J. Kramer), Wiley-VCH, Weinheim, 1999, p. 403. (d) A. W. Bosman, H. M. Janssen and E. W. Meijer, *Chem. Rev.*, in press (1999).

Chapter 3

Supramolecular Structures with Macromolecules

UWE BEGINN AND MARTIN MÖLLER

Universität Ulm, Germany

1. INTRODUCTION

Macromolecular chemistry has evolved as a field of chemical sciences dealing with intermolecular interactions and supramolecular structures. Early ideas considered polymers to consist of a large number of individual small molecules which associated or aggregated to colloidal particles [1]. Progress was made when Staudinger established the concept of main valence bonded long chain molecules for which he never allowed another name than macromolecules [2]. Based on this concept, step growth and chain growth polymerization were developed to yield a vast number of synthetic polymers which are now valuable, energy efficient materials [3,4].

Because of the focus on new materials, macromolecular chemists are concerned with the relation between molecular structure and the material properties, which results from intermolecular interactions and the organization within supramolecular architectures. However, the structures of synthetic macromolecules are polydisperse and not well defined, and the dominant intermolecular interactions, such as entanglements, are mostly not directed and localized [5]. So far, it must be stated that our ability to prepare high molar mass molecules lacks the perfection which is necessary for the reproducible assembly of well-defined supramolecular units [4,6].

In contrast, supramolecular chemistry is directed towards the predictable formation of exactly defined structures, relying mostly on small molecules. Thus, the molar mass of a macrocyclic molecule is up to several orders of magnitude smaller

than that of a cyclic macromolecule. Moreover, well-defined supramolecular complexes are typically assembled by rather strong directed interactions and have a limited ability to undergo complex changes depending on slight variations of the chemical environment. This impedes one of the main objectives, namely to provide highly functional molecular devices, e.g. switches, self-replicating structures, signal transducers, pores, or even molecular motors [7,8]. In all these cases the underlying molecular action requires some variance in the structural response of the supramolecular assembly, as is realized in biomolecular systems by the principle of quasiequivalency [9–13].

Regarding the functionality and structural perfection of biomolecules as the ultimate objective of supramolecular and macromolecular chemistry, it can be easily anticipated that the current situation is an intermediate state. Supramolecular chemistry will include the formation of structurally more flexible molecular assemblies of increased size, while macromolecular chemists will develop new means of approaching the structural exactness of biomolecules and low molecular weight chemistry ultimately leading to standards where the traditional classifications in chemistry will become obsolete.

An important contribution of macromolecular chemistry to functional supramolecular systems and devices is the limitation of ordering typical for macromolecular compounds and, of course, the long-range interconnectivity between different molecular subunits.

The covalent linkage of monomer molecules within a molecular chain causes an entropy loss because of the restricted freedom of each unit. At the same time it favours disordered states because of the polydispersity of the primary structure and the enormous numbers of different conformations each molecule can adopt. As a consequence, ordering of macromolecules is usually limited either to small domains or limited in perfection. Even in systems which principally can attain a highly ordered equilibrium state, ordering is usually limited for kinetic reasons. In particular, the spatial limitation of ordering produce the well-defined superstructures in macromolecular systems, e.g. when crystallization or phase segregation occurs on the length scale within the dimension of a single macromolecule.

It is the purpose of this review to demonstrate with selected examples: supramolecular aspects in macromolecular chemistry, microdomain formation and long-range interactions in macromolecular systems as a means of extending the length scale of supramolecular chemistry, and finally a number of recent developments will be discussed where concepts from macromolecular chemistry and supramolecular chemistry have been combined. This is a rapidly growing field and so the selection we have made is necessarily incomplete.

2. PRIMARY AND SECONDARY STRUCTURES OF SYNTHETIC MACROMOLECULES

Macromolecules are formed by covalent bonding of a large number of monomeric units. This results in a wide variety of possible structural architectures, e.g. linear chains, branched chains, brush-like chains (“hairy rods”), star-like, tree-like (“hyperbranched”), perfectly branched (“dendritic”) structures (Figure 1) [14,15].

Apart from the Merrifield synthesis of peptides and oligonucleotides [19,20] and the preparation of dendrimers [15,21–25] (which are limited in molecular weight) synthetic chemistry has not been able to develop methods of making macromolecules of uniform structure. Simple homopolymers vary in molecular weight, regioselectivity and stereoselectivity of bonding of the constituent monomers. Copolymers vary in the composition of the individual macromolecules and in the sequence distribution. If the molecules are branched, we cannot control the exact distribution and length of the branches. Moreover, our ability to prepare and process macromolecules whose subunits undergo strong directional interactions is restricted because of their limited solubility and tractability. As a consequence commercially important polymers consist mostly of rather unpolar monomers which predominantly undergo dispersion interactions [14].

So-called “living polymerization” techniques, where the chemist can start and terminate the statistical growth of all molecules at the same time, give the most narrow molecular weight distributions one can achieve so far. But the largest and the smallest molecules still differ easily by a factor of two or more [6,26]. Stereoregular polymerization by insertion polymerization at transition metal complexes is practically limited to nonpolar monomers, broad molecular weight distributions and does not allow controlled variations of the stereostructure within one chain. Only recently, development of single site catalysts opened new avenues of controlled polymerization by coordination complex catalysts [49,462].

Ultimate progress in the control of the primary structure of synthetic macromolecules might be expected if it were possible to develop a template type synthesis, in analogy to the polymerase chain reaction [27]. In spite of many efforts, no successful concept has yet been developed, which is no surprise regarding the complicated supramolecular interactions involved in the necessary steps, i.e. preorganization of the template, binding of the monomer, initiation and termination of the polymerization, and the release of the formed macromolecule from the template [28,29].

Most synthetic polymers in which the monomer units are connected via single bonds have rather flexible chains. The bond torsion energy is relatively small and the units can rotate around their bonds [14,30,31]. Each molecule can adopt a large number of energetically equivalent conformations and the resulting molecular geometry is that of a statistical coil, approximately described by a Gaussian density distribution. This coil conformation is the characteristic secondary structure of macromolecules in solution and in the melt. It is entropically favoured because of its

statistical probability. Extension or collapse of the coil requires external forces or strong intersegmental interactions. The shape of a statistical coil can be visualized as an irregular bean-like shape with approximate axes-ratios of 1 : 16 : 2.8 [32,33]. The size of the coil is characterized by the average end-to-end distance \overline{l}_0 , which can be calculated from the degree of polymerization \overline{P}_n [3]:

$$\overline{l}_0^2 = \overline{P}_n \cdot \overline{b}_0^2 \cdot \alpha \cdot \delta = \overline{P}_n \cdot \overline{l}_{\text{seg}}^2 \quad (1)$$

In Equation 1, \overline{b}_0 is the bond length of a monomer-unit, δ is a “sterical factor” accounting for short-range restrictions in bond-angles and bond-torsionability. Long-range interactions between the polymer segments and the polymer chain and solvent molecules, which compete for the same volume element within the coil are considered by the factor α . Both effects cause an expansion of the coil beyond the size of the so called “freely jointed chain”. Long-range repulsion can be balanced by the segmental attraction, e.g. in a relatively bad solvent, resulting in ideal or Θ -conditions where the end-to-end distance can be calculated merely based on the bond length and the rotational isomeric states (Figure 2) [3]. The non-ideality effects are combined in the “statistical segment length”, l_{seg} .

As stated by Equation 1, the end-to-end distance of a polymer coil increases with increasing degree of polymerization \overline{P}_n impeding the formation of ring molecules by cyclization reactions [34,35]. For the preparation of relatively small macrocycles in supramolecular chemistry this can be overcome by using the respective host molecule as a template [28]. Generally, high molecular weight cyclic macromolecules have to be prepared under conditions of extreme dilution. This is labour-intensive and costly. Recently a first example of macromolecular ring expansion has been reported with the preparation of syndiotactic cyclic poly(lactones) by polymerization of butyrolactone with cyclic dibutyltin initiators [36]. The concept was expanded to obtain poly(lactides) [37] or poly(lactone) “nanopretzels” by means of a spirocyclic tin-initiator derived from pentaerithrol [38]. Further advances toward the controlled “living” macrocyclic polymerization are promising [39]. Presently it is possible to polymerize ϵ -caprolactone at 80 °C in the presence of the 2,2-dibutyl-1,3-dioxepane initiator, yielding complete monomer conversion without the destruction of the active centres [40].

Stiff polymer chains can be prepared by introduction of conformational rigid units in the backbone, i.e. triple bonds, *p*-phenylene-groups, aromatic ester and amide groups. Distortion of valence bonds and angles causes a chain length deviation from a rod-like conformation and can be described by the so-called persistence length, a_0 . This is the length of a chain segment over which the cosine between the tangents drops by a factor of e . A finite persistence length leads to a “wormlike” or Kratky–

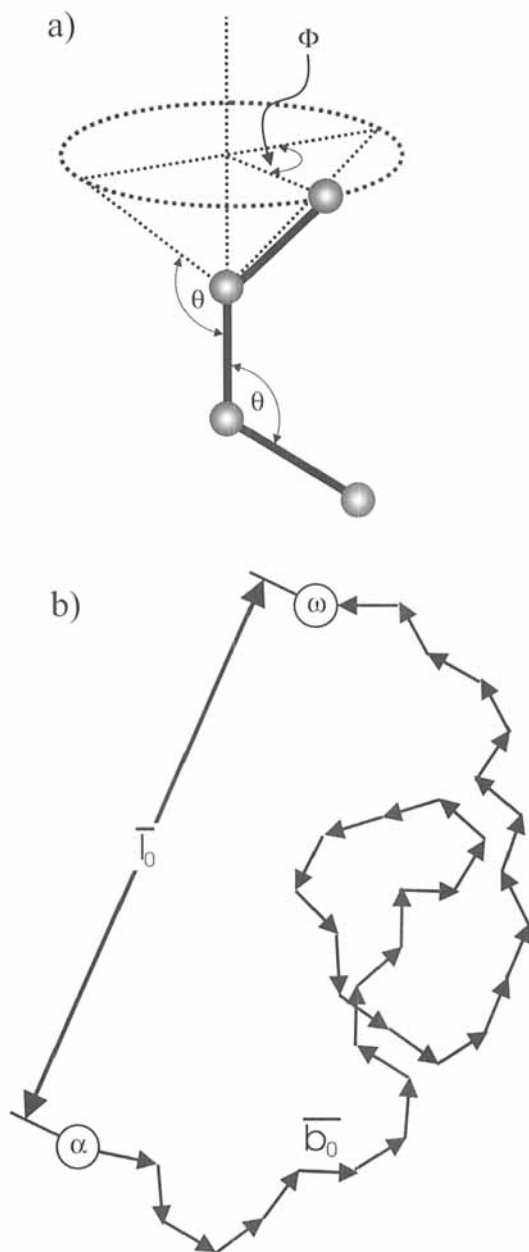


Figure 2 (a) Sketch of the variables determining the rotation isomeric state model of a statistical coil: θ = bond angle, ϕ = bond torsion angle [3]. (b) Representation of one of the possible conformations of a two-dimensional statistical coil (33 monomers) with bond-angle restriction ($-90^\circ < \theta < 90^\circ$) [3].

Porod chain [41] with random conformations and a mean square end-to-end distance given by Equation 2 [42]:

$$\overline{l_0^2} = 2 \cdot L_K \cdot a_0 - 2a_0^2[1 - \exp(-L_K/a_0)] \quad (2)$$

L_K = contour length of the chain

Chain rigidity can cause partial ordering of the macromolecules. While flexible macromolecules yield amorphous solutions and melts in which the individual coils interpenetrate each other, semiflexible macromolecular systems order in nematic domains [43].

Rod like conformations can also be formed by macromolecules which adopt a helical chain conformation. Helical secondary structures are so far the only higher structures which can be achieved in a rather controlled way in macromolecular chemistry, e.g. poly(benzylglutamate) [44,45], poly(isocyanides) [46,47] and poly(isocyanates) [48]. Helix formation by isolated macromolecules in dilute solution required directed cooperative interactions along the chain, by π -stacking and multiple hydrogen bonding. Due to their mostly nonpolar nature, many synthetic macromolecules lack this ability. Provided their primary structure is regular, however, they tend to form helices upon crystallization. In this case, the necessary cooperativity originates from three dimensional ordering and does not rely on specific and directed interactions. Examples are the helical crystal structures of poly(α -olefines) [49]. Another way to stiffen a macromolecular chain is by dense substitution with sterically demanding side chains (see below the discussion on cylindrical brushes and polymer acid–base complexes).

As a general statement it can be concluded that macromolecular conformations different from the predominant coil structure are still the exception. Defined spherical secondary-structures have not been obtained by means of noncovalent interactions, since there is no synthetic concept available, distinguishing between inter- and intra-molecular interactions. Formation of globular structures by linear macromolecules is still a privilege of biomolecules where intermolecular interactions are counteracted by well-coordinated intermolecular interactions [50,51]. Synthetic nanospheres can be obtained by the stepwise synthesis of dendrimers [15] or by polymerization of microgels [52] (see below).

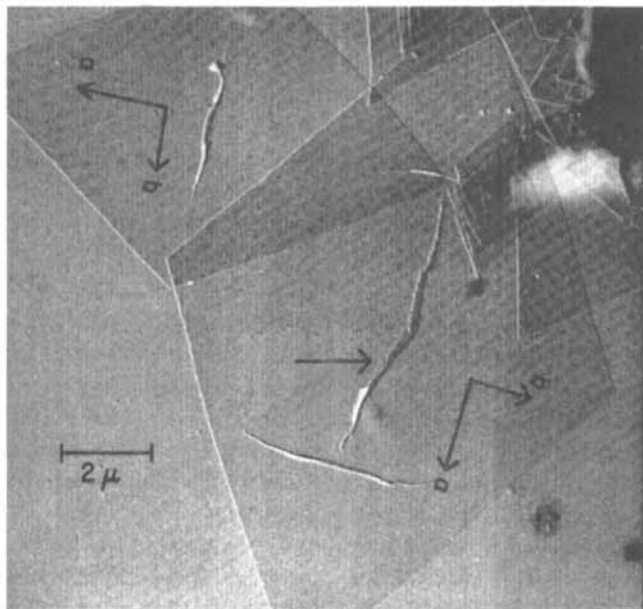
3. SUPRAMOLECULAR ORGANIZATION IN BULK

Macromolecular crystallinity differs in three important ways from low-molecular weight molecular crystallinity: polymers never crystallize completely, the unit cells are always smaller than the macromolecule, i.e. the crystal lattice is formed by the subunits rather than by the whole molecule and a long polymer chain can thread through different crystallites. Complete crystallization is impeded because of the structural polydispersity and the topological constraints resulting from the fact that

one chain can be part of different crystallites. As a consequence, kinetic effects can never be neglected and rather peculiar phenomena of supramolecular order can be observed [53].

A chemically distinct crystalline polymer is polyethylene consisting of $-\text{CH}_2-$ units. The molecules crystallize as they adopt an extended all-trans planar zig-zag

a)



b)

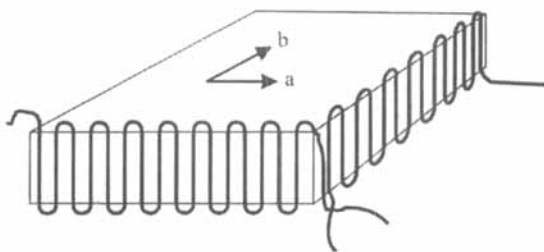


Figure 3 Polyethylene lamellar crystals grown from tetrachloroethylene. The pleats (arrow) are formed after cessation of growth [54]. Reproduced with permission from [54]. © 1960 American Institute of Physics

conformation. However, because of competition with the entropically favoured coiled conformation, it is impossible to form a nucleus whose length can match the contour length of the macromolecular chain. The contour length is the overall length of the stretched macromolecule. The system overcomes this problem by forming chain-folded crystals whose perfection differs whether they are formed from a dilute or entangled solution melt. Figure 3 shows single crystals of polyethylene formed in dilute solution. Each chain is neatly folded up and adjacent steps are connected by a tight re-entry fold. Typically the thickness of the lamellae is 10–20 nm and, controlled primarily by the undercooling temperature during crystallization. The width of single crystals can easily exceed several micrometers [55–58].

The structures of molecular crystals are not necessarily rigid but can undergo complex dynamic rearrangement. Two examples are demonstrated in Figure 4. When lamellar crystallites of long *n*-alkanes, e.g. *n*-dotriacontane and the corresponding deuterated *n*-dotriacontane, are prepared from separate solutions and the corresponding suspensions are mixed, a mat of lamella crystals is formed after removing the solvent by filtration. In those preparation deuterated crystals alter arbitrarily with non-deuterated ones. Annealing such a crystal mat below its melting temperature will alter the structure as the deuterated chains diffuse into the non-deuterated lamellae and vice versa (Figure 4a) [59].

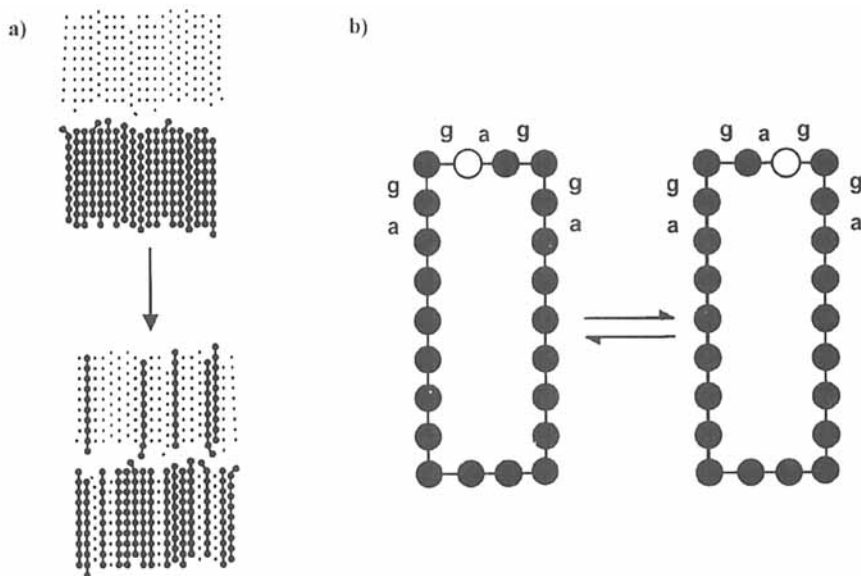


Figure 4 (a) Sketch of the intermixing of long chain *n*-alkane molecules from different crystals in contact below the melting temperature [59]. (b) Molecular motion in cyclododecane yielding the exchange of single chain segments [60]

Figure 4b shows schematically another example of molecular motion in the crystal state. Below their melting point cycloheptacontane and cyclohexanonadecane were shown by solid state NMR experiments to undergo a chain rotation which results in the exchange of single chain segments between the tight folds and the stems of the molecules within the lamella crystal (Figure 4b) [60].

As a consequence of the molecular mobility even below the melting transition, a chain folded crystal will alter its structure upon annealing, trying to extend the length of the stems and thus increase the ordered inner volume and minimize the crystal surface [61–63]. The question arises of how the length of the folds is determined. Detailed experiments on poly(ethyleneoxides) and poly(methylenes) with narrow molecular weight distributions and of moderate molar mass (2000–6000) demonstrated that the thickness of the crystals always corresponded to an integral number of folds, indicating that the endgroups are not incorporated within the crystal but lie at the surface. The thickness of the crystals depends with remarkable precision on the crystallization temperature. High temperatures favour the formation of extended chain crystals. Changes as small as 0.01°C can cause the transition from one to twice folded chains in a responsible manner. Figure 5 depicts crystals of poly(ethylene)oxide which have been grown isothermally within thin layers of melt. The crystal edges, as well as steps and protrusions in the basal plane, have been made visible between crossed polarizers by self-decoration with secondary crystallites formed after quenching the sample to a lower temperature [65]. Upon increasing the crystallization temperature, formation of thicker crystals was observed starting in the centre of the first grown lamellae. The thickened portion overgrew the original layer in a variety of habits (from left to right: hexagon, lozenge, and star) and the height difference was an integral fraction of the chain length, i.e. $1/2$, $1/3$ corresponding to the integral folding of the chains [66]. The example is one of a number of possibilities for forming lateral steps and patterns by chain folding crystallization of polymers.

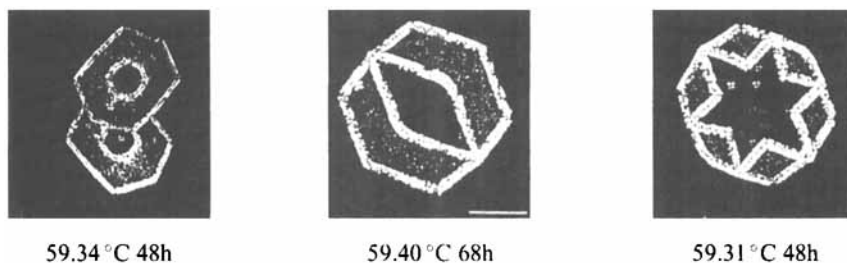


Figure 5 Poly(ethylene)oxide lamella crystals grown within thin layers of melt (the white bar corresponds to $20\ \mu\text{m}$) [64,460]. Reproduced from [64] with kind permission of Elsevier Science NL. The crystal edges, the crystal steps and protrusions in the basal plane have been made visible between crossed polarizers by self-decoration with secondary crystallites formed after quenching the sample to a lower temperature [65]

If crystallization occurs in a flow-gradient, the polymer chains are oriented along the laminar flow and the growth of long, rod-like fibrillar structures occurs. Between the fibrils, the shear forces are diminished and the fibre crystals act as nucleation centres for the growth of lamellar structures. Consequently lamellae, oriented perpendicular to the fibre axis, epitaxially grow in regular distances on the fibres resulting in “shish-kebab”-like structures (Figure 6a) [67]. The transmission electron micrographs show shish-kebab fibres as they form when a polymer of

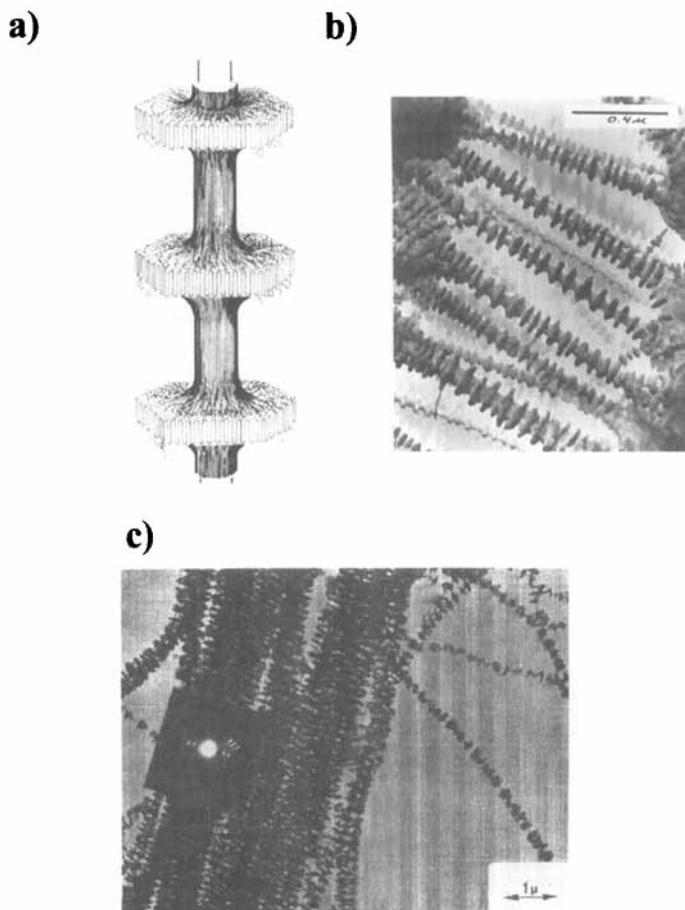


Figure 6 (a) Sketch of the chain arrangement in shish-kebab structures. Reproduced from [67] with permission. (b) Polyethylene shish-kebabs crystallized from solution [68]. Reproduced with permission from H. D. Keith, © 1996 American Institute of Physics. (c) Mannan-lamellae, epitaxially grown on cellulose fibres [69]. Reproduced from H. Chanzy, reprinted with permission from John Wiley & Sons, Inc.

very high molecular weight is crystallized from a stirred solution. Figure 6b depicts shish-kebab crystals of polyethylene [68]. Upon stirring, the coiled chains get elongated which can be regarded as a preorganization effect for the crystallization. Some of the chains form extended chain crystallites (the shish) which then serve as a nucleus on which chain folded lamellae grow (the kebab). The example in Figure 6c shows a hetero-shish-kebab where a core of extended cellulose crystals is decorated by lamellar crystals from mannan [69].

Crystallization plays an important role for the production of fibre-materials. Simple melt crystallized or solution cast semicrystalline polymers have poor mechanical properties due to the formation of non-oriented folded-chain crystallites, lamellae, spherulites or shish-kebabs. Only a small number of molecular chains bear an external load [70]. Strong fibres can be manufactured by mechanical stretching and molecular orientation during spinning [71]. Microstructures of technically used synthetic fibres like poly(amides), poly(esters) or poly(ethylene) are shown in Figure 7 [72]. The fibre consists of about 90% of ordered crystalline domains, oriented parallel to the fibre axis. The crystallites are interconnected by disordered domains and surrounded by extended, but non-crystalline macromolecules. The crystals act as cross-linking units, responsible for the mechanical strength of the fibre, while the flexibility is supported by the disordered regions [71]. The stability of the crystals is determined by how the single macromolecular chains stick together: poly(ethylene) chains crystallize due to van-der-Waals interactions and since these forces are weak, the polymer chains have to be as long as possible to maximize the chain-to-chain contact area. Consequently, only ultrahigh molecular weight poly(ethylenes)

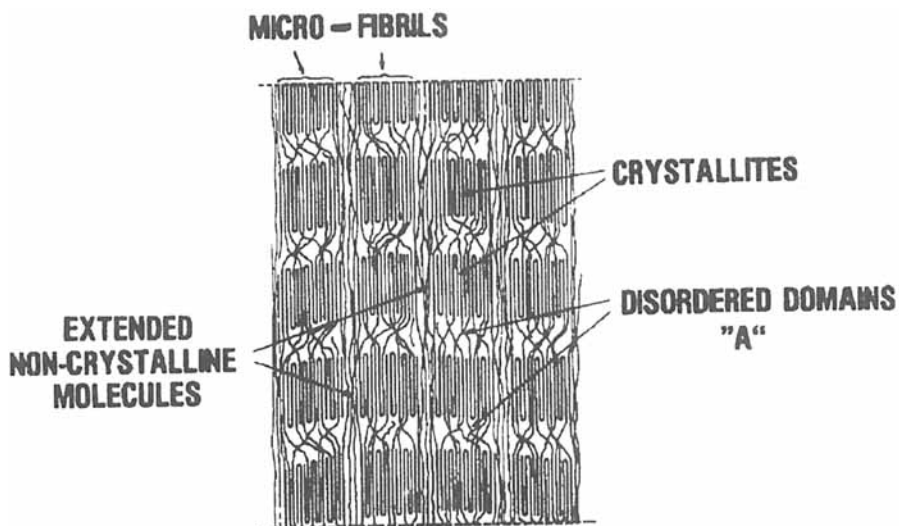


Figure 7 Schematic structure of nylon-6 fibre [72]. Reproduced from [72] with permission of Chapman & Hall

($M_n > 10^6 \text{ g mol}^{-1}$) give rise to high strength fibres. In poly(amides) the polymer chains are linked together via $\text{C}=\text{O} \cdots \text{H}-$ hydrogen-bonds. Because of the relative high bond-energy (about 25 kJ mol^{-1}) the macromolecules are strongly tied together, though the degree of polymerization in poly(amides) seldom exceeds 400. In contrast to natural silk, being flexible and strong at the same time, strength and elasticity are contradictory properties in synthetic fibres, since a high crystallinity always leads to strong, but stiff materials.

Thus we are far from accomplishing the perfection, performance, and complexity of natural fibres like keratin or spider silk [71]. The latter demonstrates the fundamental lack of structural control we still have to overcome. Spider silk is stronger than steel, its tensile-strength approaches that of KevlarTM while the toughness (energy required to break a fibre) exceeds all known synthetic high performance fibres by a factor of ten [72,74]. The unique combination of strength and elasticity in spider silk is the result of a specific superstructure of entangled amorphous domains structurally stabilized by hydrogen bonds and small crystallites (Figure 8) [75].

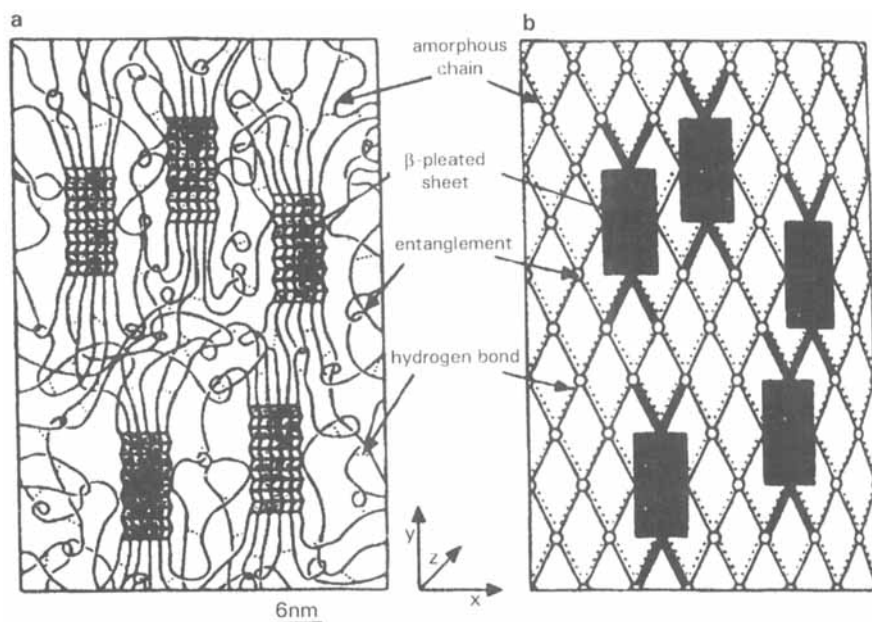


Figure 8 (a) Schematic drawing of the proposed structure of the dry dragline silk of *Nephila clavipes*, consisting of β -pleated nanocrystallites, connected via amorphous chains. (b) Simplified model, investigated by Termonia [75]. Reproduced with permission from [75]. © 1994 American Chemical Society

Spider silk consists of protein macromolecules with a block-like structure, containing hydrophilic poly(glycine) enriched blocks and hydrophobic poly(alanine) segments. Though the details of spider silk structure are not elucidated completely [76] it is generally believed that the reinforcing crystalline domains consist of β -pleated sheets of hydrophobic poly(alanine) sequences. These crystallites are remarkably small, with a mean size of $2 \times 7 \times 5$ nm and totally isolated by the hydrophilic amorphous segments, nevertheless they are highly oriented already before stretching [77,78,79]. Hydrogen bonding within the amorphous phase is responsible for the initial modulus. After extension, the nanocrystallites are hardly altered [76]. By investigation of computer-models, Termonia was able to show that the size of the nanocrystallites plays a crucial role: the mechanical properties of the silk are optimal if the crystallite sizes do not exceed the experimentally proven size [75].

In man-made fibres, any stretching will irreversibly alter the crystallinity and there is no control of the lateral size of polymer crystals. Semicrystalline polymer networks typically consist of platelet type crystals whose width exceeds their thickness by several order of magnitudes because only the thickness is controlled by the chain folding [61]. In contrast to synthetic fibres, spider silk does not need any mechanical treatment by external forces: the constituents self-assemble directly during the spinning-process. These examples clearly demonstrate the need for more detailed control of the mesoscopic structures for further development of man-made materials.

The examples in Figures 2–8 demonstrate how the chain structure and the competition between entropy-driven disordering and enthalpy-driven ordering can result in the formation of rather well-defined superstructures and dynamic exchange processes where segments of the same macromolecule are involved in different states of order. In all cases the essential molecular interactions are weak forces, and it is the multiplicity of these interactions in rather extended microdomains which causes the stability of the superstructures. Stronger interactions like dipole–dipole forces, hydrogen bonding and extended π -stacking can even endanger the reversibility and lead to intractable insoluble products (as in the case of some high performance materials like poly(aramides), poly(etherketones) and poly(benzthiazoles) [80]).

The principal according to which weak interactions between small building blocks are organized and amplified by connecting them within a long chain, also forms the basis for supramolecular organization of block copolymers. Because of the reduced entropy of mixing, many polymers undergo phase segregation although their low molecular weight analogues are well miscible. If two polymers are linked by a covalent bond, a block copolymer is formed whose constituent blocks cannot demix macroscopically. As a consequence, microdomains are formed whose structure or morphology mainly depends on the volume fraction of the segments. In the limit of strong segregation (high molecular weight and a positive interaction parameter, $\chi = \Delta H_{\text{segment}}/kT > 0$) highly ordered domain structures are formed whose geometry is controlled by minimizing the interfacial surface and the deformation of the coil

structure [81,82]. At higher temperatures, the blocks may mix homogeneously, but as the temperature is lowered, they segregate on a microscopic scale forming A- and B-rich domains separated by an extensive amount of internal interface. The classical structures are lamellae, hexagonally packed cylinders, and body centred cubic arrays of spheres [83,84]. More recently bicontinuous cubic structures [85,86] and a hexagonally perforated lamellar phase [87] have been observed. An overview of these structures is given in Figure 9 [89–91]. Ordering can extend over large

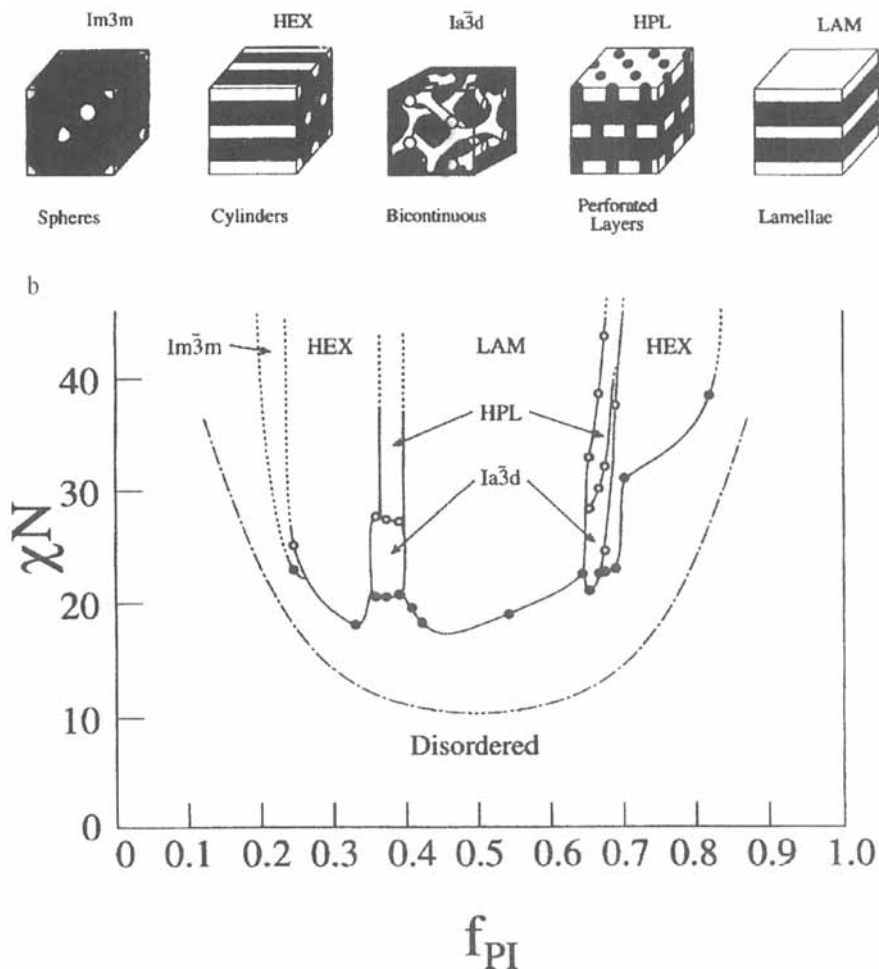


Figure 9 (a) Sketch of the phase segregated microstructures of binary block copolymers. (b) Existence regions of the different microphases, depending on the volume ratio of the blocks (f_{PI}) and the interaction parameter χ^N [88]. Reproduced with permission from [88]. © 1995 American Chemical Society

volumes with few defects and grain boundaries. Typical periodicities are in the range 15–150 nm. Recently it has been shown that the multiplicity of phase structures can be understood by means of mean-field theories [81,92,93] and that the main features of AB-block copolymer phase diagrams can be predicted [90].

“Miktoarm” block copolymers are star shaped polymers with chemically different arms [16,94–96], which permit study of the influence of the chain architectures on the microphase behaviour of the macromolecules. These new materials can exhibit interesting morphological features, either by moving the borders of the classical morphology map or by forming new morphologies. This was demonstrated with examples of styrene/isoprene (S/IP) miktostars. At the same S:IP ratio where a linear poly(styrene-*b*-isoprene) block copolymer shows a lamellar structure, in a PIP₂PS mikto-star bicontinuous structures were observed and a PIP₃PS mikto-star shows hexagonally packed cylinders [97]. A three-mikto star (PIP₂PS), containing 81% poly(styrene) segments, exhibits a randomly oriented “worm micelle” morphology never observed in linear block copolymer systems [98].

“Rod-Coil” AB block copolymers consisting of rigid and flexible blocks expand the complexity of mesomorphic ordering of polymers further [99,100,101,309]. The geometrically different spatial requirement of rods and coils affect the domain segregation. While the rod-like blocks tend to form sheet like domains, the coils favour curved interfaces. Thomas *et al.* observed zig-zag like layers [102]. Rather unique honeycomb pattern and 3D ordering of rod like domains were reported for well-defined rod-*b*-polyisoprenes with varying composition [103].

The morphology is not significantly altered if the molecular structure is changed from a diblock to a triblock copolymer, as long as the polymer still consists of only two components (ABA-triblock copolymer) [104,105]. If the block structure consists, however, of three different components (ABC-triblock copolymers), the situation changes remarkably. Now the phase morphology depends on three interaction parameters χ_{AB} , χ_{BC} , χ_{AC} and two independent volume fraction parameters. Minimizing the interfacial surface and the surface energy is not the same and a large variety of peculiar structures can be formed [88,106,107].

Such ABC-triblock systems offer the opportunity of creating ordered morphologies containing simultaneously mesoscopic structures of different dimensionality, some selected examples are depicted in Figure 10. Yet, scope and limitations in the morphologies of ternary block copolymers are not fully explored [107–109,110] and theoretical approaches for their quantitative understanding are still at the beginning [111].

The examples mentioned so far demonstrate only part of the intriguing versatility of block copolymers for the controlled formation of periodical nanostructures. It has been suggested that block copolymers could be used in the development of new electronic devices [113], the synthesis of mesoporous solids [114,115], or the fabrication of nanofibres [116].

Self-ordering caused by segregation is also observed in the case of the so called “ionomers”. Ionomers are water-soluble copolymers from hydrophobic monomers

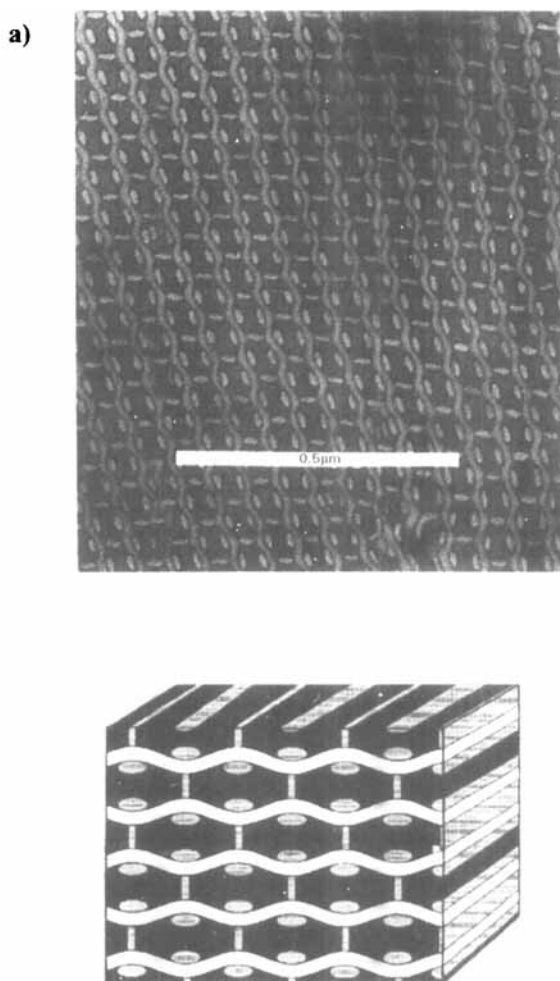


Figure 10 Examples for phase segregate microstructures in ABC triblock copolymers. Transmission electron micrograph and schematic three dimensional representation of (a) the “knitting pattern morphology” [107]. Reproduced from [107] with permission of Hüthig & Wepf Verlag.

and small amounts (<10%) of ionic comonomers. Within the non-polar matrix, the ionic groups form tightly bound ion pairs which interact with each other as strong dipoles. Clustering of the ionic groups gives rise to the formation of physical, thermoreversible gels. In most cases the cluster structures are not well understood [117–119]. According to the Eisenberg–Hind–Moore (EHM) model (Figure 11a), the ionic groups associate in “multiplets”. The multiplet sizes are governed by the

b)

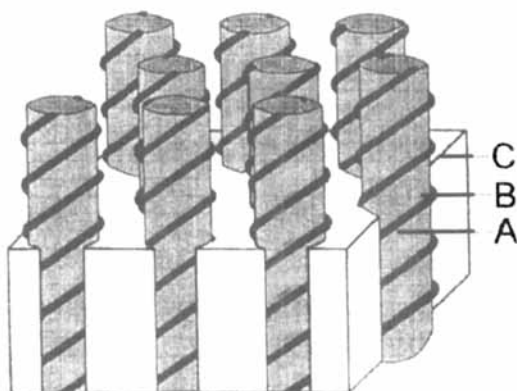


Figure 10 (b) A helical morphology [112]. Reproduced with permission from R. Stadler. © 1995 American Chemical Society

type of ionic groups, their distance to the polymeric backbone and by steric effects arising from the limiting condition, that all polymer chains have to be found outside the aggregates [120]. The chains attached to the multiplets show a constrained mobility and this hindrance increases with decreasing distance between chain and multiplet. Though the typical diameter of a multiplet is 3 nm, the less mobile chain regions start to overlap at higher ion concentrations ($>3\%$) forming an independent “cluster phase” (Figure 11b) [119,121].

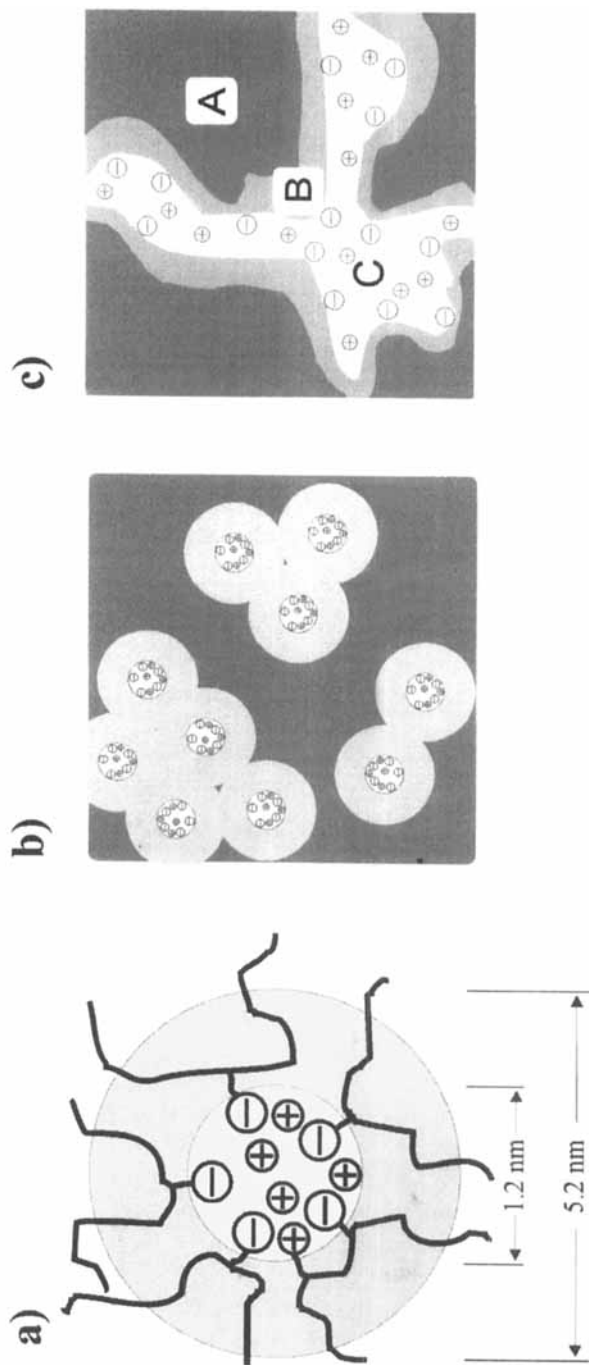


Figure 11 (a) Schematic representation of an ion-cluster ("multiplet") and the region of restricted chain mobility according to the EHM-model [119]. (b) Increasing volume fraction of the "cluster phase" with increasing ion-concentration in an ionomer [119]. (c) Schematic structure of the phase-segregated morphology of Nafion™ [119]. A, perfluorinated bulk polymer phase; B, water-swollen boundary phase; C, aqueous inner phase

Practically important ionomers are a copolymer of polyethylene and methacrylic acid which is only partially neutralized (SurlynTM) [122,123] and a tetrafluoroethylene copolymer with sulfonate groups (NafionTM) [124,125]. In the first case, careful balance of a relatively low molecular weight, the fraction of methacrylic acid groups and the degree of polymerization results in a polymer which has elastic properties like very high molecular weight materials at ambient conditions and can be processed like any other low molecular weight polymer at elevated temperature [119,126]. The phase segregation behaviour of perfluorinated ionomers (NafionTM) has been utilized for the preparation of ion-exchanging systems. The inert heterogeneous resin has been used as a strong acid polymeric catalyst for a wide variety of reactions in synthetic organic chemistry [127]. Since the phase segregated regions percolate the structure (Figure 11c), perfluorinated ionomers have been used for the preparation of ion-selective membranes [128,129]. The observation, that the ion-selectivity of Nafion-membranes can exceed the well understood Donnan-permselectivity has been marked as the “superselectivity-effect” [130,131]. It is well known that the superselectivity relates to the microphase separated morphology of the perfluorinated ionomers and theoretical concepts to explain the effect have been proposed [132–135].

Another area of superstructure formation in bulk polymers is the wide field of “liquid crystalline” polymers. Here the synthesis, structure and properties of liquid crystal polymers will only be touched on briefly, and this subject is reviewed in detail in the literature [10,43,80,136–141]. Liquid crystals or “mesomorphic” compounds exhibit ordering intermediate between crystals and liquids [142]. Liquid crystalline phase behaviour is generated by anisometric groups, called “mesogenes”, typically rod-like (“calamitic”) or disk-like (“discotic”) [143]. In a nematic liquid crystalline phase, the mostly calamitic mesogenes are all oriented along one main direction, while their centres of mass are distributed randomly in space. In case of additional long-range order, e.g. a positional order along parallel planes, the mesophase is a “smectic” one. A “cholesteric” phase is observed when plies of nematic phases change their direction from ply to ply [144]. To create liquid crystalline polymers the mesogenic groups can either be incorporated into the polymeric backbone (“main chain liquid crystal polymers”, MCLCP) or be attached to the side groups (“side chain liquid crystalline polymer”, SCLCP). The main principles of LCP molecular architectures are depicted in Figure 12 [137].

Side chain liquid crystals are investigated for their functional properties, e.g. for displays, optronics [139,145,146,] or for the production of effect-pigments, exploiting the angle dependent, wave length selective light reflection of chiral nematic phases [147,148]. Main chain liquid crystals are important materials for structural applications offering high performance mechanical properties [80], i.e. high performance fibres like poly(phenyleneterephthalamide) (KevlarTM, TwaronTM) [149] or aromatic polyesters like VectraTM which are also used for the assembling of electronic devices [150], as metal coatings [151] and adhesives [152]. The peculiar properties of main chain polymer liquid crystals are achieved by macroscopic

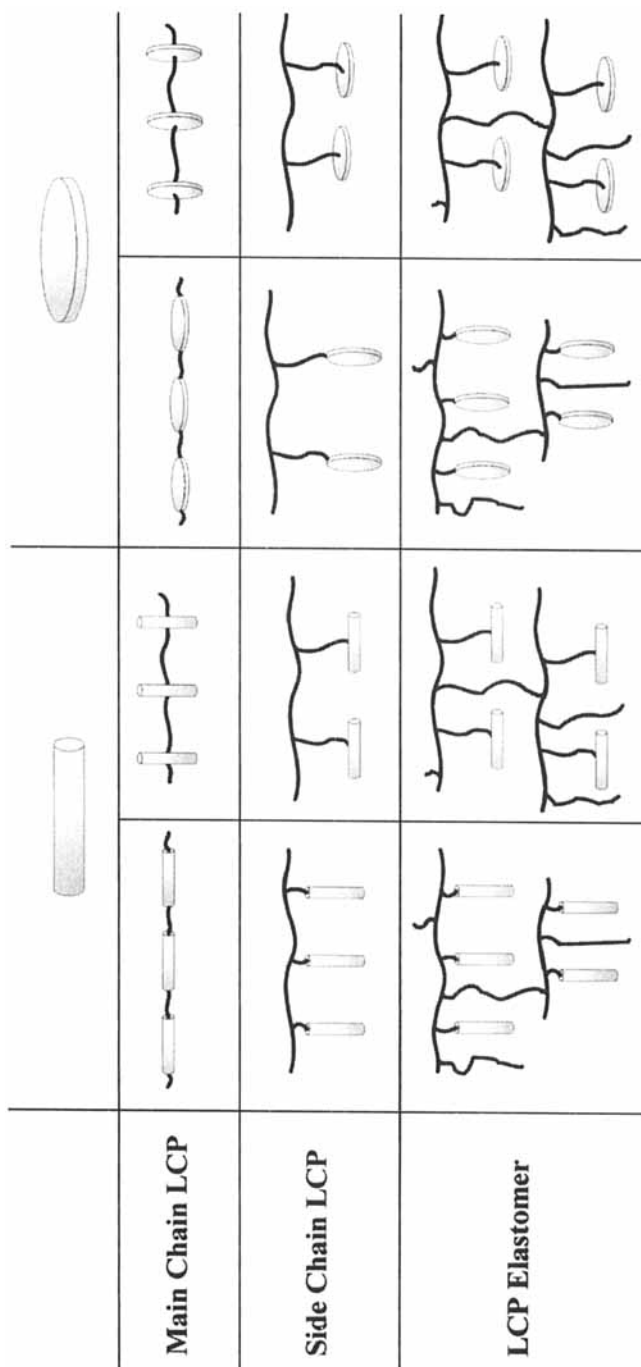


Figure 12 Molecular architectures of liquid-crystalline polymers [137]

orientation during mechanical shear and elongation. In the case of the poly-(aramides), this is done by spinning the nematic polymer solution in sulfuric acid. Aromatic polyesters can be processed in the melt. The orientation of the mesophase still remains after cooling below the glass transition temperature. The low thermal expansion coefficients parallel to the molecular axis allow the combination with ceramic materials or the application over a wide temperature range [70].

Recent work focuses on “non-classical mesogenes” which are built up by self-assembly. One example is a family of polymers containing disk-like groups which form no liquid crystalline phase, but can act as an electron acceptor or donor. Charge transfer complexation with a complementary low molecular mass compound induces nematic or columnar discotic liquid crystalline order [153,154]. Figure 13 demonstrates this with the example of a polyester, bearing electron-rich tetra(alkoxy)tri-phenylene-units in the main chain, mixed with the electron deficient aromatic 2,4,7-trinitro-9-fluorenone (TNF). While the pure polymer shows a non-ordered isotropic melt, a columnar phase appears on addition of TNF.

With the exception of the last example we have mainly dealt with supramolecular assemblies and structures of polymers which are formed by dispersion interaction forces so far. Self-assembly of polymers by more specific interactions, which justifies the denotation as “supramolecular complexes” is still limited in number and mostly poorly defined.

An important example is the polyelectrolyte complexes, e.g. between poly(vinyl-*N*-butylpyridiniumbromide) and poly(sodium styrene sulfonate) [155]. Stoichiometric polyelectrolyte-complexes are insoluble in organic solvents and water, while non-stoichiometric polyelectrolyte-complexes can be dissolved in water, containing considerable concentrations of salts [156]. The entangled, non-ordered precipitates are believed to be metastable states, due to the extremely fast complexation reaction preventing proper structural arrangement [157]. Formation of more ordered complexes, containing cation–anion “ladder” structures has been possible [156,158], resulting in a fibrillar morphology [159–161].

Isolated structurally defined polymer–polymer electrolyte complexes can only be obtained with very well-defined biological macromolecules. Rather well-defined complexes can, however, be prepared by adding synthetic polyelectrolytes and low molecular weight surfactants [WA86] (Figure 14). In the bulk state, these complexes form regular microdomain morphologies. For a recent review see [162]. Many of the structure elements are characterized by a periodical deformation which can be assigned to a mismatch of the geometrical shape of the surfactant and the phase geometry (see Figure 15). It has been shown, that the complexes are formed by a zipper-mechanism [163–167]. They can be re-dissolved and cast to homogeneous films of good optical quality and stability. A discernible example are complexes of perfluorinated cationic surfactants and anionic poly(acrylate/methacrylate)s, yielding smectic ordered materials, possessing surfaces with low energies [168].

Complexes of sodium poly(α ,L-glutamate) with salts of various fatty acids form a lamellar structure, consisting of alternating layers of polymer-chain and double-

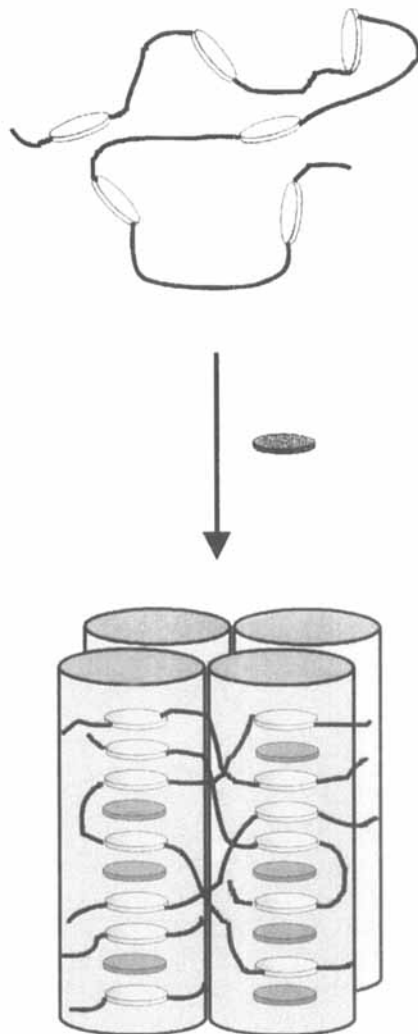


Figure 13 Induction of liquid-crystalline order via electron donor/acceptor complexation [154]

layers of the surfactant [170]. Detailed X-ray analysis proved that the polymer chain adopts an α -helical conformation, while the ordering of the surfactant chains depended on their length: short chains (C_{12} – C_{16}) were extended but disordered, while longer chains ($>C_{18}$) were packed in hexagonal order [170].

In bulk we may not forget the so called stereocomplexes between stereoregular polymers. In 1961 Watanabe reported that mixing syndiotactic poly(methylmethacrylate) (*s*-PMMA) and isotactic poly(methylmethacrylate) (*it*-PMMA) leads to the

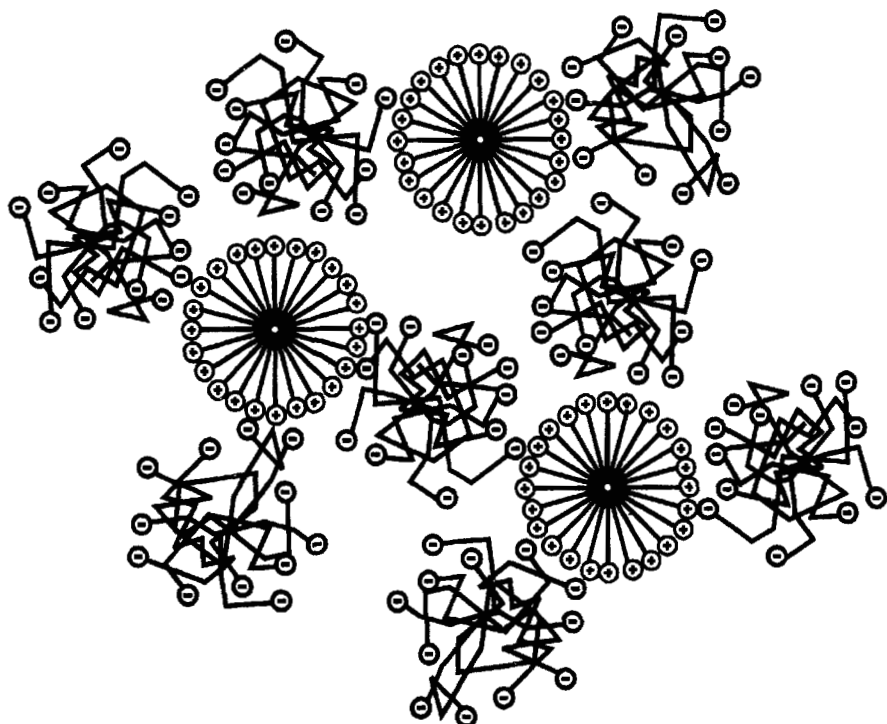


Figure 14 Schematic structure of the complex between a spherical poly(anion) and a low molecular weight cationic surfactant [171]. With permission of the American Chemical Society

formation of aggregates, which he called “stereocomplex” PMMA [172]. Since then, a vast amount of literature has been designated to the PMMA systems [173]. Thermoreversible gelation can be observed if the stereocomplex is formed from solution [174].

Stereocomplexation also occurs in blends of isotactic polymers of opposite configurations, such as poly(alkylthiirane)s [175,176], poly(benzylglutamate) [177], and poly(lactide) [178]. Poly(lactide) homo- and copolymers have gained great interest as synthetic biodegradable polymers. They are prepared by ring-opening polymerization from the various lactide stereoisomers and mixtures thereof. As the polymerization proceeds with only acyl-oxygen cleavage, the configuration of the chiral centres in the lactide is retained enabling the preparation of highly crystalline stereoregular and totally amorphous *meso* and *rac* poly(lactide). Though racemic poly(lactides) are amorphous materials, blending of poly(lactides) of opposite configuration leads to the formation of crystalline stereocomplexes. The melting temperature of the 1 : 1 D/L-complex (230°C) is about 50°C higher than the

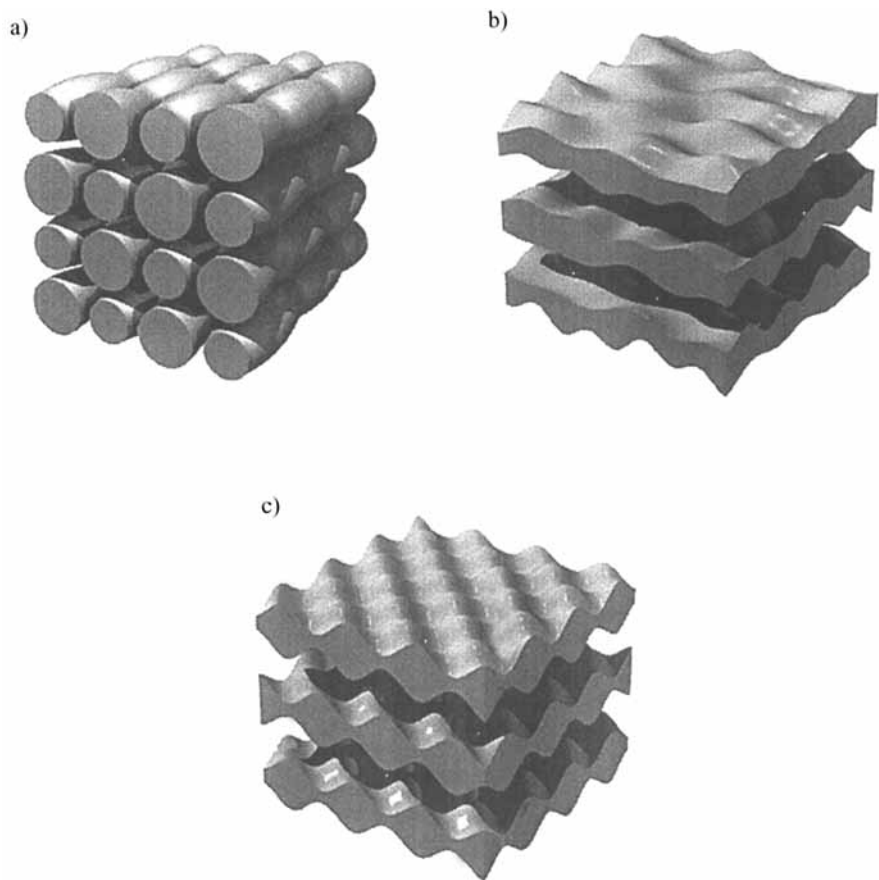


Figure 15 “Undulated” phases of different polyelectrolyte/surfactant complexes. (a) Cylinder-phase. Reproduced from [169] with permission. © 1995 Wiley–VCH. (b) Mattress-phase. (c) Egg-carton phase [167]. Reproduced from [167] with permission of Academic Press

melting temperature of the stereoregular homopolymers [179]. The stereocomplex formation is even preferred to the homopolymer crystallization if an enantiomeric pure poly(L-lactide) is mixed with a poly(D-lactide) at only 80% enantiomeric excess [180]. The complex crystallizes in regular triangular shaped single-crystals (Figure 16a), the molecular structure (Figure 16b) was elucidated by combinations of X-ray analysis and force-field calculations [181,182]. The racemic crystal is formed by packing β -form 3_1 -helices of opposite absolute configuration alternatively side by side. The increased melting temperature is explained by more densely packing of the enantiomeric polymer chains, resulting in stronger attractive interactions.

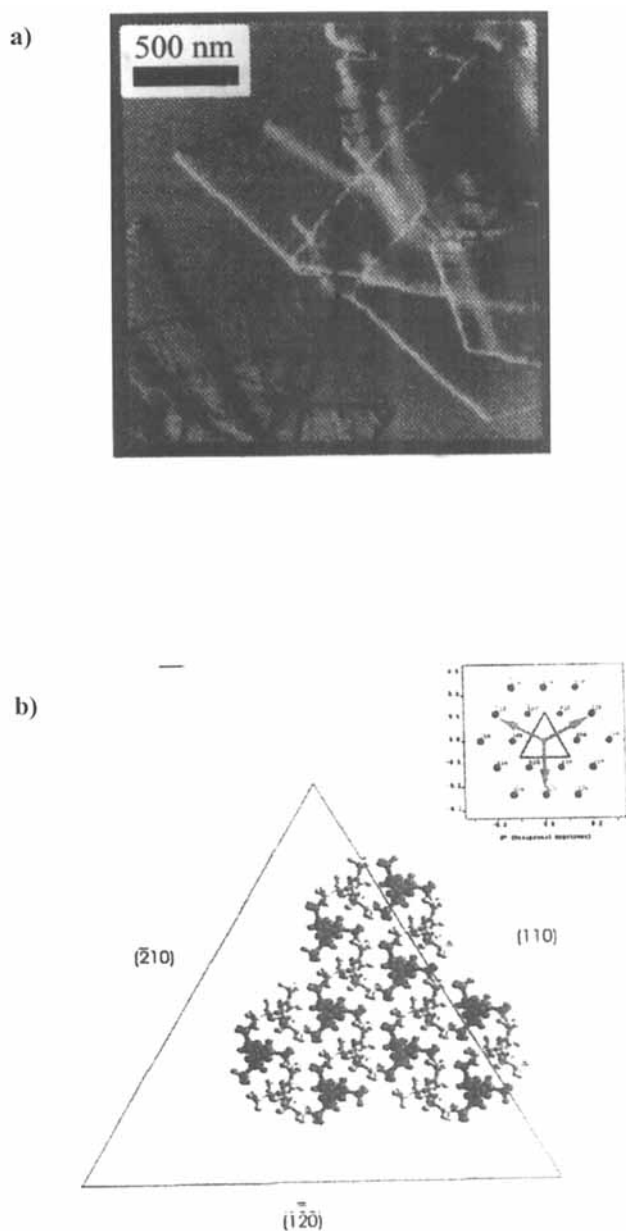


Figure 16 (a) Morphology of solution-grown poly(lactide) stereocomplexes and (b) the proposed crystal structure [181]. Reproduced from [181] with permission. © 1996 American Chemical Society

Although the stereocomplex formation of poly(lactide) represents an intriguing example of a superstructure, the question must be raised whether this can be regarded as a congenial complex formation as it occurs between individual molecules in solution not affected by the cooperativity implicated in crystalline ordering. With respect to this question, however, a recent report must be noted which describes that intermolecular and intramolecular stereocomplexed PMMA molecules can be distinguished by gel-permeation-chromatographic measurements, indicating true complex formation in dilute solution [183].

Regarding supramolecular organization in bulk, topochemical polymerization reactions must not be forgotten, i.e. reactions which occur in the three-dimensional ordered state and which require that the monomers are preorganized. Topochemical polymerization of monomers with conjugated triple bonds yields crystalline polymers of high molecular weight, with semiconducting properties ($E_A < 1 \text{ eV}$) [184,185]. The thermal or radiation induced reaction occurs as an 1,4-addition polymerization of the conjugated triple bonds giving rise to macromolecules with three cumulated double bonds per monomer unit.

Crystalline poly(oxymethylenes) with peculiar morphologies were produced via γ -initiated topochemical polymerization of trioxane. Depending on the crystal modification of the trioxane, porous poly(oxymethylene) crystals, showing cylind-



Figure 17 (a) Topochemically polymerized poly(oxymethylene) exhibiting cylindrical voids. Reproduced from [186,187]. © 1981 John Wiley & Sons Inc., with permission.

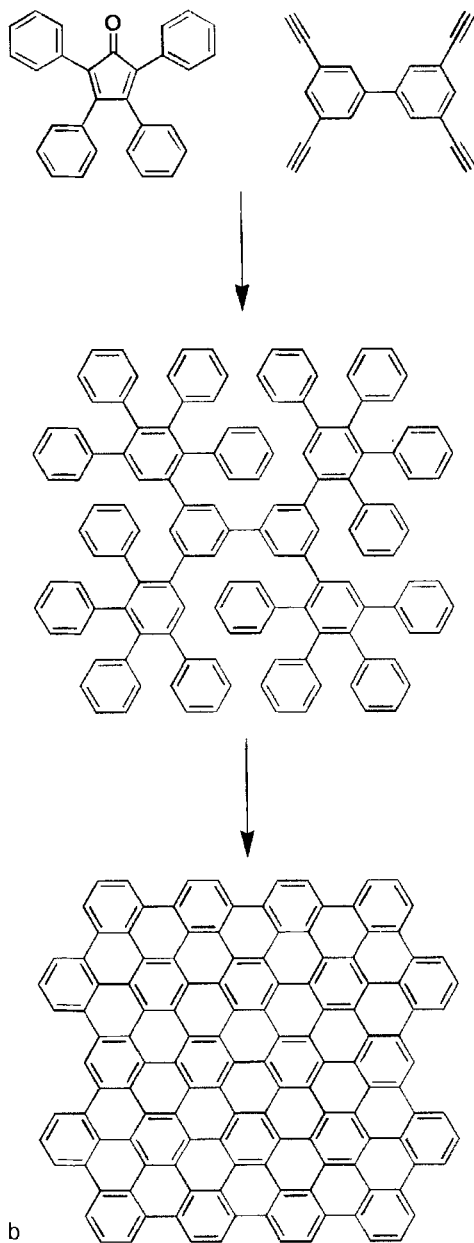


Figure 17 (b) Large polycyclic aromates via topochemical cyclization [188]

rical voids (Figure 17a) or fibre-like polymer microfibrils were synthesized [186]. In a similar way, polymer/polymer composites have been prepared by solid-state polymerization of trioxane crystals grown from binary trioxane/poly(caprolactone) or trioxane/poly(ethyleneoxide) mixtures [187].

Cyclohydrogenation of poly(phenylene) dendrimers has to be mentioned as a special case of topochemical polymerization proceeding in solution. The reaction yielded extended polycyclic aromatic hydrocarbons containing up to 132 carbon atoms (Figure 17b) [188].

Another example of supramolecularly controlled polymerization is the inclusion polymerizations. Several organic compounds like cyclodextrins, cholic acids or perhydrotriphenylene exhibit regular channels with angstrom-wide diameters (0.5–0.7 nm) inside their crystal structures, capable of including molecules with the right shape, fitting inside (Figure 18a) [189]. Other guest compounds like urea, thiourea or cyclotriphosphazenes built up the channels only in the presence of a guest [190,191]. Numerous organic monomers can be included into such channels and polymerized therein by irradiation, mostly with γ -rays, via radical polymerization. The primary product is a composite material made from a polymer, surrounded by the low-molecular host crystal. Due to the confinement in the crystalline matrix, isolated fully stretched macromolecules are generated (Figure 18). The polymers can be isolated by dissolution of the low molecular weight host compound [194].

Because of the necessity for high-intensity γ -sources (dose rate >1000 Ci), the discontinuous process and the low polymer/host ratio in the clathrates ($\cong 100$ mg polymer per gram host material), the inclusion polymerization process was never of practical importance. However, inclusion polymerizations exhibit some important features of a template polymerization (see also point 7 of this chapter) and it might be worthwhile to consider the design of new inclusion complexes for this purpose. Peculiar examples are: 1,3-butadienes can be converted into pure trans-1,4-poly-(butadienes) and from vinyl and diene monomers highly iso- or syndiotactic macromolecules were prepared. The stereoregularity of inclusion polymerized poly(acrylonitrile) exceeded that of products prepared by stereospecific coordination complexes [195]. Optically active polymers could be prepared by combination of prochiral monomers and chiral hosts [194,196,197]. The radical polymerization of allyl-inhibited monomers like isobutylene, dimethylbutene or propen has been enabled by the confinement [198]. Copolymerization parameters were found to differ from those of the corresponding bulk-copolymerizations. The composition of inclusion copolymers is determined by the sequence of entrance of the monomers into the host-channel and by the relative stability of the comonomer/host complexes [198]. Since the growing polymer chains are isolated from each other, chain-termination reaction are suppressed. The occurrence of “living” radicals, trapped in the complex and stable over months, have been shown [196,199] and successfully used to prepare block-copolymers [200].

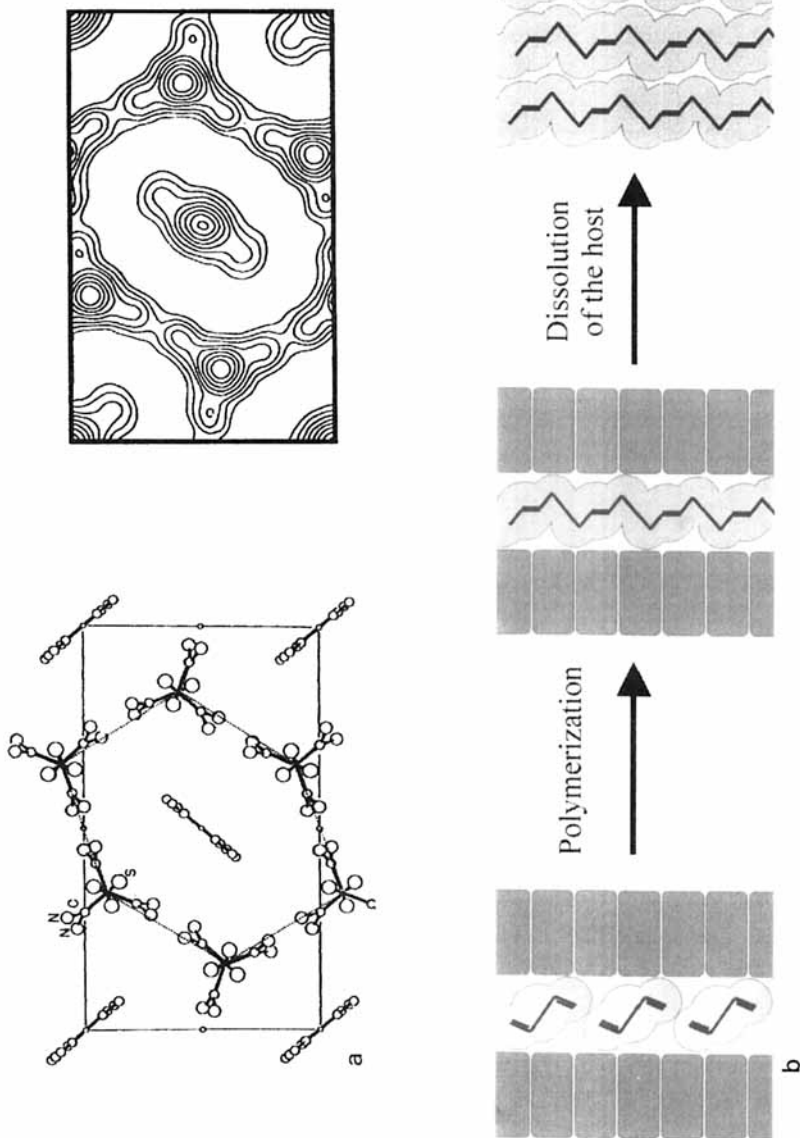


Figure 18 (a) Sketch of the thiourea/dimethylbutadiene-inclusion complex structure and electron density map of the cross-section of the thiourea channel [192]. (b) Schematic drawing of the inclusion polymerization process. Reproduced with permission from [193]. © 1972 American Chemical Society

4. SUPRAMOLECULAR ORDERING AND SELF-ASSEMBLY OF DISSOLVED POLYMERS

The examples of the superstructures formed in bulk polymers demonstrate a certain richness which has its origin in the chain structure of the polymers. Corresponding well-defined superstructures with macromolecules in solution are, however, more scarce. Again, this is explained by the fact that we can handle systems well which interact predominantly by weak dispersion forces, while in the case of multiple more strongly interacting forces like hydrogen bonding or dipole–dipole interactions, we mostly lack the necessary precision in the design of the primary structure. Besides helix forming polymers and the yet not satisfactorily investigated stereocomplexes in dilute solution which have been described above, the most important example is certainly the formation of micelles and vesicles [21,201–204].

Fixation of hydrophilic units as side-groups of a hydrophobic macromolecular chain leads to water-soluble “polysoaps” [205], exhibiting a similar diversity of self-organized structures like the monomeric analogues. A detailed review can be found in [206]. In contrast to polyelectrolytes and ionomers described above, the association of the amphiphilic groups of polysoaps occurs preferentially intramolecularly. As a consequence the solution viscosity remains low, even for highly concentrated solutions [207] and no critical micelle concentration (CMC) can be found up to extreme dilutions [208,209].

The synthesis of “giant” amphiphiles was recently reported by Meijer *et al.*, who linked a linear hydrophobic poly(styrene) block to a dendritic poly(propyleneimine) as a polar head group. The association structure was found to vary with the dendrimer generation changing from inverse micelles for poly(styrene-*dendr*-(NH₂)₄) through vesicles and rod-like micelles to spherical aggregates for poly(styrene-*dendr*-(NH₂)₃₂) [210].

Also macromolecules with a blocky structure tend to associate to micelles. Because of the chain length dependent solubility, association is not restricted to hydrophilic/hydrophobic systems. Micelle formation can be effected by choice of a solvent *and* a high molecular weight of the constituent blocks. Provided the molecular weight is not too low, all kinds of block copolymers do form micelles when they get dissolved in a solvent which is not equally good for the constituent blocks [211,212]. In most cases the formation of micelles can be described as a closed association process, i.e. unimers are in equilibrium with a defined multimer. Due to the strong influence of the molecular weight, critical micelle concentrations can be several orders of magnitude smaller than for low molecular weight surfactants. In practice, the inevitable variation in the molar mass, even of the most narrowly distributed block copolymers, leads to a smeared CMC as molecules of smaller molecular weight associate at higher concentrations than those of higher molecular weight [213]. Another important aspect of micelle formation by macromolecules is the elastic contribution to the entropy as the coiled chains get partially stretched upon association. Increased incompatibility or a more selective solvent can balance a larger penalty in entropy caused by this elastic contribution and thus allows the formation of

micelles with a larger core than corona volume [88,91]. As a general rule it has been shown that the radius of gyration of diblock copolymer micelles is proportional to $N_A^{4/25} \cdot N_B^{3/5}$ [214,215,216], where the core-forming block is denoted by A.

Generally, block copolymers with rather monodisperse block length form predominantly globular micelles [e.g. 121,201,203,204,217,218]. Formation of cylindrical or plate-like micelles as well as the corresponding lyotropic liquid crystalline phases is well-established only for blockcopolymers of poly(ethyleneoxide) and the higher poly(alkyleneoxide)s, e.g. poly(propyleneoxide), in aqueous solution [219,220,221]. For high molecular weight polymers and in organic solution the formation of other structures like cylinders and vesicles has been observed only recently (Figure 19) [222–225]. So far these investigations refer to non-equilibrium systems and we do not know whether, and under which conditions, the structures are thermodynamically stable. There is little doubt, however, that the same structural richness known for the self-assembly of low molecular weight surfactants will be also realized with amphoteric macromolecules.

It is an important aspect that block-copolymer micelles are characterized by much longer relaxation times than compared to low molecular surfactants. Non-equilibrium morphologies can easily be obtained in a vitrified state due to the efficient suppression of structural reorganization, because of the corresponding very slow response of the micelles to changes of temperature, solvent and concentration. In the case of a block-ionomer, i.e. a diblock copolymer where one block consists of ionic units, it was observed that micelles which formed in non-polar solution needed weeks to re-equilibrate after dilution of the solvent [226–228].

Block copolymer micelles can solubilize other compounds very well. Because of the elastic nature of the coiled chains and the chemical interaction with the core segments, the micelles can take up relatively large loads. Solubilization by micellar solutions of block copolymers has been reviewed in a number of papers [229–231]. The resulting nanodispersions are of considerable interest because of distinct differences in physical and chemical properties of bulk and highly dispersed systems. In a confined volume, reactants can meet more frequently, eventually undergoing a reaction much faster [232]. Compartmentization can be used to prepare ultrasmall particles of uniform size and controlled composition [233]. Such nanoparticles are of great current interest because of the size-dependent properties observed for dimensions below 10 nm, e.g. the surface bulk ratio increases rapidly with decreasing dimensions, confining electronic states into nanometer volumes gives rise to quantum size effects [234–237].

As an example, tetrachloroaurate salts have been solubilized within the cores of poly(styrene-*b*-2-vinylpyridine) block copolymer micelles in toluene. Subsequent reduction of the gold ions yielded metallic nanocrystals of uniform size inside the micellar cores. The stability of the dispersion was sufficient to cast thin films in which the gold particles were arranged within rather equal distances forming a regular two-dimensional pattern. Controlled destabilization of the micelles allowed defined coagulation of several micelles bringing together a rather defined number of particles. Even the formation of strings of particles could be achieved. Figure 20

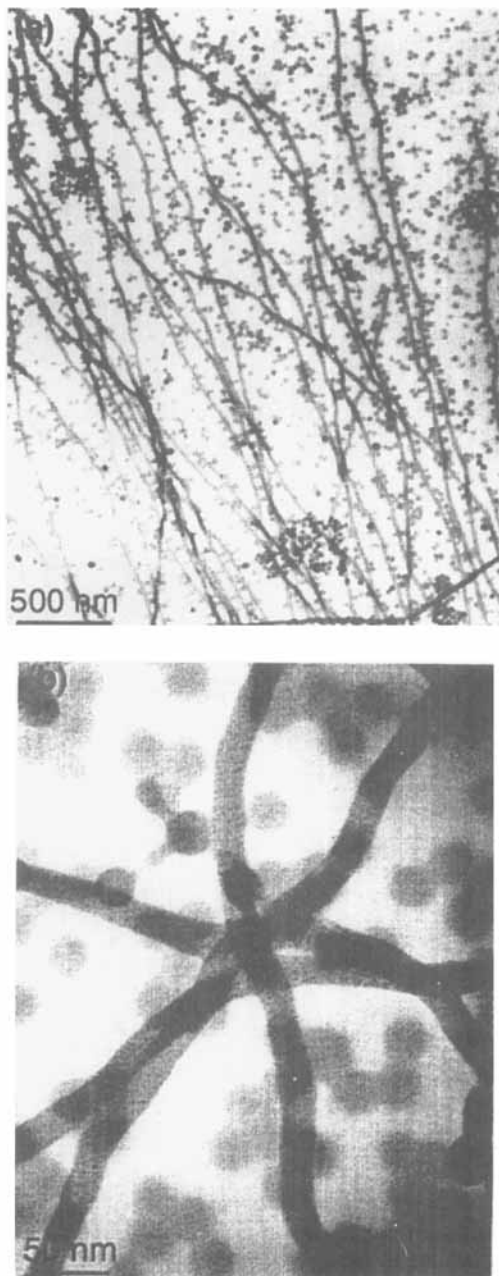


Figure 19 Metastable cylindrical micelles from poly(styrene-*b*-2-vinylpyridine) block copolymer [222]

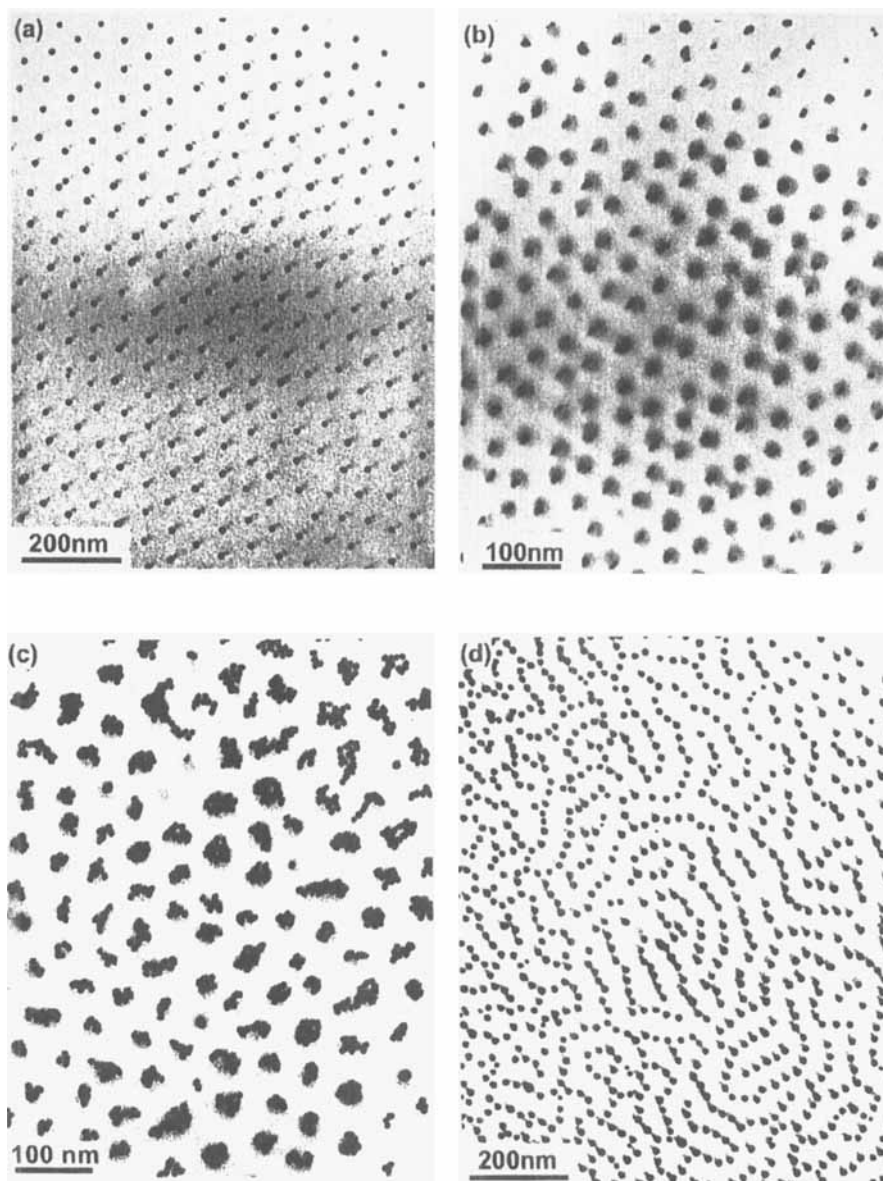


Figure 20 (a–d) Two-dimensional hexagonal array of gold-nanocrystals, deposited from a block copolymer micellar solution [222]

depicts 9 nm gold crystallites incorporated into thin films of poly(styrene-*b*-2-vinylpyridine) block copolymer [238,239].

In similar approach it was possible to obtain cadmium sulfide nanocrystals in block copolymer micelles of poly(styrene-*b*-2-vinylpyridine) [240–242]. Further approaches have been described recently by Antonietti [243].

Corresponding compartmentization effects can also be achieved with cascade branched polymers [244] and microgels. Whetten prepared highly regular films of silver crystallites which were embedded in silica microgel particles of uniform size [245]. Meijer and de Brabander-van den Berg produced a “dendritic box” by substituting a poly(propylene-imine) dendrimer with a dense layer of bulky nonpolar groups [246,247]. These “inverted unimolecular dendritic micelles” were able to encapsulate permanently up to eight molecules of the hydrophilic dye “Bengal Rose”. The loaded micelles could be dissolved in non-polar solvents, indirectly introducing a polar dye in a non-polar environment [248]. Similarly, 3-carboxypropyl-radicals have been enclosed in these monomolecular micelles and the spin–spin interactions were studied by means of electron spin resonance spectroscopy [249].

The most important compartmentization example in polymer chemistry is still polymerization in emulsion demonstrating how a chemical conversion can be controlled by supramolecular organization. Compared to solution polymerization, the reaction rate of the polymerization and the molecular weight of the obtained polymer do not depend on the initiator concentration but are controlled by the surfactant concentration [4,250,251]. In a typical emulsion process, a water insoluble monomer, dispersed by means of an emulgator is polymerized using a water-soluble initiator. Three stages of the reaction can be distinguished: in the initial-phase, the system contains emulsified monomer drops (diameter $\approx 5\text{--}10\ \mu\text{m}$), surfactant micelles (diameter $\approx 5\text{--}10\ \text{nm}$), and small amounts of water-dissolved monomer molecules (Figure 21a, phase-I). The polymerization starts in the aqueous phase with the decomposition of the initiator. The free radicals produced initiate polymerization by reaction with the water dissolved monomer molecules. As the resulting polymer radicals grow, they become insoluble in water and become absorbed by the micelles of the surfactant molecules. Within the thus-formed compartment, the polymerization rapidly proceeds [31]. The rate of the polymerization increases during this “nucleation period” (phase I in Figure 21b), until no more new locii of polymerizations can be stabilized due to a lack of surfactant. Whenever a radical enters such a microreactor, containing a growing chain radical, the two radicals combine immediately and the polymerization stops until a new radical enters. The number of “active” polymerization centres remains constant and the overall rate of polymerization becomes independent of the formation of radicals, but a function of the surfactant concentration. Because monomer which is consumed inside the active compartments gets replaced on the expense of the dispersed monomer droplets, the monomer concentration within the microreactor is also kept constant and the rate of polymerization does not change until all monomer drops are empty (phase-II in Figure 21a, 21b). In the last phase, the reaction rate decreases, obeying a pseudo first-order kinetic law (phase III in Figure 21a, 21b).

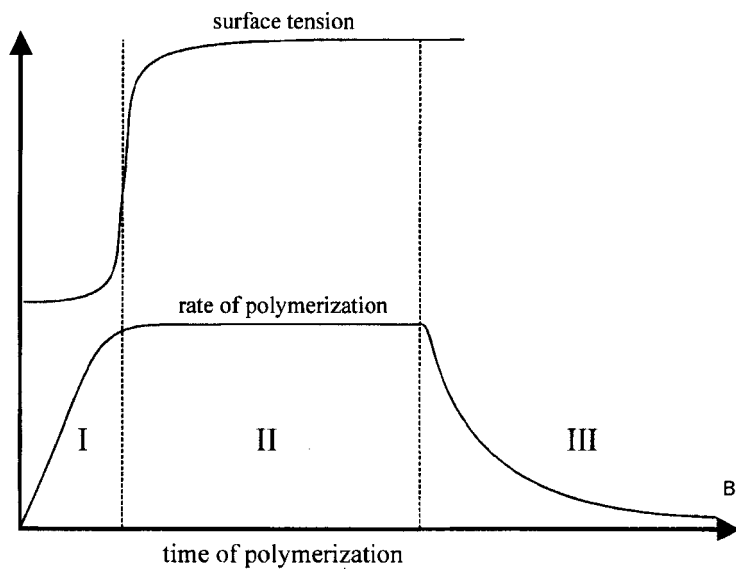
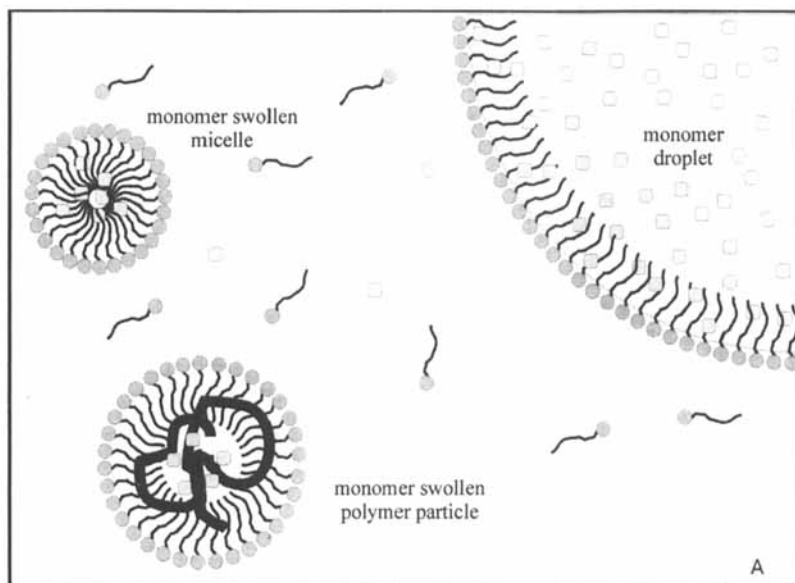


Figure 21 (a) Schematic diagram of the components determining a typical emulsion polymerization [80]. (b) Rate of polymerization in the different intervals of emulsion polymerization [4]

Typical particle sizes of the resulting lattices are between 50 nm and 500 μm . Generally, the size distribution of the latex particles is broad [252]. Lattices with a very narrow size distribution can be achieved by a short nucleation period followed by a long growth period in the absence of coagulation [250]. Because the polymerization takes place within the outer periphery (shell) of the particle, latex polymers with a core-shell structure can be prepared, the core consisting of a cross-linked polymer, surrounded by a shell of tethered linear non-cross-linked polymer of different chemical composition. Recent reviews deal with the preparation and application of these "core-shell" polymers [212,253].

Copolymerization with diazo-functionalized monomers in emulsion has been employed for the preparation of highly cross-linked poly(methylmethacrylate) lattices with diazo groups covalently fixed to the core (Figure 22). Thermal decomposition of the diazo groups allowed selective grafting of a shell [254–256].

As a consequence of the continuous feed of monomers from the dispersed monomer droplets to the growing particle, the size of the lattices obtained by emulsion polymerization exceeds that of the surfactant micelles by up to several orders of magnitude. So-called microemulsion polymerizations have been developed in order to prepare particles smaller than 50 nm, whose size is related to that of the monomer loaded micelles [463]. Because of the small size of the surfactant stabilized particles, a microemulsion is stable and might even be in thermodynamic equilibrium. In the presence of a large amount of surfactant, the monomer can be spontaneously dispersed within nanometer scale colloidal particles each surrounded by a monolayer of surfactant molecules [257]. Polymerization, however, destroys the stability of the original microemulsion system, because an osmotic pressure builds up and the polymer containing micelles inevitably swell on the expense of the micelles with monomer molecules only. The gain in free energy, caused by the swelling ($\approx 10 k_{\text{B}}T$ per macromolecule), exceeds the minimum free energy of a micelle and drives the whole system away from the equilibrium state. As a consequence the particle size gets determined by kinetic factors [52].

The polymerization process can be described qualitatively by the Candau–Leong–Fitch (CLF) model [258,259], depicted schematically in Figure 23. Polymerization is initiated either by entry of radicals into the primary microemulsion droplets (in the case of a water soluble initiator) or by decay of an oil soluble initiator. During polymerization, the nucleated particles can grow by transport of monomer through the water phase or by particle collision (Figure 23a). New active micelles are formed continuously throughout the course of the polymerization. Consequently no period of constant reaction rate can be observed. At the end of the polymerization, latex particles which are about 50% bigger than the initial monomer droplets coexist with empty micelles (Figure 23c).

The inherent instability of a polymerizing particle can be overcome by adding a cross-linking, bifunctional comonomer. This way microgels are formed, which cannot take up monomer by swelling. Recent experiments have demonstrated that the size of the microgel particles still depends on the absolute rate of polymerization,

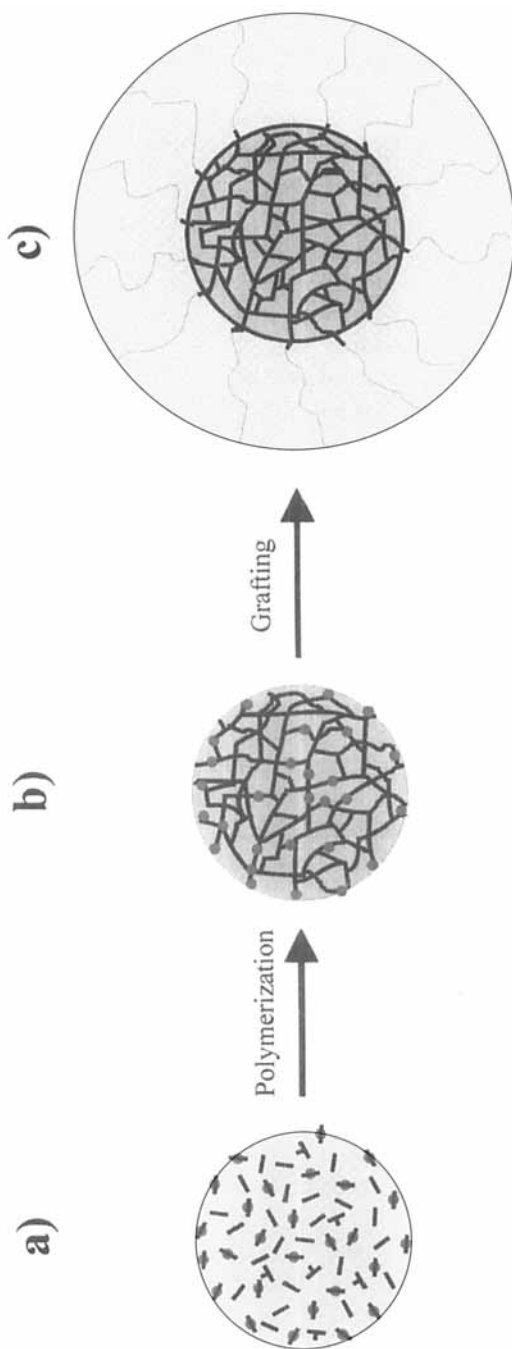


Figure 22 Sketch of the preparation of macromolecular core-shell particles via grafting of a monomer on a initiator-group containing a cross-linked core. (a) Mixture of monomer, cross-linker and azo-group emulsified in water. (b) Reactive cross-linked core. (c) Core-shell particle [254,255]

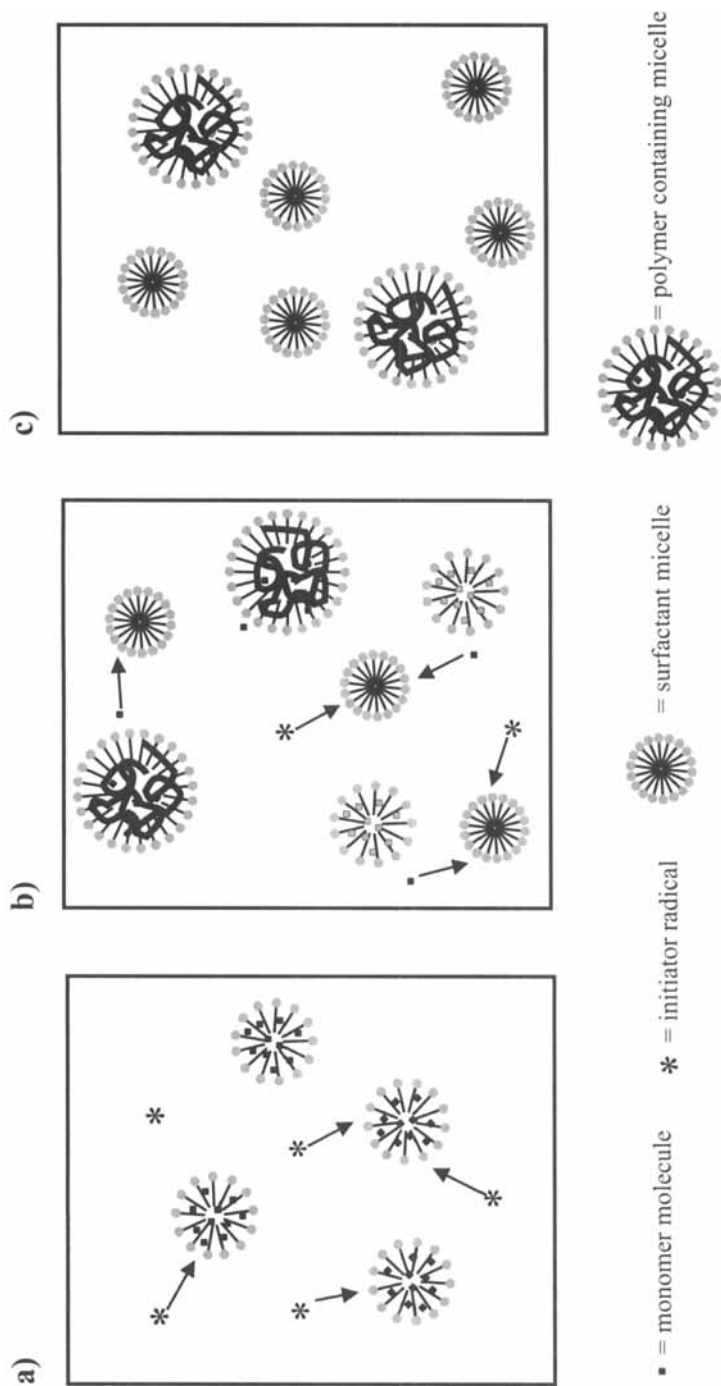


Figure 23 Diagram of the three intervals of micro-emulsion polymerization, according to Candau [258]

but the polydispersity of the particle diameters can be kept low ($\sigma < 0.3$) [52]. Apparently, the monomer transport into the active, monomer consuming particles, caused by the enormous difference in osmotic pressure, cannot completely be suppressed. Microgel particle radii down to 5 nm have been obtained [260].

Utilization of microgel particles has been proposed as colloidal drug carriers, highly functionalized polymer particles, and as calibration standards [4,261]. For many applications claimed for dendrimers, they represent a highly competitive alternative.

5. SUPRAMOLECULAR ORGANIZATION OF POLYMERS IN THIN FILMS AND AT SURFACES

Preparation and structure control of thin organic films involves a number of intriguing problems and challenges in supramolecular, as well as in macromolecular chemistry. This includes the tailoring of the interfacial interactions by suitable functional chemical groups to control the adsorption of the molecules and the stability of thin films. Lateral interactions within the organic layer provide a further means of controlling ordering and film formation. Furthermore, the fact that thin films possess a surface makes them accessible either for the purpose of characterization or as a platform on which other molecules can be assembled in a sort of molecular "Lego".

Characterization of surfaces and thin films has been revolutionized by the invention of scanning probe microscopes, i.e. scanning force microscopy, scanning tunnelling microscopy, and scanning near field optical microscopy [262–264]. These methods not only allow imaging of molecular and supramolecular details, but can also be employed to probe and to manipulate chemical properties on a nanoscopic or molecular scale, e.g., mechanical SFM [265], chemical SFM [266], electrochemical STM [267,268].

Utilization of thin organic films as a platform for defined supramolecular assemblies offers new perspectives as different chemical functionalities can be arranged in a lateral pattern. However, at the molecular or nanoscopic scale, this will only be possible by chemical strategies complementary and in combination with lithographic techniques for which the microcontact printing technique, developed by Whitesides, is a leading example [269–272,465,466]. Macromolecular chemistry can contribute to this task in several ways. Particular aspects are: the length scale spanned by a single macromolecule, the competition between segmental ordering and the entropically driven coiling limiting the size of ordered domains at the other domains, and the possibility of designing macromolecular architectures which are especially suitable for the formation of well-defined and stable thin films, e.g. macromolecular sheets, rods, disks and spheres [273–275].

Stability and formation of thin films has become an important issue of current activities in physics [276–279]. If the film thickness is below the bulk equilibrium

dimensions of the macromolecules, the necessary deformation results in a positive entropic contribution to the free energy [280,211]. A hard flat wall requires additional ordering and alignment of the molecular segments in its direct neighbourhood [281,282]. Furthermore, the stability of thin films is affected by long range van der Waals interactions across the film [283–286].

Under certain conditions, rather well-defined ring and honeycomb patterns can be formed by solution casting of thin films. Recently Nolte described the formation of isolated rings with diameters of several micrometers formed by stacked porphyrin molecules [287]. Phase segregation or eruption of gas bubbles was assumed to be responsible for the peculiar assembly of the “porphyrin wheels”. However, the regular shape of the solute molecules was also considered to be of crucial importance. Another example is the honeycomb pattern of star shaped poly(styrene)-block-poly(*p*-phenylene) films described by François [288]. In this case, the peculiar molecular shape was emphasized to be of crucial importance besides the proper choice of solvent and evaporation conditions [289].

It must be pointed out, however, that the formation of rings and honeycomb pattern is a consequence of the instability of thin films to convection, caused by the fast evaporation of the solvent [290]. It does not require complex shaped molecules or even depend on some molecular recognition process.

Ring formation occurs as the liquid film becomes unstable as its thickness falls short of a critical value upon solvent evaporation and holes form. The observed rim is caused by the de-wetting process. Occurrence, regularity and the size of the holes depends primarily on the interfacial energies and the viscosity of the liquid film [291–293]. An important aspect is also that the rings mark the contact line between the substrate air and organic film liquid film. Molecules, or even nanoparticles, can be adsorbed preferentially at the contact line during the process and thus get regularly arranged along this lines [294].

Formation of various patterns like the honeycomb structure mentioned above can originate from gradients in surface tension or density due to temperature variations caused by solvent evaporation. Both effects can produce convection instability, namely Marangoni [295] and Rayleigh [296] convection. In thin films Marangoni convection predominates.

If a film forming material is not homogeneous in its composition or contains amphiphilic molecules with groups of different affinity towards the interfaces, a thin film gets structured in such a way that the components orient themselves to the interfaces minimizing the interfacial energy, e.g. polar groups towards a polar substrate and non-polar groups to the air. On a smooth substrate incompatible polymer mixtures tend to form a lamellar structure [297,298]. Similarly the microdomains of block copolymers orient parallel to the surface [299–301]. Due to the surface–polymer interaction, layered structures can even be preferred, though copolymers exhibit different morphologies in the bulk [302]. Thus, a diblock copolymer with equally long constituent blocks which forms a lamellar morphology in the bulk, forms alternating layers parallel to the substrate with a periodicity equal to that of the bulk morphology [303].

If the amount of material for the film does not match the amount necessary for $L/2 + n \cdot L$ layers, with n being an integer, the top layer cannot become complete, resulting in holes with a depth equal to L (Figure 24a).

In the case that the film is constrained between the two flat surfaces whose distances does not match a length of $L/2 + n \cdot L$ the layers have to adjust in thickness, which requires some deformation of the coiled polymer conformation resulting in some penalty in the free energy. If the surfaces exhibit similar affinity to both blocks, the perpendicular orientation of the domains become more favourable because the elastic deformation is reduced (Figure 24b) [273–275,304,306,307]. A similar situation results if the film thickness becomes less than $L/2$. The polymer chains are deformed at the expense of an elastic contribution to the free energy to ensure maximum coverage of the substrate. In the case of block copolymers where the blocks are not equally long and which form a cylindrical bulk morphology it has been demonstrated that the cylinders get oriented perpendicularly to the surface in the case of ultrathin films (Figure 24c) [308,309].

A further example of surface induced morphology is observed when a substrate is covered by an ultrathin layer of a diblock copolymer containing one block which interacts selectively and strongly with the substrate, i.e. wets the substrate. This is demonstrated in Figure 25a for a poly(styrene)-block-poly(2-vinylpyridine) with two equally long blocks on mica. The amount of block copolymer was much smaller than required for covering the surface with a layered structure as shown in Figure 24a. In this case the poly(2-vinylpyridine) block gets tightly adsorbed resulting in an ultrathin layer with very small loops, which has a thickness of only about 1 nm. Because of the enthalpically unfavourable interaction between the chemically connected polystyrene and poly(vinylpyridine) the poly(styrene) dewets the adsorbate layer, several blocks aggregate into one cluster and form small nanoscopic islands of poly(styrene) (Figure 25c). Depending on the chain length and the interaction strength of the adsorbing block with the substrate, regular point or line patterns can be formed spanning a width of 80–500 nm [310,311].

Only recently first reports appeared describing the potential of the nanostructured thin block copolymer films for lithographic etching. A thin film of polystyrene-block-polybutadiene with a hexagonal cylindrical morphology where the poly-(butadiene) cylinders were oriented perpendicular to the substrate was deposited on a silicon wafer and selectively decomposed by treatment with ozone or converted with osmium tetroxide. By a subsequent reactive ion etching process the pattern could be inscribed into the surface of the silicon wafer yielding small holes or islands with a lattice constant of 27 nm and hole/island sizes of 13 nm [305,312].

In another report, a 50 nm thick poly(styrene-*b*-methylmethacrylate) block copolymer film with spherical domains was prepared on a sodium chloride monocrystal and coated by a thin layer of gold, replicating the domain pattern. Similar results were also obtained with poly(styrene-*b*-2-vinylpyridines) [113].

Nanostructured thin films can also be prepared by deposition of polymer micelles from solution. In the case of a short core block, the thermodynamic stability is little

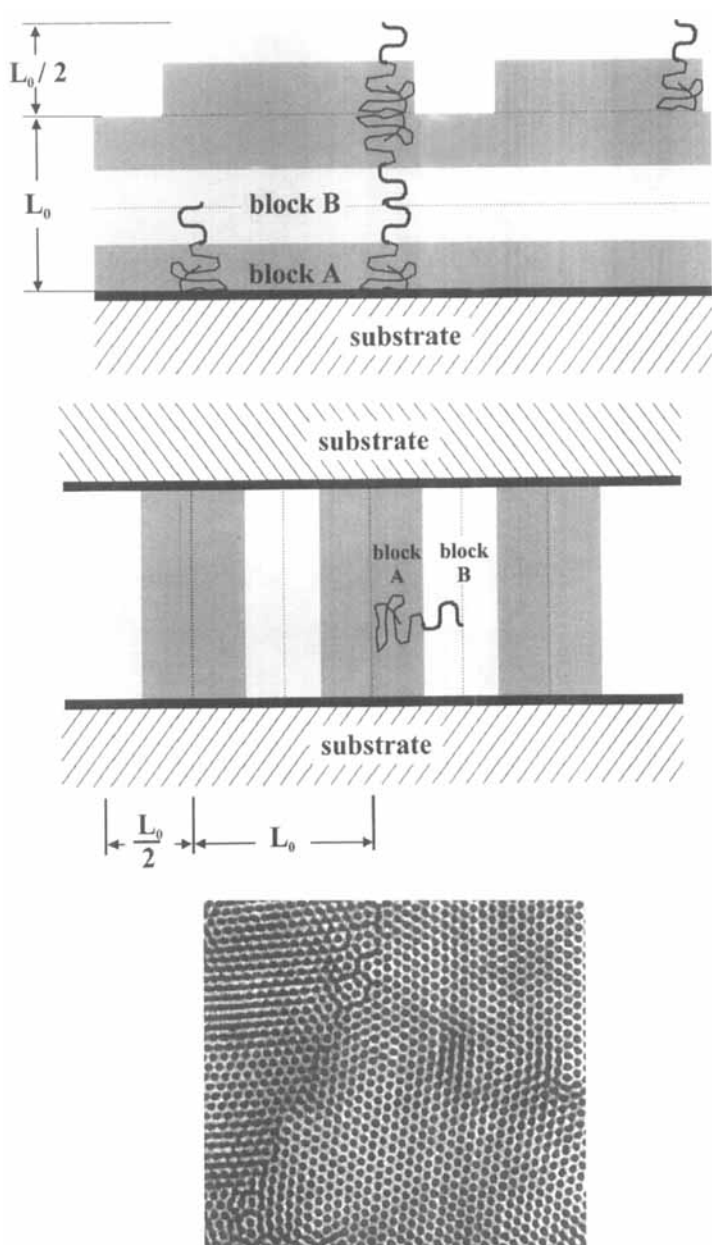


Figure 24 (a) Layered structures of AB diblock copolymers. (b) Vertical confinement causing the lateral orientation of block copolymer layers [304]. (c) Cylindrical morphology (cylinder diameter = 13 nm) [305]. Reproduced with permission from [305]. © 1996 American Institute of Physics

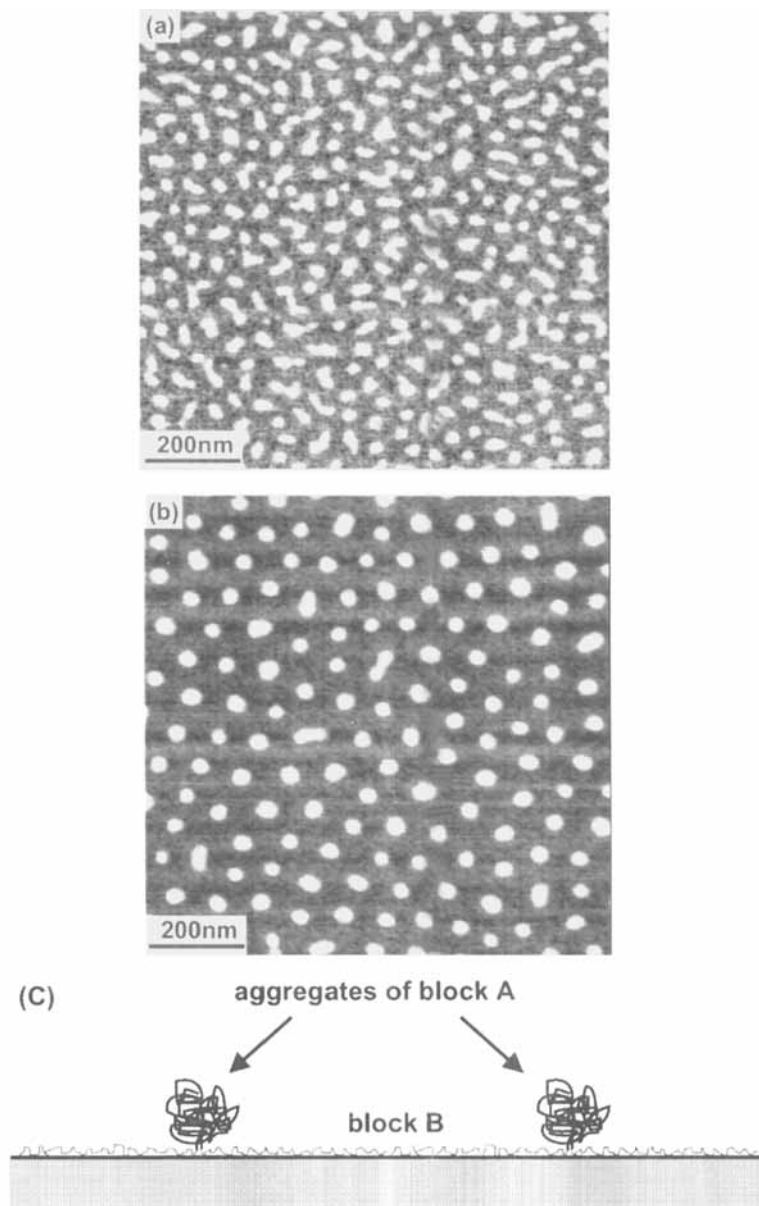


Figure 25 (a) Scanning force micrograph of a poly(styrene-*b*-2-vinylpyridine) copolymer thin film as cast on mica. (b) After annealing of the film, showing a regular arrangement of small poly(styrene) islands. (c) Because the amount of block copolymer is smaller than necessary to produce a closed layered structure, the poly(2-vinylpyridine) block, strongly adsorbed on mica, forms a very thin layer from which the incompatible poly(styrene) block segregates [310]

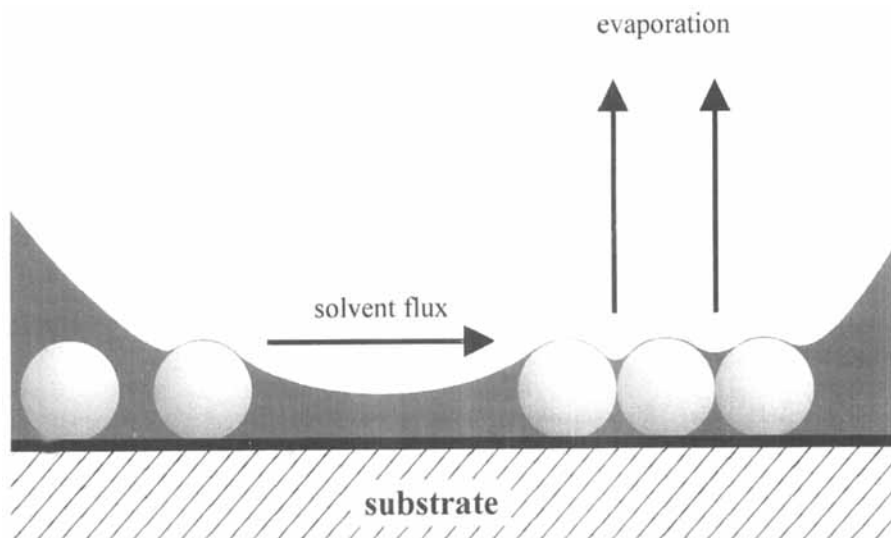


Figure 26 Formation of two-dimensional lattices of spherical particles like block copolymer micelles on a flat substrate [313]

effected by the evaporation of the solvent as the polymers adopt a spherical equilibrium morphology in the bulk (Figure 26 [88]). If the inner block is equally long or even longer than the outer block, the kinetic stability can be sufficient for the micelles to remain intact until the film vitrifies irrespective of the presence of the solvent. This requires high molecular weights and strongly incompatible blocks [213,311,314,315].

The peculiar aspect of these micellar films is their stability and easy preparation. Mono-micellar films are sufficiently thick to overcome van der Waals forces between the interfaces which might destabilize film formation [476]. Adsorption of the particles on the substrate and subsequent evaporation of the solvent gives rise to long-range capillary forces which act parallel to the substrate and drag the particles together [316]. As a result, well-defined regular films of block copolymers can be prepared by simple spreading, dipping or spin coating techniques where the film thickness and two-dimensional order is controlled by the concentration of the casting solution and, for example, by the rate with which a substrate is pulled out of the solution (Figure 27) [311,313,317].

A discussion on thin films must not omit multilayer films prepared by Langmuir–Blodgett techniques. The field of Langmuir–Blodgett films from low molecular weight amphiphiles like surfactants or lipids has been reviewed in a number of excellent reports [318,319].

A macromolecular chemistry contribution to this area concerns fixation of the layers by introduction of monomeric surfactants which can be polymerized in the

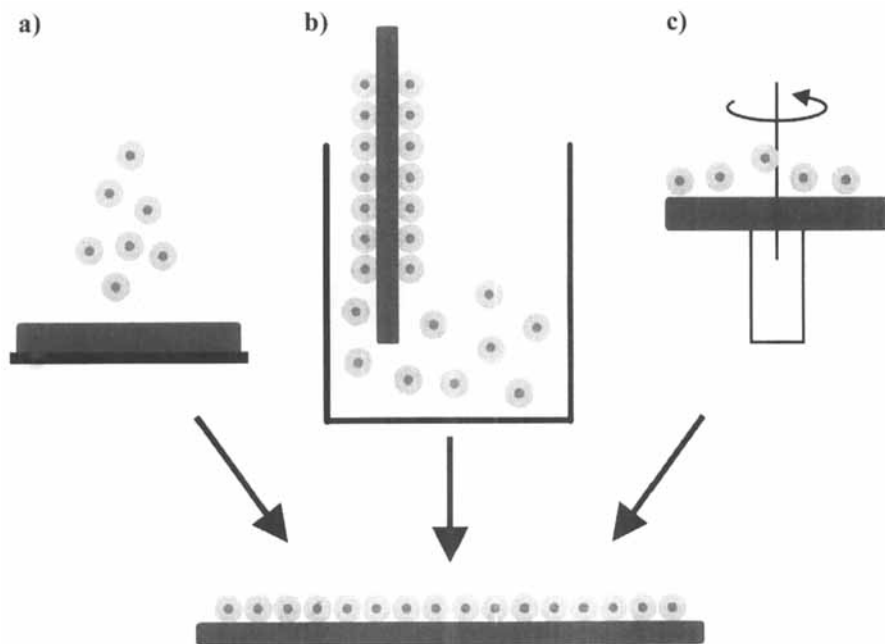


Figure 27 Sketch of the preparation of well-defined micellar monolayers by (a) spreading, (b) dipping/pull-casting, or (c) spin-casting-techniques

ordered state, e.g. by the incorporation of diene, diacetylene or (meth)acrylate units [320–327]. In this way it has been possible to prepare multilayered materials with excellent mechanical stability. Model studies on membranes and vesicles have also been performed, in which functional groups like biological receptor molecules can be incorporated [328,329]. In addition, functional guest molecules have been included in the layers exhibiting e.g. non-linear optical effects [330,331,332]. Recent reviews, describing the field of surface organized assemblies including supramolecular polymeric systems can be found in [333,335].

Another original macromolecular contribution for the preparation of highly defined multilayer structures is the preparation of Langmuir–Blodgett films with “hairy-rod” macromolecules. “Hairy rods” consist of a polymer backbone of high conformational rigidity, e.g. poly(phthalocyaninosiloxanes) [336], poly(glutamates) [45], cellulosis [337], poly(isocyanides) [338], poly(4-hydroxybenzoic ester) or poly(phenylene), all bearing flexible alkyl- or oligoglycoether side chains. These “hairs” are necessary in order to achieve sufficient solubility in common solvents [324]. The polymers are spread on a water surface in a solution of a volatile solvent. Upon compression of the film the rod-like molecules order nematically. Transfer to a substrate introduces a macroscopically uniform orientation along the drawing direction (Figure 28) [324]. Multilayer-formation and incorpora-

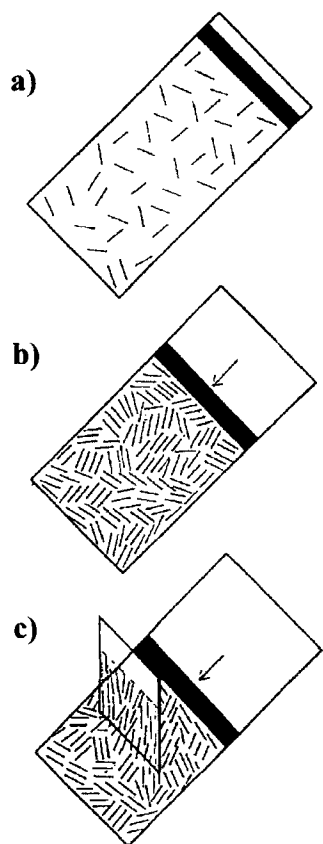


Figure 28 Sketch of the formation of Langmuir–Blodgett films using rod-like polymers.

(a) Rods-like molecules on the water surface. (b) Formation of nematically ordered domains by compression of the film. (c) Transfer of the macromolecules to the substrate and orientation in drawing direction [324,462]. Reproduced from [462] with permission of Elsevier Science

tion of guest molecules within the layers is easily possible [335] and the macroscopic orientation during the processing allows the preparation of well-ordered anisotropic films [335,339].

A very versatile approach to the formation of multilayer films has been developed by Decher, based on polyelectrolytes. If a solid substrate with ionic groups at the surface is dipped into a solution of a complementary polyelectrolyte, an ultrathin, essentially monomolecular film of the polyion is adsorbed [340]. The adsorption is based on pairing of surface bound ionic sites with oppositely charged ions, bound to the macromolecule. The polymers adsorb in an irregular flattened coil structure and only part of the polymer ions can be paired with the surface ions (Figure 29a). Ionic sites which remain with small counterions provide anchor points for a next layer formed by a complementary polyelectrolyte [342,343]. This way multilayer polyelectrolyte films can be prepared “layer-by-layer” just by dipping a suitable substrate alternately in an aqueous solution of polyanions and polycations. The technique can be employed with nearly all soluble charged polymers and results in films with a

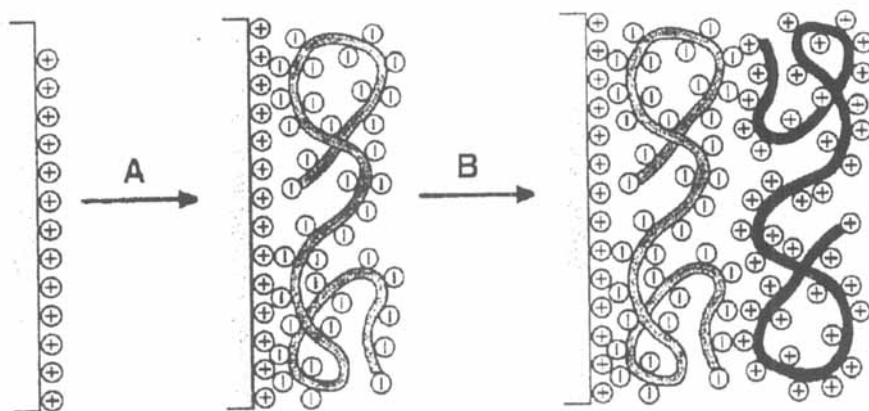


Figure 29 Self-assembled polyelectrolyte thin film via the “layer-by-layer” adsorption technique [341]. With permission of Elsevier Science

regular layer thickness (Figure 29b) [341]. The films adhere strongly to the substrate and can even undergo reversible swelling when they are immersed in aqueous solution of different ionic strength [343].

As most material surfaces have anionic surface charges, a large variety of substrates can be employed. In many cases the “layer-by-layer” adsorption technique provides an alternative for Langmuir–Blodgett films [344–347]. Multilayered polyelectrolyte films have been prepared with biopolymers like DNA and proteins [342,348–350] as well as with inorganic macromolecules [351]. Even charged viruses have been assembled in alternating layers of polyelectrolytes [352]. Another interesting example is composite films with an electrically conductive polymer, i.e. poly(para-phenylene-vinylene), PPV. A cationic PPV-precursor was deposited in alternating layers with an anionic polyelectrolyte (cellulose sulfate or poly(vinyl-sulfate)). Afterwards the multilayer film was thermally converted to a poly(para-phenylene-vinylene) composite [341].

6. SUPRAMOLECULAR CHEMISTRY CONCEPTS WITH MACROMOLECULES

Lately many new approaches have been reported which concern supramolecular chemistry concepts with high molecular weight macromolecules. A strong influence on these developments which can only be discussed by a few examples was exerted by the synthesis of cascade type dendrimers already mentioned above [15,23–25]. A typical supramolecular approach in this field is the preparation of metallodendrimers reported by Reinhoudt *et al.* where the monomer units have been linked by non-

covalent palladium-complexes with a tridentate sulfur-carbon-sulfur (“SCS”) pincer type ligand (Scheme 1).

The fourth coordination site at the palladium centre is used to bind the next monomer via coordination of a nitrile group. Formation of the metallo-dendrimer was achieved in a step-by-step one-pot procedure with the α,α' -bis-(3,5-bis(phenylthiomethyl)phenoxy- α -cyanomesitylene (BB-Cl) in which the fourth Pd-coordination site is protected by a chloride-ligand. Activation is performed by removing the chloride-ligand with AgBF_4 [353,354]. Balzani reported the preparation of coordination complex dendrimers with Ru(II) and Os(II) based on 2,3-bis(2-pyridyl)pyrazine ligands (Scheme 2) [355,356]. Dendrimers, self-assembled via hydrogen-bonds have also been described [357,358].

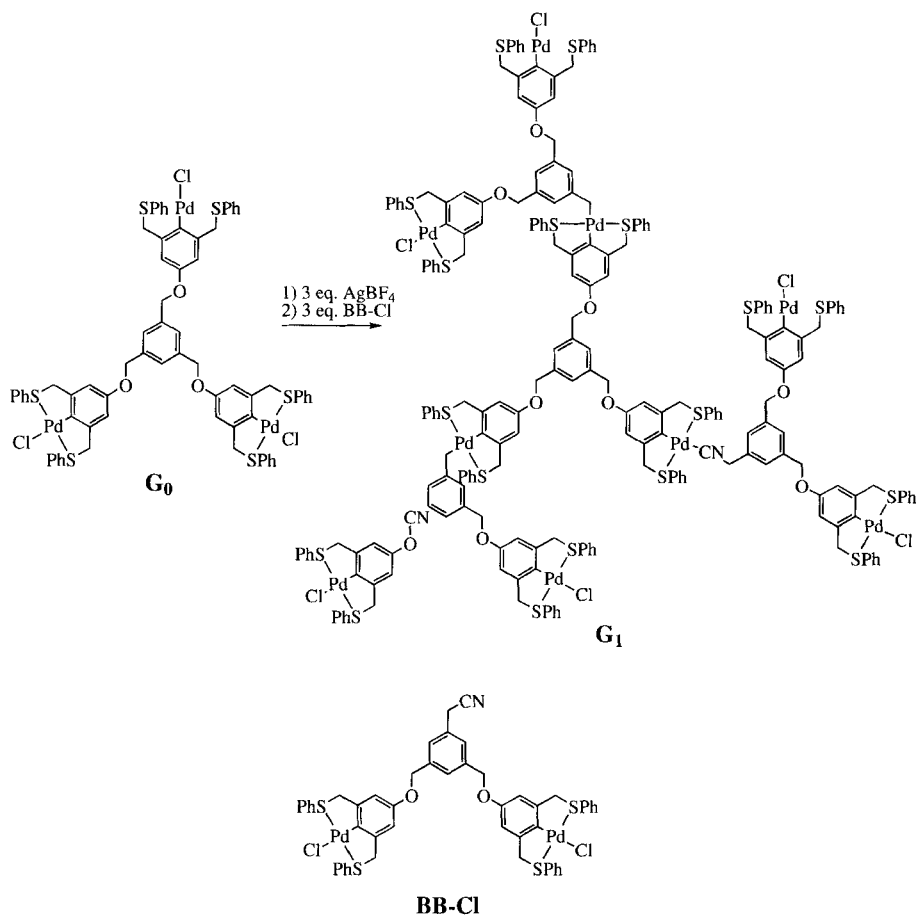
Besides the divergent synthesis where the molecules are built up shell-by-shell starting from the centre, a convergent approach has been developed in which wedge like subunits, so called “dendrons”, are employed. The dendrons are prepared first and become assembled to the final dendrimer via a multifunctional core (Scheme 3) [15,359]. The dendrons are versatile building blocks for molecules with a distinct tertiary structure (Scheme 4).

Structural features of a dendron are the rather soft geometrically defined shape, the definition of an outer rim B and a terminal (inner) functional group A (Figure 30). Whether or to what extent the dendron adopts a wedge like conformation depends only partially on the rigidity of the subunits but mostly on the sterical constraints by the surrounding.

This adaptability or softness of the cascade type dendrons represents peculiar perspectives for the formation of supramolecular structures related to the well-known quasiequivalency in biomolecular systems. Quasiequivalent building blocks are chemically identical subunits which can switch between different conformational states [9]. Examples are the protein coats which jacket a nucleic acid during self-assembly of rod like and icosahedral viruses [11–13]. By attaching rather soft or flexible monodendrons with one to three alkyl chains as terminal units to a flexible macromolecular backbone, Percec *et al.* demonstrated that this principle can be transferred to synthetic polymers. Depending on the degree of polymerization spherical or cylindrical macromolecular substructures were formed [360,361]. This change in shape is accompanied by a change in backbone conformation from random coil to extended [362,363] (Figure 31). Preparation of rod-like poly(phenylenes) with Fréchet type dendrons of the first and second generation was recently described by Schlüter [364–367].

A completely different, nevertheless intriguing concept, for the jacketing of a macromolecular chain has been developed based on rotaxane complexes. In a rotaxane a macrocycle is thread on a linear molecule [368]. If the ends of the linear molecule get blocked by sterically demanding substituents, both molecules are permanently linked without formation of a direct chemical bond [368–370].

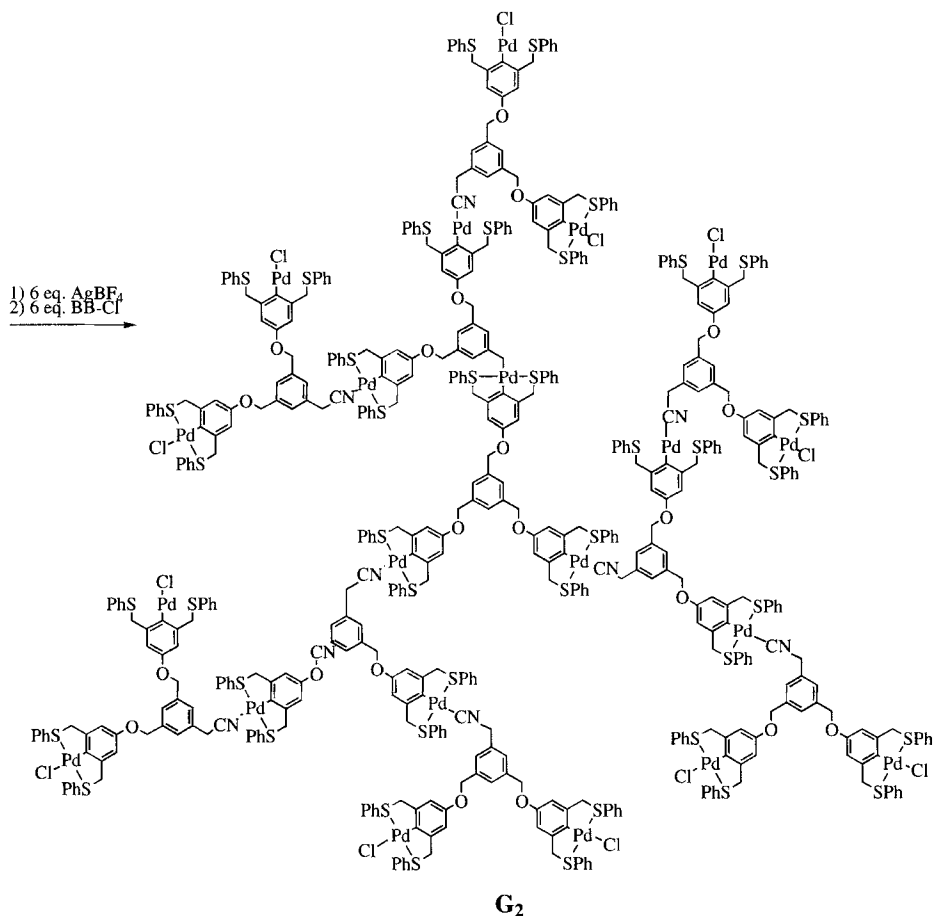
In polyrotaxanes, a large number of macrocycles are thread on the macromolecular chain. The rings can only move along the backbone and therefore are confined



Scheme 1

in a one-dimensional space [371]. Cyclodextrines (i.e. cyclic oligosaccharides consisting of six (α -CD), seven (β -CD) or eight (γ -CD) glucopyranose-units [372]), have been used frequently for the formation of polyrotaxanes. Two strategies have been described to thread the rings on the polymer backbone: in the first approach macrocycles are mixed with suitable macromolecules and the polyrotaxanes form by themselves [373,378]. Due to the sequential threading process, the complex formation requires an increasingly longer time, the higher the degree of polymerization of the macromolecule chosen [377] (Figure 32).

A second route to polyrotaxanes is the polymerization of monomeric rotaxanes. This synthesis is only possible if the lifetime of the monomeric rotaxane exceeds the time required for the polymerization. The polymer can be formed by radical

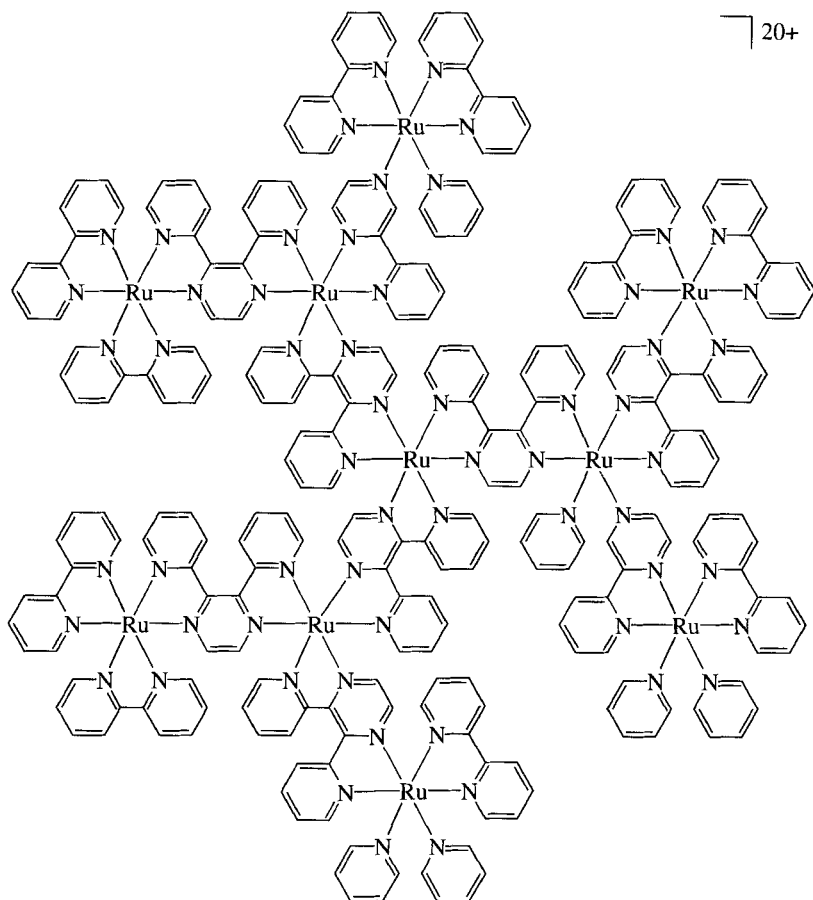


Scheme 1 (continued)

polymerization [379], inclusion polymerization [380] or polycondensation [381,382], but defined, soluble adducts have only seldomly been obtained [383].

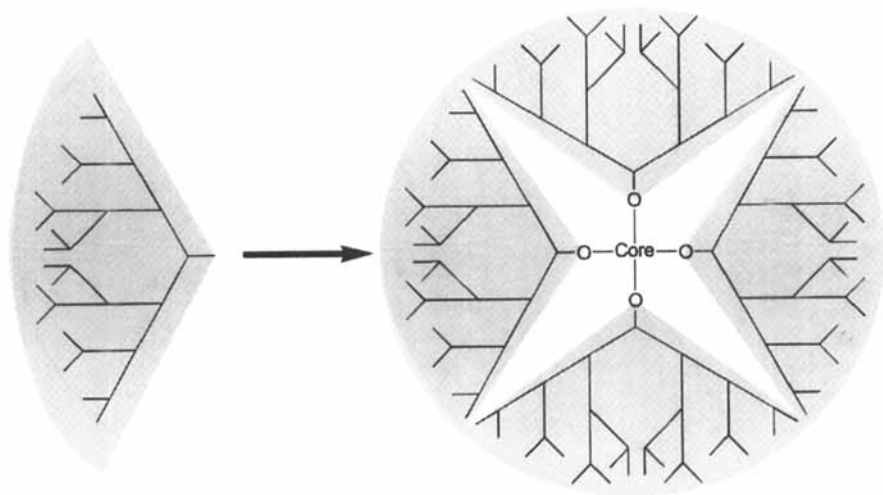
Harada linked the threaded α -cyclodextrines of poly(ethyleneoxide)/ α -cyclodextrine-rotaxanes with epichlorohydrin. After removing the poly(ethyleneoxide)-template, he obtained tube-like carbohydrate compounds [376]. Similar attempts have also been reported with β - and γ -CD [378,384].

“Pseudo” polyrotaxanes consist of low molecular weight rotaxanes which can assemble via non-covalent interactions. An illustrative example has recently been described by Stoddart, using a tetra-cationic bis(bipyridyl-phenyl)-cyclophane as macrocyclic ring component and phenylene-1,4-bis(oxy-oligoethyleneoxy)- ω -carboxylic acid [385].

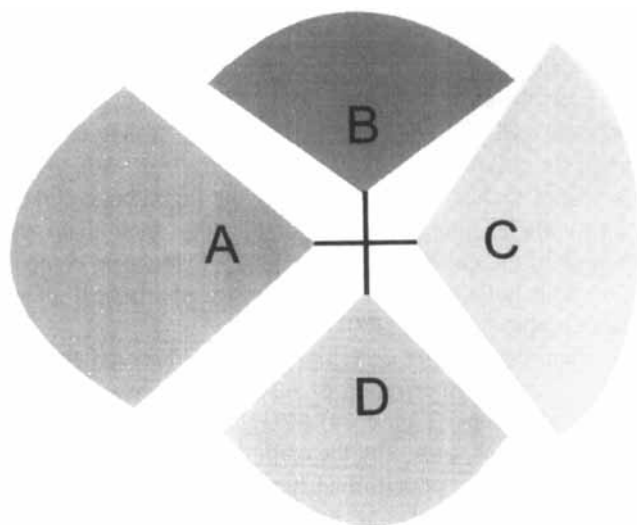


Scheme 2

Another again, completely different, concept for the jacketing of a linear macromolecule is based on the formation of acid–base complexes of a low molecular weight compound with macromolecules. A prominent example are complexes of camphor sulfonic acid or dodecyl sulfonic acid with poly(aniline) (Figure 33) [386–389]. Poly(aniline) and its conducting form the “emeraldine salt” are intractable and in most solvents insoluble materials. When the protonating counterion, however, acts simultaneously as a surfactant, miscibility with a large number of organic solvents and even some polymers can be achieved allowing film formation and melt processing. Together with the inherent chemical stability this results in an outstanding position of poly(aniline) as an electronically conducting polymer [389,390–394].



Scheme 3



Scheme 4

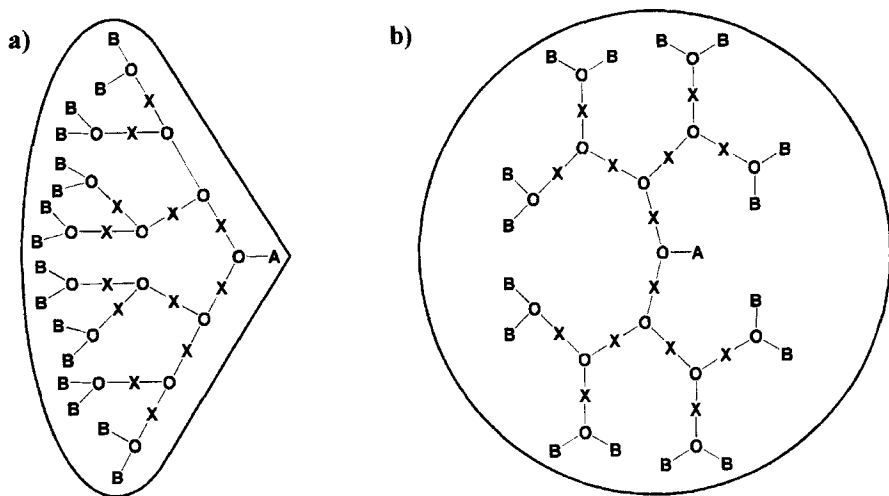


Figure 30 Second generation dendron in (a) a wedge like conformation and (b) in a more spherical open shape

Recently it even was possible to obtain optically active poly(aniline) complexes with a helical secondary structure using (+)- and (-)-camphor sulfonic acids [395].

The sterical crowding of the complexing units causes the transformation of the macromolecular conformation from a statistical coil into a semiflexible rod and induces the occurrence of a lyotropic liquid-crystalline order [388]. Stiffening of a macromolecular chain by sterically demanding side chains and the formation of liquid-crystalline order has been described for a number of similar acid-base and polymer/surfactant complexes, i.e. poly(vinylpyridines) and Nylon-6 complexed with zinc dodecylbenzene sulfonate [396,397], pentadecylphenol [398], dodecylbenzene sulfonic acid [399] or lauryl gallate [400]. Near-to-complete stretching was also observed for poly(ethyleneoxide) upon interaction with sodium dodecylsulfate [401]. Theoretical studies demonstrated how the liquid-crystalline order depends on the degree of complexation of the macromolecules, their chain length and also the molecular mass of the complexing agent [402]. Systematic comparison of different surfactants and phenolic cosurfactants demonstrated a critical interaction strength to induce mesomorphic ordering [400].

Lyotropic liquid-crystalline ordering was also observed for cylindrical brushes formed by the homopolymerization of macromonomers, i.e. macromolecules with polymerizable endgroups (Figure 34) [403]. The extended conformation of these cylindrical brushes is controlled by the coiling and steric repulsion of the side chains and is independent of the unperturbed flexibility of the backbone segments [402].

A further example for jacketing macromolecules by complexation refers to the work of Nolte who has developed a “molecular clip” based on diphenylglycoluril

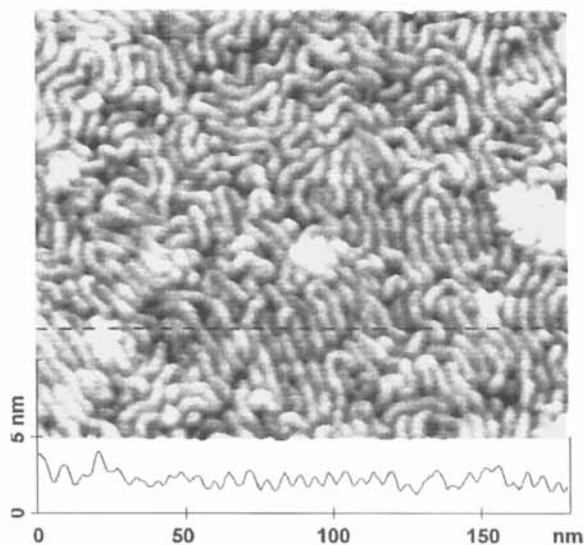
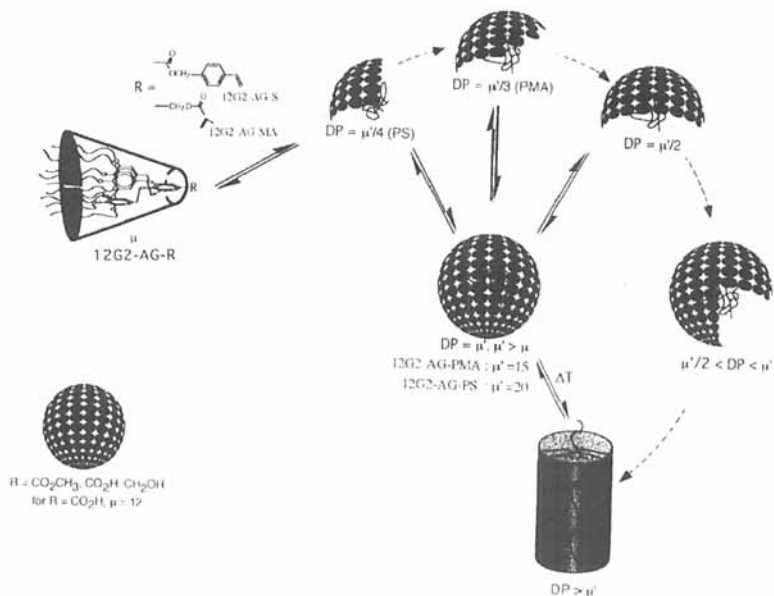


Figure 31 (a) Controlling the secondary structure of a linear macromolecule by quasi-equivalent side groups. Three dimensional scanning force microscopy images of monolayers of (b) high molecular weight ($M_w = 440.110 \text{ g/mol}^{-1}$) 12G2-AG-PS and (c) low molecular weight ($M_w = 14.680 \text{ g/mol}^{-1}$) prepared by spin casting from cyclohexane and chloroform solutions respectively. The cross-sectional height profiles of the monolayers were recorded along the reference lines in (b) and (c) [363]

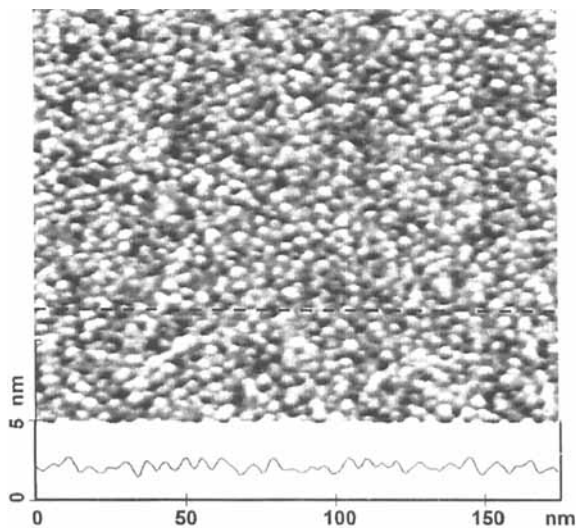


Figure 31 (continued)

building blocks. These molecules complex, i.e. “clip” to suitable electron-deficient aromatic units in a sort of sandwich structure. If they get bound to a macromolecular chain, as in the case in poly(styrene-co-3,5-dihydroxystyrene) or poly(styrene-co-4-hydroxystyrene-co-4-(3,5-dihydroxy-1-carboxyl-oxy)-styrene) a sterically crowded situation occurs and liquid crystalline order (Figure 35) is induced. Also in this case it is indicated, how recognition processes on a molecular level can generate a macroscopic effect [287].

Controlled formation of highly defined macromolecular superstructures by hydrogen bonding is of paramount importance for biopolymers. In the world of synthetic polymers, examples are very limited and the rational design of higher macromolecular structures based on hydrogen bonding is perhaps one of the most difficult tasks in macromolecular chemistry. This is because of: the relatively small bond strength which requires multiple cooperative bonding for the formation of stable structures; the directed nature of the hydrogen bonds which requires a considerable preorganization of the molecular conformation, in particular in the case of macromolecules undergoing multiple bonds, and the hydrogen bonds have to be shielded against interaction with polar low molecular weight compounds like water by a non-polar jacket around the binding site.

Developments in supramolecular chemistry provide a number of very intriguing examples of rather complex, but nevertheless well-defined, hydrogen bonded superstructures which present new building blocks for conjugation with macromolecular systems. Figures 36a and b give two examples of finite assemblies based on

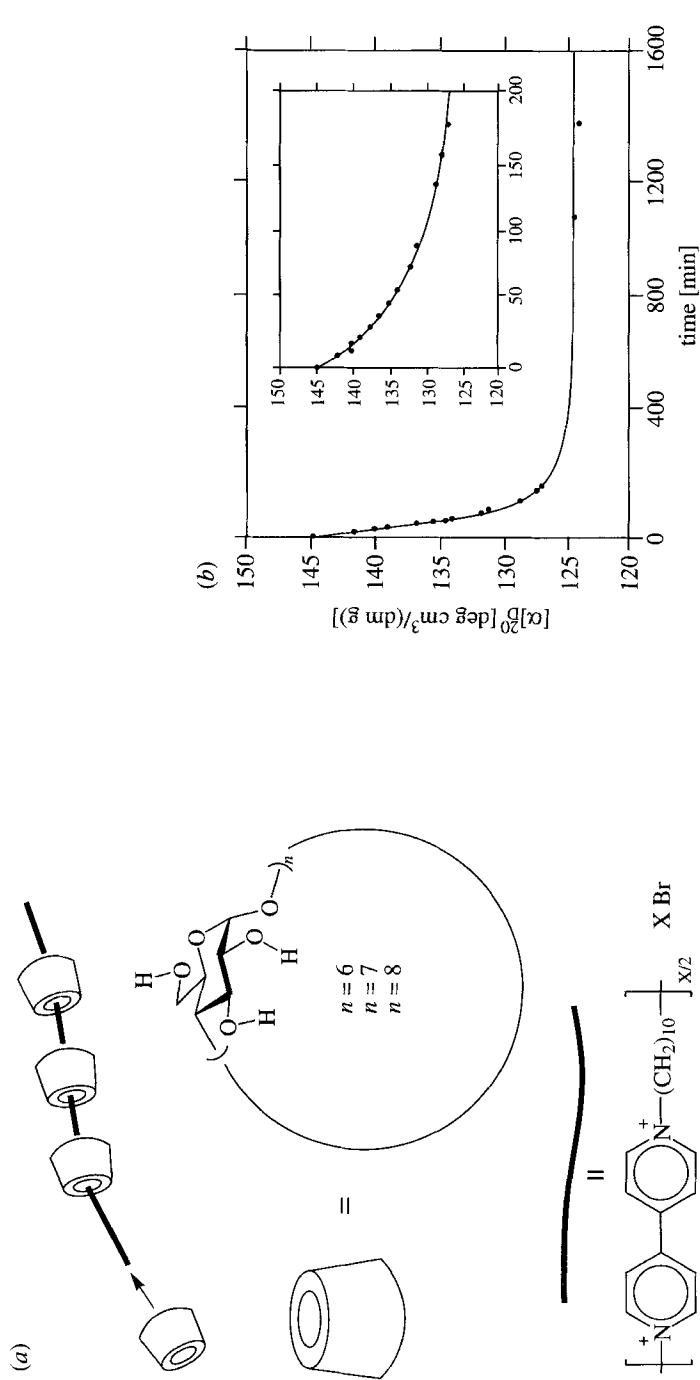


Figure 32 (a) Preparation of polyrotaxanes by threading of α -cyclodextrine on the macromolecular chain. (b) Rate of threading as determined by optical rotation dispersion of the cyclodextrine [378]. Reproduced from [378] with permission. © 1996 American Chemical Society

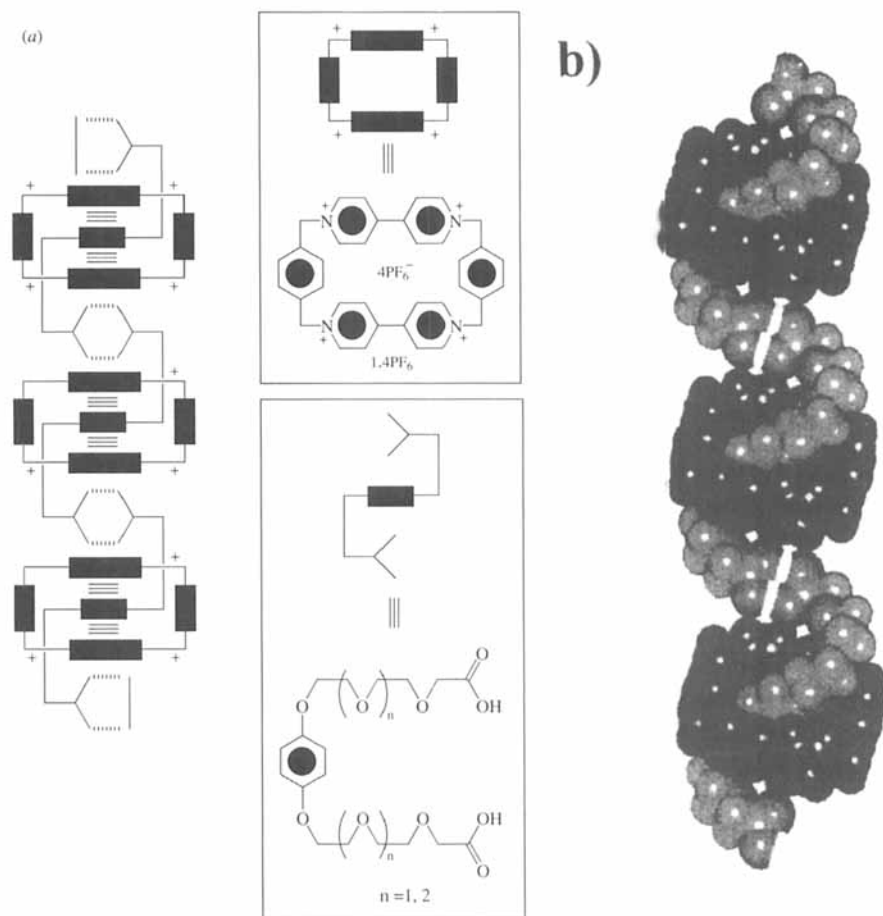


Figure 33 (a) Sketch of a pseudo-polyrotaxane from a bis(biphenyl-phenylene) cyclophane threaded on phenylene-1,4-bis(oxy(oligoethylenoxy)carboxylic acid). (b) Space filling model, calculated from crystal structure data [385]. With permission of Wiley-VCH

hydrogen bonding. Combination of three barbituric or cyanuric acid and three melamine units gives cyclic hexameres, so called rosettes (Figure 36a). The cyclic structure is stabilized by 18 hydrogen bonds [272,405]. Hexameric hydrogen-bonded assemblies of isophthalic acid derivatives were described by Hamilton [406]. Bulky substituents at the 5-position of isophthalic acid disrupt linear packing and prefer the ring formation (Figure 36b).

Discussing finite assemblies, one may not forget the nanogrids developed by Lehn. Complexation of multi-binding site ligands containing catenated bipyridine

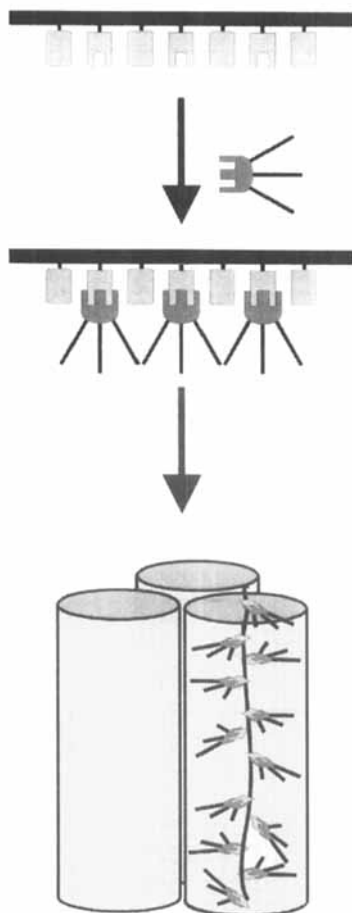


Figure 34 Jacketing of a macromolecule by “molecular clipping” induces a mesophase via steric overcrowding [287]

phenanthroline and pyrimidine units with metal ions yielded a series of different racks, ladders and grids like the 3×3 grid shown in Figure 36c. Spontaneous formation of the closed structure is ensured by the rather strong complexation [407].

Modification of macromolecular material properties by hydrogen bond formation has been demonstrated at the example of thermoreversible networks: Stadler modified poly(butadiene) elastomers with urazole groups to introduce hydrogen-bonded cross-links into the system. In fact, thermoreversible cross-linking appeared due to the urazole–urazole molecular recognition, causing intermolecular cross-links [408,467]. The group of Meijer expanded the approach by the synthesis of two

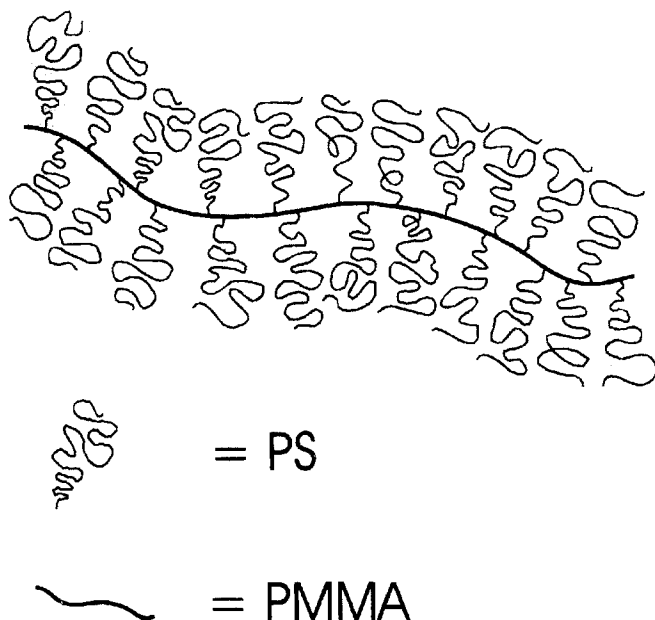


Figure 35 Sketch of a “brush-polymer”, illustrating the sterical overcrowding of the side-chains to force the macromolecular backbone into a stretched conformation [404]

complementary copolymers, one of them containing 2,4-diamino-1,3,5-triazine units, the other one bore maleic-imide groups (Scheme 5). Blending of the two copolymers yielded a material behaving like an highly cross-linked resin. The occurrence of defined 1 : 1 intermolecular maleic-imide : triazine hydrogen-bonded complexes was proven with NMR-spectroscopy [409,410]. In a second series of experiments, the maleic-imide containing polymer was doped with melamine. Though melamine is quite insoluble in organic compounds, the melamine was found to be molecularly dissolved in the polymeric matrix, up to a content of 20wt%. This was explained by participation of the melamine molecules in triple-hydrogen bonded complexes, linking together the imide-containing macromolecules [409]. Rather well-defined intermolecular links of high stability can be formed by the self complementary unit **1** (Scheme 5) for which the dimerization constant in chloroform was reported to exceed 10^6 .

Recently, alkyl chain substituted main chain poly(hydrazides) were synthesized, exhibiting a hexagonally ordered columnar mesophase. In this polymer always two hydrazide-monomers are jointed together via hydrogen bonds and consequently the compound has to be considered as a thermoreversible highly cross-linked network [411].

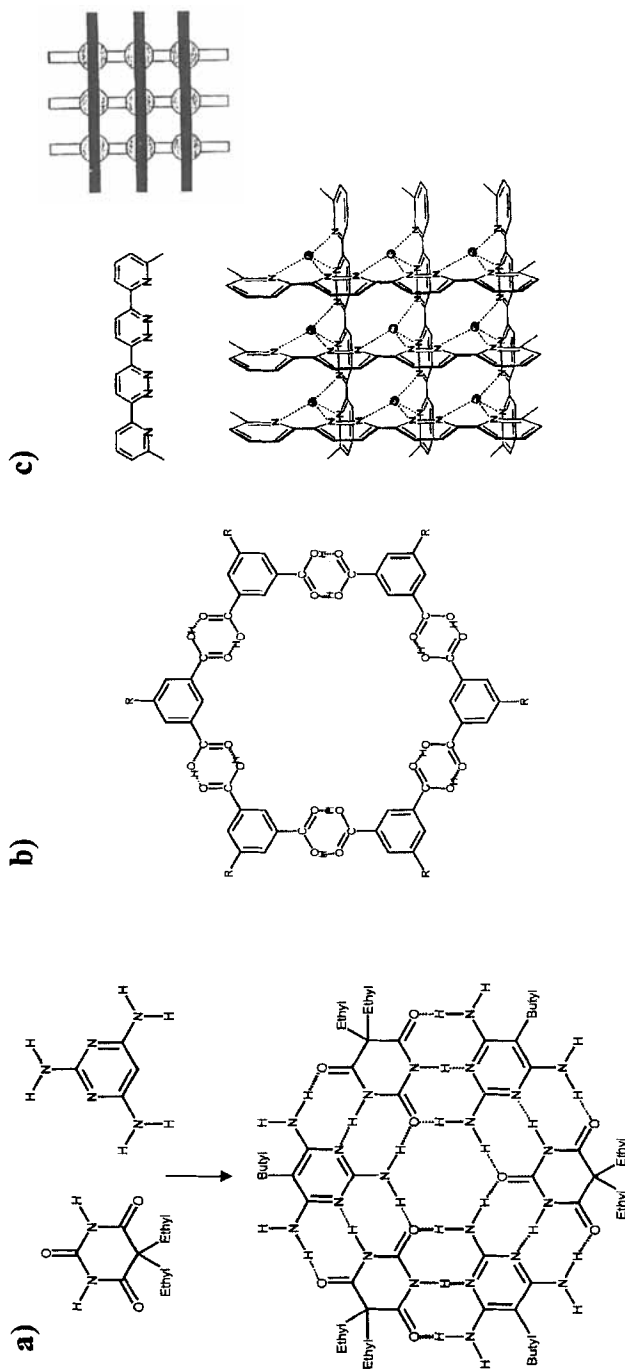
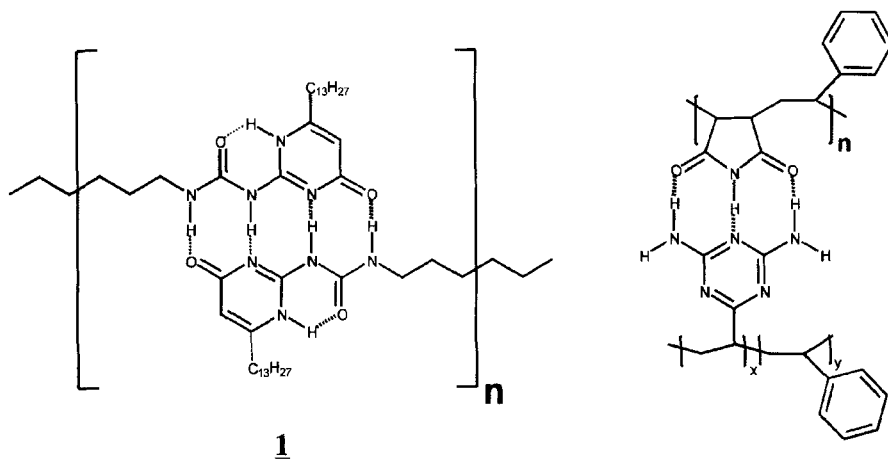


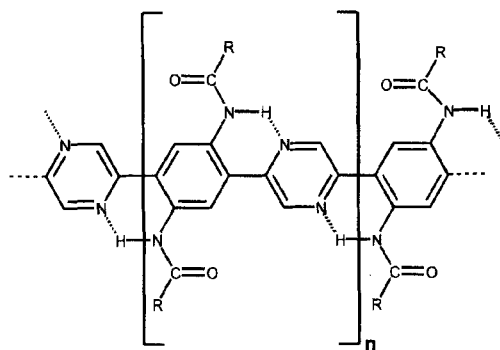
Figure 36 Supramolecular assemblies of finite size: (a) "rosettes" from melamine and cyanuric acid [272,405]. (b) Cyclic hexamers from isophthalic acid bearing bulky substituents in 5-position. (c) "3 x 3" grid from metal-complexed biphenyl phenanthrolines [407]. With permission of Wiley-VCH



Scheme 5

Also a π -conjugated polymer with intra-chain hydrogen bonds has been synthesized. The polymer contains aromatic nitrogen atoms in one monomer and an amide group in every subsequent unit. The hydrogen bonds between the amide and aromatic nitrogen forced the macromolecular backbone in a planar and rigid ladder structure, increasing the conjugation length of the fully aromatic polymer (Scheme 6) [412].

The examples discussed above refer to finite assemblies or conjugates with linear macromolecules. Based on the pioneering work by Jean Marie Lehn a number of approaches have been developed in which secondary bonds are employed to build up chain molecules. Different supramolecular chain polymers, made up from hydrogen-



Scheme 6

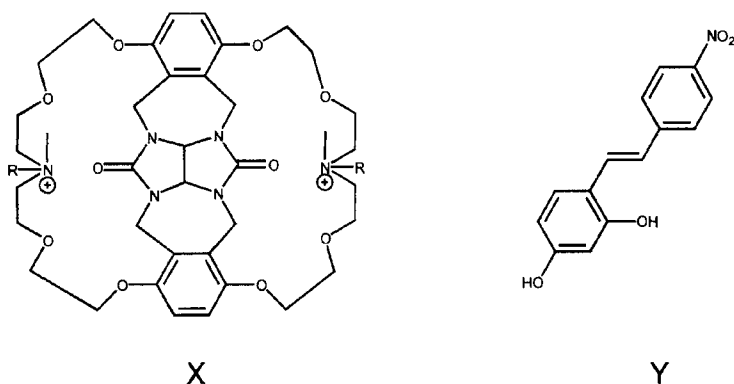
bonded units were reported [370,385,413,414]. Similar to the metal complexes shown in Figure 36c, two- and three-dimensional hydrogen bonded association polymers have been found [415–417]. Substitution of the outer periphery of β -cyclodextrines by nitrophenol has been used to obtain an association polymer as the β -cyclodextrines forms stable inclusion complexes with nitrophenols [418].

A great variety of self-assembled supramolecular structures can be found in “supramolecular gels”. Association of low molecular weight compounds in a topologically defined way yields long fibres with often well defined diameters [420]. An amazing variety of very complex superstructures has been described, i.e. rods and tubes formed from concentric or would up lamellae, helices, or braid-like structures. In all cases we can assume a hierarchy of superstructures which ultimately link the molecular structure to the nanoscopic assembly. However, this has only been investigated in detail in a few cases so far.

Most frequently, the formation of such supramolecular gels is observed upon cooling aqueous solutions [419–423]. In Figure 37a self-assembled thin fibres of a carbohydrate substituted porphyrin are depicted, while Figure 37b shows a multi-layered fibre of a octylmannonamide [424].

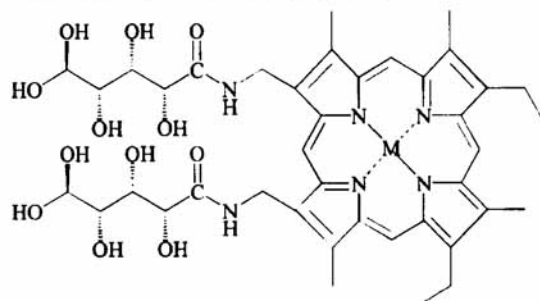
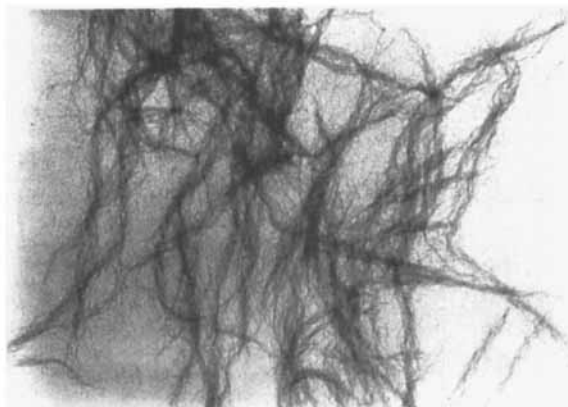
Fibrillar superstructures were also obtained when the amphiphilic diphenylglucosuril X was used to complex magnesium, Y, by clipping onto the dihydroxyphenyl unit. The clip molecules X formed globular associates, which transformed to nanotubes upon complexation of Y [426,427] Scheme 7.

Due to the lack of the “hydrophobic effect” [428] the formation of well-defined aggregates from organic solvents, “supramolecular organogels”, is observed less frequently (Figure 37c and 37d) [429–432]. Formation of “association copolymers” has been reported upon cooling mixtures of triaminotriazines with barbituric acid derivatives in an organic solvent. The fibrillar morphology and gelation is supposed to originate from intermolecular hydrogen bonding between the triazine and the barbituric acid [433]. Another very beautiful example is the stacks of cyclic peptide



Scheme 7

a)



b)

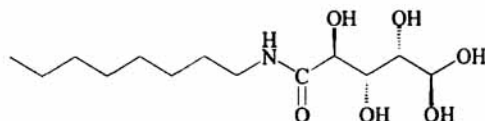


Figure 37 Electron micrographs of self-assembled fibres. (a) Porphyrine-fibres with a diameter of 6 nm. (b) *N*-octyl-*D*-mannonamide multilayered fibre, negatively stained with phosphotungstate, the central dark hole has a diameter of 50 nm. (a) and (b) were obtained from aqueous solution [424].

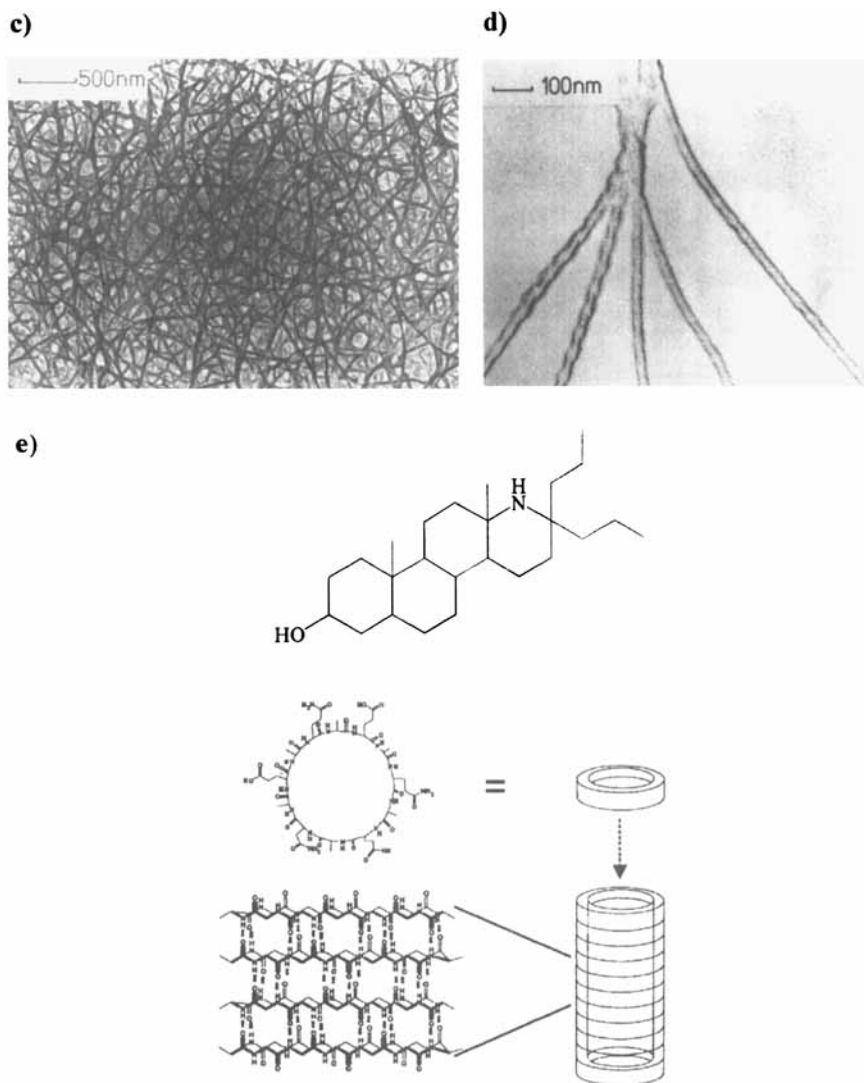


Figure 37 Electron micrographs of self-assembled fibres. (c) Electron micrograph showing the dense network of long helical fibres in a steroid/cyclohexane organogel. (d) Preparation of single fibres, demonstrating their helical superstructure [425]. (e) Cyclic oligopeptides, self-assembling into nanofibres [435,436]. Reproduced with permission of The Royal Society of Chemistry and The American Chemical Society. Parts (c) and (d) © 1986 American Chemical Society

structures of alternating D- and L-amino acids, which have been shown to stack to nanotubes of micrometer length [434]. These nanotubes were incorporated into lipid bilayers and shown to be capable of transporting sodium and potassium ions through the membrane (Figure 37e) [435,436].

As a final example of a highly defined supramolecular assembly, the mushrooms of S. Stubb have to be mentioned. “Miniaturized” triblock copolymers with the sequence $A_nB_nC_{9-n}$ have been prepared from stiff aromatic polyester segments A, a polystyrene segment B and a short polyisoprene chain C. The polyester block is highly incompatible with the other constituents and crystallizes. As a consequence, the molecules have to assemble in layers. Although not fully understood, this occurs in small very well-defined nanodomains giving rise to the mushroom-like superstructure of about $200\,000\text{ g mol}^{-1}$ depicted in Figure 38. Optically transparent thin

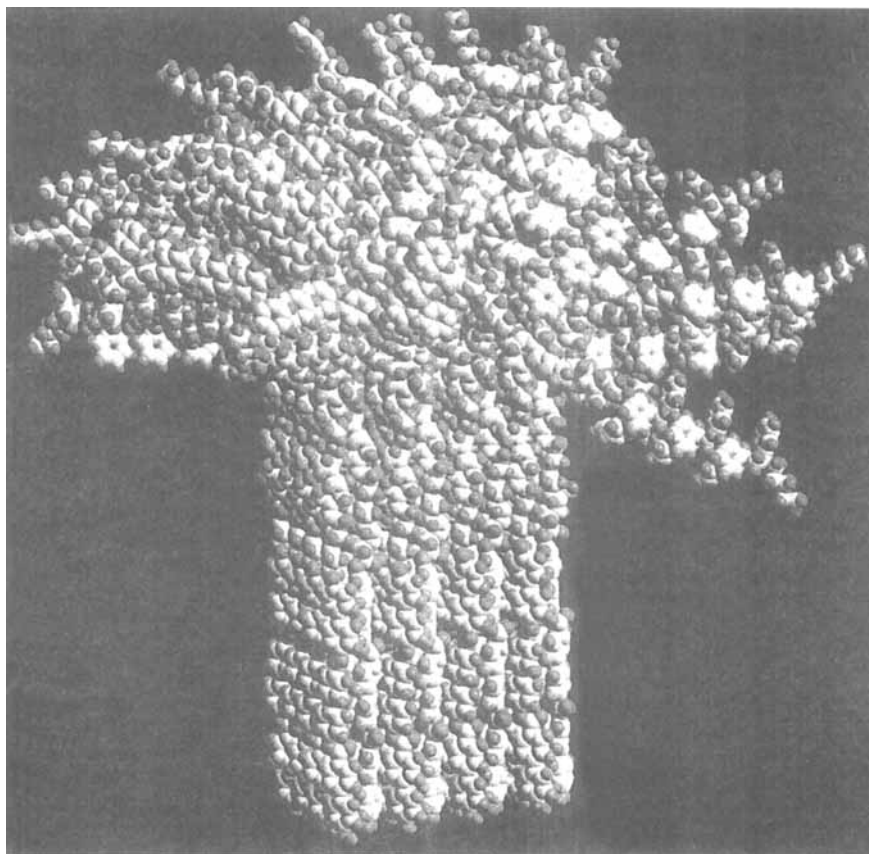


Figure 38 Self-assembled “molecular mushrooms” from miniaturized ABC-triblock copolymers [437]. With permission of the American Association for the Advancement of Science

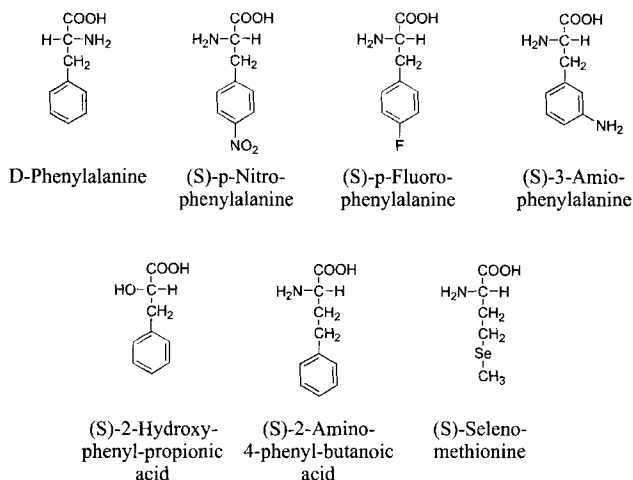
films containing 100 or more layers in a polar arrangement have been formed. The two surfaces of the films were clearly distinguished with one being non-adhesive and hydrophobic while the opposite surface was hydrophilic and sticky [437].

7. TEMPLATE SYNTHESSES

The different examples and aspects discussed so far, demonstrated a delicate balance between ordering and disordering effects for the supermolecular organisation of macromolecules. In order to improve the design of functional macromolecular structures, we need a much higher developed ability to control the primary structure of synthetic macromolecules. In the introduction and also in Section II, it was already pointed out that the synthetic means we have at hand are not sufficient to prepare macromolecules whose functionality and structural perfection equals that of biomolecules. Perfect structural control of biomolecules is achieved by replication and template synthesis, e.g. the polymerase chain reaction for the biosynthesis of peptides [27,438,439]. Hence, the development of template type polymerizations may be regarded as an ultimate objective for a future supramolecular chemistry with macromolecules. However, the problems encountered are barely solved i.e. preorganisation of the template, binding of the monomer, starting and termination of the polymerization, and the release of the formed macromolecule from the template [28,29]. Because of the central importance and the intriguing scientific challenges, this last section gives a short overview on template approaches in polymer science.

One possibility which has been developed rather successfully so far is based on using living cells for the preparation of new macromolecules. This has been achieved by feeding biocompatible monomers to bacteria which synthesize polyesters or by genetical modification of bacteria. In the first attempt the polymer structure is manipulated simply by the supply of suitable monomers to the fermenter which are barely discriminated by the living organism (cf. Scheme 8). In the second approach the genetic code is manipulated by genetical engineering allowing to determine the sequence in which rather different amino acids can be assembled.

Escherichia coli bacteria were modified with a synthetic genome, affecting the cells to produce a poly(peptide) with the sequence (alanine-glycine)₃-para-fluorophenylalanine-glycine₁₃. The bacteria were grown in a batch-reactor and were fed with para-fluormethylalanine in addition to their normal feed. The biosynthesis yielded poly(peptides), exhibiting a β -platelet structure and bearing the fluoro-groups oriented to one side of the platelet only [440]. Tirrell described the multi-gram-scale bio-synthesis of poly(2-alanyl-glycine), the "parent" polymer of the crystalline domains of silk-like proteins. The desired amino-acid sequence was coded in a synthetic DNA, and introduced into *Escherichia coli* using the "Recombinant DNA" technology [441]. The polymer was shown to crystallize in chain-folded lamellae of 3.2 nm thickness. In these structures the chain conformation was described as α - β -sheets, folded through γ -turns [442]. On proceeding this



Scheme 8

approach, it can be expected to obtain much better defined polymers with programmable secondary structures in the near future.

It has been attempted to perform template polymer syntheses without using biological sources. Concepts focus on the formation of a complex between monomer molecules and a present macromolecule [4,480]. This way the monomer will get preorganized and the polymerization is supposed to follow a “zip” mechanism controlled by the length and the configuration of the template polymer, offering replication of the molecular weight and control of the stereo structure. Polymerization of acrylic acid in the presence of poly(ethyleneimine), N-vinylimidazole/poly(methacrylic acid) or acrylonitrile with poly(vinylacetate) have been described [469,470,471,472,473]. Recently the preparation of solid polyelectrolyte complexes from chitosan and sodium-styrenesulfonate has been reported [481].

So far two major scenarios can be discussed in template polymerisation [4,482,483]. In the limiting case of extremely strong complexation and a ratio of monomer to polymer-segments that is smaller than one all monomer will be complexed and the polymerization will proceed only along the preorganized strings of monomer molecules (see Figure 39). Compared to polymerization in solution an enhancement of the rate of polymerization by a factor up to 5–7 has been observed [4]. This can be explained by the preorganization and eventually by a decreased rate of termination in radical polymerization. Replication of the parents molecular weight is rather poor and would require that the initiation has to occur selectively at the ends of the chain of monomer-complexed polymer, in addition the solution polymerization of the free monomer has to be negligible slow compared to the template polymerization [484]. No doubtless proved example for this mechanism has been stated in the literature.

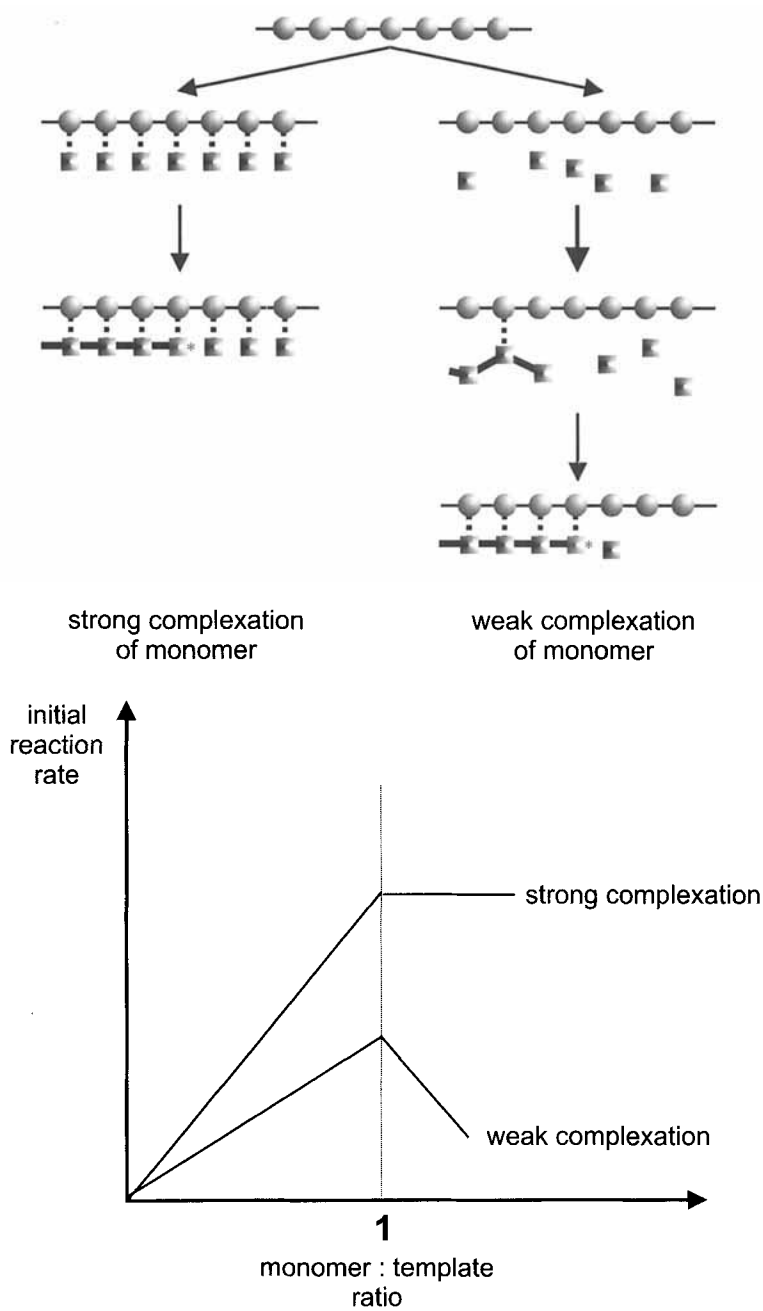


Figure 39

Frequently the complexation of the monomer is weak, and only oligomers exceeding a critical degree of polymerization can become complexed to the template-chain (Figure 39). Because the polymerization simultaneously proceeds in the solution and along the template complex, a lower over-all rate enhancement is observed. If the number of monomer molecules exceeds the available complexation sites, the reaction rate is decreased. Virtually all investigated template polymerizations seem to obey this mechanism [484].

These template polymerizations suffer from three fundamental problems: (i) In most cases the binding of the polymer to the template is stronger than the binding of the monomer due to the cooperativity of the interaction between the polymers. As a consequence the newly formed macromolecules are not released from the template and multiple replication is not possible without multiple separation steps. (ii) We lack the possibility to start the polymerisation reaction at the terminal group of the monomer-template complex. (iii) While a weak interaction between the template and the monomer is favourable to allow easy separation of the template and the newly formed macromolecule, it leads to incomplete complexation of the template and interruption of the polymerisation along the chain. A solution of these problems would require a relatively strong complexation of the monomers in combination with sufficient anticooperativity in the complexation of the polymer. The latter however would inevitably impede the polymerisation reaction and require therefore a living polymerisation mechanism which does not suffer from a slowed down rate of polymerisation.

Another rather successful kind of template polymerizations, the so called inclusion polymerisations, have been addressed earlier in this chapter (see Figure 18).

A templating concept which is not directed to polymerization but to separation of different molecules and catalysis is the so called "molecular imprinting" technique. Selective recognition sites can be formed by crosslinking polymerization of suitable functional monomers in the presence of a compound whose structure is to be recognised and which can be leached out of the polymer matrix leaving back its "molecular imprint" [443,458,459] (cf. Figure 40a). The method yields a solid material containing functional "holes" complementary in shape and functionality to the template molecule [445]. Scope, limitations and applications of molecular imprinting has recently been reviewed [444,445,446,459,485].

Specific interactions between the template and the substrate which have been described include covalent bonds, ligand-metal binding complexation, electrostatic interactions, hydrogen bonds, charge-transfer- and hydrophilic interactions. The most selective sites were obtained by means of ionic interactions, covalent- and hydrogen bonds [444,486].

The matrix polymer has to be rather rigid to conserve the empty imprinted sites after extraction of the template, this is achieved by extensive crosslinking. Generally, the crosslinker content of a mixture has to exceed a threshold value (>40%) to obtain selectivity [444,447]. Further, the chemical structure of the polymer network is of minor importance for the selectivity, though its polarity should be adapted to the imprinting molecule [444]. To obtain a maximum number of accessible sites,

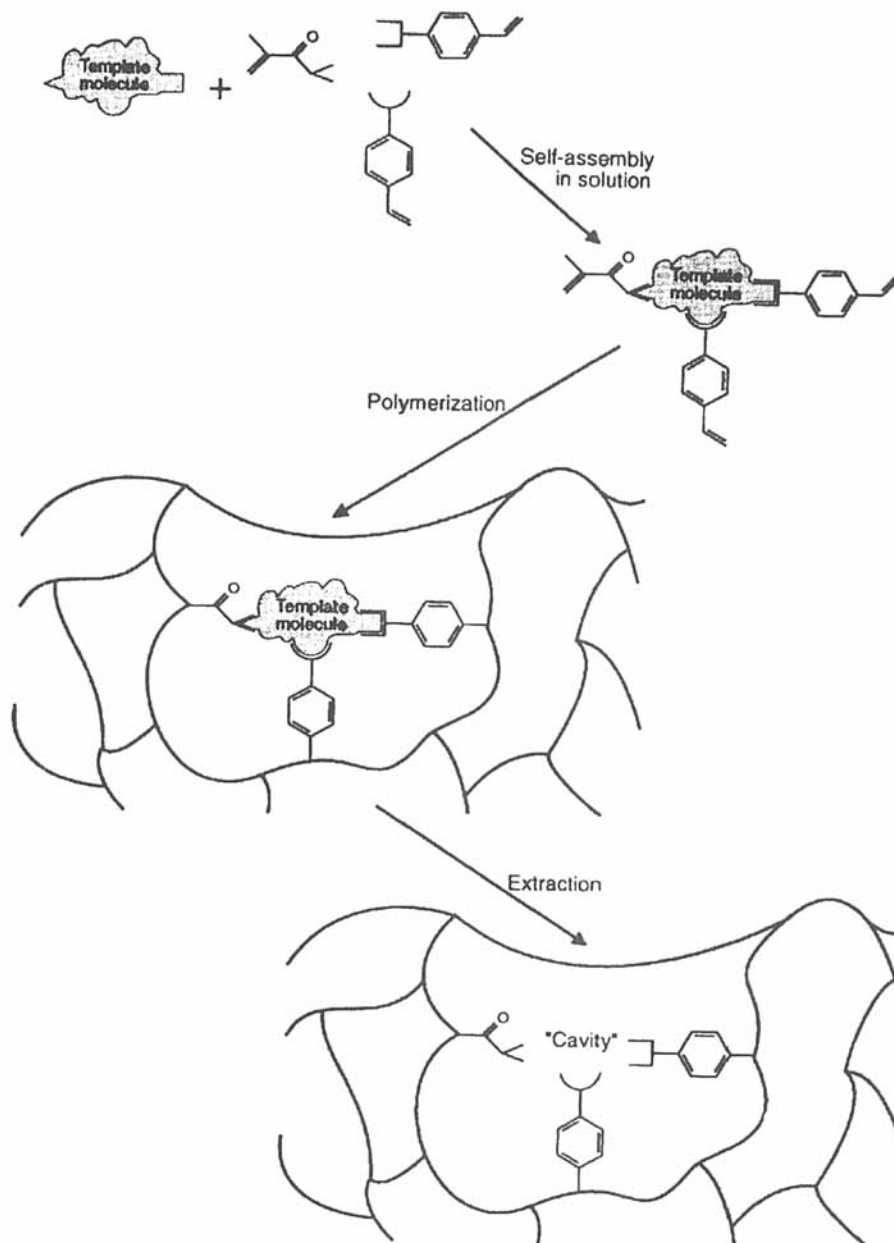


Figure 40 (a) Sketch of the molecular imprinting process [444].

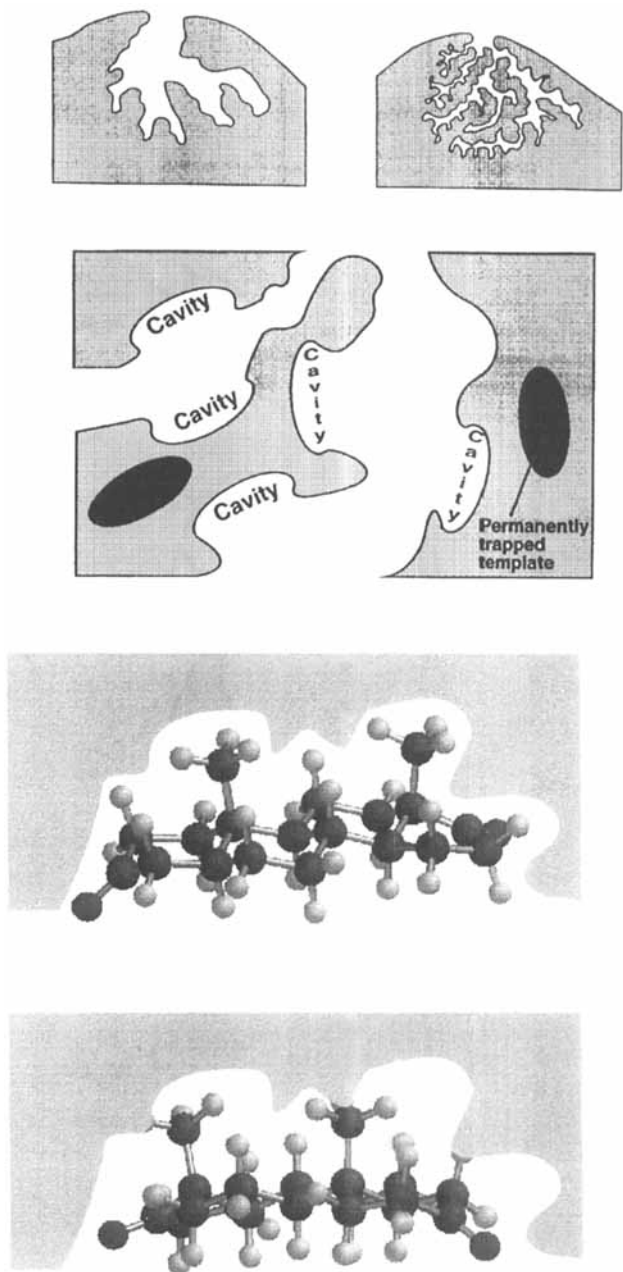


Figure 40 (b) Sketch of the morphology of an imprinted polymer matrix [444]. Parts (a) and (b) reproduced from [444] by permission of Springer-Verlag. (c) Illustrative drawing, showing how imprinted cavities can act as selective catalysts [445]. With permission of Wiley-VCH

porous matrices are prepared via polymerization in the presence of a inert liquid "porogene" [464]. The porogene determines the size, shape and the distribution of the cavities but must not influence the selectivity of the recognising sites [445]. The morphology of the porous imprinted polymer is schematically depicted in Figure 40b: large pores percolate through the polymer matrix and contain the selective sites at their inner walls [444]. In order to enhance the rates of the guest-host inclusion/ejection reaction, imprinted polymers are used at elevated temperatures [445].

Imprinted polymers have been used as stationary phase in liquid chromatographic separations and allowed the enantiomer separation for a wide range of compounds [445]. Improved chiral chromatographic resolution factors have been archived by means of gradient-elution [448]. Imprinted polymer thin films have been tested as selective membranes [450,487], including enantiomer separation [451].

The quantitative determination of drugs by radio-immunoassay techniques using imprinted polymers instead of natural antibodies was investigated by Mosbach. Theophyllin, Diazepam and Morphine were recognised and cross-reaction tests with other but sterical similar molecules, gave similar results like the established antibody reactions [449]. Eventually the expensive antibodies can be replaced by cheap synthetic imprinted polymers [474].

Another important research direction is the mimicking of enzymes and the construction of selective catalysts. For these purposes, the polymer is imprinted with the desired reaction-product or better, a molecule which resembles the transition state of the reaction adducts. If the educts bind specifically to the recognition site, they become confined into these "micro-reactors" and are supposed to react faster and more defined than outside the cavities [445]. Examples for reactions in the presence of such "synthetic enzymes" can be found in [452,453,454,455,456,457] (cf. Figure 40c). First positive results have been reported, e.g. an "synthetic esterase", increasing the rate of alkaline hydrolysis of substituted phenyl-(2-(4-carboxy-phenyl)-acetic esters for 80 times [488] and Diels-Alder catalysis functional holes containing titanium lewis-acids [489]

8. Conclusion

The examples represented here have demonstrated our increasing ability to design and to manipulate ever larger supramolecular systems and merge concepts from supramolecular and polymer chemistry. Yet we are still far from approaching the perfection and versatility and, most important, the functionality of biomolecules and their superstructures. Like in biology, macromolecules and the competition between macromolecular order and disorder will play a dominant role in the preparation of functional molecular devices and nanoscopic objects.

Aspects that are peculiar for macromolecules are manifold. This is the length allowing intermolecular entanglements and the bridging of distances exceeding the range of chemical interactions. The mass and dimension give rise to long range

interaction forces typically observed for colloidal particles. Antagonistic molecular subunits can be linked covalently within one molecule. The conformational flexibility is the cause for a delicate balance between entropic and enthalpic effects on the molecular structure. This can yield cooperativity and also anticooperativity in the molecular interaction. The interplay of cooperative and anticooperative effects, however, is an important principle for the finite growth of supramolecular objects and a means to adjust and even to switch the strength of an interaction or a secondary linkage over wide ranges. An important aspect of the variability in the conformation and the interaction forces is the principle of quasi-equivalent tertiary structures that has been pointed out by Aaron Klug at the example of the tobacco mosaic virus [12].

Due to the coupling of segmental modes of motion, macromolecular dynamics cover a range of 10 orders in magnitude in time. Slow dynamics, however, allow the formation of persistent metastable and intermediate states. Still supramolecular organization under nonequilibrium conditions is a rather unexplored field and there is an urgent need to learn about the scope and the limitations for the formation of supramolecular structures far away from the equilibrium state.

Yet we lack the ability to synthesize macromolecules with the structural perfection known from biomacromolecules and which is inevitable for the formation of well defined tertiary and quarternary structures. However, major macromolecular design achievements have occurred over the past decade with important discoveries in the areas of catalysis, macromolecular architecture, supramolecular chemistry and macromolecular biosynthesis. The biological synthesis of unnatural polypeptides pursued by D. Tirrell is an example of a new approach for the synthesis of copolymers with a specified monomer sequence. Further progress may come from developments in the field of catalysis and from hybrids combining synthetic and biomolecular units. In the future the systems to be designed will become functional and be able to fulfill specific tasks involving templating, self-regulation, and replication. Within this context, supramolecular chemistry of polymers is an emerging area bridging chemistry, biology and nanoscopic material sciences.

9 REFERENCES

1. H. Morawetz, *Polymers, The Origin and Growth of a Science*, Wiley Interscience, New York, 1980.
2. H. Staudinger, *From Organic Chemistry to Macromolecules*, Wiley, New York, 1970.
3. P. J. Flory, *Principles of Polymer Chemistry*, Cornell University Press, Ithaca, London, 1953.
4. G. Odian, *Principles of Polymerization*, Wiley, New York, 1991.
5. P.-G. de Gennes, *Scaling Concepts in Polymer Physics*, Cornell University Press, 1979.
6. P. Rempp and E. Merrill, *Polymer Syntheses*, Hüthig & Wepf, Basel, 1986.
7. F. Jülicher and J. Prost, *Cooperative Molecular Motors*, *Phys. Rev. Lett.*, **75**, 2618 (1995).

8. R. B. Vallee (ed.), *Molecular Motors and the Cytoskeleton, Methods in Encymology*, **196**, Academic Press, San Diego, 1991.
9. D. L. D. Casper, *Biophysical J.*, **32**, 103 (1980).
10. G. Ungar, *Polymer*, **34**, 2050 (1993).
11. A. J. Levine, *Viruses*, W. H. Freeman, New York, 1992.
12. A. Klug, *Angew. Chem., Int. Ed. Engl.*, **22**, 565 (1983).
13. A. W. Ackermann and L. Berthiaume, *Atlas of Virus Diagrams*, CRC Press, New York, 1995.
14. H.-G. Elias, *Makromoleküle*, Hüthig & Wepf, Basel, 1990.
15. G. R. Newkome, C. N. Moorefield and F. Vögtle (eds.), *Dendritic Molecules, Concept, Synthesis, Perspectives*, VCH, Weinheim, Germany, 1996.
16. N. Hadjichristidis, Y. Tselikas, H. Iatrou, K. S. Liang, K. Mohanty and D. J. Lohse, *J. Chem. Phys.*, **103**, 2456 (1996).
17. M. Gauthier and M. Möller, *Macromolecules*, **24**, 4548 (1991).
18. S. S. Sheiko, M. Gauthier and M. Möller, *Macromolecules*, **30**, 2343 (1997).
19. R. B. Merrifield, *J. Am. Chem. Soc.*, **85**, 2149 (1963).
20. R. B. Merrifield, *Automated Synthesis of Peptides, Science*, **150**, 178 (1965).
21. J. W. Feast and N. M. Stainton, *Mater. Chem.*, **5**, 405 (1995).
22. G. R. Newkome, Z. Yao, G. R. Baker and V. K. Gupta, *J. Org. Chem.*, **50**, 2003 (1990).
23. D. A. Tomalia, A. M. Naylor and W. A. Goddard, *Angew. Chem.*, **102**, 119 (1990).
24. P. R. Dvornic and D. A. Tomalia, *Curr. Opin. Coll. Interf. Sci.*, **1**, 221 (1996).
25. B. I. Voit, *Acta Polymerica*, **46**, 87 (1995).
26. M. Swarc, *Ionic Polymerization Fundamentals*, Hanser Publishers, Munich, 1996.
27. T. K. Blackwell and H. Weintraub, *Science*, **250**, 1104 (1990).
28. F. Vögtle and R. Hoss, *Angew. Chem.*, **106**, 389 (1994).
29. J. P. Sauvage, (Vol. ed.), *Comprehensive Supramolecular Chemistry* (eds. J. L. Atwood, J. E. D. Davies, D. D. MacNicol, F. Vögtle and J. M. Lehn), Vol. 9, *Templating, Self-Assembly, and Self-Organization*, Pergamon Press, Oxford, 1996.
30. P. J. Flory, *Statistical Mechanics of Chain Molecules*, Interscience, New York, 1969.
31. P. C. Hiemenz, *Polymer Chemistry, The Basic Concepts*, Marcel Dekker Inc., New York and Basel, 1984.
32. H. Kuhn, F. Moning and W. Kuhn, *Helv. Chim. Acta*, **36**, 731 (1953).
33. P. J. Ludovice and U. W. Suter, *Polym. Prep.*, **30**, 13 (1989).
34. H. Jacobson and W. H. Stockmeyer, *J. Chem. Phys.*, **18**, 1600 (1950).
35. R. J. Cotter and M. Matzner, *Ringforming Polymerizations*, Academic Press, New York, 1969.
36. H. R. Kricheldorf and S.-R. Lee, *Macromolecules*, **28**, 6718 (1995).
37. H. R. Kricheldorf, S.-R. Lee, and S. Bush, *Macromolecules*, **29**, 1375 (1996).
38. H. R. Kricheldorf and S.-R. Lee, *Macromolecules*, **29**, 8689 (1996).
39. H. R. Kricheldorf, S.-R. Lee and N. Schittenhelm, *Macromol. Chem. Phys.*, **198**, 1753 (1997).
40. H. R. Kricheldorf and S. Eggerstedt, *Macromol. Chem. Phys.*, **198**, 1767 (1997).
41. O. Kratky and G. Porod, *Recl. Trav. Chem.*, **68**, 1106 (1949).
42. H. Yamakawa, *Modern Theory of Polymer Solutions*, Harper & Row, New York, 1971.
43. P. J. Flory, *Adv. Polym. Sci.*, **59**, 1 (1983).
44. H. Block, *Poly(γ -benzyl-L-glutamate) and other Glutamic Acid Containing Polymers*, Gordon & Breach Science Publishers, New York, 1983.
45. T. R. Vierheller, M. Foster, A. Schmidt, K. Mathauer, W. Knoll, G. Wegner, S. Satija and C. F. Majkrzak, *Macromolecules*, **27**, 6893 (1994).
46. R. J. M. Nolte, *Chem. Soc. Rev.*, **23**, 11 (1994).

47. M. N. Teerenstra, J. G. Hagting, A. J. Schouten, R. J. M. Nolte, M. Kauranen, T. Verbiest and A. Persoons, *Macromolecules*, **29**, 4876 (1996).
48. S. Lifson, M. M. Greene, C. Anderola and N. C. Peterson, *J. Am. Chem. Soc.*, **111**, 8850 (1989).
49. H. H. Britzinger, D. Fischer, R. Mülhaupt, B. Rieger and R. Waymouth, *Angew. Chem.*, **107**, 1255 (1995).
50. C. A. Ianeway and E. Merler, *The Gamma Globulines*, Little, Brown & Co., Boston, 1967.
51. F. Franek (ed.), *Gamma Globulines, Structure and Biosynthesis*, Academic Press, London, 1969.
52. M. Antonietti, R. Basten and R. Lohmann, *Macromol. Chem. Phys.*, **196**, 441 (1995).
53. K. Armistead and H. Goldbeck-Wood, *Adv. Polym. Sci.*, **100**, 219 (1992).
54. P. H. Geil and D. H. Reneker, *J. Appl. Phys.*, **31**, 1916 (1960).
55. P. H. Geil, *Polymeric Single Crystals*, Interscience Publishers Inc., 1963.
56. H. J. Hall, *Structure of Crystalline Polymers*, Elsevier, Amsterdam, 1984.
57. B. Wunderlich, *Crystalline High Polymers: Molecular Structure and Thermodynamics*, American Chemical Society Symposium Series (ACS), Washington DC, 1969.
58. L. H. Sperling, *Introduction to Physical Polymer Science*, 2nd edn., Wiley Interscience, New York, 1992.
59. G. Ungar and A. Keller, *Coll. Polym. Sci.*, **257**, 90 (1979).
60. M. Möller, G. Kogler, D. Oelfin and H. Drotloff, *Molecular Motions in Crystalline and Mesomorphous Phases of Large Size Cycloalkanes as a Model for Polyethylene* (ed. L. J. Mathias), Plenum Press, New York, 1988, Chap. 14, p. 245.
61. H. Tadokoro, *Structure of Crystalline Polymers*, Wiley, New York, 1979.
62. A. Keller, *Philos. Mag.*, **2**, 1171 (1957).
63. B. Wunderlich, *Macromolecular Physics*, Vol. I: *Crystal Structure, Morphology, Defects*, Academic Press, New York, 1973.
64. A. J. Kovacs, A. Gonthier and C. Straupe, *J. Polym. Sci.*, **C50**, 283 (1975).
65. C. P. Buckley and J. A. Kovacs, in *Structure of Crystalline Polymers* (ed. I. H. Hall), Elsevier Appl. Science, London, 1984, p. 261.
66. A. Keller and G. Goldbeck-Wood, *Polymer Crystallization: Fundamentals of Structure and Crystal Growth of Flexible Chains*, in *Comprehensive Polymer Sci.*, Second Suppl. (eds. G. Allen, S. L. Aggarwal and S. Russo), Pergamon, New York, 1996.
67. A. J. Pennings, J. M. M. A. van der Mark and A. M. Kiel, *Koll. Z. Z. Polym.*, **237**, 336 (1970).
68. H. D. Keith, F. J. Padden Jr and R. G. Vadimsky, *J. Appl. Phys.*, **37**, 4027 (1966).
69. H. Chanzy, R. H. Marchessault and J. F. Revol, *Biopolymers*, **18**, 887 (1979).
70. V. A. Marikhin and L. P. Myasnikova, *Structural Basis of High-Strength High-Modulus Polymers*, in *Oriented Polymeric Materials* (ed. S. Fakirov), Hüthig & Wepf, Zug, 1996, Chap. 2.
71. H. F. Mark, N. M. Bikales, C. G. Overberger, G. Menges and J. I. Kroschwitz (eds.), *Encyclopedia of Polymer Science and Engineering*, Vol. 6, p. 646 ff, John Wiley & Sons, New York, 1996.
72. D. C. Prevorsek, Y. D. Kwon and R. K. Sharma, *J. Mater. Sci.*, **12**, 2310 (1977).
73. M. W. Denny, *J. Exp. Biol.*, **65**, 483 (1976).
74. J. M. Gosline, M. W. Denny and M. E. DeMont, *Nature*, **309**, 551 (1984).
75. Y. Termonia, *Macromolecules*, **27**, 7378 (1994).
76. T. D. Grubb and L. W. Jelinski, *Macromolecules*, **30**, 2860 (1997).
77. K. Kerkham, C. Viney, D. Kaplan and S. Lombardi, *Nature*, **349**, 596 (1991).
78. P. Calvert, *Nature*, **340**, 266 (1989).
79. W. Burchard, *Chemie in unserer Zeit*, **23**, 69 (1989).

80. J. C. Salamone (ed.), *Polymeric Materials Encyclopedia*, CRC Press, New York, 1996.
81. L. Leibler, *Macromolecules*, **13**, 1602 (1980).
82. A. E. Likhtman and A. N. Semenov, *Macromolecules*, **27**, 3103 (1994).
83. G. H. Frederickson and F. S. Bates, *Ann. Rev. Mater. Sci.*, **26**, 501 (1996).
84. Y. Nishikawa, H. Kawada, H. Hasegawa and T. Hashimoto, *Acta Polym.*, **44**, 247 (1993).
85. M. F. Schulz, F. S. Bates, K. Almdel and K. Mortensen, *Phys. Rev. Lett.*, **73**, 86 (1994).
86. D. A. Hajduk, P. G. Harper, S. M. Gruner, L. C. Honeker, G. Kim, E. L. Thomas and L. J. Fetters, *Macromolecules*, **27**, 4063 (1994).
87. S. Förster, A. K. Khandpur, J. Zhao, F. S. Bates, I. W. Hamly, A. J. Ryan and W. Bras, *Macromolecules*, **27**, 6922 (1994).
88. M. W. Matsen and F. S. Bates, *Macromolecules*, **28**, 8796 (1995).
89. J. Zhao, B. Majumdar, M. F. Schulz, F. S. Bates, K. Almdal, K. Mortensen, D. A. Hajduk and S. M. Gruner, *Macromolecules*, **26**, 1204 (1996).
90. M. W. Matsen and F. S. Bates, *Macromolecules*, **29**, 1091 (1996).
91. M. W. Matsen and M. Schick, *Curr. Opin. Coll. Interf. Sci.*, **1**, 329 (1996).
92. S. T. Milner and P. D. Olmsted, *Phys. Rev. Lett.*, **L74**, 829 (1993).
93. M. Muthukumar, *Macromolecules*, **26**, 5259 (1993).
94. N. Hadjichristidis and H. Iatrou, *Macromolecules*, **26**, 2479 (1993).
95. N. Hadjichristidis, H. Iatrou and A. Averopoulos, *Macromolecules*, **27**, 6232 (1994).
96. D. J. Lohse and N. Hadjichristidis, *Curr. Opin. Coll. Interf. Sci.*, **2**, 171 (1997).
97. N. Hadjichristidis, A. Averopoulos, Y. Poulos and J. Roovers, *Macromolecules*, **29**, 6076 (1996).
98. D. J. Pochan, S. P. Gido, S. Pispas, J. W. Mays, A. J. Ryan, J. P. A. Fairclough, J. W. Hamley and J. N. Terril, *Macromolecules*, **29**, 5091 (1996).
99. J. Adams and W. Gronski, *Macromol. Chem. Rapid Comm.*, **15**, 879 (1994).
100. S. I. Stupp and L. H. Radzilowski, *Macromolecules*, **27**, 7747 (1994).
101. P. Bohnert and H. Finkelmann, *Macromol. Chem. Phys.*, **195**, 685 (1994).
102. J. T. Chen, E. L. Thomas, C. K. Ober and S. S. Hwang, *Macromolecules*, **28**, 1688 (1995).
103. L. H. Radzilowski, B. O. Carragher and S. I. Stupp, *Macromolecules*, **30**, 2110 (1997).
104. T. Hashimoto, M. Fujimura, H. Kawai, J. Diamont and M. Shen, *Polym. Prep.*, **19**, 81 (1978).
105. T. Hashimoto, M. Fujimura, K. Saijo, H. Kawai, J. Diamont and M. Shen, *Adv. Chem. Ser.*, **176**, 257 (1979).
106. R. Stadler, C. Auschra, J. Beckmann, U. Krappe, J. Voigt-Martin and L. Leibler, *Macromolecules*, **28**, 3080 (1995).
107. R. Stadler, U. Breiner and U. Krappe, *Macromol. Rapid Commun.*, **17**, 567 (1996).
108. T. Hashimoto, S. Sakurai and L. J. Fetters, *Macromolecules*, **29**, 740 (1996).
109. R. Stadler, C. Neumann and V. Abetz, *Poly Bull.*, **36**, 43 (1996).
110. Z.-G. Wang and W. Zheng, *Macromolecules*, **28**, 7215 (1995).
111. T. M. Birshtein and Y. V. Lyatskaya, *Polymer*, **36**, 975 (1995).
112. U. Krappe, R. Stadler and I. Voigt-Martin, *Macromolecules*, **28**, 4558 (1995).
113. T. L. Morkved, P. Wiltzius, H. M. Jaeger, D. C. Grier and T. A. Wilten, *Appl. Phys. Lett.*, **64**, 422 (1994).
114. D. D. Archibald and S. Mann, *Nature*, **364**, 430 (1993).
115. C. T. Kresge, M. E. Leonowicz, W. J. Roth, J. C. Vartuli and J. S. Beck, *Nature*, **359**, 710 (1992).
116. G. Liu, *Adv. Mater.*, **9**, 437 (1997).
117. R. A. Weiss, W. J. MacKnight, R. D. Lundberg, K. A. Mauritz, C. Thies and D. A. Brant, *Structure and Application of Ion-Containing Polymers*, in *Coulombic Interactions in*

- Macromolecular Systems* (eds. A. Eisenberg and F. E. Bailey), American Chemical Society Symposium Series (ACS), **302**, Washington DC, 1986, p. 2.
118. M. Pineri and A. Eisenberg (eds.), *Structure and Properties of Ionomers*, NATO ASI-Series, Reidel, Dordrecht, 1987.
 119. A. Eisenberg and J.-S. Kim, Ionomers, in *Polymeric Materials Encyclopedia*, (ed. J. C. Salamone), CRC Press, New York, 1996, Vol. 5, p. 3435.
 120. A. Eisenberg, B. Hind and R. B. Moore, *Macromolecules*, **23**, 4098 (1990).
 121. J. S. Kim, R. J. Jackmann and A. Eisenberg, *Macromolecules*, **27**, 2789 (1994).
 122. R. W. Rees and D. J. Vaughan, *Polym. Prep.*, **6**, 287 (1965).
 123. H. Tachino, H. Hara, E. Hirasawa, S. Kutsumizu, K. Tadano and S. Yano, *Macromolecules*, **27**, 372 (1994).
 124. A. Eisenberg and S. C. Yeo, *Appl. Polym. Sci.*, **21**, 875 (1977).
 125. A. Eisenberg and H. L. Yeager (eds.), *Perfluorinated Ionomer Membranes*, American Chemical Society Symposium Series (ACS), **180**, Washington DC, 1982.
 126. B. Hird and A. Eisenberg, *J. Polym. Sci. Phys. Ed.*, **28**, 1665 (1990).
 127. F. J. Waller, *Catalysis with a Perfluorinated Ion-Exchange Polymer*, in *Polymeric Reagents and Catalysts* (ed. W. T. Ford), American Chemical Society Symposium Series (ACS), **308**, Washington DC, 1986, Chap. 3, p. 42.
 128. F. Helfrich, *Ion Exchange*, McGraw Hill, New York, 1962, Chap. 6.
 129. C. W. Martin, P. J. Nandapurkar and S. V. Katti, *Ionomeric Membranes, Perfluorinated*, in *Polymeric Materials Encyclopedia* (ed. J. C. Salamone), CRC Press, New York, 1996, Vol. 5, p. 3427.
 130. H. Reiss and I. C. Bassignana, *J. Membr. Sci.*, **11**, 219 (1982).
 131. H. Reiss, *J. Membr. Sci.*, **23**, 11 (1985).
 132. T. Hashimoto, M. Fujumura and H. Kawai, in *Perfluorinated Ionomer Membranes* (eds. A. Eisenberg and H. L. Yeager), American Chemical Society Symposium Series (ACS), **180**, Washington DC, 1982.
 133. W. Y. Hsu, J. R. Barkley and P. Makin, *Macromolecules*, **29**, 198 (1996).
 134. H. L. Yeager and E. A. Steck, *J. Elektrochem. Soc.*, **128**, 1880 (1981).
 135. H. L. Yeager and M. A. F. Robertson, *Macromolecules*, **29**, 5166 (1996).
 136. J. Economy and K. Goranor, *Adv. Polym. Sci.*, **117**, 221 (1994).
 137. H. Finkelmann, *Angew. Chem.*, **99**, 840 (1987).
 138. Y. K. Godovsky and V. S. Papkov, *Adv. Polym. Sci.*, **88**, 129 (1989).
 139. J. Lin and D. C. Sherrington, *Adv. Polym. Sci.*, **111**, 177 (1994).
 140. K. Müller, K.-H. Wassmer and G. Kothe, *Adv. Polym. Sci.*, **95**, 1 (1990).
 141. M. G. Northolt and D. J. Sikkema, *Adv. Polym. Sci.*, **98**, 115 (1991).
 142. H. Kelker and R. Hatz, *Handbook of Liquid Crystals*, Verlag Chemie, Weinheim, 1980.
 143. S. Chandrasekhar, *Liquid Crystals*, 2nd edn., Cambridge University Press, Cambridge, 1992.
 144. R. Schledjewski and K. Friedrich, *Orientation Effects on the Thermal, Mechanical and Tribological Performance of Neat, Reinforced and Blended LCP*, in *Oriented Polymer Materials* (ed. F. Sokyö), Hüttig & Wepf Verlag, Zug, 1996, Chap. 17.
 145. M. Gordon and N. A. Platé (ed.), *Liquid Crystal Polymers*, Vol. I, *Adv. Polym. Sci.*, **59** (1983).
 146. M. Gordon and N. A. Platé (ed.), *Liquid Crystal Polymers*, Vol. II/III, *Adv. Polym. Sci.*, **60/61** (1984).
 147. AG, Daimler-Benz, Wacker-Chemie GmbH, German Patent No. DE 4418076A1, 1995.
 148. M. Müller, R. Zentel and H. Keller, *Adv. Mater.*, **9**, 159 (1997).
 149. J. R. Schaefgen, T. J. Bair, J. W. Ballow, S. L. Kwolek, P. W. Morgan, M. Panar and J. Zimmenmann, in *Ultra-high Modulus Polymers* (eds. A. Cifferi and J. M. Ward), Applied Science, London, 1979.

150. J. Kachidza, G. Serpe and J. Economy, *Macromol. Chem. Macromol. Symp.*, **53**, 65 (1992).
151. D. Frich and J. Economy, *Polym. Mater. Sci. Engl.*, **69**, 438 (1993).
152. J. Economy and A. Andreopoulos, *J. Adhesion*, **40**, 115 (1993).
153. H. Ringsdorf, M. Ebert, J. H. Wendorff and R. Wuestefeld, *Polym. Prep.*, **30**, 479 (1989).
154. H. Ringsdorf, G. Frick, C. Baehr, J. H. Wendorff and R. Wuestefeld, *Liq. Cryst.*, **11**, 923 (1992).
155. R. M. Fuoss and H. Sadek, *Science*, **110**, 552 (1949).
156. T. Eishun and K. Abe, *Polyelectrolyte Complexes*, Chap. 5 in Vol. 2 of *Developments in Ionic Polymers* (eds. A. D. Wilson and H. J. Press), Elsevier Applied Science Publishers, London, 1986, p. 191.
157. A. S. Michaels, *Ind. Engl. Chem.*, **57**, 32 (1965).
158. E. Trudida, K. Abe and M. Honma, *Macromolecules*, **9**, 112 (1976).
159. A. Blumstein, S. R. Kakivaya, R. Blumstein and T. Suzuki, *Macromolecules*, **8**, 435 (1975).
160. V. Kabanov, O. V. Kargina and M. V. Ulyanova, *J. Polym. Sci., Polym. Chem. Ed.*, **14**, 2351 (1976).
161. J. C. Salamon, S. Poulin, A. C. Watterson and A. P. Olson, *Polymer*, **20**, 611 (1979).
162. C. K. Ober and G. Wegner, *Adv. Mater.*, **9**, 17 (1997).
163. E. D. Goddard, *Coll. Surf.*, **19**, 301 (1986).
164. H. Hoffmann, O. El-Seoud, G. Huber and R. Bocher, *Polyelectrolyte-Surfactant-Complexes*, in *Integration of Fundamental Polymer Science and Technology* (eds. P. J. Lemstra and L. A. Kleintjens), Elsevier Applied Science, London, 1988, Vol. 2, p. 317.
165. K. Hayagawa and J. C. T. Kwak, *J. Phys. Chem.*, **86**, 3866 (1982).
166. B. Phillip, W. Dawydoff and K. Linow, *Z. Chem.*, **22**, 1 (1982).
167. M. Antonietti and A. Thünemann, *Curr. Opin. Coll. Interf. Sci.*, **1**, 667 (1996).
168. M. Antonietti, S. Henke and A. Thünemann, *Adv. Mater.*, **8**, 41 (1996).
169. M. Antonietti, C. Burger and J. Effing, *Adv. Mater.*, **7**, 751 (1995).
170. E. Dessipri, D. Tirrell and E. D. T. Atkins, *Macromolecules*, **29**, 3545 (1996).
171. C. Wu, R. Ma, B. Zhou, J. Shen, K. K. Chan and K. F. Woo, *Macromolecules*, **29**, 228 (1996).
172. W. H. Watanabe, C. F. Ryan, P. C. Fleischer and B. S. Garret, *J. Phys. Chem.*, **65**, 896 (1961).
173. J. Špeváček and B. Schneider, *Adv. Coll. Interf. Sci.*, **27**, 81 (1987).
174. J. M. Yu and R. Jerome, *Macromolecules*, **29**, 8371 (1996).
175. P. Dumas, N. Spassky and P. Sigwalt, *Macromol. Chem.*, **156**, 55 (1972).
176. N. Spassky, P. Dumas, M. Sépulchre and P. Sigwalt, *J. Polym. Sci., Polym. Symp.*, **52**, 327 (1975).
177. F. Fukuzawa and I. Uematsu, *Polym. J. Tokyo*, **6**, 537 (1974).
178. K. Hatada, S. Shimizu, Y. Terawaki, K. Ohta and H. Yuki, *Polym. J. (Tokyo)*, **13**, 811 (1981).
179. G. L. Loomis, J. R. Murdoch and K. H. Gardner, *Polym. Prep.*, **31**, 55 (1990).
180. R. E. Prud'homme, I. Barakat, S. Brochu and R. Jerome, *Macromolecules*, **28**, 5230 (1995).
181. D. Brizzolara, H.-J. Cantow, K. Diederich, E. Kelter and A. J. Domb, *Macromolecules*, **29**, 191 (1996).
182. T. Okihara, T. Masa, K. Akiyoshi and K. J. Ken-ichi, *Macromol. Sci. Phys.*, **B30**, 119 (1991).
183. T. Nishiura, T. Kitayama and K. Hatada, *Polym. J.*, **28**, 1021 (1996).
184. G. Wegner, *Macromol. Chem.*, **154**, 35 (1972).
185. G. Wegner, *Mol. Cryst. Liq. Cryst.*, **52**, 535 (1979).

186. G. Kiss, K. Kiss, A. J. Kovacs and J. C. Wittmann, *J. Appl. Polym. Sci.*, **26**, 2485 (1981).
187. G. Kiss, A. J. Kovacs and J. C. Wittmann, *J. Appl. Polym. Sci.*, **26**, 2665 (1981).
188. K. Müllen, F. Morgenroth and E. Reuther, *Angew. Chem.*, **109**, 647 (1997).
189. J. L. Atwood, J. E. D. Davies and D. D. McNicol, *Inclusion Compounds*, Academic Press, London, 1984.
190. F. Cramer, *Einschlussverbindungen*, Springer Verlag, Heidelberg, 1954.
191. W. Schlenk, *Angew. Chem.*, **62**, 446 (1950).
192. Y. Chatani, *Prog. Polym. Sci. Japan*, **7**, 149 (1974).
193. Y. Chatani and S. Nakatani, *Macromolecules*, **5**, 597 (1972).
194. M. Farina, *Inclusion Polymerization*, in *Inclusion Compounds* (eds. J. L. Atwood, J. E. D. Davies and D. D. McNicol), Academic Press, London, 1984, Vol. 3, p. 297.
195. B. Rehbold, Thesis, Cologne University, Germany, 1988.
196. M. Farina, U. Pedretti, M. T. Gramengna and G. Audisio, *Macromolecules*, **3**, 475 (1970).
197. M. Miyata, S. Akizuki, H. Tsutsumi and K. Takemoto, *J. Polym. Sci. C, Polym. Lett.*, **26**, 229 (1988).
198. M. Miyata, in *Comprehensive Supramolecular Chemistry* (ed. D. Reinhoudt), Pergamon Press, Oxford, 1996, Vol. 10, Chap. 19, p. 557.
199. W. Kempf, Thesis, Cologne University, Germany, 1989.
200. G. DiSilvestro, P. Sozzani and M. Farina, *Polym. Prep.*, **27**, 92 (1986).
201. J. Israelachvili, *Intermolecular and Surface Forces*, Academic Press, San Diego, 1991.
202. D. Myers, *Surfactant Science and Technology*, 2nd edn., VCH, New York, 1992.
203. A. Halperin, M. Tirrell and T. P. Lodge, *Adv. Polym. Sci.*, **100**, 31 (1992).
204. G. Gast, *Curr. Opin. Coll. Inter. Sci.*, **2**, 258 (1997).
205. E. A. Bekturov and Z. K. Bakauova, *Synthetic Water-Soluble Polymers in Solution*, Hüthig & Wepf, Basel, 1986.
206. A. Laschewski, *Adv. Polym. Sci.*, **124**, 1 (1995).
207. U. P. Strauss and N. L. Gershfeld, *J. Phys. Chem.*, **108**, 1242 (1996).
208. A. Laschewski and I. Zerbe, *Polymer*, **32**, 2081 (1991).
209. B. Boyer, G. Lamaty, A. Leydet, J. P. Roque and P. Sama, *New J. Chem.*, **16**, 887 (1992).
210. S. Stevelmans, J. C. M. van Hest, I. F. G. A. Jansen, D. A. F. J. van Baxtel, E. M. M. de Brabender van den Berg and E. W. Meijer, *Adv. Mater.*, **7**, 561 (1996).
211. G. J. U. Fleer, M. A. Cohen-Stuart, J. M. H. M. Scheutjens, T. Cosgrove and B. Vincent, *Polymers at Interfaces*, Chapman & Hall, London, 1993, Chap. 6, p. 301.
212. J. L. Gardon, *Technology for Water Borne Coatings* (ed. J. E. Glass), American Chemical Society Symposium Series (ACS), **663**, 27 (1997).
213. Z. Gao and A. Eisenberg, *Macromolecules*, **26**, 7353 (1993).
214. P.-G. de Gennes, *Solid State Physics*, Academic Press, New York, 1978.
215. A. Halperin, *Macromolecules*, **20**, 2943 (1987).
216. S. Förster, M. Zisenis, E. Wenz and M. Antonietti, *J. Chem. Phys.*, **104**, 9959 (1996).
217. Z. Tuzar and P. Kratochvil, *Surface and Colloid Science* (ed. E. Matijevic), Plenum Press, New York, 1993, Vol. 15.
218. F. S. Bates, *Science*, **251**, 898 (1991).
219. M. Almgren, W. Brown and S. Hvidt, *Coll. Polym. Sci.*, **273**, 2 (1995).
220. K. Mortensen, *J. Phys.*, *Condens. Matter*, **8**, A103 (1996).
221. P. Alexandridis and T. A. Hatton, *Association of Pluronic Polyols in Aqueous Solutions in Dynamic Properties of Interfaces and Association Structures* (eds. V. Pillai and D. O. Shah), AOCS Press, Champaign, 1996, p. 231.
222. J. P. Spatz, S. Mößmer and M. Möller, *Angew. Chem. Int. Ed. Engl.*, **35**, 1510 (1996).
223. L. Zhang and A. Eisenberg, *Science*, **268**, 1728 (1996).
224. Y. Kui and A. Eisenberg, *Macromolecules*, **29**, 6359 (1996).

225. J. P. Spatz, S. Mößmer and M. Möller, *Angew. Chem.*, **108**, 1673 (1996).
226. D. Nguyen, S. K. Varshneg, C. E. Williams and A. Eisenberg, *Macromolecules*, **27**, 794 (1994).
227. D. Nguyen, C. E. Williams and A. Eisenberg, *Macromolecules*, **27**, 5090 (1994).
228. D. Nguyen, Z. Goo and A. Eisenberg, *Macromolecules*, **27**, 5173 (1994).
229. P. W. Hurter, *Solubilization in Amphiphilic Block Copolymer- Solutions*, in *Solubilization in Surfactant Aggregates* (eds. S. D. Christian and J. F. Scamekorn), Marcel Dekker, New York, 1995.
230. R. Nagarajan, *Solubilization of Hydrophobic Substances by Block Copolymer Micelles in Aqueous Solution*, in *Solvents and Self-Organization of Polymers* (eds. S. E. Webber, P. Munk and Z. Tuzar), Kluwer Publishers, Amsterdam, 1988.
231. R. Nagarajan and K. Ganesh, *Macromolecules*, **22**, 4312 (1989).
232. C. M. Palcos (ed.), *Polymerization in Organized Media*, Gordon & Breach, Philadelphia, 1992.
233. J. P. Spatz, M. Möller, R. D. Behm and M. Pietralla, *Macromolecules*, **30**, 3874 (1997).
234. D. S. Godovsky, *Adv. Polym. Sci.*, **119**, 79 (1995).
235. U. Kreibitz and M. Volme, *Optical Properties of Metal Clusters*, Springer Ser. Mat. Sci., Vol. 25, Berlin, 1995.
236. H. Weller, *Angew. Chem., Int. Ed. Engl.*, **35**, 1079 (1996).
237. A. P. Alirsatos, *Science*, **271**, 933 (1996).
238. J. P. Spatz, S. Mößmer and M. Möller, *Chem. Europ. J.*, **1**, 1552 (1996).
239. J. P. Spatz, A. Roescher and M. Möller, *Adv. Mater.*, **8**, 337 (1996).
240. H. Kunstle, M. Kunz and M. Möller, *Synth. Meth.*, **41-43**, 1159 (1991).
241. J. Yue, V. Sankaran, R. E. Cohen and R. R. Schrock, *J. Am. Chem. Soc.*, **115**, 4409 (1993).
242. M. Moffit and A. Eisenberg, *Chem. Mater.*, **7**, 1185 (1995).
243. M. Antonietti, S. Förster, J. Hartmann and S. Oestreich, *Macromolecules*, **29**, 3800 (1996).
244. S. C. Zimmerman, *Curr. Opin. Coll. Interf. Sci.*, **2**, 89 (1997).
245. S. A. Harfenist, Z. L. Wang, R. L. Whetten, I. Vezmar and M. M. Alvarez, *Adv. Mater.*, **9**, 817 (1997).
246. J. F. G. A. Jansen, E. M. M. de Brabender van den Berg and E. W. Meijer, *Science*, **266**, 1226 (1994).
247. J. F. G. A. Jansen, R. A. J. Jansen, E. M. M. de Brabender van den Berg and E. W. Meijer, *Science*, **266**, 1226 (1995).
248. E. W. Meijer, J. C. M. van Hest, D. A. P. Delnoye, M. W. P. L. Baars, C. Elissen-Roman and M. H. P. van Genderen, *Chem. Europ. J.*, **2**, 1616 (1996).
249. J. F. G. A. Jansen, E. W. Meijer and E. M. M. de Brabender van den Berg, *J. Am. Chem. Soc.*, **117**, 4417 (1995).
250. H. F. Mark, N. M. Bikales, C. G. Overberger, and G. Menges, *Encyclopedia of Polymer Science and Engineering*, Wiley, New York, 1989, Vol. 6, p. 1.
251. J. Piirno, *Emulsion Polymerization*, Academic Press, New York, 1982.
252. D. N. Napper and R. G. Gilbert, *Polymerization in Emulsions*, in *Comprehensive Polymer Science* (eds. G. Allen and J. C. Barrington), Pergamon Press, Oxford, 1989, Vol. 4, Chap. 11, p. 171.
253. Y. Nakamura, M. Ohta and M. Okubo, *Nipp. Setch. Gakk.*, **32**, 104 (1996).
254. O. Nuyken, R. Bayer, W. Billig-Peters, B. Voit and D. Yang, *Kautsch. Gumm. Kunstst.*, **47**, 903 (1994).
255. O. Nuyken, S.-K. Ko, B. Voit and D. Yang, *Kautsch. Gumm. Kunstst.*, **48**, 784 (1995).
256. O. Nuyken, W. Billig-Peters, B. Voit and D. Yang, German Patent No. DE 4406002 A1 950831.

257. Z. A. Schelly, *Curr. Opin. Coll. Interf. Sci.*, **2**, 37 (1997).
258. F. Candau, Y. S. Leong and R. M. Fitch, *J. Polym. Sci., Polym. Chem. Ed.*, **23**, 193 (1985).
259. F. Candau, *Polymerization in Inverse Microemulsions*, in *Comprehensive Polymer Science* (eds. G. C. Eastmond, A. Ledwith, S. Russo and P. Sigwalt), Vol. 4, Pergamon Press, Oxford, 1989, Chap. 13, p. 225.
260. M. Antonietti, W. Bremser, D. Mischenborn, C. Rosenauer, B. Schupp and M. Schmidt, *Macromolecules*, **24**, 6636 (1991).
261. M. Antonietti, S. Lohmann and C. von Neil, *Macromolecules*, **25**, 1139 (1992).
262. O. Marti, in *STM and SFM in Biology*, Academic Press, New York, 1993, Chap. 1, p. 1.
263. S. N. Magonov and M.-H. Wanbo, *Surface Analysis with STM and AFM*, VCH, Weinheim, 1996.
264. R. Wiesendanger and H.-J. Güntherodt (eds.), *Scanning Tunneling Microscopy*, Springer Series in Surface Science, Springer-Verlag, Heidelberg, 1996.
265. M. Radmacher, R. W. Tillmann, M. Fritz and H. E. Gaub, *Science*, **257**, 1900 (1992).
266. C. D. Frisbie, L. F. Rosznyi, A. Noy and C. M. Lieber, *Science*, **265**, 2071 (1994).
267. D. M. Kolb, *Prog. Surf. Sci.*, **51**, 109 (1996).
268. D. M. Kolb, *J. Chem. Soc., Faraday Trans. (Special Issue)*, **92**, 20 (1996).
269. A. Khumar and G. M. Whitesides, *Appl. Phys. Lett.*, **63**, 2002 (1993).
270. A. Khumar, H. A. Biebuyck and G. M. Whitesides, *Langmuir*, **10**, 1498 (1994).
271. J. H. Wilbur, A. Khumar, E. Kim and G. M. Whitesides, *Adv. Mater.*, **6**, 600 (1994).
272. A. Kumar, N. L. Abbot, E. Kim, H. A. Biebuyck and G. M. Whitesides, *Acc. Chem. Res.*, **28**, 219 (1995).
273. G. J. Kellog, D. G. Walton, A. M. Mayes, P. Lambooy, T. P. Russel, P. D. Gallagher and S. K. Satija, *Phys. Rev. Lett.*, **76**, 2503 (1996).
274. P. Mansky, T. P. Russel, C. J. Hawker, J. Mays, D. C. Cook and S. K. Satija, *Phys. Rev. Lett.*, **79**, 237 (1997).
275. Y. Liu, E. Huang, T. P. Russel and C. Hawker, *Science*, **275**, 1458 (1997).
276. P.-G. de Gennes, *Rev. Mod. Phys.*, **57**, 827 (1985).
277. J. C. Berg, *Wettability*, Marcel Dekker, New York, 1993.
278. K. Binder, *Adv. Polym. Sci.*, **112**, 181 (1994).
279. T. Russel, *Curr. Opin. Coll. Interf. Sci.*, **1**, 107 (1996).
280. C. H. Marques and J. Joenny, *J. Phys. France*, **49**, 1103 (1988).
281. R. G. Horn and J. N. Israelachvili, *Macromolecules*, **21**, 2836 (1988).
282. J. Klein and E. Kumacheva, *Science*, **269**, 816 (1995).
283. F. Heslot, A. M. Cazabat and P. Levinson, *Phys. Rev. Lett.*, **62**, 1286 (1989).
284. G. Reiter, *Phys. Rev. Lett.*, **68**, 75 (1992).
285. P. Siberzan and L. Leger, *Macromolecules*, **25**, 1267 (1992).
286. C. Redon, J. B. Brzoska and F. Brochard-Wyart, *Macromolecules*, **27**, 468 (1994).
287. I. L. M. van Nunen, B. F. B. Folmer and R. J. M. Nolte, *J. Am. Chem. Soc.*, **119**, 283 (1997).
288. G. Widawski, M. Rawiso and B. Francois, *Nature*, **369**, 387 (1994).
289. B. Francois, O. Pitois and J. Francois, *Adv. Mater.*, **7**, 1041 (1995).
290. C. Normand, Y. Pomeau and M. G. Velarde, *Rev. Mod. Phys.*, **49**, 581 (1977).
291. F. Brochard-Wyart and J. Daillant, *Can. J. Phys.*, **68**, 1084 (1990).
292. G. Reiter, *Phys. Rev. Lett.*, **68**, 75 (1992).
293. G. Reiter, *Langmuir*, **9**, 1344 (1993).
294. P. C. Ohara, J. R. Heath and W. M. Gelbart, *Angew. Chem.*, **109**, 1120 (1997).
295. H. Bénard, *Compt. Rend. Acad. Sci. (Paris)*, **185**, 1109 (1927).
296. (Lord) Rayleigh and J. J. Thomson, *Phil. Mag.*, **32**, 59 (1916).
297. G. H. Frederickson, *Macromolecules*, **20**, 2535 (1987).
298. G. Krausch, *Mater. Res. Rep.*, **14**, 1 (1995).

299. C. M. Marques, L. Leibler and J. F. Joong, *Macromolecules*, **21**, 1051 (1988).
300. R. A. L. Jones, L. J. Norton, E. J. Kramer, F. S. Bates and P. Wiltzins, *Phys. Rev. Lett.*, **66**, 1326 (1991).
301. G. Krausch, C. A. Dai, E. J. Kramer and F. S. Bates, *Phys. Rev. Lett.*, **73**, 3669 (1993).
302. M. S. Turner, M. Rubinstein and C. M. Marques, *Macromolecules*, **24**, 4986 (1994).
303. G. Coulon, T. Russel, V. R. Deline and D. C. Miller, *Macromolecules*, **22**, 4600 (1989).
304. A. Menelle, T. Russel, S. H. Anastasiadis, S. K. Satija and C. F. Majkrzak, *Phys. Rev. Lett.*, **68**, 67 (1992).
305. P. Mansky, C. K. Harrison, P. M. Chaikin, R. A. Register and N. Yao, *Appl. Phys. Lett.*, **68**, 2586 (1996).
306. D. G. Walton, G. J. Kellog, A. M. Mayes, P. Lambooy and T. P. Russel, *Macromolecules*, **27**, 6225 (1994).
307. M. Kikuchi and K. Binder, *J. Chem. Phys.*, **101**, 3367 (1994).
308. M. A. Van Dijk and R. Van den Berg, *Macromolecules*, **28**, 6773 (1995).
309. C. Harrison, M. Park, P. Chaikin, R. A. Register and D. H. Adamson, *Polym. Prep.*, **37**, 821 (1996).
310. J. P. Spatz, S. Sheiko and M. Möller, *Adv. Mater.*, **8**, 513 (1996).
311. J. P. Spatz, S. Sheiko and M. Möller, *Macromolecules*, **29**, 3220 (1996).
312. M. Park, C. K. Harrison, P. M. Chaikin, R. A. Register and D. H. Adamson, *Science*, **276**, 1401 (1997).
313. P. A. Kralchovsky and K. Nagayama, *Langmuir*, **10**, 23 (1994).
314. Z. Gao, X. F. Zong and A. Eisenberg, *Macromolecules*, **27**, 794 (1994).
315. A. Roescher and M. Möller, *Adv. Mater.*, **7**, 151 (1995).
316. A. S. Dimitrov, C. D. Dushkin, H. Yoshimura and K. Nagayama, *Langmuir*, **10**, 432 (1994).
317. J. Haier, G. J. Kramers, S. Walkeirs and G. Kranich, *Macromolecules*, **30**, 6610 (1997).
318. G. Roberts (ed.), *Langmuir-Blodgett-Films*, Plenum Press, New York, 1990.
319. A. Ulman, *An Introduction to Ultrathin Organic Films from Langmuir-Blodgett to Self-assembly*, Academic Press, Boston, 1991.
320. A. Cemel, T. Fort Jr and J. B. Lando, *J. Polym. Sci.*, **A1**, 2061 (1972).
321. V. Enkelmann and J. B. Lando, *J. Polym. Sci., Polym. Chem. Ed.*, **15**, 1843 (1977).
322. C. Bubeck, B. Tieke and G. Wegner, *Mol. Cryst. Liq. Cryst.*, **96**, 109 (1983).
323. F. Embs, D. Funhoff, A. Laschewsky, U. Licht, H. Ohst, W. Prass, H. Ringsdorf, G. Wegner and R. Wehrmann, *Adv. Mater.*, **3**, 25 (1991).
324. G. Wegner, *Mol. Cryst. Liq. Cryst. Sci. Technol. A*, **216**, 7 (1992).
325. A. Laschewsky and H. Ringsdorf, *Macromolecules*, **21**, 1936 (1988).
326. D. Naegele, J. B. Lando and H. Ringsdorf, *Macromolecules*, **10**, 1339 (1977).
327. J. H. Fendler, *Polymerization in Organized Surfactant Assemblies*, in *Surfactants in Solution* (eds. K. L. Mittal and B. Lindman), Plenum Press, New York, 1982, Vol. 3, p. 1947.
328. H. Ringsdorf, B. Schlarb and J. Venzmer, *Angew. Chem.*, **100**, 117 (1988).
329. J. H. Fendler, *Adv. Polym. Sci.*, **113**, 1 (1995).
330. L. M. Blinov, *J. Nonlinear Opt. Phys. Mater.*, **5**, 165 (1997).
331. Z. Sekkat and W. Knoll, *Proc. SPIE Int. Soc. Opt. Engl.*, 164 (1997).
332. H. Nakanishi and S. Okada, *Organic Nonlinear Optical Crystals*, in *Organic Molecular Solids* (ed. W. Jones), CRC Press, Boca Raton, 1997, p. 243.
333. P. Calvert and P. Rieke, *Chem. Mater.*, **8**, 1715 (1996).
334. S. I. Stupp, S. Son, L. S. Li, H. C. Lin and M. Keser, *J. Am. Chem. Soc.*, **117**, 5212 (1995).
335. V. V. Tsukrik, *Prog. Polym. Sci.*, **22**, 247 (1997).
336. E. Orthmann and G. Wegner, *Angew. Chem., Int. Ed. Engl.*, **25**, 14 (1986).

337. M. Seufert, M. Schaub, G. Wenz and G. Wegner, *Angew. Chem.*, **107**, 363 (1995).
338. M. N. Teerenstr, J. G. Hagting, A. J. Schouten, R. J. M. Nolte, M. Kauranen, T. Verbiest and A. Persoons, *Macromolecules*, **28**, 4876 (1996).
339. R. K. Thomas and J. Penfold, *Neutron and X-ray Reflectometry of Interfacial Systems in Colloid and Polymer Chemistry, Curr. Opin. Coll. Interf. Sci.*, **1**, 23 (1996).
340. R. K. Iller, *J. Coll. Interf. Sci.*, **21**, 569 (1966).
341. J. D. Hong, K. Lowack, J. Schmitt and G. Decher, *Supramol. Sci.*, **2**, 201 (1996).
342. J. D. Hong, K. Lowack and J. Schmitt, *Prog. Coll. Polym. Sci.*, **93**, 98 (1993).
343. G. B. Sukhorukov, J. Schmitt and G. Decher, *Ber. Bunsenges. Phys. Chem.*, **100**, 948 (1996).
344. A. Katsuhiko, Y. Lvov and T. Kunitake, *J. Am. Chem. Soc.*, **119**, 2224 (1997).
345. D. Yoo, J.-K. Lee and M. F. Rubner, *Mater. Res. Soc. Symp. Proc.*, **413**, 395 (1996).
346. X. Zhang, M. Gao, X. Kong, Y. Sun and J. Shen, *J. Chem. Soc., Chem. Commun.*, 1055 (1994).
347. K. Araki, M. J. Wagner and M. S. Wrighton, *Langmuir*, **12**, 5393 (1996).
348. Y. Lvov, K. Ariga, I. Ichinose and T. Kunitake, *J. Chem. Soc., Chem. Commun.*, 2312 (1995).
349. M. Onada, Y. Lvov, K. Ariga and T. Kunitake, *Biotechnol. Bioeng.*, **51**, 163 (1996).
350. G. Decher, J.-D. Hong, K. Lowack, Y. Lvov and J. Schmitt, *Layer-by-layer adsorption: The solid/liquid interface as a template for the controlled growth of well-defined nanostructures of polyelectrolytes, Proteins, DNA and polynucleotides*, in *Self-Production of Supermolecular Structures*, NATO ASI Series, **C446**, 267 (1994).
351. Y. Lvov, K. Ariga, I. Ichinose and T. Kunitake, *Langmuir*, **12**, 3038 (1996).
352. Y. Lvov, H. Haas, G. Decher and H. Möhwald, *Langmuir*, **10**, 4232 (1994).
353. W. T. S. Huck, F. C. J. M. van Veggel, B. L. Kropmann, D. H. A. Blank, E. G. Keim, M. M. A. Smithers and D. N. Reinhoudt, *J. Am. Chem. Soc.*, **117**, 8293 (1995).
354. W. T. S. Huck, F. C. J. M. van Veggel and D. N. Reinhoudt, *Angew. Chem., Int. Ed. Engl.*, **108**, 1304 (1996).
355. S. Serroni, G. Deuti, S. Campagna, A. Juris, M. Ciano and V. Balzani, *Angew. Chem. Int. Ed. Engl.*, **31**, 1493 (1992).
356. S. Campagne, G. Deuti, S. Serroni, A. Juris, M. Venturi, V. Riceruti and V. Balzani, *Chem. Eur. J.*, 211 (1995).
357. W. T. S. Huck, R. Hulst, P. Timmermann, F. C. J. M. van Veggel and D. N. Reinhoudt, *Angew. Chem.*, **109**, 1046 (1997).
358. S. C. Zimmermann, F. Zeng, D. E. C. Reichert and S. V. Kolotuchin, *Science*, **271**, 1095 (1996).
359. C. J. Hawker and J. M. J. Frechet, *J. Am. Chem. Soc.*, **112**, 7638 (1990).
360. V. Percec, G. Johansson, J. Heck, G. Ungar and S. V. Batty, *J. Chem. Soc., Perkin Trans. 1*, 1411 (1993).
361. V. S. K. Belagurasamy, G. Ungar, V. Percec and G. Johansson, *J. Am. Chem. Soc.*, **119**, 1539 (1997).
362. V. Percec, M. N. Holerca, G. Johansson, G. Ungar and D. J. P. Yearley, *Polym. Prep.*, **38**, 478 (1997).
363. V. Percec, C. H. Ahn, G. Ungar, D. J. P. Yearley, M. Möller and S. Sheiko, *Nature*, **391**, 161 (1998).
364. V. Hensel and A. D. Schlüter, *dieb. Ann.*, **303** (1997).
365. A.-D. Schlüter, P. Liess and V. Hensel, *Lieb. Ann.*, 1037 (1996).
366. A.-D. Schlüter, R. Klopsch and P. Franke, *Chem. Eur. J.*, **2**, 1330 (1996).
367. A.-D. Schlüter, B. Karakaya, W. Claussen, K. Gessler and W. Saenger, *J. Am. Chem. Soc.*, **119**, 3296 (1997).
368. G. Schill, *Catenanes, Rotaxanes and Knots*, Academic Press, New York, 1971.

369. J. P. Sauvage, *Topology in Molecular Chemistry, New. J. Chem.*, **10–11**, 17 (1993).
370. D. Philip and J. F. Stoddart, *Angew. Chem.*, **108**, 1242 (1996).
371. G. Wenz, *Angew. Chem.*, **106**, 851 (1994).
372. W. Saenger, *Angew. Chem.*, **82**, 343 (1980).
373. Y. S. Lipatov, T. E. Lipatova and S. T. Kosynachuk, *Adv. Polym. Sci.*, **88**, 49 (1989).
374. H. W. Gibson, M. C. Bheda and P. T. Engen, *Prog. Polym. Sci.*, **19**, 843 (1994).
375. A. Harada and M. Komochi, *J. Chem. Soc., Chem. Commun.*, 1322 (1990).
376. A. Harada, J. Li and M. Kamochi, *Nature*, **370**, 126 (1994).
377. G. Wenz and B. Keller, *Angew. Chem.*, **104**, 201 (1992).
378. L. P. Meier, M. Heulle, W. R. Caseri, R. Shelden, U. W. Suter, G. Wenz and B. Keller, *Macromolecules*, **29**, 718 (1996).
379. M. Maciejewski, A. Gwidzowski, P. Peczak and A. Pietrzak, *J. Macromol. Sci., Chem.*, **A13**, 87 (1979).
380. H. H. Greve, Thesis, Cologne University, 1986.
381. N. Ogata, K. Sanui and J. Wada, *J. Polym. Sci., Polym. Lett. Ed.*, **14**, 459 (1976).
382. H. Chakikara, N. Kunieda and M. Kinoshita, *Mem. Fac. Engr. Osaka City Chem.*, **28**, 121 (1987).
383. M. B. Steinbrunn and G. Wenz, *Angew. Chem.*, **104**, 201 (1992).
384. G. Li and R. S. McGown, *Science*, **264**, 249 (1994).
385. M. Asakawa, P. R. Ashton, G. R. Brown, W. Hayes, B. Menzer, J. F. Stoddart, A. J. P. White and D. J. Williams, *Adv. Mater.*, **8**, 37 (1996).
386. Y. Cao, P. Smith and A. J. Heeger, *Synth. Meth.*, **48**, 91 (1992).
387. Y. Cao, G. M. Treacy, P. Smith and A. J. Heeger, *Appl. Phys. Lett.*, **60**, 2711 (1997).
388. Y. Cao and P. Smith, *Polymer*, **34**, 3139 (1993).
389. C. Y. Yang, P. Smith, A. J. Heeger, Y. Cao and J. E. Osterholm, *Polymer*, **35**, 1143 (1994).
390. N. S. Sariciftci, L. Smilowitz, Y. Cao and A. J. Heeger, *J. Chem. Phys.*, **98**, 2664 (1992).
391. G. Gustafsson, Y. Cao, G. M. Treacy, F. Klavetter, N. Colaneri and A. J. Heeger, *Nature*, **357**, 477 (1992).
392. Y. Yang, E. Westerweele, C. Zhong, P. Smith and A. J. Heeger, *J. Appl. Phys.*, **77**, 694 (1995).
393. Y. Xia, A. G. MacDiarmid and A. J. Epstein, *Macromolecules*, **27**, 7212 (1994).
394. Y. Cao, N. Colaneri, A. J. Heeger and P. Smith, *Appl. Phys. Lett.*, **65**, 2000 (1994).
395. M. R. Majidi, L. A. P. Kane-Maguire and G. G. Wallace, *Polymer*, **36**, 3597 (1995).
396. J. Ruokolainen, J. Tanner, G. ten Brinke, O. Ikkala, M. Torkkeli and R. Serimaa, *Macromolecules*, **28**, 7779 (1995).
397. O. Ikkala, J. Ruokolainen, M. Torkkeli, R. Serimaa and G. ten Brinke, *Macromol. Symp.*, **112**, 191 (1996).
398. J. Ruokolainen, G. ten Brinke, O. Ikkala, M. Torkkeli and R. Serimaa, *Macromolecules*, **29**, 3409 (1996).
399. O. Ikkala, J. Ruokolainen, G. ten Brinke, M. Torkkeli and R. Serimaa, *Macromolecules*, **28**, 7088 (1995).
400. J. Ruokolainen, M. Torkkeli, R. Serimaa, S. Vahvaselkä, M. Saariaho, G. ten Brinke and O. Ikkala, *Macromolecules*, **29**, 6621 (1996).
401. C. Maltesh and P. Somasundaran, *Langmuir*, **8**, 1926 (1992).
402. G. H. Frederickson, *Macromolecules*, **26**, 2825 (1993).
403. M. Wintermantel, K. Fischer, M. Gerle, R. Ries, M. Schmidt, K. Kajiwara, H. Urakawa and J. Wataoka, *Angew. Chem.*, **107**, 1607 (1995).
404. S. S. Sheiko, M. Gerle, K. Fischer, M. Schmidt and M. Möller, *Langmuir*, **19**, 5368 (1997).

405. G. M. Whitesides, E. E. Simak, J. P. Mathias, C. T. Seto, D. N. Chin, M. Mammen and D. M. Gordon, *Acc. Chem. Res.*, **28**, 37 (1995).
406. J. Yang, J.-L. Marundez, S. J. Geib and A. D. Hamilton, *Tetrahedron Lett.*, **35**, 3655 (1994).
407. J. M. Lehn, *Supramolecular Chemistry*, VCH Weinheim, 1995, Chap. 9.4.2–9.4.3.
408. R. Stadler, *Kautsch. Gummi. Kunstst.*, **46**, 619 (1993).
409. R. F. M. Lange and E. W. Meijer, *Macromolecules*, **28**, 782 (1995).
410. R. F. M. Lange and E. W. Meijer, *Macromol. Symp.*, **102**, 301 (1996).
411. G. Lattermann and U. Beginn, *Polymer Preprints*, **37**, 70 (1996).
412. A. P. Delnoye, R. P. Sijbesma, J. A. J. M. Vehemens and E. W. Meijer, *J. Am. Chem. Soc.*, **118**, 8717 (1996).
413. T. Gulik-Krzywicki, C. Fouquey and J. M. Lehn, *Proc. Natl. Acad. Sci. USA*, **90**, 163 (1993).
414. J. Michl, in *Mesomolecules* (eds. G. D. Mendenhall, A. Greenberg and J. F. Liebmann), Chapman & Hall, New York, 1995.
415. M. Simard, D. Su and J. D. Wuest, *J. Am. Chem. Soc.*, **113**, 4696 (1991).
416. S. B. Copp, S. Subramanian and M. J. Zaeorotko, *J. Chem. Soc., Chem. Commun.*, 1078 (1993).
417. C. T. Seto and G. M. Whitesides, *J. Am. Chem. Soc.*, **113**, 712 (1991).
418. K. Hirotsu and T. Higuchi, *J. Org. Chem.*, **47**, 1143 (1982).
419. J.-H. Furhop and W. Helfrich, *Chem. Rev.*, **93**, 1565 (1993).
420. R. J. H. Hafkamp, Thesis, Twente University, 1996.
421. N. Kimizuka and T. Kunitake, *Adv. Mater.*, **8**, 89 (1996).
422. R. J. H. Hafkamp, M. Feiters and R. J. M. Nolte, *Angew. Chem.*, **106**, 1054 (1994).
423. B. Pfannemüller and W. Welte, *Chem. Phys. Lip.*, **37**, 227 (1985).
424. J.-H. Furhop and J. Köning, *Membranes and Molecular Assemblies: the Synkinetic Approach* (ed. J. F. Stoddart), The Royal Society of Chemistry, Oxford, 1994.
425. P. Terech, *Physical Gelation of a Steroid-Cyclohexane System: Kinetic Phenomenological Approach*, in *Reversible Polymeric Gels and Related Systems* (ed. P. Russo), American Chemical Society Symposium Series (ACS), **350**, 115 (1987).
426. A. P. H. J. Schenning, B. de Bruin, M. C. Feiters and R. J. M. Nolte, *Angew. Chem.*, **106**, 1741 (1994).
427. I. L. M. van Nunen, R. S. A. Stevens, S. J. Picken and R. J. M. Nolte, *J. Am. Chem. Soc.*, **116**, 8825 (1994).
428. M. E. Paulatis, G. Shekhar and H. S. Ashbaugh, *The Hydrophobic Effect, Curr. Opin. Coll. Interf. Sci.*, **1**, 376 (1996).
429. B. W. Hotten and D. H. Birdsall, *Coll. Interf. Sci.*, **7**, 821 (1952).
430. T. Tashibana and H. Kambara, *Bull. Chem. Soc. Jpn.*, **42**, 3422 (1969).
431. T. Terech and V. Rodriguez, *Prog. Coll. Polym. Sci.*, **97**, 151 (1994).
432. Y. Xia, X.-M. Zhao and G. M. Whitesides, *Microelectron. Engineering*, **32**, 255 (1996).
433. K. Hanabusa, Y. Watanabe, M. Kimura, T. Koyama and H. Shirai, *Seni Gakkai Shi, Tokyo*, **52**, 129 (1996).
434. M. R. Ghadiri, *Adv. Mater.*, **7**, 489 (1995).
435. J. R. Granja and M. R. Ghadiri, *J. Am. Chem. Soc.*, **116**, 10785 (1994).
436. M. R. Ghadiri, J. R. Granja and L. K. Buehler, *Nature*, **369**, 301 (1994).
437. S. I. Stupp, V. LeBonheur, K. Walker, L. S. Li, K. E. Huggins, M. Keser and A. Amstutz, *Science*, **276**, 385 (1997).
438. G. Czihak, H. Langer and H. Ziegler, *Biologie*, Springer, Berlin, 1981.
439. B. Alberts, D. Bray, J. Lewis, M. Raff, K. Roberts and J. D. Watson, *The Molecular Biology of the Cell*, 3rd edn., Garland Publishing Inc., New York, 1994, Chap. 6, p. 223.

440. E. Dessipri and D. A. Tirrell, *Macromolecules*, **27**, 5463 (1994).
441. K. A. Bauer, A. Ben-Bonat, M. Dawson, V. De Laj Puente and I. O. Neway, *Appl. Environ. Microbiol.*, **56**, 1296 (1987).
442. A. Pnitch, K. Matsuki, E. J. Cantor, S. J. Cooper, E. D. T. Atkins, M. J. Fournier, T. L. Manson and D. A. Tirrell, *Macromolecules*, **30**, 42 (1997).
443. G. Wulff and A. Sarhan, *Angew. Chem., Int. Ed. Engl.*, **11**, 554 (1972).
444. J. Steinke, D. C. Sherrington and J. R. Dunkin, *Imprinting of Synthetic Polymers Using Molecular Templates*, *Adv. Polym. Sci.*, **123**, 81 (1995).
445. G. Wulff, *Angew. Chem.*, **107**, 1958 (1995).
446. Y. Ito, *Molecular Shape Recognition*, in *Polymeric Materials Encyclopedia* (ed. J. C. Salamone), CRC Press, New York, 1996, Vol. 5, p. 4473.
447. B. Sellergreen, M. Lepisto and K. Mosbach, *J. Am. Chem. Soc.*, **110**, 5853 (1988).
448. G. Wulff and M. Minarik, *J. Liq. Chromat.*, **13**, 2987 (1990).
449. G. Vlatakis, I. L. Andersson, R. Müller and K. Mosbach, *Nature*, **361**, 645 (1993).
450. J. Mathew-Krotz and K. J. Shea, *J. Am. Chem. Soc.*, **118**, 8154 (1996).
451. S. A. Piletzki, Y. P. Parkometz, N. V. Lavyryk, T. L. Panasyuk and A. V. Elskaya, *Sens. Actuators*, **B18-19**, 629 (1994).
452. Y. N. Belokon, V. I. Tararov, T. F. Seveleva, M. M. Vorobev, S. V. Vitt, V. F. Sizoi, N. A. Suknacheva, G. V. Vasilev and V. M. Belikov, *Macromol. Chem.*, **184**, 2213 (1983).
453. S. E. Bystöm, A. Boerje and B. Akermark, *J. Am. Chem. Soc.*, **115**, 2081 (1993).
454. J. Damen and D. C. Neckers, *J. Am. Chem. Soc.*, **102**, 3265 (1980).
455. K. J. Shea and E. A. Tompson, *J. Org. Chem.*, **43**, 4253 (1978).
456. G. Wulff and J. Vietmeier, *Macromol. Chem.*, **190**, 1717 (1989).
457. K. J. Shea, *Trends in Polymer Science*, **2**, 166 (1994).
458. G. Wulff, *Molecular Recognition in Polymers Prepared by Imprinting with Templates*, in *Polymeric Reagents and Catalysts* (ed. W. T. Ford), American Chemical Society Symposium Series (ACS), **308**, Washington DC, 1986, p. 186.
459. K. Mosbach, *Trends in Biochem. Sci.*, **19**, 9 (1994).
460. A. J. Kovacs and C. J. Straupe, *Cryst. Growth*, **48**, 210 (1980).
461. G. Wegner, *Thin Solid Films*, **216**, 105 (1992).
462. B. Rieger and M. Hackmann, *CaTEch.*, **2** (1997), p. 79.
463. J. Eastoe and B. Warne, *Curr. Opin. Coll. Interf. Sci.*, **1**, 800 (1996).
464. G. Wulff, J. Vietmeier and H.-G. Poll, *Macromol. Chem.*, **188**, 731 (1987).
465. A. Khumar, H. A. Biebyck and G. M. Whitesides, *Langmuir*, **10**, 1498 (1994).
466. J. H. Wilbur, A. Khumar, E. Kim and G. M. Whitesides, *Adv. Mater.*, **6**, 600 (1994).
467. R. Stadler, C. Auschra, J. Beckmann, U. Krappe, J. Voigt-Martin and I. Leibler, *Macromolecules*, **28**, 3080 (1995).
468. C. Tanford, *The Hydrophobic Effect*, Wiley, New York, 1980.
469. J. Gons, L. J. P. Straatnam and G. Challa, *J. Polym. Sci., Polym. Chem. Edn.*, **16**, 427 (1978).
470. J. Matuszewski-Czewik and S. Polowinski, *Europ. Polym. J.*, **26**, 549 (1990).
471. N. Tewari and A. K. Srivastava, *J. Polym. Sci., Polym. Chem. Edn.*, **27**, 1065 (1989).
472. Y. Y. Tan and G. Challa, in *Encyclopedia of Polymer Science* (eds H. F. Mark, N. M. Bikales, C. G. Overberger and G. Meares), Vol. 16, p. 544, Wiley Interscience, New York, 1988.
473. H. T. van de Grepel, Y. Y. Tan and G. Challa, *Macromol. Chem. Macromol. Symp.*, **20/21**, 83 (1988).
474. R. J. Ansell, D. Kriz and K. Masbach, *Curr. Opin. Biotechnol.*, **7**, 89 (1996).
475. O. T. Ikkala, L. O. Pietilä, L. Ahjopalo, H. Österholm and P. J. Passimiemi, *J. Chem. Phys.*, **103**, 9855 (1995).

476. J. P. Spatz, A. Roescher, S. Sheiko, G. Krausch and M. Möller, *Adv. Mater.*, **7**, 731 (1995).
477. K. N. Bakeev, S. A. Chugunov, T. A. Larina, W. J. MacKnight, A. B. Zenin and V. A. Kabanov, *Macromol. Symp.*, **106**, 19 (1996).
478. I. Yamakawa, K. Osakada and T. Yamamoto, *J. Am. Chem. Soc.*, **118**, 1811 (1996).
479. C. Wu, R. Ma, B. Thou, J. Shen, K. K. Chan and K. F. Woo, *Macromolecules*, **29**, 228 (1996).
480. M. Shwarz, *J. Polym. Sci.*, **13**, 317 (1954).
481. P. Cerrai, G. D. Guerra, M. Tricoli, S. Maltinti, N. Barbani and L. Petarca, *Macromol. Chem. Phys.*, **197**, 3567 (1996).
482. S. Polowinski, Template Polymerization in *Polymeric Materials Encyclopedia*, (ed. J. C. Salamone), **6**, 4038, CRC Press, New York (1996).
483. I. M. Papisov, Matriux Polymerization in *Polymeric Materials Encyclopedia*, (ed. J. C. Salamone), **6**, 4038, CRC Press, New York (1996).
484. J. Ferguson and J. Smyllie, Template Polymerization (Kinetics) in *Polymeric Materials Encyclopedia*, (ed. J.C. Salamone), **6**, 4038, CRC Press, New York (1996).
485. O. Ramström and R. J. Ansell, *Chirality*, **10**, 195 (1998).
486. D. A. Spivak and Shea, K.J., *Macromolecules*, **31**, 2160 (1998).
487. J.-M. Hong, P. E. Anderson, J. Qian and C. R. Martin, *Chem. Mater.*, **10**, 1029 (1998).
488. G. Wulff, T. Groß and R. Schönfeld, *Angew. Chem.*, **109**, 2051 (1957).
489. B. P. Santora, A. O. Larsen and M. R. Gagne, *Organometallics*, **17**, 3138 (1998).

Chapter 4

Chemosensors: Synthetic Receptors in Analytical Sensing Applications

ANTHONY W. CZARNIK* AND JUYOUNG YOON‡

Illumina, San Diego, CA, USA

Submission received: October 1997

1. INTRODUCTION

The field of molecular recognition deals with all aspects of the way in which two or more molecules associate noncovalently, or “bind”. Such binding is similar to “bonding” in that the forces involved hold atoms, or groups of atoms, near one another despite the entropy cost. Both types of association can involve either directional (orbital) or nondirectional (polar) components. And while bonding interactions tend to be stronger in general than binding interactions, this is not an absolute; many covalent species (e.g. peroxides) break their bonds under conditions under which two complementary strands of DNA continue to bind. However, in the general case covalent bonds do not dissociate spontaneously under ambient conditions, while many reversibly formed noncovalent complexes do.

Reversibility begets *reusability*. The transient nature of complexes is an absolute requirement for all molecules that function as *reusable machines*. Enzymes are molecule-sized lathes that bind to their substrates, catalyze a reaction, and release the product; when done, the enzyme is ready for reuse. Indeed, any chemical catalyst must meet this criterion based on the very definition of a catalyst: “a species that enhances the rate of a chemical process *without itself being changed*.” Enzymatic

‡ Silla University, Pusan, Korea

catalysis can be simple – as in one protein, one substrate. Or it can be more complex – as in a set of proteins that must self-assemble before the catalytic action can occur (e.g. transcriptional activation complexes). Such self-assembly requires reversible complexation made specific by molecular recognition, and exemplifies complexes that function as *reusable construction materials*.

In the same way, the host of a host–guest complex can function as, or as part of, a sensor. Sensors are devices that “announce” the presence of analytes via reversible, real-time signals discernible by one of the human senses. Molecular recognition complexes utilized toward this end function as *reusable indicators*. One school of thought holds that a sensor is a macroscopic device with wires and the like; a pH meter is one such embodiment. We prefer the view that molecules themselves can be sensing devices as well. A solution of a colorimetric pH indicator fulfills all the requirements of a sensor: the solution “announces” the presence of protons via a reversible, real-time signal discernible by one of the human senses (sight).

Regardless of the reader’s view on what comprises a “device,” it is absolutely clear that the sensing of one analyte in a mixture of analytes requires molecular recognition. A signal-producing receptor (a host) must complex only one analyte (a guest) in a mixture in order to be useful. Of course, absolute selectivity is never achievable and not necessary; selectivity sufficient for the application is all that’s called for. Sometimes, that application only requires selectivity for a class of analyte, such as hydrocarbons in water. The situation in which several mixture components bind but only yields a signal is not a safe one, except in that unusual case in which the absolute number of receptors is in large excess over all binding guests.

Where do receptors with useful properties for sensor construction come from? The answer depends on your definition of the word “useful.” If “useful” requires only selectivity, then nature provides both a wealth of biotic receptors (enzymes and other proteins) and powerful tools for discovering unnatural macromolecular receptors. For the purposes of this chapter, a sensor that utilizes a polypeptide, polysaccharide, or polynucleotide as the recognition element is referred to as a *biosensor*. By contrast, any sensor utilizing a different (usually synthetic) recognition element is referred to as a *chemosensor*. For the purposes of this article, these terms will apply to any device, molecule-sized or larger, that utilizes such compounds for its molecular recognition function.

Chemosensors utilize receptors that do not denature. Furthermore, the biotic macromolecules utilized in biosensors are materials that every cell in every living organism has evolved to metabolize. Thus, the hazard of introducing a biosensor into a biotic milieu is the same as that of using biochemicals as drugs – their half-life tends to be short. Abiotic molecules can also be metabolized, but most of this activity occurs only in the liver of higher organisms. It can be seen that there are significant benefits to the use of abiotic vs. biotic receptors based on stability. Given this, why are there thousands of reported studies utilizing biosensors and only a few dozen utilizing chemosensors? Again to us, this is a prototypical example of the “lost key” phenomenon. The story goes like this. A man walking at night came

across another man on hands-and-knees searching the ground under a lamp post. “What are you looking for?” said the walking man. “My keys,” said the searching man. “Let me help you search,” said the walking man. “Where did you lose them?” The searching man pointed out into the darkness, “About twenty yards that way.” “Well, why are you looking here under the lamp post?” queried the walking man. “Because I can see here,” was the reply.

Nature has required the evolution of usefully selective hosts, and proteins (in the forms of enzymes, receptors, and antibodies) provide them. However, no individual protein molecule lasts in a cell for very long. All proteins are constantly anabolized and catabolized, with constant concentrations achieved via homeostasis. Nature never demanded permanence of its molecular recognition machinery. When we utilize biotic receptors for one-time, batch analytical applications, the receptors clearly meet the “useful” criterion. However, if a receptor must have an extended lifetime in a sensing device, then we propose that biotic receptors represent the easiest place in which to search instead of the right place to search. If a biotic receptor cannot reasonably be made stable enough to survive weeks of service, then it will not be “useful” for a sensing application no matter how avid or selective.

With that diatribe, what is the hope of finding the key at all? Can abiotic receptors be designed or discovered that meet the “useful” litmus test? The clear answer is “yes,” and the purpose of this chapter is to highlight several published reports describing chemosensor creation. It is not the authors’ purpose to review this field. Instead, we have chosen examples of chemosensors yielding different signal types that exemplify each approach to coupling a receptor with a signaling function. In the strictest sense, the coupling of a receptor in solution with an NMR tube and an NMR spectrometer yields a sensor. Indeed, the binding ability of most synthetic receptors has been monitored in this way. However, the most useful sensors will be those for which the necessary hardware is less expensive and more mobile. This confers special design and synthetic challenges on chemosensors’ creators, but these challenges are both interesting and conquerable. All solutions require integrating a receptor element with a signaling element. The signal types we will focus on here are: absorption (colorimetry), emission (fluorimetry), delayed emission (phosphorimetry), optical rotation (polarimetry), and electrical potential (potentiometry). A volume resulting from a NATO symposium on this topic is available [1].

2. CHROMOGENIC (COLORIMETRIC) CHEMOSENSORS

2.1 Example 1

Cram, Czech *et al.* [2] reported the development of chemosensors **1–4** (Figure 1) for commercial use as Na^+ and K^+ assays in serum and other solutions. When a cation binds to the crown portion of these compounds, the complexation is coupled to an increase in acidity of the conjugated aniline NH; deprotonation at constant pH

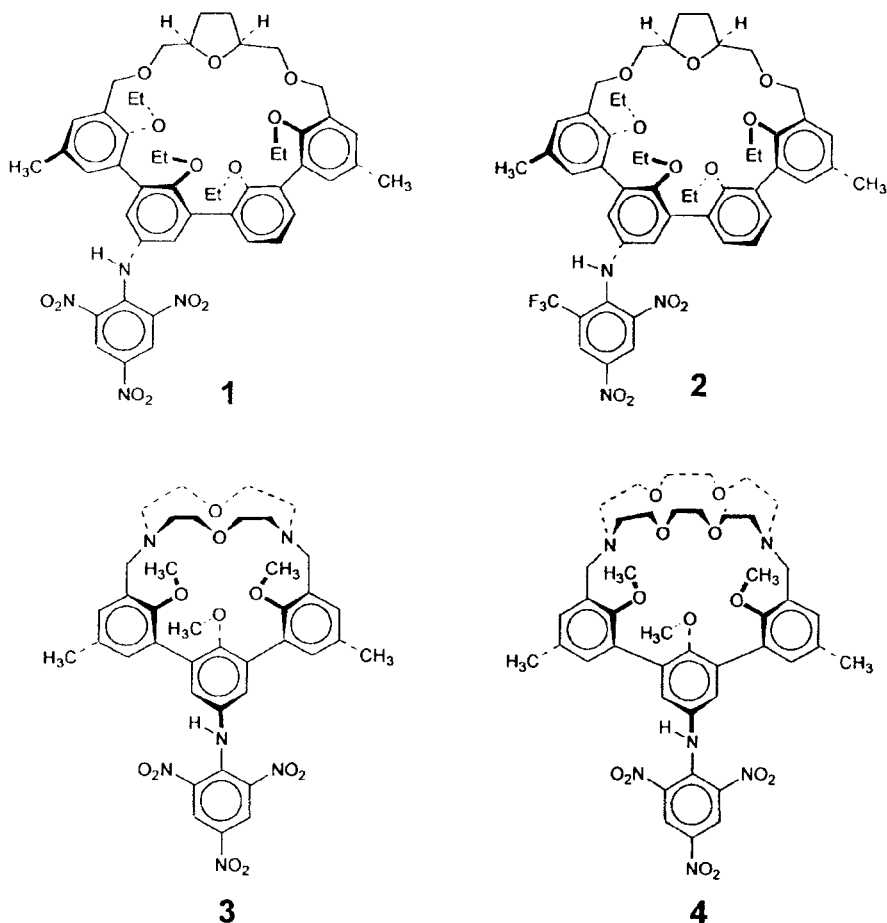


Figure 1 Structures 1, 2, 3, and 4

results in color development. Compounds **1** and **2** show usefully high affinity for K^+ (detection to 10^{-5} M) and high selectivity for K^+ over Na^+ in 80% dioxane–20% water. Compounds **3** and **4** exhibit high sensitivity (detection limits of $\approx 4 \times 10^{-7}$ M for K^+ and 2×10^{-5} M for Na^+) and selectivities estimated to be greater than 1000 for both $[K^+]/[Na^+]$ and $[Na^+]/[K^+]$, respectively. From the pK_a values of compound **1**, the authors determined that the dioxane-rich medium provides the greater selectivity of **1** for K^+ over Na^+ . For example, in 80% dioxane–20% water (v/v), the acidity of **1** ($pK_a = 11.10$) is ≈ 0.34 pK_a unit higher than that of its Na^+ complex ($pK_a = 10.76$), which is ≈ 1.5 unit higher than that of the K^+ complex

($pK_a = 9.35$). Figure 2 shows visually how much more sensitive **1** is to the presence of K^+ than to Na^+ in pH 10 buffer in 80% dioxane–20% water (v/v). Figure 3 provides a graphic measure of how **1** responds to incremental additions of KCl at pH 10 in 80% dioxane–20% water (v/v). The authors conclude that **1** is a potentially useful colorimetric system for measuring K^+ ion concentrations in the 10^{-4} – 10^{-5} M range in the presence of Na^+ at pH 10 in 80% dioxane–20% water (v/v). Also, the pK_a values of $4 \cdot NaBr$, $4 \cdot NaBr$ in the presence of 100 equivalents of NaBr, and $4 \cdot NaBr$ in the presence of 100 equivalents of KCl, were 7.75, 7.75 and 7.05, respectively. Thus, $4 \cdot K^+$ is about pK_a 0.7 units more acidic than $4 \cdot Na^+$. The UV-visible spectrum of $4 \cdot Na^+$ and $4 \cdot K^+$ in water buffered at pH 7.0 showed a similarly substantial difference as in the case of Figure 2. At pH 7.3 [3% $CH_3(OCH_2-CH_2)_2OH$ –97% H_2O (v/v)], a plot of concentration of K^+ against absorbance at $\lambda = 500$ nm was nicely linear. From these data, the authors concluded that $4 \cdot Na^+$ has close to ideal characteristics for use as a chromogenic indicator system for measuring K^+ concentrations in serum; it is operable at close to physiological pH, sensitive at low concentrations of K^+ , and not affected by the presence of physiological concentrations of Na^+ , Ca^{2+} , and Mg^{2+} or other ions present in serum.

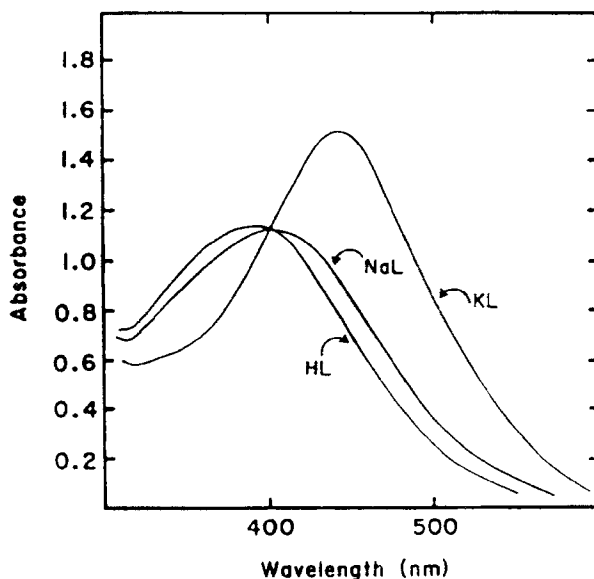


Figure 2 Differences in electronic spectra of **1** (**1** = HL) at pH 10.0 in 80% dioxane–20% water (v/v), 1.07×10^{-4} M in **1**, 0.1 M in CHES buffer: no added salt (curve HL); 0.01 M in NaCl (curve NaL); 0.01 M in KCl (curve KL)

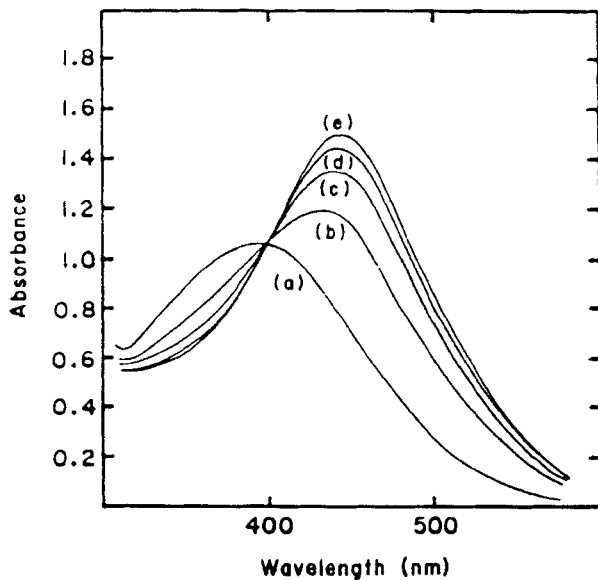


Figure 3 Potassium ion response curves in 80% dioxane–20% water (v/v), 0.020 M in CHES buffer at pH 10.0: (a) 0.0 equiv of KCl/equiv of **1** at 1.07×10^{-4} M; (b) 0.5; (c) 1.0; (d) 2.0; (e) 4.0

2.2 Example 2

Bell *et al.* [3] developed a chemosensor-based chromogenic assay for creatinine (**6**) based on host–guest chemistry. Receptor **5** was designed to bind creatinine utilizing the three hydrogen bonds available in the **5·6** complex (Figure 4). Notably, this process induces proton transfer of the phenolic hydrogen to the end nitrogen in **5**. The resulting dipolar complex gives rise to a color change. Creatinine was extracted from aqueous solution into a dichloromethane solution of **5** with a concomitant change of the organic layer from yellow to brownish-orange. Figure 5 shows that this color change corresponds to the appearance of a broad band in the UV-visible absorption spectrum (400–500 nm). The authors also showed that the intensity of absorbance of this band is clearly correlated with the concentration of **6** at pH 6.0 under conditions of excess **5**. This chromogenic response was found to be selective for creatinine with no color changes occurring under the same conditions with histidine, proline, uric acid, urea, or creatinine as guests. The dissociation constant of complex **5·6** in water-saturated chloroform was calculated to be $0.5 \mu\text{M}$. Also, weak responses to cationic analytes were observed. The authors concluded that this new analytical method is sufficiently sensitive for the measurement of creatinine at normal blood serum levels [40–130 μM], with correction for background levels of Na^+ [130–150 mM].

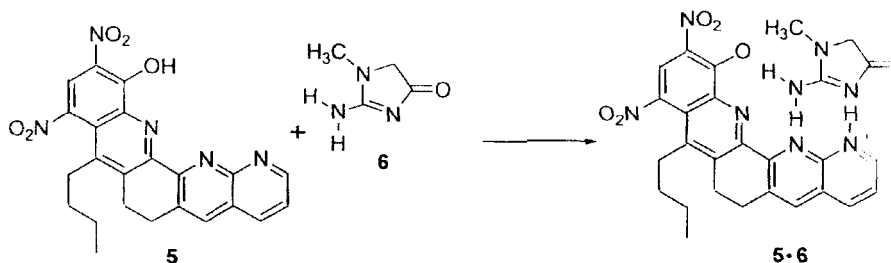


Figure 4 Reversible binding of creatinine (6) to the designed receptor 5, forming a more deeply colored complex (5-6)

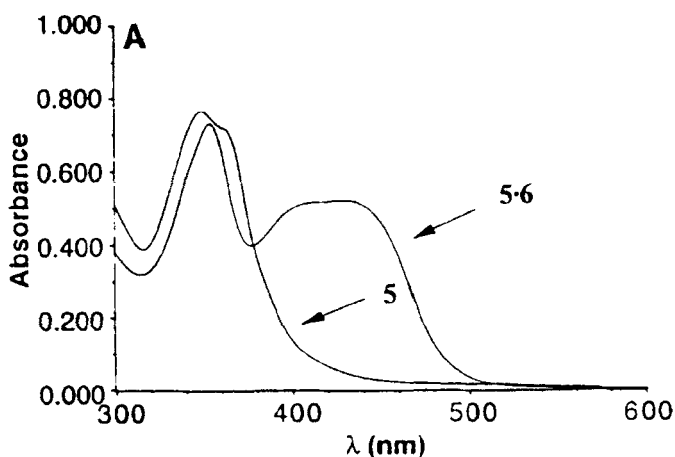
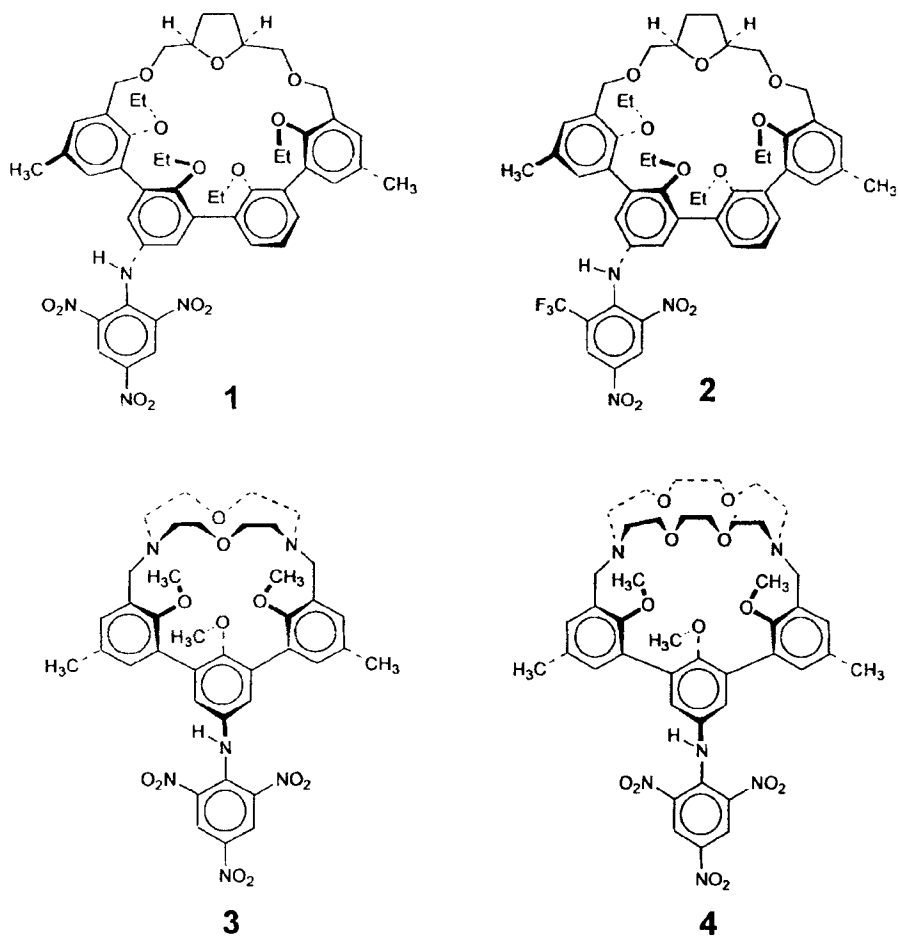


Figure 5 UV-visible absorption spectra of 5 (51 μM) and 5-6 (51 μM 5 + 43 μM 6) in water-saturated CH_2Cl_2

3. FLUORESCENT CHEMOSENSORS

3.1 Example 1

Shinkai *et al.* [4] reported the chiral discrimination of D- and L-monosaccharides using a designed molecule [7 (R or S)] that acts as a chemosensor by virtue of its fluorescent response to the binding of available polyol guest species (Scheme 1). This receptor [7 (R or S)] contains boronic acid groups that bind saccharides by covalent interactions and also incorporates a fluorescent naphthyl moiety (as such, this work expands upon a similar, previously reported approach by the writers of this review [5]). The authors hypothesized that for 7 (R or S), chiral recognition might be transduced into changes in fluorescence emission. Electron transfer from nitrogen to the naphthyl unit, and thus quenching efficiency, is dependent on the relative



Scheme 1 Possible complexes of **7** (R or S) with saccharides at pH 7.7

orientation of amine and aryl units. The authors also proposed that chiral recognition with **7** (R or S) might be possible if an unfavorable interaction or twist around the binaphthyl bond occurs on binding D- or L-monosaccharides. Table 1 gives the reported stability constants, $\log K$, for **7** (R or S) with monosaccharides in partially aqueous solution as well as D/L fluorescence intensity ratios. The fluorescence intensity of **7** (1.0×10^{-5} M) was measured at pH 7.77 (33.3% MeOH/H₂O). As shown in Table 1, using **7R** the 1:1 complex stabilities of D-monosaccharides are

Table 1 Stability constants and fluorescence enhancements for saccharides with **7** (one enantiomer; isomer not assigned)

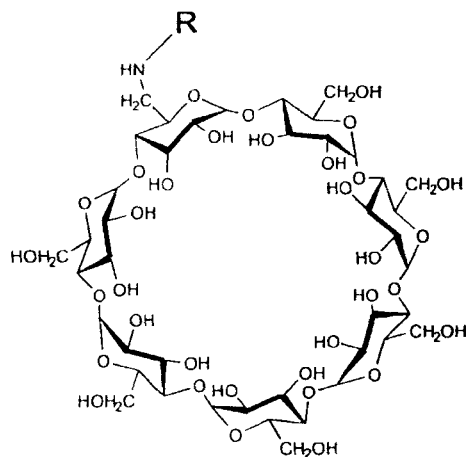
Saccharide	D log K (± 0.05)	L log K (± 0.05)	D/L fluorescence intensity ratio
Fructose	4.0 (3.7)	3.5 (4.0)	1.47 (0.69)
Glucose	3.3 (3.4)	3.1 (3.5)	1.93 (0.53)
Galactose	3.1	3.3	0.82
Mannose	< 2.4	—	—

greater than those of L-monosaccharides and using **7S** the 1 : 1 complex stabilities of L-monosaccharides are greater than those of D-monosaccharides. In this way, the authors have shown that chemosensors can be obtained that display selective response towards one optical isomer of a monosaccharide.

3.2 Example 2

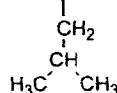
Ueno *et al.* have prepared β -cyclodextrin derivative **10** (β -DA; Figure 6) bearing a *p*-(dimethylamino)benzoyl (DMAB) moiety as a fluorescent chemosensor of molecular recognition [6]. β -DA shows a strong twisted intramolecular charge transfer (TICT) emission that decreases upon the formation of intermolecular inclusion complexes with added guest compounds (Figure 7). The binding constants of **10** with various cholic acid derivatives included $51\,000\text{ M}^{-1}$ for chenodeoxycholic acid (CDCA; Figure 8), $178\,000\text{ M}^{-1}$ for ursodeoxycholic acid (UDCA), and $158\,000\text{ M}^{-1}$ for lithocholic acid, respectively. It is interesting that deoxycholic acid (DCA, $47\,000\text{ M}^{-1}$) was not effectively detected by the host in spite of the fact that it is regioisomeric with CDCA and UDCA with one hydroxyl group at C-12 of the steroidal framework in place of C-7 of CDCA and UDCA.

Dansyl is known as a hydrophobic probe which exhibits fluorescence more strongly in a hydrophobic environment than in an aqueous milieu [7]. The authors prepared dansylglycine-modified β -CD [**9** (β -DG), Figure 6] as a chemosensor, and observed that its fluorescence intensity at 560 nm decreased upon guest addition [8]. This result suggests that the host undergoes a conformational change associated with inclusion of a guest molecule (Figure 7), changing the location of the dansyl moiety from inside to outside of the cavity. This implies that the dansyl moiety is excluded from the hydrophobic environment of the CD cavity to water environment when the guest molecule is accommodated in the cavity. As in the case of β -DA, among the steroidal compounds the host is not sensitive to ketosteroids such as progesterone, corticosterone, cortisone, prednisolone, and hydrocortisone while relatively sensitive to chenodeoxycholic acid and ursodeoxycholic acid. *l*-Borneol was detected with a comparable sensitivity to that of CDCA, while compounds such as menthol, fenchone, nerol, and cyclohexanol were detected with moderate sensitivities. Ueno has also prepared dansyl-*L*-leucine-modified β -CD (**10**, β -DL), and found that its



8 (β -DG): R = -CO-CH₂-NH-C

9 (β -DL): R = -CO-CH-NH-O₂



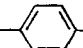
10 (β -DA): R = -CO-

Figure 6 Structures 8, 9, and 10

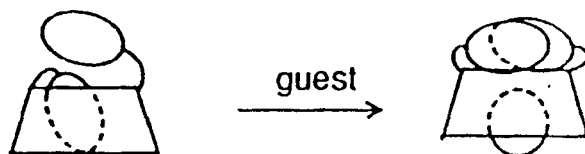


Figure 7 Sketch of the guest-induced conformational change of chromophore-modified cyclodextrins that causes the fluorescence

molecular recognition abilities are similar to those of dansyl-D-leucine-modified β -CD although its reported affinities are roughly twice those of β -DD. Because these cyclodextrin chemosensors are composed of chiral molecules, the potential for signaling via optical rotation exists. In fact, each of these systems displays changes in optical rotation upon guest binding.

A description of work by the authors of this review on fluorescent chemosensors is available [9]. An excellent review by de Silva has recently been published [10]. A symposium volume on the topic from 1992 is also available [11].

4. PHOSPHORESCENT CHEMOSENSORS

Cyclodextrins have been used for enhancing the phosphorescence of guests by encapsulation [12]. de Silva *et al.* employed cyclodextrins as transparent shields to protect the phosphor molecule sterically from contact with its environment (especially O₂) while allowing access to photons. Sensing remains viable because the proton receptor module is not enveloped (Figure 9) [13]. The authors used this system as a phosphorescent PET (photoinduced electron transfer) chemosensor for

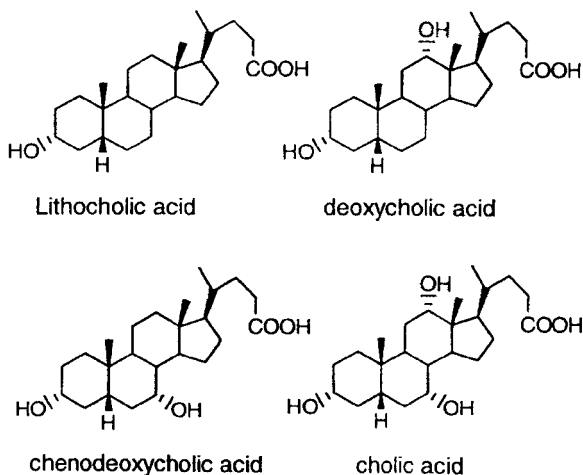


Figure 8 Structures of cholic acids

proton monitoring. The phosphorescence of the bromonaphthyl module of **11** (Figure 10) can be expected to be quenched by the diethylamino moiety; retrieval of phosphorescence is expected upon protonation of the amine electron pair [14]. Chemosensor **11** thus signals pH via phosphorescence in the range 5.5–8.0 with a pK_a (T_1) value of 6.9. The phosphorescence life-time (τ_p) was measured as 0.40 ms. β -Cyclodextrin encapsulation has a marked effect on the phosphorescence of **11**. When compared to simple aqueous solution at pH 3.0, the β -cyclodextrin induced phosphorescence enhancement (PE_{CD/H_2O}) was four-times larger. Compound **12**, a structural isomer of **11**, showed no binding with β -cyclodextrin in dilute solution as evidenced by the nearly identical phosphorescence life-times in water and in β -cyclodextrin solution at pH 3.0 ($\tau_p = 0.45$ and 0.48 ms, respectively). On the other hand, **12** in γ -cyclodextrin solution showed $PE_{CD/H_2O} = 1.3$, suggesting significant complexation. Under these conditions, the phosphorescence was smoothly pH-dependent with pK_a (T_1) = 7.6, $\tau_p = 0.42$ and 1.32 ms at pH 3.0 and 11.0, respectively. Compound **13** is less hydrophobic than **11** or **12** and showed no inclusion in β - or γ -cyclodextrin under phosphorimetric conditions, but nevertheless exhibited useful phosphorescent pH sensing behavior [$\lambda_p = 553$ nm, $\tau_p = 0.42$ ms, pK_a (T_1) = 6.0].

5. ELECTROCHEMICAL CHEMOSENSORS

The first example of chemically modified field-effect transistors (CHEMFETs) was reported by Janata *et al.* [15] in 1978 for ion-sensitive field-effect transistors (ISFETs) in which the gate oxide was covered with a PVC membrane containing

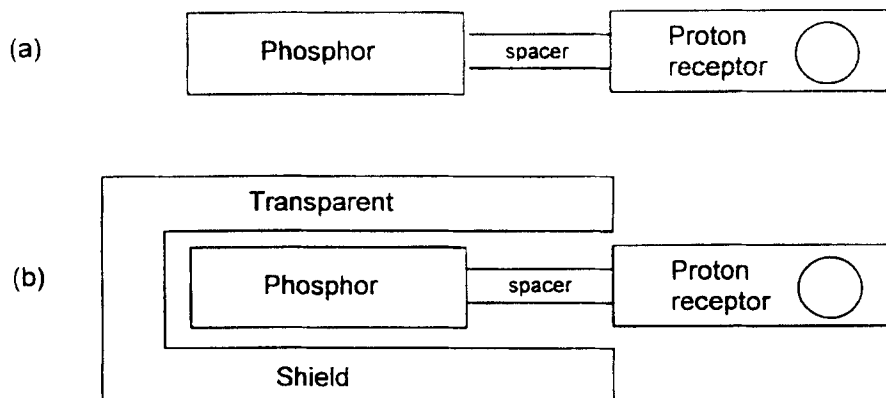


Figure 9 Sketches of (a) phosphorescent PET pH sensor and (b) sterically protected phosphorescent PET pH sensor

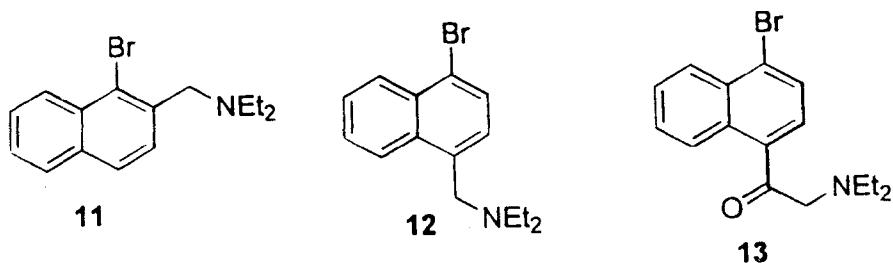


Figure 10 Structures 11, 12, and 13

the K^+ selective ionophore valinomycin. For practical applications of these systems, the basic problems are selectivity and durability. Reinhoudt *et al.* [16] solved the first problem by design of a series of calix[4]arene-based receptors for Na^+ , K^+ , Cs^+ , Ag^+ , Cd^{2+} , and Pb^{2+} . The second problem was solved by covalent anchoring of a combined membrane system to the gate oxide of the field-effect transistor, and by copolymerization of the electroactive components both the ionophore and the lipophilic anions is tuned to buffer the hydrophobic membrane with respect to the ion that is measured. This approach is outlined in Figures 11 and 12. The architecture of these CHEMFETs is depicted in Figure 11. As mentioned before, the mixture of polysiloxane, methacrylated ionophore, and tetraphenylborate is photopolymerized on the top of the polyHEMA layer (Figure 12). This system exhibited a Nernstian response ($54\text{--}56\text{ mV decade}^{-1}$) toward K^+ with selectivity coefficient [$\log(K_{i,j})$] of -3.0 for Na^+ , -4.0 for Mg^{2+} and -3.5 for Ca^{2+} . The broad range of useful analyte concentrations afforded by this electrochemical chemosensor highlight an advantage of Nernstian potentiometry as compared to optical signaling. The CHEMFETs in this paper with covalently bound hemispher- and exhibited an almost constant response during a period of 20 weeks.

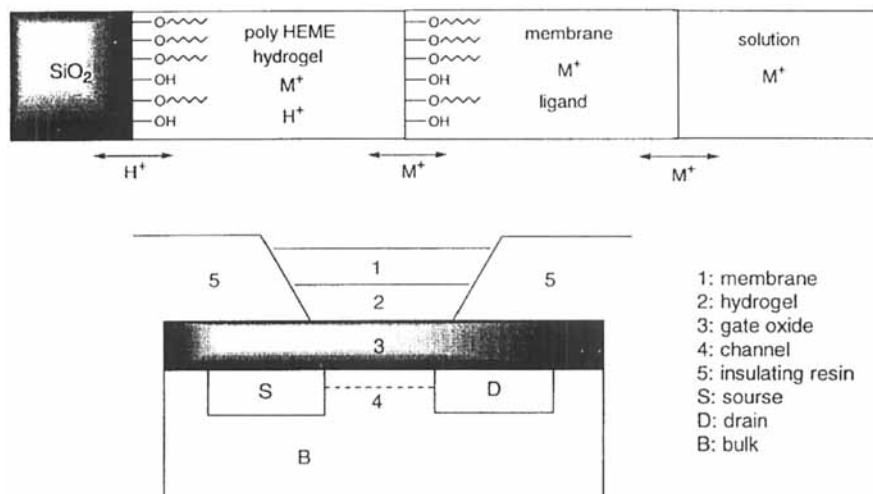


Figure 11 Cross-section of a CHEMFET

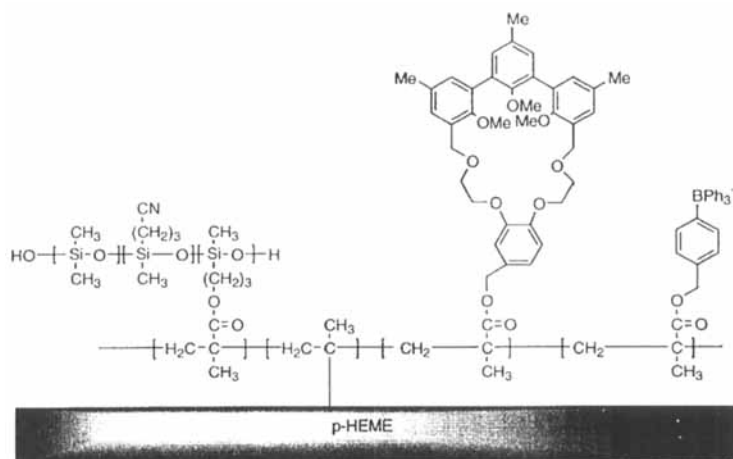


Figure 12 Schematic composition of a polysiloxane membrane with covalently linked hemispherand and tetraphenylborate

6. THE FUTURE OF CHEMOSENSOR DISCOVERY: COMBINATORIAL APPROACHES

Each of these examples of chemosensor creation either required extensive synthesis effort to discover the receptor or benefited from such an effort previously published. Indeed, it is precisely this effort that makes the use of biotic receptors so appealing. Is there hope that usefully selective chemosensors can be discovered with less time

and effort? The question has direct relevance to the drug discovery process as it has been practiced for 50 years. Tremendous synthetic effort goes into the discovery of one drug, but the economic reward of discovery of a “useful” drug is so high that the investment is sustained. Very few sensor projects hold the economic potential of a blockbuster drug. However, very few drugs hold the potential of a blockbuster drug, and new techniques for speeding the discovery process have been invented to meet the challenge.

Drug discovery has recently been revolutionized by combinatorial chemistry, which is in essence a set of tools enabling use of a small set of reactions to combine a few reagents together in all possible combinations with the formation of a matrix of products [17]. At its heart is the premise that host–guest complexation energetics cannot yet be predicted with accuracy, and so facilitated empiricism is a valuable approach to discovery. Drug discovery is host–guest research, in which the host is known and the right guest is desired.

Chemosensor discovery is also host–guest research, in which the guest is known and the right host is required. The issues are really quite the same in both endeavors. As antibody libraries are assembled combinatorially via biosynthesis, so synthetic receptor libraries can now be assembled combinatorially via organic synthesis. The strategy must be to start with a very poor synthetic receptor, and to elaborate its structure with a broad diversity of potentially binding groups. The work of Still is amongst the best reporting this approach to date [18].

The library will have been prepared with a careful eye towards its facile screening for both the best binder overall and the best binders obtained under conditions of competing guests. In this regard, libraries of optical chemosensors truly provide an unusual synergy of form and function. If the library is composed of the chemosensor molecules themselves, then the process of screening for binding ability is made enormously simpler using the signal of the chemosensor itself. For example, consider the case of a bead-based library of chemosensors for glucose in which the fluorescence is expected to increase upon glucose complexation. One simply adds glucose to a mixture of the beads in water until a few of the beads fluoresce, then pull out those beads and establish (perhaps via an encoding scheme) which chemosensor was on it. Chemosensors selective for glucose vs. galactose would be discovered by taking all glucose-binding beads and subjecting them to a solution of galactose; beads that did *not* fluoresce are good candidates for selective chemosensors.

7. CONCLUSIONS

The use of abiotic receptors for sensor creation warrants a renaissance. A myriad of important applications awaits the creation of sensors with useful selectivity and stability properties. The discovery of molecules with such properties is invigorated

by the combinatorial approach. It would seem that a great deal of discovery awaits those who join the chase.

8. REFERENCES

1. J.-P. Desvergne and A. W. Czarnik, *Chemosensors of Ion and Molecular Recognition*, NATO Symposium Series, Kluwer, Dordrecht, 1997.
2. R. C. Helgeson, B. P. Czech, E. Chapoteau, C. R. Gebauer, A. Kumar and D. J. Cram, *J. Am. Chem. Soc.*, **111**, 6339 (1989).
3. T. W. Bell, Z. Hou, Y. Luo, M. G. B. Drew, E. Chapoteau, B. P. Czech and A. Kumar, *Science*, **269**, 671 (1995).
4. T. D. James, K. R. A. S. Sandanayake and S. Shinkai, *Nature*, **374**, 34 (1995).
5. J.-Y. Yoon and A. W. Czarnik, *J. Am. Chem. Soc.*, **114**, 5874 (1992). The term "chemosensor" was coined by the authors in this paper to distinguish the synthetic receptor approach from the biosensor approach.
6. K. Hamasaki, H. Ikeda, A. Nakamura, A. Ueno, F. Toda, I. Suzuki and T. Osa, *J. Am. Chem. Soc.*, **115**, 5035 (1993).
7. E. M. Kosower and D. Huppert, *Annu. Rev. Phys. Chem.*, **37**, 127 (1986).
8. A. Ueno, S. Minato, I. Suzuki, M. Fukushima, M. Ohkubo and T. Osa, *Chem. Lett.*, 605 (1990).
9. A. Czarnik, *Acc. Chem. Res.*, **27**, 302 (1994).
10. A. P. de Silva, H. Q. N. Gunaratne, T. Gunnlaugsson, A. J. M. Huxley, C. P. McCoy, J. T. Rademacher and T. E. Rice, *Chem. Rev.*, **97**, 1515 (1997).
11. A. W. Czarnik, *Fluorescent Chemosensors for Ion and Molecule Recognition*, ACS Books, Washington, 1993.
12. (a) N. J. Turro, J. D. Bolt, Y. Kuroda and I. Tabushi, *Photochem. Photobiol.*, **35**, 69 (1982). (b) N. J. Turro, T. Okubo and C. Chung, *J. Am. Chem. Soc.*, **104**, 1789 (1982). (c) N. J. Turro, G. S. Cox and X. Li, *Photochem. Photobiol.*, **37**, 149 (1983). (d) S. Scypinski and L. J. Cline Love, *Anal. Chem.*, **56**, 332 (1984). (e) R. A. Femia and L. J. Cline Love, *J. Colloid Interf. Sci.*, **108**, 271 (1985). (f) S. Hamai, *J. Am. Chem. Soc.*, **111**, 3954 (1989).
13. R. A. Bissell and A. P. de Silva, *J. Chem. Soc., Chem. Commun.*, 1149 (1991).
14. (a) G. S. Cox, N. J. Turro, N. C. Yang and M. J. Chem, *J. Am. Chem. Soc.*, **106**, 422 (1984). (b) A. J. Bryan, A. P. de Silva, S. A. de Silva, R. A. D. D. Rupasinghe and K. R. A. S. Sandanayake, *Biosensors*, **4**, 169 (1989). (c) S. A. de Silva and K. R. A. S. Sandanayake, *Tetrahedron Lett.*, **32**, 421 (1991).
15. S. D. Moss, J. Janata and C. C. Johnson, *Anal. Chem.*, **47**, 2338 (1975).
16. D. N. Reinhout, *Recl. Trav. Chim. Pays-Bas*, **115**, 109 (1996), and references cited therein.
17. A. W. Czarnik, *Chem. Tracts., Org. Chem.*, **8**, 13 (1995).
18. W. C. Still, *Acc. Chem. Res.*, **29**, 155 (1996).

Chapter 5

Selective Ion Recognition with Durable Sensors

RONNY J. W. LUGTENBERG AND DAVID N. REINHOUTD

University of Twente, The Netherlands

1. INTRODUCTION

From the agrotechnical, clinical, and environmental fields, there is a large demand for chemical sensors that are able to monitor metal ion concentrations in aqueous solutions. The type of sensor, e.g. potentiometric, amperometric, or optical, depends on the chemical species to be monitored and on the environment in which it will be applied [1]. For monitoring a large dynamic range of ion-activities in aqueous media potentiometric sensors are suitable. Potentiometric sensors respond to a physical or chemical stimulus and transduce the resulting signal into a potential change. Such sensors require the integration of a selective detection element and a transducing element. As selective detection elements ion-selective membranes are used that contain synthetic receptor molecules which selectively recognize a guest species. As a transducing element the ion-sensitive field effect transistor (ISFET) is very interesting because the gate oxide can be modified for the covalent attachment of ion-sensitive membranes. Such chemically modified field effect transistors (CHEMFETs) have been investigated for ten years and the literature has been reviewed extensively [2]. CHEMFETs and ion-selective electrodes (ISEs) belong to the same family of potentiometric sensors and have in common an ion-selective membrane as the source of the sensing signal. Technological development has become focused more and more on the CHEMFETs, because these have the advantage of a fast response time and *in situ* impedance transformation. Furthermore, CHEMFETs can be made very small with the available planar integrated circuit technology which

gives rise to the possibility of constructing multi-ion sensing systems [3]. The use of multi-ion sensing systems requires sensors with lifetimes of the order of months or longer. Consequently, receptor molecules in the sensing membrane must be sufficiently hydrophobic or they leach from the membrane to the contacting aqueous solution. To overcome this problem several solutions have been suggested, but large scale applications of CHEMFETs have still not been achieved. The problems and solutions dealing with the application of these sensors will be the first topic discussed in this Chapter. The second part deals with the design of functionalized receptor molecules mainly based on calix[4]arenes which can be used as the selective recognition element in the sensor.

2. CHEMFET ARCHITECTURE

The basic building block of all CHEMFETs is the ion-sensitive field effect transistor (ISFET), introduced in 1970 by Bergveld [4]. In an ISFET the gate metal of a metal oxide semiconductor field effect transistor (MOSFET) is removed and the resulting gate oxide surface (2) is directly exposed to the electrolyte solution (Figure 1).

A reference electrode (1) is present in the solution to achieve a stable and measurable potential. The gate oxide (e.g. SiO_2) acts as an insulator for the p-type silicon semiconductor material (B) in which two n-type conducting paths are implanted, the source (S) and drain (D). By applying a voltage between source and drain (V_{ds}) a current is established, which is dependent on the density of charge carriers present in the semiconductor channel (4) that connects source and drain. The electrical field perpendicular to the gate oxide surface influences the density of charge carriers in the channel and, therefore, the conductance between source and

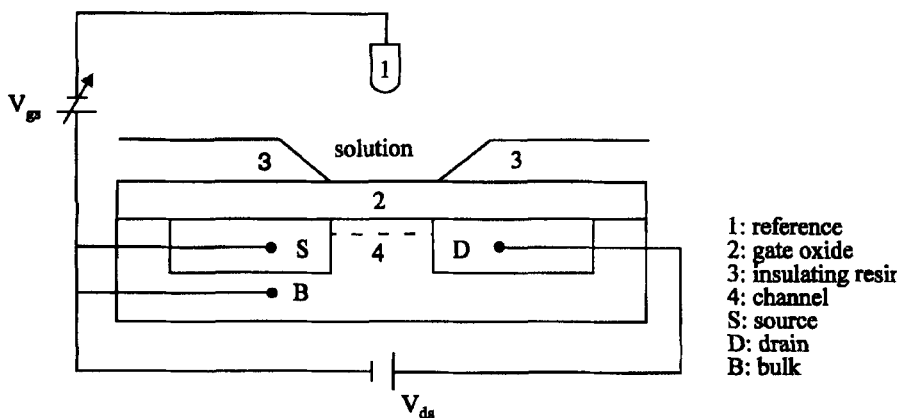


Figure 1 Measuring set-up for an ISFET

drain of the ISFET [5]. In contact with an aqueous solution, the state of ionization of the surface hydroxyl groups (SiOH groups in case of a SiO₂ gate oxide) is dependent on the pH of the solution. This state of ionization determines the surface potential, and modulates the electrical field perpendicular to the gate oxide. In this way, the pH of the solution can be measured. A theoretical site-dissociation model applied to the ISFETs was described by Siu and Cobbold [6], and Bousse and Bergveld [7]. The model correctly describes Nernstian (59.2 mV decade⁻¹) and sub-Nernstian (< 59.2 mV decade⁻¹) behavior of different oxides (SiO₂, Al₂O₃, Ta₂O₅) depending on the surface hydroxyl group dissociation and association constants and the surface concentration of the oxide groups [8,9].

For the detection of ionic species other than protons, it is necessary to introduce receptor molecules which can selectively bind guest species on top of the gate of the ISFET. Direct attachment of ion-selective moieties to the surface, e.g. by silylation with (3-cyanopropyl)dimethyl(dimethylamino)silane resulted in some sensitivity towards Ag⁺ ions (20 mV decade⁻¹), but the sensor was still sensitive towards protons (15 mV decade⁻¹) [10]. Chemical grafting with ammonium phosphonate (1–3) and phosphate sites (4) (Figure 2) or with phthalocyanine-based ionophores bearing crown-ether moieties resulted in a sensitivity towards alkaline (earth) ions, but the pH dependency remained [11,12].

Ion sensitivity can also be introduced by the adhesion of a hydrophobic membrane over the gate oxide area (MEMFET). In these membranes an ion-selective receptor molecule and lipophilic anionic sites can be incorporated which gives the membrane its ion sensitivity and permselectivity [13]. In contact with an aqueous phase a membrane potential is established, which is determined by the electrochemical thermodynamic equilibrium between ions in solution and the hydrophobic membrane. The membrane potential modulates the potential over the gate oxide, and therefore, the electric resistance of the channel. The first membrane-covered ISFET, developed by Moss *et al.*, was selective for K⁺ [14]. This MEMFET was based on a plasticized PVC membrane incorporating the natural ionophore valinomycin. Using different ionophores a number of cation-selective MEMFET devices have been constructed. However, these sensors showed interfering pH and CO₂ sensitivity due to the (uncontrolled) ionization of the surface silanol groups of the gate oxide [15]. We have solved these problems by chemical modification of the ISFET (CHEMFET); a buffered poly(2-hydroxyethyl methacrylate)[polyHEMA]

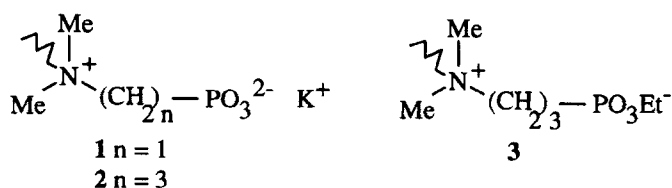


Figure 2 Different phosphonate (1, 2 and 3) and phosphate (4) groups

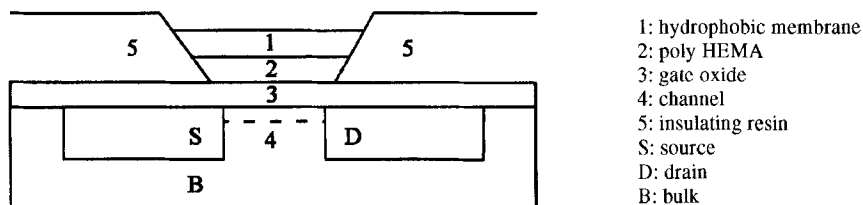


Figure 3 Schematic representation of the CHEMFET

hydrogel is introduced between the gate oxide surface and the sensing membrane layer which keeps the dissociation of the surface silanol groups constant (Figure 3) [16]. The hydrogel is covalently attached to the gate oxide by prior functionalization of the gate oxide with (3-methacryloxypropyl)trimethoxysilane. The resulting methacryloxy groups at the surface react in the photo(co)polymerization of a cast layer of a mixture of 2-hydroxyethyl methacrylate and ethylene glycol dimethacrylate under the formation of a covalently attached hydrophilic cross-linked hydrogel layer of 10–20 μm thickness. The resulting polyHEMA layer is then soaked in a pH-buffer solution containing a fixed concentration (0.1 M) of the primary cation. Due to the presence of this polyHEMA hydrogel, the surface potential is kept constant and the CO_2 interference is eliminated. Because the hydrogel contains hydroxyethyl functional groups, *covalent* anchoring of the hydrophobic membrane to the hydrogel is also possible by functionalization of part of the hydroxyl groups at the surface of the hydrogel.

3. PRINCIPLES OF THE MEMBRANE POTENTIAL

For the interpretation of the parameters that influence the membrane potential (E_M) a general three-segment model of Teorell [17], Meyer and Sievers [18] (TMS model) is often used (Figure 4). The membrane potential (Equation 1) is given by the potential of the (inner) reference solution (Φ_r) minus the potential of the sample solution (Φ_s) and is dependent on the diffusion potential (E_D) and the boundary (or Donnan) potentials ($E_{B,s}$ and $E_{B,r}$):

$$E_M = \Phi_r - \Phi_s = -E_{B,r} - E_D + E_{B,s} \quad (1)$$

$E_{B,s}$ and $E_{B,r}$ are determined by the ratios of the activities of ionic species in the solution (a_i) and the membrane phase (\tilde{a}_i) according to Nernst's law:

$$E_B \sim \frac{RT}{zF} \cdot \ln \frac{a_i}{\tilde{a}_i} \quad (2)$$

When the partition of cations in the membrane is higher than the partition of anions a positive excess of charge is built up at the interface in the membrane phase and the

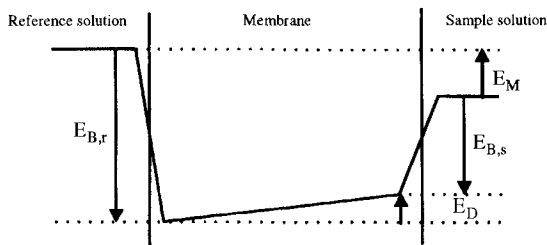


Figure 4 The membrane potential (E_M) as a function of the two interfacial potentials ($E_{B,r}$ and $E_{B,s}$) and the diffusion potential (E_D)

solution is left with an excess of negative charge. This charge separation creates a boundary potential (E_B), which reduces the rate of penetration of positive ions into the membrane and favors the initial rate of anion penetration. This process continues until a steady state boundary potential is established. When the membrane contains lipophilic anionic groups, the extraction of cations is enhanced and a higher boundary potential (E_B) is built up which effectively prevents anions in solution from entering the membrane (the so-called Donnan exclusion principle) [19,20].

By conditioning of the polyHEMA layer in a buffer of fixed pH and primary ion concentration prior to use, the activity of the ions (a_i) in the polyHEMA layer is constant. This fixes the inner boundary potential of the ion sensitive membrane ($E_{B,r}$). For an accurate measurement of an unknown activity of the primary ion in the sample solution based on Nernst law, it is essential that the primary ion activity in the membrane phase (\tilde{a}_i) remains constant. This can be achieved by the introduction of proper amounts of primary ion-selective receptor molecules (ligands, L) in the membrane. The extraction of a particular ion in the membrane phase is then determined by the product of the partition of the ion over membrane and aqueous phase (K_p) and the association constant of the ion-ionophore complex in the membrane (β_i). The association constant β_i determines the free cation activity in the membrane:

$$\beta_i = \frac{[L\tilde{a}_i^+]}{\tilde{a}_i^+[L]} \quad (3)$$

The ratio of complexed and uncomplexed receptor molecules can be fixed by the concentration of lipophilic anionic sites in the membrane. When, for monovalent primary ions, the concentration of lipophilic anionic groups is approximately 50 mol% with respect to the concentration of receptor, the ratio of complexed to free ionophore will be close to unity and consequently $\tilde{a}_i \approx \beta_i^{-1}$. Under these circumstances, the association equilibrium acts as an effective ion buffer system which keeps the activity of the free ion involved in the equilibrium in the membrane constant. The consequence is that changes of the activity of that particular ion in solution will not cause changes of activity of that ion in the membrane phase but will

cause a change of the boundary potential according to Nernst Law given in Equation 2 [21,22]. In order to fulfil an effective buffering, β_i must be sufficiently high ($>10^4 \text{ M}^{-1}$). At values $<10^4 \text{ M}^{-1}$ the amount of the primary cation–ligand complex is lower and varying, and as a result a sub-Nernstian response is observed [22].

In practice, ideal Nernstian behavior often cannot be attained in the presence of interfering ions. The degree of interference caused by other cations is determined by the selectivity of the ion receptor for the primary ion, by the partition coefficients of the different ions over the membrane and aqueous phase, and by the relative activities of the ions in the sample solution. This imposes a second important role to the ion receptor for obtaining ion selectivity in the membrane. By selective complexation of the primary ions i , other cations j are largely excluded from the membrane, with the result that the primary ion becomes the potential determining species. When interfering ions are not completely excluded from the membrane, their contribution to the membrane potential can be treated in terms of an apparent increase of the activity of the primary ion. This is expressed in the semi-empirical Nickolsky–Eisenman equation (Equation 4):

$$E = E^0 + \frac{RT}{z_i F} \cdot \ln(a_i + K_{ij}^{\text{pot}} a_j^{z_i/z_j}) \quad (4)$$

In this equation, E is the potentiometric response, E^0 is the standard potential, and K_{ij}^{pot} is the potentiometric selectivity coefficient [23]. The Nickolsky–Eisenman equation is *only valid if ions of the same valency are compared* [24]. If that is not the case, if a divalent cation is interfering the measurement of a monovalent ion or vice versa, a new selectivity factor K_{ij}^{sel} is recommended [24,25] which more accurately describes the degree of interference; $\log K_{ij}^{\text{sel}}$ is derived graphically from the horizontal distance of the separately measured calibration curves towards the two ions, i and j , of interest (Figure 5) and is formulated as follows:

$$K_{ij}^{\text{sel}} = a_i(I)^{1-(z_j/z_i)} (K_{ij}^{\text{pot}})^{(z_j/z_i)} \quad (5)$$

in which $a_i(I)$ is the activity of primary ions if only primary ions are present in the sample. However, the potentiometric selectivity coefficient K_{ij}^{pot} is still generally accepted and recommended by IUPAC [26], even for the description of ions with different charges.

Besides the boundary potentials at the two interfaces of the membrane, the membrane potential (E_M) is also dependent of the diffusion potential (E_D) (Equation 1). When there is a difference in ion activity between both sides of the membrane, ions start to diffuse from the high to the low activity side. A diffusion potential (E_D) is then created, caused by differences in mobility of cationic and anionic species in the membrane. This diffusion potential can be calculated with the use of the

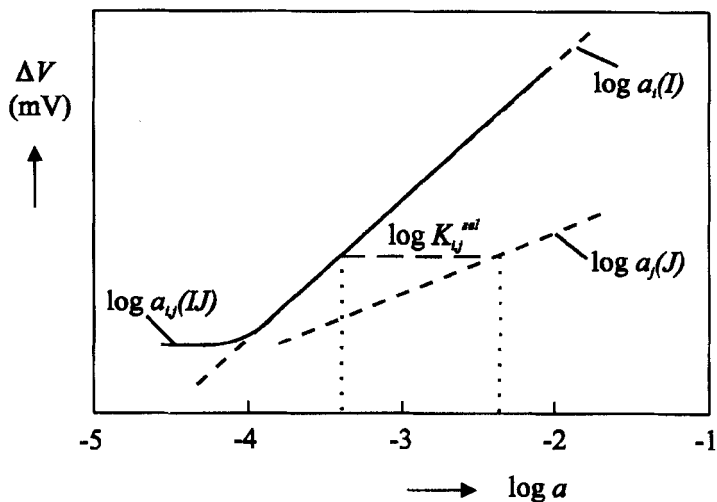


Figure 5 Calculated electrode responses as a function of primary ion [$\log a_i(I)$] and interfering ion alone [$\log a_j(J)$] and of the primary ion together with a constant interfering ion background [$\log a_{i,j}(IJ)$]

Henderson approximation [27], which assumes a *linear concentration profile* of the ions in the membrane (Equation 6):

$$E_D = \frac{RT \sum |z_+| \cdot \mu_+ \cdot \Delta \tilde{a}_+ - \sum |z_-| \cdot \mu_- \cdot \Delta \tilde{a}_-}{F \sum z_+^2 \cdot \mu_+ \cdot \Delta \tilde{a}_+ + \sum z_-^2 \cdot \mu_- \cdot \Delta \tilde{a}_-} \times \ln \frac{\sum z_+^2 \cdot \mu_+ \cdot \tilde{a}_+(r) + \sum z_-^2 \cdot \mu_- \cdot \tilde{a}_-(r)}{\sum z_+^2 \cdot \mu_+ \cdot \tilde{a}_+(s) + \sum z_-^2 \cdot \mu_- \cdot \tilde{a}_-(s)} \quad (6)$$

- in which μ_+ = mobility of a cationic species in the membrane,
- μ_- = mobility of an anionic species in the membrane,
- $\tilde{a}_+(r)$ = activity of a cationic species on the reference side in the membrane,
- $\tilde{a}_-(r)$ = activity of an anionic species on the reference side in the membrane,
- $\tilde{a}_+(s)$ = activity of a cationic species on the sample side in the membrane,
- $\tilde{a}_-(s)$ = activity of an anionic species on the sample side in the membrane,
- $\Delta \tilde{a}_+ = \tilde{a}_+(s) - \tilde{a}_+(r)$,
- $\Delta \tilde{a}_- = \tilde{a}_-(s) - \tilde{a}_-(r)$.

A too small association constant β_i in the membrane ($<10^4 \text{ M}^{-1}$) gives a relative large concentration of free ions in the membrane and can give rise to a diffusion potential (E_D) generated by the free ions in the membrane. The association constant

must be sufficiently high ($>10^4 \text{ M}^{-1}$) to fulfil an effective buffering which will give a low activity of free ions at both interface sides of the membrane resulting in a low diffusion gradient of these ions in the membrane. In that case the diffusion potential (E_D) can be neglected. However, when the concentration of anionic sites in the membrane is too low, sample anions can also be co-extracted into the membrane and a diffusion potential is generated (Donnan exclusion failure). This results in a sub-Nernstian response. A sub-Nernstian response can also be generated when the association of the ligand with the cation is too strong ($\beta_i > 10^{13} \text{ M}^{-1}$) [22,28]. An increase in the primary cation activity in the sample solution then severely changes the ratio of free to primary cation-ionophore complex due to strong complexation of the ionophore with the primary cation. The limited buffer capacity of the free ionophore and the primary ion-ionophore complex towards the primary ion results then in a gradual decrease in the membrane potential. At sufficiently high primary ion activities in the sample solution (usually $>10^{-2} \text{ M}$) nearly all ionophore in the membrane is complexed with primary cation and this complex starts functioning as a cationic site, extracting sample anions into the membrane, resulting in an *anion response*.

In our group the TMS model was upgraded by including divalent cations and ion-pair association in the system [22] and by the introduction of free and immobilized electroactive components in the membrane (i.e. receptor molecules and anionic sites) [21,29]. The effect of immobilization is of special importance for the sensor design, because covalent attachment of the electroactive components to the membrane seems to be an attractive possibility to obtain durable sensors.

4. ION-SENSITIVE MEMBRANES

In 1970 Thomas *et al.* described for the first time the use of plasticized PVC membranes in ion-selective electrodes [30] and within a few years this was followed by the construction of the first K^+ selective MEMFET [14]. The working mechanism of the plasticized PVC-type ion-selective electrode has been studied extensively [31] and from this work some general features for the design of ion-selective membrane materials can be defined:

- The membrane must be an elastomer in which the electroactive components (receptor molecules and anionic sites) can be dissolved. This is mainly achieved by the addition of external solvent mediators to polymeric materials.
- The membrane must be hydrophobic.
- For cation permselectivity anionic sites must be present, and vice versa.

The compatibility of all electroactive components of the membrane is an obvious requirement. Furthermore, the polymer, solvent mediator, and the electroactive components should possess a high lipophilicity in order to prevent leaching to the contacting sample solution. The latter process will result in a gradual loss of

sensitivity and selectivity and a very restricted lifetime [32]. Lipophilic anionic sites in the membrane can be introduced by the addition of tetraphenyl borate salts and cationic sites can be introduced by addition of tetra-alkyl ammonium salts. The presence of these ionic sites also lowers the electrical membrane resistance [20] and reduces the response time. Moreover, the addition of anionic groups lowers the activation barrier for the cation-exchange at the membrane-solution interface [33]. In PVC-based membranes inherent anionic sites like sulfonate and carboxylate anions are present [34]. These groups are residual impurities from the polymerization process. The impurity concentrations in commercially available PVC membranes have been reported to be about $0.063 \text{ mmol kg}^{-1}$ [35]. The amount of added ionic sites should be carefully adjusted in order to reach the desired improvement in selectivity without too much interference from counter ions [36]. The selectivity change induced by anionic additives agrees very well with model calculations [37].

An ion-sensing membrane which is suitable for long-life CHEMFETs also requires a good adhesion or a covalent attachment of the membrane layers to the underlying surface. Physical interaction of plasticized PVC membranes to the gate oxide or to the encapsulation material of the field effect transistor (FET) is insufficient to obtain durable sensor devices. These sensors only function well for some weeks when the ionophores are sufficiently hydrophobic [38]. The adhesion to the silicon oxide surface of Langmuir-Blodgett (LB) films is improved compared with PVC membranes. The LB films are well defined and highly ordered. Selectivity was achieved by the use of covalently or physically attached ionophores in the LB membrane [39]. The first durable Na^+ selective CHEMFET based on LB membranes was sensitive for 60 days in permanent contact with an electrolyte [40]. CHEMFETs with Ca^{2+} selective ionophores covalently attached to LB membranes have also been reported [41]. The use of LB films of substituted phthalocyanato-polysiloxanes gave promising results for the construction of a durable CHEMFET [42,43]. Also, mixed films of polyglutamate and a sodium ionophore were investigated as ion-sensitive materials, but these sensors were not very selective and had sensitivities around $50 \text{ mV decade}^{-1}$ [43].

4.1 Plasticized Membrane Materials

Besides the membrane materials described above, several other membrane materials have been investigated. Aminated [44,45] and carboxylated [46,47] PVC membranes were used for covalent attachment of ionophore to the matrix and showed to have improved adhesion to the gate oxide. These membranes were also used in ion-selective electrodes and showed to be ion-sensitive up to about 50 days, but had the disadvantage of being pH dependent. Membrane adhesion to the gate oxide can also be enhanced by using Urushi latex as membrane material. Urushi latex mainly consists of Urushiol which is a mixture of 3-substituted pyrocatechol derivatives

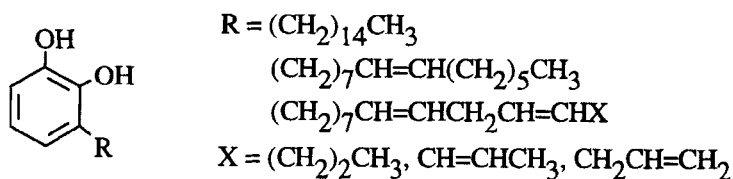


Figure 6 Chemical structure of Urishiol

with a saturated or an unsaturated chain of 15 carbon atoms (Figure 6). In combination with a plasticizer, Urushi membrane based Ca^{2+} selective CHEMFETs maintained a sensitivity of $25 \text{ mV decade}^{-1}$ for over one month [48]. The polymerization of the Urushi membrane normally takes 10 days, but could be reduced to 3 days by the addition of formaldehyde as a cross-linking agent [49]. A further reduction of curing time to 18 h was possible by an increase of the temperature of hardening up to 100°C [50].

For mass production, all chemical binding steps on the FET require photopolymerization in order to make sensor fabrication compatible with integrated circuit technology. Therefore, membranes are necessary which are photopolymerizable. Photocurable (meth)acrylates were used as membrane material because they have both good adhesion to the gate oxide surface as well as good mechanical strength [51]. The latter property makes this membrane suitable for CHEMFETs in flow injection analysis [52]. Compared to plasticized PVC membranes the amount of plasticizer in acrylate membranes can be lower [53]. Photocurable oligomers based on urethane and Bisphenol A (epoxy) diacrylates were studied for K^+ selective membranes of CHEMFETs [54]. These membranes showed very good adhesion during 5 months of contact with 10^{-2} M KCl solution. A CHEMFET with plasticized acrylate membrane with ammonium groups showed nitrate sensitivity with a lifetime >2 months [55].

4.2 Non-plasticized Membrane Materials

All of the membrane materials described above still need an external solvent mediator which can leach from the membrane to the sample solution. This reduces the plasticizing properties of the membrane and increases the electrical resistance giving rise to noisy responses. Membrane materials that function without addition of an external plasticizing group have also been investigated. A copolymer from toluene 2,4-diisocyanate, triethylene glycol, and 2-hydroxyethyl methacrylate was used in the construction of a potassium [56] and a lead sensitive ISFET [57]. Although this polymer is expected to be too hydrophilic in nature, it was claimed to perform well as an ion-selective membrane. Unfortunately, the authors are not very clear in this respect. Silicone rubbers may also be used without plasticizer owing to

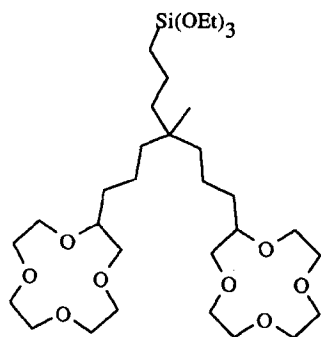
their low glass transition temperature. Silicone rubbers adhere strongly to most solid surfaces and exhibit less interference from lipophilic anions present in biological fluids [58–60]. Therefore, silicone rubber based membranes have been applied in sodium and glucose assays in human body fluids [61,62]. Silicone rubber based CHEMFETs were also used in dynamic systems, like flow injection analysis [63,64]. Silicone rubber membrane, in which nonactin is incorporated, on top of the ISFET showed a durability of at least 4 weeks. However, the commercially available room temperature vulcanizing (RTV) silicone rubbers have higher resistances and slower response times than PVC membranes [65–67]. A high membrane resistance imposes severe restrictions to the membrane thickness and results in high noise levels of the sensor. Sometimes plasticizers were added to RTV silicone rubber to decrease the bulk resistance of the membrane and to increase the solubility of electroactive components in the membrane [68,69]. However, the intrinsic advantage of silicone rubber having a low glass-transition temperature is eliminated by adding plasticizers. To overcome these problems commercially available fluorosilicone rubber (e.g. RTV Dow Corning 730) was suggested as membrane material [70–72]. The advantages over “conventional” silicones are the higher conductivity and the high relative permittivity. Another approach is the modification of silicones with cyanopropyl groups [3,72–74]. The polarity of the membrane can be tuned by variation of the number of cyanopropyl groups. The physical properties were characterized by measuring the membrane resistance and dielectric constant by impedance measurements. Impedance measurements of commercially available siloxane copolymer with 97 mol% dimethyl groups and about 3 mol% cyanopropyl groups showed that the membrane resistance is 10–20 times smaller than the polysiloxanes without these polar moieties [67].

In our group we developed siloxane terpolymers composed of dimethylsiloxane, cyanopropylsiloxane (for modulation of the polarity of the membrane) and methacryloxypropylsiloxane (enabling covalent linkage of receptor and/or ionic sites) [73]. The siloxane terpolymers were initially synthesized by emulsion polymerization of a mixture of octamethylcyclotetrasiloxane, the trimer and tetramer of (3-cyanopropyl)methylcyclodisiloxanes, and (3-methacryloxypropyl)methyldichlorosilane [75]. These polysiloxane membranes were used for CHEMFETs applied for measurements of ion activity in nutrition water in closed loop systems of greenhouses [76–78]. K^+ and Na^+ selective CHEMFETs with polysiloxane membranes were tested for sensitivity, selectivity and durability and good responses with lifetimes of 3–10 months were obtained [29,79,80]. However, the yield of well-functioning CHEMFETs was too low for mass production, mainly caused by the low reproducibility in the polysiloxane preparation. By synthesizing the polysiloxane polymers starting from only cyclotetrasiloxane monomers the reproducibility in the production of well-functioning Na^+ selective CHEMFETs was improved significantly [81]. A further improvement of the homogeneity of the polymers was obtained by the use of only cyclotrisiloxane monomers. Cyclotrisiloxanes can be purified by distillation and polymerize in a kinetically controlled reaction yielding a more

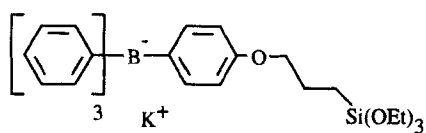
narrow molecular weight distribution than obtained with the thermodynamic controlled reaction of cyclotetrasiloxanes [82]. These polymers offer the possibility of tuning the polarity and the character of the membrane by changing the amount and the type of the polar substituent. Novel siloxane terpolymers with cyano, amido, ester or ketone moieties revealed that the nature of the polar substituents in the polysiloxane membranes has a large influence on the sensor characteristics and well-functioning CHEMFETs were obtained for selective detection of Ca^{2+} [83] and various heavy metal ions, like Ag^+ , Cd^{2+} and Pb^{2+} [82,84].

4.3 Sol-gel Based Membranes

Another way to obtain an ion-sensitive layer is the use of ion-sensing membranes based on sol-gel derived glasses. Such membranes were investigated for detection of K^+ and Na^+ ions and a good adhesion with inorganic materials was observed [85]. The sol-gel glass membranes were obtained by polymerization of tetraethoxysilane and diethoxydimethylsilane in ethanol in the presence of HCl. The response times of the sensors are fast (≤ 3 s) and the selectivities for K^+ (membranes with valinomycin incorporated) and Na^+ (membranes with bis 12-crown-4 ether incorporated) are comparable to those of ISFETs based on the corresponding plasticized PVC membranes. In this methodology the receptor molecule and the borate anion can also be chemically attached to the sol-gel glass membrane [86], e.g. with the alkoxy silyl biscrown ether derivative **5** in the presence of the silylated borate anion **6**. The sensor exhibits a Nernstian response ($59 \text{ mV decade}^{-1}$) and is Na^+ selective in the presence of K^+ ($\log K_{\text{Na,K}} = -2.6$). No data were given about the pH sensitivity of the membrane. The sensor was reported to be stable for several months, however, no experimental data were given.



5



6

4.4 Conclusions

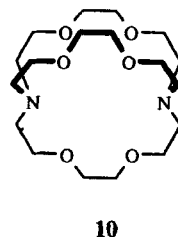
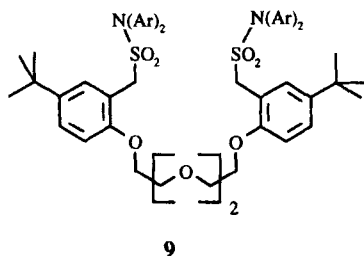
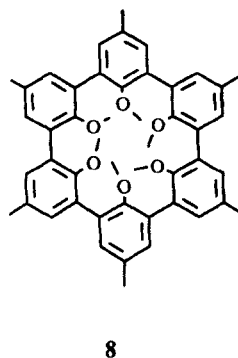
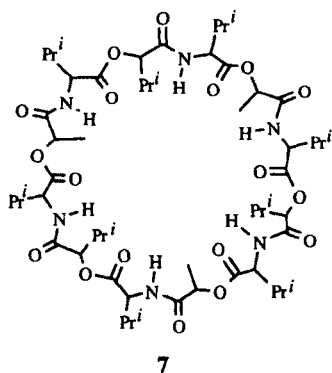
In summary, various polymeric materials have been studied for use as sensing membranes in CHEMFETs, mainly focused on improvement of the adhesion to the surface to prevent detachment of the membrane. Only limited attention has been paid to development of photopolymerizable membrane materials which enables chemical anchoring of the membrane to the gate oxide surface. Membranes based on sol-gel glasses, (meth)acrylates or polysiloxanes allow the covalent attachment to the gate oxide and this offers the possibility of binding the electroactive components covalently in the membrane. CHEMFETs with polysiloxane membranes showed the most promising results for development of durable sensors. The use of polysiloxane membranes also opens the possibility of constructing plasticizer-free membrane based CHEMFETs for heavy metal ions.

5. RECEPTOR MOLECULES FOR SELECTIVE RECOGNITION

In the previous sections the working of the CHEMFET and the state of the art of durable CHEMFET membranes have been discussed. The following sections deal with the receptor molecules that are used as the selective recognition elements of the CHEMFET. The properties of these molecules are essential for the overall performance of the chemical sensor as these determine the characteristics of the device, that is, its selectivity, lifetime and response time [87]. A number of requirements have to be fulfilled to obtain ionophores that possess highly selective complexation properties. Firstly, the size of the hydrophobic cavity of the ionophore created by the coordinating atoms should be complementary with the size of the ion to be complexed. A better fit of the cation radius and the cavity corresponds to a higher enthalpy of binding. The conformational changes upon complexation must also be minimized which requires a high degree of preorganization. Secondly, the ionophore should be highly lipophilic to prevent leaching of the ionophore from the membrane phase. CHEMFETs have a thin membrane layer (40–60 μM) and therefore the lipophilicity of the ionophore is much more important than for conventional ion-selective electrodes which possess a much thicker membrane. Thirdly, a stability constant of the ion ligand complex (β_i) between about 10^4 M^{-1} and 10^{13} M^{-1} ensures that a constant free ion concentration in the membrane can be maintained in a large dynamic range of sample ion activity. The constant concentration of free ions in the membrane is a prerequisite for Nernstian behavior, which has been described in the previous section. Finally, a fast (de)-complexation rate is required to obtain sufficiently short response times, in the range of milliseconds.

As already mentioned, the first K^+ selective MEMFET was based on the natural ionophore valinomycin (7).

In the 1970s and 1980s, Simon and coworkers identified groups of compounds for use as ionophore in ion-selective electrodes [88]. Synthetic ionophores, like crown

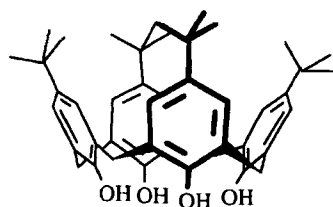
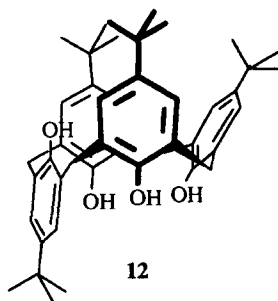
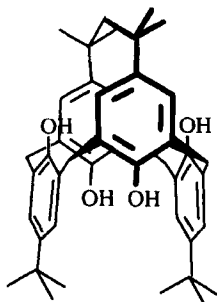
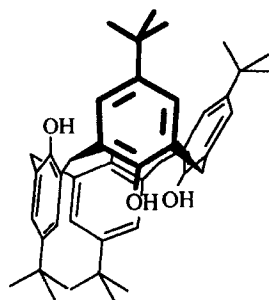


ethers and acyclic amides which are known for recognition of alkaline and alkaline earth metal ions, have been applied in ISEs. Also (hemi-)spherands (**8**) [89–91], podands (**9**) [92], and cryptands (**10**) [93] have been used. A more recently developed strategy for the synthesis of receptor molecules is the use of lipophilic molecules as platforms to which appropriate functionalities can be attached. A very versatile class of these building blocks are the calix[4]arenes. These receptor molecules will be discussed next.

6. RECEPTOR MOLECULES BASED ON CALIXARENES

The calix[*n*]arene (*n* indicates the number of aromatic units in the metacyclophane) building block provides a three-dimensional skeleton that is needed to fix different donor ligands in the optimal spatial positions for binding one ion selectively [94,95]. Calix[*n*]arenes are easily accessible from the base-catalyzed condensation of *p*-tert-butylphenol and formaldehyde [96]. Gutsche proposed to define the two faces of a calix[4]arene molecule as the *lower* (phenolic groups) and the *upper rim*. The calix[4]arene with free hydroxyl groups is conformationally flexible and the

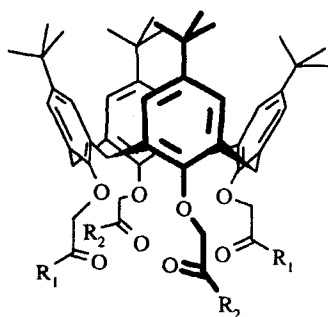
molecule can adopt four different extreme conformations viz.: *cone* (**11**), *partial cone* (**12**), *1,3-alternate* (**13**) and *1,2-alternate* (**14**) [96,97]. The introduction of substituents larger than ethyl at the *lower rim* results in conformationally fixed calix[4]arenes [98,99]. Selective de-*t*-butylation and/or reaction of one or more of the phenolic groups leads to a rapidly increasing number of possible functionalized calix[4]arenes. A large variety of substituents, including alkyl, ester, ketone, amido, phosphoryl and heterocyclic groups, can be positioned by (selective) *O*-alkylation or *O*-acylation at the *lower rim* [100]. Both the size and the shape of the hydrophilic cavity created by the coordinating atoms of the ionophore can be matched with the size of the ion. In this way a large variety of calix[4]arene derivatives can be synthesized and applied as selective detection elements in CHEMFETs.

**11****12****13****14**

Calix[4]arene derivatives with hard donating atoms, like oxygen, have a high affinity for hard alkaline and alkaline earth metal ions [101]. This type of calix[4]-arene derivatives will be described first. Subsequently, the calix[4]arene derivatives with soft donating atoms, like sulfur, will be discussed. These compounds have a preference for soft metal ions.

6.1 Cation Interaction with Carbonyl Functionalized Calix[4]arenes

Hard alkaline and alkaline earth metal ions have only s-orbital interactions with the ionophore and need a high degree of preorganization of the hard donating atoms in the ionophore. The first successful ionophores based on calix[4]arenes were obtained from derivatives with ester (**15**) or ketone (**16**) functionalities [102,103]. The interaction of the hard donating carbonyl atoms and four etheral oxygen atoms is the highest with hard cations [101]. Picrate extraction experiments showed that stable complexes are formed with different alkaline metal ions (e.g. Li^+ , K^+ , Na^+ , Rb^+ and Cs^+) with stability constants (β) in the range 10^2 – 10^6 M^{-1} [104,105].



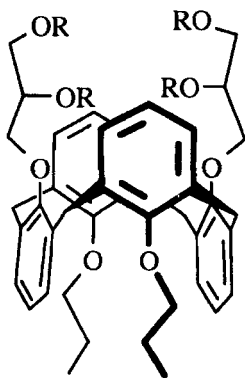
- 15** $\text{R}_1 = \text{R}_2 = \text{OAlkyl}$
16 $\text{R}_1 = \text{R}_2 = \text{Alkyl}$
17 $\text{R}_1 = \text{R}_2 = \text{N(Alkyl)}_2$
18 $\text{R}_1 = \text{OEt}$ $\text{R}_2 = \text{N(Me)}_2$

In all cases, Na^+ has the highest affinity with these calix[4]arene derivatives [103]. In plasticized PVC membranes such calix[4]arenes show Na^+/K^+ selectivities of -2.5 to -2.7 [106–108]. The flexibility of the calix[4]arene with four alkylester moieties (**15**) was reduced by the introduction of different lengths of diametrically bridged methylene units at the *upper rim*, but this rigidification did not enhance the Na^+/K^+ selectivity [109,110]. The amidocarbonyl oxygens of calix[4]arene **17** are more electron donating than ester and ketone carbonyl groups and do give more stable Na^+ complexes [111,112]. However, the stability of the K^+ complex is also increased, and no enhancement of the Na^+/K^+ selectivity was found in extraction experiments and CHEMFET measurements [113–115]. The Na^+ selectivity of calix[4]arene derivatives was further optimized by the introduction of mixed and bis(*syn-distally*)-*O*-functionalized substituents. In these calix[4]arenes two opposite phenolic positions are functionalized with ethylester substituents whereas the other two positions are substituted with different alkylesters [108,114,116] alkylamides [108,114,116] and methylketone groups [114,117]. A maximum selectivity of $\log K_{\text{Na,K}} = -3.1$ was obtained for CHEMFETs with the bis(*syn-distally*)-*O*-functionalized calix[4]arene derivative **18** having two ethylester and two dimethylamido moieties.

A further enhancement of the stability of the cation complexes was obtained by the introduction of carboxylate moieties. However, a bis(*syn-distally*)-*O*-functiona-

lized calix[4]arene with two diethylamido and two carboxylic acid substituents exhibits a decreased Na^+/K^+ selectivity. These receptor molecules preferentially complex alkaline earth metal ions [118].

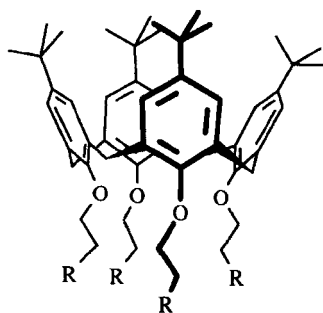
More recently, the *1,3-alternate* calix[4]arene with four amido moieties (**19**) was reported to be selective for Ca^{2+} ions. Polysiloxane based CHEMFETs with calix[4]arene **19** are selective for Ca^{2+} in the presence of Na^+ , K^+ , and Mg^{2+} ions ($\log K_{\text{Ca,Na}} = -1.9$, $\log K_{\text{Ca,K}} = -2.5$, and $\log K_{\text{Ca,Mg}} = -3.2$, respectively).



19 $\text{R} = \text{CH}_2\text{C}(\text{O})\text{N}(\text{Me})_2$

6.2 Cation Interaction with Phosphine Oxide Functionalized Calix[4]arenes

A further enhancement of the hardness of donating atoms by introduction of phosphine oxide ligands **20** did not give more stable Na^+ complexes but resulted in selectivity for di- and trivalent cations.



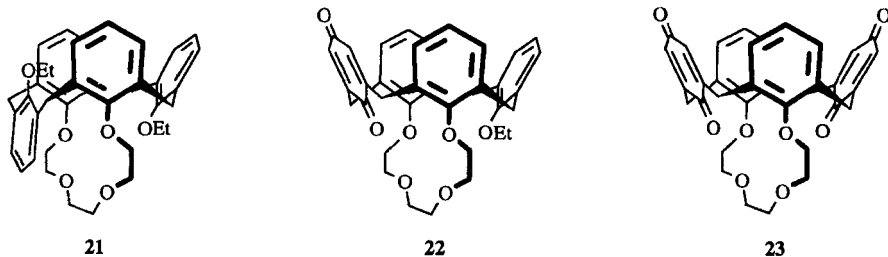
20 $\text{R} = \text{P}(\text{O})(\text{Ar})_2$

PVC membranes with calix[4]arene **20** are selective for Ca^{2+} in the presence of Na^+ and Mg^{2+} ($\log K_{\text{Ca,Na}} = -2.2$, $\log K_{\text{Ca,Mg}} = -2.6$) [119]. The same calix[4]arene was also applied for the extraction of tri- and tetravalent cations like Eu^{3+} , Th^{4+} and Pu^{3+} and Am^{4+} [120]. Ion-selective electrodes with plasticized PVC membranes with calix[4]arene tetraphosphine oxide **20** also showed selectivity for Eu^{3+} ions [121]. This was the first reported electrode which is selective for a trivalent cation; however, the electrode showed a sub-Nernstian slope of $15 \text{ mV decade}^{-1}$ over the range 10^{-4} – 10^{-1} M EuCl_3 . The authors attributed the sub-Nernstian behavior to the reaction of a hydroxyl group with the lanthanides, causing a low free-ion concentration in the membrane. However, the reaction with a hydroxyl group probably gives mono- and/or divalent cationic species, which should result in an increased voltage response. No Eu^{3+} selectivity was measured in the presence of Ca^{2+} [83].

6.3 Cation Interaction with Calix[4]arene Crown Ethers

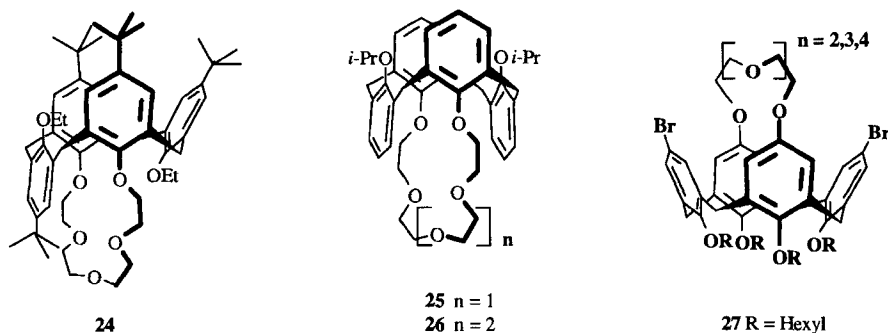
As already described, the selectivity of receptor molecules is not only dependent on the number and type of the donating atoms, but also on the preorganization of donating atoms. Preorganization of the receptor molecule can be further optimized by introduction of a rigid bridge at the *lower rim*. Calix[4]arene crown ethers have been used for the selective complexation of alkaline metal ions. Shinkai *et al.* reported calix[4]arene **21** bridged with three ethyleneoxy units, for the selective complexation of Na^+ ions and applied this calixarene derivative as receptor molecule in ion-selective electrodes [122]. The *cone* conformer (not shown), exhibits a selectivity of $\log K_{\text{Na,K}} = -4.1$. The *partial cone* conformer **21** exhibits an even higher selectivity ($\log K_{\text{Na,K}} = -5.1$). For the same ionophore (**21**) Suzuki *et al.* reported a much lower Na^+/K^+ selectivity ($\log K_{\text{Na,K}} = -2.8$) [123].

The reason for this difference was attributed to a non-steady-state response in the earlier measurements of Shinkai *et al.*, due to omitting the preconditioning of the sensor. A calix[4]arene with one quinone moiety (**22**) was also investigated as receptor molecule in ion-selective electrodes and the Na^+/K^+ selectivity ($\log K_{\text{Na,K}} = -3.4$) was higher than obtained with calix[4]arene derivative **18**



[124]. However, the ionophore with two quinone moieties (**23**) has a lower Na^+/K^+ than **22**.

When the ring size of ethyleneoxy bridged calix[4]arene is further increased by one or two oxyethylene units the preference is changed in favor of larger ions, e.g. K^+ (**24**, **25**) and Cs^+ (**26**), respectively [125–127]. With picrate extraction experiments it was shown that the *partial cone* calix[4]arene crown-5 derivative **24** has a very high affinity ($\Delta G = -13.5 \text{ kcal mol}^{-1}$) for K^+ ions [127]. CHEMFET measurements with this calix[4]arene also showed a high K^+ selectivity ($\log K_{\text{K,Na}} = -3.9$) [128]. More recent investigations pointed out that substituents at the calix[4]arene and the conformation of the calix[4]arene conformations influence the selectivity of the ion receptor [126]. Picrate extraction experiments with *1,3-alternate* 25,27-diisopropoxy-calix[4]arene-crown-5 (**25**) showed that this receptor extracted K^+ even better ($4.0 \times 10^4 \text{ M}^{-1}$) than the *partial cone* derivative **24** ($2.8 \times 10^4 \text{ M}^{-1}$). The Na^+/K^+ selectivity of CHEMFETs with calix[4]arene **24** ($\log K_{\text{Na,K}} = -4.2$) is even better than that observed with CHEMFETs containing the natural ionophore valinomycin ($\log K_{\text{K,Na}} = -3.9$). The 1,3-dialkoxycalix[4]arene-crown-6 (**26**) binds cesium almost more than four thousandfold stronger than sodium in picrate extraction experiments [129]. PVC based CHEMFETs with **26** showed a higher selectivity for Cs^+ ions in the presence of Na^+ ($\log K_{\text{Cs,Na}} = -3.3$) than observed for PVC based CHEMFETs with bis(18-crown-6)derivatives ($\log K_{\text{Cs,Na}} = -3.0$) [130].

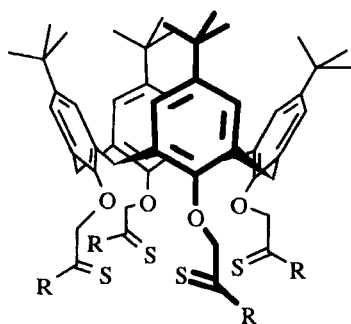


The preorganization of the receptor molecule by introduction of an ethyleneoxy bridge unit at the *upper rim* was also described [131]. The cavities of these bridged calixarenes (**27**) were larger than the *lower rim* bridged calixarenes and extraction experiments were done with both solid alkali metal and ammonium picrates into chloroform. The measurements showed that these calixarenes have a lower affinity for alkali metal ions (extraction <3%) than the *lower rim* bridged calix[4]arenes. However, primary ammonium ions were efficiently extracted with efficiencies of 27–57%.

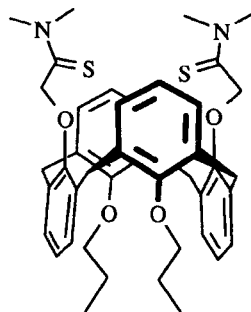
6.4 Cation Interaction with Sulfur Containing Calix[4]arenes

In the previous section the alkaline (earth) metal ion interaction with hard donating atoms was discussed. Compared to the hard metal ions the physical and chemical properties of transition metal ions are significantly different. Most of the transition metal ions have a divalent positive charge, or even higher, and therefore the partition of the metal ion from the aqueous phase to the hydrophobic membrane phase is lower than for univalent cations. Moreover, soft metal ions also interact via their polarizable d-orbitals with the donor atoms of a ligand. For binding a transition metal cation not only the specific requirements for the preorganization have to be fulfilled, but also for the coordination number, bond angle, and distance of the donor atoms. Soft metal ions tend to have a higher affinity towards soft donor atoms like nitrogen and sulfur. There are only a few reports in the literature describing ion-selective electrodes for transition metal ions based on the use of selective receptor molecules in polymeric membranes. Previous work has mainly been performed in our group and several Pb^{2+} selective calix[4]arene derivatives **28** and **29** functionalized with thioamido moieties were synthesized and applied in both plasticized PVC [132,133] and polysiloxane based ion sensors [82,84]. Polysiloxane based CHEMFETs with *cone* calix[4]arene **28** are highly selective for Pb^{2+} in the presence of Cd^{2+} and Cu^{2+} ions ($\log K_{\text{Pb,Cd}} = -4.2$ and $\log K_{\text{Pb,Cu}} = -3.0$, respectively) [133,134]. The $\text{Pb}^{2+}/\text{Cu}^{2+}$ is slightly enhanced by using the *1,3-alternate* calix[4]arene **29** with two thioamido moieties. In polysiloxane membranes calix[4]arene **29** exhibits a $\text{Pb}^{2+}/\text{Cu}^{2+}$ selectivity of -3.3 . Thioamido derivatives **30** and **31** are highly selective for Cd^{2+} ions. CHEMFETs with calix[4]arene (**30**) showed high selectivity for Cd^{2+} ions in the presence of Ca^{2+} or K^{+} ions ($\log K_{\text{Cd,Ca}} = -4.1$ and $\log K_{\text{Cd,K}} = -2.6$, respectively) [82]. However, no Cd^{2+} selectivity was obtained in the presence of Cu^{2+} ions. CHEMFETs with the *1,3-alternate* calix[4]arene **31**, utilizing two pairs of vicinal thioamide functionalities at the same face of the molecule, showed the highest Cd^{2+} selectivities ever reported ($\log K_{\text{Cd,Ca}} = -4.2$ and $\log K_{\text{Cd,K}} = -3.0$) and is even selective in the presence of Cu^{2+} ions ($\log K_{\text{Cd,Cu}} = -1.6$) [84].

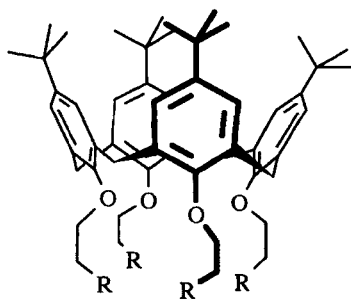
ISEs and CHEMFETs with calix[4]arene **32**, bearing two thioether functionalities, are highly selective for Ag^{+} in the presence of alkaline earth ions (K^{+} , Ca^{2+}) and transition metal ions (Cu^{2+} , Cd^{2+}), with selectivities $\log K_{\text{Ag},j}$ varying from -4.2 to -4.7 [133,135]. The CHEMFETs with **32** also showed selectivity for Ag^{+} in the presence of Hg^{2+} ions ($\log K_{\text{Ag,Hg}} = -2.7$), which is quite unique since both ions have the same coordination number and preference for a linear interaction with soft donor atoms [133]. McKervey *et al.* reported Ag^{+} selectivity for calix[4]arene **33** in PVC membrane based ISEs [136]. These ISEs show a moderate Ag^{+} selectivity (-1.1 to -2.1). Due to the presence of the hard donating carbonyl atoms in the molecule, a sub-Nernstian response ($50 \text{ mV decade}^{-1}$) was obtained in the presence of alkaline metal ions [137]. Moreover, the sensor was not selective for Ag^{+} in the presence of Hg^{2+} ions.



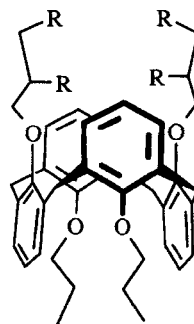
28 R = N(Me)₂



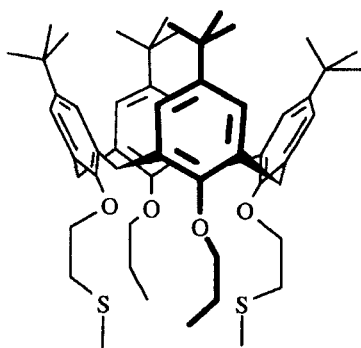
29



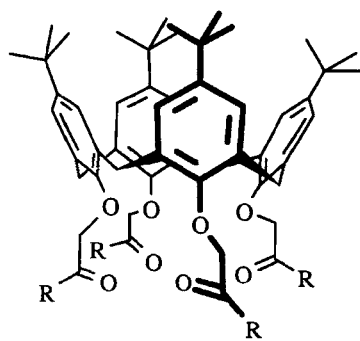
30 R = OCH₂C(S)N(Me)₂



31 R = OCH₂C(S)N(Me)₂

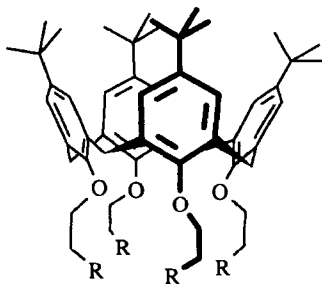


32



33 R = OCH₂CH₂SCH₃

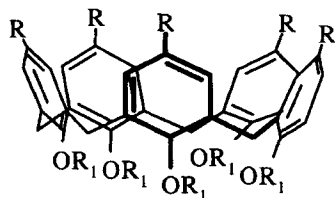
Only one calix[4]arene derivative is known which selectively complexes Cu^{2+} ions [133]. CHEMFETs based on a calix[4]arene **34** functionalized with four thiocarbamoyl moieties, respond selectively to Cu^{2+} ions in the presence of Ca^{2+} , Cd^{2+} and Pb^{2+} . The selectivities ranged from $\log K_{\text{Cu},j} = -1.6$ to -2.0 . Extraction experiments with calix[4]arene **34** also showed affinity for other soft metal ions like Hg^{2+} and Ag^+ [138].



34 $\text{R} = \text{SC}(\text{S})\text{N}(\text{Et})_2$

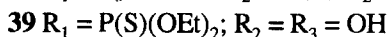
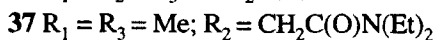
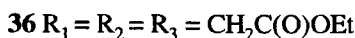
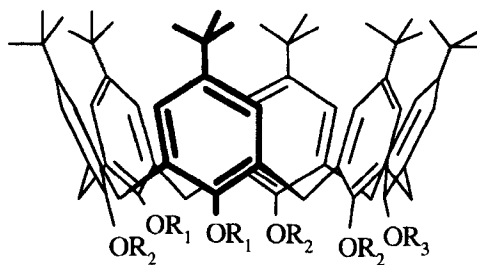
6.5 Receptor Molecules Based on Calix[5]- and Calix[6]arenes

The calixarene building block can be enlarged by increasing the ring size to, e.g. calix[5]- and calix[6]arenes, having five and six methylene phenol units in the ring, respectively. The flexibility of the aromatic rings in these compounds, however, is much larger than that of the aromatic rings in calix[4]arenes. This makes calix[5]- and calix[6]arenes less useful for spatial positioning of ligands unless bulky substituents are used to restrict the flexibility. There is only one example known of a calix[5]arene, functionalized with ethyl ester moieties (**35**), which is selective for metal ions [139]. Picrate extraction experiments with calix[5]arene **35** showed a preference for large cations like K^+ , Rb^+ , and Cs^+ over Na^+ . However, the derivative has not been tested as receptor molecule in ion-selective electrodes or CHEMFETs.



35 $\text{R} = t\text{-butyl}$ $\text{R}_1 = \text{CH}_2\text{C}(\text{O})\text{OEt}$

Four examples are known of calix[6]arene derivatives which have been used as receptor molecules in potentiometric measuring devices. Calix[6]arene **36** functionalized with six ethylester moieties showed a moderate selectivity for hexylammonium ions in the presence of smaller primary alkylammonium ions ($\log K = -1.0$ to -1.4) in ion-selective electrodes [140]. The same derivative **36** also proved to be sensitive towards Cs^+ ions [141]. CHEMFETs with calix[6]arenes, functionalized with three diethylamido moieties (**37**) or with three phosphate moieties (**38**), are selective for guanidinium ions [142]. The fourth example is calix[6]arene **39** functionalized with two thiophosphoryl groups which is selective for Pb^{2+} ions [143]. Ion-selective electrodes with **39** showed $\text{Pb}^{2+}/\text{Cd}^{2+}$ selectivities of $\log K_{\text{Pb,Cd}} = -2.5$.



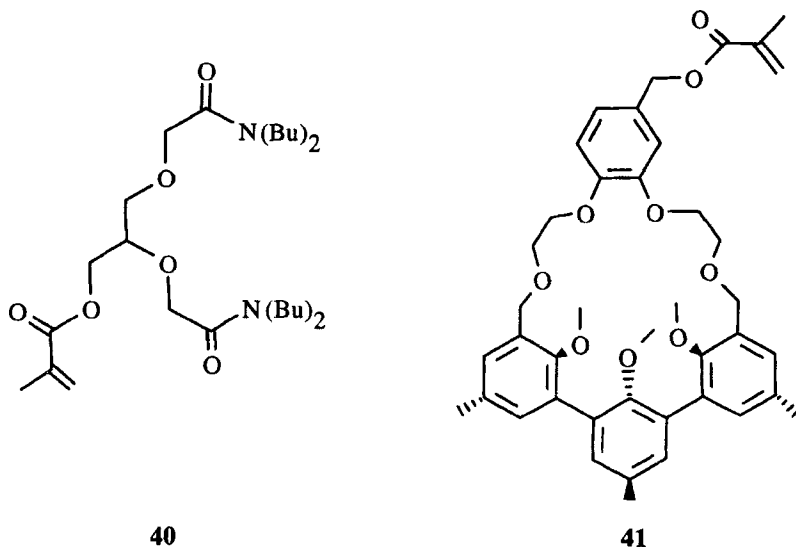
6.6 Conclusions

Calix[4]arenes have a high potential for application as receptor molecules in chemical ion-sensing devices. Functionalization of this building block allows the development of a great variety of lipophilic receptor molecules suitable for selective complexation of metal ions. The variation of conformation of the calix[4]arene derivative has shown an important tool for the optimization of its selectivity. Calix[4]arenes functionalized with hard donating atoms have been reported as receptor molecule for the selective determination of alkaline (earth) metal ions. Calix[4]arenes functionalized with soft donating atoms showed to be very selective for heavy metal ions, like Cu^{2+} , Ag^+ , Cd^{2+} and Pb^{2+} . More recent investigations also showed the ability of using calix[5]- and calix[6]arenes as receptor molecule in ion-sensing devices.

7. PHOTOPOLYMERIZABLE RECEPTOR MOLECULES

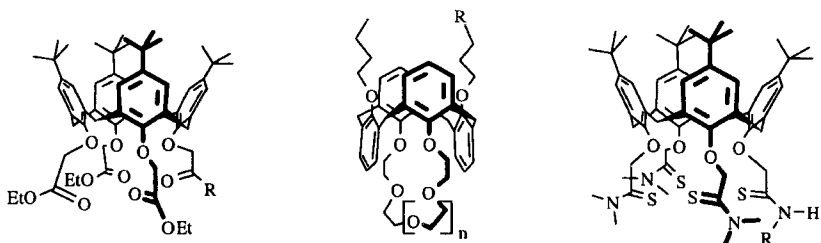
For the development of durable ion-sensing devices the leaching of the ion-selective receptor molecule is prevented by their covalent attachment to the membrane material. A methacrylate moiety can be attached to the electroactive component, which is polymerized together with the membrane material to form a covalently linked network. However, covalent binding of receptor molecules in the membrane can have counteracting effects on the selectivity and sensitivity of the sensor. The influence of the decrease in mobility of the receptor molecule on the formation of the membrane potential was simulated by van den Berg *et al.* [21]. They concluded that decrease in mobility of the receptor molecule results in a *counteracting diffusion potential* caused by interfering ions at low primary ion activities. This diffusion potential results in a decrease in the selectivity of the CHEMFET as compared with CHEMFETs with free receptor molecules in the membrane. The counteracting diffusion potential can be prevented by the provision of certain mobility to the ligand, e.g. by attaching the receptor molecule to the polymer backbone via a spacer.

Receptor molecules for Ca^{2+} , and K^+ ions (**40** [144], **41** [79], respectively) were covalently attached in the membrane matrix by photopolymerization in the presence of a photoinitiator [145].



Until now, only a restricted number of photopolymerizable calix[4]arene-based receptor molecules are known. Calix[4]arene **42** showed to be selective for Na^+ ions in the presence of different interfering ions [29]. More recently, we also synthesized

photopolymerizable calix[4]arene derivatives for K^+ , Cs^+ , and Pb^{2+} ions (**43**, **44**, and **45**, respectively) and applied these receptors in polysiloxane-based CHEMFETs [146]. The covalent attachment of the receptor molecule does not change the selectivity and Nernstian responses are obtained for K^+ , Cs^+ or Pb^{2+} ions. Durability studies with polysiloxane-based CHEMFETs with free or covalently attached receptor molecules and selective for Na^+ , K^+ and Pb^{2+} ions showed that in all cases polysiloxane membranes are suitable for the construction of durable CHEMFETs. The best performance was obtained with polysiloxane-based CHEMFETs containing covalently attached receptor molecules.



42 R = $NH(CH_2)_2OC(O)C(CH_3)CH_2$

43 n = 1

R = $CH_2OC(O)C(CH_3)CH_2$

44 n = 2

R = $CH_2OC(O)C(CH_3)CH_2$

45 R = $(CH_2)_6NHC(O)C(CH_3)CH_2$

8. OUTLOOK

The quantitative transduction of the recognition process at the molecular level into a measurable, reliable signal is not a trivial process. For real application of sensor systems problems of selectivity and durability have to be overcome. The first has been achieved by design of various calix[4]arene based receptor molecules selective for Na^+ , K^+ , Cs^+ , Ca^{2+} , Ag^+ , Cd^{2+} , Cu^{2+} , and Pb^{2+} ions. The second has been achieved by the use of covalently attached receptor molecules and membranes made of homogeneous siloxane terpolymers. The incorporation of different types and amounts of polar substituents made it possible to tune the membrane properties in order to achieve optimal selectivity of the sensor. The next challenge is the design of CHEMFETs that can detect anions. The potentiometric detection of anions is far less developed than cation sensing. Anion selectivity closely following the Hofmeister series can be obtained by the addition of lipophilic cationic sites (e.g. tetraoctylammonium ions) to the membrane [147]. Durable polysiloxane based CHEMFETs with these cationic sites are selective for NO_3^- [148]. The design of ion-sensing devices with selectivity for anions which are more hydrophilic than NO_3^- requires the synthesis of selective anion receptors. Until now, only a few anion receptors are

known which are based on organometallic ligands. Simon *et al.* developed Cl^- selective ISEs applying organometallic trialkyl tin derivatives as neutral anion receptor [149]. Ion sensors with di- or tetradentate organotin derivatives showed selectivity for H_2PO_4^- even in the presence of lipophilic anions, e.g. SCN^- and ClO_4^- [150]. The first cobalt porphyrines applied in polysiloxane membrane based CHEMFETs showed to be selective for NO_2^- in the presence of Cl^- and Br^- ions [151]. The latest results in the field of anion recognition are directed towards other neutral receptors like uranyl salophene derivatives [151–153].

9. ACKNOWLEDGEMENTS

This work summarizes the contribution of the chemical sensor group of the MESA Research Institute at the University of Twente. Albert van den Berg, Peter van der Wal, Peter Cobben, Felix Kremer, Jos Brunink, Herman Holterman, Gerard Honig, Udo Verkerk, Martijn Antonisse, Richard Egberink, Johan Bomer, Jan Haak, Zbigniew Brzozka, Ernst Sudhölter, and Johan Engbersen have all made original and creative contributions to this research program. Professor Piet Bergveld and Hans van der Vlekkert are acknowledged for their continuous interest and stimulating discussions. The work would not have been possible without the excellent facilities of the MESA cleanroom and the financial support of the Technical Foundation (STW), Technical Science Branch of the Dutch Organization for Advanced and Pure Research (NWO), Priva BV, and Twente Transfer Technology BV.

10. REFERENCES AND NOTES

1. For a recent review about chemical sensors see: J. Janata, M. Josowicz and D. M. DeVaney, *Anal. Chem.*, **66**, 207R (1994).
2. For recent reviews see (a) K. Domansky, J. Janata, M. Josowicz and D. Petelenz, *Analyst*, **118**, 335 (1993); (b) J. Janata, *Analyst*, **119**, 2275 (1994); (c) P. Bergveld, *Sens. Actuators B*, **4**, 125 (1991); (d) D. N. Reinhoudt, *Recl. Trav. Chim. Pays-Bas*, **115**, 109 (1996).
3. P. D. van der Wal, A. van den Berg and N. F. de Rooij, *Sens. Actuators B*, **18–19**, 200 (1994).
4. P. Bergveld, *IEEE Trans. Biomed. Eng.*, **BME-17**, 70 (1970).
5. In practice the source–drain current is kept constant by adjusting the potential between the reference electrode and bulk of the semiconductor.
6. W. H. Siu and R. S. C. Cobbold, *IEEE Trans. Electron. Devices*, **ED-26**, 1805 (1979).
7. L. Bousse and P. Bergveld, *Sens. Actuators*, **6**, 65 (1984).
8. (a) A. van den Berg, P. Bergveld, D. N. Reinhoudt and E. J. R. Sudhölter, *Sens. Actuators*, **8**, 129 (1985); (b) J. F. Scherder, *J. Coll. Interf. Sci.*, **61**, 569 (1987).
9. R. E. G. van Hal, J. C. T. Eijkel and P. Bergveld, *Sens. Actuators B*, **24–25**, 201 (1995).
10. P. Clechet and N. Jaffrezic-Renault, *Adv. Mater.*, **2**, 293 (1990).
11. N. Jaffrezic-Renault, J. M. Chovelon, H. Perrot, P. Le Pershec and Y. Chevalier, *Sens. Actuators B*, **5**, 71 (1991).

12. T. Thami, J. Simon, N. Jaffrezic, A. Maillard and S. Spirkovitch, *Bull. Soc. Chim. Fr.*, **133**, 759 (1996).
13. D. N. Reinhoudt and E. J. R. Sudhölter, *Adv. Mater.*, **2**, 23 (1990).
14. S. D. Moss, J. Janata and C. C. Johnson, *Anal. Chem.*, **47**, 2238 (1975).
15. E. J. Fogt, D. F. Untereker, M. S. Norenberg and M. E. Meyerhoff, *Anal. Chem.*, **57**, 1995 (1985).
16. E. J. R. Sudhölter, P. D. van der Wal, M. Skowronska-Ptasinska, A. van den Berg, P. Bergveld and D. N. Reinhoudt, *Anal. Chim. Acta*, **230**, 59 (1990).
17. T. Teorell, *Proc. Soc. Exp. Biol. Med.*, **33**, 282 (1935).
18. K. H. Meyer and J. F. Sievers, *Helv. Chim. Acta*, 649 (1936).
19. W. E. Morf, G. Kahr and W. Simon, *Anal. Lett.*, **7**, 9 (1974).
20. T. A. Nieman and G. Horvai, *Anal. Chim. Acta*, **170**, 359 (1985).
21. A. van den Berg, P. D. van der Wal, M. Skowronska-Ptasinska, E. J. R. Sudhölter and D. N. Reinhoudt, *J. Electroanal. Chem.*, **284**, 1 (1990).
22. P. L. H. M. Coben, R. J. M. Egberink, J. G. Bomer, P. Bergveld and D. N. Reinhoudt, *J. Electroanal. Chem.*, **368**, 193 (1994).
23. A. Lewenstam and A. Hulanicki, *Sel. Elec. Rev.*, **12**, 161 (1990).
24. E. Bakker, R. K. Meruva, E. Pretsch and M. E. Meyerhoff, *Anal. Chem.*, **66**, 3021 (1994).
25. Y. Umezawa, K. Umezawa and H. Sato, *Pure Appl. Chem.*, **67**, 507 (1995).
26. R. P. Buck and E. Lindner, *Pure Appl. Chem.*, **66**, 2527 (1994).
27. W. E. Morf, *The Principles of Ion-Selective Electrodes and of Membrane Transport. Studies in Analytical Chemistry*, Vol 2, Elsevier, Amsterdam, 1981, p. 247.
28. R. P. Buck, K. Toth, E. Graf, G. Horvai and E. Pungor, *J. Electroanal. Chem.*, **223**, 51 (1987).
29. J. A. J. Brunink, R. J. W. Lugtenberg, Z. Brzozka, J. F. J. Engbersen and D. N. Reinhoudt, *J. Electroanal. Chem.*, **378**, 185 (1994).
30. G. J. Moody, R. B. Oke and J. D. R. Thomas, *Analyst*, **95**, 910 (1970).
31. For recent reviews see (a) T. Rosatzin, E. Bakker, K. Suzuki and W. Simon, *Anal. Chim. Acta*, **280**, 197 (1993); (b) A. Lewenstam and A. Hulanicki, *Sel. Elec. Rev.*, **12**, 161 (1990); (c) E. Pungor, *Electroanalysis*, **8**, 348 (1996); (d) R. P. Buck, T. M. Nahir, V. V. Cosofret, E. Lindner and M. Erdosy, *Anal. Proc. Incl. Anal. Commun.*, **31**, 301 (1994).
32. U. Oesch and W. Simon, *Anal. Chem.*, **52**, 602 (1980).
33. P. Gehrig, W. E. Morf, M. Welti, E. Pretsch and W. Simon, *Helv. Chim. Acta*, **73**, 203 (1990).
34. A. van den Berg, P. D. van der Wal, M. Skowronska-Ptasinska, E. J. R. Sudhölter, D. N. Reinhoudt and P. Bergveld, *Anal. Chem.*, **59**, 2827 (1987).
35. M. Nagele and E. Pretsch, *Microchim. Acta*, **121**, 269 (1995).
36. R. Eugster, P. M. Gehrig, W. E. Morf, U. E. Spichiger and W. Simon, *Anal. Chem.*, **63**, 2285 (1991).
37. P. C. Meier, W. E. Morf, M. Läubi and W. Simon, *Anal. Chim. Acta*, **156**, 1 (1984).
38. Z. Brzozka, P. L. H. M. Cobben, D. N. Reinhoudt, J. J. H. Edema, J. Buter and R. M. Kellog, *Anal. Chim. Acta*, **273**, 139 (1993).
39. K. B. Blodgett, *J. Am. Chem. Soc.*, **57**, 1007 (1935).
40. R. Erbach, B. Hoffmann, M. Schaub and G. Wegner, *Sens. Actuators B*, **6**, 211 (1992).
41. F. Kauffmann, B. Hoffmann, R. Erbach, L. Heiliger, H.-U. Siegmund and M. Völker, *Sens. Actuators B*, **18-19**, 60 (1994).
42. A. Vogel, B. Hoffmann, T. Sauer and G. Wegner, *Sens. Actuators B*, **1**, 408 (1990).
43. M. J. Schöning, M. Sauke, A. Steffen, M. Marso, P. Kordos, H. Lüth, F. Kaufmann, R. Erbach and B. Hoffmann, *Sens. Actuators B*, **26-27**, 325 (1995).
44. V. V. Cosofret, E. Lindner, R. P. Buck, R. P. Kusy and J. Q. Whitley, *Electroanalysis*, **5**, 725 (1993).

45. R. P. Buck, V. V. Cosofret and E. Lindner, *Anal. Chim. Acta*, **282**, 273 (1993).
46. (a) V. V. Cosofret, R. P. Buck, M. Erdosy, *Anal. Chem.*, **66**, 3592 (1994); (b) V. V. Cosofret, M. Erdosy, R. P. Buck, W. J. Kao, J. M. Anderson, E. Lindner and M. R. Neuman, *Analyst*, **119**, 2283 (1994).
47. S. Daunert and L. G. Bachas, *Anal. Chem.*, **62**, 1428 (1990).
48. (a) S. Wakida, M. Yamane and K. Hiiro, *Sens. Mater.*, **2**, 107 (1988); (b) S. Wakida, M. Yamane, K. Higashi, K. Hiiro and Y. Ujihara *Sens. Actuators B*, **1**, 412 (1990).
49. S. Johnson, G. J. Moody and J. D. R. Thomas, *Anal. Proc.*, **27**, 79 (1990).
50. S. Ito, K. Baba, Y. Ansano, H. Takesako and H. Wada, *Talanta*, **43**, 1869 (1996).
51. R. W. Cattrall, P. J. Iles and I. C. Hamilton, *Anal. Chim. Acta*, **169**, 403 (1985).
52. G. J. Moody, J. M. Slater and J. D. R. Thomas, *Analyst*, **113**, 103 (1988).
53. L. Y. Heng and E. A. H. Hall, *Anal. Chim. Acta*, **324**, 47 (1996).
54. A. Bratov, N. Abramova, J. Munoz, C. Domínguez, S. Alegret and J. Bartoli, *Anal. Chem.*, **67**, 3589 (1995).
55. C. Dumschat, R. Frömer, H. Rautschek, H. Müller and H.-J. Timpe, *Anal. Chim. Acta*, **243**, 179 (1991).
56. M. Battilotti, R. Colilli, I. Giannini and M. Ciongo, *Sens. Actuators B*, **17**, 209 (1989).
57. M. Battilotti, R. Mercure, G. Mazzamurro, I. Giannini and M. Giongo, *Sens. Actuators B*, **1**, 438 (1990).
58. E. Lindler, Z. Niegreis, K. Toth, E. Pungor, T. R. Berube and R. P. Buck, *J. Electroanal. Chem.*, **259**, 67 (1989).
59. I. A. Mostert, P. Anker, H.-B. Jenny, U. Oesch, W. E. Morf, D. Amman and W. Simon, *Microchim. Acta*, **1**, 33 (1985).
60. P. D. van der Wal, M. Skowronska-Ptasinska, A. van den Berg, P. Bergveld, E. J. R. Sudhölter and D. N. Reinhoudt, *Anal. Chim. Acta*, **231**, 41 (1990).
61. Y. Tsujimura, M. Yokoyama and K. Kumura, *Sens. Actuators B*, **22**, 195 (1994).
62. A. Saito, N. Ito, J. Kumura and T. Kuriyama, *Sens. Actuators B*, **20**, 125 (1994).
63. S. Ufer and K. Cammann, *Sens. Actuators B*, **7**, 572 (1992).
64. P. D. van der Wal, E. J. R. Sudhölter and D. N. Reinhoudt, *Anal. Chim. Acta*, **245**, 159 (1991).
65. E. Lindler, K. Tóth, E. Pungor, W. E. Morf and W. Simon, *Anal. Chem.*, **50**, 1627 (1978).
66. E. Lindler, Z. Niegreis, K. Toth, E. Pungor, T. R. Berube and R. P. Buck, *J. Electroanal. Chem.*, **259**, 67 (1989).
67. P. D. van der Wal, E. J. R. Sudhölter, B. A. Bouwkamp, H. J. M. Boumeester and D. N. Reinhoudt, *J. Electroanal. Chem.*, **317**, 153 (1991).
68. B. K. Oh, C. Y. Kim, H. J. Lee, K. L. Rho, G. S. Cha and H. Nam, *Anal. Chem.*, **68**, 503 (1996).
69. E. Malinowska, V. Oklejas, R. W. Hower, R. B. Brown and M. E. Meyerhoff, *Sens. Actuators B*, **33**, 161 (1996).
70. M. Knoll, K. Cammann, C. Dumschat, C. Sundermeier and J. Eshold, *Sens. Actuators B*, **18-19**, 51 (1994).
71. C. Dumschat, S. Alazard, S. Adam, M. Knoll and K. Cammann, *Analyst*, **121**, 527 (1996).
72. A. Bouazizi, H. Maaref and N. Jaffrezic-Renault, *Anal. Chim. Acta*, **295**, 283 (1994).
73. E. J. R. Sudhölter, M. Skowronska-Ptasinska, P. D. van der Wal, A. van den Berg and D. N. Reinhoudt, *Eur. Pat. Appl.*, 285 591, 1986.
74. C. Soulié, J.-C. Favier, P. Hemery and J. Simon, *J. Mater. Chem.*, **2**, 1271 (1992).
75. D. N. Reinhoudt, *Biosensors and Chemical Sensors. Optimizing Performance through Polymeric Materials* (ACS symposium series 487), (eds P. G. Edelman and J. Wang), ACS, Washington, DC, 1992, p. 202.
76. H. H. van den Vlekkert, U. H. Verkerk, P. D. van der Wal, A. van Wingerden, D. N.

- Reinhoudt, J. R. Haak, G. W. N. Honig and H. A. J. Holterman, *Sens. Actuators B*, **6**, 34 (1992).
77. T. H. Gieling and H. H. van den Vlekkert, *Adv. Space Res.*, **18**, 135 (1996).
 78. U. H. Verkerk, H. H. van den Vlekkert, D. N. Reinhoudt, J. F. J. Engbersen, G. W. N. Honig and H. A. J. Holterman, *Sens. Actuators B*, **13–14**, 221 (1993).
 79. D. N. Reinhoudt, J. F. J. Engbersen, Z. Brzózka, H. H. van den Vlekkert, G. W. N. Honig, H. A. J. Holterman and H. Verkerk, *Anal. Chem.*, **66**, 3618 (1994).
 80. Z. Brzózka, H. A. J. Holterman, G. W. N. Honig, U. H. Verkerk, H. H. van der Vlekkert, J. F. J. Engbersen and D. N. Reinhoudt, *Sens. Actuators B*, **18–19**, 38 (1994).
 81. H. Gankema, R. J. W. Lugtenberg, J. F. J. Engbersen, D. N. Reinhoudt and M. Möller, *Adv. Mater.*, **6**, 944 (1994).
 82. R. J. W. Lugtenberg, M. M. G. Antonisse, R. J. M. Egberink, J. F. J. Engbersen and D. N. Reinhoudt, *J. Chem. Soc.: Perkin Trans. II*, 1937 (1996).
 83. R. J. W. Lugtenberg, R. J. M. Egberink, J. F. J. Engbersen and D. N. Reinhoudt, *Anal. Chim. Acta*, **357**, 225 (1997).
 84. R. J. W. Lugtenberg, R. J. M. Egberink, J. F. J. Engbersen and D. N. Reinhoudt, *J. Chem. Soc.: Perkin Trans. II*, 1353 (1997).
 85. K. Kimura, T. Sunagawa and M. Yokoyama, *Chem. Lett.*, 967 (1995).
 86. S. K. Srivastava, V. K. Gupta and S. Jain, *Anal. Chem.*, **68**, 272 (1996).
 87. For a recent review about molecular recognition see: B. König, *J. Prakt. Chem.*, **337**, 339 (1995).
 88. For a review of Simon's contribution to the development of chemical sensors see: H. M. Widner, *Anal. Meth. Instrum.*, **1**, 3 (1993).
 89. P. J. Dijkstra, H. J. den Hertog Jr., B. J. van Steen, S. Zijlstra, M. Skowronska-Ptasinska, D. N. Reinhoudt, J. van Eerden and S. Harkema, *J. Org. Chem.*, **52**, 2433 (1987).
 90. E. J. R. Sudhölter, P. D. van der Wal, M. Skowronska-Ptasinska, A. van den Berg, P. Bergveld and D. N. Reinhoudt, *Recl. Trav. Chim. Pays-Bas*, **109**, 222 (1990).
 91. D. J. Cram, *Angew. Chem.*, **29**, 1304 (1990).
 92. M. Bochenska and J. F. Biernat, *J. Incl. Phenom. Molec. Recognit. Chem.*, **16**, 63 (1993).
 93. (a) E. Lindler, K. Tóth, M. Horvath, E. Pungor, B. Agai, I. Bitter, L. Töke and Z. Hell, *Fresenius Z. Anal. Chem.*, **322**, 157 (1985); (b) J.-M. Lehn, *Angew. Chem.*, **100**, 91 (1988).
 94. For recent review articles on the inclusion properties of calixarenes see (a) M. Takeshita and S. Shinkai, *Bull. Chem. Soc. Jpn.*, **68**, 1088 (1995); (b) D. Diamond, *J. Incl. Phenom. Molec. Recognit. Chem.*, **19**, 149 (1994).
 95. For optimizing the cation selectivity for calix[4]arene based ion selective electrodes see: T. Sakaki, T. Harada, Y. Kawahara, S. Shinkai, *J. Incl. Phenom. Molec. Recognit. Chem.*, **17**, 377 (1994).
 96. C. D. Gutsche, *Calixarenes: Monographs in Supramolecular Chemistry* (ed J. F. Stoddart), Royal Society of Chemistry, Cambridge, UK, 1989.
 97. For a comprehensive review see: J. Vicens and V. Böhmer, Eds, *Calixarenes*, Kluwer Academic Press, Dordrecht, 1991.
 98. K. Iwamoto, K. Araki and S. Shinkai, *J. Org. Chem.*, **56**, 4955 (1991).
 99. L. C. Groenen, J.-D. van Loon, V. Verboom, S. Harkema, A. Casnati, R. Ungaro, A. Pochini, F. Ugozzoli and D. N. Reinhoudt, *J. Am. Chem. Soc.*, **113**, 2385 (1991).
 100. For a recent review see: V. Böhmer, *Angew. Chem. Int. Ed. Engl.*, **34**, 317 (1995).
 101. R. G. Pearson, *J. Am. Chem. Soc.*, **85**, 3533 (1963).
 102. (a) A. Arduini, A. Pochini, S. Reverbi and R. Ungaro, *J. Chem. Soc.: Chem. Commun.*, 981 (1984); (b) A. Arduini, A. Pochini, S. Reverberi, R. Ungaro, G. D. Andreetti and F. Ugozzoli, *Tetrahedron*, **7**, 2089 (1986).
 103. F. Arnaud-Neu, E. M. Collins, M. Deasy, G. Ferguson, S. J. Harris, B. Kaitner, A. J.

- Lough, M. A. McKervey, E. Marques, B. L. Ruhl, M.-J. Schwing-Weill and E. M. Seward, *J. Am. Chem. Soc.*, **111**, 8681 (1989).
104. M. A. McKervey, E. M. Seward, G. Ferguson, B. Ruhl and S. J. Harris, *J. Chem. Soc.: Chem. Commun.*, 388 (1985).
105. S.-K. Chang and I. Cho, *J. Chem. Soc.: Perkin Trans. I*, 211 (1986).
106. (a) J. A. J. Brunink, J. R. Haak, J. G. Bomer, D. N. Reinhoudt, M. A. McKervey and S. J. Harris, *Anal. Chim. Acta*, **254**, 75 (1991); (b) J. A. J. Brunink, J. G. Bomer, J. F. J. Engbersen, W. Verboom and D. N. Reinhoudt, *Sens. Actuators B*, **15-16**, 195 (1993).
107. M. Telting-Diaz, D. Diamond, M. R. Smyth, E. M. Seward and A. M. McKervey, *Electroanalysis*, **3**, 371 (1991).
108. K. M. O'Connor, M. Cherry, G. Svehla, S. J. Harris and M. A. McKervey, *Talanta*, **41**, 1207 (1994).
109. F. Arnaud-Neu, V. Böhmer, L. Guerra, M. A. McKervey, E. F. Paulus, A. Rodriguez, M.-J. Schwing-Weill, M. Tabatabai and W. Vogt, *J. Phys. Org. Chem.*, **5**, 471 (1992).
110. V. Böhmer, W. Vogt, H. Goldmann, M. A. McKervey, M. Owens, S. Cremin and E. M. Collins, *J. Org. Chem.*, **55**, 2569 (1990).
111. S.-K. Chang, S.-K. Kwan and I. Chao, *Chem. Lett.*, 477 (1984).
112. A. Arduini, E. Ghidini, A. Pochini, R. Ungaro, G. D. Andreotti, G. Calestani and F. Ugozzoli, *J. Incl. Phenom.*, **6**, 119 (1988).
113. (a) F. Arnaud-Neu, M.-J. Schwing-Weill, K. Ziat, S. Cremin, S. J. Harris and M. A. McKervey, *New J. Chem.*, **15**, 33 (1991); (b) M.-J. Schwing-Weill, F. Arnaud-Neu, M. A. McKervey, *J. Phys. Org. Chem.*, **5**, 496 (1992).
114. J. A. J. Brunink, PhD Thesis, University of Twente, 1993.
115. M. Careri, A. Casnati, A. Guarinoni, A. Mangia, G. Mori, A. Pochini and R. Ungaro, *Anal. Chem.*, **65**, 3156 (1993).
116. (a) K. Kimura, T. Matsuba, Y. Tsujimura and M. Yokoyama, *Anal. Chem.*, **64**, 2508 (1992); (b) K. Kimura, Y. Tsujimura and M. Yokoyama, *Pure Appl. Chem.*, **67**, 1085 (1995); (c) Y. Tsujimura, M. Yokoyama and K. Kimura, *Anal. Chem.*, **66**, 2401 (1995); (d) Y. Tsujimura, M. Yokoyama and K. Kimura, *Electroanalysis*, **5**, 803 (1993).
117. E. M. Collins, M. A. McKervey, E. Madigan, M. B. Moran, M. Owens, G. Ferguson and S. J. Harris, *J. Chem. Soc.: Perkin Trans. I*, 3137 (1991).
118. M. Ogata, K. Fujimoto and S. Shinkai, *J. Am. Chem. Soc.*, **116**, 4505 (1994).
119. T. McKittrick, D. Diamond, D. J. Marrs, P. O'Hagan and M. A. McKervey, *Talanta*, **43**, 1145 (1996).
120. J. F. Malone, D. J. Marrs, M. A. McKervey, P. O'Hagan, N. Thompson, A. Walker, F. Arnaud-Neu, O. Mauprivez, M.-J. Schwing-Weill, J.-F. Dozol, H. Rouquette and N. Simon, *J. Chem. Soc.: Chem. Commun.*, 2151 (1995).
121. T. Gady, S. Maskala, D. Diamond, D. J. Marrs, M. A. McKervey and P. O'Hagan, *Anal. Proc. Incl. Anal. Comm.*, **32**, 471 (1995).
122. H. Yamamoto and S. Shinkai, *Chem. Lett.*, 1115 (1994).
123. K. Suzuki, K. Hato, H. Hisamoto, D. Siswanti, K. Hayashi, N. Kasahara, K. Watanabe, N. Yamamoto and H. Sasakura, *Anal. Chem.*, **68**, 208 (1996).
124. H. Yamamoto, K. Ueda, H. Suenga, T. Sakaki and S. Shinkai, *Chem. Lett.*, 39 (1996).
125. E. Ghidini, F. Ugozzoli, R. Ungaro, S. Harkema, A. Abu El-Fadl and D. N. Reinhoudt, *J. Am. Chem. Soc.*, **112**, 6979 (1990).
126. A. Casnati, A. Pochini, R. Ungaro, C. Bocchi, F. Ugozzoli, R. J. M. Egberink, H. Struijk, R. J. W. Lugtenberg, F. de Jong and D. N. Reinhoudt, *Chem. Eur. J.*, **2**, 436 (1996).
127. A. Casnati, A. Pochini, R. Ungaro, F. Ugozzoli, F. Arnaud, S. Fanni, M.-J. Schwing, R. J. M. Egberink, F. de Jong and D. N. Reinhoudt, *J. Am. Chem. Soc.*, **117**, 2767 (1995).
128. Z. Brzózka, B. Lammerink, D. N. Reinhoudt, E. Ghidini and R. Ungaro, *J. Chem. Soc.: Perkin Trans. II*, 1037 (1993).

129. R. Ungaro, A. Casnati, F. Ugozzoli, A. Pochini, J.-F. Dozol, C. Hill and H. Rouquette, *Angew. Chem. Int. Ed. Engl.*, **33**, 1506 (1994).
130. R. J. W. Lugtenberg, Z. Brzozka, A. Casnati, R. Ungaro, J. F. J. Engbersen and D. N. Reinhoudt, *Anal. Chim. Acta*, **310**, 263 (1995).
131. K. Peak and H. Ihm, *Chem. Lett.*, 311 (1996).
132. E. Malinowska, Z. Brzózka, K. Kasiura, R. J. M. Egberink and D. N. Reinhoudt, *Anal. Chim. Acta*, **298**, 253 (1994).
133. P. L. H. M. Cobben, R. J. M. Egberink, J. G. Bomer, P. Bergveld, W. Verboom and D. N. Reinhoudt, *J. Am. Chem. Soc.*, **114**, 10573 (1992).
134. Calix[4]arene derivative **28** could also be used for the construction of a ClO_4^- selective CHEMFET which has been described in: W. Wróblewski and Z. Brzózka, *Anal. Chim. Acta*, **326**, 163 (1996).
135. E. Malinowska, Z. Brzózka, K. Kasiura, R. J. M. Egberink and D. N. Reinhoudt, *Anal. Chim. Acta*, **208**, 245 (1994).
136. K. O'Connor, G. Svehla, S. J. Harris and M. A. McKervey, *Talanta*, **39**, 1549 (1992).
137. K. N. Koh, T. Imada, T. Nagasaki and S. Shinkai, *Tetrahedron Lett.*, **35**, 4157 (1994).
138. (a) A. T. Yordanov, J. T. Margue and D. M. Roundhill, *Inorg. Chem.*, **34**, 5084 (1995); (b) A. T. Yordanov and D. M. Roundhill, *New J. Chem.*, **20**, 447 (1996).
139. G. Barrett, M. A. McKervey, J. F. Malone, A. Walker, F. Arnaud-Neu, L. Guerra, M.-J. Schwing-Weill, C. D. Gutsche and D. R. Stewart, *J. Chem. Soc.: Perkin Trans. II*, 1475 (1993).
140. W. H. Chan, K. K. Shiu, X. and H. Gu, *Analyst*, **118**, 863 (1993).
141. A. Cadogan, D. Diamond, M. R. Smyth, G. Svehla, M. A. McKervey, E. M. Seward and S. J. Harris, *Analyst*, **115**, 1207 (1990).
142. F. J. B. Kremer, G. Chiosis, J. F. J. Engbersen and D. N. Reinhoudt, *J. Chem. Soc.: Perkin Trans. II*, 677 (1994).
143. W. Wróblewski, Z. Brzózka, R. G. Janssen, W. Verboom and D. N. Reinhoudt, *New J. Chem.*, **20**, 419 (1996).
144. D. N. Reinhoudt, *Sens. Actuators B*, **6**, 179 (1992).
145. R. Cacciapaglia, A. R. van Doorn, L. Mandolini, D. N. Reinhoudt and W. Verboom, *J. Am. Chem. Soc.*, **114**, 261 (1992).
146. R. J. W. Lugtenberg, R. J. M. Egberink, J. F. J. Engbersen, D. N. Reinhoudt, *J. Electroanal. Chem.*, **452**, 69 (1998).
147. D. Wegman, H. Weiss, D. Amman, W. E. Morf, E. Pretsch, K. Sugahara and W. Simon, *Microchim. Acta*, **3**, 1 (1984).
148. M. M. G. Antonisse, R. J. W. Lugtenberg, R. J. M. Egberink, J. F. J. Engbersen and D. N. Reinhoudt, *Anal. Chim. Acta*, **332**, 123 (1996).
149. (a) U. Wuthier, H. V. Pham, E. Pretsch, D. Ammann, A. K. Beck, D. Seebach and W. Simon, *Helv. Chim. Acta*, **68**, 1822 (1985); (b) U. Wuthier, H. V. Pham, R. Zünd, D. Welte, R. J. J. Funck, A. Bezegh, D. Ammann, E. Pretsch and W. Simon, *Anal. Chem.*, **56**, 535 (1984).
150. (a) J. K. Tsagatakis, N. A. Chaniotakis and K. Jurkschat, *Helv. Chim. Acta*, **77**, 2191 (1994); (b) N. A. Chaniotakis, K. Jurkschat and A. Ruhlman, *Anal. Chim. Acta*, **282**, 345 (1993).
151. M. M. G. Antonisse, B. H. M. Snellink-Ruël, J. F. J. Engbersen, D. N. Reinhoudt, *J. Chem. Soc.: Perkin Trans. II*, 772 (1998).
152. D. M. Rudkevich, W. Verboom, Z. Brzozka, M. J. Palys, W. P. R. V. Stauthamer, G. J. van Hummel, S. M. Franken, S. Harkema, J. F. J. Engbersen, D. N. Reinhoudt, *J. Am. Chem. Soc.*, **116**, 4341 (1994).
153. J. J. A. M. Scheerder, M. Fochi, J. F. J. Engbersen and D. N. Reinhoudt, *J. Org. Chem.*, **59**, 7815 (1994).

Chapter 6

Ion Separation in Membrane and Solid Phase Extraction Systems

REED M. IZATT, JERALD S. BRADSHAW AND RONALD L. BRUENING†

Brigham Young University, UT, USA

1. INTRODUCTION

The field of chemical separation provides many opportunities for the introduction of innovative new technologies. The need for innovation in chemical separation was recognized by the National Academy of Sciences in a special report [1] that stressed the requirement for new selective separations reagents based on host-guest recognition at the molecular level. These reagents should be capable of the selective removal of ions present at low levels from large volumes of solutions, often containing high concentrations of solutes. Accomplishment of these goals and the commercialization of resulting molecular recognition processes requires the combined efforts of those trained in molecular design, organic synthesis, coordination chemistry, chemical engineering, and chemical marketing. The design and synthesis steps incorporate to a significant degree the principles embodied in supramolecular chemistry [2].

The need for new technologies capable of an increased level of host-guest selectivity and capability has become increasingly evident during the past two decades. Traditional separation technologies were not designed to achieve high selectivities of ions over chemically similar species or to remove traces of ions from dilute solutions. Successful functioning of traditional separation procedures is

† IBC Advanced Technologies, UT, USA

Table 1 Some traditional and novel separation methods

Procedure	Basis	Advantages	Disadvantages
Traditional			
Precipitation	Precipitation of target species with added reagent	Inexpensive reagents	Separation and disposal of precipitate, coprecipitation, new contaminants added, decreased effectiveness with decreased concentration of target species, limited selectivity options
Ion exchange	Exchange on a resin of a species by the target species	Inexpensive resins, no loss of resin to environment	Selectivity based on ion charge, new contaminants added, decreased selectivity with decreased concentration of target species, large space requirements, hydrophobic support, slow kinetics
Solvent extraction	Selective transfer of target species to a second immiscible solvent	Selectivity for target species by host extractant	New contaminants added, large space requirements, organics contaminate aqueous stream, hydrophobicity requirements for ligand can add to cost and development, slow kinetics
Chromatographic	Differing retention times by column packing material	Large separation factors	Limited to small scale separations, pressure and equipment requirements may be severe, sensitive to solids
Reverse osmosis	Target species passes through pore, other species do not	Suitable for large scale operation when applicable	Selectivity based on size of species to be separated limiting selectivities, large energy costs, sensitive to solids

Novel				
Solid phase extraction	Design of ligands labor intensive, usually not applicable to simultaneous removal of a wide range of metal ions	No loss of resin to environment, high selectivity for target species, large scale operation feasible, minimal environmental effects, continuous automated operation, hydrophilic or hydrophobic support, rapid kinetics	Recognition on molecular level of target species by extractant	
Membranes	Membrane fouling, automation difficult	Selectivity for target species by host carrier, large separation factors possible, rapid kinetics	Selective transfer of target species across membrane	
Biological	Difficult to recover metal, microorganisms may be sensitive to surrounding, difficult to automate procedure or use it in an operating plant	Minimal environmental effects, low cost	Selective ingestion or adsorption by biological material	
Ion exchange chelation	Some limitations to selectivities, not hydrophilic, slow kinetics, some matrix limitations	No loss of reagents to environment, some added selectivity, operational in some added matrices, capable of element removal to low levels	Incorporate high affinity chelating agents into resin	
Supercritical (SC) carbon dioxide	Difficult to use with liquid and gas separations, limited by polarity of the solute	SC CO ₂ moves chelating agent through interstices of solid materials, recovery involves lowering pressure with loss of CO ₂ , promising for solid matrix applications, CO ₂ is environmentally benign	Chelating agent incorporated in CO ₂ binds species, CO ₂ carries complex	

especially difficult in highly acidic or highly basic solutions or in the presence of large amounts of other solutes. Increased awareness of environmental damage by trace amounts of ions, the need to increase the cost-effectiveness of product manufacture, and the requirement for increased purity of industrial products have provided the impetus for the development of new technologies.

A variety of novel procedures has been developed that are aimed at effective separation of trace amounts of elements. Table 1 is a list of some common traditional and novel separation procedures together with the basis, advantages, and disadvantages for each procedure. In general, traditional procedures rely on inexpensive reagents and are not designed to achieve the highly effective and selective separations required by modern industry. Several novel separation technologies have been developed in attempts to overcome deficiencies in traditional systems. Although these new separation procedures have their own shortcomings, they represent significant advances in achieving selectivities in chemical separations. The new technologies have specific niches in which they fit. In general, they are not competitive with low cost procedures such as precipitation unless other overriding factors are present. A significant effort to commercialize solid phase extraction (SPE) technology using an approach based on specificity of host-guest recognition is being made by IBC Advanced Technologies, Inc. (IBC).

In Table 2, some desirable features of an effective separation system are given. It is apparent that these requirements pose severe challenges for any separation procedure. Traditional technologies fail on many of the points given in Table 2. However, the molecular recognition technology (MRT) approach has enabled IBC to develop new separation systems tailored to specific needs in several industries. Examples of these systems will be presented and discussed.

Table 2 Desirable features of an effective separation system

-
1. Have sufficient specificity for the target species even if present at ppm/ppb level in the presence of high concentrations of other similar species.
 2. Have sufficient specificity for a given oxidation state of an element when the element has multiple oxidation states.
 3. Have sufficient selectivity for the target species when it is in a difficult matrix, such as strong acid, strong base, F^-/HF , redox agents, other complexing agents, high solute concentrations.
 4. Be capable of operation without adding potential contaminants, such as solvents, replacement ions, precipitants.
 5. Be capable of removing target species to sufficiently low target levels.
 6. Be capable of handling large solution volumes at rapid flow rates.
 7. Have rapid separation kinetics for diffusion, host-guest interaction, and host-guest dissociation.
 8. Have adequate longevity due to resistance/stability to matrix chemical effects, including, if applicable, intense nuclear radiation, acid/base, redox, and other chemical reactants.
 9. Be capable of automation in a continuous mode.
 10. Be capable of concentrating desired species by large factors leading to rapid and efficient recovery of highly purified product.
-

The demand for highly effective separation procedures is high and is found in many commercial operations. This demand is a result of greater environmental awareness resulting in actual or impending litigation, the need to increase cost-effectiveness, the need for products of increased purity, and the often deleterious effect of the build-up of impurities in the ultimate product. Thus, in commercial operations the separation of unwanted elements can be cost-effective for a number of reasons. An additional economic incentive is that a trace species can often be concentrated, recovered, and sold as a pure product.

A necessary requirement for effective separation of trace amounts of a chemical species in the presence of other similar species and/or difficult matrices is the availability of the correct complexing agent. Among the most effective selective complexing agents in single phase systems are macrocyclic ligands. In recent reviews [3–5], we have discussed the characteristics of macrocycles which cause them to have these ion-selective properties. An advantage of these compounds is the ability to design the molecule for optimal interaction with the ion of interest. This ability places the problem of creating new, selective reagents in the realm of the organic chemist and opens up the possibility of the preparation of reagents capable of highly selective ion separations. There is a need for such reagents in a variety of large scale commercial operations. In addition, the need for highly selective reagents extends to the separation of precious and other metals where a high level of purity is required and in analytical applications where there is a need for highly selective separations of target ions prior to their analysis.

2. EXPERIMENTAL TECHNIQUES

The basic requirement for the separation of ions from a matrix and from each other is that the target ion be transferred, preferably alone, into a new phase from which it may be separated after the first phase has been removed. Traditional technologies (Table 1) are designed to accomplish this task on a large scale using inexpensive reagents. Systems used in commercial applications must be cost-effective. Therefore, the traditional technologies have appeal for many applications. In general, these technologies do not have many of the desirable features listed in Table 2. Their mode of operation results in new ions and/or reagents being added to the system with potential environmental problems or further separation needs. These methods usually have large space requirements and reagent inventories, and involve the handling of large volumes of often corrosive reagents. They are generally incapable of accomplishing many of the requirements of modern separations. These requirements (Table 2) include the selective recovery of trace amounts of target ions in concentrated form from large volumes of solution, the avoidance of adding additional pollutants to the system, and the carrying out of the separation on a continuous, real time basis.

Similar arguments apply to the separations necessary to recover primary metal products in metallurgical and refining operations. However, in most of these cases

the value of the purified metal product does not justify the additional expense of more sophisticated techniques. An exception is the purification of precious metals such as platinum and gold. In several of these cases, the value of the product justifies the use of new separation techniques of improved selectivity with greater cost-effectiveness.

The new techniques (Table 1) are aimed at achieving one or more of the desirable features noted in Table 2 for separations systems. The biological systems show promise in the selective removal of several of the heavy metals, such as mercury, cadmium, and lead, either by adsorption on algae [6], feedstock for bacteria [7], or adsorption on biomass [8]. These techniques have shown promise in the remediation of industrial streams, soil, and contaminated dumps. The biological materials are relatively inexpensive. For example, favorable pricing has resulted in 30% of the copper produced in the USA being extracted by microbes [9]. However, microorganisms capable of a given separation must be found and treated with care to keep them alive and functioning. Significant disadvantages of biological material are the difficulty of recovering the separated element(s) and the inability to automate the procedure. It is improbable that such methods could be used to separate and prepare elements for analytical procedures or to prepare a variety of pure metal products on a large scale.

The use of complexing agents in a supercritical CO₂ solvent to effect selective ion separation is of great interest [10–14]. The advantages of these systems have led to an interest in their use for commercial applications. This procedure may be especially effective in cases of removal of target ions from complex solid matrices, such as soils. Supercritical CO₂ has properties similar to those of a gaseous fluid allowing it to penetrate effectively into pores of a solid matrix. The recently discovered ability to dissolve appreciable amounts of reagents capable of highly selective complexation with target ions makes this technique a promising one [10]. The relatively high density of the supercritical CO₂ allows movement of the reagent throughout the matrix. Following removal of the target species, the CO₂ is separated by lowering the pressure. This procedure has great promise, especially in systems involving solid matrices, such as soil. Its development is in its infancy.

Much effort has been expended in attempting to use membranes for separations. Reverse osmosis membranes are used worldwide for water purification. These membranes are based on size selectivity depending on the pores used. They do not have the ability to selectively separate target species other than by size. Incorporation of carrier molecules into liquid membrane systems of various types has resulted in achievement of highly selective separations on a laboratory scale. Reviews of the extensive literature on the use of liquid membrane systems for carrier-mediated ion separations have been published [15–20]. A variety of liquid membranes has been studied including bulk (BLM), emulsion (ELM), thin sheet supported (TSSLM), hollow fiber supported (HFSLM), and two module hollow fiber supported (TMHFSLM) types. Of these liquid membranes, only the ELM and TMHFSLM types are likely to be commercialized. Inadequacies of the remaining

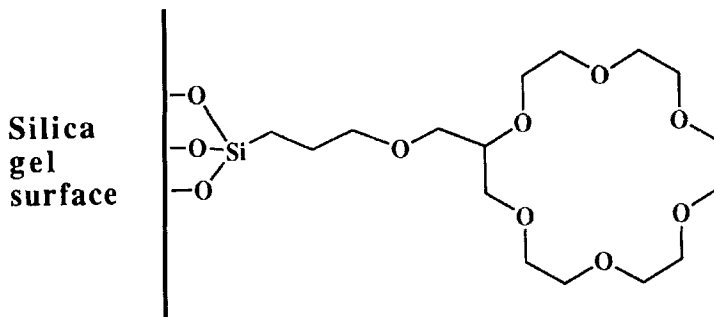


Figure 1 Macrocycle host attached to a solid support (silica gel) using a connector arm

systems include slow transport (BLM, TSSLM), and the need for extremely hydrophobic carriers and membrane solvents (TSSLM, HFSLM). All of the systems would require inventories of solvent and ligand with likely subsequent loss to the environment. Difficulties encountered with these systems have been presented and discussed [21]. The TSSLM system has well-defined geometry. Transport results calculated from models of this system agree well with those determined experimentally [20]. SPE procedures for the competitive and selective removal of ions from industrial streams have been developed at Brigham Young University and commercialized by IBC. The SPE process is based on the concept of molecular recognition of a particular host molecule permanently attached by a chemical bond to a solid support for a specific guest ion in a stream. The attachment of the host to the support is illustrated in Figure 1 and the separation of Pb^{2+} from a multi-cation mixture is shown in Figure 2 for the column mode of operation. The resulting Pb^{2+} may be recovered using a small volume of eluent solution in a concentrated and purified form. This process meets the requirements set forth in Table 2. It is termed molecular recognition technique (MRT). It has been commercialized, is competitive with traditional techniques, and in many cases, it is superior to these techniques.

3. COMMERCIAL SEPARATIONS USING MOLECULAR RECOGNITION TECHNOLOGY

Commercial separations using MRT as developed by IBC have been accomplished in several areas, e.g. environmental, metallurgical, precious metals, nuclear, and analytical [20,22]. In the material that follows, examples of separations are given in each of these areas. The solid phase host–connector–support materials used by IBC for commercial separations are termed SuperLig[®].

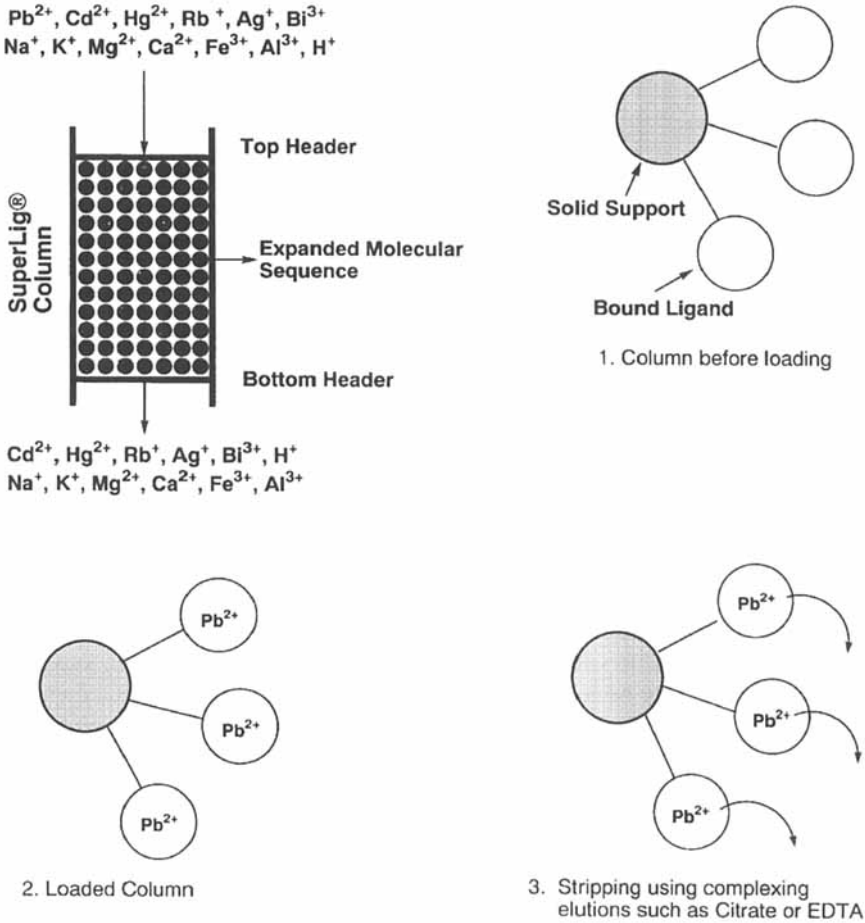


Figure 2 Illustration of the solid phase extraction system involving the selective removal of Pb^{2+} from a matrix typically found in acidic high-level or low-level nuclear waste. Following selective removal of the Pb^{2+} (Step 2), the column is washed to remove the solution remaining in the dead volume, and the Pb^{2+} is eluted in highly purified form with a complexing agent such as citrate ion or ethylenediaminetetraacetic acid (EDTA)

3.1 Environmental

Environmental contamination has existed as long as natural forces have operated on the earth. Increases in the use of certain metals such as lead beginning in Greek and Roman times and continuing to the present, are well documented in Greenland ice cores [23]. The beginning of the modern industrial revolution is likewise well

documented in environmental samples. Early examples abound of environmental contamination, particularly by heavy metals in mining districts. Some of the best documentation is found in the literature concerning early mines in Wales [24].

During the past three decades, there has been an increased awareness of the dangers of environmental contamination. This awareness has led to increasingly stringent US governmental laws and regulations respecting effluents. Of particular concern were the effects on the environment and on human health of heavy metals present in industrial wastewaters. Peters, Ku, and Bhattacharyya have reviewed traditional techniques for the removal of these metals [25]. These techniques include chemical precipitation, coagulation, complexation, activated carbon adsorption, ion exchange, solvent extraction, foam flotation, electrodeposition, cementation, and membrane operations. Comparisons of their applications in industry have been given, together with advantages and disadvantages of each technique [25].

MRT operates from a different base from traditional techniques. In general, traditional techniques are not based on specific host-guest recognition as is MRT. The specificity of MRT allows separations to be accomplished in the presence of high concentrations of matrix species, acid, and base. Also, particular species can be separated in the presence of other species having similar chemistry. The capability of MRT is now illustrated with recent studies of a Superfund Site (Berkeley Pit) [26] and wastewaters from a Navy operation.

(a) *The Berkeley Pit*

Berkeley Pit is a large Superfund Site located in Butte, Montana. The discovery of large Cu, Pb, and Zn deposits at Butte in the 1880s led to the development of one of the most important mining complexes in the world [26–29]. The initial mining operations were underground, but open pit mining began in the mid-1950s and lasted until 1982. Upon closure of the operation, the resulting Berkeley Pit began to fill from underground water contaminated with metals. During its excavation, over $300 \times 10^6 \text{ m}^3$ of rock were removed from the pit, which reached a depth of 542 m [28]. At the rim, its lateral extent was approximately $1.8 \times 1.4 \text{ km}$ [29]. The pit is filling from ground and surface water sources at a rate of approximately $23 \times 10^6 \text{ l}$ per day [27,28]. The water level in the pit is rising at a rate of approximately 8 m per year [28] and is expected to reach a level at which surrounding ground water will be contaminated by about 2012 [27,28]. The composition of the Berkeley Pit water at approximately the 60 m level has been given [27]. The main metals present are Al, As, Cd, Ca, Cu, Fe, K, Mg, Mn, Ni, Na, Pb, Zn, and Si. The anions are Cl^- and SO_4^{2-} . The pH is approximately 3 and the reduction potential is approximately 620 mV. The solute concentrations generally increase with time. The pH and ion levels exceed discharge regulations as defined by the US Environmental Protection Agency Gold Book (environmental standards for pristine water supplies) by large,

often orders of magnitude, amounts. The drainage into the pit has raised the depth of solution to 250 m. The pit contains approximately 80×10^{10} l of waste solution. There is clearly a need for action before large scale contamination of the environment occurs.

In 1994 and 1995, IBC participated in a program sponsored by MSE, Inc. (Butte, MT) and funded by the U.S. Department of Energy to test new technologies for their effectiveness in removing metal contaminants from actual Berkeley Pit solutions. As would be expected, the Berkeley Pit contains a variety of metals. The five major contaminants excluding Na and Ca, all present at levels greater than 100 mg l^{-1} (p.p.m.), are iron (II/III), copper (II), aluminum (III), zinc (II), and manganese (II) [26–29]. The Berkeley Pit represents a commercial opportunity for any technology that can recover these metals selectively from the solution and purify them. However, in order to meet environmental requirements any process would need to be capable of removing the metals to low p.p.b./p.p.t. levels, of not adding any new undesirable contaminant(s) during the processing, and of processing large quantities of solution rapidly. In addition the process should be economically feasible.

Specifically, the criteria for a successful procedure are five-fold. First, the metals must be removed to or below levels acceptable from an environmental standpoint. Second, the target elements must be separated and recovered in sufficient purity (> 95%) and yield (> 95%) to make it economically feasible to return them to commercial use rather than storing them as hazardous waste. Third, the process should use operating chemicals that are readily available, inexpensive, and pose minimal environmental hazard. Fourth, in its operation the process should result in a significant volume reduction and add no undesirable ions to the system. Finally, the process should be inexpensive, environmentally friendly, and easy to operate. The MRT separation system achieved high metal recovery and product purities as indicated in Table 3. Effluent water quality met the EPA Gold Book specifications

Table 3 MRT separation system results for Berkeley Pit solutions

Metal	Feed concentration (mg l^{-1})	Treated effluent concentration ^a (mg l^{-1})	Recovery (%)	Eluent purity (%)
Cu	180	< 0.02	> 99	96–98
Fe	994	< 0.1	> 99	99.5
Al	270	< 1	> 99 ^b	97–98
Zn	554	< 0.05	> 99	99–99.5
Mn	194	< 1	> 99	75–80 ^b
Cd	2	< 0.02	—	—
As	0.3	< 0.1	—	—

^a All below detection by analytical methods used.

^b Some Al slipped past the Al system but was recovered with the Mn. Total Al recovery was > 99%.

and/or regulatory drinking water standards. The required criteria were met by the SuperLig[®] materials. These data demonstrate that MRT is effective in the removal of heavy metals and transition metals from difficult matrices under field operating conditions. The resulting separated metal products are of sufficient purity to allow them to be marketed, if desired.

(b) Navy plating operation

The Department of Defense has many operations that produce wastewater containing heavy metals. Chrome wastewater and acid/alkali wastewater solutions from a US Navy plating operation were studied by IBC. While the main focus of the investigation was to remove the undesirable metal-containing ions for environmental reasons, it was also desirable to recover the target metals as purified concentrates to allow for their possible reuse. Mimic solutions were prepared using the following chemicals: Na_2CrO_4 , $\text{Cr}(\text{NO}_3)_3$, $\text{Cu}(\text{NO}_3)_2$, $\text{Ni}(\text{NO}_3)_2$, $\text{Cd}(\text{NO}_3)_2$, AgNO_3 , and H_2SO_4 . The target ions were Ag^+ , Cu^{2+} , Cr^{3+} , Ni^{2+} , Cd^{2+} , and CrO_4^{2-} . Solutions of NaNO_3 and Na_2SO_4 were added to the acid/alkali solution to mimic the excess Na^+ present in the actual acid/alkali solution.

The metal ions sequentially removed from the acid/alkali solutions were silver, copper, chromium(III), and cadmium/nickel. The cadmium and nickel were later separated from each other. The first separation performed with the chrome solution involved the selective separation of Cr(VI) as CrO_4^{2-} from the feed solution. Chromium(III) remained in the solution in small amounts after Cr(VI) was removed. Neither the Cr(VI) nor the Cr(III) SuperLig[®] material is capable of removing the other chromium species. The second separation from the chrome solution involved copper removal. The third separation was the removal of the remaining chromium as Cr(III). The final separation was the removal of nickel.

The separation results for the acid/alkali and chrome solutions are given in Table 4. The data show that excellent recovery of the target elements is achieved. The only byproducts of the system are the treated streams (now virtually devoid of heavy metals) and the concentrated metal products in H_2SO_4 that may be recovered, if desired. The chemicals added are a base, $\text{Ca}(\text{OH})_2$, for pH adjustment, water and H_2SO_4 for making eluents.

3.2 Metallurgical

Removal of metals from their ores and their subsequent purification typically results in the production of significant amounts of waste materials. In the purification process, removal of unwanted elements can have significant economic consequences for three reasons. First, the value of the final product may be enhanced significantly as its purity increases. This criterion applies particularly to elements designed for high technology uses where component purity is essential. The presence of

Table 4 MRT separation system results for Navy acid/alkali and chrome waste solutions

Feed stream	Ion	Average feed concentration (mg l ⁻¹)	Treated effluent concentration ^a (mg l ⁻¹)	Recovery (%)	Eluent purity (%)
Acid/alkali	As ⁺	2.6	< 0.1	> 99	> 99
Acid/alkali	Cu ²⁺	1.5	< 0.02	> 99	> 99
Acid/alkali	Cr(III)	0.9	< 0.1	> 99	> 99
Acid/alkali	Ni ²⁺	6.4	< 0.02	> 99	> 99
Acid/alkali	Cd ²⁺	7.1	< 0.02	> 99	> 99
Chrome	CrO ₄ ²⁻	25	< 0.1	> 99	> 99
Chrome	Cu ²⁺	2.1	< 0.02	> 99	> 99
Chrome	Cr ³⁺	25	< 0.1	> 99	> 99
Chrome	Ni ²⁺	1.3	< 0.02	> 99	> 99

^a All below detection by flame atomic absorption or inductively coupled plasma spectroscopy.

significant amounts of an impurity usually leads to products with inferior properties. Second, the recovered impurity may have commercial value. A process capable of selectively removing the impurity and recovering it in concentrated form could have important economic value. Third, the ability to selectively recover an impurity and thus remove it from the process in a pure form has important environmental consequences. This ability represented an important phase of the Berkeley Pit study. The inadequacy of traditional separations procedures to achieve this goal has resulted in many of the Superfund Sites found in the USA and in many of the pollution problems present world wide.

MRT has made significant progress in the selective removal and subsequent recovery of impurities in primary metallurgical processes [30–34]. The development of commercial units capable of these operations represents a significant advance in separations technology as applied to this industry. In Table 5, a listing is given of metallurgical operations in which the separation capability of MRT has been demonstrated. An example of the effectiveness of MRT is given in Table 6 for the removal of Bi from Cu electrolyte.

Table 5 Examples of commercial metallurgical operations where MRT effectiveness for impurity removal and recovery has been demonstrated

Primary element(s)/compound(s)	Element(s) removed	Ref.
Copper	Bismuth, iron, antimony, lead, cobalt	31,32
Silver	Palladium	30
Tin	Lead, iron	31,32
Zinc	Fluoride, germanium, chloride	
Sulfuric acid	Mercury	32
Nickel	Lead, copper, silver	32

Table 6 Removal of Bi from a copper refinery tankhouse solution

Processing stream ^a	Metal concentration	
	Bi (mg l ⁻¹)	Cu (mg l ⁻¹)
Feed	275	29,611
Barren feed after SuperLig [®] treatment	^b	29,117
0.1 M H ₂ SO ₄ wash	^b	14,802
Elution	19,960	^b

^a Solutions are in a H₂SO₄ matrix.

^b Below analytical detection limits.

Bismuth at high levels in copper tankhouse electrolyte can reduce the quality of the cathode copper, causing excessive breakage of copper wire. Classical methods of bismuth control include using a bleed stream, ion exchange, control in the smelter, or reliance on low bismuth concentrates. MRT has proven to be superior to any of these methods and is now in use at several copper smelters. In the MRT procedure, a portion of the tankhouse electrolyte is filtered and fed to a SuperLig[®] column where bismuth is extracted. The purified bismuth-free solution is returned to the tankhouse. After the SuperLig[®] column is loaded, the feed is switched to a second column. The first column is then treated with an 8 M H₂SO₄ eluent to remove the bismuth for recovery. Simple precipitation, filtration, and drying steps produce a high purity bismuth product and recover the eluent for recycle to the process. The volume of the H₂SO₄ used in the elution step is approximately one percent of that of the volume of electrolyte treated although in actual operations this percentage may be lower. This results in the collection of a small volume of Bi concentrated in a pure form. Bismuth sulfate product is produced at > 95% purity and the H₂SO₄ is recycled to give a closed loop separation system with no contamination of the environment.

A significant feature of these separations is that they can be automated making continuous operation possible. Thus, the level of an impurity can be maintained within desired limits on a continuing basis. This feature is important in cases where the ore contains trace amounts of one or more impurities that follow the primary element through its purification steps and accumulate in the finished product in unacceptable levels. A number of the impurities listed in Table 5 fall into this category. Impurities present in a variety of commercial operations have been listed [30].

3.3 Precious Metals

Precious metals such as platinum, gold and silver have great commercial importance. Their uses include personal adornment, incorporation into objects or devices where long life and resistance to corrosion are desired, catalysts for laboratory and

Table 7 Palladium recovery from silver nitrate electrolyte using a Pd SuperLig[®] system [35]

Processing stream	Metal Concentration (mg l ⁻¹) (p.p.m.)			
	Pd	Ag	Pb	Cu
Feed	275	400,000	5,000	40,000
Barren feed following SuperLig [®] treatment	^a	396,000	4,950	39,600
0.1 M H ₂ SO ₄ wash	^a	184,300	2,328	19,400
Elution	19,458	^a	^a	^a

^a Below analytical detection limits.

industrial use, and as monetary reserves. Their value derives in large part from their ability to withstand corrosion and the possession of certain distinctive chemical properties that enable them to catalyze effectively many chemical reactions. In addition, their inherent beauty has appeal to many individuals for personal uses.

The distinctive properties of the precious metals make their separation from other elements present in their ores relatively straightforward. However, production of highly purified (99.95% or higher) individual precious metals requires the removal of other noble metals. Traditional separation techniques such as solvent extraction and ion exchange are able to accomplish these separations. However, a significant disadvantage of these techniques is the large inventory of separation reagents required and the large floor space needed. MRT overcomes both of these disadvantages while enabling the required purity to be achieved. A significant fraction of the world's palladium is now produced by an MRT process. The recovery of palladium from silver nitrate electrolyte is illustrated in Table 7 [35]. The SuperLig[®] used in this process is seen to be highly selective for the palladium.

SuperLig[®] materials have been used to recover at high purity Rh, Pt, and Pd from spent catalyst [36]. These individual elements can be recovered at purity levels of > 99.9%. The separation and recovery of rhodium is particularly difficult because of the similarity of its chemical properties to those of the remaining platinum metals. An MRT process has been developed that is effective for rhodium separations and recovery. This process is used commercially for rhodium production. An example of rhodium separation and recovery is given in Table 8. Another case of precious metal

Table 8 Separation of rhodium from platinum, palladium, and base metals

Processing stream	Volume (l)	Metal Concentration (mg l ⁻¹)			
		Rh	Pt	Pd	Base metals
Feed	2	8,042	7,045	15,300	26,000
Barren feed	2	13	4,650	11,475	19,000
0.1 M HCl wash	1	8	4,790	7,650	14,000
Elution	0.7	11,500	2	^a	^a

^a Below analytical detection limits.

separations using MRT is the recovery of gold at a primary gold mining operation [37]. The development of separations based on MRT represents an important advance in simplifying the recovery and purification procedures for precious metals. Significant savings in time, resources, and personnel are achieved.

3.4 Nuclear Waste Applications

The past half-century has witnessed an enormous accumulation of nuclear wastes. This accumulation continues today, but on a smaller scale, due to peacetime uses of nuclear energy. Some of the largest repositories of nuclear waste are derived from atomic weapons development and are found in the USA. These repositories often date back to the 1940s and 1950s and contain a mixture of radioactive and non-radioactive constituents reflecting past efforts to modify the original waste.

A concentrated effort is now underway to find effective procedures for the separation of selected components from these wastes. IBC has participated in this effort with support from the US Department of Energy [38]. Effective procedures have been developed for the use of MRT to accomplish several desired separations. MRT has significant advantages over competing technologies for a number of the needed separations. First and foremost among these advantages is the capability to bring the power of molecular design and modern organic synthesis to bear in the preparation of new ligands designed specifically to accomplish predetermined separations. This achievement is illustrated in Table 9 by the separation of Cs⁺ from an alkaline Hanford (Washington) waste solution. The requirements for this separation are threefold. First, the SuperLig[®] material must be capable of at least 10³ and preferably higher selectivity of Cs⁺ over Na⁺ and K⁺. This requirement arises because the waste solution (see footnote a in Table 9) contains large amounts

Table 9 Separation of Cs⁺ from a Hanford nuclear waste solution mimic^{a,b}

Sample description	Metal concentration (mg l ⁻¹)(p.p.m.)
Original solution	10
0–150 ml feed after passage through columns ^c	<0.1
0–2 ml 0.5 M HNO ₃ eluent ^d	750
2–4 ml 0.5 M HNO ₃ eluent ^d	2

^a Composition, g l⁻¹: NaOH, 136; NaNO₃, 21.93; NaF, 3.74; NaNO₂, 29.67; Na₂CO₃, 24.38; Na₂HPO₄·7H₂O, 6.7; Na₂SO₄, 21.31; Al(NO₃)₃·9H₂O, 161.31; RbNO₃, 0.00737; KNO₃, 12.13.

^b Support used was a hydrophobic polymer-bound pH sensitive SuperLig[®] material (0.1 g SuperLig[®] in an Empore[™] membrane disk).

^c Flow rate, 40 ml min⁻¹.

^d Following an appropriate wash between the loading and elution steps, the Na⁺ and K⁺ levels were below detection limits.

of these ions, which are chemically similar to Cs^+ . Second, the affinity of the SuperLig[®] material for Cs^+ must be large enough to reduce the overall Cs^+ concentration often to the low p.p.b./high p.p.t. range with large radioactive Cs decontamination factors (> 500). Third, the SuperLig[®] material must retain its integrity in the presence of the highly basic solution. In addition to these requirements, the material must be able to resist degradation from the radioactive solution. The data in Table 9 show that a SuperLig[®] material selective for Cs^+ is capable of accomplishing the separation under the difficult conditions and requirements. This material also is satisfactory with respect to the radiation requirement. The ability to design materials with predetermined separation properties makes MRT a desirable procedure for creating new separation materials for specific uses.

The MRT approach has already been used to design and prepare new SuperLig[®] materials capable of separating and recovering Sr^{2+} , Ra^{2+} , and Tc(VII) with success on I(V), Am(III), Pu(IV), and U(VI) also possible. Separations for several of the elements are feasible in strongly acidic, neutral, and strongly basic conditions. These materials also have promise for the separation and recovery of specific components from waste solutions produced at operating nuclear energy generating operations. These operations are important sources of electric energy in a number of nations including (percentage of total energy output obtained from nuclear source in 1995 in parentheses) Lithuania (86%), France (76%), Belgium (55%), Sweden (47%), Bulgaria (46%), Korea (36%), Japan (33%), UK (25%), Canada (17%), and USA (23%) [39]. An effective means of separating and recovering the radioactive elements produced would be useful in these cases. These elements represent a resource that could have economic significance [40,41]. Several of the platinum metals produced in nuclear reactions are not radioactive. Nuclear wastes represent a potentially important source of these metals.

3.5 Anion Separations

Novel separations procedures for anions have been developed at IBC with support from the National Institute of Standards and Technology through their Advanced Technology Program. This research has resulted in commercial or near commercial analytical procedures for anions such as RhCl_6^{3-} , TcO_4^- , F^- , and $\text{Au}(\text{CN})_2^-$. Removal of F^- is important for environmental cleanup in several industries.

3.6 Analytical Uses

There is a need at the laboratory level for reagents capable of selective removal of chemical species from other similar species, often in difficult matrices. These separations may be required for preparing solutions for subsequent analysis by concentrating a primary ion or to remove interfering constituents. MRT has found application in several of these uses and has promise to be used in others [42].

IBC and 3M have jointly developed a Sr Rad Disk product that is capable of separating and concentrating $^{80}\text{Sr}^{2+}$ from radioactive samples for subsequent analysis. This device recently won an R&D 100 Award for the development of a product of high technological significance [43]. The separation of Sr^{2+} is achieved using a disk composed of a specific SuperLig[®] material imbedded in Empore[™]. Use of this disk eliminates extensive separations procedures, time, and reagents required in traditional procedures. The entire operation from separation to counting takes about 20 min. Similar materials are available for radioactive Ra^{2+} and TcO_4^- . Similar devices for the separation of Pb^{2+} and Hg^{2+} from field samples and their preparation for subsequent analysis are being marketed jointly with Hach Corporation.

4. FUTURE PROSPECTS

There will be increased emphasis in the future on developing ligands that are highly selective for particular target ions. This selectivity will need to be maintained even in high or low pH conditions, in the presence of ions having similar chemical properties, and in the presence of much higher concentrations of competing ions. Emphasis will be placed on clean separations that do not add additional pollutants to the system. Many of the recovered elements may have economic value. Thus, recycling of elements will be a priority to minimize environmental problems encountered with present technologies. Future separation procedures will be automated allowing rapid, efficient, and continuous separations to be made in a cost-effective manner. Since separations will be targeted to particular species, there will be fewer waste materials and the operations will have much smaller space requirements. There will be increased interest in the development of novel separations materials targeted at particular species. The impetus for these developments will be increased environmental awareness and the need for greater cost effectiveness in separations procedures.

REFERENCES

1. G. J. King, *Separation and Purification*, National Academy of Sciences, USA, 1987.
2. J. M. Lehn, *Supramolecular Chemistry*, VCH, New York, 1995.
3. R. M. Izatt, K. Pawlak, J. S. Bradshaw and R. L. Bruening, *Chem. Rev.*, **95**, 2529 (1995).
4. R. M. Izatt, K. Pawlak, J. S. Bradshaw and R. L. Bruening, *Chem. Rev.*, **91**, 1721 (1991).
5. R. M. Izatt, J. S. Bradshaw, S. A. Nielsen, J. D. Lamb, J. J. Christensen and D. Sen, *Chem. Rev.*, **85**, 271 (1985).
6. L. R. Drake and G. R. Rayson, *Anal. Chem.*, **22A** (1996).
7. K. A. Matis, A. I. Zouboulis and I. C. Hancock, *Bioresource Tech.*, **49**, 253 (1994).
8. C. A. Maban and J. A. Holcombe, *Anal. Chem.*, **64**, 1933 (1992).
9. M. Merson, *New Scientist*, 4 January 1992, pp. 17–19.

10. Y. Lin, C. M. Wai, F. M. Jean and R. D. Brauer, *Environ. Sci. Technol.*, **28**, 1190 (1994).
11. J. Wang and W. D. Marshall, *Anal. Chem.*, **66**, 1658 (1994).
12. C. M. Wai and S. Wang, *Anal. Chem.*, **68**, 3516 (1996).
13. N. Smart, Y. Lin, and C. M. Wai, *Am. Environ. Lab.*, February 1996, pp. 38, 41, 42.
14. H. Black, *Environ. Sci. Technol.*, **30**, 124A (1996).
15. F. de Jong and H. C. Visser, in *Comprehensive Supramolecular Chemistry, Vol. 10, Supramolecular Technology*, (ed D. N. Reinhoudt) Pergamon, Tarrytown, 1996, pp. 13–51.
16. *Chemical Separations with Liquid Membranes*, (eds R. A. Bartsch and J. D. Way) ACS Symp. Ser., **642**, American Chemical Society, Washington, DC, 1996.
17. In *Liquid Membranes: Theory and Applications* (eds R. D. Noble and J. D. Way) ACS Symposium Series 347; American Chemical Society, Washington, DC, 1987, Ch. 7, pp. 98–108.
18. R. M. Izatt, J. S. Bradshaw, J. D. Lamb and R. L. Bruening, in *Liquid Membranes; Chemical Applications* (eds T. Araki and H. Tsukube) CRC Press, Boca Raton, FL, 1990, Chapter 7.1, pp. 123–140.
19. R. M. Izatt, J. D. Lamb, R. L. Bruening, *Sep. Sci. Tech.*, **23**, 1645 (1988).
20. R. M. Izatt, *J. Incl. Phenom. Mol. Recognit. Chem.*, **29**, 197 (1997).
21. R. M. Izatt, R. L. Bruening, M. L. Bruening, G. C. LindH and J. J. Christensen, *Anal. Chem.*, **61**, 1140 (1989).
22. R. M. Izatt, J. S. Bradshaw, R. L. Bruening, B. J. Tarbert and M. L. Bruening, in *Comprehensive Supramolecular Chemistry, Vol. 10, Supramolecular Technology*, (ed D. N. Reinhoudt), Pergamon, Tarrytown, NY, 1996.
23. S. Hong, J. P. Candelone, C. C. Patterson and C. F. Boutron, *Science*, **265**, 1841 (1994).
24. R. Rees, *History Today*, **43**, 38 (1993), ch. 7, pp. 1–11.
25. R. W. Peters, Y. Ku and D. Bhattacharyya, in *Separation of Heavy Metals and Other Trade Contaminants* (eds R. W. Peters and B. M. Kim), Am. Institute of Chem. Eng., New York, NY, 1985.
26. D. Baum and M. L. Knox, *Smithsonian*, **23**, 46 (1992).
27. H. H. Huang and Q. Liu, in *Emerging Technologies in Hazardous Waste Management V* (eds D. W. Tedder and F. G. Pohland), American Chemical Society, Washington, DC, 1995, pp. 196–209.
28. R. W. Hammack, H. M. Edenborn and D. H. Dvorak, *Wat. Res.*, **28**, 2321 (1994).
29. A. Davis and D. Ashenberg, *Appl. Geochem.*, **4**, 23 (1989).
30. R. M. Izatt, J. S. Bradshaw, R. L. Bruening, B. J. Tarbet and K. E. Krakowiak in *Emerging Separations Technologies for Metals and Fuels*, (eds V. I. Lakshmanan, R. G. Bautista and P. Somasundaran), TMS, Warrendale, PA, 1994.
31. R. M. Izatt, J. S. Bradshaw, R. L. Bruening, B. J. Tarbet and M. L. Bruening, *Pure Appl. Chem.*, **67**, 1069 (1995).
32. N. E. Izatt, R. L. Bruening, L. Anthian, L. D. Griffin, B. J. Tarbet, R. M. Izatt and J. S. Bradshaw, *Proceedings: Metallurgical Processes for Early 21st Century*, (ed H. Y. Sohn), TMS, Warrendale, PA, 1994, pp. 1001–1018.
33. R. L. Bruening, N. E. Izatt, W. Young and P. Soto, in *Clean Technology for the Mining Industry* (eds M. A. Sanchez, F. Vergara and S. H. Castro) University of Concepción, Concepción, Chile, 1996.
34. R. L. Bruening, J. B. Dale, N. E. Izatt and W. Young, in *Hidden Wealth*, South African Institute of Mining and Metallurgy, Johannesburg, 1996, pp. 45–54.
35. C. Wright and R. L. Bruening, in *Precious Metals Recovery and Refining* (ed L. Manziek) Historical Publications, Austin, 1990, pp. 95–106.
36. R. L. Bruening, J. B. Dale, R. M. Izatt and S. R. Izatt, paper presented at Spring National AIChE Meeting, March 19–23, 1995.

37. R. L. Bruening, J. B. Dale, N. E. Izatt and W. Young, in *Hidden Wealth*, South African Institute of Mining and Metallurgy, Johannesburg, 1996, pp. 143–149.
38. R. M. Izatt, J. S. Bradshaw and R. L. Bruening, *Pure Appl. Chem.*, **68**, 1237 (1996).
39. R. Famighetti, ed. *The World Almanac and Book of Facts*, World Almanac Books, Mahwah, NJ, 1997, 239.
40. S. Jurisson, D. Berning, W. Jia and D. Ma, *Chem. Rev.*, **93**, 1137 (1993).
41. R. J. Kowalsky and A. F. Parr, in *Encyclopedia of Pharmaceutical Technology*, (eds J. S. Warbrick and J. C. Boylan), Marcel Dekker, New York, NY, Vol. 11, 1988, pp. 1–42.
42. R. M. Izatt, J. S. Bradshaw, R. L. Bruening and M. L. Bruening, *Am. Lab.*, **26**, 28C–28M (1994).
43. Anon, *R&D Magazine*, **38**, 21 (1996).

Chapter 7

Porphyrin- and Expanded Porphyrin-based Diagnostic and Therapeutic Agents

TARAK D. MODY* AND JONATHAN L. SESSLER†

* *Pharmacyclics Inc., Sunnyvale, CA, USA*

† *The University of Texas at Austin, TX, USA*

1. INTRODUCTION

The year 1998 marks the 10th anniversary of when the first texaphyrin, namely the Cd(II) system **1**, was reported [1]. While great progress has been made in terms of understanding and exploiting this class of porphyrin derivatives in the intervening decade, even at the time of their initial synthesis it was recognized that the texaphyrins possessed special properties that might make them useful in several biomedical applications [2]. First, they were found to possess a pentadentate macrocyclic core that was about 20% larger than those found in more normal porphyrins; this allows the texaphyrins to form planar 1:1 complexes with the trivalent lanthanide cations [e.g. Gd(III) and Lu(III)]. Second, these 22 π -electron aromatic macrocycles were found to absorb light in the far-red portion of the visible spectrum and produce singlet oxygen in good quantum yield. Third, like their endogenous counterparts (i.e., the porphyrins) it was suspected that they would exhibit significant biolocalization in neoplastic cells and atheromatous plaque. Taken together, these properties, as detailed in this Chapter, led to the consideration that the texaphyrins could function as tumor-selective magnetic resonance imaging (MRI) enhancing agents and photodynamic therapy (PDT) sensitizers. Later on, it was appreciated that the same materials (i.e. **2–4**), useful for MRI and PDT, might also

function as sensitizers for X-ray radiation therapy and as useful dyes for fluorescence-based tumor detection. At present, therefore, the texaphyrins are viewed as showing promise in at least four oncology-related areas, as well as being of potential interest in the treatment of cardiovascular disease.

Not surprisingly, given the propitious timing and inspired by the encouraging results obtained to date, it was a desire to highlight the above promise that led the authors to write the present review. However, once approached about writing an article for the present book, it became apparent that a fair and unbiased treatment of our own work could only be made in the context of a general overview of the porphyrin-based cancer and cardiovascular treatment fields. This, then, is what we have tried to do. Specifically, we have tried to summarize porphyrin and porphyrin-like approaches to the generation of contrast agents for MRI enhancement, radiation sensitizers, photodynamic therapy agents, and fluorescence tumor detection. We have tried to be comprehensive in our review, but as a means of restricting the scope of the project, we have elected to focus our attention on systems that are either currently approved for use by the US Food and Drug Administration (FDA) or in the process of undergoing FDA-allowed clinical testing. While this has proved expedient, wherever possible reference to work at an earlier stage of development is also made. Thus, the hope is that the reader will obtain an appreciation for the current state-of-the-art while deriving some sense of how this research area is evolving.

2. MAGNETIC RESONANCE IMAGING

2.1 Background: Utility of Contrast Agents

Magnetic resonance imaging (MRI) is now firmly entrenched as a clinical tool of considerable importance. It is a noninvasive, nonradiative method that continues to have increasing application in the diagnosis and treatment planning of many diseases [3–11]. Unfortunately, however, the difference between MRI signals for diseased and normal tissues is often small. This has limited the utility of MRI in certain clinical situations, including many associated with cancer and cardiovascular diagnosis. To address this issue, considerable effort is currently being devoted to the preparation of MRI contrast reagents for the detection and delineation of tumors and atheromatous plaque. As will be discussed below, manganese(III) and iron(III) complexes of functionalized porphyrins (e.g. TPPS₄) [12–20] and other derivatized porphyrin-like macrocycles, such as manganese(II) phthalocyanine [21] and gadolinium(III) texaphyrins [22–26] (Figure 1, structures **2** and **3**), have recently attracted significant attention as potential tumor-localizing MRI contrast media.

The extent to which a contrast agent acts to effect MRI enhancement, termed relaxivity [6–8,10,11], is highly dependent on the magnitude of the dipole–dipole interactions between the electron spin on a paramagnetic metal complex and the proton spin on the water molecule in question. The development of an effective MRI

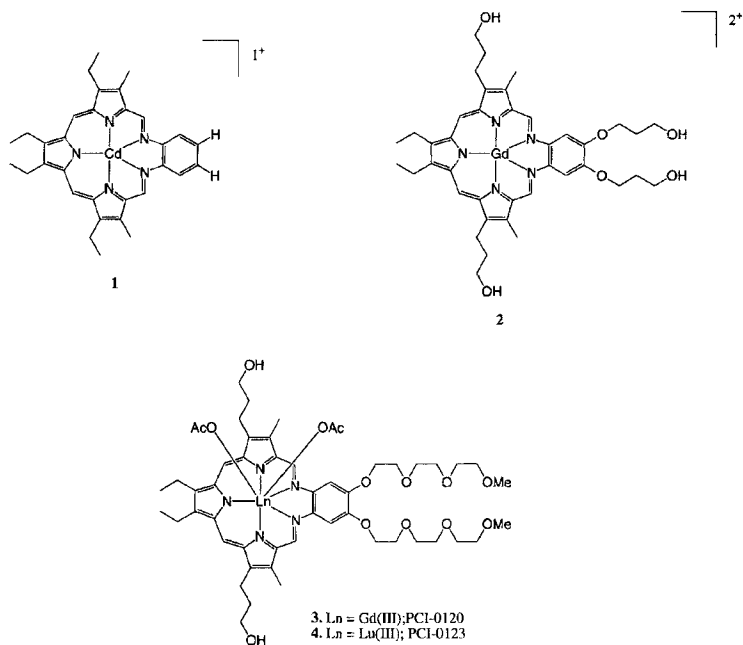


Figure 1 Structures 1–4

contrast agent requires finding a highly paramagnetic species that: binds water molecules directly in a so-called inner sphere fashion, allows fast aqua-ligand exchange (such that the effects on the water spins are magnified and the overall relaxivity phenomenon is optimized), has acceptable chemical and biochemical stability *in vivo*, and displays appropriate tissue selectivity and low *in vivo* toxicity [6–8,10,11].

Currently, the paramagnetic cations iron(III), manganese(II) and gadolinium(III) have received the most attention due to their high magnetic moments (i.e. 3, 5, 7 unpaired electrons, respectively). Of these, most effort has perhaps been devoted to the study of gadolinium(III), since this cation is the single most paramagnetic mononuclear species known. Exchange of water about gadolinium(III) centers is also generally quick. *A priori*, it thus engenders a high relaxivity [6–8,10,11,27]. Unfortunately, however, the aquo ion of Gd^{3+} is too toxic to allow for its unmodified use *in vivo*. As a consequence, considerable effort has been devoted in recent years to the preparation of Gd(III) complexes that might be less toxic and hence suitable for use in clinical situations. Indeed, several such pharmaceutical products are now approved for human use in the USA: namely, the bis-*N*-methylglucamine salt of Gd(III) diethylenetriaminepentaacetic acid (DTPA) (MagnevistTM), the bis-*N*-methylamide of Gd(III) DTPA (OmniscanTM), and the Gd(III) complex of 10-(2-hydroxypropyl) derivative of 1,4,7,10-tetraazacyclododecane-*N, N', N'*-triacetic acid (DO3A)

(Prohance) [28–44]. It is important to appreciate, however, that these FDA-approved agents rely on polydentate oxyanion-based chelation. This generates agents that are of high water solubility and of relatively low relaxivity. Thus, even though these so-called extracellular agents have been considerable application, their use has remained limited when it comes to problems involving tumor detection or atherosclerotic plaque enhancement that would necessarily involve drug uptake or retention in biological loci of a rather hydrophobic nature.

Recently, a few nongadolinium(III)-based MRI contrast agents have been approved by the FDA for human use in the USA. Two such agents, developed by Advanced Magnetics, Inc., are based on ultrasmall superparamagnetic iron oxide (USPIO) particles and go by the tradenames *Gastromark*TM and *Feridex I.V.*TM, respectively. These have been used for the MR imaging of the gastrointestinal tract and detection of liver cancer [45–49]. Another nonGd(III) chelate is the agent, Mn(II)DPDP (dipridoxyl diphosphate) [50–52]. MnDPDP has been documented to be an effective agent for the detection of focal liver lesions [16,53]. These nonporphyrin systems, however, fall outside the scope of this review.

2.2 Porphyrins as MRI Contrast Agents

One feature of porphyrins, long appreciated in the photodynamic therapy (PDT) area, is that certain of these tetrapyrrolic macrocycles, including hematoporphyrin derivative (HpD), do in fact show specificity for neoplasms, including sarcomas and carcinomas, as well as for atheromatous plaque [54–62]. While the reasons for this site-selective accumulation and/or retention remain obscure, this fact has made porphyrin and other porphyrin-like macrocycles, such as the phthalocyanines and the texaphyrins, logical candidates as possible tumor-selective MRI contrast agents. The major requirements for an effective tumor-selective contrast agent are that it should have a high *in vivo* stability, elicit high molar relaxivity, and localize preferentially in tumors [21].

As described above, most of the work in the MRI contrast development field has focused on tissue nonspecific extracellular agents derived from gadolinium(III) polydentate oxyanion-based chelands. Nonetheless, there has been considerable research interest in the development of intracellular tumor-localizing MRI contrast agents. The first work in the area was reported by Chen *et al.* in 1984; these workers noted that manganese(III) porphyrins show high relaxivity and further suggested that water-soluble metalloporphyrins could prove useful as tumor-specific contrast-enhancing contrast agents for magnetic resonance (MR) imaging [12]. Since then, a number of investigations have been undertaken by a number of workers employing a variety of porphyrins and a plethora of tumor models [12–15,18–20,63–71]. Given the inherent coordination chemistry of the porphyrins and related systems (e.g. phthalocyanines), much of this effort has been devoted to the study of manganese(III) and iron(III) tetrapyrrolic complexes [12–15,18–21,63–71]. Considerable

attention, however, has also been devoted to the study of gadolinium(III) texaphyrins [22,25,26], especially in the context of developing MRI-detectable radiation sensitizers.

The potential of Fe(III) porphyrins as MRI contrast agents has been greatly compromised by their propensity to form low-spin adducts and their tendency to dimerize at physiological pH [72]. Dimerization is accompanied by loss of relaxivity due to the antiferromagnetic coupling often manifest in stacked or μ -oxo linked dimers. For instance, Patronas *et al.* have found that, compared to their Mn(III) analogs, Fe(III) porphyrins were less than half as effective in the 300–500 mg kg⁻¹ dose range as judged by their ability to enhance the detection of a human colon carcinoma model in nude mice [14]. Likewise, based on a L1210 tumor model, Fiel *et al.* have reported MnTPPS₄ (**5**) (Figure 2) to be much more effective than FeTPPS₄ (**6**) [63]. It was suggested by Yushmanov *et al.* that the difference in binding and aggregation properties of metalloporphyrins may not only be relevant to their ability to mediate relaxivity effects *in vivo*, but also could adversely affect their blood transport and biodistribution properties [72].

In view of the above, only Mn(III) porphyrin derivatives are currently being considered as being promising porphyrin-based relaxation agents [12–14,19, 20,63,66,67,69,70,73]. Supporting this selection is work from Lyon and coworkers [13]. These researchers have noted that a number of water-soluble Mn(III) porphy-

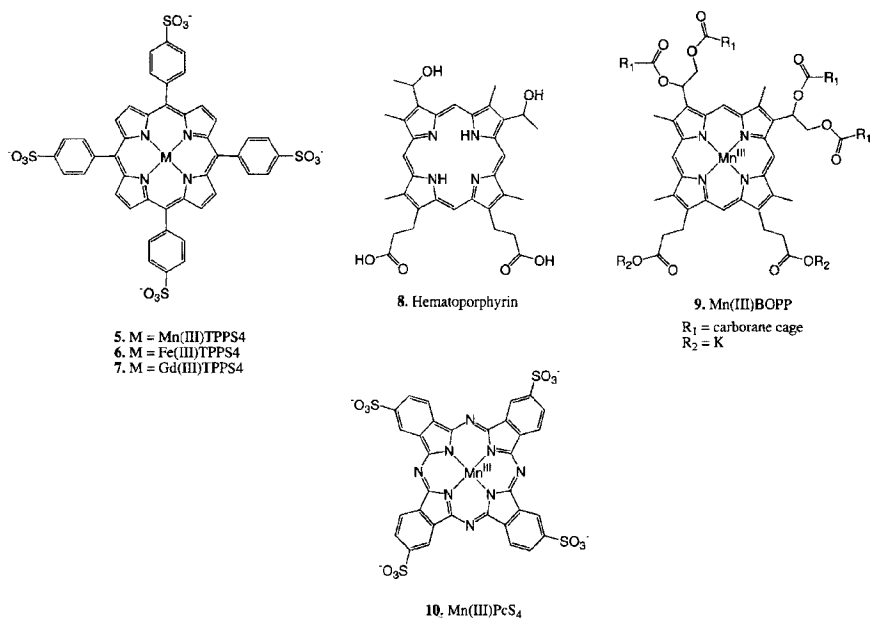


Figure 2 Structures 5–10

rins exhibit good kinetic stability and high relaxivities at 10.7 MHz (0.25 T) [12,13]. In particular, they found that Mn(III) *meso*-tetrakis(4-sulfonatophenyl)porphyrin (MnTPPS₄, **5**, (Figure 2) and Mn(III) *meso*-tetrakis(*N*-(methyl-4-pyridyl)porphyrin (MnTMPyP) complexes act to enhance the MRI detectability of transplanted human colon carcinomas in mice. In their study, the relaxivity of MnTPPS₄ was determined to be 10.3 mM⁻¹ s⁻¹ in water, compared to 11.1 mM⁻¹ s⁻¹ and 10.7 mM⁻¹ s⁻¹, respectively, after 1 h and 9 days of incubation at 37°C in human plasma [13]. By contrast, the corresponding Fe(III)TPPS₄ derivative exhibited a relaxivity of only 3.9 mM⁻¹ s⁻¹ at 10.7 MHz in water, a value which was further reduced at pH ≥ 6 due to μ-oxo-dimer formation.

Another reason attention has focused on Mn(III) porphyrins is that the corresponding Gd(III) complexes are unstable [13,74]. While Gd(III)TPPS₄ (**7**, Figure 2) does display a high relaxivity in water and human plasma (e.g. 22.8 mM⁻¹ s⁻¹ and 20.0 mM⁻¹ s⁻¹ after 1 h incubation, respectively, at 10.7 MHz), this desirable relaxivity is severely diminished by metal dissociation [13]. Further, and more importantly, this metal dissociation and the resulting metal-based toxicity makes GdTPPS₄ and other gadolinium(III) porphyrins unsuitable for use *in vivo*, a point that has been explicitly established by experiment [3].

In contradistinction to GdTPPS₄, the corresponding Mn(III) complex (**5**) was found to be stable for 9 days in human plasma at pH 7.5 [13]. Further, upon *i.v.* injection into mice bearing subcutaneous human colon carcinoma xenografts, MnTPPS₄ was found to provide for good contrast enhancement of subsequently excised mouse tissues such as liver, kidney and tumor [13]. In these latter studies, no evidence was found of either free Mn(II) or protein-bound Mn(II) complexes being present [note: Mn(III)_{aq} is unstable and reduced to Mn(II) by water; therefore, any free manganese, arising from complex breakdown, should be present in the divalent state] [6].

Bohdiewicz *et al.* have reported *in vivo* toxicity results and magnetic resonance imaging properties with a Mn(III) complex of hematoporphyrin (**8**, Figure 2) (MnHp). In their acute and subacute toxicity studies (involving rats), no deaths resulted when the agent was administered at doses of 13 or 19 μmol kg⁻¹ of MnHp. At a dose of 38 μmol kg⁻¹, however, a 33% mortality rate was noted. Under a standardized MRI protocol, there was a mean signal intensity increase of 37% in the liver-to-muscle contrast ratios for four rats injected with 25 μmol kg⁻¹ MnHp 24 h before MRI analysis as compared to paired controls (*P* < 0.0050) [69].

In work that also involves the use of a Mn(III) porphyrin, Huang *et al.* published a report on the manganese chelate of the tetrakis(carborane carboxylate ester of 2,4-(α, β-dihydroxylethyl)deuteroporphyrin IX (MnBOPP, **9**, Figure 2) [19]. The free-base form of this derivative, BOPP, has demonstrated potential as an agent for boron neutron capture therapy (BNCT) [75,76] and photodynamic therapy (PDT) [77] and is known to localize selectively in cerebral glioma tumors at ratios as high as 400:1 relative to normal brain tissue [19,78]. Like the free-base, MnBOPP also selectively localizes in tumor tissue. Specifically, it has been shown to enhance preferentially the

tumor-to-normal brain contrast of T_1 -weighted images of rat 9L gliosarcomas for at least 92 h. Interestingly, Huang *et al.* found that the initial uptake in 9L glioma was slower with MnBOPP than with MnTPPS₄ [19,64,67]. However, it was likewise found that MnBOPP is retained in the tumor longer. As a consequence, the maximum tumor-to-normal tissue contrast for MnBOPP and normal brain was observed at 24 h compared to 5 min for MnTPPS₄ at a comparable dose of 20 $\mu\text{mol kg}^{-1}$ [19]. However, the molar relaxivity of MnBOPP (determined to be 3.60 and 4.43 $\text{mM}^{-1} \text{s}^{-1}$ at 25°C and 37°C, respectively) is considerably lower than that of MnTPPSA₄ (12.21 and 10.16 $\text{mM}^{-1} \text{s}^{-1}$ at 25°C and 37°C, respectively) [19]. Nonetheless, MnBOPP represents the first agent that can both enhance the MRI-based contrast between neoplastic and normal tissue and serve as a possible sensitizing agent for BNCT.

A related class of tetrapyrrolic macrocycles are known to localize in tumors. These are the phthalocyanines (Pc) which have been extensively studied as second generation PDT agents, especially in their sulfonated forms [21,79–93]. In general, these compounds display high chemical and thermal stability when administered *in vivo* and show preferential retention in tumors when the degree of sulfonation is high [94,95]. Appreciating this, Saini *et al.* evaluated the Mn(III)PcS₄ complex **10** (Figure 2) as a potential tumor-localizing MRI contrast agent. In their study, MnPcS₄ was found to display a molar relaxivity of 10.1 $\text{mM}^{-1} \text{s}^{-1}$ in water at 10.7 MHz, 37°C. This relaxivity is twice that of GdDTPA and comparable to that of MnTPPS₄ [13,19,21]. Saini *et al.*'s study included tests of toxicity and biodistribution in mice. The LD₅₀ of MnPcS₄ was determined to be 600 mg kg^{-1} body weight compared to 500 mg kg^{-1} of MnTPPS₄. The biodistribution of MnPcS₄ in tumor-bearing mice showed a selective tumor-to-muscle retention ratio of 9.2:1 at 24 h. MR imaging done on the animals using a 1.5 T superconducting clinical imager showed an approximate mean percentage increase of 130% in the tumor and about 70% increase in tumor-to-muscle ratio over the pretreatment value, at 24 h. MnPcS₄ was found to accumulate in normal liver tissue more than any other tissue both at 1 h and 24 h after injection; this is similar to what is observed with MnTPPS₄ [21,63,73].

Although a considerable amount of effort has been invested in studying metallated tetrapyrrolic macrocycles, especially MnTPPS₄, as potential tumor-specific MR contrast agents, to date, the authors remain unaware of any complexes that have been subject to actual FDA-allowed human clinical trials for this indication. The reasons for this lack of clinical testing are surely varied. However, it could reflect the fact that TPPS₄ is known to engender neurological dysfunction, progressing to structural damage, when administered to mice [96,97].

As noted above, the porphyrins fail to form stable complexes with gadolinium(III) [13,74,98]. Since Gd(III) is inherently more paramagnetic than Mn(III), it is intrinsically more attractive for use in MRI contrast applications [6]. In view of this, the authors proposed that a larger “porphyrin-like” macrocycle, capable of coordinating gadolinium(III) in a stable, nonlabile manner, could prove useful as an

MRI contrast agent. In particular, it was suggested that such a system would prove useful for cancer diagnosis, provided it could be made to retain the special tumor-localizing characteristics of the porphyrins, and could be rendered biocompatible (i.e. water-soluble and nontoxic). In fact, it was a desire to test this hypothesis that provided much of the early impetus to develop the texaphyrins as lanthanide(III) ligating agents [1,2,23,24,99,100]. As detailed below, these particular expanded porphyrins do coordinate gadolinium(III) with seemingly unsurpassed kinetic stability [23] and show considerable promise as tumor-localizing MRI-detectable contrast agents.

2.3 Gadolinium(III) texaphyrins

There are several chemical properties that were originally considered as making the gadolinium(III) texaphyrins attractive as potential MRI contrast agents. First, the novel pentadentate nature of the texaphyrins allows them to form remarkably stable 1:1 nonlabile complexes with this highly paramagnetic lanthanide(III) cation. (It also allows the texaphyrin macrocycle to form strong, nonlabile complexes with other Ln(III) ions.) [23,101]. Second, as judged from single crystal X-ray diffraction analysis (Figure 3), the texaphyrins coordinate this metal center in such a way (meridinal, nearly in plane) that fast and efficient exchange of 4–5 water molecules might be expected at the apical ligation sites [23]. In accord with this expectation, a first generation water-soluble texaphyrin **2** (Figure 1) was found to show an exceptionally high relaxivity in aqueous medium ($R_1 = 16.9 \pm 1.5 \text{ mM}^{-1} \text{ s}^{-1}$; 50 MHz; room temperature) [22,23,102]. At the time it was obtained, this important result was considered to augur well for the ultimate *in vivo* utility of **2**; it meant that MRI enhancing efficacy could be expected at doses considerably lower than those required for carboxylate-derived gadolinium(III) chelates.

The *in vivo* efficacy of the first generation system **2** (code **PCI-0101**) was demonstrated by Young *et al.* using a number of tumor model systems, including a V2 carcinoma implanted into the thigh of a New Zealand white rabbit [22,26,103]. Specifically, these workers found that good tumor-depicting MRI enhancement could be achieved when complex **2**, in its bis-acetate form (**PCI-0101**), was administered intravenously at a dose level of $5 \mu\text{mol kg}^{-1}$ (Figure 4). Under these conditions, little contrast enhancement of the surrounding muscle tissues was seen. Further, no signs of acute toxicity were observed in the context of these studies, and indeed, no serious toxicity was observed in healthy rats given thrice weekly $20 \mu\text{mol kg}^{-1}$ doses of **2** for a period of 21 days [26]. Using this same agent, Young and coworkers were also able to demonstrate *ex vivo* the MRI enhancement of atheromatous plaque in human aorta [104] as well as acute cerebral ischemia in a rabbit model [105]. Thus, these initial studies served to show that the gadolinium(III) texaphyrin approach to MRI contrast enhancement had potential merit in the context of evaluating a wide range of important diseases.

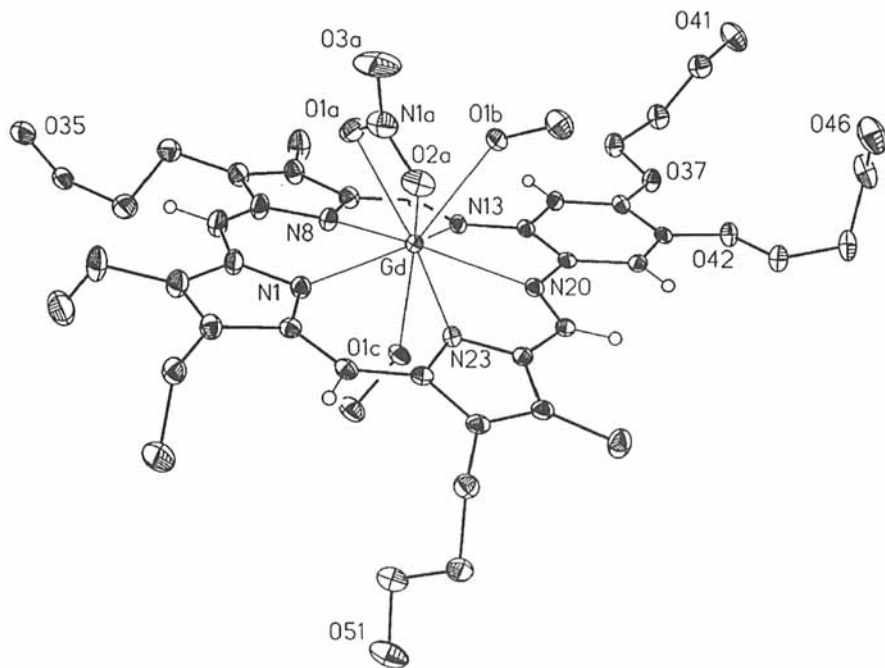


Figure 3 Single crystal X-ray diffraction structure of the gadolinium texaphyrin complex **PCI-0101 (2)** (bis-nitrate form) showing the planar nature of the basic monoanionic texaphyrin macrocycle and the four putative inner sphere coordination sites for water (occupied by two apical methanol molecules and a bidentate nitrate anion in this structure). The Gd(III) ion is nine-coordinate and lies 0.60 Å out of the plane through the five nitrogen atoms of the macrocycle. Most hydrogen atoms have been omitted for clarity. Thermal ellipsoids have been scaled to the 30% probability level. Reproduced from [22] with permission. © 1993 American Chemical Society

Further support for the above preliminary conclusions has come from studies involving a second generation gadolinium(III) texaphyrin complex **3** (Figure 1). This pharmaceutical drug product, to which the code name **PCI-0120** has been assigned, is being developed as an MRI-detectable radiation sensitizer by Pharmacyclics Inc. (Sunnyvale, CA) [25]. In a Phase I human clinical study involving the gadolinium texaphyrin complex, **PCI-0120**, selective tumor localization was established *via* MRI in patients receiving a single drug dose of 0.75–25.8 $\mu\text{mol kg}^{-1}$. Selective tumor uptake was seen in patients with brain metastasis, multiple myeloma, small and nonsmall cell lung cancer, pelvic leiomyosarcoma, ovarian cancer and in normal liver and kidney [106,107]. For instance, as illustrated in Figure 5, MRI scans of a patient enrolled in this Phase I trial indicate that the imaging of a large lung cancer may be enhanced by the use of **PCI-0120**, with the enhancement being found to persist for several hours [106,107]. As the result of these studies and other

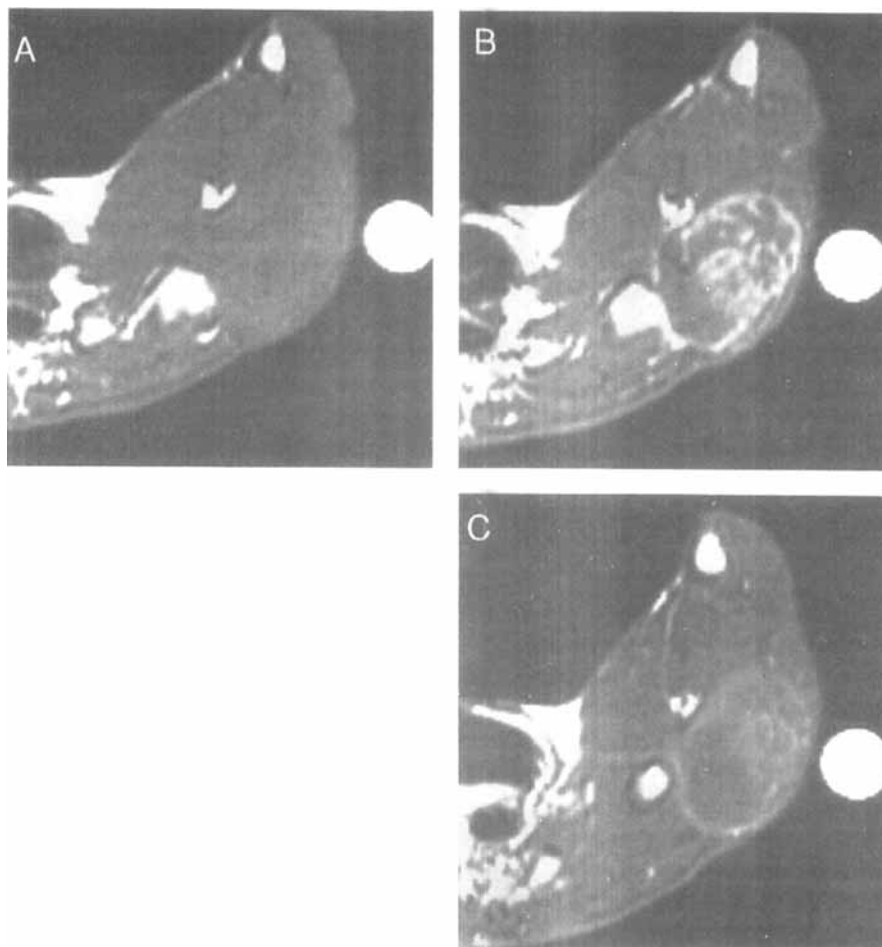


Figure 4 A series of magnetic resonance imaging scans obtained through the left thigh of a New Zealand white rabbit bearing a V2 carcinoma before (A), immediately after (B), and 3½ h after (C) the administration of 5 µmol/kg of **PCI-0101** (complex **2**; bisacetate counter anions). Noteworthy is the persistent, marked increase in contrast enhancement of the V2 carcinoma compared with surrounding muscle obtained under these conditions (1.5 T; T₁-weighted pulsing sequence; 300/15 repetition time/echo time). Reproduced from [26] by permission of Lippincott–Raven Publishers

predicative preclinical ones [25,108], it is now clear that this new gadolinium(III) texaphyrin-based agent (**PCI-0120**) facilitates the MRI-based detection of neoplastic tissues at doses much below those needed to engender a toxic response [106]. This, it is thought, could serve to augment its utility in the context of the therapeutic applications for which it is currently being developed.

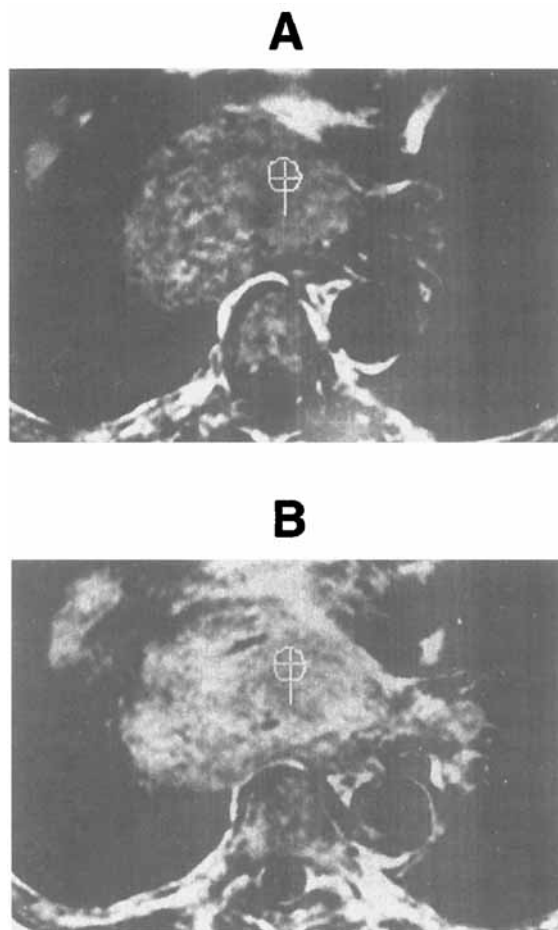


Figure 5 These MRI scans show a large lung cancer that was imaged before (A) and after (B) intravenous administration of gadolinium texaphyrin **PCI-0120 (3)** to a patient in the Pharmacyclics, Inc. sponsored Phase I clinical trial. **PCI-0120** localizes in the tumor, producing a “whitening” of the tumor image (B)

3. X-RAY RADIATION THERAPY (XRT) ENHANCEMENT

3.1 General Overview: Potential Benefit of Sensitizers

Every year, roughly 1 400 000 new cancer cases are recorded in the USA alone [109]. Of these, roughly one half undergo radiation therapy in one form or another [110–112]. Unfortunately, in all too many instances the hoped-for curative effects are not

realized. Thus, there is a constant, ongoing search for ways to improve the efficacy of this time-honored approach. One avenue being explored involves the use of radiosensitizers, compounds specifically designed to enhance the effects of localized, tumor-targeted radiation [113–117].

A major difference between many solid tumors and surrounding normal tissue is the presence in tumors of chronically hypoxic (i.e. subject to a reduced oxygen supply), yet still viable cells. Hypoxic cells have been observed to be 2.5–3.0 times more resistance to the damaging effects of ionizing radiation [118–120]. While cure or control rates of a tumor can be elevated with an effective increase in the radiation dose, such an increase also tends to damage adjacent, fully-oxygenated (i.e. normal) tissues as well as the targeted neoplastic ones. Consequently, failure of conventional radiation therapy and local recurrences are common events that are in large measure attributed to the presence of radiation-resistant hypoxic cell populations in solid tumors. Specific modification of tumor radiation sensitivity has been pursued through alteration of the tumor oxygenation state. This can be achieved through the use of fractionation, wherein the total radiation dose is divided into multiple smaller doses. It can also be achieved, at least in principle, by the use of so-called radiation sensitizers, a class of material with which this review is in part concerned [114,121].

Radiation sensitizers are pharmacologic agents that increase the lethal effects of radiation when administered in concert with it. An ideal radiation sensitizer should: augment the cytotoxicity of radiation applied to malignant loci but not engender enhanced killing of normal cells, operate *via* a mechanism that is active towards oxic and hypoxic cell regions, and have a low inherent *in vivo* toxicity.

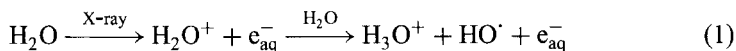
During the past 25 years, several chemical agents and drug products approved for other indications have been studied as possible radiosensitizers. Some of these agents have been studied extensively and been the subject of several reviews [113–115]. The authors of one such review, Shenoy and Singh, have classified radiosensitizers into the following categories: DNA-based analogs, agents with electron affinity, membrane-active drugs, and miscellaneous agents [114]. Apart from the authors' and collaborators' work on texaphyrins, only two types of sensitizers have progressed to the point of being studied clinically: the halogenated pyrimidines, and hypoxic cell sensitizers [115].

The first class of radiation sensitizer alluded to above, namely the halogenated pyrimidines, includes such materials as 5-bromodeoxyuridine (BUdR) [122], 5-iododeoxyuridine (Iudr), and 5-fluorouracil (5-FU). These compounds have shown a certain degree of efficacy due, presumably, to the fact that they are incorporated into DNA [113,114,123]. Indeed, a new drug application (NDA) for one member of this class, BUdr (also known as BroxineTM), has recently been filed by Neopharm with the FDA [124].

The second class of materials that has been the subject of clinical study in the context of XRT sensitization is the so-called hypoxic sensitizers. These agents are electron-affinic compounds that exacerbate damage induced by ionizing radiation

under hypoxic conditions. In this way they are thought to mimic oxygen [113–115, 125]. The most prototypic of all hypoxic cell sensitizers are the nitroimidazoles, including, to name a few, metronidazole, misonidazole and ethanidazole [113–115, 126]. Although these agents have been the subject of extensive investigation *in vitro* and *in vivo*, including numerous clinical trials [113–115, 125–141], to date, no compound in this class has been approved as a radiation sensitizer in the USA. While anecdotal efficacy has been demonstrated, toxicity effects have limited the maximum individual or cumulative dose that can be administered *in vivo*.

The idea that an easy-to-reduce species could function as a radiation sensitizer is not new [113–117]. Indeed, there is considerable precedent for it both in the radiation sensitization literature *per se* [113–115, 118, 125–129, 132–135, 138, 139, 142] and in classic mechanistic explanations of radiation-induced cytotoxicity [143–145]. While the biological effects of radiation therapy are certainly complex, it is well established that exposure of bodily tissues to high energy gamma- and X-ray radiation (i.e. of the type commonly used clinically [112]) causes the ejection of one or more high energy electrons from water (the most prevalent available target). These electrons can exert a cytotoxic effect directly by, e.g. breaking the sugar phosphate bonds in DNA [112]. More frequently, however, they exert their effect indirectly *via* the follow-up formation of solvated electrons and hydroxyl radicals (Equation 1).



Of these daughter products, it is the hydroxyl radical, HO^\cdot , that constitutes the dominant cytotoxin [112, 143]. Hydroxyl radicals are highly reactive, oxidizing entities that cause damage (chromosomal or otherwise) within about ± 4 nm three-dimensional radius of where they are formed [112, 143]. The hydrated electrons, on the other hand, are strongly reducing, rather mobile, and relatively long-lived ($T_{1/2} \approx 25$ ns) [112, 143]. Although these latter hydrated electrons can cause DNA damage themselves (in analogy to the direct, electron-mediated process described above), they are also capable of recombining with hydroxyl radicals (Equation 2) [112, 143].



Such an $\text{e}_{\text{aq}}^- + \text{HO}^\cdot$ deactivation process produces hydroxide anion (HO^-) and thus serves effectively to deactivate both cytotoxic daughter products, namely e_{aq}^- and HO^\cdot . In the presence of oxygen, on the other hand, the solvated electrons get trapped, at least initially, in the form of superoxide anion (Equation 3) [112, 143]. This trapping precludes recombinatorial deactivation of the hydroxyl radicals, leaving the latter free to carry out cell killing,



The above chemistry explains why hypoxia is a major contributor to the failure of radiation therapy. Hypoxic cells in solid tumors contain a lower oxygen tension (and correspondingly reduced number of e_{aq}^- traps) than their highly vascularized, rapidly growing “outside neighbors”. For this reason, so-called fractionation, wherein the total chosen radiation dose (generally on the order of 3–5 Gy) is administered in multiple daily or semidaily doses, is generally employed clinically [118–120,146]. This protocol allows healthy tissues time to undergo cell repopulation and permits reoxygenation of hypoxic regions originally distant from functional vasculature [114,121]. Unfortunately, even this approach, does not provide a complete, satisfactory solution to the problems of hypoxic-region cancer control. Hence the appeal of electron-deficient species, such as nitroimidazole. These, by virtue of “soaking up” the unwanted e_{aq}^- (i.e., by acting as “oxygen surrogates”), could serve to increase substantially the clinical benefit of X-ray radiation therapy (XRT) [113–115, 118,125–129,134,135,138,139,142].

The use of porphyrins and porphyrin-like macrocycles, namely the texaphyrins, which show good selectivity towards tumor cells, could be used to overcome the limitations of the current sensitizers, namely a lack of suitable biolocalization and a consequent high toxicity at the needed therapeutic doses [25]. The strengths and weaknesses of this approach are detailed below.

3.2 Porphyrins as Radiation Sensitizers

As will be described below in the context of the PDT discussion, Samuel Schwartz was the first to develop hematoporphyrin derivative (HpD) by manipulating and testing various fractions of the original hematoporphyrin preparation [59]. In the context of this exploratory work, more than 100 preparations were tested in tumor models. In fact, 55 human cancer patients, more than 20000 mice, several dogs, rabbits, paramecia, and some enzymes were included in his studies [147]. The dogs and mice received local and total body radiation. This is the first recorded evidence of porphyrin in a radiation sensitization study. Schwartz and coworkers found that cytotoxicity due to ionizing radiation depended on three factors: porphyrin dose, porphyrin type, and tissue type. They determined that the porphyrin dose was very critical. For instance, while small doses of certain porphyrins were found to enhance the radiosensitivity of tumors (but not normal tissues), large doses of these same porphyrins were found to be radioprotective for these same tumor types. Eventually Schwartz and his colleagues were granted an investigative new drug (IND) application in the 1960s for testing copper hematoporphyrin in conjunction with radiation therapy of hepatic, pancreatic, and brain tumors. Unfortunately, these studies were never done. Rather, the testing actually carried out had as its focus the task of finding ways to overcome the radioprotection or radioresistance that was found to occur at high porphyrin doses. Interestingly, these studies, while not so relevant to the goal of radiosensitization, led to the evolution of phototherapy or what we call today, photodynamic therapy (PDT) [59,147–152].

More recently, effort has focused on studying monomeric metalloporphyrins in combination with ionizing radiation [153–157]. For instance, O'Hara *et al.* tested a series of cationic and anionic porphyrins, namely tetrakis(4*N*-methylpyridyl)porphyrin (TMPyP) and tetrakis(4-sulfonatophenyl)porphyrin (TPPS₄) containing a range of metal cations [e.g Co(III), Fe(III), Cu(II), Rh(III), Mn(III), Sn(IV), Pd(II)], using both hypoxic and oxic membranes of Chinese hamster fibroblast (V79N) cells as their model [153]. The metal-free analogues of these two porphyrins were also included in this study. The study demonstrated that the most active compounds effecting radiation-induced cell kill in hypoxic cells, measured by the radiation sensitizer enhancement ratio (SER), were the cobalt(III) complexes. Specifically, at porphyrin concentrations of 100 μM and X-ray doses of 16 Gy, SER values of 2.3 and 2.4 were achieved using CoTPPS₄ and CoTMPyP, respectively [153].

In a similar study, James and coworkers reported weak sensitization towards Chinese hamster ovary (CHO) cells with cationic cobalt(III) porphyrin derivatives [154]. Their best agent was the cobalt(III) complex of 5,10-bis(4-methylpyridinium)-15,20-bis-(4-nitrophenyl)porphyrin, which had an SER of 1.22 at 50 μM towards CHO hypoxic cells. This complex was actually the most promising of over 50 studied. Using this CHO tumor cell line and identical XRT conditions (i.e. oxic and hypoxic; 100 μM porphyrin concentration; 16 Gy), O'Hara *et al.* found that the cobalt(III) complexes, CoTPPS and CoTMPyP, exhibited a weak sensitization effect (SER = 1.05–1.22, with or without serum-containing medium). These workers also concluded that the introduction of nitro and/or positively charged substituents on the porphyrin periphery serves to augment the net radiosensitization effect for these kinds of Co(III) porphyrins [153,154]. Unfortunately, even when enhanced in this way, the net sensitization effect is small.

3.3 Gadolinium(III) texaphyrins

Currently, in spite of a great deal of effort and a number of promising leads [113,115,118,123,127–135,138,139,142,158–163] not a single agent has been approved as a radiation sensitizer in the USA. The texaphyrins, by virtue of their special electronic character, may serve to fill this gap. In fact, the gadolinium(III) texaphyrin-based experimental drug, **PCI-0120 (3)**, is the only porphyrin or porphyrin-like molecule undergoing XRT-related human clinical trials in the USA [106]. Given the importance of radiation therapy as a cancer treatment modality, there is naturally a great deal of interest attendant to these trials.

There are two critical features of the texaphyrins that led to the consideration that it could function as a radiation sensitizer. First, this class of molecules, like the porphyrins, is known to localize with high selectivity in cancerous tissues. Second, the texaphyrins are known to contain a low-lying LUMO; in comparison to porphyrins and most other endogenous species, they are thus very easy to reduce

($E_{1/2} \approx 0.08$ vs. NHE; aqueous, pH 7) [25,164,165]. Taken together, these two facts led to the proposal that the water-soluble, MRI-detectable gadolinium(III) texaphyrin agent **PCI-0120** (complex **3**, Figure 1) could function as a good radiation sensitizer [25].

As detailed in the context of the hypoxic sensitizer discussion above, the idea that an easy-to-reduce species could function as a radiation sensitizer is not new [113–117]. Indeed, there is considerable precedent for it both in the radiation sensitization literature *per se* [113–115,118,125–129,132–135,138,139,142] and in classic mechanistic explanations of radiation-induced cytotoxicity [143–145]. However, as has also been made clear in the context of this earlier discourse, this idea has yet to translate into an FDA-approved XRT sensitizing product. However, as noted above, **PCI-0120** (**3**) possesses special features that led to the consideration that it

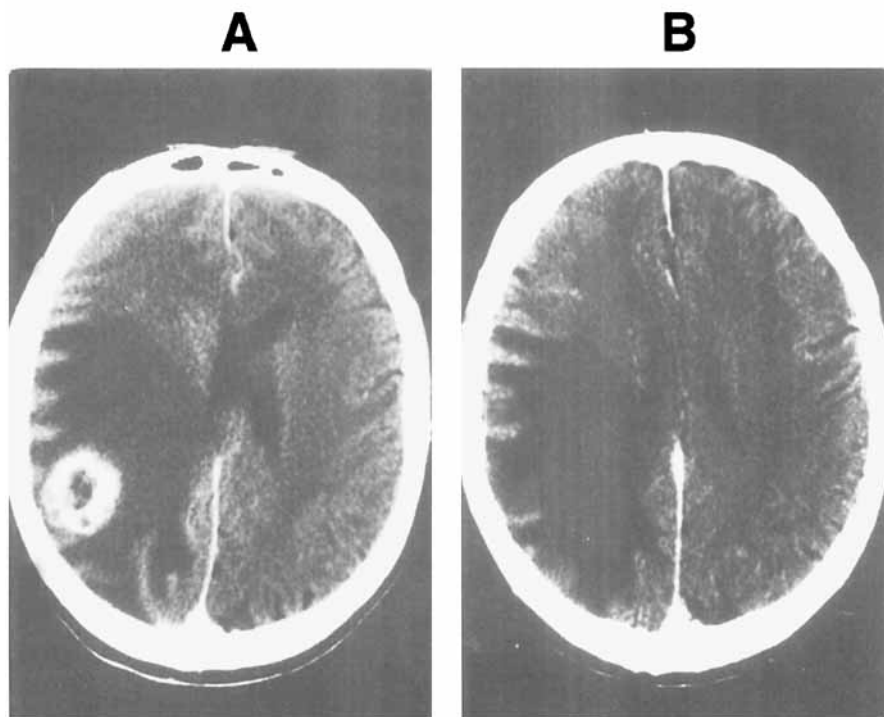


Figure 6 These CT (computerized tomography) scans of the head show a large metastatic cancer of the brain (A) in a patient enrolled in a Pharmacyclics, Inc. sponsored gadolinium(III) texaphyrin (**PCI-0120**) Phase Ib/II clinical trial. The tumor mass and surrounding edema cause the brain tissue to shift across the midline in (A). After intravenous injection of **PCI-0120** (ten treatments) and radiation therapy (ten treatments, total radiation dose of 30 Gy), the tumor is eliminated, leaving some residual edema with the reduction of the shift, as illustrated in (B)

might work where other agents have failed. Currently, this agent XCYTRIN™ is being tested as a radiation sensitizer in a Phase III clinical study involving multiple sites in the USA, Canada and Europe [106,166]. So far, the results from the completed Phase 1b/II trial have been quite promising. As shown in Figure 6, a CT head scan of a patient enrolled in the Phase 1b/II study displays a tumor mass and surrounding edema, which cause the brain tissue to shift across the midline [166]. However, after **PCI-0120** administration and radiation therapy, the tumor is eradicated, leaving some residual edema with reduction of the shift (Figures 6a and 6b).

In addition to the above exciting, but anecdotal, findings, a considerable body of preclinical data exists that supports the contention that this agent will emerge as a good, clinically useful radiation sensitizer. For instance, it is known to react at near diffusion controlled rates with hydrated electrons [25]. Additionally, under *in vivo* conditions, it was found to improve significantly the long-term survival of DBA/2N mice containing implanted SMT-F tumors under single dose irradiation conditions (Figure 7), as well as BALB/c mice bearing EMT6 neoplasms treated in accord with a fractionation protocol [25].

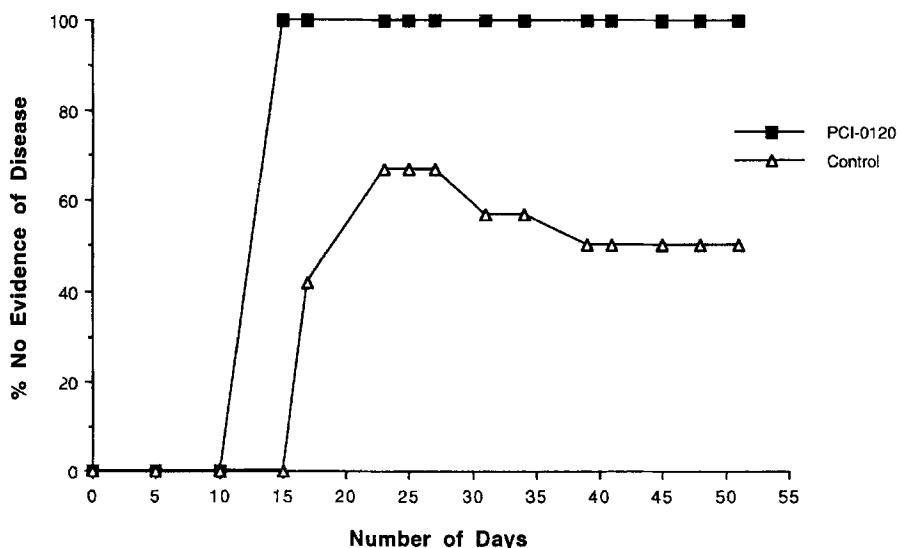


Figure 7 Single dose radiation sensitization study following intravenous (i.v.) administration of **PCI-0120** (gadolinium(III) complex 3). Twelve DBA/2N mice were injected intravenously *via* the tail vein with 10 $\mu\text{mol}/\text{kg}$ of **PCI-0120**, 4–7 days after intramuscular injection of SMT-F tumor cells into the hind flank of the right rear leg. After 2 h, a single dose of 30 Gy of radiation was administered. A control group of twelve DBA/2N mice with implanted SMT-F tumors were treated with 30 Gy of radiation only. The results show that after 51 days all of the animals given the **PCI-0120** as a putative radiation sensitizer were alive and without evidence of disease while four of the twelve irradiation-only animals had died and of the remaining eight mice, only six were without evidence of disease

While the above results are encouraging, it is important to appreciate that they do not necessarily serve to confirm (or refute) the mechanistic analyses that led this particular gadolinium(III) texaphyrin **PCI-0120 (3)** to be considered as being a potential radiation sensitizer. Indeed, many other explanations for the observed sensitization effects, including ones involving inhibition of DNA repair, reactive oxygen species-induced apoptosis, or cell cycle modification, can be conceived. Interestingly, not all of these determinants of action would show up on clonogenic *in vitro* assays. Still, the very fact that **PCI-0120 (3)** appears to work as a radiation sensitizer serves to highlight what could prove to be an important new biomedical application for porphyrin and porphyrin-like macrocycles.

4. PHOTODYNAMIC THERAPY AND PHOTODYNAMIC VIRAL INACTIVATION

4.1 Introduction: History of Photodynamic therapy

Photodynamic therapy (PDT) involves the use of an exogenous photon-absorbing sensitizer to mediate a therapeutic effect, and has a long history in the medical arts. Psoralens (e.g. **11** in Figure 8) were used in India as early as 1400 BC for repigmentation of vitiliginous skin [167,168]. Around the 12th century AD, the Egyptians obtained psoralens from a plant which grew on the banks of the Nile River and used it in the treatment of leucoderma [168]. In 1834, Kalbrunner isolated 5-methoxypsoralen (MOP) from bergamot oil. However, it was not until 1974 that the use of psoralen dyes, activated by ultraviolet A radiation (i.e. light of 320–400 nm), was established rigorously as being effective in the treatment of psoriasis [168,169].

The origin of cancer phototherapy dates to the beginning of the 20th century. For instance, in early 1900, Professor Von Tappeiner of Munich and a dermatologist named Jesionek published clinical data using eosin (**12**, Figure 8) as a photosensitizer in the treatment of skin cancer, lupus of the skin, and chondylomata of female genitalia [170,171]. This study established *inter alia* that oxygen was required for the biological effect (i.e. photosensitization). This oxygen-dependent photochemical

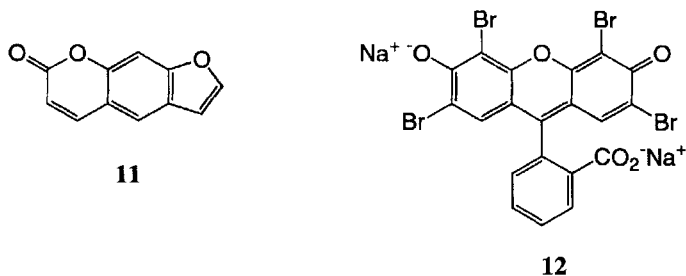


Figure 8 Structures **11** and **12**

process was termed “photodynamic action” by Von Tappeiner. Von Tappeiner was also the first to attempt to treat tumors using phototherapy [170,172].

The history of porphyrins and their role in medicine is, by contrast, quite brief. Hematoporphyrin **8** (Hp) was first prepared by Scherer in 1841 [173]. The first proof of the photosensitizing ability of porphyrins in humans came when Meyer-Betz (1913) self-administered 200 mg Hp to determine its biological effects [174]. Within minutes after light exposure, Meyer-Betz noticed severe pain and swelling localized at the light-exposed areas. He also remained photosensitive for several months [174]. Over the next 40 years, a number of investigators studied the *in vivo* properties of administered porphyrins. This led to observations that neoplastic, embryonic, and traumatized tissues either have a higher intrinsic affinity for, or are better able to retain, a variety of porphyrins and metalloporphyrins. Taken together, this early work played an important role in advancing the concept that a combination of porphyrins (or related tetrapyrrolic macrocycles) and light could be useful in cancer detection and therapy [54–59,61,168].

In 1955, Schwartz *et al.* found that hematoporphyrin (Hp) “as isolated” was composed of a crude, variable mixture of porphyrins, many with different chemical, physical, and biological properties. Schwartz focused on the nonhematoporphyrin component, which he found to be more active (i.e. tumor-localizing). This component he enriched by treating with acetic–sulfuric acid, followed by dilute base. This afforded what has come to be known as hematoporphyrin derivative (HpD) [59,175–177]. In 1966, Lipson and coworkers at the Mayo Clinic were the first to treat a cancer patient photodynamically with this new HpD formulation [178–180]. The patient, suffering from a large recurrent breast carcinoma, was treated with multiple injections of HpD and local exposure of the diseased area with filtered light from a xenon arc lamp. While a localized response was achieved, the cancerous lesion later recurred [178]. Diamond and coworkers were credited with the first effective destruction of tumor cells *in vivo* using hematoporphyrin-glioma cells implanted subcutaneously in rats, followed by fluorescent lamp exposure. They termed this effect “photodynamic therapy” (PDT) [83,181]. Coincidentally, Dougherty *et al.* became the first to show long-term cures in animal models. In their initial studies, hematoporphyrin-sensitized mice and rats bearing a variety of tumors were irradiated with a xenon lamp (filtered to produce light with a wavelength above 600 nm) [182]. This regime was found to be nontoxic to the animals and was found to result in minimal damage to the surrounding skin. Following up on their seminal animal studies, Dougherty and coworkers then pioneered the clinical use of PDT by treating 28 patients in 1978 with a combination of HpD (injected *i.v.* at doses of 2.5 and 5.0 mg kg⁻¹) and light (irradiation 1–78 days after injection using a 5000 mW xenon arc lamp, filtered to produce 600–700 nm light). This protocol was found to afford a complete or partial response in 111 of 113 cutaneous or subcutaneous cancerous lesions studied. The tumors themselves ranged from carcinomas of the breast, colon, prostate, to squamous cell, basal cell, and melanoma [183]. While these results were remarkable in their day, the field of PDT has grown significantly since 1978. Some

of this progress is reviewed below, in the context of discussing, as befits this chapter, the various PDT sensitizers that are now in the clinic at some stage of the FDA-required testing process.

4.2 Current Status of PDT in the Clinic

Presently, photodynamic therapy (PDT) stands as one of the more promising new modalities currently being explored for use in the control and treatment of tumors [59,79,80,83,172,184–196]. As implied above, this technique is based on the use of a photosensitizing dye, such as a porphyrin [54–59,61], which localizes at, or near, the tumor site, and which produces cytotoxic materials, such as singlet oxygen, when irradiated in the presence of oxygen. Much of the current excitement associated with PDT derives from this property since it means a level of control and selectivity may be attained that is not otherwise possible. In addition, PDT is attracting attention because it may be used for the treatment of solid tumors, such as lung cancer (178 000 cases per year USA), and primary melanoma (40 300 cases per year and 7300 deaths per year) for which good curative strategies are often lacking [109].

One more development has PDT poised to take on a prominent role in oncology: In December of 1995, the FDA granted its first approval in the PDT area. It went to QLT Phototherapeutics of Vancouver, BC, Canada, and has allowed them to market the light-sensitizing drug, Photofrin[®] (porfimer sodium) for the palliative treatment of obstructive esophageal cancer. Using a standard protocol (drug dose of 2–5 mg kg⁻¹ and 100–200 J cm⁻², 24–72 h after i.v. injection), Photofrin[®] has proven quite effective for a variety of indications (e.g. bladder cancer, lung cancer, malignant diseases of the skin and upper aerodigestive tract, head and neck, brain, etc.) [186,197–202]. However, many in the medical community feel that the best prospects for PDT lie with the next generation of photosensitizing drugs (i.e. those now in clinical development) [187]. Given this sentiment, a goal in writing this section of the present chapter is to provide a review of these so-called second generation porphyrin and porphyrin-like PDT agents. For the sake of brevity, we will limit the discussion to those systems currently undergoing clinical trials in the USA.

As stated above, Photofrin[®] is the only approved PDT agent in the USA. It has also been approved in Canada for the treatment of bladder and esophageal cancer. In France and in The Netherlands, Photofrin[®] is approved for early and late stage esophageal and lung cancers. In Japan, it is used to treat early cancers of the esophagus, lung, stomach, and cervix, as well as cervical dysplasia [187]. This drug is prepared by purifying the hematoporphyrin derivative of Schwartz and Lipson by gel filtration chromatography. This affords the fractions rich in the oligomeric species that are known to have the best tumor-localizing ability [176,188]. While this tumor-localizing ability has led to important clinical advances, the fact that Photofrin[®] is a mixture is seen as a drawback. Further, Photofrin[®] is known to

engender prolonged cutaneous photosensitivity in patients long after the PDT treatment course is finished (i.e. $t_{1/2}$ in serum fits a three-compartmental model, α , β , γ , are ≈ 16 h, 7.5 days, and 115.6 days, respectively; Table 1) [184,203–206]. While the reasons for this deleterious photosensitivity remain recondite, it could derive in part from the fact that Photofrin[®] contains hard-to-catabolize and/or hard-to-excrete oligomers within its overall mixed constitution. To the extent this is true, it suggests ways in which this FDA-approved agent might be improved. Another way Photofrin[®] could be improved is by shifting its lowest energy absorption maximum (λ_{\max}) further to the red. This is because Photofrin[®], with a lowest energy λ_{\max} at 630 nm, absorbs but poorly in the red part of the electronic spectrum (i.e. $\lambda_{\max} \geq 700$ nm) where blood and other bodily tissues are most transparent [207]. Taken together, the deficiencies inherent in Photofrin[®] have prompted efforts to develop new, so-called “second generation” PDT photosensitizers [83] (Figure 9). These include systems as diverse as benzoporphyrin derivative mono-acid ring A (**13**, BPD-MA, $\lambda_{\max} = 690$ nm) [81,208–212], tin(IV) ethyletiopurpurin (**14**, SnET2, $\lambda_{\max} = 659$ nm) [213–218], mono-l-aspartyl chlorin *e*₆ (**15**, NPe6, $\lambda_{\max} = 664$ nm) [81,219–224], *meso*-(tetrahydroxyphenyl)chlorin (**16**, *m*-THPC, Foscan[®], $\lambda_{\max} = 652$ nm) [225–231], 5-aminolevulinic acid (**17**)-induced protoporphyrin IX (**18**, $\lambda_{\max} = 630$ nm) [80,232–238], and lutetium(III) texaphyrin (**4**, PCI-0123,

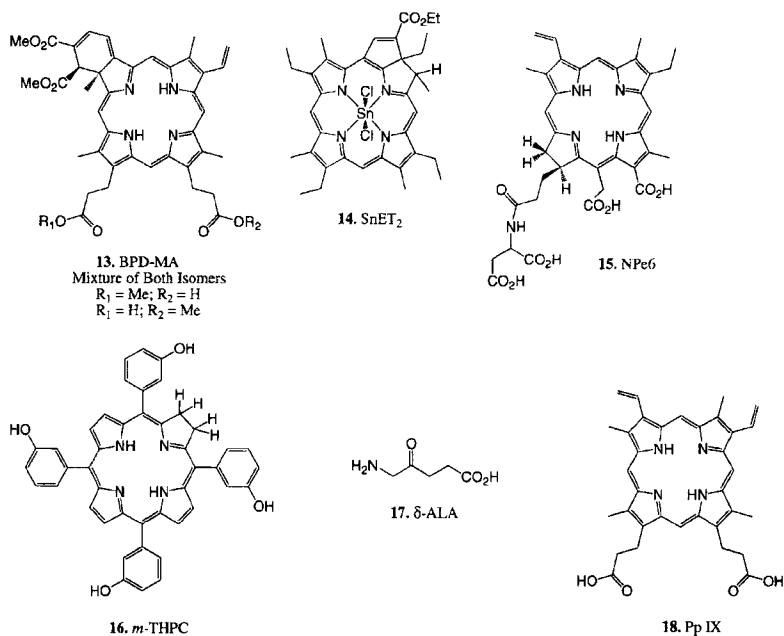


Figure 9 PDT clinical photosensitizers, structures 13–18

Table 1 Characteristics of clinical photosensitizers

Photosensitizer	Hydrophobicity	λ_{\max} (nm) ^a	ϵ (M ⁻¹ cm ⁻¹) ⁻¹	$\phi_{\Delta}({}^1\text{O}_2)$	$t_{1/2}$ (PK serum)	Clinical Status (US)	Refs.
Photofrin [®] (PF)	Water-soluble	630 ($\sim 3.0 \times 10^3$)		0.89 ^b	250 h \pm 285 h ^c	Approved ^d	204, 267
BPD-MA	Hydrophobic	690 (3.4×10^4)		0.84 ^b	5.5 h ^c	Phase II/III	266–268
SnET2	Hydrophobic	659 (3.0×10^4)		—	—	Phase II/III	216, 269–270
NPe6	Water-soluble	664 (4.0×10^4)		0.77 ^e	9 h and 134 h	Phase I	271, 219
<i>m</i> -THPC (Foscan [®])	Amphiphilic	652 (2.2×10^4)		0.87 ^e	45.4 h	Phase III	225, 279–280
δ -ALA---PpIX	Hydrophilic	630 (5.0×10^3)		0.56 ^b	30 min ^f	Phase II/III	267, 232
LuTex (PCI-0123)	Water-soluble	732 (4.2×10^4)		0.58 ^b	0.25 h and 8.8 h	Phase II	108, 295–296

^a Extinction coefficients were measured in various media; for Photofrin[®] (PBS), BPD-MA (MeOH), SnET2 (CH₂Cl₂), NPe6 (phosphate buffer, pH 7.4), *m*-THPC (MeOH), and PCI-0123 (MeOH), see references for further details.

^b The singlet oxygen quantum yields were measured by Grossweiner and coworkers at the relevant absorption maximum for each photosensitizer (PF, BPD-MA, PpIX, and PCI-0123). The technique employed by these researchers utilizes the photosensitization of lysozyme (LYS, 20 μM) as an internal actinometer. The singlet oxygen measurements of the photosensitizers (PF, 9 μM ; BPD-MA, 1.1 μM ; PpIX, 10 μM ; PCI-0123, 8.8 μM) were conducted at pH 7.4 phosphate buffer plus 1% Triton X-100 and methylene blue was used as the standard ($\phi_{\Delta} = 0.52$). For more details, please see ref. 267. The singlet oxygen quantum yields for these photosensitizers have been determined by using other photophysical methods and have given sometimes disparate values. For BPD-MA and PCI-0123, see refs. 268 and 244, respectively.

^c Bellnier and Dougherty have recently reported a preliminary pharmacokinetic study of IV Photofrin[®] (PF) in patients. These researchers determined that their data, taken from a 19 patient study involving the administration of 1 mg PF/kg, for a three-compartmental pharmacokinetic model. The α , β and γ half-lives were \sim 16 h, 7.5 days, and 156 days, respectively. For more details, see ref. 203. The pK data obtained for BPD-MA was obtained by personal communication with David Mitchell, Director of Regulatory Affairs, QLT Phototherapeutics.

^d Photofrin[®] has been approved by the U.S. FDA for limited PDT applications. Specifically, Photofrin[®] is indicated for palliation of patients with completely obstructing esophageal cancer, or of patients with partially obstructing esophageal cancer who, in the opinion of their physician, cannot be satisfactorily treated with Nd:YAG laser therapy (see ref. 204).

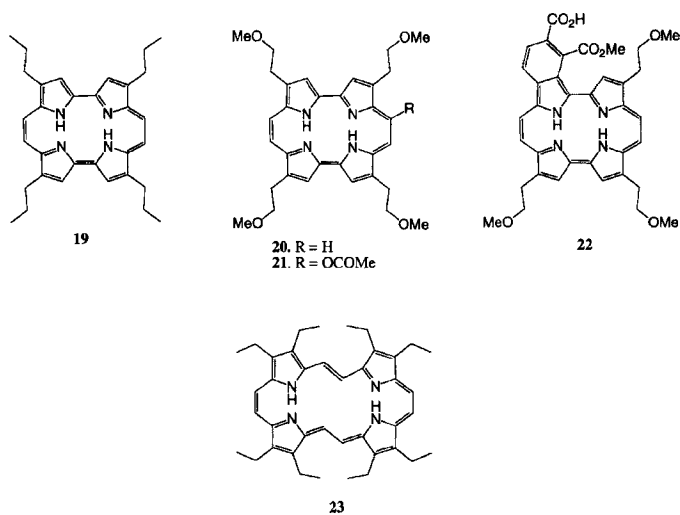
^e The singlet oxygen quantum yield for NPe6 (in air-saturated D₂O) was determined by Spikes and Bommer using Rose Bengal as a standard under conditions of laser flash photolysis (see ref. 271). The singlet oxygen quantum yield for *m*-THPC was measured by Vonarx-Coinsmann *et al.* in an air-saturated 50:30:20 v/v D₂O/ethanol/polyethylene glycol mixture (see ref. 270).

^f Private communication with Dr Stuart Markus, DUSA Pharmaceuticals, Inc.

Table 2 Idealized criteria for PDT or PDI photosensitizers

1. Readily available.
2. Chemically pure and stable.
3. Easily subject to synthetic modification.
4. Soluble in water such that administration can be effected without resorting to the use of an ancillary carrier.
5. Intrinsically nontoxic in the absence of light.
6. Taken up or retained selectively in diseased tissues or other targeted biological loci.
7. Cleared quickly after administration.
8. Free of lingering phototoxicity effects, cutaneous or otherwise.
9. Endowed with one or more strong absorption bands in the ≥ 700 nm spectra region.
10. Capable of acting as an efficient singlet oxygen photosensitizer when irradiated with near-infrared light.

$\lambda_{\max} = 732$ nm) [23,24,108,239–244], that might better fulfill what are considered to be an idealized set of desiderata (Table 2) [83,245,246]. While this Chapter will primarily focus on the PDT agents currently under clinical investigations, there are numerous porphyrin and porphyrin-like (e.g. expanded porphyrins) macrocycles not covered by this review in preclinical development. These include phthalocyanines (i.e. zinc and aluminum) or the naphthalocyanines [79–93,247], carborane-derived porphyrins [75–77], pyropheophorbides [248,249], porphycene and cumulene porphycenes [218,250–262], (e.g. **19–23**; Figure 10) sapphyrins [245,263], (e.g.

**Figure 10** Structures **19–23**

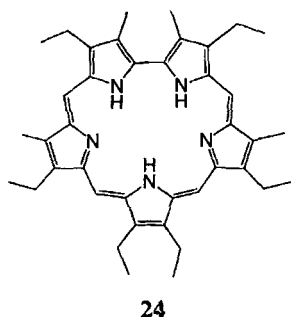


Figure 11 Structure 24

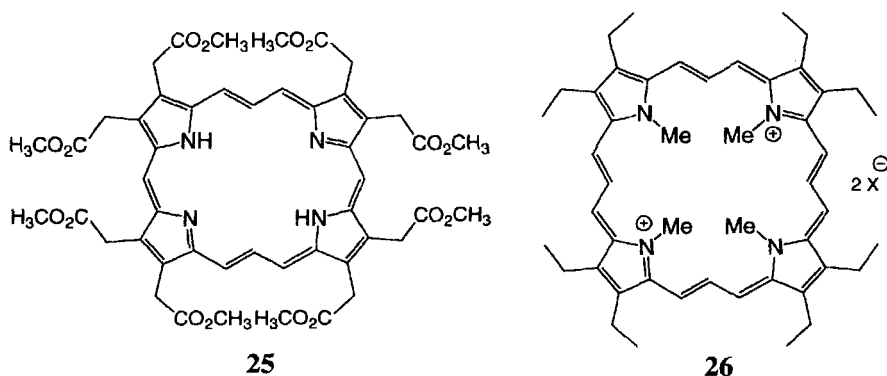


Figure 12 Structures 25–26

24; Figure 11) and vinyllogous porphyrins [246,264], (e.g. **25** and **27**; Figure 12), which appear attractive because they too appear to overcome many of the deficiencies seen with Photofrin^(®). In particular, many of these agents are monomeric species that absorb in the far-red spectral region and which show favorable (i.e. low) toxicity characteristics *in vivo*.

The ability to absorb in the near-infrared is important. It means more of the activating light, administered at a wavelength of ≥ 700 nm, is available for singlet oxygen production [207,265]. This is because, as can be appreciated from an inspection of Figure 13, a switch in activation wavelength from ≤ 630 nm to ≥ 700 nm serves to increase the viable depth of light penetration by 2–6 fold [207,265]. To the extent this is true, it would make PDT more efficacious for treating both deep-seated tumors and/or highly pigmented ones such as melanoma. This assumes, of course, that the other criteria of Table 2 are appropriately met.

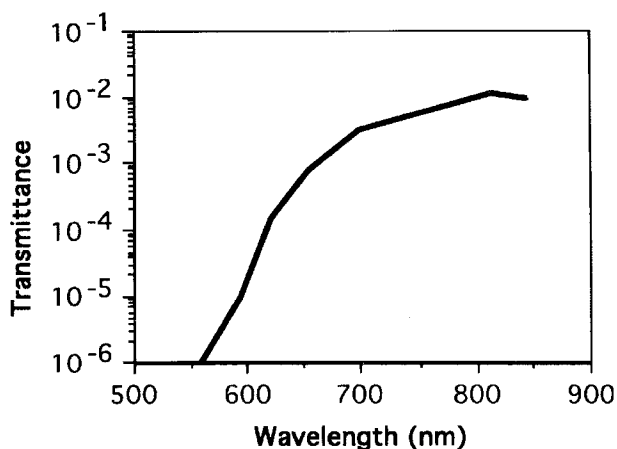


Figure 13 Spectral transmittance through human chest wall with rib thickness of 22 mm. Redrawn from [207] by permission of the American Society of Photobiology.

4.3 Second-Generation PDT Agents in Oncological Applications

(a) Benzoporphyrin derivative

Benzoporphyrin derivative monoacid ring A (BPD-MA, verteporfin **13**) is currently being evaluated in the clinic by QLT Phototherapeutics (Vancouver, BC) as a PDT agent for the treatment of nonmelanoma skin cancer, psoriasis, age-related macular degeneration (AMD) and endometrial ablation. BPD-MA is a chlorin with extended conjugation, first synthesized by Dolphin and coworkers in 1987 from protoporphyrin [81,208–212]. As illustrated in Figure 9, BPD-MA is composed of two regioisomers (i.e. $R_1 = \text{Me}$, $R_2 = \text{H}$ or $R_1 = \text{H}$, $R_2 = \text{Me}$), which have shown identical pharmacological behaviour [266]. Levy *et al.* have reported that subsequent to injection the “mixture of regioisomers” are converted to diacids (i.e. $R_1 = R_2 = \text{H}$) in the liver. Therefore, these researchers argue that this issue of “mixture of regioisomers” should not present a problem with the FDA [266].

It has been reported that BPD-MA associated with lipoproteins *in vivo* and that this uptake abets the documented localization in tumor cell membranes [80]. Furthermore, BPD-MA absorbs light strongly at 690 nm (in MeOH, $\epsilon = 3.4 \times 10^4 \text{ M}^{-1} \text{ cm}^{-1}$ for this Q-type band). The absorption of this species at this wavelength is thus approximately four times greater than that of Photofrin[®]. BPD-MA also displays a good singlet oxygen quantum yield (Table 1) [266–268]. In humans, the pharmacokinetic plasma clearance rate (i.e. pK half-life) of BPD-MA is on the order of 5.5 h (personal communication with David Mitchell, Director of Regulatory Affairs, QLT Phototherapeutics, Inc.)

As is true for several other second-generation agents, BPD-MA is hydrophobic. Therefore, for the purposes of testing its utility under clinical conditions, it has been formulated in unilamellar liposomes. While further clinical studies involving BPD-MA are ongoing, results from a Phase I/II clinical trial for cutaneous metastases (e.g. basal cell carcinomas) have been published. In this study, involving the controlled escalation of drug dose ($0.15\text{--}0.50\text{ mg kg}^{-1}$) and binary changes in light fluence (i.e. $50\text{--}100\text{ J cm}^{-2}$ at 100 mW cm^{-2}), 47% of the lesions treated showed complete responses with minimal skin sensitivity side effects being observed. A 100% complete response rate was obtained in patients treated at higher doses (i.e. at 0.3 mg kg^{-1} and 75 J cm^{-2} ; at 0.375 mg kg^{-1} and 50 J cm^{-2} ; and at 0.50 mg kg^{-1} and 50 J cm^{-2}) [266]. In this trial, PBD was infused into the patients for 45 min, with laser treatment (argon ion pumped dye laser) at 3–5 h after injection. Levy and coworkers at QLT have also reported the results of early stage clinical studies involving the use of BPD in the treatment of psoriasis and AMD. These latter trials are still ongoing [266].

(b) *Tin(IV) ethyl etiopurpurin*

Tin ethyl etiopurpurin (SnET2, **14**, Figure 9), codeveloped by Miravant Medical (Santa Barbara, CA) and Pharmacia-Upjohn (Italy/USA) is presently in Phase II/III clinical PDT trials for cutaneous metastatic breast cancer in the USA and Europe, as well as in Phase II/III clinical trials for AIDS-related Kaposi's sarcoma (KS) and basal cell skin cancer [187]. Although the purpurins have been known since the early 1940s as a degradation product of chlorophyll, it was only in 1986 that Morgan and Tertel first synthesized SnET2 [213]. This chlorin analogue possesses a low energy Q-type band at 659 nm (in CH_2Cl_2 , $\epsilon = 3.0 \times 10^4\text{ M}^{-1}\text{ cm}^{-1}$) and a high singlet oxygen quantum yield (Table 1) [213–218]. This agent is hydrophobic and requires solubilization in a suitable drug delivery system, such as a lipid emulsion, for use *in vivo* [80]. In the clinic, this kind of SnET2 formulation (1 mg ml^{-1}) is co-infused into the patient with normal saline. According to published results, typical infusion times are 30 min to 2+ hours per total administered dose [269].

Currently, results from the phase I/II skin cancer study and the phase I/II KS clinical study are available. These two combined studies were performed to evaluate the safety of the drug and the optimum light regime required to achieve tumor response. Follow-up examinations (below) were therefore made to judge the efficacy of the treatment. Lesions were graded as follows: a complete response (CR), which is the absence of clinically visible and/or palpable residual tumor at treatment site for at least 4 weeks; a partial response (PR), which is greater than or equal to a 50% reduction of the lesion; or stable disease, which means not fulfilling criteria for partial response or progressive disease (i.e. an increase in lesion by $\geq 25\%$).

The skin cancer study included 46 patients with 418 lesions. From this study population, it was concluded that the threshold drug dose is 0.8 mg kg^{-1} with an

optimum dose being 1.2 mg kg^{-1} at a light fluence of 200 J cm^{-2} . In view of these conclusions, the phase II portion of this skin cancer study was designed to utilize the 1.2 mg kg^{-1} and 200 J cm^{-2} drug/light regime. Under these conditions, 96% of the patients presenting with cutaneous metastases (i.e. basal cell carcinomas, basal cell nevus syndrome, and metastatic adenocarcinomas) showed complete response 3 months after treatment [187,269].

The KS study involved 45 patients with a total of 404 lesions. The phase I portion evaluated drug and light doses, while the phase II trial utilized one drug dose (1.2 mg kg^{-1}) and two light doses (200 and 300 J cm^{-2}). At the higher light dose, 63% of the evaluable tumors showed responses [37.8% complete response (CR) and 25% partial response (PR)]. Side effects from the treatment were minimal with mild, transient sun sensitivity being observed in some cases (i.e. 10% of the patients in the skin cancer study and 15% of the patients in the KS study) [187,269,270]. Currently, Miravant and Pharmacia Upjohn are sponsoring a nationwide Phase III clinical study with SnET2 (tradename, PurelytinTM) for age-related macular degeneration (AMD).

(c) *Mono-L-aspartyl chlorin e6*

In recent years, a limited body of clinical data has been published on the PDT agent known as NPe6 (mono-L-aspartyl chlorin e6, ME2906, or MACE, **15**, Figure 9). This water-soluble chlorin is currently being developed by Nippon Petrochemicals Co. Ltd. (Japan). The actual formulation being used clinically is obtained by dissolving the solid drug substance in physiological saline so as to obtain a final 1.0 mg ml^{-1} sterile aqueous solution. An advantage of this approach (and the agent itself) is that it leaves the administering physician with a drug product that is free of the limitations of liposomal formulation that are inherent to BPD-MA and SnET2. NPe6 has the further advantage of being fluorescent, absorbing light at 664 nm, and producing singlet oxygen in good quantum yield upon photoirradiation (Table 1) [271,272].

In 1992, Allen and coworkers reported the results of a study designed to test the PDT potential of NPe6 in patients with superficial malignancies. Patients in this study had diagnoses of primary or metastatic skin, oro- and nasopharynx cancer [273–275]. NPe6 was injected 4–8 h before irradiation with 664 nm light. Complete responses were seen in 11 of 20 tumors treated; four partial responses were also noted. This drug displayed good selectivity and, in all patients, drug elimination was complete within 4 weeks [80,275]. The pharmacokinetics of NPe6 drug elimination from plasma were measured by Kessel. He found that the elimination profile could be fit to a two-compartmental model. This gave half-lives for clearing of approximately 9 h (α) and 153 h (β) [219] (Table 1). It is important to note that the persistence of NPe6 in plasma was not associated with extended skin photosensitization, a finding which is in marked contrast to what was observed for Photofrin[®].

More recently, Wieman *et al.* reported results from a dose escalation phase I trial with NPe6 in patients with superficial lesions [276]. Twelve patients with a total of 15 malignant lesions (i.e. recurrent adenocarcinoma of the breast, basal cell, and squamous cell carcinoma) were treated with PDT using NPe6. The phototherapy protocol consisted of i.v. injection of NPe6 ($0.5\text{--}3.5\text{ mg kg}^{-1}$) followed 4 h after injection by irradiation with 664 nm light ($50\text{--}100\text{ J cm}^{-2}$). For drug doses of 1.65 mg kg^{-1} and below, the studied tumors were found to regress (but not disappear) within the 12-week observation period. At higher drug doses, 2.5 or 3.5 mg kg^{-1} (100 J cm^{-2} of 664 nm light), 6 of 90 patients (66% of the population) were observed to be tumor-free during the observation period. Unfortunately, these same studies revealed an apparent lack of tissue selectivity (tumor destruction vs. sensitization of normal skin) at NPe6 doses above 2.5 of mg kg^{-1} [276]. Further clinical studies of NPe6, sponsored by Nippon Petrochemicals Co. Ltd., are ongoing.

The above clinical research is also being (and has been) supported by various preclinical studies [81,220–224]. For instance, Roberts and Berns have reported that NPe6 localized in lysosomes of Chinese hamster ovary cells (CHO-K1) after ingestion by endocytosis. In other preclinical work, NPe6 was evaluated *in vivo* using an EMT6 tumor model in BALB/c mice. The animals received i.p. injections of NPe6 formulated in PBS (2.5 mg ml^{-1} at pH 7) at doses ranging of $0.5\text{--}100\text{ mg kg}^{-1}$ followed by irradiation with 664 nm light (100 J cm^{-2} , 100 mW cm^{-2}). In this study, all animals that received the PDT treatment at $8\text{--}100\text{ mg kg}^{-1}$ drug dose were cured. Ancillary studies, designed to probe skin photosensitivity, demonstrated no evidence of cutaneous erythema even at a light dose of 1000 J cm^{-2} (664 nm) [81,222,223]. Why this is the case is currently unclear. However, it could be because of photobleaching. Spikes and Bommer have published that NPe6 photobleaches about 15-fold more quickly than Photofrin[®], meaning there would be less material in the skin to mediate a photoeffect. In spite of this, it was found to be as efficacious as Photofrin[®] in these mice tumor studies [272].

(d) *Meso*-(tetrahydroxyphenyl)chlorin (*m*-THPC, Foscan[®])

Another promising new PDT agent being developed by Scotia Pharmaceuticals Ltd., (Guildford, UK) is *meso*-(tetrahydroxyphenyl)chlorin (Temoporfin, Foscan[®] 16, Figure 9) [225–227,229,230,277,278]. This amphiphilic sensitizer has several potential advantages for use in PDT applications, including: the fact that it is obtainable in $> 98\%$ purity; displays good photophysical properties, including a relatively high absorption coefficient at 652 nm and good singlet oxygen quantum yield (Table 1), demonstrates efficient phototoxicity, and engenders reduced photosensitization in the skin as compared to what is seen with Photofrin[®] [228,231,279]. Given these properties, it is not surprising that Foscan[®] has been the subject of clinical testing [225,226,230,231,277,278]. The results of one such study, designed to test the application of *m*-THPC to the treatment of cancers of the upper aerodigestive tract, has been reported by Grosjean and coworkers. In this study,

27 patients with early squamous cell carcinomas (SCC) and four patients with more advanced (T_1 or T_2) cancers were studied with drug doses of *m*-THPC at 0.075 mg kg^{-1} , 0.15 mg kg^{-1} , and 0.30 mg kg^{-1} using a variety of light doses at 652 nm ($6\text{--}16 \text{ J cm}^{-2}$, $40\text{--}150 \text{ mW cm}^{-2}$) or 514 nm ($30\text{--}100 \text{ J cm}^{-2}$, $40\text{--}150 \text{ mW cm}^{-2}$) laser light. Since *m*-THPC is sparingly soluble in water at pH 7, the drug formulation used was obtained by dissolving 20 mg of *m*-THPC in a 5 ml solution of a 20%:30%:50% ethanol:polyethylene glycol 400:water (v/v/v) mixture [personal communication with Professor Raymond Bonnett, Queen Mary & Westfield College, University of London] [280]. After sterile filtration, the resulting drug product was i.v. injected into patients within 30 min of preparation, being administered over the course of 5–10 min. Of the 36 SCC lesions evaluated after PDT treatment, thirty (83%) showed no recurrence during a follow-up period lasting up to 35 months. Of the four patients with T_1 or T_2 cancers (i.e. more advanced cancers), one showed a complete response after this *m*-THPC-based and PDT regime. Based on these and related studies, it was concluded that *m*-THPC is potentially effective for the treatment of early carcinomas of upper aerodigestive tract but may be less efficacious when applied to more advanced cancers [231,281].

Recently, Ronn *et al.* reported results from a Phase I clinical study with Foscan[®] (*m*-THPC). In this study, 25 patients with bronchial cancer (1 case), prostate cancer (6 cases), mesothelioma (1 case), laryngeal cancer (8 cases), nasopharyngeal cancer (3 cases), laryngeal papilloma (5 cases), and basal cell nevus syndrome (1 case) were selected and subjected to a drug-dose escalation trial (0.0375 , 0.075 , 0.15 , and 0.30 mg kg^{-1}) and pharmacokinetic analysis [225,226]. Light treatment was performed 6 days after i.v. injection of the drug, formulated as above. Several patients received multiple treatments for a total of 36 treatments. There were several conclusions about *m*-THPC that were derived from this study; first, the half-life ($t_{1/2}$) of *m*-THPC in human plasma is about 45.4 h. Second, drug levels in the plasma peak at 24 h after injection. Third, the drug is completely cleared from the bloodstream after 8–10 days. Fourth, the ratio of drug in tumor compared to normal adjacent mucosa was in the range 2–3, and fifth, for further trials it would be advantageous to use a drug dose of 0.15 mg kg^{-1} , followed by PDT treatment 6 h after injection.

Several preclinical studies, originally designed to support the above clinical trials, have been carried out. From these it was determined that *m*-THPC is not metabolized *in vivo* and virtually all the drug is eliminated *via* the liver. Pharmacokinetic data derived from animal studies with *m*-THPC led to the prediction that this substance would show rapid clearance from plasma in humans. Surprisingly, however, this was *only* observed in the animal models (dog, rabbit, rat), not in the human populations. This dichotomy stands as a cogent reminder that caution must always be exercised in translating animal-model data into human-dosing decisions [225].

(e) δ -ALA (LevulanTM) induced protoporphyrin IX

δ -Aminolevulinic acid (LevulanTM, 17, Figure 9) is currently being developed by DUSA Pharmaceuticals, Inc. (NY, USA) as a PDT agent. LevulanTM when

administered *in vivo* results in the accumulation of the endogenous photosensitizer protoporphyrin IX (PpIX, **18**, Figure 9) *via* the heme biosynthetic pathway [80,232–238]. It is this latter species (i.e. PpIX) that is thought to be the basis for the photodynamic effect observed when LevulanTM is administered and exposed to 630 nm light [282,283]. δ -ALA (LevulanTM) is the only PDT agent under clinical development that is assumed to be a metabolic precursor of the actual photosensitizer. Currently, it is being investigated in various clinical dermatological protocols, namely, cutaneous T-cell lymphoma, superficial nodular basal cell carcinoma, Bowen's disease (SCC, squamous cell carcinoma *in situ*), and actinic (solar) keratoses [232,233]. As will be discussed later, this PDT agent is also being used as a fluorescence detection marker for photodynamic photodiagnosis (PDD) of cancer and dysplastic conditions of the urinary bladder and other organs [232,233].

On the PDT front, early preclinical studies were carried out with a view to investigating the efficacy of δ -ALA when administered by topical application, intradermal injection, subcutaneous injection, intravenous (i.v.), intraperitoneal (i.p.) injection and oral dosing. Initially, Kennedy and Pottier developed a topical cream formulation of 20% (v/v) δ -ALA that, when applied to superficial basal cell carcinoma followed by exposure to broad-band red light (600–800 nm) from a Kodak[®] slide projector equipped with a red filter, produced a significant clinical response in 90% of the cases [283]. Based on this seminal work, the topical use of δ -ALA for dermatological applications has become widespread in recent years [233]. In the context of this use, it has been found that the PDT effect is greatest when the administered light is applied when the ratio of PpIX in the lesion (measured by, e.g. fluorescence) compared to normal surrounding tissue is the highest [284].

Since Kennedy and Pottier treated the first patients with superficial basal cell carcinoma (sBCC) using their topical δ -ALA treatment, several clinical investigators have published their results [232,233]. Wolf *et al.* also used a slide projector (light dose of 30 J cm⁻²) to treat 37 sBCC lesions and reported a 97% complete response (CR) rate in a study involving four patients [285]. Carinduff *et al.* used a copper vapor/dye laser (total light dose 125–200 J cm⁻² at 630 nm) to irradiate 16 sBCC lesions in four patients; these researchers reported a 88% complete response rate. However, after a long follow-up period of 4–21 months, they found a 50% recurrence in the treated lesions [286]. Svanberg *et al.* treated 55 skin lesions (21 patients) with a Nd:YAG pumped dye laser at 630 nm (60 J cm⁻²). They reported a 100% complete response rate with no regrowth being observed after 6–14 months of follow up [287]. Warloe *et al.* [319] treated a few hundred sBCC lesions with 20% ALA and ALA/DMSO (2–20%)/EDTA (2–4%) and 40–200 J cm⁻² of 630 nm light provided by a copper vapor-pumped laser light. The two formulations produced similar response rates (i.e. on the order of 90%) [232,233]. In further clinical work, Calzavara-Pinton administered ALA topically to patients with sBCC and then carried out a PDT treatment every other day until the treated area appeared eroded without clinical evidence of tumor. A 100% complete response was achieved under this protocol [288].

Other clinical investigation of topical ALA+PDT in nonbasal cell carcinoma, and squamous cell carcinoma (*in situ*) have also shown encouraging results (i.e. 89–100% CR) [257,285–287]. For instance, in a recent, DUSA Pharmaceuticals-sponsored Phase I study of patients with actinic keratoses (AK), the lesions were exposed to varying concentrations of ALA (LevulanTM) in a oil-in-water emulsion under occlusion for 3 h and then treated with 630 nm laser light (dose range 10–150 J cm⁻²) [232,233].

In general, most clinical investigators using δ -ALA reported patient discomfort (described as mild to strong itching, or burning sensations) during the irradiation and a few reports described the use of a topical local anesthetic to ease the pain associated with treatment [232,233]. In spite of this potential problem, DUSA Pharmaceuticals has recently sponsored a multi-site Phase II clinical trial designed to treat actinic keratoses with topical δ -ALA (LevulanTM); results should be forthcoming.

4.4 Lutetium(III) texaphyrin (PCI-0123)

One of the authors of this Chapter (J.L.S.) was apparently the first to suggest that expanded porphyrins could be useful as PDT photosensitizers [2,164]. This proposal was made based on a consideration of the photophysical properties of the first-generation cadmium(II) texaphyrin **1** (Figure 1) [164]. This species, in its mono-nitrate form, was found to have a far-red absorption (lowest energy $\lambda_{\max} = 759$ nm) with good efficiency ($\epsilon = 3.9 \times 10^4$ M⁻¹ cm⁻¹) in MeOH [164,289]. It was also found to produce singlet oxygen in relatively high quantum yield ($\Phi_{\Delta} = 0.69 \pm 0.09$ in MeOH) [164]. Subsequent *in vitro* studies confirmed that this substance could be used to effect the efficient photodynamic eradication of K562 human leukemia cells [289,290] and both Gram-positive *Staphylococcus aureus* [289,291,292] and Gram-negative *Escherichia coli* bacteria, provided the latter was treated concurrently with polymyxin nonapeptide [292]. However, the fact that **1** is not appreciably water-soluble coupled, with residual concerns about cadmium toxicity, served to limit follow-up *in vivo* studies with this texaphyrin complex [293].

However, in view of the promising photophysical and cellular data amassed with **1**, a considerable effort was focused on developing what might be a *bona fide* texaphyrin-based PDT agent. This effort culminated in the synthesis of the lutetium(III) texaphyrin complex, **PCI-0123** (**4**) (Figure 1) [294]. This water-soluble, monomeric, and completely synthetic substance is being developed by Pharmacyclics, Inc; it possesses many of the characteristics expected of an ideal photosensitizer. For instance, it displays a far-red absorbance band ($\lambda_{\max} = 732$ nm; $\epsilon = 42\,000$ M⁻¹ cm⁻¹ in MeOH) [108,294]. It also serves to produce singlet oxygen in high quantum yield ($\Phi_{\Delta} = 0.58 \pm 0.04$ in PBS/1% Triton X-100, pH 7.4; Table 1) [267,295] when irradiated with red light.

In vivo lutetium texaphyrin (**PCI-0123**, tradename LUTRINTM) is known to be a fluorescent, tumor-localizing agent that may be activated for a PDT effect with low energy red light (i.e. 732 nm) [108,239]. Indeed, this novel pharmaceutical has completed a Phase I human clinical trial in the USA. This latter study involved a dose escalation trial focused on the PDT treatment of patients with unresectable or incurable cancer malignancies accessible to light illumination. Here, a single 5 min intravenous injection of lutetium texaphyrin **PCI-0123** at doses in the range 0.5–6.2 $\mu\text{mol kg}^{-1}$, was made followed by 732 nm irradiation at 150 J cm^{-2} and 75 mW cm^{-2} , 3–8 h after injection. A total of 35 patients were enrolled in the study, 15 with breast cancer, 7 with melanoma, and 13 with other types of tumors. Over the course of this study, 127 lesions were evaluated [296]. In patients with breast cancer, 52 lesions were treated. This resulted in 55% complete responses and 23% partial responses, for a total tumor response rate of 78% [296]. Among the melanoma patients, 32 lesions were treated. In this case, a 44% complete response and a 6% partial response rate were recorded, for a total tumor response rate of 50%. The dose-limiting toxicity observed at 6.2 $\mu\text{mol kg}^{-1}$ was found to be pain localized at the treatment site during light illumination [296]. At doses lower than this, all the treatments were well-tolerated with, *inter alia*, no significant systemic skin photosensitization being observed in the treated patients [240,241]. In work to be published shortly, researchers at Pharmacyclics, Inc. determined that the maximum tolerated dose (MTD), as defined by the Phase I protocol, was 4.7 $\mu\text{mol kg}^{-1}$.

The above Phase I trial has served to demonstrate in preliminary fashion that the lutetium texaphyrin **PCI-0123** is an effective PDT photosensitizer active against a variety of cancers, including pigmented melanoma (including patients with failed isolated limb perfusion), breast cancer, AIDS-related Kaposi's sarcoma, and basal cell carcinoma [241]. In fact, more than half of the patients with skin metastases followed in this trial (about 50% of the total population) showed complete responses [187]. Interestingly, the Phase I trial utilized two light sources for **PCI-0123** photoactivation, a Lambda Plus[®] argon pumped dye laser (Coherent, Palo Alto, CA) and a QBeamTM QBMEDXM-728 LED array (Quantum Devices, Inc., Barneveld, WI). The use of the LED (Light Emitting Diode) as a light source was included in the clinical protocol because LEDs are inexpensive, highly portable, reliable, and convenient in treating larger diseased surface areas [242].

Not surprisingly, the above Phase I and current Phase II human clinical studies are supported by numerous preclinical studies. These have served to show, for instance, that complete cures of implanted fast-growing spontaneous mouse mammary tumors (SMT-F) in female DBA/2N mice can be achieved using a proper combination of light fluence, **PCI-0123** (4) drug dose, and post-administration irradiation time (Figure 14) [108]. Such studies have also shown that **PCI-0123** is photo-active against other murine cancer models including the EMT6 mammary sarcoma and the B16 pigmented melanoma [239,243].

Some of this work has focused on elucidating the proposed mechanism of action of lutetium texaphyrin **PCI-0123** *in vitro* and *in vivo* as well as on understanding its

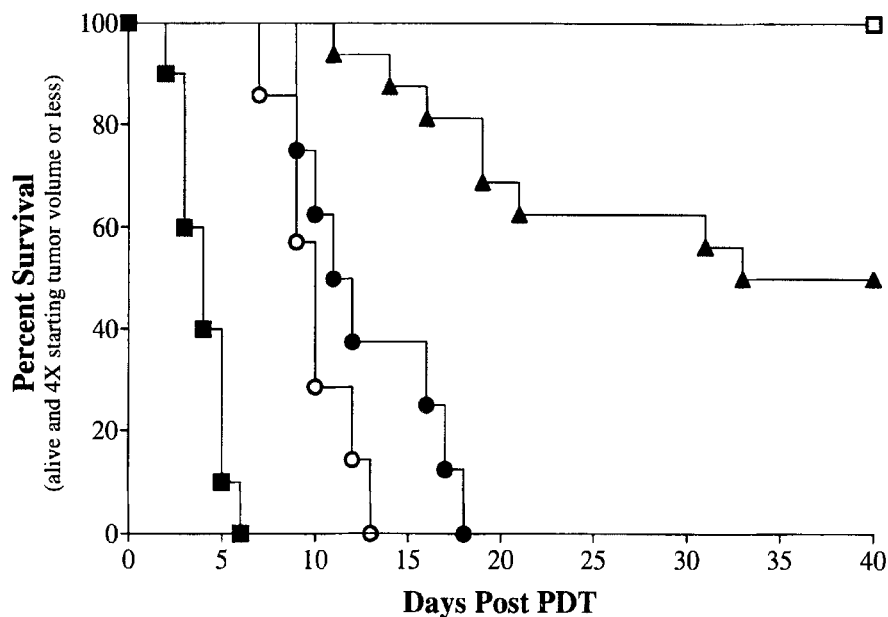


Figure 14 Kaplan-Meier survival curves for SMT-F tumor bearing mice treated with $10 \mu\text{mol/kg}$ **PCI-0123** (4). The mice were irradiated 3 h ($n=9$, \square), 5 h ($n=16$, \blacktriangle), 12 h ($n=8$, \bullet) and 24 h ($n=7$, \circ) post injection of **PCI-0123** with 150 J/cm^2 @ 150 mW/cm^2 at 732 nm . A matched set of control animals received light irradiation alone ($n=10$, \blacksquare). Tumor volumes were $70 \pm 35 \text{ mm}^3$. All animals at day 40 that were still in the study displayed no evidence of disease at the tumor site. Reproduced from [108] by permission of the American Society of Photobiology

biolocalization properties. Woodburn and coworkers have reported *in vitro* cellular uptake studies. They used confocal laser scanning microscopy to demonstrate that the intracellular localization site of **PCI-0123** is in lysosomes [240]. Subsequent illumination of the EMT6 cells with **PCI-0123**, led to lysosomal break up, extensive cytoplasmic blebbing and subsequent cell death. Interestingly, *in vivo* PDT treatment of EMT6 neoplasms in BALB/c mice with **PCI-0123** (i.e. $10 \mu\text{mol kg}^{-1}$, 150 J cm^{-2} and 150 mW cm^{-2} , 3 or 5 h after injection) followed by histologic examination of photoirradiated tumors, revealed apoptosis (i.e. “programmed cell death”) as judged by the observation of a DNA “ladder-type” fragmentation pattern [240]. In other preclinical work, Miles *et al.* have recently reported that repetitive PDT treatments (i.e. drug dose and light fluence) with **PCI-0123** in C3H mice bearing RIF-1 tumors gives rise to an improved response compared to a single treatment, with sequential daily treatments providing the greatest efficacy. This has led to the suggestion that such a “fractionated approach” could prove useful clinically [297].

4.5 PDT of Atherosclerotic Disease

Atherosclerotic vascular disease is the leading cause of death in the USA [298]. As described above, PDT has traditionally encompassed the treatment of tumors only [195]. Recently, however, efforts have focused on the possibility that PDT could prove useful for the removal of atheromatous plaque [60,243,299–305]. This impetus can be attributed to: advances in device technology, and the synthesis of second generation photosensitizers that, taken together, are making PDT far more effective. From a medical perspective, the possibility of treating cardiovascular disease *via* PDT stems from the observation that porphyrin and porphyrin-like compounds are taken up or retained more in atheromatous plaque than on the walls of normal vessels. Using HpD, Spears was first to report porphyrin uptake in atherosclerotic lesions. Specifically, he found localization in experimentally induced atheromatous plaque in rabbit and monkey models and noted PDT eradication of this plaque upon irradiation [60–62]. However, clinical testing was not successful [62,240,299].

More recently, several second generation photosensitizers (e.g. BPD-MA, **13**, SnET2, **14** and **PCI-0123**, **4**) have also been studied for use in the fluorescence-based diagnosis and/or PDT treatment of atherosclerotic disease. Of these, the lutetium texaphyrin complex **PCI-0123** appears to be the most promising. For instance, SnET2 does not appear to be particularly plaque-selective [304]. Further, Hsiang and coworkers have reported that BPD-MA shows only a 3.5–1 plaque-to-normal vessel wall ratio in the miniswine *in vivo* model [303]. One reason for the poor selectivity of SnET2 and BPD-MA, it has been suggested [240], derives from the fact that solubilizing vehicles need to be used to administer these hydrophobic PDT agents. Consistent with this hypothesis is the finding by Hsiang *et al.* that Photofrin[®] displays a 8:1 localization differential between atherosclerotic lesions and control vessels in the miniswine model [302]. Unfortunately, the lowest energy absorption of Photofrin[®] falls at 630 nm ($\epsilon = \approx 3 \times 10^3 \text{ M}^{-1} \text{ cm}^{-1}$) and light transmission at this wavelength is substantially reduced by the presence of blood [299,305]. This could limit the extent of the antiatherosclerotic PDT effect obtained when this agent is used *in vivo*.

In recent clinical and preclinical work, researchers at Pharmacyclics Inc., have demonstrated that texaphyrins selectively localize in atheromatous plaque and not in the normal aortic wall [243,300,301]. In the case of gadolinium texaphyrin **PCI-0120** (**3**), this has been shown in human populations *via* MRI. With lutetium texaphyrin **PCI-0123** (**4**), spectral bioimaging of intact rabbit aortas (i.e. after **PCI-0123** injection and subsequent sacrifice) served to reveal plaque-to-normal vessel retention ratios on the order of 34 to 1 [300]. Further, extensive preclinical studies have helped establish that **PCI-0123** (**4**) may be used in a PDT sense to effect selective photodamage of atheromatous plaque lesions in diet-induced hypercholesterolemic New Zealand white rabbits [243,300,301]. For instance, Woodburn *et al.* reported that a protocol involving i.v. injection of **PCI-0123** ($10 \mu\text{mol kg}^{-1}$ per day

for 3 days) and illumination with 200 J cm^{-2} , 250 mW cm^{-2} and 732 nm laser light 5 h after the last injection, will give rise to very effective plaque eradication (e.g., atheromatous plaque at the illuminated site was reduced by as much as 80–100%, Figure 15) and does so without apparently inducing photodamage to the normal aortic wall. Thus, while the mechanism of **PCI-0123** photoangioplasty of the atheromatous lesions is still unclear, it is equally apparent that this approach could evolve into what might become a new treatment modality for the control of atherosclerosis [243,300]. Currently, Pharmacyclics' Lutetium texaphyrin product, ANTRINTM Photosensitizer is undergoing a Phase I clinical trial in patients with atherosclerotic peripheral arterial disease. Preliminary results from the two-centre US trial are quite encouraging.

4.6 Applications of PDT to Blood Purification

There is a considerable body of evidence that PDT can be used effectively to eliminate pathogenic enveloped viruses from infected cells, cell-free suspensions, and whole blood [245,246,306–312]. In particular, HIV-1, herpes simplex I/II (HSV-1 or HSV-2), human cytomegalovirus (CMV), measles, and simian virus (SIV) can be destroyed using a PDT-type approach [80,313–315]. More recently, this general viral-killing strategy has been evaluated in the context of a blood transfusion sterilization system targeted against blood-borne pathogenic organisms. For instance, Matthews and coworkers, pioneers in this area, have reported the “photodynamic cleansing” of blood, cells and viral suspensions using dihematoporphyrin ether (DHE) and BPD-MA (**13**, $\lambda = 690 \text{ nm}$), *via* a light-activated process that, reportedly, causes no damage to erythrocytes, complement factors, and immunoglobulins [315]. In a separate study, however, North *et al.* reported that a PDT-like treatment of red blood cells with BPD-MA led to potassium leakage and IgG binding [313].

In addition to DHE and BPD-MA, both Sessler's sapphyrin **22** [245,316] and Franck's vinylogous porphyrins **23** and **24** [246,264] have been proposed as possible sensitizers for photodynamic viral inactivation of (Figures 11 and 12). In both cases the critical, predicative cell work has been done in the context of collaboration involving Dr J. L. Matthews and coworkers at the Baylor Research Foundation in Dallas, TX. From these studies it has emerged that sapphyrin (lowest energy $\lambda_{\text{max}} \approx 680 \text{ nm}$) is a highly effective photosensitizer for the light-based *in vitro* eradication of both Herpes simplex virus (HSV) and human immunodeficiency virus (HIV) [245,316]. For instance, at a light fluence of 10 J cm^{-2} ($\lambda_{\text{excit}} = 680 \text{ nm}$) and dye concentrations of $34 \mu\text{mol}$ and $16 \mu\text{mol}$, respectively, sapphyrin **22** was found to eradicate $\geq 99.999\%$ and $\geq 99\%$ of these two viruses. In the case of the vinylogous porphyrins **23** and **24**, the corresponding viral inhibition studies are apparently not yet complete. However, it is to be noted that one of these dyes, the bisvinylogous system **23**, was found, upon photolysis, to be very effective at preventing the *in vitro*

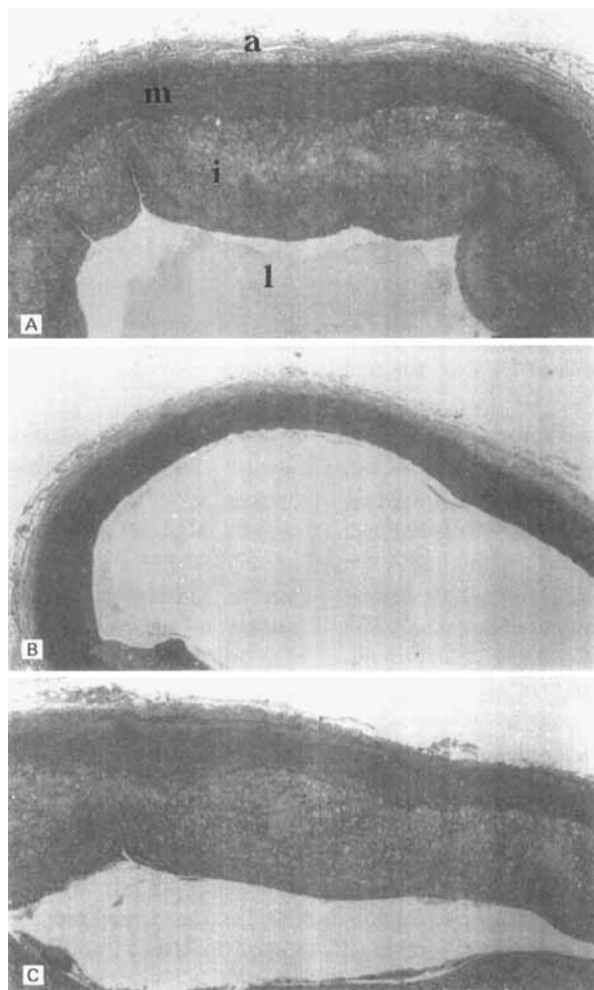


Figure 15 Three microscopic hematoxylin and eosin (H&E) stained cross-sections of a rabbit artery two weeks post PDT treatment with lutetium(III) texaphyrin **PCI-0123** ($10\ \mu\text{mol}/\text{kg}$ per day for three days and illumination with $200\ \text{J}/\text{cm}^2$, $250\ \text{mW}/\text{cm}^2$ and $732\ \text{nm}$ laser light 5 h post injection). Here, (A) and (C) are above and below the treatment site and (B) is at the treatment site. The aorta, above the treatment zone, is shown. The intima (i) is extensively thickened and heavily laden with foam cells. The atheroma completely lines the wall, thereby significantly narrowing the lumen (l). The outer wall, adventitia (a), and media (m) are normal and show no evidence of infiltrating disease. The photoirradiated site (B) is now normal (i.e., devoid of lesions), while the media muscular wall is intact with no necrotic regions being visible. The field below the treatment site (C) is heavily burdened with plaque ($\times 40$). Reproduced from [243] by permission of Mary Ann Liebert, Inc. Publishers

growth of certain leukemic cell lines [246]. This augurs well for the eventual use of this compound and its analogues in both photodynamic viral inactivation and light-based tumor therapy applications.

5. PHOTODYNAMIC DIAGNOSIS (PDD)— FLUORESCENCE-IMAGING

5.1 Background

Tumor localization plays a critical role in the control of cancer. Early clinical diagnosis improves the prognosis and, at any level, staging is important in terms of treatment planning. Current clinical methods rely on X-ray, CT-scanning, and MR imaging. If the tumor lesions are in an embryonic stage (i.e. *in situ* or dysplastic), the visualization achieved using extant methods may be quite limited. Thus, there remains a need for a minimally invasive procedure that would allow for early tumor detection.

One new diagnostic approach that appears attractive is Photodynamic Diagnosis (PDD) [232,233]. This technique has its origin in the fact that porphyrin-like materials both localize in tumors and fluoresce. Thus, by adding different tumor-marking substances, such as various porphyrin or porphyrin-like pharmaceutical agents, the hope is that the demarcations between malignant and normal tissue can be better defined. Over the course of the past decade, several spectroscopic techniques, such as laser-induced fluorescence (LIF) and fluorescence spectral bioimaging, have emerged as methods that make this approach potentially more viable. Nonetheless, until recently the most commonly used substance for PDD has been Photofrin[®]. As noted above, this substance absorbs at 630 nm. It also displays a dual-peaked fluorescence at 630 and 690 nm. Since Photofrin[®] is taken up by, and/or retained in, malignant tumor sites to a greater extent than it is in normal tissue, the fluorescence signal obtained from it may be used to effect tumor localization.

Unfortunately, as described in Section IV, Photofrin[®] is not a perfect PDT agent; it has the deleterious side effect of engendering prolonged photosensitivity for several weeks after administration in humans, and this same problem is restricting its use as a PDD agent. Accordingly, considerable effort has been devoted to exploring whether the various second generation “PDT agents” now available might serve as improved second generation fluorescent diagnostic markers [80,81,108,208–211,213–243].

5.2 Newer Approaches

In the course of their clinical evaluation of NPe6 (15), Okunaka and coworkers used a PDD-type fluorescence assay (i.e. monitored at 664 nm) to demonstrate that this

drug shows its maximal concentration in cancerous lesions 3 h post injection (1 mg kg^{-1}) in humans [317]. In fact, after 24 h, there was no evidence of fluorescence. This finding is consistent with the idea that NPe6 is cleared rapidly from the body. Kennedy *et al.* have shown that PpIX (**18**), induced by topical application of δ -ALA (**17**), may be used as a fluorescence marker for the photo-diagnosis of cancer and dysplastic conditions of the urinary bladder and other organs [232,233]. The high fluorescence yield of PpIX (635 nm) has allowed visual confirmation (using hand-held UV lamps) of the accumulation of PpIX in skin lesions after application of δ -ALA. Evaluation of PpIX in patients by laser-induced fluorescence (LIF) techniques, has also proved useful in demonstrating that the ratios of tumor-to-normal skin fluorescence vary from 9:1 (for Bowen's disease) to 15:1 in the case of cutaneous T-cell lymphoma [232,233]. Using LIF, Wang and coworkers [320] have documented an increase in fluorescence 4–6 h after the application of topical 20% δ -ALA to 24 lesions (twelve superficial basal cell carcinoma, seven nonbasal cell carcinoma, three Bowen's disease and five cutaneous T-cell lymphoma) in 24 patients [232,233]. Svanberg *et al.* [287,321] also observed PpIX fluorescence after the oral administration of δ -ALA to 30 patients. The maximum fluorescence intensity was observed at 5–8 h in their study with initial visualization being possible as early as 30 min after administration [232,233].

Pharmacyclics, Inc. has also benefited from the use of spectral bioimaging in their Phase I clinical trial involving the lutetium texaphyrin complex **PCI-0123** (**4**) [240,300]. This technique involves exciting a fluorophore, specifically this diamagnetic texaphyrin, and then capturing the resulting fluorescence using a CCD camera coupled to a Sagnac interferometer. The resultant signal is then Fourier transformed so as to obtain a pixel-by-pixel fluorescence emission profile [240,300,318]. One of the reasons this technique is attractive in the case of **PCI-0123** is that this substance displays a strong, broad fluorescence emission at 757 nm, when irradiated at $\leq 730 \text{ nm}$. This allows quantitative analyses to be performed without interference from endogenous chromophores.

Under Pharmacyclics aegis, to date, fluorescence spectral bioimaging has been performed on three cancer patients. In all three cases, good delineation between normal and malignant tissue was observed following injection with **PCI-0123** [300]. More recently, Woodburn *et al.* have demonstrated the utility of this noninvasive technique in several preclinical studies [240,300]. Specifically, spectral imaging analysis of **PCI-0123** fluorescence has been used to establish the selective uptake of **PCI-0123** in EMT6 tumor-bearing BALB/c mice [240]. This is illustrated in Plate 2. Here, a tumor-bearing mouse was tail vein injected with $10 \mu\text{mol kg}^{-1}$ **PCI-0123** then subjected to fluorescence spectral imaging 4.5 h later. The results of this study augur well for the use of this PDD technique not only for performing routine quantitative pharmacokinetic analyses of **PCI-0123**, but also for the design and implementation of therapy-targeted clinical protocols. This provides a new exciting wrinkle to the evolving history of this exciting new drug candidate.

Note added in Proof:

“QLT Phototherapeutics (Vancouver, BC) and CIBA Vision recently reported that Verteporfin (BPDMA), Visudyne™, has been shown to preserve vision in a significant number of patients with the “wet” form of age-related macular degeneration (AMD). These results come from randomized Phase III clinical trials involving 609 patients and 22 centres in North America and Europe.”

6. ACKNOWLEDGEMENTS

The authors wish to thank Dr Kathryn Woodburn (Pharmacyclics, Inc.) for providing fluorescence spectral bioimaging photos, as well as for her helpful discussions and review of this work. We appreciate the assistance of Drs Markus Renschler and Richard Miller, of Pharmacyclics, Inc. for providing texaphyrin-related clinical photos (in MRI and XRT sections). We also wish to thank Drs William Dow, Richard Miller, Stuart Young, and Ms Jackie Larson, of Pharmacyclics, Inc. for their critical review of this work. We are grateful to Mr David Mitchell (QLT Phototherapeutics), Dr Leonard Grossweiner (Wenske Laser Center, Ravenswood Hospital, Chicago, IL) and Professor Raymond Bonnett (Queen Mary & Westfield College, University of London) for their help with Table 1 in this chapter. Special thanks go to Dr Vincent Lynch (UT Austin) for assistance with X-ray structure in Figure 3. We also wish to thank Dr Alexander Cross (Cytopharm, Inc.) and Dr Kurt Schaffner (Max-Planck Institute für Strahlenchemie) for providing copies of related porphycene prepublication references. J.L.S wishes to acknowledge research support from the NIH (CA68682) and Pharmacyclics, Inc.

7. REFERENCES

1. J. L. Sessler, T. Murai, V. Lynch and M. Cyr, *J. Am. Chem. Soc.*, **110**, 5586 (1988).
2. S. Stinson, *C & EN News*, August 8, 26 (1988).
3. R. Edelman and S. Warach, *N. Engl. J. Med.*, **328**, 708 (1993).
4. C. T. Moonen, P. C. van-Zijl, J. A. Frank, D. Le Bihan and E. D. Becker, *Science*, **250**, 53 (1990).
5. S. W. Young, *Magnetic Resonance Imaging: Basic Principles*, Raven Press, New York, 1988.
6. R. B. Lauffer, *Chem. Rev.*, **87**, 901 (1987).
7. J. S. Mann and R. C. Brasch, in *Handbook of Metal-Ligand Interactions in Biological Fluids: Vol 2* (ed G. Berthon) Dekker, New York, 1995, pp. 1358–1373.
8. M. F. Tweedle, H. G. Brittain, W. C. Eckelman, G. T. Gaughan, J. J. Hagan, P. W. Wedeking and V. M. Runge, in *Magnetic Resonance Imaging, 2nd ed., Vol 1* (ed C.L. Partain) WB Saunders, Philadelphia, 1988, pp. 793–809.
9. P. G. Morris, *Nuclear Magnetic Resonance Imaging in Medicine and Biology*, Clarendon Press, Oxford, 1986.
10. S. H. Koenig and R. D. Brown III, *Magn. Reson. in Med.*, **1**, 437 (1984).

11. S. H. Koenig and R. D. Brown, in *Handbook of Metal-Ligand Interactions in Biological Fluids*, Vol. 2 (ed G. Berthon) Dekker, New York, 1995, pp. 1093-1108.
12. C. W. Chen, J. S. Cohen, C. E. Myers and M. Sohn, *FEBS Lett.*, **168**, 70-74 (1984).
13. R. C. Lyon, P. J. Faustino, J. S. Cohen, A. Katz, F. Mornex, D. Colcher, C. Baglin, S. H. Koenig and P. Hambright, *Magn. Reson. Med.*, **4**, 24 (1987).
14. N. J. Patronas, J. S. Cohen, R. H. Knop, A. J. Dwyer, D. Colcher, J. Lundy, F. Mornex, P. Hambright, M. Sohn and C. E. Myers, *Cancer Treat. Rep.*, **70**, 391 (1986).
15. D. A. Place, P. J. Faustino, P. C. M. Van Zijl, A. Chesnick and J. S. Cohen, *Invest. Radiol.*, **25**, S69 (1990).
16. A. N. Øksendal and F.-A. Hals, *J. Magn. Reson. Imag.*, **3**, 157 (1993).
17. M. D. Ogan, D. Revel and R. C. Brasch, *Invest. Radiol.*, **22**, 822 (1987).
18. S. B. Kahl, M.-S. Koo, R. M. Straubinger, L. R. Huang, R. J. Fiel, R. Mazurchuk and J. J. Alletto, in *Advances in Neutron Capture Therapy* (eds A. H. Soloway, R. F. Barth and D. Carpenter) Plenum Press, New York, NY, 1992.
19. L. R. Huang, R. M. Straubinger, S. B. Kahl, M.-S. Koo, J. J. Alletto, R. Mazurchuk, R. I. Chau, S. L. Thamer and R. J. Fiel, *J. Magn. Reson. Imag.*, **3**, 351 (1993).
20. L. S. Jackson, J. A. Nelson, T. A. Case and B. F. Burnham, *Invest. Radiol.*, **20**, 226 (1985).
21. S. K. Saini, A. Jena, J. Dey, A. K. Sharma and R. Singh, *Magn. Reson. Imag.*, **13**, 985 (1995).
22. J. L. Sessler, T. D. Mody, G. W. Hemmi, V. Lynch, S. W. Young and R. A. Miller, *J. Am. Chem. Soc.*, **115**, 10368 (1993).
23. J. L. Sessler, T. D. Mody, G. W. Hemmi and V. Lynch, *Inorg. Chem.*, **32**, 3175 (1993).
24. J. L. Sessler, G. Hemmi, T. D. Mody, T. Murai, A. Burrell and S. W. Young, *Acc. Chem. Res.*, **27**, 43 (1994).
25. S. W. Young, F. Qing, A. Harriman, J. L. Sessler, W. C. Dow, T. D. Mody, G. W. Hemmi, Y. Hao and R. A. Miller, *Proc. Natl. Acad. Sci. U.S.A.*, **93**, 6610 (1996).
26. S. W. Young, M. K. Sidhu, F. Qing, H. H. Muller, M. Neuder, G. Zanassi, T. D. Mody, G. Hemmi, W. Dow, J. D. Mutch, J. L. Sessler and R. A. Miller, *Invest. Radiol.*, **29**, 330 (1994).
27. S. Fosshem, C. Johansson, A. K. Fahlvik, D. Grace and J. Klaveness, *J. Magn. Reson. Med.*, **35**, 201 (1996).
28. V. M. Runge, J. R. Parker, *Eur. Radiol.*, **7** (Suppl 5), (1997).
29. M. Oudkerk, P. E. Sijens, E. J. R. V. Beek and T. J. A. Kuijpers, *Invest. Radiol.*, **30**, 75 (1995).
30. M. F. Tweedle, P. Wedeking and K. Kumar, *Invest. Radiol.*, **30**, 372 (1995).
31. P. T. Normann and P.-A. Hals, *Eur. J. Drug Metab. Pharmacokin.*, **20**, 307 (1995).
32. K. L. Nelson, L. M. Gifford, C. Lauber-Huber, C. A. Gross and T. A. Lasser, *Radiology*, **196**, 439 (1995).
33. W. T. C. Yuh, D. J. Fisher, V. M. Runge, S. W. Atlas, S. E. Hams, K. R. Maravilla, N. A. Mayr, J. E. Mollman and A. C. Price, *Am. J. Neuroradiol.*, **15**, 1037 (1994).
34. M. Van Wagoner and D. Worah, *Invest. Radiol.*, **28**, S44 (1993).
35. P. Akeson, E. Jonnson, I. Haugen and S. Holtas, *Neuroradiol.*, **37**, 229 (1995).
36. P. Akeson, E.-M. Larsson, D. T. Kristoffersen, E. Jonnson and S. Holtas, *Acta Radiol.*, **36**, 300 (1995).
37. S. Ekholm, E. Jonnson, L. Sandvik, M. Fagerlund, S. Holtas, B. Isberg, D. Lindell, B. Linden, S. Sjoberg, K.-A. Thuomas and P. O. Tollesson, *Acta Radiol.*, **37**, 223 (1996).
38. S. Hanquinet, C. Christophe, D. De Greef, P. Gordon and N. Perlmutter, *Pediatr. Radiol.*, **26**, 806 (1996).
39. A. D. Elster, *Radiology*, **176**, 225 (1990).
40. S. Engelter, P. Lyrer, E. W. Radu and A. J. Steck, *J. Neurol.*, **243**, 191 (1996).

41. R. I. Grossman, B. H. Braffman, J. R. Brorson, H. I. Goldberg, D. H. Silberberg and F. Gonzalez-Scarano, *Radiology*, **169**, 117 (1988).
42. V. P. Matthews, M. A. Kuharik, M. K. Edwards, B. Azzarelli and R. G. Dressen, *Am. J. Roentgenol.*, **152**, 131 (1989).
43. P. B. Crino, R. Zimmerman, D. Laskowitz, E. C. Raps and A. M. Rostami, *Neurol.*, **44**, 1334 (1994).
44. M. L. H. Whiteman, B. K. Dandapani, R. T. Shebert and M. J. D. Post, *J. Comput. Assist. Tomogr.*, **18**, 7 (1994).
45. Reuters News Service for Advanced Magnetics, Inc., September 3, 1996.
46. PR Newswire for Advanced Magnetics, Inc., December 9, 1996.
47. J. Rogers, J. Lewis and L. Josephson, *Invest. Radiol.*, **29(Suppl. 2)**, S81 (1994).
48. W. K. Johnson, C. Stoupis, G. M. Torres, E. B. Rosenberg and P. R. Ros, *Magn. Reson. Imag.*, **14**, 43 (1996).
49. T. J. Vogl, R. Hammerstingl, W. Schwartz, M. G. Mack, P. K. Mueller, W. Pegios, H. Keck, A. Eibl-Eibesfeldt and J. Hoelzl, *Radiology*, **198**, 881 (1996).
50. S. M. Rocklage, W. P. Cacheris, S. C. Quay, F. E. Hahn and K. N. Raymond, *Inorg. Chem.*, **28**, 477 (1989).
51. H. Brurok, J. Schoejtt, K. Berg, J. O. G. Karlsson and P. Jynge, *Invest. Radiol.*, **30**, 159 (1995).
52. W. F. Blsazak, G. L. Brown, T. J. B. Gray, K. A. Treinen and K. H. Dennys, *Fundam. Appl. Toxicol.*, **33**, 11 (1996).
53. K. O. Lim, D. D. Stark, P. T. Leese, A. Pfeffebraum, S. M. Rocklage and S. C. Quay, *Radiology*, **178**, 79 (1991).
54. A. Policard, *CR Soc. Biol.*, **91**, 1423 (1924).
55. H. Auler and G. Banzer, *Z. Krebsforsch.*, **53**, 65 (1942).
56. F. H. J. Figge, G. S. Weiland and L. O. J. Manganiello, *Proc. Soc. Exp. Med.*, **68**, 640 (1948).
57. D. S. Rasmussen-Taxdall, G. E. Ward and F. H. Figge, *Cancer*, **8**, 78 (1955).
58. R. L. Lipson, E. J. Baldes and A. M. Olsen, *J. Natl. Cancer Inst.*, **26**, 1 (1961).
59. T. J. Dougherty, B. W. Henderson, S. Schwartz, J. W. Winkelman and R. L. Lipson, in *Photodynamic Therapy, Basic Principles and Clinical Applications* (eds B. W. Henderson and T. J. Dougherty) Dekker, New York, 1992, pp. 1–18.
60. J. R. Spears, J. Serur, D. Shropshire and S. Paulin, *J. Clin. Invest.*, **71**, 395 (1983).
61. D. Kessel and E. Sykes, *Photochem. Photobiol.*, **40**, 59 (1984).
62. A. Spokojny, J. R. Serur, J. Skillman and J. R. Spears, *J. Am. Coll. Card.*, **8**, 387 (1986).
63. R. J. Fiel, T. M. Button, S. Gilani, M. E. H., D. A. Musser, R. M. Henkelman, M. J. Bronskill and J. G. van Heteren, *Magn. Reson. Imag.*, **5**, 149 (1987).
64. K. Bockhorst, M. Hoehn-Berlage, R.-I. Ernestus, T. Tolxdorff and K.-A. Hossman, *Magn. Reson. Imag.*, **11**, 655 (1993).
65. K. Bockhorst, T. Els and M. Hoehn-Berlage, *J. Magn. Reson. Imag.*, **4**, 451 (1994).
66. K. Bockhorst and M. Hoehn-Berlage, *Tetrahedron*, **50**, 8657 (1994).
67. L. J. Wilmes, M. Hoehn-Berlage, T. Els, K. Bockhorst, M. Eis, Bonnekoh and K.-A. Hossmann, *J. Magn. Res. Imag.*, **3**, 5 (1993).
68. J. H. McMillan, G. G. Cox, B. F. Kimbler, J. S. Spicer and S. Batnitzky, *Magn. Reson. Imag.*, **9**, 553 (1991).
69. P. J. Bohdiewicz, D. K. Lavallee, R. A. Fawwaz, J. H. Newhouse, S. F. Oluwole and P. O. Alderson, *Invest. Radiol.*, **25**, 765 (1990).
70. D. A. Place, P. J. Faustino, K. K. Berghmans, P. C. M. van Zijl, A. S. Chesnick and J. S. Cohen, *Magn. Reson. Imag.*, **10**, 919 (1992).
71. P. Furmanski and C. Longley, *Cancer Res.*, **48**, 4604 (1988).

72. V. E. Yushmanov, T. T. Tominaga, I. E. Borissevitch, H. Imasato and M. Tabak, *Magn. Reson. Imag.*, **14**, 255 (1996).
73. R. J. Fiel, D. A. Musser, E. H. Mark, R. Mazurchuk and J. J. Alletto, *Magn. Reson. Imag.*, **8**, 255 (1990).
74. P. Hambright, C. Adams and K. Vernon, *Inorg. Chem.*, **27**, 1660 (1988).
75. S. B. Kahl and M.-S. Koo, *J. Chem. Soc., Chem. Commun.*, **24**, 1769 (1990).
76. S. B. Kahl and M.-S. Koo, in *Progress in Neutron Capture Therapy for Cancer* (ed B. J. Allen) Plenum Press, New York, 1992, pp. 223–226.
77. G. P. Spizzirri, J. S. Hill, S. B. Kahl and K. P. Ghigginio, *Photochem. Photobiol.*, **64**, 975 (1996).
78. J. S. Hill, S. B. Kahl, A. H. Kaye, S. S. Stylli, M.-S. Koo and M. F. Gonzales, *Proc. Natl. Acad. Sci. USA*, **89**, 1785 (1992).
79. D. Phillips, *Pure Appl. Chem.*, **67**, 117 (1995).
80. A. M. R. Fisher, A. L. Murphree and C. J. Gomer, *Lasers Surg. Med.*, **17**, 2 (1995).
81. R. W. Boyle and D. Dolphin, *Photochem. Photobiol.*, **64**, 469 (1996).
82. G. Jori, *J. Photochem. Photobiol. A: Chem.*, **62**, 371 (1992).
83. M. Kreimer-Birnbaum, *Sem. Hematol.*, **26**, 157 (1989).
84. W. G. Love, S. Duk, R. Biolo, G. Jori and P. W. Taylor, *Photochem. Photobiol.*, **63**, 656 (1996).
85. K. A. Hahn, M. Panjehpour and X. Lu, *Photochem. Photochem.*, **63**, 117 (1996).
86. P. Margaron, M.-J. Gregoire, V. Scasnar, H. Ali and J. E. van Lier, *Photochem. Photobiol.*, **63**, 217 (1996).
87. R. Biolo, G. Jori, M. Soncin, B. Rihter, M. E. Kenney and M. A. Rodgers, *Photochem. Photobiol.*, **63**, 224 (1996).
88. M. M. Zuk, B. D. Rihter, M. E. Kenney and M. A. Rodgers, *Photochem. Photobiol.*, **63**, 132 (1996).
89. R. Biolo, G. Jori, M. Soncin, R. Pratesi, U. Vanni, B. Rihter, M. E. Kenney and M. A. Rodgers, *Photochem. Photobiol.*, **59**, 362 (1994).
90. Q. Peng, J. Moan, Kongshaug, J. F. Evensen, H. Anholt and C. Rimington, *Int. J. Cancer*, **48**, 258 (1991).
91. I. Rosenthal, *Photochem. Photobiol.*, **53**, 859 (1991).
92. N. L. Oleinick, A. R. Antunez, M. E. Clay, B. D. Richter and M. E. Kenney, *Photochem. Photobiol.*, **57**, 242 (1993).
93. P. A. Firey and M. A. Rodgers, *J. Photochem. Photobiol.*, **45**, 535 (1987).
94. W. S. Chan, J. F. Marshall, Y. F. G. Lam and I. R. Hart, *Cancer Res.*, **48**, 3040 (1988).
95. W. S. Chan, M. F. Marshall, R. Svensen, J. Bedwell and I. R. Hart, *Cancer Res.*, **50**, 4533 (1990).
96. K. Boekelheide, J. Eveleth, A. H. Tatum and J. W. Winkelman, *Photochem. Photobiol.*, **46**, 657 (1987).
97. J. W. Winkelman and G. H. Collins, *Photochem. Photobiol.*, **46**, 801 (1987).
98. S. Haye and P. Hambright, *J. Chem. Soc.: Chem. Commun.*, 666 (1988).
99. J. L. Sessler, T. Murai and G. Hemmi, *Inorg. Chem.*, **28**, 3390 (1989).
100. J. L. Sessler, A. K. Burrell, H. Furuta, G. W. Hemmi, B. L. Iverson, V. Král, D. J. Magda, T. D. Mody, K. Shreder, D. Smith and S. J. Weghorn, in *Transition Metals in Supramolecular Chemistry (NATO ASI Series C)* Vol. 48, (eds L. Fabbrizzi and A. Poggi) Kluwer, Dordrecht, 1994, pp. 391–408.
101. T. D. Mody, PhD Dissertation, University of Texas at Austin, 1993.
102. C. F. G. C. Geraldies, A. D. Sherry, P. Vallet, F. Maton, R. N. Muller, T. D. Mody, G. Hemmi and J. L. Sessler, *J. Magn. Reson. Imag.*, **5**, 725 (1995).
103. S. W. Young and Q. Fan, *Invest. Radiol.*, **31**, 280 (1996).
104. G. W. Hemmi, PhD Dissertation, University of Texas at Austin, 1992.

105. S. W. Young, Q. Fan, D. M. Kunis and G. K. Steinberg, *Invest. Radiol.*, **31**, 353 (1996).
106. D. I. Rosenthal, C. R. Becerra, P. Nurenberg, S. W. Young, R. A. Miller, J. F. Engel, D. P. Carbone and E. P. Frenkel, *Abstracts of the 1996 American Society for Clinical Oncology, Annual Meeting*, **15**, May 18–21, 1996.
107. Pharmacyclics, Inc. Press Release January 29, 1996; *Pharmacyclics Initiates Phase Ib/II Trial of GdTex for Use in Treatment of Cancer Patients Receiving Radiation Therapy: Phase I Clinical Study Confirms Tumor Selective Localization*.
108. S. W. Young, K. W. Woodburn, M. Wright, T. D. Mody, Q. Fan, J. L. Sessler, W. C. Dow and R. A. Miller, *Photochem. Photobiol.*, **63**, 892 (1996).
109. S. L. Parker, T. Tong, S. Bolden and P. A. Wingo, *CA—A Cancer Journal for Clinicians*, **47**, 5 (1997).
110. S. E. Otto, *Oncology Nursing*, Mosby—Year Book, St. Louis, 1991.
111. J. J. Felmeier, in *Clinical Oncology* (ed G. R. Weiss) Appleton & Lange, Norwalk, 1993, pp. 74–88.
112. F. R. Hendrickson and H. R. Withers, in *American Cancer Society Textbook of Clinical Oncology* (eds A.I. Holleb, D. J. Fink and G. P. Murphy) American Cancer Society, Washington, DC, 1991, pp. 35–37.
113. C. J. Beard, C. N. Coleman and T. Kinsella, in *J. Cancer: Principles and Practice of Oncology* (eds V. T. Devita, Jr., S. Hellman and S. A. Rosenberg) Lippincott, Philadelphia, 1993, pp. 2701–2713.
114. M. S. Shenoy and B. B. Singh, *Cancer Invest.*, **10**, 533 (1992).
115. E. J. Hall, (ed.) in *Radiobiology for the Radiobiologist*, Lippincott, Philadelphia, 1994, pp. 165–181.
116. A. Russo, J. Mitchell, T. Kinsella, G. Morstyn and E. Glatsetin, *Semin. Oncol.*, **12**, 332 (1985).
117. M. Brada and G. Ross, *Curr. Opin. Oncol.*, **7**, 214 (1995).
118. J. M. Brown, in *Modification of Radiosensitivity in Cancer Treatment* (ed T. Sugahara) Academic, San Francisco, 1984, pp. 139–176.
119. I. F. Tannock, *Br. J. Radiol.*, **45**, 515 (1972).
120. E. R. Watson, K. E. Halnan, S. Dische, M. I. Saunders, I. S. Cade, J. B. McEwan, F. Wienik, D. J. D. Perrins and I. Sutherland, *Br. J. Radiol.*, **51**, 879 (1978).
121. C. C. Wang, in *Clinical Radiation Oncology: Indication, Techniques, and Results* (ed Wang, C. C.) PSG Publishing, Littleton, MA, 1988.
122. J. M. Robertson, W. D. Ensminger, S. Walker and T. S. Lawrence, *Int. J. Radiat. Oncol. Biol. Phys.*, **37**, 331 (1997).
123. T. E. Goffman, L. J. Dachowski, H. Bobo, E. H. Oldfield, S. M. Steinberg, J. Cook, J. B. Mitchell, D. Katz, R. Smith and E. Glatstein, *J. Clin. Oncol.*, **10**, 264 (1992).
124. RDC Report, *The Pink Sheet*, January 13, 1997.
125. S. Dische, *Radiother. Oncol.*, **3**, 97–115 (1985).
126. S. Dische, *Int. J. Radiat. Oncol. Biol. Phys.*, **16**, 1057 (1989).
127. R. O. Abratt, P. Craighead, V. B. Reddi and L. A. Sarembock, *Br. J. Cancer*, **64**, 968 (1991).
128. F. Baillet, M. Housset, B. Dessard-Diana and G. Boisserie, *Int. J. Radiat. Oncol. Biol. Phys.*, **16**, 1073 (1989).
129. J. M. Brown, *Int. J. Radiat. Oncol. Biol. Phys.*, **16**, 98 (1989).
130. D. Chassagne, H. Sancho-Garnier, I. Charreau, F. Eschwege and E. P. Malaise, *Radiother. Oncol. Suppl.*, **20**, 121 (1991).
131. D. Chassagne, I. Charreau, H. Sancho-Garnier, F. Eschwege and E. P. Malaise, *Int. J. Radiat. Oncol. Biol. Phys.*, **22**, 581 (1992).

132. C. N. Coleman, R. C. Urtasan, T. H. Wasserman, S. Hancock, J. W. Harris and V. K. Kirst, *Int. J. Radiat. Oncol. Biol. Phys.*, **10**, 1749 (1984).
133. C. N. Coleman, T. H. Wasserman, R. C. Urtasun, J. Halsey, V. K. Hirst, S. Hancock and T. L. Phillips, *Int. J. Radiat. Oncol. Biol. Phys.*, **12**, 1105 (1986).
134. C. N. Coleman, J. Halsey, R. S. Cox, V. C. Hirst, T. Blasahke, A. E. Howes, T. H. Wasserman, R. C. Urtasun, T. Pajak, S. Hancock, T. L. Phillips and L. Noll, *Cancer Res.*, **47**, 319 (1987).
135. S. Dische, M. I. Saunders, M. H. Bennett, B. Chir, E. P. Dunphy, C. Des Rochers, M. R. L. Stratford, A. I. Minchinton and P. A. Wardman, *Br. J. Radiol.*, **59**, 911 (1986).
136. J. Fazekas, T. F. Pajak, T. Wasserman, V. Marcial, L. Davis, S. Kramer, M. Rotman and J. Stetz, *Int. J. Radiat. Oncol. Biol. Phys.*, **13**, 1155 (1987).
137. L. T. Komarnicky, T. L. Phillips, K. Martz, S. Asbell, S. Isaacson and R. Urtasun, *Int. J. Radiat. Oncol. Biol. Phys.*, **20**, 53 (1991).
138. H. F. V. Newman, R. Ward, P. Workman and N. M. Bleehen, *Int. J. Radiat. Oncol. Biol. Phys.*, **15**, 1073 (1988).
139. M. I. Saunders, P. J. Anderson, M. H. Bennett, S. Dische, A. Minchinton, M. R. Stratford and M. Tothill, *Int. J. Radiat. Oncol. Biol. Phys.*, **10**, 1759 (1984).
140. L. N. Shulman, L. Buswell, L. Kalish and C. N. Coleman, *Int. J. Radiat. Oncol. Biol. Phys.*, **29**, 541 (1994).
141. L. N. Shulman, L. Buswell, H. Goddman, M. Muto, R. Berkowitz, B. Teicher, T. Kusumoto, S. J. Hurwitz, L. A. Kalish and C. N. Coleman, *Int. J. Radiat. Oncol. Biol. Phys.*, **29**, 545 (1994).
142. J. T. Roberts, N. M. Bleehen, P. Workman and M. I. Walton, *Int. J. Radiat. Oncol. Biol. Phys.*, **10**, 1755 (1984).
143. R. T. Mulcahy, D. W. Siemann and R. M. Sutherland, in *Clinical Oncology: A Multidisciplinary Approach for Physicians and Students* 7th Edition (ed P. Rubin) WB Saunders, Philadelphia, 1993, pp. 51–69.
144. T. W. Kensler, M. A. Trush and K. Z. Guyton, in *Free Radicals as Targets for Cancer Chemoprevention Prospects and Problems* (eds T. W. Kensler, M. A. Trush and K. Z. Guyton) CRC Press, Boca Raton, 1992, pp. 173–192.
145. P. Rubin and D. W. Siemann, in *Clinical Oncology: A Multidisciplinary Approach for Physicians and Students*, 7th edn. (ed P. Rubin) Saunders: Philadelphia, 1993, pp. 87–88.
146. J. M. Brown and M. J. Lemmon, *Int. J. Radiat. Oncol. Biol. Phys.*, 1991, **20**, 457–461.
147. S. Schwartz, 3rd Biennial Meeting of the International Photodynamic Association, Buffalo, New York, July 18, 1990.
148. G. Grasczew and M. Shopova, *Lasers Med. Sci.*, **1**, 193 (1986).
149. H. Kostron, M. R. Swartz, D. C. Miller and R. L. Martuza, *Cancer*, **5**, 964 (1986).
150. C. Prinze, L. C. Penning, T. M. A. R. Dubbelman and J. VanSteveninck, *Cancer Res.*, **52**, 117 (1992).
151. D. A. Bellnier and T. J. Dougherty, *Int. J. Radiat. Biol.*, **50**, 659 (1986).
152. G. Kavarnos, R. Nath and P. Bongiorno, *Radiat. Res.*, **137**, 196 (1994).
153. J. O'Hara, E. B. Double, M. J. Abrams, D. J. Picker, C. M. Giandomenico and J. F. Vollano, *Int. J. Radiat. Oncol. Biol. Phys.*, **16**, 1049 (1989).
154. B. R. James, G. G. Meng, J. J. Posakony, J. A. Ravensbergen, C. J. Ware and K. A. Skov, *Metal-Based Drugs*, **3**, 85 (1996).
155. G. G. Meng, B. R. James, K. A. Skov and M. Korbelik, *Can. J. Chem.*, **72**, 2447 (1994).
156. K. P. Valuckas, Didziapetriene, V. Atkocius, L. Gričiute, Z. Luksiene, L. Zaleckaite, R. Rotomskis, and V. Smilgevičius, *Proc. SPIE Int. Opt. Eng.*, **1881**, 76 (1993).
157. Z. Luksiene and B. Juodka, *Proc. SPIE Int. Opt. Eng.*, **1881**, 67 (1993).

158. T. J. Kinsella, A. Russo, J. B. Mitchell, J. Rowland, J. Jenkins, J. Schwade, C. E. Myers, J. M. Collins, J. Speyer, P. Kornbluth, B. Smith, C. Kufra and E. Glatstein, *Int. J. Radiat. Oncol. Biol. Phys.*, **10**, 69 (1984).
159. T. J. Kinsella, A. Russo, J. B. Mitchell, J. M. Collins, J. Rowland, D. Wright and E. Glatstein, *Int. J. Radiat. Oncol. Biol. Phys.*, **11**, 1941 (1984).
160. M. J. O'Connell, J. A. Martenson, H. S. Wicand, J. E. Krook, J. S. MacDonald, D. G. Haller, R. I. Mayer, L. L. Gunderson and T. A. Rich, *N. Engl. J. Med.*, **331**, 502 (1994).
161. F. Landoni, A. Maneo, G. Zanetta, A. Colombo, S. Nava, F. Placa, G. Tancini and C. Mangioni, *Gynecol. Oncol.*, **61**, 321 (1996).
162. A. L. Fields, P. S. Anderson, G. L. Goldberg, S. Walder, J. Beitler, B. Sood and C. D. Runowicz, *Gynecol. Oncol.*, **61**, 416 (1996).
163. M. Suzuki, Y. Saga, I. Sekiguchi and I. Sato, *Curr. Therap. Res.*, **57**, 430 (1996).
164. A. Harriman, B. G. Maiya, T. Murai, G. Hemmi, J. L. Sessler and T. E. Mallouk, *J. Chem. Soc., Chem. Commun.*, 314 (1989).
165. B. G. Maiya, A. Harriman, J. L. Sessler, G. Hemmi, T. Murai and T. E. Mallouk, *J. Phys. Chem.*, **93**, 8111 (1989).
166. Pharmacyclics, Inc. *Annual Report 1996* pp. 1–48.
167. T. B. Fitzpatrick and M. A. Pathak, *J. Invest. Dermatol.*, **23**, 229 (1959).
168. M. D. Daniell and J. S. Hill, *Aust. NA J. Surg.*, **61**, 340 (1991).
169. L. C. Harber and D. R. Bickers, *Photosensitivity diseases*, Saunders, Philadelphia, 1981.
170. H. Von Tappeiner and A. Jesionek, *Munch. Med. Wochenschr.*, **47**, 2042 (1904).
171. H. Von Tappeiner, *Munch. Med. Wochenschr.*, **47**, 5 (1900).
172. T. J. Dougherty, *J. Clin. Laser Med. Surg.*, **14**, 219 (1996).
173. H. Scherer, *Ann. d. Chem. u. Pharm.*, **40**, 1 (1841).
174. F. Meyer-Betz, *Dtsch. Arch. Klin. Med.*, **112**, 476 (1913).
175. S. K. Schwartz, K. Absolon and H. Vermund, *Univ. Minn. Med. Bull.*, **27**, 7 (1955).
176. T. J. Dougherty, *Photochem. Photobiol.*, **46**, 569 (1987).
177. D. Kessel, *Photochem. Photobiol.*, **39**, 851 (1984).
178. R. L. Lipson, E. J. Baldes and M. J. Gray, *Cancer*, **20**, 2255 (1967).
179. R. L. Lipson and E. Baldes, *J. Arch. Dermatol.*, **82**, 517 (1960).
180. R. L. Lipson, E. J. Baldes and A. M. Olsen, *J. Thorac. Cardiovasc. Surg.*, **42**, 623 (1961).
181. I. Diamond, S. G. Granelli, A. F. McDonah, S. Nielson, C. B. Wilson and R. Jaenicke, *Lancet*, **ii**, 1175 (1972).
182. T. J. Dougherty, G. Grindley and R. Flel, *J. Natl. Cancer Inst.*, **55**, 115 (1974).
183. T. J. Dougherty, J. E. Kaufman, A. Goldfarb, K. R. Weishaupt, D. Boyle and A. Mittleman, *Cancer Res.*, **38**, 2628 (1978).
184. B. W. Henderson and T. J. Dougherty, *Photochem. Photobiol.*, **55**, 145 (1992).
185. D. Kessel, *Drugs of Today*, **32**, 385 (1996).
186. J. J. Schuitmaker, P. Baas, H. L. L. M. van Leengoed, F. W. vander Meulen, W. M. Star and N. van Zandwijk, *J. Photochem. Photobiol., B: Biol.*, **34**, 3 (1996).
187. T. Reynolds, *J. Natl. Cancer Inst.*, **89**, 112 (1997).
188. T. Dougherty, *Adv. Photochem.*, **17**, 569 (1992).
189. T. J. Dougherty, *Photochem. Photobiol.*, **58**, 895 (1993).
190. S. B. Brown and T. G. Truscott, *Chem. in Brit.*, 955 (1993).
191. M. J. Manyak, A. Russo, P. D. Smith and E. Glatstein, *J. Clin. Oncol.*, **6**, 380 (1988).
192. D. Kessel, *Spectrum*, **3**, 13 (1990).
193. C. J. Gomer, *Semin. Hematol.*, **26**, 27 (1989).
194. N. A. Buskard and B. C. Wilson, *Semin. Oncol.*, **21(6)**S15, 1 (1994).
195. H. I. Pass, *J. Natl. Cancer Inst.*, **85**, 443 (1993).
196. A. R. Morgan, *Curr. Med. Chem.*, **2**, 604 (1995).
197. U. O. Nseyo, *J. Clin. Laser Med. Surg.*, **14**, 271 (1996).

198. J. S. McCaughan, *J. Clin. Laser Med. Surg.*, **14**, 223 (1996).
199. H. Kato, T. Okunaka and H. Shimatani, *J. Clin. Laser Med. Surg.*, **14**, 235 (1996).
200. M. Biel, *J. Clin. Laser Med. Surg.*, **14**, 239 (1996).
201. B. F. Overholt and M. Panjehpour, *J. Clin. Laser Med. Surg.*, **14**, 245 (1996).
202. P. J. Muller and B. C. Wilson, *J. Clin. Laser Med. Surg.*, **14**, 263 (1996).
203. D. A. Bellnier and T. J. Dougherty, *J. Clin. Laser Med. Surg.*, **14**, 311 (1996).
204. Sanofi Winthrop Pharmaceuticals, *Photofrin[®] (porfimer sodium) for Injection*, Package Insert, May 1996.
205. T. J. Dougherty, *Photochem. Photobiol.*, **45**, 879 (1987).
206. T. Christensen, T. Sandquist, K. Feren, H. Waksvik and J. Moan, *Br. J. Cancer*, **48**, 35 (1983).
207. S. Wan, J. A. Parrish, R. R. Anderson and M. Madden, *Photochem. Photobiol.*, **34**, 679 (1981).
208. A. Richter, B. Kelly, J. Chow, D. J. Liu, G. H. N. Towers, D. Dolphin and J. G. Levy, *J. Natl. Cancer Inst.*, **79**, 1327 (1987).
209. A. M. Richter, A. K. Jain, M. Obochi, H. Meadows, A. J. Canaan and J. G. Levy, *Photochem. Photobiol.*, **59**, 350 (1994).
210. A. Richter, E. Strenberg, E. Waterfield, D. Dolphin and J. G. Levy, *Proc. SPIE Int. Opt. Eng.*, **997**, 132 (1988).
211. A. M. Richter, E. Waterfield, A. K. Jain, B. Allison, E. D. Sternberg, D. Dolphin and J. G. Levy, *Br. J. Cancer*, **63**, 87 (1991).
212. L. Cincotta, D. Szeto, E. Lampros, T. Hasan and A. H. Cincotta, *Photochem. Photobiol.*, **63**, 229 (1996).
213. A. R. Morgan and N. C. Tertel, *J. Org. Chem.*, **51**, 1347 (1986).
214. C. F. Borland, D. McGarvey, T. G. Truscott and A. R. Morgan, *J. Photochem. Photobiol. B, Biol.*, **59**, 427 (1988).
215. A. R. Morgan, G. M. Garbo and T. G. Truscott, *Proc. SPIE Int. Opt. Eng.*, **997**, 139 (1988).
216. A. R. Morgan, G. M. Garbo, R. W. Keck and S. H. Selman, *Cancer Res.*, **48**, 194 (1988).
217. A. R. Morgan, A. Rampersaud, G. M. Garbo, R. W. Keck and S. H. Selman, *J. Med. Chem.*, **32**, 904 (1989).
218. Y. Luo, C. K. Chang and D. Kessel, *Photochem. Photobiol.*, **63**, 528 (1996).
219. D. Kessel, *J. Photochem. Photobiol. B: Biol.*, **39**, 81 (1997).
220. T. A. Katsumi, K. Aizawa, Y. Kuroiwa, K. Saito, Y. Kurata, Y. Ii, T. Okunaka, C. Konaka and H. Kato, *Photochem. Photobiol.*, **64**, 671 (1996).
221. C. J. Gomer and A. Ferrario, *Cancer Res.*, **50**, 3985 (1990).
222. W. G. Roberts and M. W. Berns, *Lasers Surg. Med.*, **90** (1989).
223. J. S. Nelson, W. G. Roberts and M. W. Berns, *Cancer Res.*, **47**, 4681 (1987).
224. A. Ferrario, D. Kessel and C. J. Gomer, *Cancer Res.*, **52**, 2890 (1992).
225. A. M. Ronn, M. Nouri, L. A. Lofgren, B. M. Steinberg, A. Westerborn, T. Windhal, M. J. Shikowitz and A. L. Abramson, *Lasers Med. Sci.*, **11**, 267 (1996).
226. A. M. Ronn, L. A. Lofgran and A. Westerborn, *Proc. SPIE Int. Opt. Eng.*, **2625**, 118 (1996).
227. S. Andrejevic Blant, A. Woodtil, G. Wagnières, C. Fontolliet, H. van den Bergh and P. Monnier, *Photochem. Photobiol.*, **64**, 963 (1996).
228. M. C. Berenbaum, R. Bonnett, E. B. Chevretton, S. L. Akande-Adebakin and M. Ruston, *Lasers Med. Sci.*, **8**, 235 (1993).
229. R. Whelpton, A. T. Michael-Titus, S. S. Basra and M. Grahn, *Photochem. Photobiol.*, **61**, 397 (1996).
230. A. M. Ronn and L. A. Lofgren, *Proc. SPIE: Int. Opt. Eng.*, **2133**, 112 (1994).

231. P. Grosjean, J.-F. Savary, J. Mizeret, C. Wagnieres, H. van den Bergh and P. Monnier, *J. Clin. Laser Med. Surg.*, **14**, 281 (1996).
232. J. C. Kennedy, S. L. Marcus and R. H. Pottier, *J. Clin. Laser Med. Surg.*, **14**, 289 (1996).
233. S. L. Marcus, R. S. Sobel, A. L. Golub, R. L. Carrol, S. Lundahl and D. G. Shulman, *Proc. SPIE: Int. Opt. Eng.*, **2675**, 32 (1996).
234. R. Sroka, W. Beyer, L. Gossner, T. Sassy, S. Stocker and R. Baumgartner, *J. Photochem. Photobiol. B: Biol.*, **34**, 13 (1996).
235. W. Dietel, K. Bolsen, E. Dickson, C. Fritsch, R. Pottier and R. Wendenberg, *J. Photochem. Photobiol. B: Biol.*, **33**, 225 (1996).
236. D. L. Campbell, E. F. Gudgin-Dickson, P. G. Forkert, R. H. Pottier and J. C. Kennedy, *Photochem. Photobiol.*, **64**, 676 (1996).
237. Z. Hua, S. L. Gibson, T. H. Foster and R. Hilf, *Cancer Res.*, **55**, 1723 (1995).
238. B. W. Henderson, L. Vaughan, D. A. Bellnier, H. van Leengoed, P. G. Johnson and A. R. Oseroff, *Photochem. Photobiol.*, **62**, 780 (1995).
239. K. W. Woodburn, S. W. Young and R. A. Miller, *Proc. SPIE: Int. Opt. Eng.*, **2675**, 172 (1996).
240. K. W. Woodburn, Q. Fan, D. R. Miles, D. Kessel, Y. Luo and S. W. Young, *Photochem. Photobiol.*, **65**, 410 (1997).
241. M. F. Renschler, A. R. Yuen, T. J. Panella, T. J. Wieman, S. Dougherty, L. Esserman, M. Panjehpour, S. W. Taber, V. H. Fingar, E. Lowe, J. S. Engel, B. Lum, K. W. Woodburn, W.-F. Cheong, R. A. Miller, *Proc. SPIE Int. Opt. Eng.*, **3247**, 35–39 (1998).
242. K. W. Woodburn, S. W. Young, F. Qing, D. R. Miles and P. Thiemann, *Proc. SPIE: Int. Opt. Eng.*, **2972**, in press (1997).
243. K. W. Woodburn, Q. Fan, D. Kessel, M. Wright, T. D. Mody, G. Hemmi, D. Madga, J. L. Sessler, W. C. Dow, R. A. Miller and S. W. Young, *J. Clin. Laser Med. Surg.*, **14**, 343 (1996).
244. J. L. Sessler, W. C. Dow, D. O'Connor, A. Harriman, G. Hemmi, T. D. Mody, R. A. Miller, F. Qing, S. Springs, K. Woodburn and S. W. Young, *Alloys and Compounds*, **249**, 146 (1997).
245. J. L. Sessler, M. Cyr, B. G. Maiya, M. L. Judy, J. T. Newman, H. Skiles, R. Boriack, J. L. Matthews and T. C. Chanh, *Proc. SPIE: Int. Opt. Eng.*, **1203**, 233 (1990).
246. B. Franck and A. Nonn, *Angew. Chem. Int. Ed. Engl.*, **34**, 1795 (1995).
247. M. Kreimer-Birnbaum, M. M. Zuk, B. Rihter, M. E. Kenney and M. A. J. Rodgers, *Proc. SPIE: Int. Opt. Eng.*, **2625**, 105 (1996).
248. R. K. Pandey, A. B. Sumlin, S. Constantine, M. Aoudia, W. R. Potter, D. A. Bellnier, B. H. Henderson, M. A. Rodgers, K. M. Smith and T. J. Dougherty, *Photochem. Photobiol.*, **64**, 194 (1996).
249. V. Rosenbach-Belkin, L. Chen, L. Fiedor, I. Tregub, F. Pavlotsky, V. Brumfeld, Y. Salomon and A. Scherz, *Photochem. Photobiol.*, **64**, 174 (1996).
250. M. Guardiano, R. Biolo, G. Jori and K. Schaffner, *Cancer Lett.*, **44**, 1 (1989).
251. C. Milanese, R. Biolo, G. Jori and K. Schaffner, *Lasers Med. Sci.*, **6**, 437 (1991).
252. K. Schaffner, E. Vogel and G. Jori, in *Biologic Effects of Light (1993)* (eds E. G. Jung and M. F. Holick) Walter de Gruyter, Berlin, 1994, pp. 312–321.
253. A. D. Cross, *Proc. SPIE: Int. Opt. Eng.*, **2625**, 262 (1996).
254. C. Richert, J. M. Wessels, M. Müller, M. Kisters, R. Benninghaus and A. E. Goetz, *J. Med. Chem.*, **37**, 2797 (1994).
255. M. Leunig, C. Richert, F. Gammara, W. Lumper, E. Vogel, D. Jocham and A. E. Goetz, *Brit. J. Cancer*, **68**, 225 (1993).
256. R.-M. Szeimies, and W. Böumler, *J. Photochem. Photobiol. B: Biol.*, **34**, 67 (1996).
257. R.-M. Szeimes, T. Sassy and M. Landthaler, *Photochem. Photobiol.*, **59**, 73 (1994).

258. C. K. Chang, I. Morrison, W. Wu, S.-S. Chern and S.-M. Peng, *J. Chem. Soc.: Chem. Commun.*, 1173 (1995).
259. L. I. Grossweiner, M. D. Bilgin, P. Berdusis, T. D. Mody, *Photochem. Photobiol.*, to be submitted.
260. D. Kessel, Y. Luo, K. Woodburn, C. K. Chang and B. W. Henderson, *Proc. SPIE: Int. Opt. Eng.*, **2392**, 122 (1995).
261. R.-M. Szeimes and W. Bäumier, *Arch. Dermatol. Res.*, **289**, 132 (1997).
262. V. Gottfried, R. Davidi, C. Averbuj and S. Kimel, *J. Photochem. Photobiol. B: Biol.*, **30**, 115 (1995).
263. L. Roitman, B. Ehrenberg, Y. Nitzan, V. Kravl, and J. L. Sessler, *Photochem. Photobiol.*, **60**, 421 (1994).
264. B. Franck, U. Schneider, D. Schröder, K. S. Gulliya and J. L. Matthews, in *Biologic Effects of Light 1993* (eds E. G. Jung and M. F. Holick) Walter de Gruyter, Berlin, 1994, pp. 289–302.
265. B. C. Wilson, in *Photosensitizing Compounds: Their Chemistry, Biology, and Clinical Use (Ciba Foundation Symposium 146)* (eds G. Bock and S. Harnett) Wiley, Chichester, UK, 1989, pp. 60–77.
266. J. G. Levy, A. Chan and H. A. Strong, *Proc. SPIE: Int. Opt. Eng.*, **2625**, 86 (1996).
267. J. M. Fernandez, M. D. Bilgin and L. I. Grossweiner, *J. Photochem. Photobiol. B: Biol.*, **37**, 131 (1997).
268. B. Aveline, T. Hasan and R. W. Redmond, *Photochem. Photobiol.*, **59**, 328 (1994).
269. N. J. Razum, A. B. Snyder and D. R. Doiron, *Proc. SPIE: Int. Opt. Eng.*, **2675**, 43 (1996).
270. G. M. Garbo, *J. Photochem. Photobiol. B: Biol.*, **34**, 109 (1996).
271. J. D. Spikes and J. C. Bommer, *J. Photochem. Photobiol. B: Biol.*, **17**, 135 (1993).
272. J. D. Spikes and J. C. Bommer, *Photochem. Photobiol.*, **58**, 346 (1993).
273. W. Volz and R. Allen, in *Photodynamic Therapy and Biomedical Lasers* (eds P. Spinelli, M. dal Fante and R. Marchesini) Elsevier Science, New York, 1992, pp. 446–448.
274. D. Kessel and R. Allen, in *Photodynamic Therapy and Biomedical Lasers* (eds P. Spinelli, M. Dal Fante and R. Marchesini) Elsevier Science, New York, 1992, pp. 526–530.
275. R. Allen and D. Kessel, in *Photodynamic Therapy and Biomedical Lasers* (eds P. Spinelli, M. Dal Fante and R. Marchesini) Elsevier Science, New York, 1992, pp. 441–445.
276. T. J. Wieman, S. W. Taber and V. H. Fingar, *Photochem. Photobiol.*, **61**, 51S (1995).
277. P. Grosjean, J.-F. Savary, C. Wagnieres, J. Mizeret, A. Woodtli, J.-F. Theuman, C. Fontolliet, H. van den Bergh and P. Monnier, *Lasers Med. Sci.*, **11**, 227 (1996).
278. M. G. Dilkes, M. L. DeJode, A. Rowntree-Taylor, J. A. McGilligan, G. S. Kenyon and P. McKelvie, *Lasers Med. Sci.*, **11**, 23 (1996).
279. V. Vonarx-Coinsmann, M. T. Foutlier, N. Cempel, L. Morlet, A. Combre and T. Patrice, *Lasers in Med. Sci.*, **9**, 173 (1994).
280. H.-B. Ris, H. J. Altermatt, R. Inderbitzi, R. Hess, B. Nachbur, J. C. M. Stewart, Q. Wang, C. K. Lim, R. Bonnett, M. C. Berenbaum and U. Althaus, *Br. J. Cancer*, **64**, 1116 (1991).
281. H. van den Bergh, in *Proceedings of the First International Symposium on Hadrontherapy* (eds U. Amaldi and B. Larsson) Elsevier Science, Amsterdam, 1994, pp. 577–621.
282. J. C. Kennedy, R. H. Pottier and D. C. Pross, *J. Photochem. Photobiol. B: Biol.*, **6**, 143 (1990).
283. J. C. Kennedy and R. H. Pottier, *J. Photochem. Photobiol. B: Biol.*, **14**, 275 (1992).
284. R. Pottier and J. C. Kennedy, *Proc. SPIE: Int. Opt. Soc.*, **2625**, 2 (1996).
285. P. Wolf, E. Rieger and H. Kerl, *J. Am. Acad. Dermatol.*, **28**, 17 (1993).
286. F. Carinduff, M. R. Stringer, E. J. Hudson, D. V. Ash and S. B. Brown, *Br. J. Cancer*, **69**, 605 (1994).

287. K. Svanberg, T. Anderssen, D. Killander, I. Wang, U. Stenram, S. Andersson-Engels, R. Berg, J. Johansson and S. Svanberg, *Br. J. Derm.*, **130**, 743 (1994).
288. P. G. Calzavara-Pinton, *J. Photochem. Photobiol.: B: Biol.*, **29**, 53 (1995).
289. J. L. Sessler, G. L. Hemmi, B. G. Maiya, A. Harriman, M. L. Judy, R. Boriak, J. L. Matthews, B. Ehrenberg, Z. Malik, Y. Nitzan and A. Rück, *Proc. SPIE: Int. Opt. Eng.*, **1426**, 318 (1991).
290. B. Ehrenberg, L. Roitman, A. Lavi, Y. Nitzan and J. L. Sessler, *Proc. SPIE: Int. Opt. Eng.*, **2325**, 68 (1994).
291. B. Ehrenberg, A. Lavi, Y. Nitzan, Z. Malik, H. Ladan, F. M. Johnson and J. L. Sessler, *Proc. SPIE: Int. Opt. Eng.*, **1645**, 259 (1992).
292. B. Ehrenberg, Z. Malik, Y. Nitzan, H. Ladan, F. M. Johnson, G. Hemmi and J. L. Sessler, *Lasers Med. Sci.*, **8**, 197 (1993).
293. K. König, F. Genze, K. Miller, A. Rück, E. Reich and D. Repassy, *Laser Surg. Med.*, **13**, 522 (1993).
294. T. D. Mody, M. Wright, V. Linqvist, S. W. Young, J. L. Sessler, A. Harriman, M. Berns and R. A. Miller, *Photochem. Photobiol.*, **59S**, 37S (1994).
295. L. I. Grossweiner, J. M. Fernandez, M. B. Bilgin, K. W. Woodburn and T. D. Mody, unpublished results.
296. Pharmacyclics, Inc. Press Release January 7, 1997: *Pharmacyclics Completes Phase I Lu-Tex Trials in Photodynamic Cancer Treatment*.
297. D. R. Miles, L. M. Parker, P. A. Thiemann, K. W. Woodburn and S. W. Young, *Proc. SPIE: Int. Opt. Eng.*, **2972**, 38 (1997).
298. K. D. O'Brien and A. Chait, *Med. Clin. N. Amer.*, **78**, 4 (1994).
299. J. R. Spears, in *Cardiovascular Laser Therapy* (eds J. M. Isner and R. H. Clarke) Raven Press, New York, 1989, pp. 107–120.
300. K. W. Woodburn, F. Qing, D. Kessel and S. W. Young, *Proc. SPIE: Int. Opt. Eng.*, **2970**, 44 (1997).
301. K. W. Woodburn, S. W. Young, Q. Fan, D. Kessel and R. Miller, *Proc. SPIE: Int. Opt. Eng.*, **2671**, 62 (1996).
302. Y. N. Hsiang, M. Fragoso, V. Tsang and W. Schreiber, *Photochem. Photobiol.*, **57**, 518 (1993).
303. Y. N. Hsiang, M. T. Crespo, A. M. Richter, A. K. Jain, M. Fragoso and J. G. Levy, *Photochem. Photobiol.*, **57**, 670 (1993).
304. H. L. Narciso, W.-F. Cheong, R. Crilley, D. R. Doiron and J. R. Spears, *Proc. SPIE: Int. Opt. Eng.*, **2130**, 30 (1994).
305. G. M. Vincent, J. Fox, G. Charlton, J. S. Hill, R. McClane and J. D. Spikes, *Lasers Med. Sci.*, **11**, 399 (1991).
306. J. L. Matthews, F. Sogandares-Bernal, M. M. Judy, H. Kiles, J. E. Levenson, A. J. Marengo-Rowe and T. C. Chanh, *Transfusion*, **28**, 81 (1988).
307. J. L. Matthews, F. Sogandares-Bernal, M. M. Judy, A. Marengo-Rowe, J. Levenson, H. Skiles, J. Newman and T. C. Chanh, *Transfusion*, **231**, 636 (1991).
308. E. Ben-Hur and B. Horowitz, *Photochem. Photobiol.*, **62**, 383 (1995).
309. E. Ben-Hur, N. E. Geacintov, B. Studamire, M. E. Kenney and B. Horowitz, *Photochem. Photobiol.*, **61**, 190 (1995).
310. S. Rywkin, E. Ben-Hur, Z. Malik, A. M. Prince, Y. S. Li, M. E. Kenney, N. L. Oleinick and B. Horowitz, *Photochem. Photobiol.*, **60**, 165 (1994).
311. P. Gottlieb, L. G. Shen, E. Chimezie, S. Bahng, M. S. Kenney, B. Horowitz and E. Ben-Hur, *Photochem. Photobiol.*, **62**, 869 (1995).
312. E. Ben-Hur, M. E. Kenney, N. L. Oleinick, J. Mulvihill and B. Horowitz, *Lasers Med. Sci.*, **11**, 221 (1996).
313. J. North, H. Neyndorff, D. King, J. G. Levy, *Blood Cells*, **18**(1), 129–140 (1992).
314. J. North, H. Neyndorff and J. G. Levy, *J. Photochem. Photobiol. B*, **17**, 99 (1993).

315. J. L. Matthews, F. Sogandares-Bernal, M. Judy, K. Gulliya, J. Newman, T. Chanh and A. Marengo-Rowe, *Blood Cells*, **18**, 117 (1992).
316. M. L. Judy, J. L. Matthews, J. T. Newman, H. Skiles, R. Boriack, M. Cyr, B. G. Maiya and J. L. Sessler, *Photochem. Photobiol.*, **53**, 101 (1991).
317. T. Okunaka, K. Furukawa, K. Tanaka, H. Shimatani, M. Harada, H. Shibuya, S. Okada, J. Usuda, C. Konaka, K. Aizawa and H. Kato, *Proc. SPIE: Int. Opt. Soc.*, **2675**, 99 (1996).
318. E. Schröck, S. du Manoir, T. Veldman, B. Schoell, J. Wienberg, M. A. Ferguson-Smith, Y. Ning, D. H. Ledbetter, I. Bar-Am, D. Soenksen, Y. Garini and T. Ried, *Science*, **273**, 494 (1996).
319. T. Warloe, Q. Peng, H. Heyerdahl, J. Moan, H. B. Steen, K.-E. Giercksky, in *International Photodynamic Association Biennial Meeting*. (ed. D. A. Cortese), Proc. SPIE 2371, 226–135 (1995).
320. I. Wang, K. Svanberg, S. Andersson-Engels, R. Berg, P. Svanberg, in *International Photodynamic Association Biennial Meeting*, (ed. D. A. Cortese), Proc. SPIE 2371, pp. 243–252 (1995).
321. K. Svanberg, I. Wang, R. Rydell, A. Einer, J. Wennerberg, L. P. Clemente, E. Cardosa, R. Pratas, N. P. Clemente, S. Andersson-Engels, S. Svanberg, in *International Photodynamic Association Biennial Meeting*, (ed. D. A. Cortese). Proc SPIE 2371, pp. 129–141 (1995).

Cumulative Author Index

This index comprises the names of contributors to Volumes 1–5 of **Perspectives in Supramolecular Chemistry**.

- Beginn, Uwe, *Supramolecular Structures with Macromolecules*, **4**, 89.
Bell, Ian M., *see* Hilvert, Donald, **1**, 73.
Benkovic, S.J., *Macrocycles and Antibodies as Catalysts*, **1**, 149.
Barawkar, Dinesh, A. *see* Ganesh, Krishna N., **3**, 263.
Bowden, Ned, *see* Issacs, Lyle, **4**, 1.
Bradshaw, Jerald, S., *see* Izatt, Reed, M., **4**, 225.
Bruce, Duncan, W., *Metallomesogens—Supramolecular Organization of Metal Complexes in Fluid Phases*, **5**, 285.
Bruening, Ronald, L., *see* Izatt, Reed, M., **4**, 225.
- Chambron, Jean-Claude, *Rotaxanes: From Random to Transition Metal-templated Threading of Rings at the Molecular Level*, **5**, 225.
Chang, Ning-Leh, *see* Davis, Raymond E., **2**, 63.
Chin, Donovan, N., *see* Issacs, Lyle, **4**, 1.
Collinson, Simon, *see* Bruce, Duncan, W., **5**, 285.
Cramer, Friedrich, *Emil Fischer's Lock-and-Key Hypothesis after 100 Years—Towards a Supracellular Chemistry*, **1**, 1.
Czarnik, Anthony, W., *Chemosensors: Synthetic Receptors in Analytical Sensing Applications*, **4**, 177.
- Dance, Ian, *Supramolecular Organic Chemistry*, **2**, 137.
Davis, Raymond E., *Molecular Shape as a Design Criterion in Crystal Engineering*, **2**, 63.
Demleitner, Bernhard, *see* Saalfrank, Rolf, W., **5**, 1.
Desiraju, Gautam R., *Crystal Engineering and Molecular Recognition—Twin Facets of Supramolecular Chemistry*, **2**, 31.
Dunitz, Jack D., *Thoughts on Crystals as Supermolecules*, **2**, 1.
- Fabbrizzi, Luigi, *Fluorescent Sensors for and with Transition Metals*, **5**, 95.
Fagan, Paul J., *Molecular Engineering of Crystals by Electrostatic templating*, **2**, 107.
Fredricks, John R., *Metal Template Control of Self-Assembly in Supramolecular Chemistry*, **3**, 1.
- Ganesh, Krishna N., *Synthetic Control of DNA Triplex Structure Through Chemical Modifications*, **3**, 263.
Glusker, Jenny P., *The Protein as a Supermolecule: The Architecture of a ($\beta\alpha$)₈ Barrel*, **2**, 235.

- Hamilton, Andrew, D., *see* Fredricks, John R., **3**, 1.
Hilvert, Donald, *New Biocatalysts via Chemical Modifications*, **1**, 73.
Horovitz, Ammon, *see* Katchalski-Katzir, Ephraim, **1**, 25.
- Issacs, Lyle, *Self-Assembling Systems on Scales from Nanometers to Millimeters: Design and Discovery*, **4**, 1.
Izatt, Reed, M., *Ion Separations in Membrane and Solid Phase Extraction Systems*, **4**, 225.
- Katchalski-Katzir, Ephraim, *Molecular recognition in Biology: Models for Analysis of Protein-Ligand Interactions*, **1**, 25.
Kim, Kimoon, *Self-Assembly of Interlocked Structures with Cucurbituril Metal Ions and Metal Complexes*, **5**, 371.
Krishnamohan Sharma, C.V., *see* Desiraju, Gautam R., **2**, 31.
Kuhn, Hans, *A Model of the Origin of Life and Perspectives in Supramolecular Engineering*, **1**, 247.
Kumar, Vijayanti, A. *see* Ganesh, Krishna N., **3**, 263.
- Lahav, Meir, *Lock-and-Key Processes at Crystalline Interfaces: Relevance to the Spontaneous Generation of Chirality*, **1**, 173.
Lancet, Doron, *see* Katchalski-Katzir, Ephraim, **1**, 25.
Lehn, Jean-Marie, *Perspectives in Supramolecular Chemistry—From the Lock-and-Key Image to the Information Paradigm*, **1** 307.
Leiserowitz, Leslie, *see* Lahav, Meir, **1**, 173.
Licchelli, Maurizio, *see* Fabbrizzi, Luigi, **5**, 95.
Lugtenberg, R.J.W., *Selective Ion Recognition with Durable Sensors*, **4**, 193.
- Maitra, Uday, *A Survey of Supramolecular Chemistry (1993–1994)*, **3**, 41.
Meijer, E.W., *see* van Genderen, Marcel H.P., **4**, 47.
Mody, Tarak, D., *Porphyrin- and Expanded Porphyrin-Based Diagnostic and Therapeutic Agents*, **4**, 245.
Möller, Martin, *see* Beginn, Uwe, **4**, 89.
Moumentau, Michel., *Models of Hemoprotein Active Sites*, **3**, 155.
- Pallavicini, Piersandro, *see* Fabbrizzi, Luigi, **5**, 95.
Parodi, Luisa, *see* Fabbrizzi, Luigi, **5**, 95.
Popovitz-Biro, Ronit, *see* Lahav, Meir, **1**, 173.
Provent, Christophe, *The Chirality of Polynuclear Transition Metal Complexes*, **5**, 137.
- Real, José Antonio, *Bistability in Iron (II) Spin-Crossover Systems: A Supramolecular Function*, **5**, 55.
Rebek Jr, Julius, *see* Wintner, Edward A., **3**, 225.
Reinhoudt, D.N., *see* Lugtenberg, R.J.W., **4**, 193.
- Saalfrank, Rolf, W., *Ligand and Metal Control of Self-Assembly in Supramolecular Chemistry*, **5**, 1.
Scrimin, Paolo., *Control of Reactivity in Aggregates of Amphiphilic Molecules*, **3**, 101.
Sessler, Jonathan, L., *see* Mody, Tarak, D., **4**, 245.
Smithrud, D.B., *see* Benkovic, S.J., **1**, 149.
- Taglietti, Angelo, *see* Fabbrizzi, Luigi, **5**, 95.

- van Genderen, Marcel H.P., *Dendritic Architectures*, **4**, 47.
- Vlassov, V.V., *Oligonucleotides: Superspecific Ligands for Targeting Nucleic Acids and Proteins and Development of Molecular Devices*, **1**, 89.
- Ward, Michael, D., *see* Fagan, Paul J., **2107**.
- Waser, Jürg, *see* Kuhn, Hans, **1**, 247.
- Weissbuch, Isabelle, *see* Lahav, Meir, **1**, 173.
- Whitesell, James, K., *see* Davis, Raymond E., **2**, 63.
- Whitesides, George, M., *see* Issacs, Lyle, **4**, 1.
- Williams, Alan, F., *see* Provent, Christophe, **5**, 137.
- Winpenny, Richard E.P., *Design and Serendipity in the Synthesis of Polymetallic Complexes of the 3d-Metals*, **5**, 195.
- Wintner, Edward A., *Recent Developments in the Design of Self-Replicating Systems*, **3**, 225.
- Wong, Man-Shing, *see* Davis, Raymond E., **2**, 63.
- Xia, Younan., *see* Issacs, Lyle, **4**, 1.
- Yoon, Juyong, *see* Czarnik, Anthony, W., **4**, 177.

Cumulative Title Index

This index comprises the titles and authors of all chapters appearing in Volumes 1–5 of **Perspectives in Supramolecular Chemistry**.

A Model of the Origin of Life and Perspectives in Supramolecular Engineering (<i>Kuhn and Waser</i>)	1	247
A Survey of Supramolecular Chemistry (1993–1994) (<i>Maitra</i>)	3	41
Bistability in Iron (II) Spin-Crossover Systems: A Supramolecular Function (<i>Real</i>)	5	55
Chemosensors: Synthetic Receptors in Analytical Sensing Applications (<i>Czarnik and Yoon</i>)	4	177
Control of Reactivity in Aggregates of Amphiphilic Molecules (<i>Scrimm</i>)	3	101
Crystal Engineering and Molecular Recognition Twin Facets of Supramolecular Chemistry (<i>Desiraju and Krishnamoran Sharma</i>)	2	31
Dendritic Architectures (<i>van Genderen and Meijer</i>)	4	47
Design and Serendipity in the Synthesis of Polymetallic Complexes of the 3d-Metals (<i>Winpenny</i>)	5	193
Emil Fischer's Lock-and-Key Hypothesis after 100 Years—Towards a Supracellular Chemistry (<i>Cramer</i>)	1	1
Fluorescent Sensors for and with Transition Metals (<i>Fabrizzi, Licchelli, Pallavicini, Parodi and Taglietti</i>)	5	95
Ion Separations in Membrane and Solid Phase Extraction Systems (<i>Izatt, Bradshaw and Bruening</i>)	4	225
Ligand and Metal Control of Self-Assembly in Supramolecular Chemistry (<i>Saalfrank and Demleitner</i>)	5	1
Lock-and-Key Processes at Crystalline Interfaces: Relevance to the Spontaneous Generation of Chirality (<i>Weissbuch, Popovitz-Biro, Leiserowitz and Lahav</i>)	1	173

Macrocycles and Antibodies as Catalysts (<i>Smithrud and Benkovic</i>)	1	149
Metallomesogens—Supramolecular Organization of Metal Complexes in Fluid Phase (<i>Collinson and Bruce</i>)	5	285
Metal Template Control of Self-Assembly in Supramolecular Chemistry (<i>Fredericks and Hamilton</i>)	3	1
Models of Hemoprotein Active Sites (<i>Momenteau</i>)	3	155
Molecular Engineering of Crystals by Electrostatic Templating (<i>Fagan and Ward</i>)	2	107
Molecular Recognition in Biology: Models for Analysis of Protein–Ligand Interactions (<i>Lancet, Horovitz and Katchalski-Katzir</i>)	1	25
Molecular Shape as a Design Criterion in Crystal Engineering (<i>Davis, Whitesell, Wong and Chang</i>)	2	63
New Biocatalysts via Chemical Modifications (<i>Bell and Hilvert</i>)	1	73
Oligonucleotides: Superspecific Ligands for Targeting Nucleic Acids and Proteins and Development of Molecular Devices (<i>Vlassov</i>)	1	89
Perspectives in Supramolecular Chemistry—From the Lock-and-Key Image to the Information Paradigm (<i>Lehn</i>)	1	307
Porphyrin- and Expanded Phorphyrin-Based Diagnostic and Therapeutic Agents (<i>Mody and Sessler</i>)	4	245
Recent Developments in the Design of Self-Replicating Systems (<i>Wintner and Rebek Jr</i>)	3	225
Rotaxanes: From Random to Transition Metal-Templated Threading of Rings at the Molecular Level (<i>Chambron</i>)	5	225
Selective Ion Recognition with Durable Sensors (<i>Lugtenberg and Reinhoudt</i>)	4	193
Self-Assembling Systems on Scales from Nanometers to Millimeters: Design and Discovery (<i>Issacs, Chin, Bowden, Xia and Whitesides</i>)	4	1
Self-Assembly of Interlocked Structures with Cucurbituril Metal Ions and Metal Complexes (<i>Kim</i>)	5	372
Supramolecular Structures with Macromolecules (<i>Beginn and Möller</i>)	4	89
Synthetic Control of DNA Triplex Structure Through Chemical Modifications (<i>Ganesh, Kumar and Barawkar</i>)	3	263
The Chirality of Polynuclear Transition Metal Complexes (<i>Provent and Williams</i>)	5	137
The Protein as a Supermolecule: The Architecture of a $(\beta\alpha)_8$ Barrel (<i>Glusker</i>)	2	235
Thoughts on Crystals as Supermolecules (<i>Dunitz</i>)	2	1

Index

- AB diblock copolymers 131
 ABC-triblock copolymers 104, 105, 154
 Acid-alkali wastewater solutions 235
 Acid-base complexes 140
 Acrylic acid 158
 Acrylonitrile 158
 Aggregation behaviour 67
 Alkanethiolates
 on Ag, Cu and GaAs 21
 on Au 15, 16, 20, 21
 Alkanethiols 28
 Alkylamides 208
 Alkyl-decorated dendrimers 49
 Alkylesters 208
 1,2-Alternate conformation 207
 1,3-Alternate conformation 207
 δ -Aminolevulinic acid (δ -ALA) 273–5, 282
 5-Aminolevulinic acid-induced protoporphyrin IX 265
 Amphiphiles 119
 Amphiphilic behaviour 67–77
 at air–water interface 70
 Amphiphilic dendrimers 80, 82
 Amphiphilic polymers 65, 66
 Anion separations 240
 Association copolymers 151
 Atramol 49
 Atherosclerotic disease, PDT 278–9
 Atomic numbering 59
 Atomistic models 34

 Barbituric acid 146, 151
 Bengal Rose molecules 62–5, 78–9, 123
 Benzoporphyrin derivative 269–70
 Berkeley Pit 232–5
 Biocompatibility 85

 Biomedical applications 85
 Biosensor 178
 Biotic receptors 178
 Biphenyl phenanthrolines 149
 Bipyridine phenanthroline 146–7
 Bis(*p*-bromophenyl)melamine 26
 α,α' -Bis-(3,5-bis(phenylthiomethyl)phenoxy- α -cyanomesitylene (BB-CI) 137
 Bis(bipyridyl-phenyl)-cyclophane 139
 5,10-Bis(4-methylpyridinium)-15,20-bis-(4-nitrophenyl)porphyrin 259
 Bismuth removal 236–7
 Bis(phenyl-phenylene) cyclophane 146
 Block copolymers 102, 103
 see also specific block polymers
 Blood purification 279
 Bond length 93
l-Borneol 185
 Boron neutron capture therapy (BNCT) 250, 251
 BPD-MA 265, 269, 278
 Branched macromolecules 48
 Brewster angle microscope (BAM) 70
 5-Bromodeoxyuridine (BUdR) 256
 Broxine 256
 Brush-polymer 148
 Buckminsterfullerene 47
 Bulk liquid membranes (BLM) 229–31
 1,3-Butadienes 117
tert-Butyloxycarbonyl (*t*-BOC)-protected L-phenyl-alanine 58
p-*tert*-Butylphenol 206

 Cadmium(II) system 245
 Calix[4]arenes 206–15
 carbonyl functionalized 208

- crown ethers, cation interaction with 209–11
- ethyleneoxy bridged 211
- phosphine oxide functionalized 209–10
- sulphur containing 212–14
- Calix[5]arenes, receptor molecules based on 214–15
- Calix[6]arenes, receptor molecules based on 214–15
- Camphor sulfonic acid 140, 142
- CA^M lattice 3–7, 24, 26, 38
- CA^M rosettes 13
- Candau-Leong-Fitch (CLF) model 125
- ε*-Caprolactone 93
- 3-Carboxy-PROXYL 60, 61
- Catalysts 177–8
- Cation interaction
 - with calix[4]arene crown ethers 210–11
 - with carbonyl functionalized calix[4]arenes 208–9
 - with phosphine oxide functionalized calix[4]arenes 209–10
 - with sulphur containing calix[4]arenes 212–14
- Cellulosis 134
- CH₂Cl₂ 64
- CH₂Cl₂-triethylamine mixture 58
- Chain rigidity 95
- CHARMm program 60
- CHEMFETs 187–8, 193–223
 - architecture 194–6
 - long-life 201
 - schematic representation 196
 - silicone rubber based 203
- Chemical separation methods 225–43
 - desirable features 228
 - experimental techniques 229–31
 - novel 227
 - trace amounts 229
 - traditional 226
 - see also* specific methods
- Chemical SFM 128
- Chemosensors 177–91, 193
 - combinatorial approaches 189–91
 - future 189–90
- Chenodeoxycholic acid (CDCA) 185, 187
- Cholic acids 187
- Chrome wastewater 235
- Chromogenic (calorimetric) chemosensors 179–82
- Circular dichroism (CD) spectra 63–4
- Cluster phase 106
- Cobalt(III) porphyrin derivatives 259
- Compartmentization effects 123
- Complexing agents 230
- Compression isotherms 82
- Conductivity measurements 67–70
- Cone conformation 207
- Copolymerization 125
- Copper refinery tankhouse solution 236–7
- Core-shell molecules 58
- Core-shell structure 125
- CoTMPyP 259
- CoTPPS₄ 259
- Counteracting diffusion potential 216
- Covalent bonds 3
- CPK models 7–8, 14, 36, 82, 83
- Creatinine 182, 183
- Critical aggregation concentration (CAC) 80
- Critical association concentration (CAC) 71–2, 77
- Critical micelle concentration (CMC) 119
- Crystal engineering 24, 28, 34, 38
- Crystalline growth 38
- Curie law 61
- Cyanuric acid 146, 149
- Cyanuric acid-melamine lattice. *See* CA^M
- Cyclic oligopeptides 153
- Cyclic ureas 24, 26
- Cyclodextrines 138, 186
- α-Cyclodextrines 139, 145
- β-Cyclodextrines 151, 185, 187
- DAB-*dendr*-(CN)_n 50–6
- DAB-*dendr*-(NH₂)_n 50–7, 78
- DAB-*dendr*-(NH-*t*-BOC-L-Phe)₆₄ 60–3
- DAB-*dendr*-(NHCOC_m)_n 78, 79
- Dansyl 185
- Dansyl-glycine-modified β-CD 185
- Dansyl-L-leucine-modified β-CD 185
- Decompression isotherms 82
- Degrees of freedom (DOF) 34
- ΔG, surrogates 35–6
- Dendrimers 48–9, 78, 83
 - nomenclature 50
 - sizes 56
 - stepwise synthesis 95
 - superamphiphiles based on 65–78
- Dendritic architectures 47–88
 - supramolecular interactions of 84
- Dendritic box 57–65, 123
 - dynamic light scattering studies 60
 - encapsulation of guest molecules 60–4

- Dendritic box (*continued*)
 organic dye molecules in 62
 shape-selective liberation of encapsulated guests 64–5
- Dendritic systems 48
- Dendrons 137
- Deoxycholic acid 187
- Deviation from planarity (DP) 35
- 1,4-Diaminobutane 50
- 2,4-Diamino-1,3,5-triazine 148
- Diazo-functionalized monomers 125
- 2,2-Dibutyl-2-stanna-1,3-dioxepane initiator 93
- Dichloromethane 78
- Diethylbarbital 26
- Differential scanning calorimetry (DSC) 54
- Diffusion-ordered spectroscopy 56
- 2,4-(α,β -Dihydroxyethyl)deuteroporphyrin (MnBOPP) 250, 251
- Diketopiperazines (DKPs) 26–8, 38
- p*-(Dimethylamino)benzoyl (DMAB) 185
- Diphenylglucoluril 151
- Diphenylglycoluril 142–4
- Dipole–dipole interactions 54
- 4,5-Disubstituted 2-benzimidazolones 24
- DNA duplex formation 28
- DNA sequences 28
- Dodecanethiol 20
- Dodecanethiolate on gold 18, 20
- Dodecyl benzene sulfonic acid 142
- Dodecyl sulfonic acid 140
- Donnan exclusion failure 200
- Drug discovery 190
- DTPA 247
- Dynamic light scattering (DLS) 67, 72–3, 80
- EDTA 230
- Eisenberg–Hind–Moore (EHM) model 105
- Electrochemical chemosensors 187–8
- Electrochemical STM 128
- Electron donor/acceptor complexation 111
- Electron spin resonance spectroscopy 123
- Electrospray ionization mass spectrometry (ES-MS) 11
- Electrospray mass spectroscopy 51–3
- Empirical potentials (EP) 34
- Emulsion liquid membranes (ELM) 230
- Emulsion polymerization 123, 124
- Enhancing agents 245
- Enthalpy 35
 calculation for molecular systems 34
- Enthalpy-driven ordering 102
- Entropy 35
 calculation for molecular systems 34
- Entropy-driven disordering 102
- Environmental contamination 232–5
- Enzymes 177
- Epichlorhydrin 139
- Eriochrome Black T 64
- Escherichia coli* 155
- Ethyleneoxy bridged calix[4]arene 211
- Feridex I.V. 248
- FeTPPS₄ 249
- Fibrillar morphology 110
- Fibrillar superstructures 151
- Field effect transistor (FET) 201
 see also ISFETs
- Fluorescence-imaging 281–82
- Fluorescence intensity ratio 72
- Fluorescent chemosensors 183–6
- 5-Fluorouracil (5-FU) 256
- Formaldehyde 206
- Formic acid 65
- Fréchet type dendrons 137
- Freely jointed chain 93
- Gadolinium(III) cations 247
- Gadolinium(III) complexes 245, 251
- Gadolinium(III) polydentate oxyanion-based chelands 248
- Gadolinium(III) texaphyrins 246, 249, 252–4
 as radiation sensitizers 259–62
- Gadolinium(III) TPSP₄ 250
- Gastromark 248
- GdDTPA 251
- Gel permeation chromatography (GPC) 51
- Glass transition temperature 53–4
- Gold
 alkanethiolates on 15, 16, 20, 21
 dodecanethiolate on 18, 20
 hexadecanethiol on 22
 hexadecathiolate on 19
- Gold colloids 28
- Gold crystallites 123
- Gold cylinders 28
- Gold nanocrystals 122
- Gold recovery 237–9
- Guest–host systems 57
- “Hairy-rod” macromolecules 134
- HB/(N – 1) 6, 35–6

- Head group modified superamphiphile 69
Helical morphology 106
Hematoporphyrin (Hp) 263
Hematoporphyrin derivative (HpD) 248, 258
Henderson approximation 199
Hexadecanethiol on gold 22
Hexadecathiolate on gold 19
High pressure liquid chromatography (HPLC) 51
Hollow fibre supported liquid membranes (HFSLM) 230–31
Honeycomb structure 129
Host–guest chemistry 182
Host–guest selectivity 225
Hydraamphiphiles 65
Hydrogen-bonded imide protons 10
Hydrogen-bonded molecular aggregates 3–14
 analysis of spokes 11–12
 buttressing groups 12
 characterization 8–11
 CPK models 7–8, 14
 design 4–8
 electrospray ionization mass spectrometry (ES-MS) 11
 future challenges and unsolved problems 13–14
 gel permeation chromatography 10–11
 $HB/(N - 1)$ 6
 isomers 12–13
 nuclear magnetic resonance 9, 10, 11
 peak width 9
 peripheral crowding 5, 12
 preorganization 5
 solubility 7
 stoichiometry by titration 10
 symmetry 7
 synthesis 8
 tetrahedral aggregates 13
 vapor pressure osmometry (VPO) 11
Hydrogenation 51, 52
Hydrogen bonding 146, 151
 in molecular organic crystals 24–8
Hydrogen-bonding-based tapes 26
Hydrophobic effect 151
Hydrophobic probe 185
N-Hydroxy-succinimide ester 38
Hydroxyl radicals 257
Hyperbranched polymers 48
Hypoxia 258
Hypoxic sensitizers 256–8
Imprinted polymer matrix 157
Imprinted polymers 159
Inclusion polymerization 139
Infrared (IR) spectroscopy 51, 52
Intermolecular interactions 48
Intramolecular interactions 48
Inverted unimolecular dendritic micelles 123
 self-assembly 78
5-Iododeoxyuridine (Iudr) 256
Ion-selective electrodes (ISEs) 193, 206, 212
Ion-sensitive field effect transistors (ISFETs) 187, 193–5, 202–4
Ion separation in membrane and solid phase extraction systems 225–43
Ionomers 104
Iron(III) cations 247
Iron(III) complexes 246
Iron(III) porphyrins 249
Iron(III) tetrapyrrolic complexes 248
Iron(III) TPPS₄ 249, 250
Isophthalic acid 149
Kevlar 101, 108
Kratky–Porod chain 93–5
 $L/2 + n^2L$ layers 130
Ladder structures 110
Langmuir–Blodgett (LB) films 20, 133–6
Langmuir–Blodgett (LB) techniques 133
Lanthanide(III) 252
Laser-induced fluorescence (LIF) 281, 282
Lauryl gallate 142
Layer-by-layer adsorption technique 135–6
Lead removal 231, 232
Lescanec-model 56
Levulan 273–5
Linear concentration profile 199
Liquid crystalline polymers 108, 109
Liquid membrane systems 230
Lithocholic acid 187
“Living polymerization” techniques 91
“Lost key” phenomenon 178–9
Lutetium(III) complexes 245
Lutetium(III) texaphyrin 265, 275–7, 282
Lyotropic liquid-crystalline ordering 142
Macromolecular architectures 92
Macromolecular chemistry 89
Macromolecular core-shell particles 126

- Macromolecular crystallinity 95
Macromolecular formation 91
Macromolecular supramolecular chemistry 136–55
Macromolecular templates 158
Magneson 151
Magnetic resonance imaging (MRI) 245–6
 background 246–8
 utility of contrast agents 246–8
Main chain liquid crystal polymers (MCLCP) 108
MALDI-TOF-MS 59
Maleic-imide groups 148
Maleic-imide:triazine hydrogen-bonded complexes 148
Manganese(II) cations 247
Manganese(II) DPDP (dipridoxyl diphosphate) 248
Manganese(II) phthalocyanine 246
Manganese(III) 251
Manganese(III) complex of hematoporphyrin (MnHp) 250
Manganese(III) complexes 246, 248
Manganese(III) *meso*-tetrakis(4-sulfonatophenyl)porphyrin (MnTPPS₄) 249–51
Manganese(III) *meso*-tetrakis(*N*-(methyl-4-pyridyl)porphyrin (MnTMPyP) 250
Manganese(III) PcS₄ 251
Manganese(III) porphyrin derivatives 249
Manganese(III) porphyrins 248, 250
Marangoni convection 129
Mark-Houwink-Sakurada rise in viscosity 48
Mechanical SFM 128
Melamine 148, 149
Membrane potential 196–200
MEMFET 195, 200, 205
MESA 28–34
 assembly of objects 33–4
 choice of material 31
 computer simulations 38–9
 design and fabrication of objects 31–2
 experimental issues 31–4
 forces 32–3
Meso-(tetrahydroxyphenyl)chlorin (*m*-THPC) 265, 272–3
Mesoscale self-assembly. *See* MESA
Metalloporphyrins 259
Metallurgical operations, MRT 235–7
Methacrylated ionophore 188
5-Methoxypsoralen (MOP) 262
Methylketones 208
2-Methyltetrahydrofuran 60
Micellar films 133
Micellar monolayers 134
Micelles
 block copolymer 120, 123
 cylindrical 120
 formation 119–20
 monomer loaded 125
 plate-like 120
Michael reactions 50
Microcontact printing (μ CP) 20–2, 24
Microemulsion 125
Microemulsion polymerization 127
Microgel particles 128
“Miktoarm” block copolymers 104
Molecular architecture 109
Molecular clipping 147
Molecular crystals 97
Molecular dynamics
 methods 34
 simulation 56
Molecular imprinting 156, 158
Molecular mechanics 60
Molecular modelling techniques 56
Molecular mushrooms 154
Molecular recognition technique. *See* MRT
Molecular volumes 56, 57, 84
Mono-L-aspartyl chlorin e6 (MACE) 271–72
Monolayer experiments 70–1, 82
Mono-micellar films 133
D-Monosaccharides 183–5
L-Monosaccharides 183–5
Monte Carlo methods 38
Monte Carlo simulations 56
MOSFET 194
MRT 175, 178, 228, 231–41
 analytical uses 240–41
 anion separations 240
 Berkeley Pit 233–5
 environmental contamination 232–5
 metallurgical operations 235–7
 nuclear waste applications 239–40
 precious metals recovery 237–9
 US Navy plating operation 235
Multilayer films 133
Multilayer-formation 134
Multiplets 105–6
Nafion 107, 108
Neopharm 256
Nephila clavipes 101

- Neutron scattering 56
Nickolsky-Eisenman equation 198
Nitroimidazole 258
Nitrophenol 151
NMR spectroscopy 7
Nongadolinium(III)-based MRI contrast agents 248
Non-plasticized membrane materials 202–4
NPe6 281
Nuclear magnetic resonance (NMR) 9–11, 51, 179
Nuclear waste applications 239–40
Nylon-6 100, 142
- N*-Octyl-D-mannonamide 152
Oligo(propylene imine) cascade structures 49
Ordered structures 14
Osmium tetroxide 130
- Palladium complexes 137
Palladium recovery 238
Para-nitrobenzoic acid 64–5
Parent–daughter approach 158
Partial cone conformation 207
PCI-0120 253–5, 259–62
PCI-0123 265, 275–7, 278–9, 282
PDMS 31
Pentadecylphenol 142
Perfluorodecalin–water interface 32
Persistence length 93
PET (photoinduced electron transfer) chemosensor 186
pH effects 73
Phenylene-1,4-bis(oxy-oligoethyleneoxy)-carboxylic acid 146
Phenylene-1,4-bis(oxy-oligoethyleneoxy)- ω -carboxylic acid 139
Phosphorescent chemosensors 186–7
Phosphotungstate 152
Photochemotherapy, history 262
Photocurable (meth)acrylates 202
Photodynamic action 263
Photodynamic diagnosis (PDD) 281–82
Photodynamic therapy (PDT) 248, 250, 258, 262–79
agents 251
atherosclerotic disease 278–9
blood purification 279
current clinical status 264–8
second-generation agents in oncological applications 269–75
sensitizers 245
Photodynamic viral inactivation 262–79
Photofrin 264, 265, 268, 281
Photopolymerizable receptor molecules 216–17
Photosensitizers 265
characteristics 266
idealized criteria 267
Phthalocyanines (Pc) 248, 251
 pK_a values 55
Plasticized membrane materials 201–202
Platinum recovery 237–9
Poisson–Boltzmann equation 35
Poly(acrylonitrile) 117
Poly(2-alanyl-glycine) 155
Poly(alkyleneoxide) 120
Poly(alkylthiirane)s 112
Poly(amides) 100, 101
Poly(aminoamide) dendrimers 49
Poly(aniline) 140–2
Poly(aramides) 102
Poly(benzothiazoles) 102
Poly(benzylglutamate) 95, 112
Poly(butadiene) cylinders 130
Polycondensation 139
Polycyclic aromates 116
Polydentate oxyanion-based chelation 248
Polydimethylsiloxane (PDMS) 20–1, 30
Polyelectrolyte complexes 110
Polyelectrolyte/surfactant complexes 113
Polyelectrolytes 135
Poly(esters) 100
Poly(etherketones) 102
Poly(ethylene) 96, 100
Poly(ethyleneimine) 158
Poly(ethylene)oxide 98, 120, 142
Poly(ethylene)oxide/ α -cyclodextrine-rotaxanes 139
Poly(glutamates) 134
PolyHEMA 197
Poly(hydrazides) 148
Poly(4-hydroxybenzoic ester) 134
Poly(2-hydroxyethyl methacrylate)-[polyHEMA] hydrogel 195–6
Poly(isocyanates) 95
Poly(isocyanides) 95, 134
Poly(D-lactide) 113
Poly(L-lactide) 113
Poly(lactide) stereocomplexes 114
Poly(lactides) 93, 112, 115
Poly(lactones) 93

- Polymerization 123, 125, 138, 158
Poly(methylenes) 98
Poly(methylmethacrylate) (PMMA) 111–12, 125
Poly(oxymethylenes) 115
Poly(para-phenylene-vinylene) (PPV) 136
Poly(phenylene) 134, 137
Poly(phenylene) dendrimers 117
Poly(phenyleneterephthalamide) 108
Poly(phthalocyaninatosiloxanes) 134
Poly(propylene imine) dendrimers 49–57, 59, 84, 123
 characterization 51–3
 large-scale synthesis 50–1
 modifications 58
 physical properties 53–5
 shape 55–6
 synthesis 66–7
 synthetic scheme 50
Poly(propyleneoxide) 120
Polyrotaxanes 137–9, 145
Polysiloxane 188
Polysoaps 119
Poly(sodium styrene sulfonate) 110
Poly(styrene) 130
Poly(styrene)-block-polybutadiene 130
Poly(styrene)-block-poly(*p*-phenylene) films 129
Poly(styrene)-block-poly(2-vinylpyridine) 130
Poly(styrene-co-3,5-dihydroxystyrene) 144
Poly(styrene-co-4-hydroxystyrene-co-4'(3,5-dihydroxy-1-carboxyl-oxy)-styrene) 144
Polystyrene-COOH 66
Polystyrene-*dendr*-(CN)₁₆ 66
Polystyrene-*dendr*-(COOH)_{*n*} 66, 67, 70, 73
Polystyrene-*dendr*-(NH₂)₄ 119
Polystyrene-*dendr*-(NH₂)₃₂ 66, 119
Polystyrene-*dendr*-(NH₂)_{*n*} 67, 71, 73
Polystyrene-dendrimer block copolymers 66
Poly(styrene-*b*-methylmethacrylate) block copolymer film 130
Polystyrene-poly(propylene imine) block copolymer superamphiphiles 49
Polystyrene-poly(propylene imine) block copolymers 66, 68
Poly(styrene-*b*-2-vinylpyridine) 120, 121, 123, 130, 132
Poly(vinylacetate) 158
Poly(vinyl-*N*-butylpyridiniumbromide) 110
Poly(vinylpyridines) 142
Porphyrin fibres 152
Porphyrin-like macrocycles 258
Porphyrin wheels 129
Porphyrins 245, 246, 258
 as MRI contrast agents 248–52
 as radiation sensitizers 258–9
 history 263
Potentiometric sensors 193
Precious metals recovery 237–9
Pressure-area isotherms 71
Protoporphyrin IX (PpIX) 265, 274, 282
Pseudo-polyrotaxane 146
PVC membranes 201, 208, 210
Pyrimidine 147

Quantum mechanics (QM) 34

Radiation-induced cytotoxicity 260
Radiation sensitizer enhancement ratio (SER) 259
Radiation sensitizers 256
 gadolinium(III) texaphyrins as 259–62
 porphyrins as 258–9
Radical polymerization 140–51
Radioimmunoassay techniques 161
Radius of gyration 56, 57, 60
Receptor molecules
 based on calixarenes 206–15
 for selective recognition 205–6
 photopolymerizable 216–17
Receptors 178
Retro-Michael reaction 51, 54
Reusability 177
Reusable construction materials 178
Reusable indicators 178
Reusable machines 177
Reverse osmosis membranes 230
Reversibility 177
Rhodium recovery 238
Ring formation 129
“Rod-Coil” AB block copolymers 104
Rod-like molecules 134
Rod-like polymers 135
Room temperature vulcanizing (RTV) silicone rubbers 203
Rose Bengal molecules 62–5, 78–9, 123

SAMS 1–3, 14–24
 applications in interface engineering and microfabrication 20–4
 degree of interaction 15

- density of defects 17–19
- DNA terminated 28
- formation 16
- fundamental studies 15–20
- hydrophilic 21
- mixed 19–20
- patterning 20–4
- pinholes in hexadecathiolate on gold 19
- prototypical 23
- scanning probe microscopy (SPM) 15
- SEM image of patterned surface of gold 22
- SEM image of test patterns of silver 23
- simulations 36–8, 37
- STM image of dodecanethiolate on gold 18
- structure and order 17
- substrates and ligands forming 15
- terminated in $-NMe_3^+$ groups 28
- SAXS 60
- Scanning force microscopy 128
- Scanning near field optical microscopy 128
- Scanning probe microscopes 128
- Scanning tunnelling microscopy 128
- Self-assembled fibres 153
- Self-assembled monolayers. *See* SAMs
- Self-assembly 1–46
 - dissolved polymers 119–28
 - experimental systems 3–39
 - inverted unimolecular dendritic micelles 78–84
 - issues in theory 34–9
 - scope and objectives of review 2–3
 - solid state 24–8
- Shape-dependent aggregation behaviour 77
- Shish-kebab structures 99–100
- Side chain liquid crystalline polymer (SCLCP) 108
- Silver
 - recovery 237–9
 - SEM images of test patterns 23
- Simulated annealing 38
- Simulations, increasing efficiency 34–5
- Single crystals 97
- Size exclusion chromatography (SEC) 55–6
- Small-angle neutron scattering (SANS) 56
- SnET2 278
- Sodium dodecylsulfate 142
- Sodium poly(α ,L-glutamate) complexes 110
- Sol-gel based membranes 204
- Solid phase extraction (SPE) 228, 231, 232
- Soluble aggregates 36
- Solution polymerization 123
- Spider silk 101–2
- Spin-lattice relaxation measurements 59
- Spin-spin relaxation measurements 59
- Starbranched polymers 48
- Starburst 49
- Stereocomplexation 112
- Sterical factor 93
- Steroid/cyclohexane organogel 153
- Styrene/isoprene (S/IP) miktostars 104
- Superamphiphiles based on dendrimers 65–78
- SuperLig system 231, 238
- Supramolecular chemistry 89
 - macromolecules 136–55
- Supramolecular complexes 110
- Supramolecular gels 151
- Supramolecular interactions of dendritic architectures 84
- Supramolecular ordering 119–28
- Supramolecular organization
 - bulk 95–117
 - polymers in thin films and at surfaces 128–36
- Supramolecular organogels 151
- Supramolecular structures with macromolecules 89–174
- Supramolecular technologies 49
- Surface characterization 128
- Surface induced morphology 130
- Surface-polymer interaction 129
- Surlyn 108
- Template syntheses 155–9
 - 1,4,7,10-Tetraazacyclododecane- N,N',N' -triacetic acid (DO3A) 247
- Tetrachloroaurate salts 120
- Tetrachloroethylene 96
- Tetraethynylmethane 47
- Tetrakis(4-sulfonatophenyl)porphyrin (TPPS₄) 259
- Tetrakis(4-*N*-methylpyridyl)porphyrin (TMPyP) 259
- Tetraphenylborate 188
- Texaphyrins 245, 248, 258
- Thermal analysis 53
- Thermogravimetric analysis (TGA) 54
- Thin organic films 128–36
- Thin sheet supported liquid membranes

- (TSSLM) 230–1
- Thiolates, patterning SAMs 21
- Thiourea/dimethylbutadiene-inclusion complex 118
- Tin(IV) ethyl etiopurpurin (SnET2) 265, 270–71
- TMS model 196
- Toluene-concentrated HCl mixture 67
- Topochemical cyclization 116
- Trans-1,4-poly(butadienes) 117
- Transmission electron microscopy (TEM) 67, 73–7, 80
- Triaminotriazine]716s 151
- 2,4,7-Trinitro-9-fluorenone (TNF) 110
- Twaron 108
- Twisted intramolecular charge transfer (TICT) 185
- Two module hollow fibre supported liquid membranes (TMHFSLM) 230–31
- Ultrasmall superparamagnetic iron oxide (USPIO) particles 248
- Unimolecular dendritic micelles 78–80
- Ursodeoxycholic acid (UDCA) 185
- Urushiol 201–202
- US Food and Drug Administration (FDA) 246, 248, 251
- US Navy plating operation 235
- Valinomycin 188
- Van der Waals interactions 100
- Van der Waals radii 56
- Van der Waals repulsions 56
- Vectra 108
- N*-Vinylimidazole/poly(methacrylic acid) 158
- Viscometry 56
- Water–perfluorodecalin (PFD) interface 30
- X-ray diffraction 82
- X-ray quality crystals 40
- X-ray radiation therapy (XRT) 246 enhancement 255–62
- Zinc dodecylbenzene sulfonate 142